THE UNIVERSITY OF
SYDNEY

THE ROLE OF THE SECONDARY LYMPHOID ORGANS IN WEST NILE VIRUS ENCEPHALITIS: IMMUNE-MODIFYING MICROPARTICLE TREATMENT

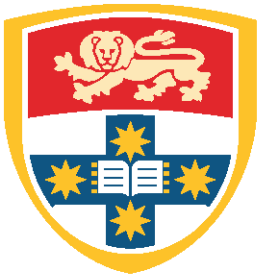

THE UNIVERSITY OF SYDNEY

Caryn van Vreden

A thesis submitted for the degree of Doctor of Philosophy

Discipline of Pathology, Sydney Medical School
The University of Sydney

2015

Declaration

I hereby declare that all work presented in this thesis describes original research work undertaken in the Discipline of Pathology, Sydney Medical School, The University of Sydney. I have been involved in the writing of review articles and book chapters, parts of which have been incorporated and rewritten in the introduction of this thesis (van Vreden et al. 2015; King et al. 2011; Ashhurst et al. 2014). The results in this thesis have not been previously submitted for any degree, and will not be submitted for any other degree or qualification. Results from this study, in particular Figure 4.15-Graph B, Figure 5.1-Graph A and Figure 5.8-Graph B, have been included in one publication by Getts et al. (Getts et al. 2014). All studies reported within this thesis were performed by the author except in the specific instances stated. Thomas Ashhurst (Discipline of Pathology, The University of Sydney) performed the immunofluorescent staining and imaging of Figure 5.1–Panel A. Luan vu Dinh (Discipline of Pathology, The University of Sydney) aided in the processing, acquisition and analysis of RT-PCR and gel electrophoresis assay in Figures 3.15-Panels A, B and C. Ethical approval was obtained for the use of mice from the Animal Ethics Committee at the University of Sydney (K20/8-2008/3/4863; K20/8-2009/3/5127; K20/11-2011/3/5660). The financial assistance of the National Research Foundation (NRF) towards this research is hereby acknowledged. Opinions expressed and conclusions arrived at, are those of the author and are not necessarily to be attributed to the NRF.

Caryn van Vreden

August 2015

Acknowledgements

Firstly, I would like to thank my supervisor Professor Nicholas King, without whom this thesis would not be possible. Nick, thank you for giving me the opportunity to do this degree in your laboratory and for your support throughout the years. I would also like to thank all the past and present King lab members, in particular: Celine Defrassnes, Rachael Terry, Amanda Yeung, Mahmoud Azar, Blanca Lee, Kanami Watabe, Victoria Jones, Darren Cox, Zheng Ling, Thomas Ashhurst, Luis Munoz-Erazo, Luan vu Dinh and Paula Niewold. All of you have helped me in someway to become a better researcher. Thanks to the staff of the Pathology department and Histopathology lab for their invaluable contribution to this thesis. Thank you to the members of the Flow cytometry facility for their invaluable technical support and training.

Paula, thank you as a colleague, but mostly as a friend, for countless hours of not only helping me with experiments, but making it fun. To my partner Phil, thanks for your patience and encouragement throughout these years and especially 3 am pickups from the lab. Also, thanks Jozi for always being happy to see me. Lastly, I would like to thank my family and friends back in South Africa: Al is julle ver weg het die pakkies, briewe en elke bemoedigende woord hierdie pad soveel makliker gemaak!

Lastly, I would like to thank the NRF South Africa and USYD for the financial support to my degree, allowing me to complete my studies in Australia.

Publications and presentations

van Vreden, C., Terry, R. L., Deffrasnes, C., Getts, D. R., Yeung, A., Getts, M. T., Davison, A. M., Munoz-Erazo, L., and King, N. J. C. (2011) "The Immunopathogenesis of Neurotropic Flavivirus infection". "Encephalitis / Book 1", ISBN 978-953-307-344-6. Accepted for publication, June 2011.

Say, J. M., **van Vreden, C.**, Reilly, D. J., Brown, L. J., Rabeau, J. R., King, N. J. C. (2011). "Luminescent nanodiamonds for biomedical applications". Biophysical Reviews 3 (4): 171-184. Accepted for publication, Oct 11, 2011.

Terry, R. L., Getts, D. R., Defrassnes, C., **van Vreden, C.,** Campbell, I. L., King, N. J. C. (2012). " Inflammatory monocytes and the pathogenesis of viral encephalitis". J Neuroinflammation 9:270. Accepted for publication, November 19, 2012.

Ashhurst, T. M., **van Vreden C.**, Munoz-Erazo, L., Niewold, P., Watabe, K., Terry, R.L., Deffrasnes, C., Getts, D.R., King, N. J. C. (2013). "Antiviral macrophage responses in flavivirus encephalitis". Indian J Med Res. 138 (5): 632-647. Accepted for publication October 18, 2012.

Getts, D. R., Terry, R. L., Getts, M. T., Deffrasnes, C., Muller, M., **van Vreden, C.**, Ashhurst, T. M., Chami, B., McCarthy, D., Wu, H., Ma, J., Martin, A., Shae, L. D., Witting, P., Kansas, G. S., Kuhn, J., Hafezi, W., Campbell, I. L., Reilly, D., Say, J., Brown, L., White, M. Y., Cordwell, S. J., Chadban, S. J., Thorp, E. B., Bao, S., Miller, S. D., King, N. J. C. (2014)."Therapeutic inflammatory monocyte modulation using immune-modifying microparticles". Sci Transl Med.6 (219): 219ra7.

Chami, B., Yeung, A. W., **van Vreden, C.,** King, N. J. C., Bao, S. (2014). "The Role of CXCR3 in DSS-Induced Colitis". PLoS One; 9(7): e101622. Accepted for publication June 10, 2014.

Ashhurst, T. M., **van Vreden, C.**, Niewold, P., King, N. J. C., (2014). "The plasticity of inflammatory monocyte responses to the inflamed central nervous system". Cell Immunol. 291(1-2): 49-57.

Terry, R. L., Deffrasnes , C., Getts, D. R., Minten, C., **van Vreden, C.**, Ashhurst, T. M., Getts, M. T., Xie, R. D., Campbell, I. L., King, N. J. C. (2015). "Defective inflammatory monocyte development in IRF8-deficient mice abrogates migration to the West Nile virus-infected brain". J Innate Immun. 7 (1): 102-12.

van Vreden, C., Niewold, P., Vu Dinh, L., Munoz-Erazo, L., Getts, D. R., King, N. J. C. (2015). "Flavivirus Encephalitis: Immunopathogenesis of disease and Immunomodulation". "Global Virology I-Identifying and investigating Viral Diseases", ISBN 978-1-4939-2410-3. Accepted for publication, June 2015.

Posters and presentations

Caryn van Vreden, Thomas Ashhurst, Paula Niewold, Wan-Chi Lee, Rachael L Terry, Celine Deffrasnes, Iain L Campbell, Nicholas JC King (2012). The contribution of CNS draining lymph nodes to the increase of lymphoid lineage cells in WNV encephalitis. Australasian Society for Immunology Annual Scientific Meeting, 2-6th December, Melbourne Vic Australia (Poster).

Caryn van Vreden, Paula Niewold, Victoria Jones, Nicholas King (2014) The recruitment of T-cell populations from non-draining lymph nodes to the adaptive immune response during viral encephalitis. Australasian Society for Immunology Annual Scientific Meeting, 1-5th December, Wollongong NSW Australia (Poster).

Caryn van Vreden, Paula Niewold, Victoria R. Jones, Rachael L.Terry, Shishan Bao, Nicholas JC King (2014). The role of the spleen in immune-modifying microparticle treatment of lethal West Nile encephalitis. 3rd International Conference on Immune Tolerance, 28-30th September, Amsterdam, The Netherlands.

Caryn van Vreden, Paula Niewold, Nicholas JC King (2014) The role of the spleen in immunemodulatory particle treatment of WNV encephalitis. Bosch Young Investigators Symposium, 9th December, The University of Sydney, Sydney NSW Australia (Oral presentation).

Caryn van Vreden, Paula Niewold, Victoria Jones, Nicholas King (2014). The recruitment of T-cell populations from non-draining lymph nodes to the adaptive immune response during viral encephalitis. 2014 MBI Colloquium, 25th November, The University of Sydney, Sydney NSW Australia (Poster).

Abstract

West Nile virus (WNV) is a neuroinvasive pathogen transmitted by mosquitoes and is one of the most widespread members of the Flaviviridae family. In some 2% of infected individuals, infection can progress to acute lethal encephalitis associated with a severe immunopathological response. Current treatments are symptomatic only and no approved vaccine exists for humans. Thus, research and design of viable treatment strategies targeting the pathological immune response in this disease are critical. Furthermore, understanding the mechanism of immunopathogenesis and development of the adaptive immune response to WNV is essential to elucidate how the virus is eventually eradicated. Very little is known about the local draining lymph node response to WNV encephalitis and, until recently, the exact lymphatic drainage pathway in the CNS has been relatively unknown. We investigated the local responses of the draining lymph nodes of the CNS, the cervical lymph nodes, as well as the non-draining inguinal and mesenteric nodes, following intranasal infection with WNV. The role of the draining lymph nodes in the development of an adaptive immune response during viral infection is well known, however, the extent to which the "non-draining" lymph nodes contribute to the adaptive immune response against a CNS viral infection has not been studied. In our model, the significant expansion of leukocyte numbers in the cervical lymph node, in response to WNV infection of the CNS, demonstrates its involvement in the immune reaction to CNS viral infection. Dendritic cell subsets in the cervical lymph node increase significantly from d5p.i., likely contributing to the significant B and T cell clonal expansion seen in these nodes. Although a certain proportion of leukocyte expansion in the cervical node is due to proliferation of cells *in situ*, leukocytes are clearly recruited from other lymphoid organs. Indeed, during WNV infection, distinct changes also occur in the mesenteric and inguinal lymph nodes. In contrast to the significant expansion of lymphocytes in the cervical lymph node, the inguinal and mesenteric nodes show a reduction of up to 50% in $CD4^+$ and $CD8^+$

T cell populations. We hypothesise that these T cells preferentially home to the cervical lymph node, contributing to T cell populations and forming part of the effector cell population in the adaptive immune response to WNV in the CNS. Tracking of peripheral node leukocytes also suggested that B cell recruitment to the CNS-draining lymph node was increased during WNV infection. Furthermore, significant upregulation of Ly6C expression occurs in both the draining and non-draining lymph nodes, in direct response to inflammation in the CNS. Further characterisation of the inflammatory response in the draining and non-draining lymph nodes will determine the kinetics of emigration of T and B cells from the non-draining lymph nodes and their specific contribution to the anti-viral immune response.

Although there is significant infiltration of lymphocyte subsets into the CNS of mice with WNV encephalitis, these cells only form some 30% of the total leukocyte infiltrate, whereas Ly6C^{hi} inflammatory monocytes can contribute up to 50%. Indeed, the recruitment of pathogenic Ly6C^{hi} inflammatory monocytes to the CNS is a hallmark of WNV encephalitis, as this subset has been shown to be the primary contributor to the lethal immunopathology seen in WNV encephalitis. We have recently shown that intravenous administration of immune-modifying microparticles (IMP) results in a halving of the numbers of Ly6C^{hi} monocytes infiltrating the brain and improves survival by up to 60% in a mouse model of intranasal WNV infection. These cells are sequestered with a significant proportion of IMP^{+} cells observed within the splenic marginal zone. Since the marginal zone macrophages phagocytose apoptosing cells and other particulate debris, including nanoparticles, we hypothesised that the spleen, in particular the marginal zone macrophages, may be crucial for the efficacy of IMP treatment.

Surgical removal of the spleen or specific depletion of splenic macrophages using clodronate-encapsulated liposomes resulted in a similar decrease in Ly6C^{hi} monocyte numbers in the CNS compared to IMP treatment, but did not result in increased survival.

In splenectomised mice, however, IMP treatment resulted in a further reduction in Ly6Chi monocyte numbers, and while not significant, this resulted in some improvement in survival.

In clodronate-depleted animals, in which marginal zone macrophages are completely ablated, IMP treatment also improved survival, with reduced Ly6C^{hi} monocyte infiltration into the brain. However, IMP treatment was still most effective in mice with an intact spleen that received no clodronate treatment. These data demonstrate that, neither the spleen as a whole, nor the marginal zone macrophages, are critical for successful IMP treatment, but the absence of these components nevertheless reduce IMP efficacy. These data highlight the fact that not all methods of Ly6C^{hi} inflammatory monocyte modulation are equal and suggests that, compared to clodronate and splenectomy-mediated reduction in Ly6C^{hi} monocytes, IMP treatment reduced this inflammatory monocyte subset specifically and with minimal impact on other components of the immune system, maintaining the ability to eradicate viral infection and promote survival. By further characterising key differences between these models we have elucidated a little further, the mechanism behind IMP treatment and expanded our understanding of the secondary lymphoid organs in the immune response to WNV encephalitis.

Abbreviations

ACE	angiotensin-converting enzyme
APC	antigen presenting cell
BBB	blood brain barrier
BrdU	Bromodeoxyuridine
CLN	cervical lymph node
CFSE	Carboxyfluorescein Succinimidyl Ester
CNS	central nervous system
CSF	cerebrospinal fluid
CTL	cytotoxic T lymphocyte
DC	dendritic cell
DENV	dengue virus
DRG	dorsal root ganglion
DNA	deoxyribonucleic acid
DLN	draining lymph node
EAE	experimental autoimmune encephalomyelitis
EDTA	ethylenediamineetraacetic acid
ER	endoplasmic reticulum
FACS	fluorescence-activated cell sorting
FCS	foetal calf serum
FRC	fibroblastic reticular cell
FSC-A	forward scatter-area
FSC-H	forward scatter-height
HEV	high endothelial venule
ICAM	intracellular adhesion molecule
IFN	interferon

IHC	immunohistochemistry
i.c.	intracranial
i.n.	intranasal
i.p.	intraperitoneal
i.v.	intravenous
IL	interleukin
ILN	inguinal lymph node
IMP	immune-modifying microparticles
ISG	interferon stimulatory genes
JEV	Japanese encephalitis virus
KO	knockout
LC	Langerhans cells
mAb	monoclonal antibody
MDM	monocyte-derived macrophages
MHC	major histocompatibility complex
MI	myocardial infarction
MLN	mesenteric lymph node
MMP	matrix metalloproteinases
MST	mean survival time
MVEV	Murray Valley encephalitis virus
MZM	marginal zone macrophages
NK cell	natural killer cell
NKT cell	natural killer T cell
NO	nitric oxide
NOS	nitric oxide synthase
PALS	peri-arteriolar lymphoid sheath
PBS	phosphate-buffered saline

PCR	polymerase chain reaction
pDC	plasmacytoid DC
PFU	plaque-forming unit
p.i.	post infection
PLN	popliteal lymph node
PMN	polymorphonuclear cells
PNS	peripheral nervous system
PRR	pattern recognition receptor
RBC	red blood cell
RLR	RIG-I-like receptor
RNA	ribonucleic acid
ROS	reactive oxygen species
RT	room temperature
$S1P_1$	sphingosine-1 phosphate receptor-1
SCS	subcapsular sinus
SSC-A	side scatter-area
TBEV	tick-borne encephalitis virus
TBST	Tris-buffered saline with Tween-20
TJP	tight junction proteins
TLR	Toll-like receptor
TNF	Tumor necrosis factor
Treg	regulatory T cell
VCAM	vascular cell adhesion molecule
WNV	West Nile virus
WT	wild type

Table of contents

1. Chapter 1 Introduction

1.1. West Nile virus

1.1.1. General introduction

West Nile virus (WNV), a single-stranded RNA virus, belongs to the Flaviridae family of viruses, representatives of which are found on all inhabited continents (Hayes 2001). WNV consists of Lineage I, II and III isolates and was first discovered in 1937 in the West Nile region of Uganda (K. C. Smithburn et al. 1940). It belongs to the Japanese encephalitis serocomplex, as do other medically important neurotropic flaviviruses such as Murray Valley encephalitis virus (MVEV), found in Australia, Saint Louis encephalitis virus (SLEV), in North America and Japanese encephalitis virus (JEV), in Asia and the subcontinent (Calisher et al. 1989; Poidinger et al. 1996). WNV is geographically the most widespread of these, being found in Africa, the Middle East, Europe, the Americas and Western Asia.

Most flaviviruses are arthropod-borne, i.e., transmitted by mosquitoes or ticks, with birds generally serving as amplifying hosts in an enzootic cycle. In general, humans are regarded as incidental hosts, since they do not appear to develop high enough viral titres to infect potential arthropod vectors (Mackenzie et al. 2004; Goldblum et al. 1957; Hayes 2001). Rare cases of viral transmission via organ transplant, blood transfusion and in utero transmission have also been documented (Iwamoto et al. 2003; Bode et al. 2006; Lindsey et al. 2009; Moreland et al. 2014; Rhee et al. 2011).

While the majority of WNV infections are subclinical, some 20% of individuals develop a mild febrile illness. The most severe form of WNV infection is seen with the development of encephalitis and/or meningitis, which occurs in less than 2% of infected individuals and, when not fatal, can leave patients with severe lifelong neurological sequelae. Initial

diagnosis of WNV infection is based on clinical symptoms and early infection is confirmed by the presence of virus-specific IgM in the cerebrospinal fluid (CSF) or serum of patients. Symptoms of WNV encephalitis can include altered mental state, malaise, myalgia, ocular manifestations, nausea, headache and fever (Rhee et al. 2011; Mostashari et al. 2001; Petersen and Marfin 2002; Haley et al. 2003). Ocular manifestations of WNV encephalitis generally present as chorioretinitis and may include blurry vision, floaters and in some cases vision loss. Although disease in the eye is usually self-limiting, patients may be left with persistent chorioretinal scars (Moreland et al. 2014; Myers et al. 2005; Beardsley and McCannel 2012).

WNV spread throughout North America in less than 10 years and subsequently into Canada and South America, following an outbreak of virulent Lineage-I strain in 1999 in New York City. It is now the most common cause of viral meningoencephalitis in North America, seemingly supplanting SLEV (Lanciotti et al. 1999; Shieh et al. 2000; Schweitzer et al. 2006). Indeed, a diagnosis of WNV encephalitis is made in approximately 60% of patients presenting with seropositive neuroinvasive disease (Samuel and Diamond 2009). The young, immunocompromised and elderly are at highest risk of developing encephalitis (Weiss et al. 2001; Iwamoto et al. 2003; Guarner et al. 2004; Bode et al. 2006; Khairallah et al. 2007; Lindsey et al. 2009) and recent estimates indicate that up to 3-million individuals were infected with WNV in the USA between 1999-2010 with up to 1100 fatal cases (Petersen et al. 2013).

Various factors impact on the increasing spread of arboviruses, including, climate change and geographic factors like the expansion of vector habitat. While the difficulty of restricting the migration of amplifying avian hosts make these viruses virtually impossible to eradicate (Schweitzer et al. 2006). Despite considerable effort, the only successful live attenuated vaccine available for humans in this serogroup is for JEV, while treatment for all other flavivirus encephalitides remains supportive.

1.1.2. WNV infection: Virus entry and initial spread

Initial infection occurs when an infected mosquito injects saliva, containing WNV, cutaneously during feeding. It is likely that saliva is locally immunosuppressive, allowing an initial viral replicative advantage (Schneider et al. 2006; Schneider et al. 2010). The first immune components to encounter the virus are Langherhans cells (LC), dermal dendritic cells (DC), which can self-renew during steady-state conditions and are present from embryonic development (Merad et al. 2008). As antigen-presenting cells (APC), both dermal DC and LC can migrate to the draining lymph node (DLN) to stimulate T cells and, when depleted, are locally renewed from $Ly6C^{lo}$ myeloid precursors in the bone marrow (Steinman 1991; Davison and King 2011). Virus may infect LC, which then change sequentially into migratory and antigen-presenting phenotypes (Johnston et al. 2000). Although active replication of WNV in LC or DC has not been shown *in vivo*, it does occur in other flavivirus infections (Ho et al. 2001). LC maturation into a migratory phenotype occurs, accompanied by increased expression of cell surface adhesion molecules major histocompatibility class-I and -II (MHC), CD45 and costimulatory molecules like CD80, which are involved in T cell activation (Johnston et al. 1996). The prevailing chemokine milieu induced by live virus mediates LC migration to the DLN in an accelerated manner (Johnston et al. 2000). Cytokines such as IL1-β have been identified as crucial for the emigration of LC from the epidermis to the DLN (Byrne et al. 2001), where evidence suggests that these LC pass antigen to $CD8\alpha^{+}$ DC, arguing for a series of collaborative interactions between initiating elements of the antiviral immune response (Allan et al. 2003; Hildner et al. 2008; Kissenpfennig et al. 2005).

Viral presence in the lymph node is accompanied by increased CCL2 expression. Also known as monocyte chemoattractant-1 (MCP-1), CCL2 attracts bone marrow monocyte-derived macrophages (MDM) to areas of infection. These MDM rapidly become TNF and

nitric oxide (NO)-producing cells known as TipDC in the DLN, which may contribute to the initiation of the type-1 immune response by inducing higher IFN-γ production from local T cells, compared to other DC subsets (Davison and King 2011). Importantly, there is also significant CCL2 production by infected cells in the skin. In a dermal model of WNV infection, CCL2 recruited large numbers of MDM from the blood. These subsequently surrounded the infected focus, becoming DC within 24h of arrival. Adoptive transfer studies showed Ly6C^{lo} MDM migrating to the infectious focus in the skin, went on to the DLN, whereas Ly6C^{hi} MDM homing to the focus of infection, remained there in this model (Davison and King 2011).

The initial innate antiviral immune response to WNV is triggered by the products of viral replication, such as extra- and intracellular double-stranded RNA and single-stranded viral RNA, detected by Toll- and RIG-I-like receptors, respectively (TLR and RLR) (Wang et al. 2004). Collectively known as pattern recognition receptors (PRR), the ensuing result of stimulation of these receptors is a downstream cascade of events, starting with the activation of latent transcription factors responsible for initiating the reaction of WNV-responsive genes, the interferon stimulatory genes (ISG) (Fredericksen et al. 2008). The result is a vigorous inflammatory response directed against WNV-infected cells and mediated by several proinflammatory cytokines and chemokines (Wacher et al. 2007). The RLR group of PRR consists of RIG-I and MDA-5 and it is the cooperative function of these receptors that maintains the innate immune response.

The balance of immune activation *versus* suppression forms a critical part of PRR function. The adaptor molecule IPS-I plays a crucial regulatory role in flaviviral infection and has been identified as the converging point of the RLR. *In vitro*, the disruption of IPS-I led to a reduced ISG response and *in vivo* its signalling has been shown to greatly influence the control of WNV tropism, replication and central nervous system (CNS) invasion (Fredericksen et al. 2008; Suthar et al. 2010). *In vivo,* the regulatory role of IPS-I is

highlighted by the fact that in its absence mice displayed considerable neuropathology due to abnormal levels of innate and humoral immune products (Suthar et al. 2010). In contrast, adaptor molecules such as Myd88, which functions independently of RLR and IPS-1, are critical for viral control and leukocyte trafficking to the CNS. Reduced leukocyte migration to the CNS in Myd88 knockout (KO) mice led to increased viral load and lethality. Similarly, WNV infection of TLR-7 KO mice showed increased viremia and susceptibility to disease, due to decreased levels of chemokines such as IL-23 impeding macrophage recruitment to the CNS (Town et al. 2009; Szretter et al. 2010).

The actions of cytokines, induced by PRR, are also critical for the initiation of the adaptive immune response. Acutely viremic human donors presented with substantial increases in serum levels of IFN-γ and -α, as well as IFN-stimulated CXCL10 and CCL2. This upregulation occurred before IgM seroconversion and might be involved in the initial management of acute viremia. Furthermore, upregulation of IL-4 occurred during the same time frame, implicating IL-4 in immunoregulation and involvement of early humoral adaptive immunity (Tobler et al. 2008).

WNV infection of various cell lines leads to an upregulation of cellular adhesion molecules either directly or co-modulated through the action of cytokines (Shen et al. 1995; Shen et al. 1997; Arnold et al. 2004). These adhesion molecules include MHC-I and –II, intracellular adhesion molecule (ICAM), vascular cellular adhesion molecule (VCAM) and E-selectin (King and Kesson 1988; Argall et al. 1991; Shen et al. 1997; Verma et al. 2009). The increase in MHC-I in mouse embryonic fibroblasts is independent of TNF (Cheng et al. 2004a) and can be induced by two signalling pathways, namely type-I IFN-dependent and -independent pathways, with the IFN-independent pathway relying on the activation of the transcription factor NF-κB (King and Kesson 1988; Kesson and King 2001; Cheng et al. 2004b). This is mirrored in the infection of human skin fibroblasts with WNV, in which human leukocyte antigen, the human analogue of MHC-I, is upregulated in a type-I IFN-

dependent, as well as independent manner (Arnold et al. 2004). It is of interest to understand how these changes in MHC expression influence the outcomes of innate immune interactions, such as with natural killer (NK) cells, and/or the ultimate affinities of later adaptive cytotoxic T cell responses.

1.1.3. WNV infection: Entry into the CNS

Virus undoubtedly spreads from the lymphatic system to the bloodstream, resulting in infection of peripheral organs, including the CNS, where neurons are the main target (Xiao et al. 2001; Shrestha et al. 2003; Cheeran et al. 2005; Samuel and Diamond 2009). The factors influencing this phase of virus spread are poorly defined. Moreover, how the virus gains access to the CNS is unclear, with evidence of both direct and indirect modes of infection across the blood brain barrier (BBB) (Wang et al. 2004). Several hypotheses exist of how viral entry into the CNS occurs, including 1) direct infection of the CNS by virus; 2) the "Trojan horse" theory of undetected viral infection through a carrier cell, usually argued to be a monocyte, and 3) retrograde axonal transport.

Some evidence favours direct viral access into the CNS via BBB breakdown, however, BBB breakdown is quite variable in flavivirus infection (Liu et al. 2008; Verma et al. 2010; Getts et al. 2008). IFN-λ was shown to be protective against WNV by inducing the tightening of the BBB. *Ifnlr* KO mice, which lack the IFN-λ receptor, showed increased BBB leakiness and viral burden in the CNS during WNV infection. Indeed, IFN-λ may preserve BBB integrity by maintaining junctional integrity, thereby reducing viral access to neurons (Lazear et al. 2015). Although certain TLR play a protective role during WNV infection (Daffis et al. 2008), they have also been implicated in aiding WNV infection into the CNS by compromising the BBB. TLR-3 KO mice have significantly lower viral levels in the brain and less BBB leakiness compared to wild type mice (WT), which coincided with higher viral load in the periphery, possibly as a result of reduced TNF production (Wang et al.

2004). Primary human macrophages isolated from 'young' individuals (20-36 years old) showed a marked reduction in TLR-3 levels during WNV infection, compared to 'elderly' donors (>55 years old). TLR-3 levels are controlled by a signal transducer and activator of transcription-1 (STAT1)-mediated pathway, which in turn is inhibited by WNV envelope-protein. The elevated TLR-3 expression in macrophages of the elderly was accompanied by increased levels of inflammatory cytokines such as TNF, suggesting that TLR-3 may play a role in the increased susceptibility of elderly individuals to WNV encephalitis (Kong et al. 2008). Despite this, more recent *in vivo* studies with TLR-3 KO mice showed increased susceptibility to infection with higher viral titres in the CNS (Daffis et al. 2008). The discrepancies in these experiments not only highlight the different outcomes of *in vitro versus in vivo*, and murine *versus* human studies, but also the use of different isolates of virus. Furthermore, it may also bear upon the use of KO mice as a model for virus infection.

Astrocytes, non-neuronal support cells of the CNS, are susceptible to WNV infection *in vitro* (Liu et al. 1988; Cheeran et al. 2005; Verma et al. 2010). In addition to the upregulation of MHC-I and –II and adhesion molecules, WNV infection of astrocytes induces the production of matrix metalloproteinases (MMP), capable of degrading tight junction proteins (TJP) such as ZO-1 and claudin-1, crucial structural components of the BBB (Verma et al. 2010). Although the combined actions of proteins like MMP and TLR in response to WNV infection might impact the barrier function of TJP, leading to BBB breakdown, this notion requires an existing viral presence in the CNS, making it unlikely to be the initial method of viral entry. Mice and hamsters infected with WNV exhibited signs of BBB leakiness, however this coincided with animals succumbing to the virus, suggesting that CNS infection preceded the degradation of the BBB (Morrey et al. 2006; Morrey et al. 2008). Furthermore, the significant BBB disruption present in an *in vivo* model of WNV infection occurred after virus was first detected in the CNS, correlating with

peak viral titres. There was a concomitant decrease in several TJP (claudin-1, ZO-1, occludin) and adherens junction proteins (β-catenin, VE-cadherin), possibly as a direct result of the inflammatory actions of increased MMP. It is likely that high rates of viral replication contributed to BBB disruption and although this was not the primary route of CNS infection, it likely facilitated leukocyte immigration and further access of virus into the CNS in this model (Roe et al. 2012). WNV infection of endothelial and epithelial cells induced the endocytosis of the TJP claudin-1, leading to the microtubule-dependent transport to a lysosome and subsequent degradation of this protein, elucidating a possible mechanism by which virus mediates BBB degradation (Xu et al. 2012).

Alternatively, virus may infect the CNS directly by crossing the BBB through endothelial trancytosis or endothelial infection. Entry of JEV is thought to occur by endothelial transcytosis of virus (German et al. 2006). However, despite the susceptibility of human endothelial cells to WNV *in vitro* (Shen et al. 1997), there are few reports of endothelial infection *in vivo* by flaviviruses.

Another hypothesis for viral entry into the CNS is the "Trojan horse" scenario in which transmission of virus into the brain is mediated by haematogenous entry of infected monocytes or other infiltrating leukocytes. Indeed, macrophages and monocytes (and to a lesser extent $CD4^+$ lymphocytes) are highly susceptible to WNV infection *in vitro* (Cardosa et al. 1986; Garcia-Tapia et al. 2006; Rios et al. 2006; Yeung et al. 2012) and the subsequent upregulation of adhesion molecules like E-selectin, VCAM-1 and ICAM-1 could undoubtedly support the extravasation of leukocytes to brain (Shen et al. 1997; Getts et al. 2012). In primary human brain microvascular endothelial cells, VCAM-1 and E-selectin upregulation is induced when viral replication peaks (Verma et al. 2009). Together with BBB breakdown and the influence of TLR, these adhesion molecules could contribute to the infiltration of infected leukocytes into the CNS (Getts et al. 2012). Interestingly, studies have shown that polymorphonuclear cells (PMN), like neutrophils, exhibited much higher

viral loads than macrophages. These cells are recruited by CXCL1 and -2 during the early stages of WNV infection. Depleting this subset prior to WNV infection resulted in delayed mortality and reduced viral levels, implicating PMN as possible reservoirs for early viral replication and dissemination during WNV infection (Bai et al. 2010). However, it is unlikely that neutrophils are the primary carrier of WNV to neurons as they only contribute up to ~3% of the CNS leukocyte infiltrate (Hickey et al. 1991; Terry 2012). Additionally, leukocyte-independent migration of WNV directly across an intact *in vitro* BBB model has been reported (Verma et al. 2009).

Lastly, there is good evidence for retrograde nerve spread of the virus from the periphery to the CNS (Engle and Diamond 2003; Getts et al. 2007). Herpes simplex and Rabies are examples of viruses capable of infecting peripheral nerve components, utilising retrograde axonal transport to enter the neurons (Finke and Conzelmann 2005; McGraw and Friedman 2009). WNV can spread between neuronal and non-neuronal cell cultures in a retrograde and anterograde manner but requires an intact axon. Viral particles assemble in axons and are subsequently released extracellularly. If the sciatic nerve of golden hamsters is transected above the site of infection, animals develop a systemic infection with less severe clinical signs normally associated with CNS invasion (Samuel et al. 2007). Treatment of mice with nocodazole, a microtubule inhibitor blocking axonal transport, prior to inoculation, delayed virus infection of the CNS by 6 days (Hunsperger and Roehrig 2009). Evidence for a similar manner of viral dissemination exists in the footpad model of infection that is designed to mimic the skin route of infection with WNV via a mosquito bite. Here, infection occurs in the subcutaneous layer of the skin, which is innervated by the sensory fibres of the dorsal root ganglion (DRG) of the peripheral nervous system (PNS). Both the PNS (*in vitro*) and the DRG (*in vivo*) have been shown to be susceptible to WNV infection, identifying this as a possible pathway of retrograde axonal transport (Hunsperger and Roehrig 2005; Hunsperger and Roehrig 2006). Our intranasal (i.n.)

model of WNV infection involves infection of the olfactory nerve and results in direct CNS infection with rostral to caudal spread via neurons only, which further supports retrograde spread of virus between neural connections in the CNS (Getts et al. 2007; Getts et al. 2008).

Although most of the data supports initial CNS viral entry via retrograde axonal transport, it is likely that more than one of these pathways are involved, and additional studies are required to demonstrate the primary and secondary routes of WNV infection of the CNS and induction of lethal WNV encephalitis conclusively.

1.1.4. WNV infection: Effects on the CNS

Whilst astrocytes, oligodendrocytes and microglia are permissible for WNV infection *in vitro* (King, Unpublished) (Liu et al. 1988; Argall et al. 1991), neurons are evidently the main viral target (Shrestha et al. 2003; Cheeran et al. 2005) with only one report of glial cell infection *in vivo* (He et al. 2009). One of the responses to viral infection of glial cells *in vitro* is the production of chemoattractants like CCL5 and CXCL10 (Cheeran et al. 2005). In humans, viral antigen is found in the cytoplasm of neurons and neuronal processes, often associated with the presence of microglial nodules (Guarner et al. 2004). Viral entry into the neuron occurs after a short latent period with the attachment of virus to plasma membrane and subsequent entry by clathrin-mediated endocytosis, resulting in the formation of endosomes and lysosomes. A pH-dependent fusion mechanism expels the nucleoplasmid and virus into the cell cytoplasm, which is then assumed to replicate in the endoplasmic reticulum (ER) (Chu and Ng 2004). The majority of animal models of WNV infection show detectable virus replicating exclusively within neurons in the CNS between day-3 and -6 post-infection (p.i.), a behaviour distinguishing it from the encephalitic DNA viruses (Steele et al. 2000; Xiao et al. 2001; Shrestha et al. 2003; Brehin et al. 2008). Following peripheral inoculation of the footpad, WNV replicated in lymphoid tissues with

increased viral load in the CNS culminating in the onset of encephalitis (Brehin et al. 2008). Importantly, as with humans, neuroinvasion can occur in animals that do not succumb to infection (Hunsperger and Roehrig 2006; Appler et al. 2010). Certain locations in the CNS, like the brainstem, become infected as early as 48-hours post-infection, before the peak of viremia and symptoms are present. There are also indications that virus can be cleared, only to be followed by re-emergence of the virus to that area (Hunsperger and Roehrig 2006). Whether this is recrudescence of the virus in the same cells infected initially or infection of new cells close by is unknown. The brain structures most susceptible to virus and developing the highest viral titres in the murine model of WNV infection are the cortex, hippocampus, brainstem and spinal cord, with humans showing involvement of the brainstem and anterior horn of the spinal cord (Xiao et al. 2001; Hunsperger and Roehrig 2006; Sejvar et al. 2003; Guarner et al. 2004).

Encephalitis, the inflammatory involvement of the CNS parenchyma, occurs due to the damage resulting from excessive virus replication and/or an over-exuberant immune response, which leads to potentially fatal outcomes. Distinguishing between viral- and immune-mediated pathology in the CNS is complicated by the increased presence of both viral antigen and leukocytes in areas of neuronal apoptosis and degeneration (Xiao et al. 2001; Shrestha et al. 2003; Brehin et al. 2008). Microglial nodules, perivascular cuffing, principally comprised of infiltrating macrophages and T cells, and in advanced disease, neuronal loss, are common neuro-histopathological and immuno-histochemical findings (Steele et al. 2000; Guarner et al. 2004; Petzold et al. 2010). Ultimately, clinical symptoms develop as a result of a combination of viral infection and the inflammatory milieu. In mice these include limbic seizures, with animals succumbing to disease soon after seizures develop. IFN-γ is a key factor in seizure development, as IFN-γ KO mice do not develop seizures. Suppression of seizures in WT mice extends survival by several days, allowing viral growth to increase ~10-fold in the CNS, indicating that viral replication may play a smaller role in lethal pathology than previously thought (Getts et al. 2007). The following

section (1.2.) considers the contributions of viral infection and leukocyte infiltration to pathology in lethal WNV encephalitis.

1.2. Flavivirus pathogenesis: Immunopathology *versus* viral contribution

Two main hypotheses exist as to the main cause of flaviviral-induced pathology in the CNS, namely, direct viral induction of apoptosis in neurons or immune-mediated pathology. The immune system is clearly involved in detrimental responses against self in autoimmune scenarios, but has only recently been implicated in a range of diseases previously not thought to be autoimmune related, such as viral infection, myocardial infarction (MI) and colitis (Getts et al. 2014). The extent to which an overactive immune response can drive pathology in viral diseases is only now becoming clear and this knowledge provides exciting opportunities for development of novel and potentially life-saving therapies. Although several cell types are permissible for flavivirus infection *in vitro* (Cheeran et al. 2005; van Marle et al. 2007; Dutta et al. 2010), CNS neurons remain the principle target for most flaviviral infections in mammals (Desprès et al. 1996; Shieh et al. 2000; Cantile et al. 2001; Getts et al. 2007). Neurons have extremely limited regenerating capacity and exhibit higher rates of apoptosis compared to other CNS cell types, with flavivirus infection (van Marle et al. 2007). Whether this virus-induced apoptosis is sufficient to induce lethality remains to be elucidated.

1.2.1. Viral contribution

The permissiveness of various cell types to WNV *in vitro* and their subsequent virus-induced apoptosis forms the basis for the hypothesis of virus-mediated disease progression (Jan et al. 2000; Shrestha et al. 2003). Examples include the concentration- and time-dependent manner in which JEV promotes apoptosis of human medullablastoma

cells, with administration of isolated viral protein also inducing caspase-3 activation, leading to mitochondrial-mediated apoptosis (Yang et al. 2009). The caspase cascade has also been implicated in mitochondrial-mediated apoptosis and generation of reactive oxygen species (ROS) in JEV- and WNV-infected neuronal cell lines (Chu 2003; Lin 2004; Tsao et al. 2008). Similarly, apoptosis has been shown in neuronal cell lines infected with dengue virus (DENV) and JEV and it is clear that accumulation of viral proteins in cells can ultimately lead to cell death (Desprès et al. 1996; Jan et al. 2000; Prikhod et al. 2002). This provides evidence that even isolated viral components can act as potent inducers of apoptosis in neural cells in the absence of exogenous immune effects.

In vivo evidence for virus induced cell death has also been shown convincingly in several murine models of flavivirus infection. Intramuscular injection of WNV capsid protein resulted in apoptosis as a consequence of the disruption of mitochondrial transmembrane potential and caspase-9 and -3 activation (Yang et al. 2002). Moreover intracranial (i.c.) infection of neonatal mice with DENV induced neuronal apoptosis concentrated in areas with high levels of virus replication. However, the minimal signs of inflammation in this model could be attributed to the immature immune response and thus cannot exclude the possibility that inflammation plays a role in DENV pathogenesis in the adult CNS (Desprès et al. 1998). In a hamster model of WNV infection, neuronal degradation occurred prior to major perivascular infiltrate and microglial nodule formation (Xiao et al. 2001). On the other hand, abrogation of macrophage migration inhibitory factor by antibody blockade, or TLR-3 deletion by gene inactivation in the form of TLR KO mice, both resulted in decreased viremia and mortality rates following WNV infection. However, whether the improved clinical outcome was attributable to decreased viral titres is hard to determine, as this occurred in conjunction with a significant reduction in leukocyte infiltration (Wang et al. 2004; Arjona et al. 2007).

It remains difficult to determine if neurological symptoms occur as a result of virus-induced apoptosis or are mediated by inflammation occurring as a secondary response to virus-induced neuronal stress. While flavivirus infection clearly induces cell death in several neuronal cell lines, evidence for virus-induced neuronal degeneration *in vivo* occurring independently of inflammation is scarce. In contrast, the contribution of the inflammatory milieu in the CNS during flavivirus encephalitis is well established in animal models and will be discussed in the following section.

1.2.2. Immune contribution

The pathogenic nature of the immune system has long been recognised, however the extent to which an over-reactive immune response contributes to pathology in viral infection is only now becoming evident (Camenga and Nathanson 1975). High levels of inflammatory mediators such as TNF, IL-8, IL-6, NO and CCL5 (RANTES) in the CSF and serum of JEV-infected patients were associated with a fatal outcome, whereas high IgM levels correlated with survival (Ravi et al. 1997; Winter et al. 2004). Generally, flaviviral encephalitis in mammals is characterised by neuronal damage occurring along with significant infiltration of inflammatory leukocytes, including monocytes, T cells, NK cells and neutrophils, with accompanying activation of CNS-resident cells (microgliosis and astrogliosis) and the concomitant release of pro- and anti-inflammatory mediators (Shieh et al. 2000; Singh et al. 2000; Cantile et al. 2001; van Marle et al. 2007; Chen et al. 2010; Petzold et al. 2010). Mounting evidence suggests that this cascade of events triggered by viral infection is responsible for the development of WNV encephalitis. Several publications from our laboratory have demonstrated that infiltrating inflammatory monocytes, rather than virus, are the main contributors to lethal encephalitis during WNV infection (Getts et al. 2008; Terry et al. 2012; Getts et al. 2014). However, along with infiltrating leukocytes, there is also evidence for CNS-resident cells such as neurons,

astrocytes and microglia, contributing to immunopathology directly and indirectly. These are represented in Figure 1.1.

1.2.2.1. Resident cells

Neurons

Although the effect of inflammatory mediators, derived from infiltrating cells, on neuronal death is widely accepted, it is likely that neurons themselves at least partially contribute to the pathogenesis of disease. Pro-inflammatory mediators such as CXCL10, TNF, IL-1β, -6 and -8, released by infected neurons may contribute directly by inducing apoptosis of neighbouring neurons. Indeed, antibody-mediated neutralisation of neuronal TNF and IL-1β decreased apoptosis of neighbouring WNV-infected neurons. Indirectly, neuron-derived cytokines also induced the activation of astrocytes, which too have been implicated in pathogenesis of disease (van Marle et al. 2007; Kumar et al. 2010). Moreover, neurons of WNV-infected mice produce significant amounts of the chemoattractant CCL2, responsible for the recruitment of pathogenic Ly6C^{hi} inflammatory monocytes (Figure 1.1) (Getts et al. 2008). Thus, virus infection and replication not only has a cytopathic effect on neurons, but also triggers an "exogenous" immunopathogenic response. Inhibition of viral entry in TLR3 KO mice and reduction of subsequent neuronal infection improved resistance of mice to WNV infection, which coincided with reduction in inflammatory responses and concurrent neurodegeneration (Wang et al. 2004). Neuronal contribution to WNV encephalitis may be limited but in an extended disease course any additional inflammatory stimulus may aid in tipping the balance of the immune response from protective to pathogenic.

Figure 1.1 Immunopathology of WNV infection

Figure 1.1 illustrates the immunopathology of WNV infection of the CNS. WNV-infected neurons (green section) secrete CCL2 which results in the recruitment of $CCR2^{+}$ $Ly6C^{hi}$ inflammatory monocytes from the bone marrow (blue section) into the bloodstream. Upon reaching the bloodstream (red section) the CCR2/CCL2–axis drives migration of $CCR2^{+}$ $Ly6C^{hi}$ inflammatory monocytes to the BBB where receptor/ligand interactions between ICAM-1/LFA-1 and VCAM-1/VLA-4 facilitate the entry of pathogenic $Ly6C^{hi}$ inflammatory monocytes into the infected CNS. $Ly6C^{hi}$ inflammatory monocytes release NO in the CNS. Furthermore, infected neurons release IL-1β and TNF, which activate CNS-resident cells such as astrocytes and resting microglia. Activated microglia can release NO, compounding the detrimental effect of the $Ly6C^{hi}$ inflammatory monocyte-derived NO, whereas activated astrocytes may also release CCL2, resulting in additional recruitment of $Ly6C^{hi}$ inflammatory monocytes.

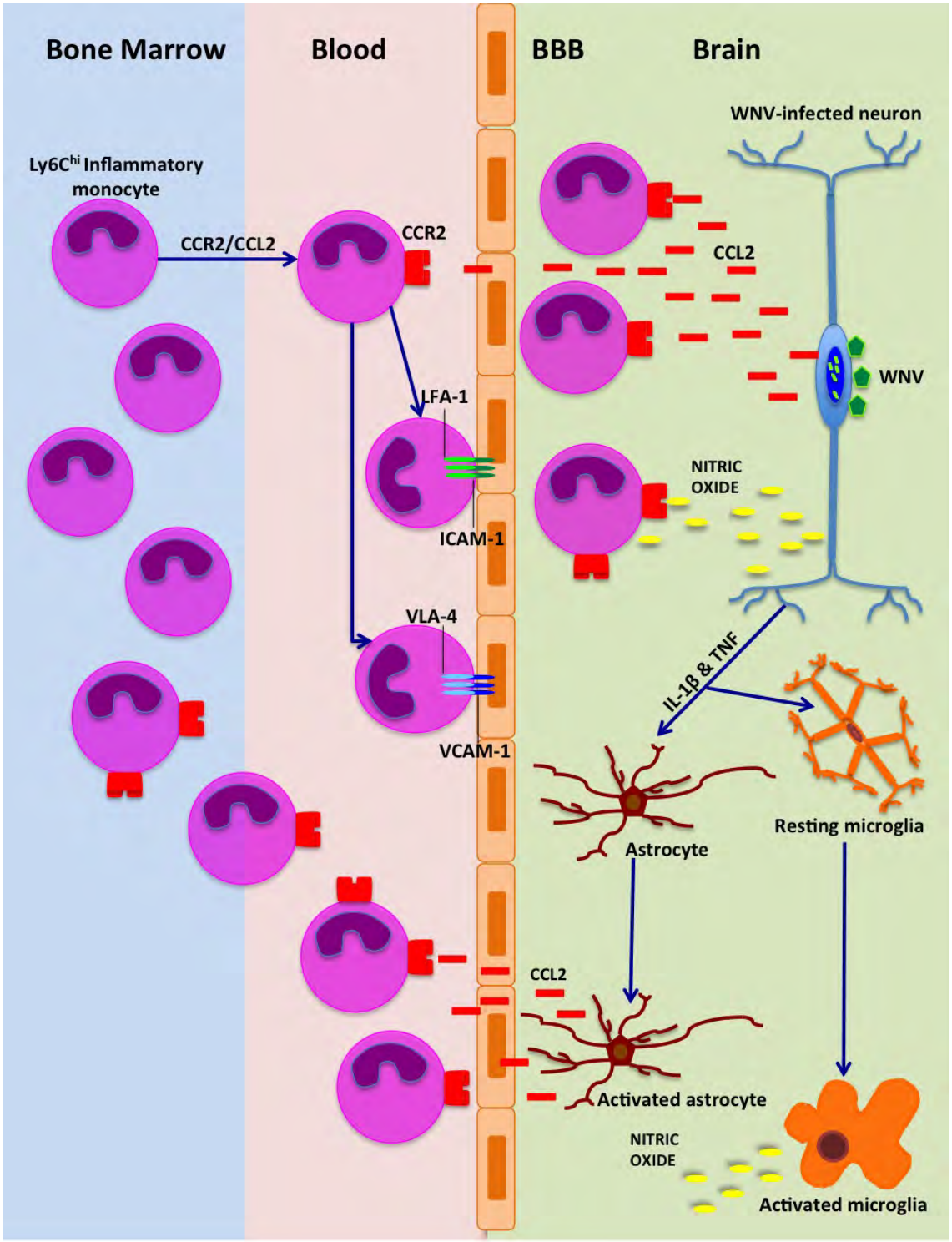

Figure 1.1 Immunopathology of WNV infection

Astrocytes

Astrocytes, the main glial cell in the CNS, play a crucial supportive role during homeostasis. Their intimate anatomical and functional relationship with neurons and their synapses, as well as their ability to produce various inflammatory mediators to regulate the surrounding CNS milieu in a neuro-stimulatory or –inhibitory manner, makes them ideal candidates to contribute to neuronal pathology during WNV encephalitis (Song et al. 2002; Barkho et al. 2009). Although evidence exists for direct infection of astrocytes by flaviviruses *in vitro* (Cheeran et al. 2005; Das et al. 2008; van Marle et al. 2007), it is unlikely that activation of this subset occurs as a result of infection by live replicating virus and they are more likely activated by cytokines such as IL-1β and TNF, released by infected neurons (Kumar et al. 2010) (Figure 1.1.). JEV- and WNV-induced astrogliosis results in the secretion of several pro-inflammatory mediators such as CXCL10, CCL2, IL-1β and CCL5 (Lieberman et al. 1989; Cheeran et al. 2005; van Marle et al. 2007; Das et al. 2008; Swarup et al. 2008; Chen et al. 2010), although the extent to which these factors contribute to pathology remains to be elucidated. Furthermore, IL-6 is significantly upregulated in WNV encephalitis and its production by astrocytes has been implicated in enhancing the inflammatory immune response and subsequent pathology during autoimmune disease, such as experimental autoimmune encephalomyelitis (EAE), a mouse model of multiple sclerosis (Getts et al. 2007; Quintana et al. 2009).

The IL-1 family of pro-inflammatory cytokines has been implicated as a crucial factor in the pathogenesis of acute and chronic neurodegenerative diseases, such as Alzheimer's and stroke (Reviewed (Griffin 2006) (Allan et al. 2005). The production of both IL-18 and IL-1β by astrocytes increase during *in vitro* and *in vivo* JEV infection of neurons. Although IL-1β stimulates neurogenesis in steady state, during JEV infection these cytokines activate glial cells, inducing pro-inflammatory cytokine release, and also increase their

own production via an autocrine-feedback loop. Indeed, the dysregulated production of these factors all results in apoptosis of neuronal cells (Barkho et al. 2009; Das et al. 2008). In contrast, the protective role of IL-1β-mediated astrocyte activation has also been shown, as this inhibited neuronal apoptosis at certain concentrations. Furthermore, studies show that the duration of astrogliosis i.e. chronic versus acute, may dictate whether the reaction is beneficial, further highlighting the dual neuro-protective or pathogenic role that immune cells can play (Sticozzi et al. 2013; Okada et al. 2006).

Similar to neurons, activated astrocytes produce CCL2, which may indirectly contribute to pathogenesis by recruiting large numbers of inflammatory monocytes. As the main cellular source of CCL2, astrocytes are responsible for initiating the inflammatory immune response during the acute stages of a spinal cord injury. CCL2 expression is mediated via the Myd88/IL-1R1 signalling pathway and recruits significant numbers of neutrophils and inflammatory monocytes to the site of injury, which have been reported to contribute to secondary tissue loss in this model (Pineau et al. 2010). Moreover, astrocyte production of CXCL10 has been implicated in the neuropathology of human- and simian immunodeficiency virus (HIV and SIV) (Sui et al. 2004; van Marle et al. 2007), a possible mechanism being the binding of CXCL10 to its cognate receptor, CXCR3, inducing Ca^{2+} release from the ER. Uptake of elevated Ca^{2+} by mitochondria can result in mitochondrial membrane permeabilisation and cytochrome c release, which induces a caspase-cascade ultimately resulting in neuronal apoptosis (Sui et al. 2006). Human brain cortical astrocytes also produce MMP that may play a role BBB disruption, further contributing to immune infiltration and subsequent immunopathology (Verma et al. 2010). Ultimately, the inflammatory mediators released by astrocytes upon activation may increase the risk of neurodegeneration by amplifying the existing pathogenic immune response in a similar manner to neurons.

Microglia

Although the inflammatory products of virus-activated astrocytes can induce neuronal cell death, this effect is much more pronounced in studies using microglia, the resident immune cells of the CNS (Das et al. 2008; Chen et al. 2010). Microglia function as local phagocytes and, upon activation, express similar cell surface markers and inflammatory mediators to circulatory macrophages. These cells replenish themselves from an *in situ* population that originates from the yolk sac and is established in the brain during early embryogenesis. (Olson and Miller 2004; Ginhoux et al. 2010). Differential CD45 and Ly6C expression distinguishes microglia from immigrant macrophages.

Thus, resident microglia express $CD45^{lo}CD11b^{+}Ly6C^{-}$, activated/infiltrating microglia become $CD45^{int}CD11b^{+}Ly6C^{int}$, whereas recently immigrant macrophages are $CD45^{hi}CD11b^{+}Ly6C^{hi}$ (Sedgwick et al. 1991; Getts et al. 2008). While microglia undoubtedly play a neuroprotective role, several studies have reported a correlation between inflammatory mediators produced by activated microglia and neuronal damage during flavivirus infections.

Although microglia can be infected by flaviviruses *in vitro,* viral replication is not supported (Cheeran et al. 2005), but the presence of pathogen induces activation and secretion of various pro-inflammatory mediators. These include cytokines (TNF, IL-1β, IL-6, IFN-γ), chemokines (CCL5, CCL2), inducible nitric oxide synthase (iNOS), cyclooxygenase-2 (Cox-2) and ROS (Wang et al. 2004; Ghoshal et al. 2007; Swarup et al. 2008; Chen et al. 2010), several of which have neurotoxic potential (Chen et al. 2010) (Figure 1.1). Furthermore, activated microglia lose their resting dendritic phenotype, developing a motile amoeboid morphology and histologically, can be seen surrounding infected neurons, forming microglial nodules soon after infection (King and Kesson 2003; Getts et al. 2008).

Microglial activation occurs prior to immune lymphocyte infiltration in the brain and is likely an indirect consequence of neuronal viral infection (Getts et al. 2008). Although direct viral activation of microglia is possible *in vitro* (Chen et al. 2010), evidence suggests that inflammatory mediator release from infected neurons is the main activator of glial cells *in vivo*. TNFR-1-associated death domain (TRADD) was identified as a crucial mediator of neuronal death during JEV infection. Inhibition of TRADD synthesis with small-interfering RNA reduced neuronal apoptosis, leading to decreased microglial activation and concomitant inflammatory mediator production and leukocyte infiltration (Swarup et al. 2008).

TNF, IL-18 and IFN-γ can inhibit the proliferation of neural precursor cells (Liu et al. 2005) and IFN-γ increased the rate of apoptotic cell death but this effect could be partially inhibited by TNF at certain concentrations (Ben-Hur et al. 2003). Conversely, in a WNV model of infection, TNF and IL-6 directly mediated bystander damage to neurons (Wang et al. 2004) and raised TNF levels were associated with mortality in tick-borne encephalitis virus (TBEV) infection (Hayasaka et al. 2009), emphasising that multiple variables are involved in determining the effect of pro-inflammatory mediators. Inhibition of Cox-2 and NOS-2 in a JEV model of infection significantly reduced neuronal death (Das et al. 2011) and aminoguanidine-mediated inhibition of NO had a significant protective effect during WNV infection (Getts et al. 2012). However, CNS-resident cells are clearly not the only source of these mediators and the significant infiltration of soluble factor-secreting leukocytes from the circulation also contributes to pathology in the brain in WNV encephalitis.

1.2.2.2. Infiltrating cells

As discussed in the previous section, it is evident that flavivirus infection of neurons and subsequent apoptosis results in the release of a range of chemotactic mediators, as well as

the activation of astrocytes and microglia. The joint action of activated resident CNS populations leads to significant leukocyte infiltration into the CNS, a hallmark of flaviviral encephalitis (Shrestha et al. 2003). CCL2 is known to play a crucial role in the recruitment of MDM, however IL-23 has also been implicated in this process (Getts et al. 2008; Town et al. 2009; Lim et al. 2011). Significant infiltration of neutrophils and mononuclear cells, like macrophages and T cells occurs in humans, as well as experimental animal models during flavivirus infection. Infiltrating leukocytes are often concentrated in the most severely affected areas of the CNS and have been associated with fatal disease outcome (Singh et al. 2000; Kelley et al. 2003). Although these cells are crucial for viral clearance, they have been implicated as the main drivers of immunopathology and cause of clinical symptoms in flaviviral encephalitis. DENV-infected mice with meningoencephalitis display distinct behavioural changes occurring at the peak of leukocyte infiltration into the CNS, (Amaral et al. 2011) and work from our laboratory has linked specific infiltrating leukocyte subsets as key mediators in the development of clinical symptoms and lethality during WNV infection.

1.2.2.2.1. Myeloid subsets

Monocytes and Macrophages

Monocytes, specifically Ly6C^{hi} inflammatory monocytes, have been established as the main contributors of immunopathology in our i.n. model of WNV encephalitis. Adoptive transfer studies have identified the bone marrow as a major source for these cells, but there is also evidence for a splenic supply of Ly6C^{hi} inflammatory monocytes (Swirski et al. 2009; Getts et al. 2008). Mice and humans have analogous monocyte subsets identified as two distinct populations based on differential cell surface marker expression. Murine patrolling monocytes (non-classical) are CCR2^{lo}CX3CR1^{hi} and Ly6C$^{lo/-}$, with a CD14^{lo}CD16^{hi} expressing human counterpart. Inflammatory monocytes (classical) are defined as Ly6C^{hi}CCR2^{hi}CX3CR1$^{lo/int}$ in mice and CD14^{hi}CD16^{lo} in humans (Geissmann et al. 2003;

Sunderkotter et al. 2004). Inflammatory conditions result in the differentiation of circulatory monocytes into either inflammatory macrophages or DC once they reach the focus of inflammation. The factors determining the fate of circulatory monocytes are complex and not well understood. However, evidence suggests that the inflammatory milieu present in viral infection of the CNS supports monocyte-to-macrophage differentiation (Uchide et al. 2002). Activated macrophages have been implicated in the pathology of several neurotropic diseases like Theiler's encephalomyelitis virus (TMEV), neurotropic mouse hepatitis virus (MHV), TBEV and WNV (Bennett et al. 2003; Gelpi et al. 2005; Gelpi et al. 2006; Templeton et al. 2008; Howe et al. 2012; Bowen and Olson 2013; Cusick et al. 2013). In contrast, DC are a major driver of autoimmune-mediated disease such as EAE (McMahon et al. 2005; Zhu et al. 2007; King et al. 2009).

The expression of ICAM-1 and VCAM-1, the ligands for LFA-1 and VLA-4 respectively, increases substantially in the CNS (Getts et al. 2012) with WNV infection and studies of WNV-infected human umbilical vein endothelial cells (HUVEC) showed pro-inflammatory cytokines further amplified VCAM-1 expression. This suggests that the combined action of infection and cytokine-induced upregulation could facilitate leukocyte infiltration into the CNS (Shen et al. 1997). The high level of CCL2 produced in the CNS during WNV infection is responsible monocyte recruitment from the bone marrow. Neutralisation of CCL2 resulted in significant reduction in inflammatory macrophages in the brain, accompanied by prolonged survival and improved clinical symptoms of WNV-infected mice. As there was no reduction in viral titre, the amelioration of disease was directly attributed to the significant decrease in inflammatory monocyte populations in the CNS (Getts et al. 2008). Although T cells form a substantial proportion of the leukocyte infiltrate during WNV encephalitis, almost 50% of leukocytes infiltrating the brain are Ly6C^{hi} MDM. Infiltration occurred mainly via the integrin, VLA-4, on these cells, with a number of these macrophages producing NO, a potent mediator of neuronal pathology (Figure 1.1) (Getts

et al. 2012). In addition, adoptive transfer experiments with Ly6C^{hi} monocytes show that some of this subset can differentiate into activated microglia, adding to the resident population (Getts et al. 2008).

JEV-activated macrophages are capable of producing several neurotoxic and chemotactic inflammatory mediators such as IL-12, CCL2, TNF, IFN-γ, NO, ROS and Cox-2 (Nazmi et al. 2011). Inflammatory macrophages in a DENV model of infection produced significant levels of IFN-γ-dependent NOS-2. Indeed, high NOS-2 levels were associated with disease lethality, as NOS-2 KO mice exhibited improved survival outcome compared to WT (de Souza et al. 2013). In contrast, NO production plays a crucial antiviral role against DENV and JEV, whilst IFN-γ-mediated NOS-2 expression and NO production were critical for survival in a mouse-adapted DENV-3 infection (Costa et al. 2012; Neves-Souza et al. 2005; Saxena et al. 2000; Saxena et al. 2001). Interestingly, in human DENV infection, low NO levels were associated with poor outcome and development of a haemorrhagic form of the disease, compared to patients with elevated NO (Valero et al. 2002). However, discrepancies in studies with DENV infection in animal models due to the use of different viral strains make definitive conclusions difficult. Ultimately, it is likely that the concentration and duration of NO and other MDM-derived inflammatory mediators present in the CNS determines whether it exerts a protective or pathogenic role.

Neutrophils

Neutrophils (Ly6G^{+}CD11b^{hi} SSC^{hi}) are members of the granulocyte family, which include basophils and eosinophils, and contribute up to 3% of the inflammatory infiltrate during WNV encephalitis (Getts et al. 2012). IL-1, CXCL2 and TNF have been implicated in the recruitment of neutrophils to the CNS (McColl et al. 2007) and the accumulation of this subset has been associated with increased levels of several inflammatory mediators such as IFN-γ, TNF, CCL2, CCL5, CXCL1, CXCL2 and iNOS (Andrews et al. 1999; Amaral et al.

2011). High neutrophil numbers and concomitant IL-8 production have been linked to severe forms of disease in JEV-infected patients (Singh et al. 2000) and neutrophils contribute significantly to the lethality of lymphocytic choriomeningitis virus infection in mice (Kim et al. 2009). Inhibition of neutrophil-derived NO increased the mean survival time (MST) of mice during flavivirus infection. However, complete neutrophil depletion was more effective, suggesting that neutrophil-mediated pathology was not limited to NO, but due to the combined action of neutrophil-derived inflammatory products (Andrews et al. 1999; Kreil and Eibl 1996; Getts et al. 2012). In contrast, neutrophils have also been shown to have a protective role in WNV, highlighting the dual role these innate cells may play in flavivirus infection (Bai et al. 2010).

Dendritic cells

Infiltrating myeloid cells can differentiate either into DC or macrophages in the inflamed CNS. Their differentiation into DC occurs in EAE, and exacerbates disease by facilitating the ongoing presentation of antigen within the CNS. However, this does not seem to occur to any significant degree in WNV and there are very few, if any, DC subsets in the brain parenchyma following i.n. lethal WNV infection. This is presumably due to an inflammatory milieu, which favours the differentiation of the majority of infiltrating Ly6C^{hi} monocytes into macrophages, in contrast to EAE. The requirement of DC in antigen presentation in CNS infection must remain with the DLN of the inflammatory focus, marking out the cervical lymph nodes for likely involvement in the immune response to WNV in the i.n. model.

1.2.2.2.2. Lymphoid subsets

CD8$^+$ T cells

CD8$^+$ cytotoxic T cells are the primary antiviral effector cell of the adaptive response and

form a significant part of the inflammatory infiltrate during viral infection. Indeed, in our model of WNV encephalitis this subset contributes ~10-15% of the inflammatory infiltrate. $CD8^+$ T cells are activated by the recognition of cognate antigen presented by MHC-I on virus-infected host $CD8^+$ DC, generally in the DLN. On recognition of infected cells, activated $CD8^+$ T cells release perforin and granzymes, which induce the apoptosis of infected cells. However, whilst crucial for viral clearance, these cells may contribute to the damage of bystander cells (Liu et al. 1989; Luna et al. 2002; Shrestha et al. 2006b). Paradoxically, flavivirus infection induces MHC-I expression on infected cells, thereby increasing $CD8^+$ T cell specific recognition and cytolysis (Liu et al. 1989; King and Kesson 1988; Douglas et al. 1994; Kesson et al. 2002)

T cells expressing chemokine receptor CXCR3 are recruited in a region-specific manner by increased expression of the ligands CXCL10, CXCL11 and CXCL9, secreted by activated astrocytes and microglia (Glass et al. 2005; Muller et al. 2007; Zhang et al. 2008). TNF has also been implicated in the recruitment of anti-viral $CD8^+$ T cells during WNV infection (Shrestha et al. 2008). WNV-infected mice deficient in $CD8^+$ T cells, and mice with impaired $CD8^+$ T cell migration, due to loss of the CXCR3 receptor, exhibit increased mortality rates, confirming the protective role of anti-viral T cells during viral encephalitis (Zhang et al. 2008; Wang et al. 2003; Wang et al. 2006; Brien et al. 2008.) In contrast, high-dose WNV infection of mice deficient in $CD8^+$ T cells resulted in improved survival indicating that this subset may contribute to pathology at a certain threshold (Wang et al. 2003). Evidently, at lower viral doses, $CD8^+$ T cells are able to efficiently clear the virus, whereas high-dose infection may recruit larger numbers of $CD8^+$ T cells and other leukocytes, resulting in immune-mediated pathology. This was also evident in the transfer of virus-specific $CD8^+$ T cells in mice infected with respiratory syncytial virus. Although $CD8^+$ T cells cleared the virus, there was a direct correlation between the number of T cells transferred and severity of respiratory distress (Cannon et al. 1988). Granzyme B-

producing $CD8^+$ T cells were associated with apoptosing neurons in TBEV infection and $CD8^+$ T cells have been identified as key players in the pathology of TBEV and DENV in clinical and experimental conditions (Kurane et al. 1991; An et al. 2004; Ruzek et al. 2011; Gelpi et al. 2006). Gene deletion of granzyme and FasL in mice with MVEV resulted in higher survival rates, indicating that these factors contribute to $CD8^+$ T cell-mediated immunopathology (Luna et al. 2002).

The relationship between protection and pathology by T cells is further complicated by the involvement of other infiltrating subsets. In our i.n. model of WNV encephalitis, the depletion of $CD8^+$ T cells did not increase survival, in contrast to an interventional reduction in monocyte populations. However, these populations evidently modulate one another as a significant reduction, but by no means ablation, of T cell numbers occurred alongside the decrease in monocyte numbers, caused by VLA-4 antibody blockade or IMP infusion (Getts et al. 2012; Getts et al. 2014; Terry 2012). Thus, T cells may, in concert with the action of monocytes, contribute to the pathology seen in the WNV-infected CNS. Nevertheless, irrespective of the extent to which they contribute to immunopathology in this model, T cells remain crucial for viral clearance and development of protective immunity.

CD4+ T cells

$CD4^+$ T cells, or helper cells, form 15-20% of the inflammatory infiltrate in the i.n. model of WNV encephalitis. Important functions of this subset pertinent to the antiviral responses include enhancing the activation of $CD8^+$ T cells and class switching of B cells, As with $CD8^+$ T cells, CXCR3 plays a major role in the recruitment of $CD4^+$ T cells (Muller et al. 2007). $CD4^+$ T cells were found to play a protective role in TBEV infection, although secretion of pro-inflammatory cytokines such as IFN-γ also influenced the production of 'macrophage-like' cells, raising the possibility of an indirect contribution to the

immunopathogenic response (Ruzek et al. 2009). Indeed, $CD4^+$ T cell production of IFN-γ was found to be crucial for $Ly6C^+$ monocyte function and activation in a peripheral model of *Toxoplasma gondii* infection (Cohen et al. 2013). $CD4^+$ T cells are also critical for survival during WNV infection, as mice deficient in, or depleted of, $CD4^+$ T cells were unable to clear virus efficiently and ultimately succumbed to infection (Sitati and Diamond 2006). In addition, $CD4^+$ T cells may play a role in specific lysis of infected cells, as shown with the transfer of $CD4^+$ T cells into WNV-infected RAG KO (deficient in both $CD4^+$ and $CD8^+$ T cells) mice. In this model $CD4^+$ T cells alone sufficiently cleared virus by specifically lysing infected cells in a perforin and FasL-dependent manner, which resulted in increased survival (Brien et al. 2008).

NK cells

NK cells are present in significant numbers in the WNV-infected brain, constituting approximately 10% of the leukocyte infiltrate (Terry 2012). These cells are able to lyse abnormal cells, e.g. virus-infected cells, independently of APC-mediated stimulation. NK cells are capable of destroying WNV-infected cells when stimulated artificially *in vitro* (Mullbacher and King 1989; Zhang et al. 2010; Hershkovitz et al. 2009) and the production of IFN-γ by NK cells has been implicated in the regulation of monocyte-to-DC differentiation in peripheral *Toxoplasma gondii* infection (Goldszmid et al. 2012; Cohen et al. 2013). However, the depletion of NK cells during WNV and DENV infection did not have any effect on survival or viral load, indicating that this subset is not crucial in resolving these infections (Shrestha et al. 2006a; Walsh et al. 2008; Yoshida et al. 2012). WNV infection of non-human primates, too, showed a marked increase in the $CD56^{dim}CD16^{bright}$ NK cell population in the bloodstream, compared to other lymphocyte populations (Verstrepen et al. 2014). Despite this information, an understanding of the role for NK cells in the innate response against WNV infection remains elusive, especially in light of the fact that WNV infection not only recruits significant numbers of NK cells to the CNS,

but also induces the upregulation of MHC-I on infected cells, which is associated with reduced NK cell recognition of infected targets.

B cells

Compared to other leukocyte subsets, B cells form only a small percentage of the total leukocyte population in the CNS during i.n. WNV infection. Nevertheless, there is some evidence of B cell infiltration into the CNS during flaviviral infection (Brehin et al. 2008; Maximova et al. 2009) and antibody production is certainly crucial for systemic protection against WNV infection (Diamond et al. 2003). They will be further discussed in the next section as part of the secondary lymphoid organ response to viral infection.

1.3. Secondary lymphoid organs

The secondary lymphoid organs, namely the lymph nodes and spleen, play a crucial role in mounting an effective immune response against invading pathogens. These organs are closely associated with the lymphatics and blood stream and are distributed throughout the body, allowing continuous tissue fluid equilibration, as well as sampling of antigens. The highly organised architecture is a defining characteristic of the secondary lymphoid organs that facilitates and maximises the likelihood of antigen encounter by an antigen-specific lymphocyte.

1.3.1. Lymph nodes

The draining lymph nodes or DLN are the first lymph nodes to encounter antigen drained from a local area of infection. Anatomically, lymphatic drainage occurs to specific lymph nodes located closest to the area of infection. Antigen-presentation will result in activation and proliferation of cells in these first-line draining nodes, whereas lymph nodes distributed further away or not in direct line of drainage via the lymphatic vessels may not

be exposed to antigen. Thus in these non-draining lymph nodes resident or immigrant cells are unlikely to undergo clonal expansion in response to infection. The initial innate immune response triggers one of two reactions in the DLN, i.e. the initiation of an anti-microbial adaptive immune response during viral or bacterial infections or the presentation of self-antigen leading to either the continued tolerance or the activation of an autoimmune response. In addition to the development of antigen-specific cells that will migrate to the inflammatory focus, the lymph node components have to minimise or prevent local infection and subsequent trans-nodal spread of pathogen. Indeed, the control of lymph-borne infections is crucial, as the lymphatic system has open access to the vascular compartment and thus to nearly the whole body. Lymph, containing cytokines, chemokines and antigen, free or loaded on APC, collected from the local catchment area, enters the lymph node via the afferent lymphatic vessel, allowing the lymphocytes in the lymph node to sample concentrated antigen. Filtered lymph then exits via the efferent lymphatic vessel. In addition, cells like fibroblastic reticular cells (FRC) are able to transport lymph fluid components with a molecular weight of less than 70kDa to the high endothelial venule (HEV). Lymph flow throughout the lymph node occurs in a directionally controlled manner, as lymph does not freely diffuse throughout the lymph node but travels from afferent lymphatics to the subcapsular sinus. It then traverses the node via the trabecular sinuses ending in the medullary sinuses, which fuse to form the efferent lymphatics, allowing egress of lymph from the lymph node hilum. Ultimately, if no antigen recognition occurs by naïve cells, lymph enriched with lymphocytes exits via the efferent lymphatic vessel, ultimately returning to circulation via the thoracic duct (Batista and Harwood 2009; von Andrian and Mempel 2003; Willard-Mack 2006). The blood supplies lymph nodes with essential nutrition and oxygen required for the maintenance of homeostatic as well as inflammatory functions. Moreover, the opposing directionality of blood and lymph flow orchestrates the increased probability of meeting of incoming antigen and cognate immune cells. The continuous drainage of interstitial fluid via the

lymphatics is crucial for maintaining fluid equilibrium throughout the body, as the occurrence of lymphedema after lymphadenectomy or the blockage of the lymphatics attests.

1.3.1.1. Architecture

An illustration of the general lymph node architecture is shown in figure 1.2. The lymph node comprises of various immune cells contained within a highly organised tissue structure. Each node is composed of several functional units called lymphoid lobules, encompassed by a collagenous capsule surrounding the lymph node. The capsule is bordered by a space known as the subcapsular sinus (SCS), which contains the SCS macrophages and allows the movement of lymph deeper into the node (Batista and Harwood 2009). These sinuses also communicate with the cortical and deeper medullary sinuses, thus facilitating the efficient movement of fluid and irrelevant cells towards the next lymph node in the chain.

The whole node is filled with FRC that form the reticular meshwork in and around the lobules. In addition to supplying structural support, the soluble mediators present in the FRC facilitate the movement of lymphocytes and other immune cells throughout the node (Moe 1963; Gretz et al. 1996; Okada et al. 2002). Histologically, each lobule has an apical cortex and a medulla at the hilum of the node. The cortex is further subcompartmentalised into the superficial and deep cortex, the latter of which is also known as the paracortex, each with very specific roles and cell types.

The vascular supply of the lymph node, much like the anatomy of the lymph nodes themselves, is variable. There is abundant interspecies variation in the entry-point of the blood supply, with differences also occurring between nodes of the same animal. Generally, arteries enter through the hilum but may have other points of entry, such as the

Figure 1.2 Anatomy of the lymph node

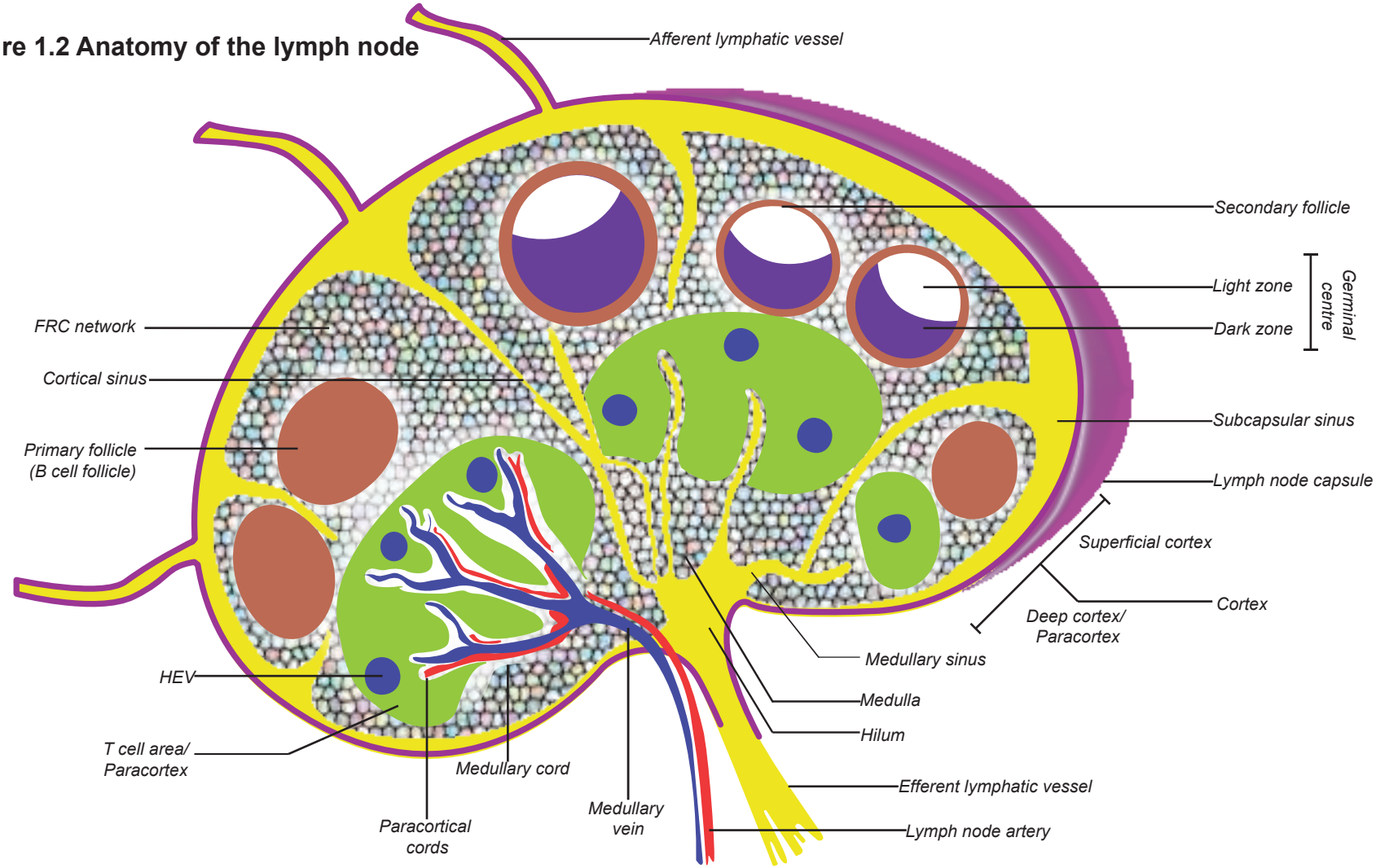

capsule, as not all nodes have an identifiable hilum. In addition, there is also significant internodal variability in the number of arteries entering a single node. Arteries entering at the hilum, branch into the medulla within the medullary cords, forming arterioles and capillaries penetrating deeper into the node, reaching the cortex in the paracortical cords, as well as the capsule. The capillaries form a network throughout the node, supplying the deep and superficial cortex. Some small cortical capillaries connect with the HEV in the paracortex, which in turn fuse and become larger HEV as they exit the cortex via the paracortical and medullary cords. At the cortico-medullary junction the HEV become medullary veins, exiting the lymph node as 2-3 hilar veins (Semeraro and Davies 1986; Belz and Heath 1995; Okada et al. 2002).

Paracortex

The paracortex or deep cortex is also known as the T cell area, due the abundance of T cells there and is situated between the medulla and superficial cortex. It is arranged into paracortical cords, originating in the B cell follicles and ending as they merge into the medullary cords in the medulla. The paracortical cords are bordered by lymph-filled cortical sinuses that communicate with the medullary sinuses. The medullary and paracortical cords are distinguishable from the sinuses by the dense cellularity and presence of arterioles and venules, compared to the lymph filled sinuses. (Belisle and Saintemarie 1981; Okada et al. 2002). In addition to numerous T cells, the paracortex is also home to large numbers of APC. This is where DC primarily present antigen to cognate T cells in order to initiate the cell-mediated immune response. The paracortex is also home to the HEV, generally situated at the centre of each paracortical cord and surrounded by concentric layers of FRC. Named after its characteristically “high” cuboidally-shaped endothelial cells, HEV are found in all secondary lymphoid organs, except the spleen, and facilitate the recruitment of naïve lymphocytes from the blood into

the lymph node in response to inflammation (Batista and Harwood 2009; von Andrian and Mempel 2003; Willard-Mack 2006).

Superficial cortex

The superficial cortex is known as the B cell area and consists of primary follicles, containing mostly B cells, with some DC (follicular DC) and follicular T helper cells. Follicular DC, expressing high levels of ICAM and VCAM are distinct from classical DC and are thought to have a mesenchymal rather than hematopoietic origin. The superficial cortex is situated in the outermost part of the lymph node and is crucial for the initiation of humoral immunity to T cell-dependent antigens and the development of long-term plasma cells (Batista and Harwood 2009). Historically, B cells activated by T cell-dependent antigen challenge, were thought to have one of two fates. They would either migrate to extrafollicular areas, becoming antibody-producing plasma cells, or develop into the germinal centres; composed of highly proliferating B cells (Allen et al. 2007). Functionally divided into a light and dark zone, the structure of the germinal centre optimises the likelihood of rare B cells interacting with their cognate antigen. The light zone is situated proximal to the lymph node capsule, in close association with follicular DC and the adjacent dark zone is located deeper in the lymph node. B cells move between these zones when they undergo affinity maturation in the germinal centre, a complex process involving the somatic mutation and selection of B cells with the highest affinity (Schwickert et al. 2007). Typically, antigen-specific B cells form the dark zone of the germinal centre, as they become rapidly proliferating centroblasts. Centroblasts give rise to centrocytes that migrate to the light zone and subsequently undergo selection as they are exposed to follicular DC and T follicular helper cells (Allen et al. 2007; Willard-Mack 2006). However, new research applying real time imaging shows that the process is much more dynamic and complicated than previously described. Indeed, the germinal centre

was found to be an open structure with bi-directional migration between the zones occurring freely (Schwickert et al. 2007).

Naïve B cells in the light zone acquire antigen from follicular DC, subsequently processing and presenting it to the T follicular helper cells. If B cells successfully present antigen they return to the dark zone, proliferating and differentiating into plasma cells capable of secreting specific antibodies against invading pathogen (Meyer-Hermann et al. 2012). Another distinction from the classic scenario is that the so-called centroblasts and centrocytes are a much more homogenous population of cells than previously thought. In fact, the B cell populations of the two zones in humans and mice are likely to have the same subset up- or downregulating specific markers such as CD83 or CXCR4 as they mature or become activated. Dark zone cells express $CD83^{lo}CXCR4^{hi}$, whereas light zone cells are $CD83^{hi}CXCR4^{lo}$. Analysis has also revealed that the genes of these subsets are highly conserved between mice and humans (Victora et al. 2012).

Medulla

The medulla, situated near the lymph node hilum, forms the innermost part of the lymph node and is organised into medullary cords, containing vasculature, and sinuses lined with endothelial cells. It is home to B and T cells with some macrophages and DC, however its function is still poorly understood (von Andrian and Mempel 2003; Batista and Harwood 2009). Lymph flow enters via the afferent lymphatic vessel into the SCS, subsequently spreading through the trabecular sinuses to the medullary sinuses where it finally exits via the efferent lymphatic vessel. Throughout this process, DC and macrophages sample lymph and remove debris whilst processing antigenic material for presentation to B and T cells (von Andrian and Mempel 2003). The medullary sinuses possess mainly medullary sinus macrophages with a few other leukocytes dispersed throughout, whereas the medullary cords consists of predominantly plasma cells and macrophages (Steer and Foot 1987). The sinus-lining macrophages separate the medullary sinuses from the cords,

which are continuous with the cortex. Macrophages in the medullary cords are an important source of IL-6 and APRIL, a proliferation inducing ligand, promoting the differentiation and maturation of antibody-secreting plasma cells (Mohr et al. 2009). Cells emigrating from the lymph node are hypothesised to exit mainly via the medullary sinus, which can occur directly from the SCS, but also from the paracortex via the trabecular and paracortical sinuses (Soderstrom and Stenstrom 1969; Grigorova et al. 2009; Nossal et al. 1968).

1.3.1.2. Leukocyte subsets of the lymph node

B lymphocytes

B cells classically form part of the adaptive immune response as drivers of humoral immunity and, in the lymph node, are mainly concentrated in the follicles. Naïve B cells express IgD and IgM. Once activated with a cognate antigen, the IgD is downregulated and proliferation is stimulated (activated/transitional B cells). The primary extrafollicular response is the secretion of mainly low-affinity IgM. Proliferating B cells give rise to the germinal centres in the follicles with subsequent class-switching of B cells occurring in conjunction with the downregulation of IgM and induction of high affinity IgG and IgA expression and secretion. Immature B cells are also identified by their expression of CD38 and, ultimately, B cells can differentiate into antibody–secreting plasma cells, identified as $CD19^{+/-}CD138^{+}$, with terminally differentiated plasma cells identified by their positive expression of CD93 (Metcalf and Griffin 2011; Banchereau et al. 1994).

Certain viruses are capable of inducing the early activation of B cells, prior to the generation of specific IgG. This function may aid in the induction of memory B cell populations and also in the subsequent retention of cells in the lymph node. This early activation is dependent on IFN-α/β but is T cell-independent (Purtha et al. 2008). Indeed, during infection, B cells can play a significant role in viral clearance, as T cell-independent

B cell activation occurs in the mesenteric lymph node (MLN) during rotavirus infection, consequently facilitating the removal of virus (Blutt et al. 2002).

In addition to the role in humoral responses, B cells also contribute to the adaptive response as potent APC. Immune complexes displayed by SCS macrophages are captured by their cognate B cells, which in turn present these to T cells. B cells can also bind antigen through complement receptors and transport antigen to the follicular DC (Phan et al. 2007; Gonzalez et al. 2010).

T lymphocytes

T cells in the paracortex become activated through the interaction with their cognate antigen, presented by either B cells or DC. Naïve T cells, arriving from the bloodstream and exposed to cognate antigen can have one of two fates. Firstly, they can become tolerant and live or they are deleted in order to avoid the development of autoimmunity. Secondly, they can mount an effector response in the form of a cytotoxic T cell and T helper response. Effector T cells thus generated will home to peripheral tissues and the inflammatory focus, after which they may become memory T cells, whereas central T cells will recirculate in the lymph node (von Andrian and Mempel 2003). Multi-photon microscopy shows T lymphocytes moving through the lymph node in a random manner picking up antigen. Once a $CD4^+$ T cell encounters antigen, it upregulates CXCR5 expression and downregulates expression of CCR7. CXCL13 then attracts these $CXCR5^+$ cells, causing the $CD4^+$ T cell to disengage from the T cell area and migrate towards the B cell follicles (von Andrian and Mempel 2003).

During viral infection the DLN play an essential role in mounting a $CD8^+$ cytotoxic T cell response. The $CD8^+$ T cell numbers in the draining mediastinal lymph node increased during i.p. LCMV infection whilst the non-draining lymph nodes decreased in T cell numbers (Olson et al. 2012). The involvement of the non-draining or distal lymph nodes

during inflammation is also evident by the presence of proliferative $CD8^+$ and $CD4^+$ T cells in the non-draining lymph node of mice immunised i.n. with *Streptococcus gordonii* (Ciabattini et al. 2010). In addition, antigen-primed T cells were present in the distal lymph node of mice immunised with OVA. The authors hypothesised that the source of proliferative T cells in the non-draining nodes was due to the dissemination of T cells primed at the site of immunisation i.e. the nose. Antibody-blocking experiments indicated that this process was highly dependent on CD62L and α4β7 integrin expression (Ciabattini et al. 2011). Regulatory T cells (Tregs) also increase significantly in the DLN during WNV infection and play an important role in the generation of the memory T cells, which are in the first line of response to reinfection (Graham et al. 2014). Furthermore, asymptomatic individuals with WNV has lower Treg frequencies in their peripheral blood than their symptomatic counterparts, speculated to be due to the ability of Tregs to downregulate the pathogenic immune response and therefore the bystander damage (Lanteri et al. 2009).

Macrophages

The macrophages of the lymph node are defined according to their location; the main two subsets are the medullary and the SCS macrophages, both of which capture lymph-borne antigens. SCS macrophages are identified by CD169 expression and, as the name suggests, can be found in the subcapsular sinus of the lymph node. These macrophages are situated in close association with the cortical and medullary sinuses, allowing direct sampling of antigen draining from the tissue and present in the lymph fluid. Although this subset is less phagocytic than their medullary counterparts, they still perform a crucial APC function, and during viral infection, play a role in preventing viral dissemination and systemic spread (Junt et al. 2007; Kastenmuller et al. 2012). Additionally, SCS macrophages are critical for the survival of mice during neurotropic viral infection like vesicular stomatitis virus, a member of rabies family, which is fatal in the absence of SCS

macrophages. In this model, the SCS macrophages function by capturing virions, protecting peripheral nerves from neuroinvasion by producing IFN-I, as well as recruiting IFN-I-producing plasmacytoid DC (pDC) (Iannacone et al. 2010). Moreover, SCS macrophages can capture antigen on their surface, subsequently presenting antigen to naïve migratory follicular B cells and inducing humoral immunity (Junt et al. 2007; Phan et al. 2007).

Although both SCS and medullary macrophages can present antigen to B cells in the follicles, they are not necessarily required to activate the humoral response in all types of viral infection. Depletion, using clodronate-encapsulated liposomes to eliminate these resident phagocytic cells subsets, did not affect humoral immunity against influenza virus (Gonzalez et al. 2010). SCS macrophages are also capable of cross-presentation of antigen to $CD8^+$ T cells and subsequent induction of specific cytotoxic T lymphocyte (CTL) responses to dying tumour cells (Asano et al. 2011). Despite this, they were not required for the activation of specific $CD8^+$ T cell responses to peripheral WNV infection but their role as gatekeeper in preventing systemic spread of WNV was of importance (Winkelmann et al. 2014). Interestingly, viral and bacterial infection leads to the disruption of the anatomical disposition of SCS macrophages due to the migration of mature DC and neutrophils to SCS. This leads to cell loss and redistribution of SCS macrophages to the inner follicular area where antigen presentation occurs. Although this likely maximises lymph node immune responses to primary infection by enhancing entry of afferent immune cells, relay of antigen to follicular DC and maximisation of antigen presentation to B cells, it also renders the lymph node temporarily unable to respond effectively infection by another organism (Chtanova et al. 2008; Braun et al. 2011; Gaya et al. 2015).

Dendritic cells

DC occur at extremely low frequencies compared to other mononuclear cells and are a highly complex group of leukocytes with extremely variable cell surface protein expression and multifarious functions, making them difficult to characterise comprehensively. The primary basic characterisation of DC in the spleen and lymph node is based on CD11c and MHC-II expression, with the spleen generally possessing lower DC heterogeneity than the lymph node. In the lymph node, DC populations are divided into "lymphoid tissue resident DC", expressing $CD11c^{hi}MHCII^{int}$ and "peripheral tissue-derived migratory DC", which are $CD11c^{int}MHCII^{hi}$. The $CD11c^{hi}MHCII^{int}$ resident population is further subdivided into a $CD8^{+}$ subset, mainly situated in the T cell zone, and a $CD11b^{+}$ population. Migratory/$CD11c^{int}MHCII^{hi}$ DC can also be subdivided into distinct populations. These include the $CD11b^{+}$ migratory dermal DC, largely inhabiting the interfollicular and outer paracortical regions once they enter the lymph node, and the $CD207^{+}CD103^{-}$ LC and $CD207^{+}CD103^{+}$ dermal DC, localised in the deeper T cell zone (Gerner et al. 2012; Elpek et al. 2011). The main function of migratory DC is to transport antigen from the site of infection to the DLN, where antigen presentation to T and B cells occur, whereas resident DC sample antigen within the lymph (Kaplan 2010). Free antigen can be recognised in the lymph node by immature DC, which then mature in the lymph node in order to present antigen to T cells (von Andrian and Mempel 2003). DC subtypes in the subcutaneous and mesenteric lymph nodes include two additional populations based on CD8 and DEC205 expression and are characterised as $CD4^{+}8^{-}DEC205^{-}$, $CD4^{-}8^{+}DEC205^{+}$ and $CD4^{-}8^{+}DEC205^{+}$(Henri et al. 2001). Other markers used to classify DC include CD4, CD8α, CD11b, CD11c, CD205, B220, MHC II and GR1, with plasmacytoid DC expressing B220 and lymphoid DC expressing CD8 (von Andrian and Mempel 2003).

While DC in the lymph node are crucial for the activation of specific T cell responses by presenting antigen to cognate T cells, they can also be involved in the humoral response. Medullary DC used SIGN-R1 to capture lymph-borne antigen, such as influenza virus, and subsequently migrated from the medulla to the B cell follicle, promoting the humoral response (Gonzalez et al. 2010). Indeed, Influenza A is similar to WNV, insofar as pathology being mainly immune-driven but, unlike the CNS where these issues are just beginning to be elucidated, the lung has a well-described lymphatic system, and DC from the lung clearly migrate to the mediastinal lymph node during infection. In this model, $CD103^{+}CD11b^{+}$ DC populations increased in the lymph node by 20% within 24h. These migrating DC served both an antigen-distributing and T cell activation role, as antigen transfer can occur between migrating and resident DC prior to T cell priming. Once activated by DC, T cell populations expanded from d3 p.i. and mature effector T cells were present in lung 6-8 days p.i., correlating with decreased lymph node T cell numbers and viral clearance. In this model, antigen delivery by DC was crucial for T cell activation and proliferation, as administration of sphingosine-1 phosphate (S1P) agonist, which interferes with DC antigen delivery to the node, significantly impacted T cell responses (Matheu et al. 2013).

Since the brain may not possess a comprehensive parenchymal lymphatic drainage system, the process of local antigen presentation in a secondary lymphoid organ is currently largely undefined. However, DC in the CSF have been shown to exhibit targeted migration to CLN during EAE, a process that will be discussed in section 1.3.2 (Hatterer et al. 2008) Furthermore, as the primary source of antibody-secreting cells for the CNS during viral infection, the cervical lymph node (CLN) is crucial for the development of humoral response to CNS infection (Metcalf and Griffin 2011).

NK, NKT cells and neutrophils

Although these cells are classically present in low numbers, their anatomical location and distribution in the lymph node indicates the potential of these subsets to play specialised roles during inflammation. Indeed, the obvious recruitment of these populations during bacterial, parasitic and viral infections to the DLN indicates a likely role in facilitating host defence. In naïve mice, innate effector NK cells are located in the medulla and paracortex in close association with DC. Parasitic infection recruits NK cells from the blood to the lymph nodes, especially the paracortex, where they colocalise with DC and $CD4^+$T cells (Bajenoff et al. 2006). The recruitment of NK cells to the lymph node is mediated by CXCR1 and the subsequent production of IFN-γ by NK cells plays a crucial role in the adaptive immune response by inducing Th1 cell responses (Martin-Fontecha et al. 2004). The NK cells present in human lymph nodes are mainly $CD56^{bright}$ and reside in the paracortex. NK cells can be induced to secrete IFN-γ and proliferate through the action of DC-derived IL-12 and IL-15, respectively. T cell-derived IL-2 also stimulates IFN-γ production by NK cells, indicating interplay between adaptive and innate systems (Fehniger et al. 2003; Ferlazzo et al. 2004). IFN-γ-producing NK and NKT cells were found in close association with SCS macrophages, resulting in the activation of these cells with IL-18 during bacterial and parasitic infections. Furthermore, depletion of NK cells resulted in increased parasitic burden in the mesenteric lymph node during *Toxoplasma gondii* infection (Coombes et al. 2012). Indeed, the absence of NK cells in the lymph node may be detrimental during HIV infection. NK cell recruitment in HIV^+ individuals was impaired due to a reduction in the expression of the NK homing receptor. This inhibited innate response was hypothesised to reduce targeting by cytolytic cells, thus allowing virus replication (Luteijn et al. 2011).

Although naïve lymph nodes possess almost no neutrophils, bacterial infection induced the recruitment of neutrophils to the lymph node in low numbers, through the action of

SCS macrophages, indicating that an innate response can be induced in rare innate lymphoid populations by the scavenging macrophages of the lymph node (Kastenmuller et al. 2012). Indeed, oral and earflap bacterial infection with *Toxoplasma gondii* resulted in significant recruitment of neutrophils to the DLN. Time-lapse imaging showed neutrophils forming distinct clusters in the SCS of the DLN, whilst disrupting the organisation of the SCS macrophage layer (Chtanova et al. 2008). In addition, bacterial infection recruits neutrophils that originate in the bone marrow to the DLN from the blood, entering the lymph node through the HEV, whereafter they migrate deeper to the medulla and between the follicles. Here, neutrophils form interactions with T helper and B cells at the follicle border and act by supressing the early humoral response through the release of TGF-β1 and disruption of SCS macrophages (Kamenyeva et al. 2015).

1.3.1.3. Leukocyte homing and trafficking to the lymph node

During homeostatic conditions, naïve lymphocytes are continuously circulating through the bloodstream with ~5% of these entering the secondary lymphoid organs via the HEV where they sample antigen and respond, or in the absence of cognate antigen, re-enter circulation (Ganusov and Auerbach 2014). In addition, memory T cells generated during infection recirculate and monitor peripheral tissues (Mackay et al. 1990). Inflammatory stimuli induce the recruitment of myeloid and lymphoid cells from blood and peripheral tissues to the DLN, in addition to the proliferation of resident lymph node lymphocytes. Much debate exists as to whether the dramatic increase in size of an antigen-stimulated lymph node is due to the significant influx of lymphocytes entering the lymph node or due to a decreased exit rate. In either case, the likelihood of specific T cells encountering cognate antigen is improved (Ganusov and Auerbach 2014; von Andrian and Mempel 2003). Three molecularly distinct steps regulate the attachment and entry of lymphocytes to the lymph node. Firstly, leukocytes bind loosely to the luminal HEV surface as they are

pushed forward by the bloodstream in a process known as “tethering and rolling”. This step is mediated by L-selectin/CD62L, expressed by both myeloid and lymphoid lineage cells, attaching to endothelial ligands or peripheral lymph node adressins on HEV and this contact is likely facilitated by the turbulence of blood caused by the raised physical profile of the HEV themselves.

Next, cellular engagement on endothelium occurs, mediated by chemotactic stimuli. Arrest of T cells is achieved by attachment of integrin LFA-1 on naïve T cells and ICAM-1 on HEV. Indeed, loss of LFA-1 leads to significantly reduced homing of T cells to the lymph node due to the disruption of firm arrest, intravascular crawling and transendothelial migration (Park et al. 2010). In a skin transplantation model, LFA-1 blockade resulted in the selective retention of effector T cells in the lymph node, but not naïve cells. This led to an increase in antigen-specific T cells ($CD62L^{lo}$) and regulatory T cells (Treg) in the lymph node and an increase in naïve T cells in the bloodstream. Importantly, LFA-1 blocking did not only affect T cell populations in the graft-draining lymph node, but also the non-draining peripheral nodes (Reisman et al. 2011). Integrin activation is mediated by CCL21, expressed on HEV, which binds to CCR7 on T cells. In addition, CCL19 and mCLCA are known to activate these integrins. However, evidence also exists for a chemokine-independent pathway of LFA-1 activation, involving Ly6C, which in addition to being a marker of inflammatory monocytes in the blood (Geissmann et al. 2003), is also found on activated T cells (Peters et al. 2014). Indeed, Ly6C-crosslinking was shown to induce LFA-1 clustering on $CD8^{+}$ T cells and increased endothelial adhesion (Jaakkola et al. 2003).

B and memory T cell attachment is governed by different signals from naïve T cells, with B cell attachment regulated by CXCL12-CXCR4 and CCL21-CCR7 interaction, although this is strain-dependent. Lastly, activation-dependent adhesion and emigration of leukocytes into the HEV is governed by different chemoattractants. Once leukocyte attachment and rolling occurs, cells need to arrest to emigrate from the intraluminal side of the HEV.

Granulocytes express L-selectin and LFA-1, allowing them to roll on the endothelial surface but the absence of a CCR7/CXCR4 interaction prevents subsequent arrest and emigration of this subset. Currently, entry of B and T lymphocyte subsets into the abluminal side of the HEV is hypothesised to occur through transendothelial diapedesis (von Andrian and Mempel 2003; Irjala et al. 2001). The interaction of mCLCA with Mac-1 on granulocytes, NK cells and macrophages may facilitate the adhesion of these subsets to lymphatic endothelium (Furuya et al. 2010). Ultimately, entry into lymph nodes via the HEV is limited to naïve B and T cells and central memory T cells, with other circulatory subsets entering at different sites and by different means.

Thus, even if cells end up interacting with each other, they may get there by different routes. For example, lymph-derived T cell entry occurs mainly via the medulla, whereas DC enter through the SCS floor. Once in the parenchyma, the migration of both these subsets into the deeper T cell zone was shown to be highly dependent on CCR7. Interestingly, DC were retained in the first lymph node encountered whilst some naïve T cells were found in downstream lymph nodes, indicating a constant redistribution of naive lymphocytes throughout the lymphatic system in the quest for cognate antigen (Braun et al. 2011).

FRC, located in the T cell zone, are also involved in homing and entry of certain subsets into the lymph node. During homeostatic conditions, these stromal cells produce CCL21 and CCL19, which interact with CCR7 on lymphocytes. Depletion of FRC reduced DC, $CD11b^+$, B, T and NK cell numbers in the lymph node. Adoptive transfer of $CD8^+$ T cells showed that the reduction in cell numbers was due to decreased homing of T cells to the lymph node as a direct result of CCL21 loss. Thus, during homeostatic conditions, homing and retention of T cells relied on CCL21 expression by FRC, however, during inflammatory conditions the loss of FRC did not affect egress of activated T cells from lymph node,

presumably due to the reacquisition of sphingosine-1 phosphate receptor-1 ($S1P_1$), a crucial signal for T cell exit (Denton et al. 2014).

After encountering an inflammatory stimulus, DC mature and express CCR7, CXCR4 and CCR4, which facilitates the access of DC into the T cell area of the DLN. In addition, pDC express L-selectin and may utilise this to migrate into the lymph node via the HEV (von Andrian and Mempel 2003). IRF4-dependent CCR7 expression is a major driver for DC migration and positioning in the lymph node (Randolph et al. 2005; Bajana et al. 2012). In response to viral infection, pDC in the spleen and lymph nodes can produce immunoregulatory cytokines IFN-α and IL-12, which may modulate T cell responses (Asselin-Paturel et al. 2001).

1.3.1.4. Leukocyte exit from the lymph node

Cellular turnover of a lymph node in steady state occurs rapidly, as recirculation of lymphocytes is essential for immune surveillance. Indeed within 24h, 70% of cells in a lymph node will have been replaced. $CD4^+$ T cells exhibit the highest rate of turnover, followed by $CD8^+$ T cells, which remain in the lymph node for up to ~12h. B cells spend roughly 24h in the lymph node, while DC show the lowest rate of exit (Tomura et al. 2008). In order to increase the likelihood of cells meeting their cognate antigen during infection, the lymph node undergoes an acute inflammation-driven short-term "lymph node shutdown" mediated in part by TNF and IL-6 (Wee et al. 2011). This phenomenon is overcome by the successful exit of activated cognate lymphocytes from the medulla of the lymph node via the efferent lymphatic vessels, and their subsequent migration to effector sites. In humans, the mannose receptor on efferent lymphatics interacts with CD62L on lymphocytes to facilitate their egress (Irjala et al. 2001; von Andrian and Mempel 2003). $S1P_1$, a G-protein-coupled receptor, is key for the efficient attachment and exit of T cells and to some extent B cells, from the lymph node. In the absence of $S1P_1$, T and B cells fail

to exit the secondary lymphoid organs. Indeed, during inflammatory conditions, activated T cells downregulate $S1P_1$, facilitating T cell retention and antigen interaction within the lymph node (Matloubian et al. 2004). Furthermore, inflammatory mediators such as IFN-α and -β act as potent inducers of cell surface activation markers like CD69 on leukocytes. CD69 negatively regulates the $S1P_1$ interaction and inhibits lymphocyte exit by forming a complex with the $S1P_1$. This complex mimics the ligand for $S1P_1$, namely S1P, and results in the downregulation, internalisation and subsequent degradation of the receptor, thereby promoting lymphocyte retention during the initial stages of inflammation i.e., lymph node shutdown (Shiow et al. 2006; Bankovich et al. 2010).

Lymphocytes from the lymph node exit back into the lymphatic circulation whereas lymphocytes from the spleen exit into the blood. The production of S1P by red blood cells in the circulation indicates that the source of S1P likely varies between blood and lymphatics (Pappu et al. 2007). The intra-nodal site of $S1P_1$ receptor-ligand interaction is the border between the lymph node parenchyma and the cortical or medullary sinuses, whereafter directional lymph flow distributes lymphocytes to the medullary sinuses and SCS, where cells eventually exit the efferent lymphatics (Grigorova et al. 2009). In addition, lymphocytes can rapidly exit the node after entry via the cortical sinuses, which are situated close to the HEV. However, during inflammation the cortical sinuses collapse, further facilitating lymphocyte retention during inflammation, resulting in the node vastly increasing in size (Grigorova et al. 2010).

1.3.2. Antigen presentation in the CNS

The structure of the CNS lymphatic system has historically been largely unknown. Therefore, the process of antigen presentation and subsequent activation of the adaptive immune system in this organ is still very much under investigation. Classically, antigen has

been thought to reach peripheral lymph nodes either via 1) draining through nasal lymphatics to CLN, 2) transport through arachnoid villi, or 3) draining through the ventricular system via the choroid plexus. However, to induce an optimal immune response, local draining APC are still needed. Recent findings identified the presence of functional lymphatic vessels in the meninges of mice draining directly into the CLN, implying that the CNS might possess its own immune surveillance, in lieu of only externally derived cells (Louveau et al. 2015).

Even though the CNS is considered immune-privileged, certain CNS sites, such as the circumventricular organs and olfactory nerve projections are obvious points of entry for pathogens. Additionally, the ability of resident cells, such as microglia, to function as DC is under investigation. Although microglia have poor antigen-presenting capacity the fact that they are a heterogeneous population raises the possibility that a subpopulation of these cells may be DC precursors. Studies with GFP have shown $CD11c^{+}$ cells in the brain co-expressing markers commonly found on microglia and macrophages. These DC-like cells were associated with specific CNS structures and increased in response to trauma. Studies have also shown the presence of choroid plexus DC, similar to classical DC in the spleen, developing from pre-DC in the choroid plexus, situated along sites of activated T cell entry (D'Agostino et al. 2012).

The use of EYFP-CD11c mice showed a $CD11c^{+}$ population in the naïve mouse, co-expressing $CD45^{int/hi}$, potentially microglia. Indeed, microglia have been shown to upregulate CD11c during inflammation. Upon stimulation with Flt3L, a potent hematopoietin, this population expands, increasing their MHCII and CD11c expression. This DC-like population was located in the choroid plexus and meninges of animals and exhibited shared gene expression profiles with splenic $CD8^{+}$ DC. Adoptive transfer showed that these DC likely arise from pre-DC in the bone marrow rather than monocytes and relied on LFA-1 expression to migrate into the CNS. In addition, this subset was able to act

as potent APC, inducing T cell activation and proliferation *in vitro* (John et al. 2011; Anandasabapathy et al. 2011). In support of this, i.c. injection with OVA protein induced the expansion of a $CD11c^{+}CD205^{+}$ population at the site of injection. The subsequent downregulation of MHC-II and increased expression of CCR7, a major driver of DC migration and positioning in the lymph node, suggests that this population was maturing and potentially preparing to migrate to a DLN. The ability of these cells to migrate to the CLN was determined by injection of GFP-expressing antigen-loaded DC into the CNS. Apart from successful migration to the CLN, these DC successfully stimulated an antigen-specific T cell response and subsequent homing of antigen-specific T cells to the CNS (Karman et al. 2004).

1.3.3. The Spleen

The spleen is the largest secondary lymphoid organ and is specialised for mounting immune responses to blood-borne pathogens. It is divided into 3 functional and anatomical compartments, namely the red pulp, white pulp and marginal zone. Due to its relationship to the blood stream, vascularity and abundance of phagocytic cells, the spleen acts as an ideal filter for any foreign material present in circulation. The first compartment to encounter the blood and its contents is the red pulp, which is highly adapted as a phagocytic filter with a multitude of macrophages, identified by the expression of F4/80 and CD11b. Bordering the red pulp and surrounding the white pulp, is the marginal zone (Sasou et al. 1982; Batista and Harwood 2009). Historically, the marginal zone has been described as part of the white pulp, however, in reality it is functionally and morphologically distinct. This compartment consists of sinus-lining reticular cells with a high concentration of non-circulating phagocytic leukocyte populations, including marginal zone macrophages (MZM), marginal metallophillic macrophages, marginal zone B cells and DC. The MZM, located on the outer rim near the red pulp, express MARCO, a

scavenger receptor, and SIGN-R1, a C-type lectin, and are hypothesised to be the splenic counterpart of the SCS macrophages (Hughes et al. 1995; Kraal and Mebius 2006; Kang et al. 2003; Phan et al. 2007). The macrophages of the marginal zone are also crucial for trapping particulate antigen in the bloodstream and limiting the haematogenous dissemination of pathogens. They are able to phagocytose apoptotic material, bacteria and nanoparticles (Demoy et al. 1999). Although the depletion of these subsets significantly affected the control of infection, they were not required for antigen presentation and specific T cell immunity against *Listeria monocytogenes* (Aichele et al. 2003). In addition, macrophages of the splenic marginal zone are important for immune regulatory responses to endogenous apoptotic material. Thus, the specific depletion of MZM severely altered the maintenance of tolerance in CNS and systemic autoimmune diseases. The absence of MZM resulted in increased uptake of apoptotic material by the red pulp macrophages and presentation to the T cell populations of the white pulp, this alteration in localisation and method of antigen presentation of apoptotic material resulted in enhanced lymphocyte responsiveness to self-antigen (Miyake et al. 2007; McGaha et al. 2011). The CCL22 production and subsequent recruitment of regulatory T cells by the CD169-expressing marginal metallophillic macrophages, situated on the inner rim of the marginal zone, was also a key regulator in the maintenance of tolerance to apoptotic material (Ravishankar et al. 2014). In contrast to what occurs in the lymph node, neutrophils in the spleen act as marginal zone B cell helpers by promoting immunoglobulin production and class switching of B cells (Puga et al. 2012).

The white pulp, surrounded by the marginal zone, contains the follicles and the periarteriolar lymphoid sheath (PALS), which can be likened to the lymph node B cell follicles and paracortex respectively (Cesta 2006). Although the white pulp is similar in structure to a lymph node (Nolte et al. 2000), there are major differences in the mechanism of antigen transport. The afferent lymphatics are the main entry point of

antigen in the lymph nodes, whereas the spleen receives antigen directly from blood, as it possesses only efferent lymphatics. Indeed, antigen picked up from blood can be presented to white pulp B and T cells by the cells of the marginal zone. In addition, the white pulp has its own conduit system, consisting of reticular fibroblasts and is connected to the marginal zone, allowing particles of low molecular weight to reach it directly. In contrast to the lymph node, the white pulp conduit system has no direct connection to the lymphatic system and is only supplied by the blood (Nolte et al. 2003). During homeostatic conditions the B and T cell distribution in the white pulp is similar, whilst the red pulp contains more B cells. In addition, ~1% of the splenic leukocytes consists of neutrophils, mostly situated in the red pulp with NK cells, which are also present in very low numbers (2-3% of splenic leukocytes) in both the white and red pulp (Nolte et al. 2000). The location of B cells in the spleen relates directly to their function, as follicular B cells ($CD21^{hi}CD23^{hi}$) produce antibody in response to T cell-mediated stimulation, whereas marginal zone B cells ($CD21^{hi}CD23^{lo}$) can promptly respond to pathogens independently of T cell stimulation (Purtha et al. 2008).

1.4. Immunomodulatory treatment of flavivirus infection

1.4.1. Background and past treatment

There are currently no effective vaccines for humans against WNV and treatment remains symptomatic. Although only a small percentage of individuals infected with WNV develop severe disease, the consequences can be life threatening and/or debilitating for the remainder of life. As vectors for flaviviruses become more widespread the need for a vaccine or successful treatment becomes critical. Considering the mounting evidence for WNV being an immunopathological disease, rather than one caused directly by the virus itself, the focus needs to shift towards research supporting immune-modulating therapies.

Importantly, treatment directed at reducing the overactive immune response will not only be applicable to WNV but a myriad of flaviviruses and potentially other viral or non-viral immune-mediated diseases.

1.4.1.1. Vaccines

Historically, the primary defence against mosquito-borne disease has been focused on preventative measures, including vaccine development. However, few vaccines for humans exist against flaviviral infections and commercially approved vaccines against WNV are limited to the treatment of horses. Effective live flavivirus vaccines exist for both JEV and yellow fever (Monath 2010; Liu et al. 2011) and formalin-inactivated whole virus vaccines are available against TBEV (Barrett et al. 2003; Heinz et al. 2007). Unfortunately, despite these exhibiting relatively good safety records, numerous cases of infection with these viruses still occur each year. Trials with formalin-inactivated WNV vaccines in murine and non-human primate models showed some protective effect, with the development of neutralising antibody after immunisation (Muraki et al. 2015). Vaccines synthesised to mimic virus, but lacking the infectious nucleus, called virus-like particles, have also been used with varying success in animal models but pose the risk of initiating a non-specific immune reaction (Pijlman 2015). Another possibility is targeting mosquitoes and ticks directly (vector management) with anti-vector vaccines (Kortekaas et al. 2010). A successful example being the stable infection of mosquitoes with the Wolbachia bacterium, which limits the spread of dengue by shortening the mosquito lifespan, without preventing breeding (McMeniman et al. 2009; Bian et al. 2010).

A different approach involves the activation of antigen-specific $CD8^+$ CTL capable of lysing WNV-infected cells (Purtha et al. 2007). Administration of a chimeric vaccine containing WNV-envelope antigen, produced antigen-specific $CD8^+$ CTL persisting for up to a year (Smith et al. 2010). Unfortunately, the short lifespan of the vaccine and activation of an

already overactive immune response makes this approach a less desirable option.

1.4.1.2. Antiviral therapies

Initial *in vitro* studies into antiviral therapies appeared promising, with antiviral treatment like ribavirin effectively inhibiting WNV infection of Vero monkey kidney and neural cell lines (Jordan et al. 2000; Anderson and Rahal 2002). However, clinical studies with ribavirin resulted in no improvement of WNV-infected patients (Chowers et al. 2001). Minocycline also showed promising antiviral effects against JEV and WNV *in vitro,* as this tetracycline significantly reduced microglial and macrophage production of inflammatory cytokines, chemokines and ROS in JEV infection (Dutta et al. 2010; Das et al. 2011). Additional *in vitro* studies show minocycline effectively promoting neurogenesis and inhibiting apoptosis of JEV- and WNV-infected neuronal cells (Michaelis et al. 2007; Mishra and Basu 2008; Das et al. 2011). Furthermore, minocycline has successfully been used in the treatment of JEV-infected mice, reducing viral titre and promoting neurogenesis. Besides the obvious antiviral effect of minocycline, the inhibition of microgliosis and subsequent pro-inflammatory mediator release is likely the main contributor of this therapeutic benefit (Mishra and Basu 2008; Das et al. 2011). Non-human primate studies treating SIV infection with minocycline also resulted in improved symptoms, which authors attributed to the reduction of the chemoattractant CCL2 and consequent decrease of inflammatory monocyte recruitment (Zink et al. 2005). Direct targeting of viral components, such as the viral helicase, with inhibitors has successfully stunted viral replication of DENV and WNV *in vitro* (Sweeney et al. 2015). Patients suffering from TBEV showed improved recovery and reduced symptoms when treated with tetracycline hydrochloride. This occurred with concurrent serum cytokine reduction (IL-6, TNF, IL-1β) in patients, indicating that the clinical effect of this antibiotic may also

be as a result of immune-modulation (Atrasheuskaya et al. 2003).

The antiviral properties of interferons have identified these proteins as potential candidates for immune-modulating therapies. IFN-α2b was established as being protective against WNV infection *in vitro* (Anderson and Rahal 2002) and type-I IFN (α/β) inhibited viral spread and replication in the periphery and CNS of WNV-infected mice, whilst also inhibiting WNV-induced neuronal death (Samuel and Diamond 2005). ISG expression and subsequent protein production increased during viral infection (Wacher et al. 2007) and inhibited viral replication by disrupting multiple steps in the life cycle of WNV and dengue viruses. For example, IFN-induced transmembrane proteins-2 and -3 can inhibit viral entry of host cells (Jiang et al. 2010).

However, as an overreactive immune response is characterised by the presence of abundant cytotoxic immune components and minimal regulatory mechanisms, the induction of inflammatory mediators with ISG-based treatments in infected individuals, should be managed in a tailored and efficient manner in order to minimise cytotoxic components without inhibiting viral clearance and resolution of disease.

1.4.1.3. Neutralising Antibody treatment

The components of the humoral immune response have also been highlighted as candidates for treating WNV infection. Although the production of numerous antibodies is induced by WNV infection, only a small proportion of these effectively neutralise WNV, limiting their therapeutic application. Protection of mice against lethal WNV infection can be achieved with the use of humanised antibodies targeting the post-attachment step of the virus. Monoclonal antibody (mAb) against the envelope protein of the virus has conferred some protection in murine studies by preventing the conformational change of the virus, critical for fusion with cellular membranes, thereby inhibiting entry into the cells (Oliphant et al. 2005; Throsby et al. 2006; Morrey et al. 2007; Zhang et al. 2009).

Further examples include the use of polyclonal antibodies to promote survival in B and T cell-deficient mice and the blocking of axonal spread of virus with neutralising antibody (Engle and Diamond 2003; Samuel et al. 2007).

Additional limitations for the use of neutralising antibody therapies in the treatment of WNV infection include the restricted capacity of antibody to cross the intact BBB (Cheeran et al. 2005; Morrey et al. 2007) and the potential development of antibody escape-mutant strains, especially considering flaviviruses in general form quasispecies. Although strains resistant to specific mAb are currently rare it needs to be closely monitored as mutations on viral epitopes can abrogate the neutralising effect and therefore the therapeutic activity of mAb against virus (Li et al. 2005; Sanchez et al. 2005; Zhang et al. 2009). Antibody treatment of flavivirus infection requires epitope binding that is both highly specific and of a high affinity (Sanchez et al. 2005). If these requirements are not met, treatment could result in exacerbation of the disease through antibody-dependent enhancement of infection. This classically occurs with recurrent infection of DENV in individuals with a different strain of DENV from the primary infection. Virus-specific antibody produced against the initial DENV strain has a lower affinity for other serotypes and, upon secondary infection, forms a complex with the virus instead of neutralising it. This leads to increased viral entry via Fc receptors on myeloid lineage cells, such as macrophages, and consequently higher numbers of productively infected cells (Halstead and O'Rourke 1977; Boonnak et al. 2011).

Administration of intravenous immunoglobulin (pooled human IgG) has been used in several clinical studies in the treatment of immunosupressed patients with severe neuroinvasive disease. This treatment has had varied success, with some patients making complete recovery from severe neuroinvasive disease. However, whether improvement was due to intravenous immunoglobulin treatment was difficult to confirm and further studies are needed (Haley et al. 2003; Shimoni et al. 2001; Rhee et al. 2011). Interestingly,

the therapeutic effect of intravenous immunoglobulin treatment is not due to the neutralising activity of antibody, but a direct consequence of immune modulation. Mice given i.p. intravenous immunoglobulin treatment survived infection with a lethal dose of WNV and neurotropic herpes simplex virus. This was directly attributed to the anti-inflammatory effect of intravenous immunoglobulin treatment, as there were significant reductions in pathogenic Ly6C^{hi} macrophages and TipDC populations in the CNS (Ramakrishna et al. 2011; Srivastava et al. 2015). How the intravenous immunoglobulin treatment modulates these subsets is still under investigation.

The primary obstacle in the treatment of WNV infection is the onset of immune-driven clinical symptoms that occur once there is an established neuronal infection. With this in mind, a therapeutic approach combining the strategies discussed above, with targeted treatment of the pathogenic immune components may be most effective.

1.4.2. Current effective treatments and Immune-modifying microparticles

Considering the immune-driven nature of WNV encephalitis, a shift in focus from antiviral to immunomodulatory therapies is more likely to be successful in unvaccinated individuals. Anti-inflammatory compounds could have significant neuroprotective effects in a disease in which pathology is mediated by inflammation and apart from targeting autoimmune diseases, it is clear that an anti-inflammatory treatment-based design could be beneficial for a multitude of diseases, including flaviviral encephalitis. Therapy can be designed to target several aspects of the disease progression, starting with the initial signals recruiting harmful cells. Intervention staged at this point, however, needs to be highly controlled, as certain infiltrating subsets remain crucial for inhibiting viral dissemination. Targeting and diverting pathogenic subsets from the CNS during later stages of disease may enable effective viral eradication and minimise damage. Lastly, the

inflammatory mediators produced by infiltrating as well as resident cells can be reduced or blocked by neutralising soluble mediators, such as NO, preventing direct oxidative stress on the CNS. Ultimately, the most likely scenario is the implementation of one or more of these strategies tailored on a patient-by-patient basis, with close monitoring of reaction to treatment.

Inhibition of ROS, Cox-2 and iNOS has been effective in reducing neuronal apoptosis during JEV infection (Nazmi et al. 2011) and neutralising antibody against TNF and IL-1β during WNV infection has a protective effect on neuroblastoma cells, reducing the apoptosis of infected cells (Kumar et al. 2010). Inhibition of NO production with aminoguanidine, was marginally protective in several models of flavivirus infection, as mice exhibited longer MST but not increased survival rates (Andrews et al. 1999; Getts et al. 2012). This indicates that it is likely the prolonged action of a combination of inflammatory mediators produced by activated leukocytes that ultimately skew the balance from a protective antiviral immune response to a pathogenic one. Ideally, treatment should be administered before this balance is tipped in favour of a pathogenic response. In our model of WNV infection, Ly6C^{hi} inflammatory MDM infiltration in the CNS correlated with weight loss and increased severity of clinical symptoms. Importantly, preventing Ly6C^{hi} inflammatory MDM from migrating to the infected CNS by blocking VLA-4 does not improve survival when administered early in infection, prior to the development of any clinical symptoms. However, administration of blocking treatment when significant weight loss occurs (>5%) increases survival of mice that would otherwise succumb to disease by up to 60% (Getts et al. 2012).

A recent breakthrough study from our laboratory targets Ly6C^{hi} inflammatory monocytes in circulation, prior to entering their target organ, where they would otherwise differentiate into either inflammatory macrophages or DC and exert a pathogenic effect.

Negatively charged, immune-modifying microparticles (IMP) are phagocytosed via MARCO expressed at high levels on Ly6C^{hi} monocytes in the circulation of WNV-infected animals (figure 1.3). As a result, these cells are mainly diverted to the spleen where they become sequestered and likely undergo apoptosis. This action, whilst reducing the immune response in the CNS, does not abrogate it, effectively allowing the virus to be cleared from the CNS whilst minimising the potentially lethal immune-mediated pathology. Intravenous infusion of IMP occurs when animals have lost >5% weight and rescues 60-70% of animals that would otherwise succumb to disease, with sterilising long-term immunity. This therapy has proven to be immensely successful in other models of disease where there is significant contribution of inflammatory monocytes to the pathology, such as MI, EAE and inflammatory bowel disease (Getts et al. 2014). This highlights the fact that immunomodulatory treatments are successful for a much greater range of therapies than just flaviviral encephalitis, if further trials prove successful this line of treatment may redefine how treatment is approached.

1.5. Objectives of this research

The primary objective of this research was to elucidate the role of the secondary lymphoid organs during lethal WNV encephalitis and subsequent immunomodulatory treatment of this disease. In particular, we focused on the contribution of the draining and non-draining lymph nodes of the CNS to the inflammatory response in WNV, with an emphasis on the lymphocyte populations. Furthermore, we aimed establish to what extent the spleen and its resident macrophages are required for the efficacy of IMP treatment in our i.n. model of WNV infection.

Figure 1.3 Immune-modifying microparticle treatment of WNV encephalitis

Figure 1.3 illustrates the proposed mechanism of action of IMP for the treatment of WNV encephalitis. IMP are injected as a bolus into the bloodstream (red section) and subsequently phagocytosed by Ly6C^{hi} inflammatory monocytes recruited by the CCL2/CCR2 axis from the bone marrow (blue section). Ly6C^{hi} inflammatory monocytes that phagocytose IMP are sequested by the spleen (yellow section) and are thus prevented from migrating to the CNS (green section). In the spleen they express apoptosis markers caspase-3 and Annexin V.

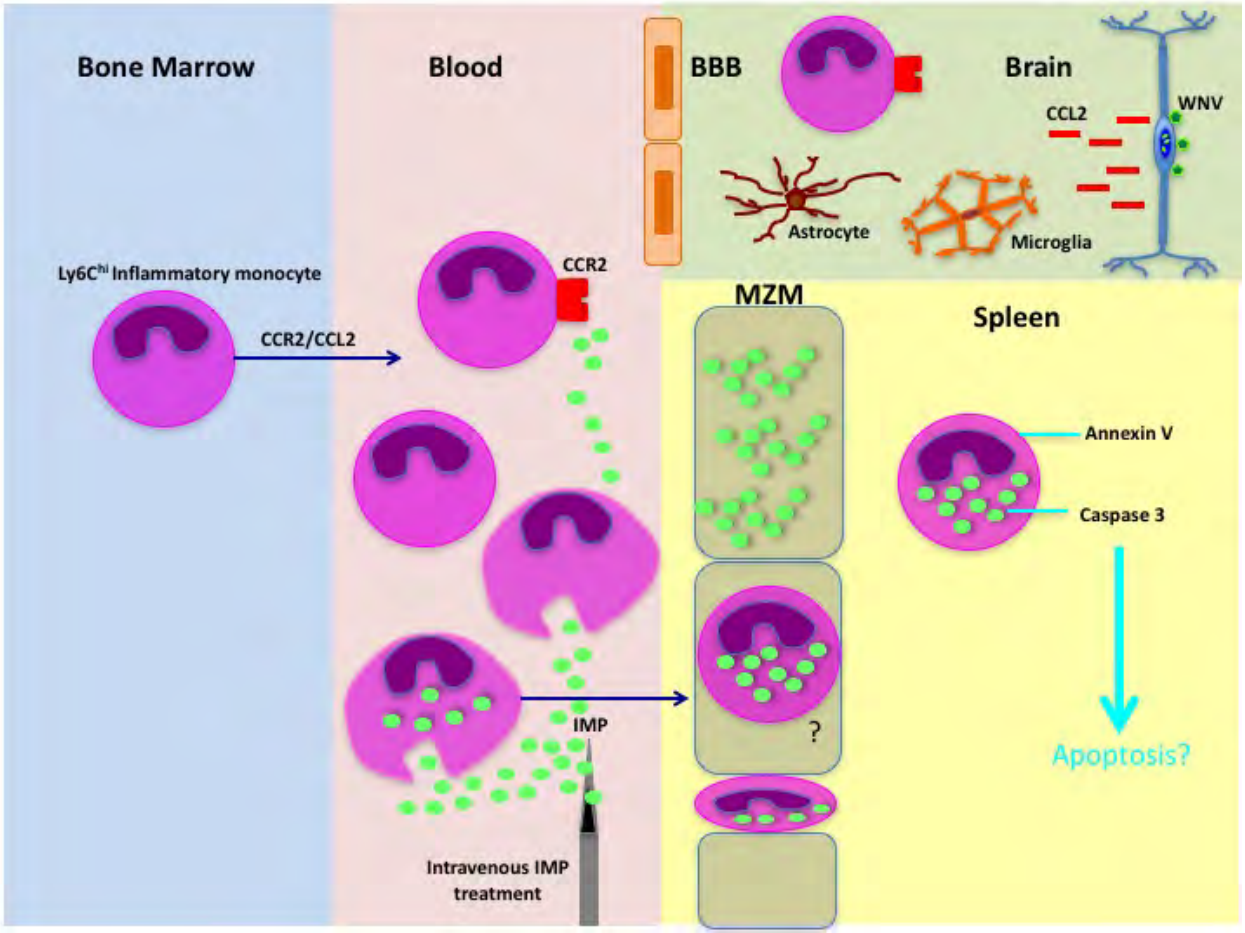

Figure 1.3 Immune-modifying microparticle treatment of WNV encephalitis

2. Materials and methods

2.1. Materials

2.1.1. Virus

Associate Professor Alison Kesson (The Children's Hospital at Westmead, Sydney, Australia) kindly provided the original WNV (Sarafend strain) stock.

2.1.2. Mice

Age matched 8-12 week old female WT C57BL/6 (CD45.2) mice and congenic B6.SJLPtprcaPep3b/BoyJ (CD45.1) mice were acquired from the Animal Resources Centre (Canning Vale, WA, Australia). Mice were housed in specific-pathogen free conditions within a PC2 animal facility in the Charles Perkins center and offered food and water *ad libitum.* Mice were treated in accordance with guidelines outlined by The University of Sydney Animal Ethics Committee under Animal ethics protocol numbers: K20/8-2008/3/4863; K20/8-2009/3/5127; K20/11-2011/3/5660.

2.1.3. Buffers, solutions and anaesthetic

Deoxyribonuclease (DNase) and Collagenase

DNase I and collagenase IV powders (Sigma Aldrich) were stored at -20°C until use. Digestion of brain tissue was performed at a concentration of 0.005 g/mL DNase I and

collagenase IV 0.05 g/mL in sterile PBS. Intracellular BrdU staining was done with DNase at a concentration of 300 µg/ml in sterile PBS.

Fluorescence-activated cell sorting (FACS) buffer

FACS buffer was made up of 5% FCS, 10% (1 mM) ethylenediaminetetraacetic acid (EDTA; Chem-Supply, SA, Australia) and sterile PBS and stored at 4°C until use.

Foetal calf serum (FCS)

Foetal calf serum (FCS; Sigma-Aldrich, MO, USA) was stored in aliquots at -20°C until use. FCS used was not heat inactivated before use.

Immune- modifying Microparticles

Fluoresbrite® YG (yellow green) Carboxylate Microspheres 0.50 µm (Polysciences, Inc, USA) were stored at 4°C until use. Stock solution ($3.64x10^{11}$ particles/ml) was diluted 1:25 in sterile PBS to a concentration of $1.46x10^{10}$ particles/ml. Each mouse was given 300 µl of working solution ($4.41x10^{9}$ particles) intravenously per dose, during once-daily treatment.

Minimum Essential Medium (MEM)

LPS-free Minimum Essential Medium containing L-glutamine and phenol red (Sigma-Aldrich) was supplemented with 20 mM Hepes (Invitrogen), 2.2 g/L sodium bicarbonate (JRH Bioscience), 4 g/L penicillin G and 0.2 g/L streptomycin sulphate (Sigma-Aldrich). MEM was supplemented with either 2% or 10% FCS as required.

Paraformaldehyde

A 4% paraformaldehyde (Sigma Aldrich) solution was prepared in PBS and stored at -20°C until required. To make 1 L of the solution, 800 ml of 1xPBS was heated to approximately ~60°C and 40 g of paraformaldehyde powder added to the heated PBS. Once the paraformaldehyde had dissolved, the solution was cooled and filtered, and the volume adjusted to 1 L by adding 1xPBS.

Percoll

Percoll (GE Healthcare, BKM, UK) was stored at 4°C. Leukocyte isolation from brain tissue was performed using Percoll solutions of 80% (to make 100 ml = 73.1 ml Percoll stock, 10 ml 1.5M NaCl and 16.9 ml of MilliQ water) and 30% (to make 100 ml = 26.32ml Percoll stock, 10 ml of 1.5M NaCl and 63.7 ml media). Leukocyte isolation from blood was performed using 70% Percoll solution (to make 100 ml = 57 ml of Percoll stock, 10ml of 1.5M NaCl, and 33 ml of MilliQ water).

Phosphate buffered Saline (PBS)

PBS powder (Sigma-Aldrich) was dissolved in MilliQ (9.57 g/L) and sterilised using a 0.22 µm filter (Corning Incorporated, NY, USA).

Red blood cell (RBC) lysis buffer

Stock solution of 10x RBC lysis (BD Pharm Lyse™; BD Biosciences, NJ, USA) was stored at 4°C and diluted to 1x working solution with MilliQ water.

TAE (Tris/acetate/EDTA) electrophoresis buffer

Stock solution (50x) was prepared by dissolving 242 g of Tris base and 37.2 g Na_2EDTA in 1l MilliQ water and adding 57.1 ml glacial acetic acid (all from Sigma Aldrich).

Tribromoethanol anaesthetic (Avertin)

Avertin was prepared by dissolving 1 g of 2,2,2-tribromoethanol in 1 ml of 2-methyl-2-butanol (Sigma-Aldrich) and adding 50 ml of pre-boiled tap water. This solution was fully dissolved by mixing then sterilised with a 0.22 filter (Corning). Aliquots were stored at 4°C, protected from light until required. An optimal dose 0.012 ml/g of body weight was used and administered i.p. to each mouse. The amount to be used for each mouse was determined based on mouse weight, from a precalculated nomogram, e.g. 250 µl/20 g mouse.

Tris-buffered saline (TBS)

TBS buffer was prepared as a 10x solution and stored at 4°C for up to a 2 months. To make 1 L TBS, 13.9 g of Tris base (Sigma Aldrich), 60.6 g Tris HCL (Sigma Aldrich) and 60.6 g of NaCl was dissolved in 1 L of MilliQ water, with 5 ml of Tween 20. Stock solution was diluted to 1x with MilliQ water for staining.

2.1.4. TaqMan primer and probe sequences

For real-time PCR of WNV NS5, the primers and probes were custom ordered from Applied Biosystems (CA, USA). The sequences were obtained from published WNV (Tang et al. 2006) primer and probe sequences, as listed in Table 2.1. WNV primers targeted the WNV 3' non-coding region. Primers and probes were reconstituted or diluted to a final stock concentration of 18 and 5µM respectively with nuclease-free water, aliquoted and stored at -20°C until use.

Table 2.1 Primer and probe sequences for WNV RNA amplification and detection by TaqMan PCR

Target		Sequence
WNV	Forward primer	AAG TTG AGT AGA CGG TGC TG
	Reverse Primer	AGA CGG TTC TGA GGG CTT AC CTC G
	Probe	AAC CCC AGG AGG ACT G

2.2. Methods

2.2.1. West Nile virus propagation

Stock WNV was propagated by injecting suckling C57BL/6 mice intracranially (i.c.) and collecting brains of mice at the first sign of illness. Brains were homogenised in DMEM+10%FCS and clarified by centrifugation. The resulting supernatant was used to infect Vero cells in Complete Medium (CM) i.e. Dulbecco's modified Eagle's medium (DMEM; Gibco, NY, USA) and 10% foetal calf serum (FCS; JRH Biosciences, KS, USA). A multiplicity of infection of 5 plaque forming units (PFU)/cell was used. Cells were propagated in a 37°C incubator, in a humidified atmosphere with 5% CO2. Virus was allowed to adsorb to Vero cells for 1 h, with rocking every 15 min to allow even distribution of virus, after which infected cells were incubated for a further 40 h at 37°C, then frozen at –80°C. Flasks were then thawed and the virus-rich supernatant clarified by centrifugation. Cell-free supernatant was stored in aliquots at –80°C until use. A final viral titre of the stock used in this project $1.7x10^9$ PFU/ml was determined by plaque assay. For 100% lethal dose infections (LD100), stock virus was diluted to $6x10^6$ PFU/ml in 10 µl (i.e. $6x10^4$ PFU/mouse). For the 50% sublethal dose of infection (LD50), stock virus was diluted a further 10-fold to $6x10^5$ PFU/ml or $6x10^3$ PFU/mouse in 10 µl.

2.2.2. West Nile virus Plaque assay

Baby hamster kidney cells (BHK) were taken out of liquid nitrogen storage and thawed. Cells were washed 3 times with CM and seeded in cell culture flasks (Corning, NY, USA). Cells were passaged until the required number of cells was obtained. Cells were then plated in 6-well plates at $1x10^6$ cells/well with 2 ml CM and incubated at 37°C for 24 h in humidified atmosphere with 5% CO2. Once cells reached an even monolayer of 80-90%

confluence, the medium was removed and 150 µl of diluted virus carefully added. Serial dilutions of virus were prepared with sterile PBS. Cells were then incubated at 37°C with virus for 60 min in a humidified atmosphere with 5%CO_2, rotating every 15 min to ensure infection occurred evenly. Agarose overlay was prepared by mixing 3% (w/v) low gelling molten agarose II (Amresco, OH, USA) with 2xMEM+10% FCS in a 1:1 ratio. After incubation of 60 min the virus was aspirated off and 2 ml of agarose mixture added to each well and allowed to solidify before returning to the incubator for 3-5 days until plaques were visible.

In order to fix cells and harden the agarose for easy removal, 3 ml of 10% Formalin (Lomb Scientific) was added to each well for 2-4 hours. Formalin was then removed and the agarose plug gently removed from the cell monolayers. Fixed cells were stained with 1 ml of 3% (w/v) of crystal violet solution in 20% (w/v) of methanol (Fronine) for 1 min and then washed with water. Well-isolated plaques were counted and the viral titre calculated as PFU/ml or PFU/mg of tissue by the following formula:

$$\frac{number\ of\ plaques\ in\ the\ well}{dilution\ factor\ x\ Volume\ diluted\ virus\ added\ in\ ml}$$

2.2.3. WNV infection

As mentioned above, two doses of virus were used for intranasal infection. These were $6x10^4$ PFU/mouse, as the LD100 dose or $6x10^3$ PFU/mouse for LD50 survival studies. Stock virus was thawed on ice and diluted to the appropriate concentration with sterile PBS. Prior to infection, mice were weighed and anaesthetised by intraperitoneal (i.p.) injection of Avertin at a concentration of 0.012 ml/g of body weight. Unconsciousness was confirmed by squeezing the hind foot of each mouse to ensure that no withdrawal reflex was observed. Once unconsciousness was established mice were given 10 µl of diluted virus or PBS for mock-infected controls, 5 µl per nostril was given intranasally (i.n.) Mice were placed on a heatpad in a supine position to prevent inoculum leaking out and

monitored until consciousness was regained. The time-course experiments described in chapter 3 and 4 were set up as follows. Infections were timed and performed on separate days, thus, mice were sacrificed and organs collected, processed, stained and acquired on the same day for each time-point. In order to test for immunity mice were re-infected intranasally with $6x10^4$ PFU (LD100), at least 3-months following primary infection, and monitored for any symptoms of disease.

2.2.4. Animal monitoring and clinical scoring

Following infection, mice were weighed twice daily and monitored for any signs of discomfort. Mice were euthanised when ≥5% weight loss was reached, compared to d0 p.i. The disease score of mice was determined according to the criteria outlined in table 2.2.

2.2.5. Tissue dissection, collection and processing

2.2.5.1. Leukocyte isolation

In any sequence of isolation and cell surface of intracellular antibody staining, all cells, alive or fixed were washed in order to remove the previous reagents used. Unless otherwise stated, this entailed a uniform approach as follows: Cells were centrifuged at 534 x g, for 5 min at 4°C, in an Allegra X-14 Beckman Coulter centrifuge. The supernatant was discarded and the resultant cell pellet gently resuspended. In addition, unless otherwise stated, the Allegra X-12R Beckman Coulter centrifuge was used for the majority of steps requiring centrifugation.

Table 2.2 Clinical scoring of WNV-infected mice

0	No weight loss
1	Weight loss of <5%. Minimal signs of disease.
2	Weight loss of >5%. Reduction in movement
3	Weight loss >5%. Significant reduction in movement, slightly hunched posture, face washing
4	Weight loss >5%, significant reduction in movement, hunched posture, ruffled fur and seizure development
5	Immobile but still alive

2.2.5.1.1. Blood

Blood was collected with a single cardiac puncture using a 27G needle and syringe containing 200 µl of heparin. Blood was then transferred to heparinised tubes. The solution was subsequently diluted to 2 ml in sterile PBS and layered on top of 3 ml Ficoll-Paque Plus or 70% Percoll (GE Healthcare). Samples were centrifuged at 1455 x g for 25 min at room temperature (RT) The purified layer of leukocytes was collected from the interface, washed twice with FACS buffer as described above. The cell pellet was subsequently resuspended in FACS buffer for cell counting and antibody staining.

2.2.5.1.2. Brain

Perfusion of mice was performed prior to collection of brain tissue by cutting the inferior vena cava and flushing the vascular system via the left ventricle with 30ml cold PBS, using a 27G needle. Brains were placed in petri dishes containing cold, sterile PBS and gently mashed through a coarse metal sieve and resuspended in 30 ml of cold PBS and centrifuged for 20 min at 524 x g. The pellet was subsequently resuspended in 20 ml of collagenase and DNase solution (described in materials) and incubated at 37°C for 60 min, with gentle agitation every 15 min. Digestion was stopped by adding 25 ml of FACS buffer containing 10% FCS and the dispersed tissue centrifuged for 20 min at 524 x g. To isolate leukocytes, the pellet was resuspended in 7 ml of a 30% Percoll solution and gently layered over 3 ml of 80% Percoll and centrifuged for 25 min at 1455 x g at RT with the brake off. Following collection of leukocytes from the interface, cells were washed and resuspended in FACS buffer for cell counting and antibody staining.

2.2.5.1.3. Bone marrow

Whole femurs were dissected and rinsed in ethanol and sterile PBS. After removing the head and lower extremity of the femur, the femurs were flushed with 10 ml cold, sterile

PBS using a 30G needle. The resultant cell suspension was centrifuged at 524 x g for 10 min and the pellet subsequently resuspended in 2 ml of 1x RBC lysis and incubated at RT for 5 min. 10 ml of FACS buffer was added to stop the reaction and the cell suspension centrifuged for 10 min at 524 x g. The cell pellet was subsequently resuspended in FACS buffer for cell counting and antibody staining.

2.2.5.1.4. Spleen

Spleens were collected in cold, sterile PBS and gently mashed through a 70 µm nylon sieve. Cells were resuspended in 10 ml PBS and centrifuged for 10 min at 524 x g. RBC lysis was performed by resuspending the pellet in 4 ml 1x RBC lysis buffer, followed by incubation for 10 min at RT. FACS buffer was added to stop the reaction and cells were centrifuged for 10 min at 524 x g. The pellet was resuspended in FACS buffer for cell counting and antibody staining.

2.2.5.1.5. Lymph nodes

Lymph nodes were removed, placed in cold, sterile PBS and gently mashed through 70 µm sieve. Cells were washed with 10 ml FACS buffer and centrifuged for 10min at 524 x g. The cell pellet was resuspended in FACS buffer for cell counting and antibody staining. Dissection and removal of mouse lymph nodes was performed based on the anatomical distribution described by Dunn (Dunn 1954).

2.2.5.2. Organ collection for PCR

Mice were perfused as described above and the brain and lymph nodes collected. Organs were place in 1 ml (whole brain) and 200 µl (for 2 lymph nodes) of RNA*later*® stabilising agent (Life Technologies, CA, USA) and stored in -80°C until required.

2.2.5.3. Organ collection for immunohistochemistry (IHC)

Once mice were anaesthetised and perfused as described above, the relevant organs were dissected and placed in Tissue-Tek cryomolds (Sakura, Netherlands) containing Optimum Cutting Temperature Compound (OCT; Sakura, Netherlands). Moulds containing organs were slowly immersed in liquid nitrogen and stored at -80°C until required.

2.2.6. Administration of immune-modifying microparticles, Enalapril and BrdU

2.2.6.1. IMP

A stock solution of IMP was kept at 4°C protected from light. The stock solution of 0.025 g/ml or $3.64x10^{11}$ particles/ml was diluted to the working IMP solution to deliver a dose of 1.4 mg/kg. For an adult mouse this is ~0.3 mg/mouse or $4.41x10^{9}$ particles per mouse. This required a 1:25 dilution (200 µl of stock IMP into 4800 µl sterile PBS)= $1.46x10^{10}$ particles/ml in sterile PBS. This working solution was kept for a maximum of 2-3days at 4°C. Mice were weighed daily and received a single dose of IMP as a 300 µl intravenous injection in the morning, depending on the treatment criteria (i.e. >5% Weight loss, time point in disease etc.). To perform the intravenous injection we dilated the tail veins in mice, either by placing them in a warmer environment (e.g. at 28-30 ºC) for up to 30 minutes, or by placing the tail in warm (30-35 ºC) water. After removing any air bubbles present in the syringe, an appropriate restraining device was used and IMP were administered with a 27-30G needle. Once the vein was located, the injection was begun at mid-length or slightly distal on the tail. Injection of a 300 µl volume was performed at a very slow rate to minimise any discomfort to the animal. Successful injection was determined by lack of resistance when pressure was placed on plunger and when

blanching of the vein was observed. If any bubbles formed around the site of injection or resistance was felt, the needle was removed and reinserted above the initial injection. After successful injection, the needle was removed slowly and pressure immediately placed on the injection site for up to 1 min to prevent bleeding. Mice were monitored daily for any discomfort. Those requiring daily treatment, received injections on alternate sides of the tail to give the tail maximum time to recover between injections, which in turn maximised the success of the injections.

2.2.6.2. Clodronate liposomes

Clodronate, a bisphosphonate, clinically used in osteoporosis to inhibit osteoclast action, does not cross the cell membrane, but enters cells through phagocytosis and possibly fluid phase pinocytosis. High intracellular concentration of clodronate induces cell death, likely as a result of interference with protein kinase C and other pathways. This results in the depletion of phagocytic subsets, in particular circulatory monocytes, as well as resident macrophages, including red pulp and marginal zone macrophages of the spleen, Kupffer cells in the liver and macrophages in the lymph nodes, but fails to deplete others, such as microglia (van Rooijen and van Nieuwmegen 1984) (Getts et al. 2008). Clodronate or control PBS-encapsulated liposomes (Nico van Rooijen, Amsterdam, Netherlands) were administered i.v. to mock-infected or LD50 ($6x10^3$ PFU i.n.) or LD100 ($6x10^4$ PFU i.n.) WNV-infected mice at a volume of 200µl per mouse on d5 p.i. as per the manufacturers instructions.

2.2.6.3. Bromodeoxyuridine (BrdU) administration

BrdU (BD, USA), 2 mg in 200 µl sterile PBS per mouse, was thawed and administered i.p. 3 hours prior to sacrificing animals.

2.2.6.4. Enalapril administration

Enalapril (Sigma-Aldrich) was administered i.p. in 200 µl to mock-infected or LD50 ($6x10^3$ PFU i.n.) or LD100 ($6x10^4$ PFU i.n.) WNV-infected mice. Enalapril was given at a dose of 100 mg/kg/day, i.e. 2 mg for a 20 g mouse (Gard et al. 1999; Leuschner et al. 2010). Mice were weighed daily and monitored for any signs of discomfort.

2.2.7. Surgery and adoptive transfer

2.2.7.1. Surgical removal of the spleen

Prior to surgery, each animal was given an i.p. injection of the analgesic anti-inflammatory drug, meloxicam (4.4 mg/kg) (Loxicom, Norbrook Laboratories, UK) and tramadol (0.7 mg/kg) (bioCSL, Victoria). Mice were sedated in a gas induction chamber with isoflurane. Once sedated, mice were fully anaesthetised under a general inhalational anaesthetic (Isoflurane, Veterinary Companies of Australia, NSW, Australia) with a facemask for surgery. Anaesthetised mice were placed on their right side, shaved and swabbed with 70% ethanol above their left kidney. A small vertical 10-15 mm incision was made through the skin and abdominal wall layers. The spleen was identified and carefully exteriorised through the incision. The splenic arteries and veins were ligated using a 4-0 synthetic silk suture (Dynek, SA, Australia), the distal tissue sectioned and the spleen removed. The abdominal muscle wall and skin incision was then sutured separately and treated with iodine. Mice were placed on a heatpad and monitored every 30 min until they recovered (Reeves et al. 2001). On d1 and d2 post-surgery, mice were given tramadol and meloxicam orally, administered per drop with a syringe. Mice were then checked twice daily for a 2-week period for any signs of infection or discomfort prior to commencing any experimental procedures.

2.2.7.2. Dye injection and Adoptive transfer experiments

2.2.7.2.1. Footpad injection of PKH26

Mock-and WNV-infected mice (i.n., $6x10^4$ PFU) were sedated in a gas induction chamber with isoflurane. Once sedated, mice were fully anaesthetised under a general inhalational anaesthetic (Isoflurane, Veterinary Companies of Australia, NSW, Australia) with a facemask for footpad injection. Once unconsciousness was confirmed by testing for the absence of the withdrawal reflex, mice were given a 50 µl injection of PKH26 (Sigma Aldrich) via the footpad on d0 p.i. Mice were sacrificed at 24 h p.i. and on d7 p.i., and the draining lymph node of the foot, the popliteal lymph node, along with the cervical and inguinal lymph nodes, brain and spleen were collected and placed in cold PBS. Samples were subsequently processed for flow cytometry as described in section 2.2.4.1.

2.2.7.2.2. Adoptive transfer of leukocytes

For adoptive transfer experiments, leukocytes were isolated under sterile conditions from the bone marrow and lymph nodes of donor (CD45.1 or CD45.2) mice as described in section 2.2.4.1. Cells were counted and cell membranes labelled according to manufacturers' instructions with PKH26 red fluorescent cell linker kit (Sigma Aldrich) and/or carboxyfluorescein succinimidy ester (CFSE) (Sigma Aldrich).

PKH26 staining: $2x10^7$ leukocytes were re-suspended in 1 ml of Diluent C, followed by addition of 1ml of 2x dye suspension, made up with 1 ml Diluent C and 4 µl PKH26. Cells were incubated for 1-2 min and the reaction terminated with 2 ml FCS. The samples were washed three times with cold, sterile PBS.

CFSE staining: up to $1x10^8$ cells/ml were resuspended in a solution containing 10 µM of CFSE and incubated for 5 min. FCS was added to the cell mixture, which was subsequently washed three times with sterile PBS. The cells were subsequently filtered through a sterile

70 µm cell strainer (Corning Incorporate, NY, USA) and injected into recipient animal. For the footpad injection of cells, each recipient animal was given $2x10^6$ cells in 50 µl of sterile PBS. Intravenous injection of cells was performed as described in section 2.2.6.1 with each animal receiving ~$2x10^6$ cells in 150-200 µl sterile PBS.

2.2.8. Flow cytometry

2.2.8.1. Cell surface staining

Once total live cell counts were determined, $1.5x10^6$ cells/sample were transferred to a 96 well U-bottom plate (BD Falcon) along with aliquots for fluorescence minus-one (FMO), single-stain and isotype controls. To determine optimal voltage parameters bead compensation controls (BD CompBeads, BD) were included for each experiment. Samples in the 96-well plates were centrifuged for 5 min at 462 x g at 4°C and supernatant discarded. The cell pellets were re-suspended in 50 µl of Fc block (anti-mouse CD16/32) (Biolegend) and 0.1 µl/sample fixable blue, dead cell staining kit (Life Technologies) and incubated on ice, protected from light. After 30 min, samples were raised in FACS buffer and washed. Samples were then re-suspended in 50 µl of prepared antibody- and isotype-cocktails, as well as single stain and FMO controls and incubated for 40 min at 4°C, protected from light. Detailed information on the antibodies used can be found in table 2.3. Cells were washed 3x in FACS buffer and either acquired the same day on the flow cytometer or fixed with 40 µl of fixation buffer (Biolegend) for 20 min at RT. Once fixed, the cells were washed 3x with FACS buffer. Cells were re-suspended in 200 µl FACS buffer, sealed and stored at 4°C until acquisition (no longer than 1-2days).

Table 2.3 Antigen specificity, isotype, clone, dilution, conjugate, application and source for each antibody used. All are specific for mouse antigens unless specified. WB = Western blotting, FC = flow cytometry, IF = immunofluorescence. The antibody source legend is listed below.

Antibody	Isotype	Clone	Dilution	Conjugate	Application	Source
CD45	Rat IgG2b	30F-11	1:200	PerCP	FC	Biolegend
CD45.1	Mouse (A.SW) IgG2a	A20	1:100	APC	FC	Biolegend
CD45.2	Mouse (SJL) IgG2a	104	5:100	PerCP	FC	Biolegend
CD3ε	Armenian Hamster IgG	145-2C11	1:200 1:100	Pe-CF594, APC, Af700	FC, IHC	BD Biosciences
CD4	Rat IgG2a	RM4-5	1:400	AF700	FC	Biolegend
CD8α	Rat IgG2a	53-6.7	1:100	BV711	FC	Biolegend
B220	Rat IgG2a	RA3-6B2	1:100	Pe , B220 BV785, PeCF594	FC, IHC	Biolegend
CD19	Rat IgG2a	ID3	1:200, 2:100	Pe-CF594, BV785	FC	BD, Biolegend
CD11b	Rat IgG2b	M1/70	1:200, 1:100	BV650,BV605 ,PeCy7, BUV395	FC	Biolegend
CD11c	Armenian Hamster IgG	N418	1:100	Pe, APC Pe/Cy7, FITC	FC	Biolegend
MHCII (I-A/I-E)	Rat IgG2b	M5/114.15.2	1:300	BV510	FC	Biolegend
Ly6G (CD45R)	Rat IgG2a	1A8	1:100	APC/Cy7, Pe, PeCy7	FC	Biolegend
Ly6C	Rat IgG2c	HK1.4	1:100	BV421	FC	Biolegend
NK1.1	Mouse IgG2a	PK136	5:100	BV510, BV605, BV711	FC	Biolegend
F4/80	Rat IgG2a	BM8	1:100	Pe	FC, IHC	Biolegend
Annexin V	-	-	5:100	PeCy7	FC	eBioscience
BrDU	-	-	5:100	APC	FC	BD; Biolegend
Biotinylated-MARCO	Rat IgG1	ED31	5:100	Af594	FC, IHC	R&D systems

2.2.8.2. Intracellular staining

Organs were collected and leukocytes isolated as described. Following cell surface staining, as described in the previous section, the samples were washed 2x with FACS buffer. After discarding the supernatant, samples were fixed and permeabilised by resuspending cells in 100 µl of BD Cytofix/Cytoperm Buffer, followed by 30 min incubation on ice. Samples were then washed with 1xBD Perm/Wash buffer, and resuspended in 100 µl of BD Cytoperm Buffer Plus, with 10 min incubation on ice. Samples were then washed with 1x BDPerm/Wash Buffer, the supernatant was discarded and the pellet resuspended in 100 µl of BD Cytofix/Cytoperm Buffer, with 30 min incubation on ice. Samples were washed again with 1xBD Perm/Wash. To expose incorporated BrdU, the samples were treated with 100 µl of DNase (300 µg/ml in sterile PBS i.e. 30 µg of DNase per 10^6 cells) and incubated for 1 hour at 37°C. Samples were washed with 1x BD Perm/Wash Buffer and intracellular BrdU staining was performed as follows. Supernatant was removed and the pellet resuspended in 50 µl of BD Perm/Wash Buffer containing diluted fluorescent anti-BrdU. Following a 20 min incubation at RT protected from light, samples were washed 3x with 1x BD Perm/Wash Buffer, and finally resuspended in 200 µl of FACS buffer and stored at 4°C until acquisition.

2.2.8.3. Sample acquisition and analysis

Fixed samples were stored at 4°C protected from light until acquisition (no longer than 1-2days). Non-fixed samples were acquired with the flow cytometer on the same day as processing. Prior to acquisition, samples were filtered through a 70 µm nytex filter to remove debris and prevent potential blockage of instruments. Samples were acquired on either a BD FACS Canto or FACS LSR-II, running FACS Diva software (BD Biosciences). Data files (.fcs) were analysed with FlowJo software (FlowJo, OR, USA) after which flow

cytometry percentages and absolute cell counts were used to calculated cell populations of interest in Microsoft Excel.

2.2.9. RT PCR

2.2.9.1. RNA extraction

Tubes were thawed; tissue removed from RNA*later*® and placed in Trizol (1 ml/50-100 mg tissue) (Life Technologies, CA, USA) with 0.25 ml Zircon beads (Biospec Products, USA) in microcentrifuge tubes. Tissue was homogenised using a Fastprep FP120 cell disruptor (ThermoElectron Corporation, MA, USA) (brain= 20 s at speed 5; LN= 2x 20 s at speed 6). Tubes were then centrifuged at 12 000 x g for 10 min at 4°C in a Microcentrifuge 5415R (Eppendorf), after which the fatty layer was removed and the clear supernatant transferred to a new 1.5 mL microcentrifuge tube. Note that all further centrifugation in this section was performed with the Eppendorf microcentrifuge described above. Phase separation was performed by adding chloroform (0.2 ml per 1 ml Trizol) and shaking the tube vigorously for 15 s by hand. Samples were centrifuged at 12 000 x g for 10 min at 4°C, followed by removal of the aqueous phase of the sample which was transferred to a new tube for RNA isolation. Next, one volume of 70% molecular-biology grade ethanol, made up in nuclease-free water, was added to the sample. The sample was then transferred to a RNA binding column (RNeasy Mini kit, Qiagen, Netherlands) with a 2 ml collection tube and centrifuged at 10 000 x g for 15 s at 4°C and the flow-through liquid discarded. Next 700 µl of RW1 buffer was added and the sample centrifuged again at 10 000 x g for 15 s and the flow-through liquid discarded. This step was repeated 2x with 500 µl RPE buffer, centrifuged for 15 s to dry the membrane and the flow-through liquid discarded. To ensure removal of the flow-through liquid and RPE buffer, the column was transferred to a

new 2 ml collection tube and centrifuged for 1 min at 16 000 x g. The column was then transferred to a 1.5 ml microcentrifuge tube and 30 µl of nuclease-free water was added directly onto the column membrane, which was centrifuged for 1 min at 9000 x g. The eluted RNA was collected in the microcentrifuge tube and tested for purity and yield. The NanoDrop ND-1000 spectrophotometer (Thermo Fisher Scientific, MA, USA) was used to measure light absorbance at 230, 260 and 280 nm. Protein contamination was determined by A_{260}:A_{280} ratio and ethanol contamination by A_{260}:A_{230} ratio.

2.2.9.2. cDNA

The SensiFAST cDNA Synthesis kit (Bioline, USA) was used for cDNA synthesis and the manufacturers protocol was followed. For the synthesis of cDNA, 1 µg of RNA was diluted to a total volume of 13 µl with nuclease-free water, 1 µl of 250 ng/ul hexamer and 1 µl of reverse transcriptase with 4 µl of TransAmp buffer. This was gently mixed by pipetting and the following program set up in the thermal cycler (Mastercycler Nexus, Eppendorf, USA): 25°C for 10 min (primer annealing), 42°C for 15 min (reverse transcription), 85°C for 5 min (inactivation) and 4°C for any hold time.

2.2.9.3. Taqman PCR

The RT reaction was performed by using the MyTaq Red DNA Polymerase kit (Bioline, UK). The setup included mixing 2 µl of template with 10 µl of 5x MyTaq Red Reaction buffer, 0.25 µl of MyTaq Red Polymerase, 1 µl of each reverse and forward primer, and raising the solution up to 50 µl in water. PCR cycling conditions were as follows: Initial denaturation at 95°C for 1 min, followed by 30 cycles of denaturation for 15 s at 95°C; Annealing for 15 s at 60°C and extension for 30 s at 72°C. This was performed on the Mastercycler Nexus (Eppendorf, USA).

2.2.9.4. Gel electrophoresis and quantitative PCR

Visualisation of PCR and identification of virus was performed with agarose electrophoresis. Agarose (Bioline, USA) was made up to 2% with TAE. Agarose mixture was transferred to a gel tray in a casting chamber and left to cool. PCR product was then loaded into each well. This included a DNA ladder, as well as a positive (RNA isolated from virus stock) and negative control (media). The gel was run for 45 min at 100 volts. The resultant gel was imaged using the Gel Doc EZ System (BioRad, CA, USA).

For quantitative PCR, each assay for the gene of interest was multiplexed with the housekeeping gene, GAPDH. Each reaction was carried out in duplicate or triplicate. Amplification was performed using the ABI Prism 7000 Sequence Detection System (Applied Biosystems). Quantitative PCR was performed and the relative RNA expression in each organ was normalised to mock-infected mice (d0) in terms of 2000 ng/µl total RNA and analysed using the $2^{-\Delta\Delta C_T}$ method.

2.2.10. Immunohistochemistry

Sections for fluorescence IHC were prepared by bringing cryomolds to temperature (-15-20°C) in the cryostat microtome and cutting 6 to 8-micron tissue sections. Slides were allowed to air dry and subsequently stored at -80°C until required.

To stain samples, slides were removed from -80°C and thawed at RT for ~20 min. Once thawed, sections were circled with a DAKO pen (DAKO, Denmark) and washed once in a Copeland jar with 1x TBS. Sections were fixed with 4% PFA in PBS and incubated for 10 min at RT, after which the washing step with TBS was repeated. Avidin/Biotin blocking was performed in any scenario in which the antibody of interest was not directly conjugated to a fluorophore. This blocked all endogenous biotin, biotin receptors and avidin binding sites. When required, Avidin block (100-150 µl) (Vector) was placed on

each section and incubated for 10 min at RT. Slides were washed for 3 min with TBS. Excess liquid was removed and 100-150 µl biotin block placed on each section and incubated for 10 min at RT, after which slides were washed for 3 min in TBS. Slides were then blocked with TNB (Tris-NaCl-blocking buffer) with 10% serum for 30 min at RT. Excess TNB was removed and 100-150 µl primary antibody or isotype control in antibody-staining buffer (45% TBS, 45% TNB, 10% FCS) was added to each section. This was incubated for either 2 hours at RT or overnight at 4°C and then washed 3x for 3 min/wash in TBS buffer. Sections were then incubated for one hour at RT with secondary antibody, diluted in antibody- staining buffer. After washing sections 3x for 3 min with TBS buffer, excess liquid was removed and one drop of DAPI with Prolong Gold added to each section. A coverslip was applied to each section, allowed to dry for ~20 min at RT and sealed. Images were acquired on an Olympus BX-51 microscope (Olympus, Tokyo, Japan), using a DP-70 camera and DP manager software (Olympus).

2.2.11. Whole blood phagocytosis assay

WNV-infected mice ($6x10^4$ PFU) were CLO-depleted at d5p.i. and blood was collected as described in section 2.2.5.1. at d6p.i. 100µl of WNV-infected control and WNV-infected CLO-depleted blood was added to 100 µl of 10% heat inactivated FCS and mixed thoroughly. 10 µl of undiluted IMP (neat) i.e. $3.64x10^9$ IMP and serially diluted 1:3 and 1:9 (with sterile PBS) IMP at 50 µl of resultant stock added to tubes of blood. Tubes containing neat and diluted IMP with blood were mixed thoroughly and placed in a 37°C waterbath for 15 min, whilst constantly being agitated. After 15 min 1 ml of cold FACS buffer was added to each tube to stop phagocytosis. Samples were then centrifuged for 5 min at 4°C at 340 x g after which the supernatant was removed and samples resuspended in 100 µl of FACS buffer. Cell surface staining was then performed as described in section 2.2.8.1. After cell surface staining was performed cells were fixed/lysed by adding 100 µl of Optilyse to

each sample and mixing. Samples were incubated for 10 min at RT in the dark. Cells were washed twice and resuspended in FACS buffer for acquisition.

2.3. Statistical analysis

Raw data was first analysed using Microsoft Excel. Graphs were generated and statistical analysis performed with GraphPad Prism 4 (GraphPad Software Inc., CA, USA). For comparison of 2 samples an unpaired, two-tailed Student's t test was used. Comparison of 3 or more samples was done using a one-way ANOVA with Tukey-Kramer (each column to the other) or Dunnet's post-test (each column to a control column, usually mock-infected), as appropriate. Survival data were analysed using Mantel-Haenszel logrank test. Significance was determined as follows: $p \leq 0.5$ was deemed statistically significant (*), $p \leq 0.1$ very significant (**) and $p \leq 0.001$ extremely significant (***).

3. Chapter 3 The role of the draining and non-draining lymph nodes following lethal WNV infection

3.1. Introduction

The critical role of the local draining lymph nodes in mounting an effective adaptive immune response during viral infection has long been recognised. In addition to inhibiting the spread of pathogens, the draining lymph nodes are crucial for the activation of cellular immunity and the development of humoral immunity through the presentation of antigen to T and B cells, respectively. Although the exact lymph drainage pathways of the CNS are relatively unknown, several publications have implicated the deep and superficial cervical lymph nodes (CLN) in the lymphatic drainage of the CNS (Yamada et al. 1991; Karman et al. 2004). The recent discovery of lymphatic vasculature in the CNS, connected to the superficial and deep CLN, has cemented a long-held belief that the CLN are the draining nodes of the CNS (Louveau et al. 2015). However, the extent to which these lymph nodes form part of the immune response to CNS inflammation, in particular during viral encephalitis, has not been studied. During lethal WNV encephalitis, there is significant infiltration of various leukocyte subsets (including lymphocytes) into the CNS. Previous work from our lab has shown that the bone marrow is a potent source of the myeloid lineage cells infiltrating the brain in this i.n. model of infection (Getts et al. 2008). However, the specific origin of lymphoid lineage cells in the inflamed CNS has not been elucidated. Considering the intimate association between the brain and CLN, these nodes would seem likely to supply the humoral and cellular immune components against WNV. Nevertheless, the lymphatic system is not an isolated organ and its constituents are distributed throughout the body, all of which are connected to some degree through the

lymphatic and blood vessels. Moreover, there is some evidence that not only the draining lymph nodes, but also the peripheral non-draining nodes may be involved during the inflammatory response (Reisman et al. 2011; Ciabattini et al. 2010). With this in mind, the aim of this chapter is to investigate the response of the CNS-draining and non-draining lymph nodes during lethal WNV encephalitis, with a particular focus on lymphoid lineage cells.

3.2. Results

3.2.1. Leukocyte population dynamics in the cervical, inguinal and mesenteric lymph nodes following lethal WNV infection

In order to investigate the kinetics of the lymph node response during WNV infection, female C57BL/6 mice, 8-12 weeks old, were infected i.n. with a lethal dose (LD100) of WNV ($6x10^4$ PFU). The intranasal model of infection was used throughout the project reported in this thesis, as it has been extremely well characterised in our laboratory, with defined LD100 and LD50 disease curves. This model allows us to specifically study the effect of immune components on the CNS and also develop detailed treatment protocols based on a well-established model. Virus can be detected in the olfactory bulb by d3 p.i. and is first evident in the neurons at d6 p.i. (Getts et al. 2007; Getts et al. 2008).While live virus can be detected in the heart, lung spleen and bone marrow, these levels were less than 0.001% of those detected in the brain (Terry 2012). In this model, d7 represents the peak of infection, characterised by maximal leukocyte infiltration into the CNS, severe clinical symptoms and, without intervention mice would die on d7p.i. (Terry 2012). Mice were sacrificed on d0, d3 d5, d6 and d7 post infection and the CNS-draining cervical lymph nodes (CLN) were harvested for flow cytometric analysis, with the inguinal (ILN) and mesenteric lymph nodes (MLN) serving as peripheral/non-draining lymph node controls.

Note that infections were performed on different days; thus, the organs from all time-points were collected, processed, stained and acquired on the same day. An example of the initial gating strategy performed for leukocyte isolation from the lymph node can be seen in Figure 3.1. In addition, a more detailed gating strategy of the lymph node, with isotype and fluorescence minus one controls, can be found in the Appendix, Figure 1 and 2. The gating steps applied followed a standardized protocol for flow cytometric data quality control, in order to ensure that all events analysed were comparable and representative. A time gate (Figure 3.1A) was implemented first to exclude any events where an uneven flow-rate compromised the signal of the data collected. Secondly, all doublets were excluded (Figure 3.1B) based on the forward scatter-area (FSC-A) and forward scatter-height (FSC-H) parameters. All cellular and tissue debris was subsequently excluded, based on size and granularity, using the side scatter-area (SSC-A) and FSC-A parameters (Figure 3.1C). Next, all dead or dying cells were removed with the use of a UV dye, which attaches to amine groups on the cell surface and intracellularly. Thus, dead or dying cells with permeable membranes will show intensely positive staining, allowing the "negative selection" of live cells (Figure 3.1D). Lastly, leukocytes were gated using the pan-leukocyte marker CD45 (Figure 3.1E). These steps ensured that only the data from live, single cell populations acquired under the same conditions were analysed.

Figure 3.1 (F) demonstrates the kinetic changes in the total leukocyte population number during a time-course of WNV infection in the CLN, MLN and ILN. A significant increase in leukocyte number was evident in the CLN from as early as d3 p.i., with cell numbers increasing by up to 6-fold, compared to d0 p.i. In contrast, the ILN and MLN exhibited a decrease in total leukocyte numbers during the course of infection, with a statistically significant decrease by d7p.i. to 50% of the leukocyte numbers seen at d0p.i.

Figure 3.1. Cellularity of the draining (CLN) and non-draining lymph nodes (MLN, ILN) of the CNS following lethal WNV infection

(A-E) Representative flow cytometric dot plots illustrating the gating strategy for leukocytes in the secondary lymphoid organs (CLN, ILN & MLN) of mice infected with LD100 WNV ($6x10^4$ PFU). In order to obtain a live single cell leukocyte population the following steps were performed during analysis: (A) Uniform events within a time period were gated, followed by exclusion of doublets with the FSC-H vs FSC-A gate (B). (C) Debris was then removed with the SSC-A vs FSC-A gate. (D) "Negative selection" of live cells, using a live/dead discriminating dye was made. Final positive selection positive selection (E) of leukocytes based on the pan-leukocyte marker (CD45) was then made by further gating. (F) Numbers of $CD45^+$cells in the CLN (red), MLN (green) and ILN (blue) of mice following lethal WNV infection ($6x10^4$ PFU) are shown on day 0, 3, 5, 6 and 7 p.i. Data are shown as the mean ±SEM of values from 3 independent experiments, with 3-4 mice/group in each experiment. Statistical analysis was conducted using one-way ANOVA with a Dunnet's multiple comparison post-test (d0 as control), and $P \leq 0.05$*; $P \leq 0.01$**; $P \leq 0.001$***.

Figure 3.1

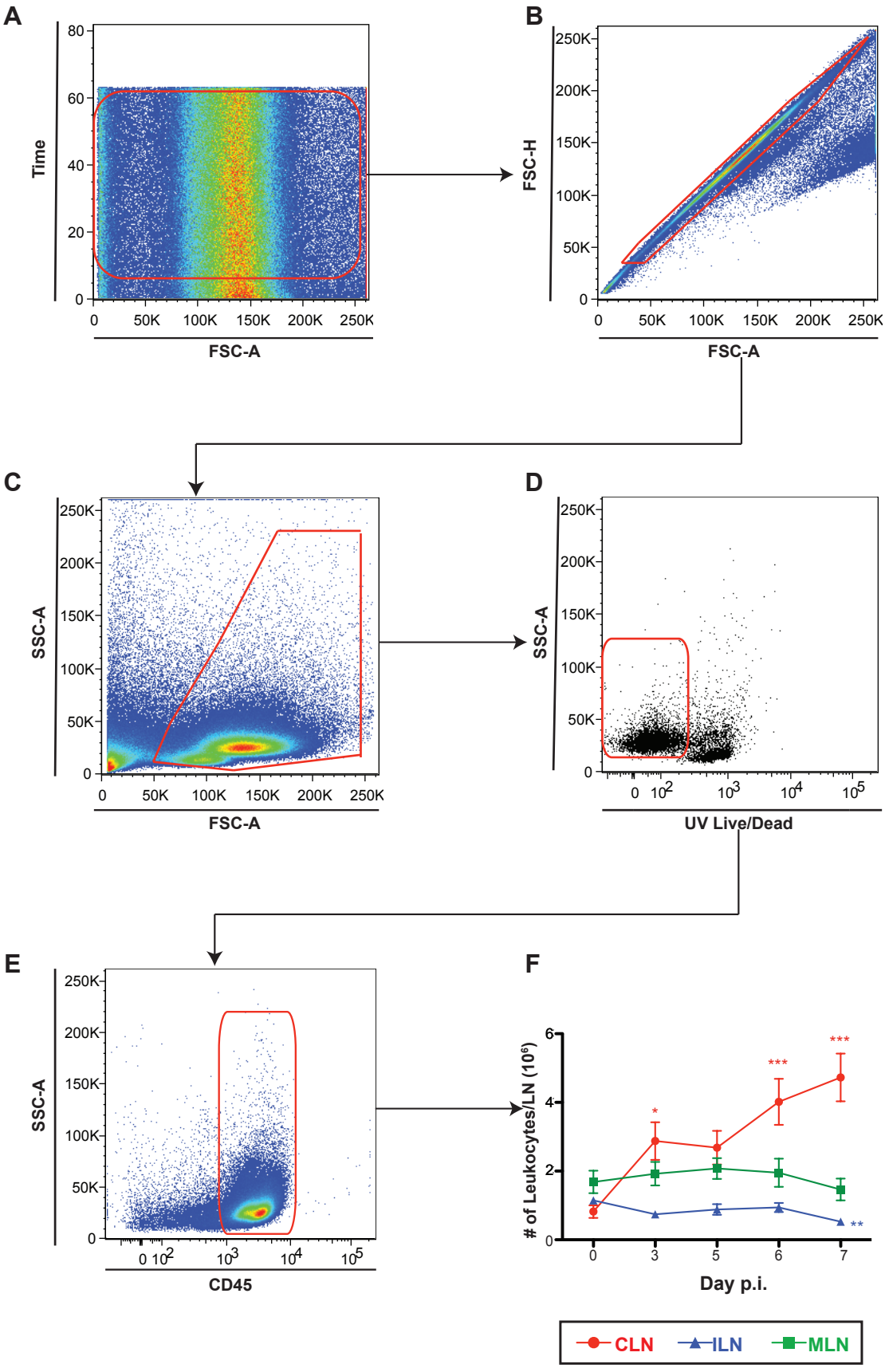
A
Time
FSC-A
B
FSC-H
FSC-A
C
SSC-A
FSC-A
D
SSC-A
UV Live/Dead
E
SSC-A
CD45
F
# of Leukocytes/LN (10⁶)
Day p.i.
CLN
ILN
MLN

3.2.1.1. T cells

An example of the gating strategy used to identify the T cell populations is illustrated in Figure 3.2 A. T cells form the bulk of the leukocyte population in the CLN, MLN and ILN during homeostatic conditions, comprising roughly 60% of the total leukocytes present (Figure 3.2C). A significant expansion in the number of T cells in the CLN was evident from as early as d3 p.i. and, despite a transient reduction in cell number between d3-d5, by d6 p.i., T cell numbers had increased significantly by 3-fold, compared to d0 p.i. Interestingly, however, the total number of T cells in both the MLN and the ILN decreased during the course of infection. A significant reduction of T cells was present as early as d3 p.i. in the ILN and by d7p.i. numbers had reduced to 30% of those present at d0 p.i. (Figure 3.2B).

Both $CD4^+$ and $CD8^+$ T cell subsets contributed to the significant increase in total T cell number in the CLN. Similarly, the reduced T cell numbers in the ILN and MLN could be attributed to similar reductions in $CD4^+$ and $CD8^+$ subset number (Figure 3.2D and F). The dynamic shift in populations of the draining and non-draining lymph nodes during WNV infection was also evident in the percentages of T cells (Figure 3.2C), including $CD4^+$ (Figure 3.2E) and $CD8^+$ subsets (Figure 3.2G), which decreased from d3 p.i. onwards in all three nodes. At d0 p.i., $CD4^+$ and $CD8^+$ T cells constituted 30-40% and 20-30% of the total leukocyte population, respectively, in all of the lymph nodes examined. By d7 p.i. the percentage of T cells in the CLN had reduced to approximately one third of the starting values, while the proportion of ILN and MLN T cells decreased by ~20%. The overall increase in T cell numbers of the CLN, as compared to the gradual decline in their percentages suggests that another leukocyte population was expanding at a greater rate than the T cells.

Figure 3.2. T cell populations in the draining (CLN) and non-draining lymph nodes (MLN, ILN) of the CNS following lethal WNV infection

Panel A demonstrates the representative flow cytometric gating of T cells in the lymph node. The sequential starting gates are listed above each panel. The number (B) and (C) percentage of total T cells ($CD45^+CD3^+NK1.1^-$) in the CLN (red), ILN (blue) and MLN (green) of mice following lethal WNV infection ($6x10^4$ PFU) on d0, 3, 5, 6 and 7 p.i. are shown. T cells were further categorised according to CD4 and CD8 expression. Panels D and E show the numbers and percentages of $CD4^+$ T cells ($CD3^+CD4^+CD8^-$) with graphs F and G representing the numbers and percentages of $CD8^+$ T ($CD3^+CD8^+CD4^-$) cells in the CLN, MLN and ILN of WNV-infected mice on d0, 3, 5, 6 and 7 p.i. Values for $CD3^+$, $CD4^+$ and $CD8^+$ T cells in panels C, E and G are expressed as a percentage of total leukocytes in the CLN, MLN and ILN. Data are shown as the mean ±SEM of values from 3 independent experiments, with 3-4 mice/group in each experiment. Statistical analysis was conducted using one-way ANOVA with a Dunnet's multiple comparison post-test (d0 as control), and $P \leq 0.05$*; $P \leq 0.01$**; $P \leq 0.001$***.

Figure 3.2

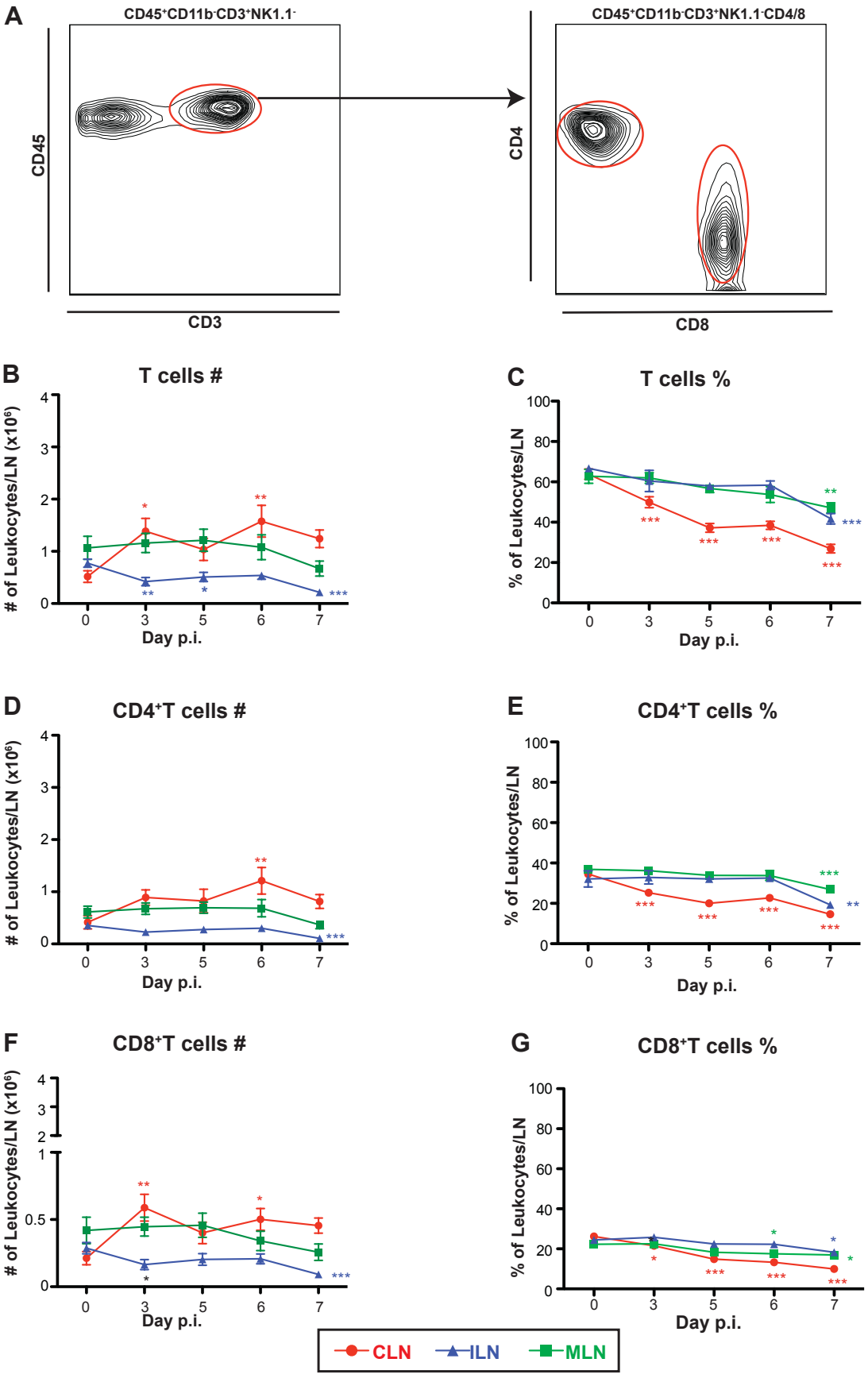
A
CD45+CD11b-CD3+NK1.1-
CD45
CD3
CD45+CD11b-CD3+NK1.1-CD4/8
CD4
CD8
B
T cells #
# of Leukocytes/LN (x10⁶)
Day p.i.
C
T cells %
% of Leukocytes/LN
Day p.i.
D
CD4+T cells #
# of Leukocytes/LN (x10⁶)
Day p.i.
E
CD4+T cells %
% of Leukocytes/LN
Day p.i.
F
CD8+T cells #
# of Leukocytes/LN (x10⁶)
Day p.i.
G
CD8+T cells %
% of Leukocytes/LN
Day p.i.
CLN
ILN
MLN

3.2.1.2. B, NK and NKT cells

B cells are critical components in the development of humoral immunity and as such form the second largest population of leukocytes in lymph nodes during homeostatic conditions. Figure 3.3 A illustrates the gating strategy for B cell identification. In this model, B cells comprised up to 20% of the total leukocyte population at d0 p.i. in all three nodes (Figure 3.3D). In a similar manner to T cells, there was a rise in B cell numbers of the CLN during the course of infection, reaching a ~15-fold increase by d7, relative to d0 p.i. (Figure 3.2C). Thus, compared to the increase in numbers of T cells, B cell expansion was markedly greater and the significant increase in B cell number is mirrored in the 40% elevation of B cell percentage in the CLN (Figure 3.3D). Parallel enumeration of MLN and ILN B cells (Figure 3.3C) demonstrated a negligible change throughout the course of infection however, the percentage contribution of ILN and MLN B cells to the total leukocyte population increased by 15-20% during this time and was significantly different from d0p.i (Figure 3.3D).

The gating strategy used to identify the innate lymphoid NK cell and heterogeneous NKT cell populations is illustrated in Figure 3.3 B. Both populations contribute to less than 0.5% of the total leukocyte population in the lymph node in each case (Figure 3.3F and H). Regardless, these cells have important effector functions during viral infection. NK (Figure 3.3E) and NKT cell (Figure 3.3G) numbers in the CLN showed similar kinetics to B and T cells, with an overall increase, relative to d0, but ILN and MLN numbers remained more or less constant during infection. The percentage of NK cells in the CLN and MLN exhibited a marginal increase, with a significant rise in the ILN by d7 p.i. (Figure 3.3F). Off all three nodes, only the MLN showed a significant rise in the percentage of NKT cells from d5-7 p.i. (Figure 3.3H). In summary, both B and T cell populations in the CLN had increased significantly, with the expansion of B cells much greater, therefore accounting for the decrease in T cell percentage. In contrast to the CLN, an absolute reduction in T cell

Figure 3.3. B, NK and NKT cell populations in the draining (CLN) and non-draining lymph nodes (MLN, ILN) of the CNS following lethal WNV infection

Panels A and B demonstrate the representative flow cytometric gating of B cells (A) and $NK1.1^+$ cells (B) in the lymph node. The sequential starting gates are listed above each panel. The number (C) and percentage (D) of total B cells ($CD45^+B220^+CD19^+CD11c^+$) in the CLN (red), ILN (blue) and MLN (green) of mice following lethal WNV infection ($6x10^4$ PFU) on d0, 3, 5, 6 and 7 p.i. are shown. Please note the change in y-axis from graphs C ($x10^6$) and D (100%), to figures E ($x10^4$) and F (0.1%). Graphs E and F show the numbers and percentages of NK cells ($CD45^+NK1.1^+CD3^-$) with graphs G and H representing the numbers and percentages of NKT ($CD45^+NK1.1^+CD3^+$) cells in the CLN, MLN and ILN of WNV-infected mice on d0, 3, 5, 6 and 7 p.i. Values of B, NK and NKT cells in panels D, F and H, are expressed as a percentage of total leukocytes in the CLN, MLN and ILN. Data are shown as the mean ±SEM of values from 3 independent experiments, with 3-4 mice/group in each experiment. Statistical analysis was conducted using one-way ANOVA with a Dunnet's multiple comparison post-test (d0 as control), and $P \leq 0.05$*; $P \leq 0.01$**; $P \leq 0.001$***.

Figure 3.3

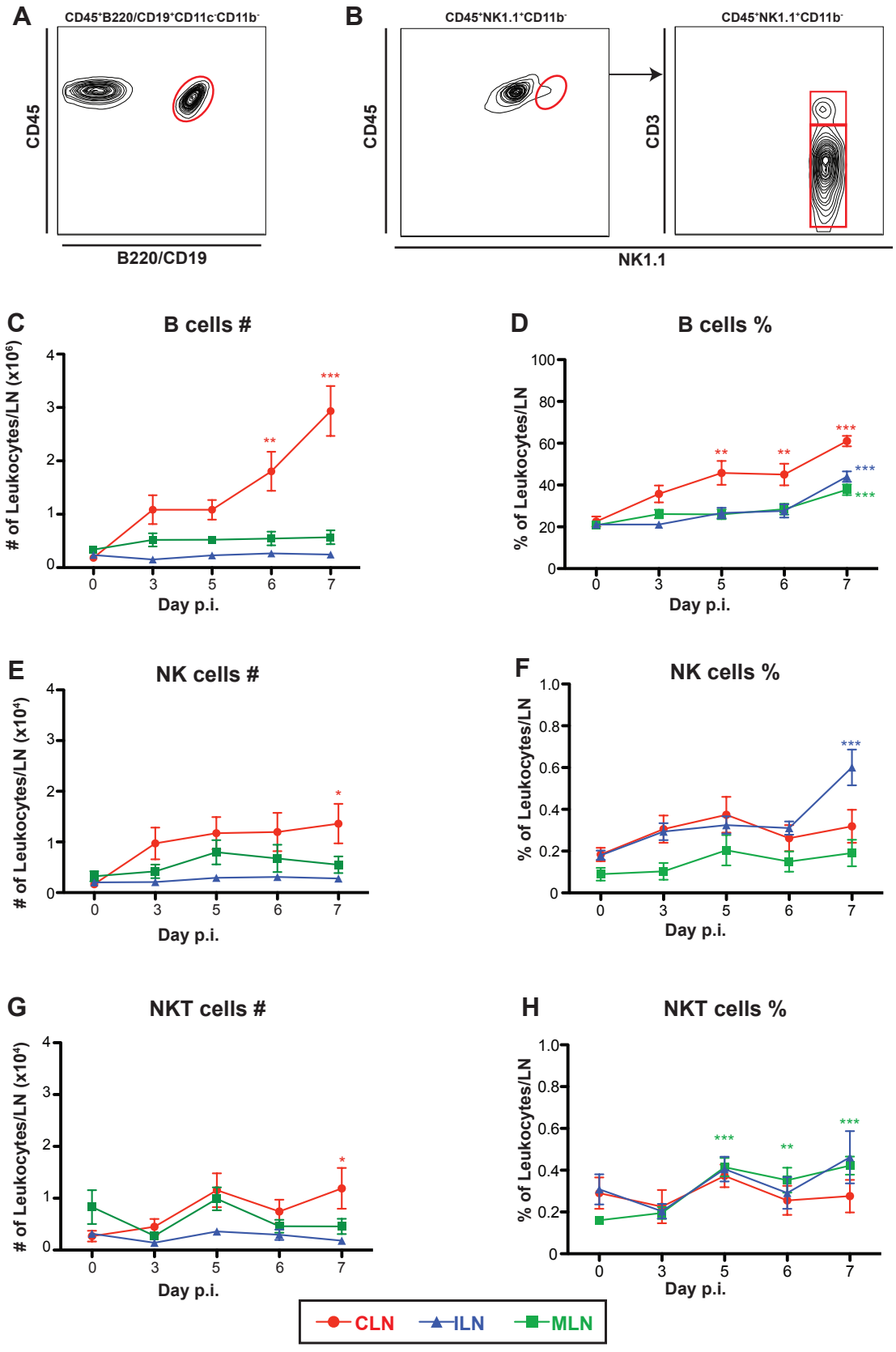
A
CD45+B220/CD19+CD11c-CD11b-
CD45
B220/CD19
B
CD45+NK1.1+CD11b-
CD45+NK1.1+CD11b-
CD45
CD3
NK1.1
C
B cells #
# of Leukocytes/LN (x10⁶)
Day p.i.
D
B cells %
% of Leukocytes/LN
Day p.i.
E
NK cells #
# of Leukocytes/LN (x10⁴)
Day p.i.
F
NK cells %
% of Leukocytes/LN
Day p.i.
G
NKT cells #
# of Leukocytes/LN (x10⁴)
Day p.i.
H
NKT cells %
% of Leukocytes/LN
Day p.i.
CLN
ILN
MLN

numbers in the ILN and MLN, rather than an increase in B cell numbers, likely accounts for the increase in B cell percentages in the non-draining nodes, since there was little, if any increase in B cell number in these nodes.

3.2.1.3. Monocytes and neutrophils

Figures A and B show the respective flow cytometry gating of neutrophils and monocytes. Similar to NK1.1$^+$ subsets, monocyte and neutrophil numbers were very low in lymph nodes during steady state (Figure 3.4C and E). Combined, these CD11b$^+$ subsets constituted less than one percent of the total leukocyte population (Figure 3.4D and F). Statistically, numbers of both remained largely unchanged in all three nodes over the course of infection (Figure 3.4C and E), notwithstanding increases seen on d7p.i. in the CLN. Neutrophils showed an increase in percentage in both MLN and ILN, with a non-significant reduction in the CLN (Figure 3.4D). Considering their low percentages in the lymph node, this change in is likely a side effect of more substantial changes in other leukocyte subsets. Statistically significant changes in the percentage of monocytes was only evident in the CLN at d3, 5 and 7 p.i. (Figure 3.4F).

3.2.1.4. Dendritic cell populations

The irreplaceable role of DC in the lymph node is remarkable, considering the low frequency of this subset in the lymph nodes, compared to B and T cells. DC are crucial for antigen presentation and activation of B and T cells, and the generation of effective immune responses are significantly impaired in the absence of DC. The DC in the lymph node were grouped according to their differential expression of CD11c, CD11b, B220 and CD8α. Based on CD11b and CD11c expression, there were 3 distinct populations of DC identified, namely CD11c$^+$CD11b$^+$, CD11c^{hi}CD11b^{int} and CD11c$^+$CD11b$^-$ (Figure 3.5A). The

Figure 3.4. Monocyte and neutrophil populations in the draining (CLN) and non-draining lymph nodes (MLN, ILN) of the CNS following lethal WNV infection

Panels A and B demonstrate the representative flow cytometric gating of neutrophils (A) and monocytes (B) in the lymph node. The sequential starting gates are listed above each panel. Graphs C and D show the numbers and percentages of neutrophils ($CD45^{+}CD11b^{hi}Ly6G^{+}SSC^{hi}$) in the CLN (red), ILN (blue) and MLN (green) of WNV-infected mice on d0, 3, 5, 6 and 7 p.i. The numbers (E) and (F) percentages of monocytes ($CD45^{+}CD11b^{+}$ $Ly6G^{-}CD11c^{-}$) in the CLN (red), ILN (blue) and MLN (green) under the same conditions described above. Values of monocytes and neutrophils in graphs D and F are expressed as a percentage of total leukocytes in the CLN, MLN and ILN. Data are shown as the mean ±SEM of values from 3 independent experiments, with 3-4 mice/group in each experiment. Statistical analysis was conducted using one-way ANOVA with a Dunnet's multiple comparison post-test (d0 as control), and $P \leq 0.05$*; $P \leq 0.01$**; $P \leq 0.001$***.

Figure 3.4

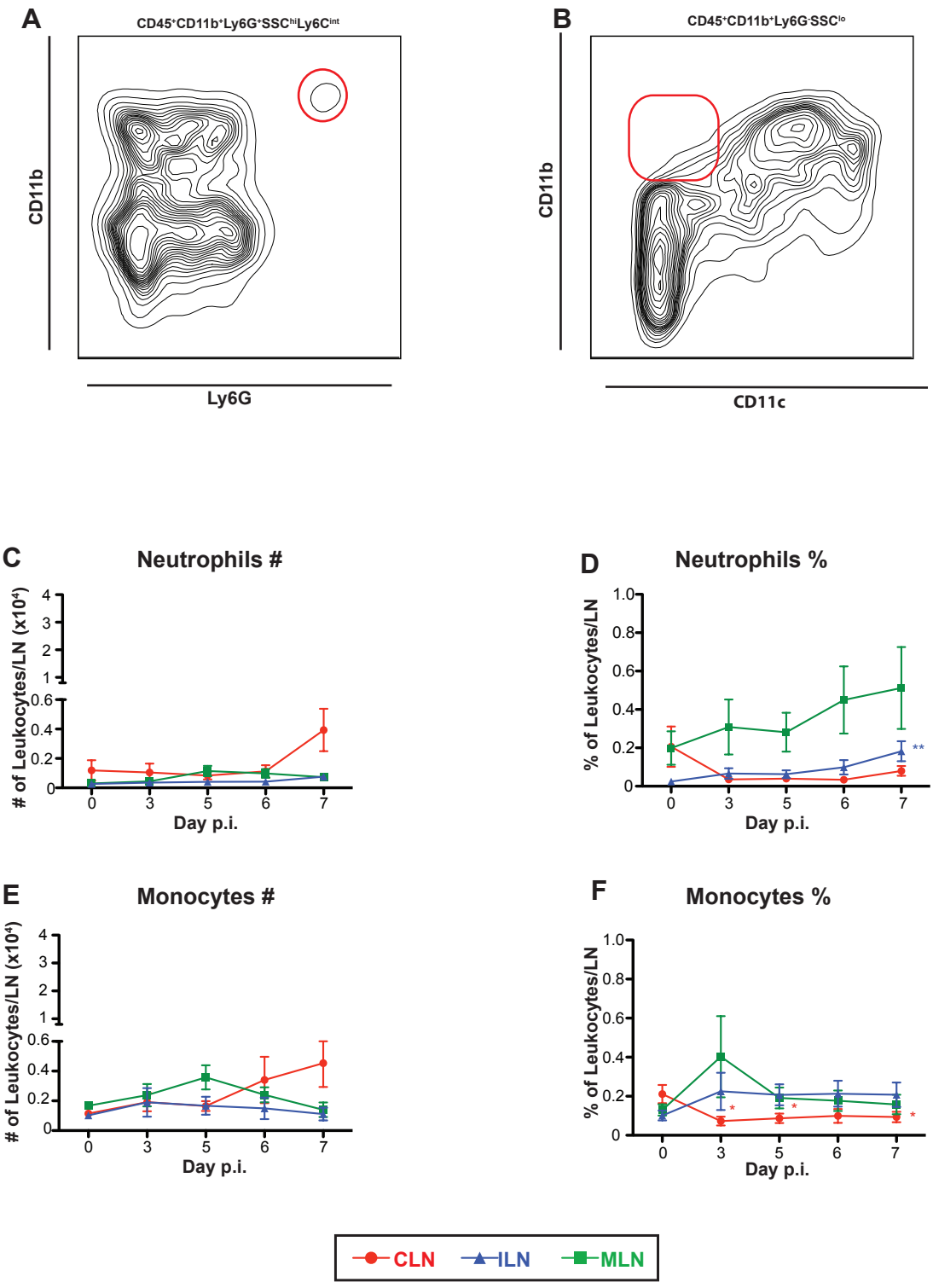
A
CD45+CD11b+Ly6G+SSChiLy6Cint
CD11b
Ly6G
B
CD45+CD11b+Ly6G-SSClo
CD11b
CD11c
C
Neutrophils #
# of Leukocytes/LN (x10⁴)
Day p.i.
D
Neutrophils %
% of Leukocytes/LN
Day p.i.
E
Monocytes #
# of Leukocytes/LN (x10⁴)
Day p.i.
F
Monocytes %
% of Leukocytes/LN
Day p.i.
CLN
ILN
MLN

Figure 3.5. Dendritic cell populations in the draining (CLN) and non-draining lymph nodes (MLN, ILN) of the CNS following lethal WNV infection

Panel A demonstrates the representative flow cytometric gating of dendritic cells in the above lymph nodes. The sequential starting gates are listed above each panel. Dendritic cell populations ($CD11c^{+}$) were defined based on differential CD11c and CD11b expression. The numbers and percentages of $CD11c^{+}CD11b^{+}$ DC (B&C), $CD11c^{hi}CD11b^{int}$ DC (D&E) and $CD11c^{+}CD11b^{-}$ DC (F&G) in the CLN (red), ILN (blue) and MLN (green) of mice following lethal WNV infection ($6x10^{4}$PFU) on d0, 3, 5, 6 and 7 p.i. was shown. Values of DC populations in graphs C, E and G are expressed as a percentage of total leukocytes in the CLN, MLN and ILN. Data are shown as the mean ±SEM of values from 3 independent experiments, with 3-4 mice/group in each experiment. Statistical analysis was conducted using one-way ANOVA with a Dunnet's multiple comparison post-test (d0 as control), and $P \leq 0.05$*; $P \leq 0.01$**; $P \leq 0.001$***.

Figure 3.5

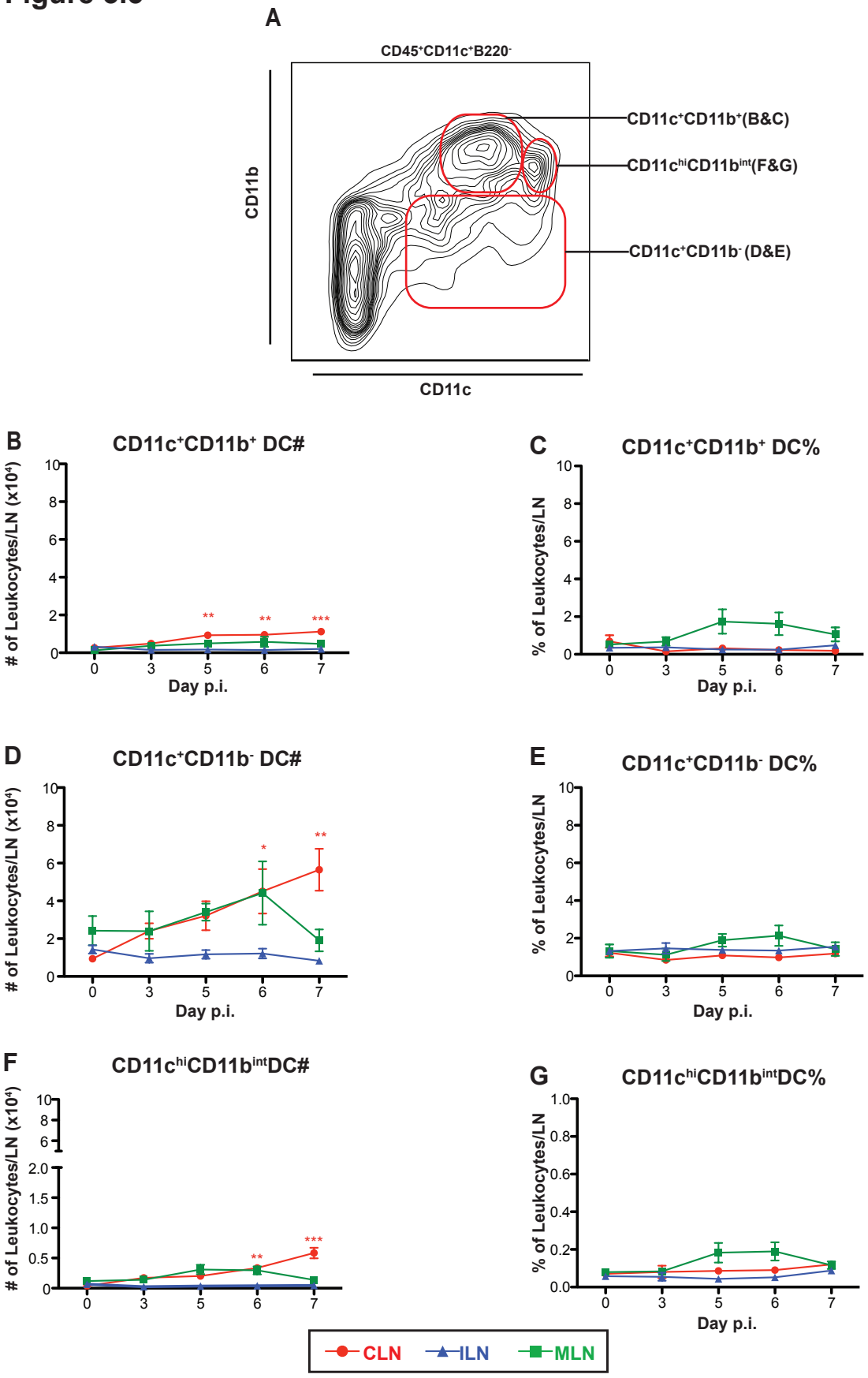
A
CD45+CD11c+B220-
CD11b
CD11c
CD11c+CD11b+(B&C)
CD11chiCD11bint(F&G)
CD11c+CD11b- (D&E)
B
CD11c+CD11b+ DC#
# of Leukocytes/LN (x10⁴)
Day p.i.
C
CD11c+CD11b+ DC%
% of Leukocytes/LN
Day p.i.
D
CD11c+CD11b- DC#
# of Leukocytes/LN (x10⁴)
Day p.i.
E
CD11c+CD11b- DC%
% of Leukocytes/LN
Day p.i.
F
CD11chiCD11bintDC#
# of Leukocytes/LN (x10⁴)
G
CD11chiCD11bintDC%
% of Leukocytes/LN
Day p.i.
CLN
ILN
MLN

number of $CD11c^{+}CD11b^{+}$ cells in the CLN increased significantly from d5 p.i., after which it plateaued, remaining high throughout the course of infection (Figure 3.5B), while numbers in the MLN and ILN remained at baseline levels throughout (Figure 3.5B). On the other hand, numbers of both the $CD11c^{hi}CD11b^{int}$ (Figure 3.5D) and $CD11c^{+}CD11b^{-}$ (Figure 3.5F) populations in the CLN continued expanding until the end of the disease course. Indeed, the number of $CD11c^{hi}CD11b^{int}$ cells in the CLN (below 500 cells at d0) had increased significantly by ~14-fold at d7 p.i. There was a transient increase of this subset in the MLN between d3 and 6 p.i., which returned to baseline by d7 p.i. but corresponding numbers in the ILN remained unchanged (Figure 3.5D). The $CD11c^{+}CD11b^{-}$ subset was the most abundant DC population present in all three lymph nodes of mice in the steady state and this number underwent a 7-fold increase in the CLN by d7, relative to d0 p.i. Similar to the $CD11c^{hi}CD11b^{int}$ subset, numbers of the $CD11c^{+}CD11b^{-}$ population in the MLN displayed a slight increase from d3 p.i., which then returned to baseline by d7 p.i., with ILN numbers remaining constant throughout the course of infection (Figure 3.5F). These DC subsets represented a small proportion of the total leukocyte population (<2%) and, except for a short-lived non-significant increase in all three subsets of the MLN at 5-6p.i., percentages of all three lymph nodes remained unchanged throughout the course of infection (Figure 3.5C, E and G).

Numbers of pDC (Figure 3.6A) in the CLN expanded from d0-7 p.i., but this was not significant (Figure 3.6C) and the percentage remained more or less constant over this time (Figure 3.6D). Numbers of pDC in the ILN and MLN remained statistically unchanged, with a reduction in percentage present only at d3 and 7p.i. in the MLN.

In addition, a $CD8\alpha^{+}$ subset could be distinguished in the $CD11c^{+}CD11b^{-}$ DC (Figure 3.6B) and showed an increase in number of 13-fold in the CLN between d5-7 p.i., with ILN and MLN numbers remaining stable during this time (Figure 3.6E). This subset represented

Figure 3.6. Plasmacytoid and resident lymphoid DC populations in the draining (CLN) and non-draining lymph nodes (MLN, ILN) of the CNS following lethal WNV infection

Panels A and B demonstrate the representative flow cytometric gating of pDC (A) and $CD8\alpha^+$ DC (B). The sequential starting gates are listed above each panel. Dendritic cell populations ($CD11c^+$) were defined based on differential CD11c, CD8α, B220 and CD11b expression. The numbers and percentages of plasmacytoid DC ($CD11c^+B220^+$) (C&D) and lymphoid-resident DC ($CD11c^+CD8\alpha^+$)(E&F) in the CLN (red), ILN (blue) and MLN (green) of mice following lethal WNV infection ($6x10^4$PFU) on d0, 3, 5, 6 and 7 p.i. are shown. Values for pDC and $CD8\alpha^+$ DC populations are expressed as a percentage of total leukocytes in the CLN, MLN and ILN. Data are shown as the mean ±SEM of values from 3 independent experiments, with 3-4 mice/group in each experiment. Statistical analysis was conducted using one-way ANOVA with a Dunnet's multiple comparison post-test (d0 as control), and $P \leq 0.05$*; $P \leq 0.01$**; $P \leq 0.001$***.

Figure 3.6

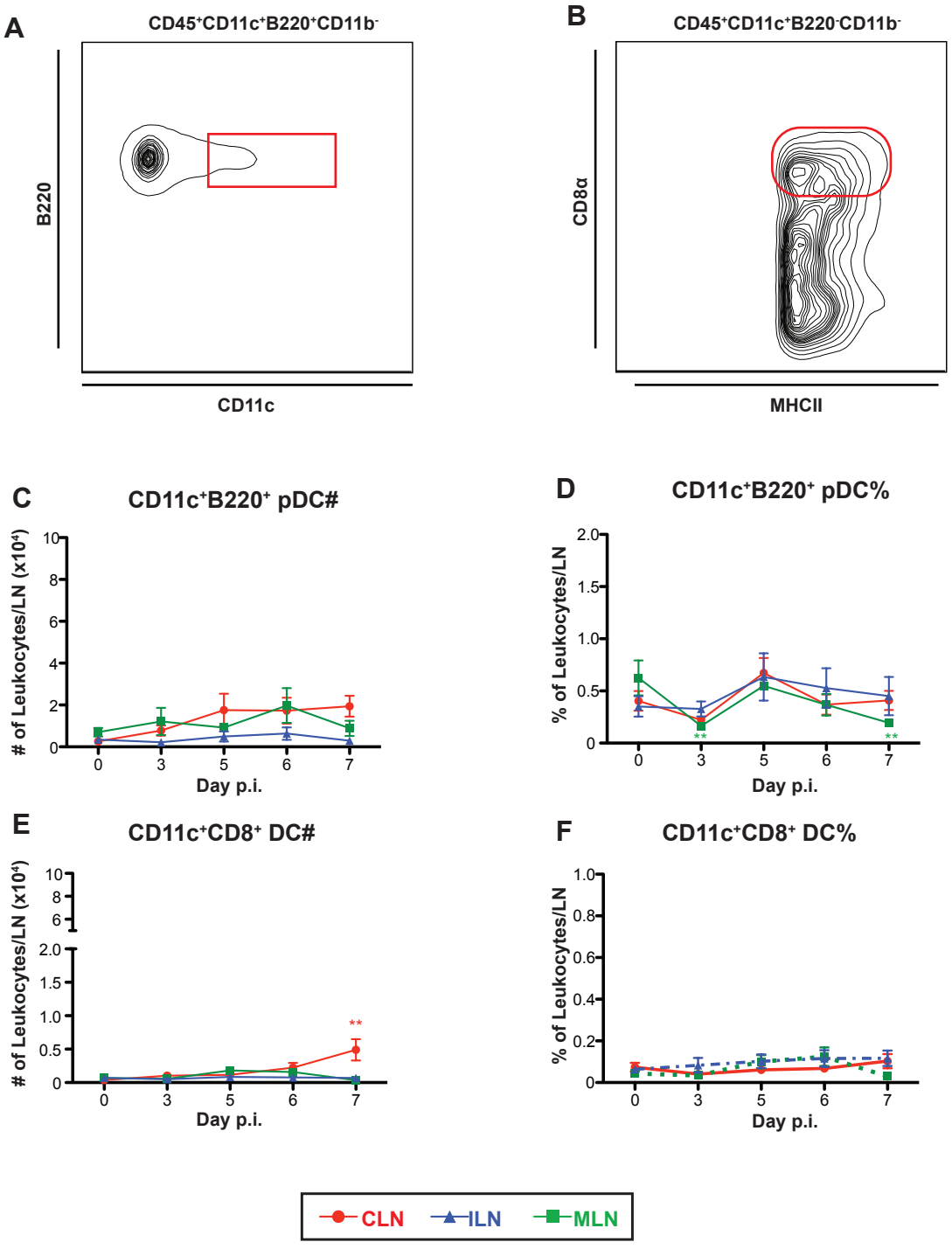
A
CD45+CD11c+B220+CD11b-
B220
CD11c
B
CD45+CD11c+B220-CD11b-
CD8α
MHCII
C
CD11c+B220+ pDC#
# of Leukocytes/LN (x10⁴)
Day p.i.
D
CD11c+B220+ pDC%
% of Leukocytes/LN
Day p.i.
E
CD11c+CD8+ DC#
# of Leukocytes/LN (x10⁴)
Day p.i.
F
CD11c+CD8+ DC%
% of Leukocytes/LN
Day p.i.
CLN
ILN
MLN

less than 0.2% of the total leukocyte population in all the nodes analysed and remained so throughout the course of infection, with no expansion in percentage (Figure 3.6F). Collectively, these data indicate that CNS inflammation does not only induce change in various leukocyte subsets in the draining CLN, but also the peripheral non-draining ILN and MLN.

3.2.2. Changes in cell surface marker expression associated with inflammation in the draining and non-draining lymph nodes during WNV encephalitis

The distinct changes associated with inflammation, occurring in both draining and non-draining lymph nodes, during the course of infection prompted us to further examine cell surface marker expression of leukocytes in these nodes. Of particular interest were the changes we identified in the levels of Ly6C expression in the draining and non-draining lymph nodes, as follows.

During the 7-day time-course of infection with an LD100 dose of WNV ($6x10^4$ PFU), there was a distinct shift in lymphocyte populations from the CLN, ILN and MLN towards an increased expression of Ly6C. Flow cytometry histograms illustrate the upregulation of the cell surface marker Ly6C in the B (Figure 3.7A) and T cell (Fig3.7-B and C) populations of all 3 nodes. Increases in Ly6C expression in B (Figure 3.7A), $CD4^+$ (Figure 3.7B) and $CD8^+$ T cells (Figure 3.7C) in the CLN could be observed from as early as d3p.i., with the $CD8^+$ T cells subset showing the highest Ly6C expression by d7p.i. Upregulation of Ly6C in the B and T cells of the ILN and MLN also occurred, however this was only evident from d5p.i. (i.e. 2 days after CLN). Similar to the Ly6C expression of the CLN, $CD8^+$ T cells isolated from the ILN and MLN also exhibited the highest Ly6C expression by d7p.i., compared to the B and $CD4^+$ T cells. Indeed, WNV infection induced a significant increase in the mean Ly6C expression of most of the leukocyte subsets at various time points in the

Figure 3.7. Ly6C expression of T and B cell populations in the draining (CLN) and non-draining lymph nodes (MLN, ILN) of the CNS following lethal WNV infection

Representative flow cytometric histograms (A-C) illustrate the change in Ly6C expression of (A) B cells ($B220^+/CD19^+$), (B) $CD4^+$ T cells and(C) $CD8^+$ T cells in the CLN, ILN and MLN on d0, 3, 5, 6 and 7p.i. following lethal WNV infection ($6x10^4$ PFU). WNV-infected samples are shown in red, while isotype controls are shown in grey.

Figure 3.7

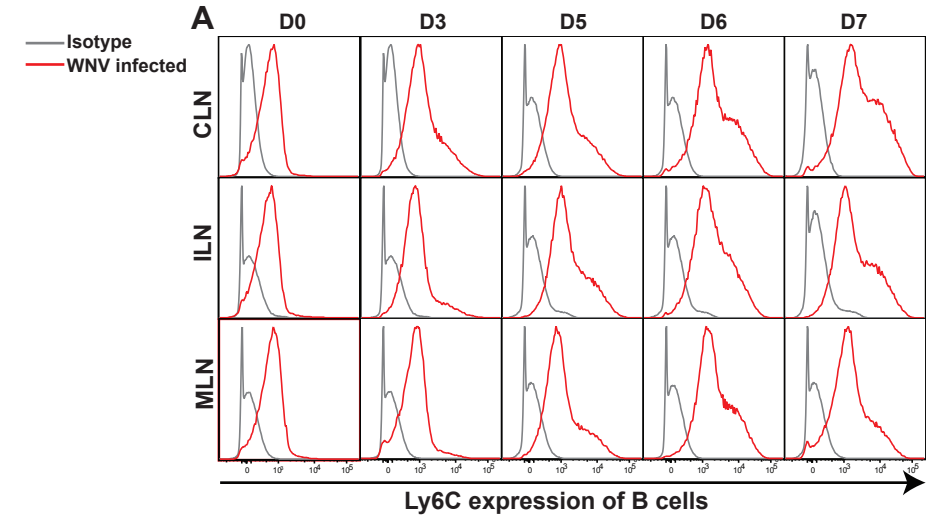
A
D0
D3
D5
D6
D7
Isotype
WNV infected
CLN
ILN
MLN
Ly6C expression of B cells

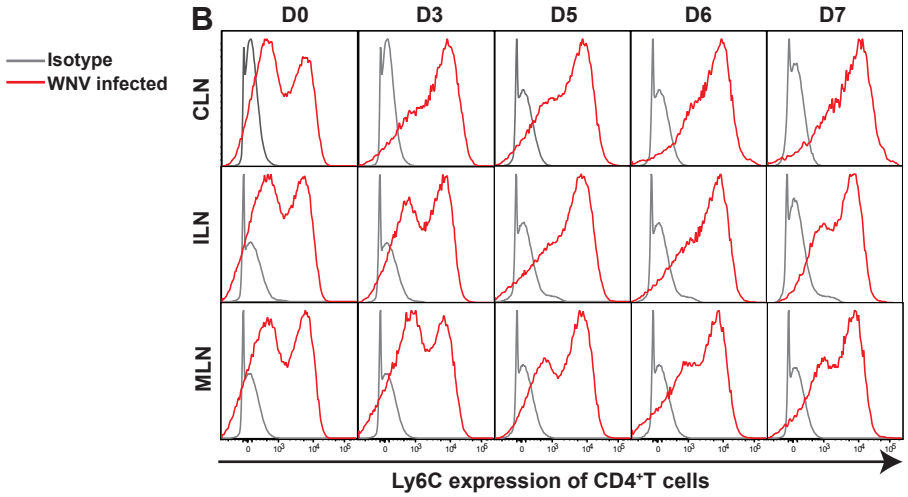
B
D0
D3
D5
D6
D7
Isotype
WNV infected
CLN
ILN
MLN
Ly6C expression of CD4+T cells

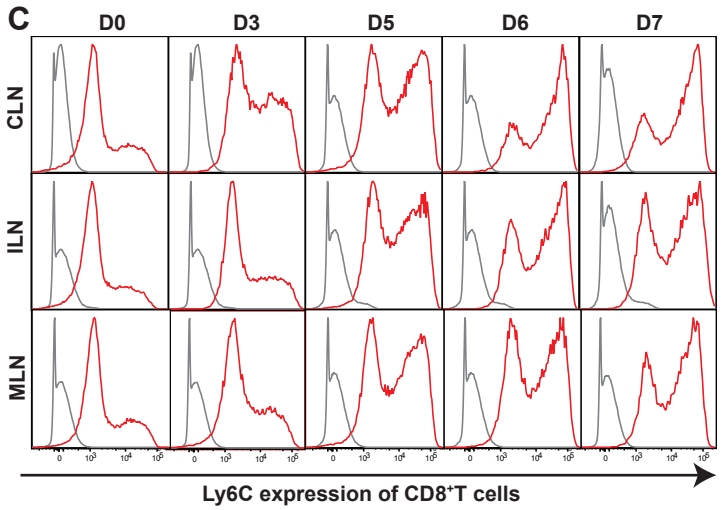
C
D0
D3
D5
D6
D7
CLN
ILN
MLN
Ly6C expression of CD8+T cells

CLN, ILN and MLN, relative to baseline (Figures 3 & 4). However, of interest here was the observation that in most cases an increase in Ly6C expression was first seen in a subset of cells, already expressing Ly6C at intermediate levels, which increased with time, both in level of expression (brightness) and number of cells contributing to this $Ly6C^{hi}$ subset. This initial data, demonstrating a shift towards higher expression of Ly6C in all the major populations of the lymph node, in particular B and T cells, prompted our further investigation into the differential upregulation of Ly6C expression in the various leukocyte subsets of the draining and non-draining lymph nodes of the CNS.

Along the lines of work previously published by our laboratory (Terry et al. 2015), leukocytes were further characterised, based on Ly6C expression, as $Ly6C^{hi}$, $Ly6C^{int}$ or $Ly6C^{-}$, and each subset enumerated (Figure 3.8A, B, C) and the kinetics of Ly6C expression shown in representative flow cytometry profiles over the duration of infection (Figure 3.8D & E). At d0p.i., B cells in the CLN were mainly $Ly6C^{-}$, (Figure 3.8D) and this was also true for the ILN and MLN on d0p.i. (data not shown). However, by d7p.i. 41%, 35% and 22% of B cells in the CLN, ILN and MLN, respectively, had become $Ly6C^{int}$, with very few $Ly6C^{hi}$ B cells present in these nodes. Enumeration of these events demonstrated a significant increase in absolute $Ly6C^{hi}$, $Ly6C^{int}$ and $Ly6C^{-}$ B cell numbers (Figure 3.8A) in the CLN by d7 p.i., however the $Ly6C^{int}$ and $Ly6C^{-}$ cell numbers exceeded those of $Ly6C^{hi}$ subset, despite a significant increase in the $Ly6C^{hi}$ subset on d7p.i. In the ILN the $Ly6C^{-}$ B cells had decreased significantly by d6p.i., although both $Ly6C^{-}$ and $Ly6C^{int}$ remained at more or less the same levels throughout, whereas the $Ly6C^{hi}$ B cell numbers had increased significantly by d7p.i. In contrast, in the MLN, while the $Ly6C^{int}$ had increased significantly by d7p.i., there was a no significant variation of other populations over the course of disease. This suggests that, similar to the CNS-draining CLN, the non-draining ILN and MLN have increased numbers of B cells expressing Ly6C at intermediate or high levels.

Figure 3.8 Differential Ly6C subsets in the B and T cell populations of the draining (CLN) and non-draining lymph nodes (MLN, ILN) of the CNS following lethal WNV infection

Leukocytes subsets in the CLN, ILN and MLN were further characterised based on Ly6C expression and subsequently classified as $Ly6C^{hi}$ (square), $Ly6C^{int}$ (triangle) or $Ly6C^{-}$ (circle). Significance, compared to d0, for each subset was defined as follows: ***$Ly6C^{hi}$ $^{+++}Ly6C^{int}$ and $^{ØØØ}Ly6C^{-}$. The number of $Ly6C^{hi/int/-}$ B cells (A) ($B220^{+}/CD19^{+}$), $CD4^{+}$ (B) and $CD8^{+}$ T (C) cells in the CLN, ILN and MLN on d0, 3, 5, 6 and 7p.i. following lethal WNV infection ($6x10^{4}$ PFU) are shown. Note the change in y-axis for B cells ($x10^{6}$) and T cells ($x10^{5}$). Flow cytometry contour plots D-E demonstrate the distributions of Ly6C expression in the CLN, ILN and MLN of WNV-infected mice ($6x10^{4}$ PFU) on d7p.i., compared to d0. Since d0 p.i. for CLN, ILN and MLN were similar, only d0 p.i. for CLN is shown. Figure D shows the change in Ly6C expression of B cells, with figure E demonstrating the change in T cells, including total T cells ($CD3^{+}$), $CD4^{+}$ and $CD8^{+}$ T cells. Note the data in panels A-C are averaged from 3 experiments, while those in D and E are representative of single animals at single time points. Thus there will inevitably be some disparity between these sets of data.

Data are shown as the mean ±SEM of values from 3 independent experiments, with 2-4 mice/group in each experiment. Statistical analysis was conducted using one-way ANOVA with a Dunnet's multiple comparison post-test (d0 as control), and $Ly6C^{hi}$ =P≤0.05*; P≤0.01**; P≤0.001***. $Ly6C^{int}$ =P≤0.05^{+}; P≤0.01^{++}; P≤0.001^{+++}. $Ly6C^{-}$ =P≤0.05^{Ø}; P≤0.01^{ØØ}; P≤0.001^{ØØØ}.

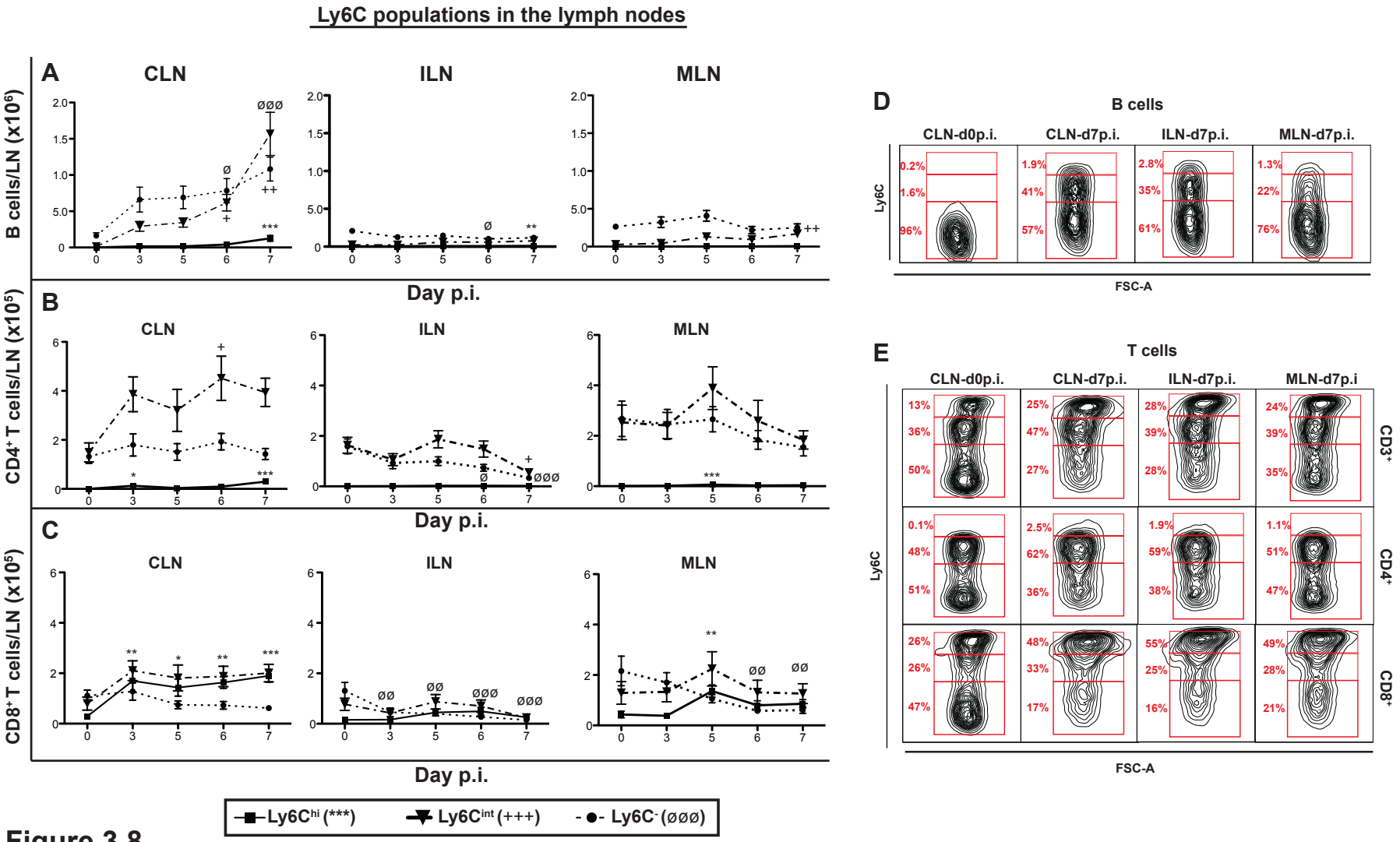
Ly6C populations in the lymph nodes
A
CLN
ILN
MLN
B cells/LN (x10⁶)
Day p.i.
B
CD4⁺ T cells/LN (x10⁵)
C
CD8⁺ T cells/LN (x10⁵)
Ly6C^hi (***)
Ly6C^int (+++)
Ly6C⁻ (øøø)
D
B cells
CLN-d0p.i.
CLN-d7p.i.
ILN-d7p.i.
MLN-d7p.i.
Ly6C
FSC-A
E
T cells
CLN-d0p.i.
CLN-d7p.i.
ILN-d7p.i.
MLN-d7p.i
CD3⁺
CD4⁺
CD8⁺

Figure 3.8

The increase in Ly6C^{hi} and Ly6C^{int} B cell numbers in the ILN and MLN, respectively, were mirrored by a similar relative decrease in Ly6C^{-} cells, with the total B cell number in these nodes remaining stable throughout the disease course. In the CLN, despite a small increase in Ly6C^{hi} cells on d7p.i., it was clearly the progressive increase in Ly6C^{int} and Ly6C^{-} cells that were responsible for the increase in total B cell number over the course of infection.

Even at d0p.i., the overall level of Ly6C expression in T cells was higher than that of B cells in the lymph nodes (Figure 3.8E). This was contributed in the case of CD4^{+} T cells, by a subpopulation that was Ly6C^{int} at this time-point, and in the case of CD8^{+} T cells by substantial Ly6C^{int} and Ly6C^{hi} populations. As a result of CNS infection, there were higher numbers of T cells expressing increased Ly6C in both CD4^{+} and CD8^{+} T cells populations. However, like the B cells, CD4^{+} T cells showed an increase primarily in the numbers of Ly6C^{int} cells, while CD8^{+} T cells showed an increase in cell numbers in both the Ly6C^{int} and Ly6C^{hi} compartments over the course of infection. Numbers of Ly6C^{int} and Ly6C^{hi} CD4^{+} T cells increased significantly (Figure 3.8B) by d6 and d7p.i., respectively, in the CLN, with no appreciable change in Ly6C^{-} CD4^{+} T cell number over the disease course. In the ILN and MLN, there was a general trend towards reduced Ly6C^{int} and Ly6C^{-} CD4^{+} T cells numbers by d7p.i., compared to mock-infected controls (Figure 3.8E). This suggests that, with the total number of T cells in the non-draining ILN and MLN decreasing, there was little change in Ly6C expression in the cells remaining in these nodes.

Notably, the Ly6C^{hi} CD8^{+} T cell subset had increased by d7p.i. (Figure 3.8E), this occurred in parallel to the increase in Ly6C^{hi}CD8^{+} T cell numbers from d3p.i. onward, plateauing until d7 p.i. (Figure 3.8C). In contrast, the ILN and MLN demonstrated a substantial reduction in total CD8^{+} T cell numbers in response to infection (Figure 3.2F), which was

mirrored in the significant reduction of Ly6C$^-$ CD8$^+$ T cells in these nodes (Figure 3.8C), relative to d0p.i.

NK and NKT cells in all three nodes showed distinct Ly6C^{hi}, Ly6C^{int} and Ly6C$^-$ subsets, enumerated in Figure 3.9 A and B and shown as representative contour plots in panels E and F. Both NK and NKT cells, in all three nodes, showed a reduction in the percentage of Ly6C$^-$ cells and increase in the percentage of Ly6C^{hi} cells by d7p.i., compared to d0p.i. Changes in numbers of Ly6C^{hi}, Ly6C^{int} and Ly6C$^-$ NK cells in the CLN were not statistically significant, but appeared to increase by d3p.i. and plateau thereafter (Figure 3.9A), while numbers of these cells in the ILN and MLN remained relatively stable over this time. Consistent with the contour plots (Figure 3.9F), numbers of Ly6C^{hi} NKT cells in the CLN, ILN and MLN (Figure 3.9B) all appeared to increase, compared to d0p.i., whereas there was a significant reduction in Ly6C$^-$ NKT cell number in the ILN from d3p.i.

Based on our gating strategy, neutrophils were mainly Ly6C^{hi} and Ly6C^{int}, with almost none of the neutrophils being Ly6C$^-$ (Figure 3.9G). Nevertheless, despite possessing relatively high baseline Ly6C expression, the neutrophils in all three nodes further upregulated Ly6C expression in response to infection. Enumeration of these neutrophils showed that Ly6C^{int} neutrophils increased significantly by d7p.i., relative to d0p.i. in the CLN (Figure 3.9C). Both Ly6C^{int} and Ly6C^{hi} neutrophils in the ILN increased substantially by d7 p.i., relative to d0, whereas only Ly6C^{int} neutrophils in the MLN increased at d5p.i.

At d0p.i., the majority of monocytes were Ly6C$^-$, however, by d7p.i. the monocytes from the draining and non-draining nodes had upregulated their expression of Ly6C to form three distinct populations (Figure 3.9H). The number of Ly6C^{hi} monocytes in the CLN increased significantly by d7, compared to d0p.i. (Figure 3.9D), whereas the Ly6C^{hi}, Ly6C^{int}

Figure 3.9 Differential Ly6C subsets in the NK1.1^{+} and CD11b^{+} cell populations of the draining (CLN) and non-draining lymph nodes (MLN, ILN) of the CNS following lethal WNV infection

Leukocytes subsets in the CLN, ILN and MLN were further characterised based on Ly6C expression and subsequently classified as Ly6C^{hi} (square), Ly6C^{int} (triangle) or Ly6C^{-} (circle). Significance, compared to d0, for each subset was defined as follows: ***Ly6C^{hi}; $^{+++}$Ly6C^{int} and ^{ØØØ}Ly6C^{-}. The number of Ly6C$^{hi/int/-}$ NK cells (A) (NK1.1^{+}CD3^{-}), NKT cells (B) (NK1.1^{+}CD3^{+}), Neutrophils (C) (CD11b^{hi}Ly6G^{+}), and monocytes (D) (CD11b^{+}CD11c^{-}), in the CLN, ILN and MLN on d0, 3, 5, 6 and 7 p.i. following lethal WNV infection (6x10^{4}PFU) are shown. Flow cytometry contour plots E-H demonstrate the distributions of Ly6C expression in the CLN, ILN and MLN of WNV-infected mice (6x10^{4} PFU) on d7p.i., compared to d0. Since d0 p.i. for CLN, ILN and MLN were similar, only d0p.i. for CLN is shown. Figure E shows the change in Ly6C expression of NK cells, with figure F demonstrating the change in NKT cells. Figures G and H are the representative flow cytometry plots of neutrophils and monocytes, respectively. Note the data in panels A-D are averaged from 3 experiments, while those in E, F, G and H are representative of single animals at single time points. Thus there will inevitably be some disparity between these sets of data.

Data are shown as the mean ±SEM of values from 3 independent experiments, with 2-4 mice/group in each experiment. Statistical analysis was conducted using one-way ANOVA with a Dunnet's multiple comparison post-test (d0 as control), and Ly6C^{hi} =P≤0.05*; P≤0.01**; P≤0.001***. Ly6C^{int} =P≤0.05^{+}; P≤0.01^{++}; P≤0.001^{+++}. Ly6C^{-} =P≤0.05^{Ø}; P≤0.01^{ØØ}; P≤0.001^{ØØØ}.

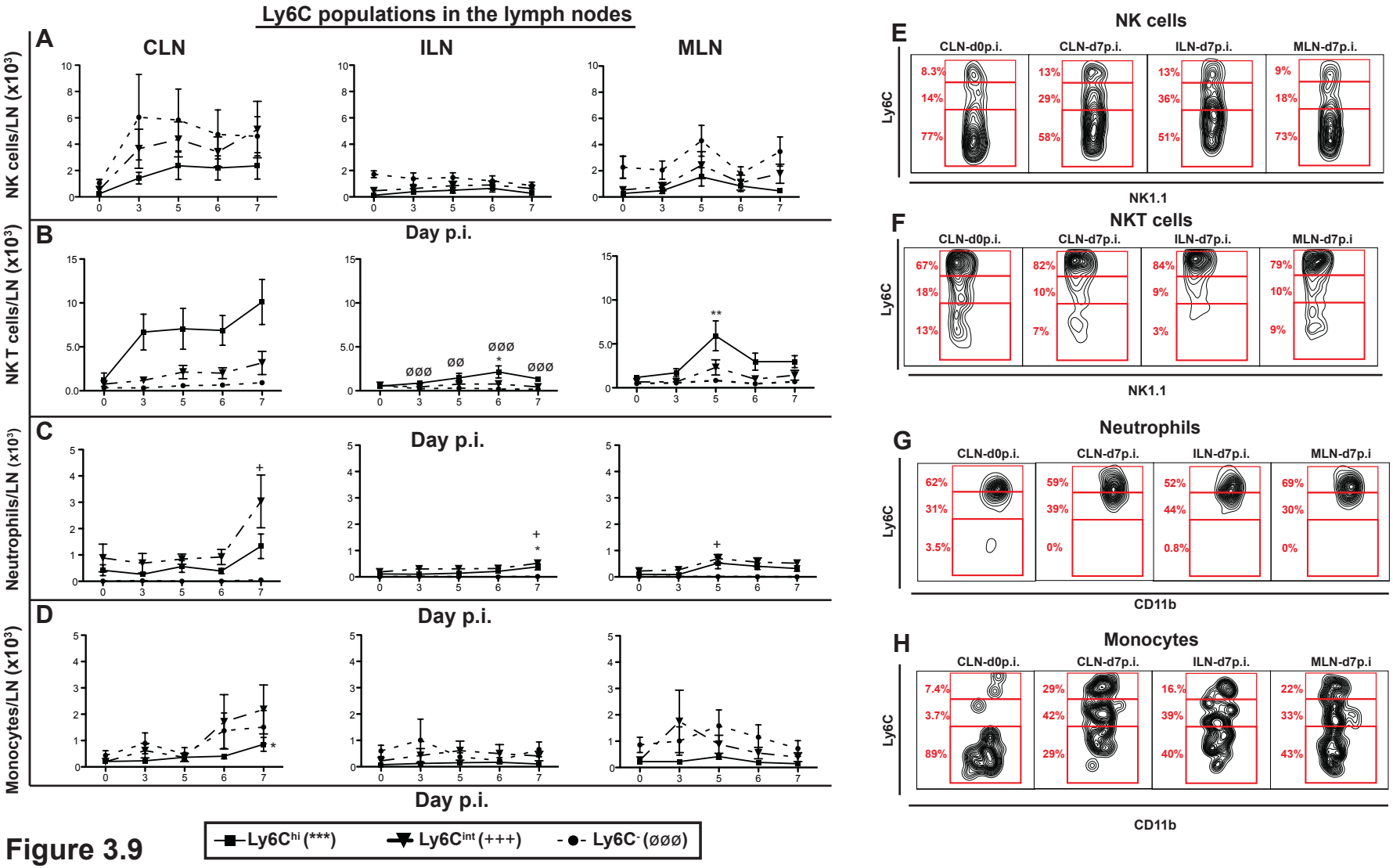
Ly6C populations in the lymph nodes
A
CLN
ILN
MLN
NK cells/LN (x10³)
B
Day p.i.
NK T cells/LN (x10³)
C
Day p.i.
Neutrophils/LN (x10³)
D
Day p.i.
Monocytes/LN (x10³)
Day p.i.
Ly6C^hi (***)
Ly6C^int (+++)
Ly6C^- (øøø)
E
NK cells
CLN-d0p.i.
CLN-d7p.i.
ILN-d7p.i.
MLN-d7p.i.
8.3%
14%
77%
13%
29%
58%
13%
36%
51%
9%
18%
73%
Ly6C
NK1.1
F
NKT cells
CLN-d0p.i.
CLN-d7p.i.
ILN-d7p.i.
MLN-d7p.i
67%
18%
13%
82%
10%
7%
84%
9%
3%
79%
10%
9%
Ly6C
NK1.1
G
Neutrophils
CLN-d0p.i.
CLN-d7p.i.
ILN-d7p.i.
MLN-d7p.i
62%
31%
3.5%
59%
39%
0%
52%
44%
0.8%
69%
30%
0%
Ly6C
CD11b
H
Monocytes
CLN-d0p.i.
CLN-d7p.i.
ILN-d7p.i.
MLN-d7p.i
7.4%
3.7%
89%
29%
42%
29%
16.%
39%
40%
22%
33%
43%
Ly6C
CD11b

Figure 3.9

and Ly6C^{-} monocyte numbers in the ILN and MLN did not change significantly over the disease course.

The various DC subsets, namely CD11c^{+}CD11b^{+}, CD11c^{hi}CD11b^{int} and CD11c^{+}CD11b^{-} also displayed differential Ly6C expression (Figure 3.10D, E, F), numbers of which varied in response to infection (Figure 3.10A, B, C). Note that the distribution of Ly6C on d0p.i., in the ILN and MLN was similar to that of the CLN, thus only the CLN d0p.i. contour plot is shown. The numbers of Ly6C^{hi} and Ly6C^{int} CD11c^{+}CD11b^{+} DC in the CLN increased significantly from d3p.i. (Figure 3.10A). In the MLN, a transient, statistically significant increase in numbers of Ly6C^{hi}, Ly6C^{int} and Ly6C^{-} CD11c^{+}CD11b^{+} cells occurred at d5p.i. but decreased on d6-7 p.i. The number of Ly6C^{hi}, Ly6C^{int} and Ly6C^{-} CD11c^{hi}CD11b^{int} cells in the CLN all increased substantially by d7p.i. (Figure 3.10B), relative to d0, whereas these cells remained unchanged in the ILN, with a short-lived, but significant, increase in Ly6C^{hi} and Ly6C^{int} cells at d5p.i. in the MLN. The CD11c^{+}CD11b^{-} DC subset (Figure 3.10F) had a lower percentages of Ly6C^{hi} cells in the CLN, ILN and MLN at d7p.i., compared to d0p.i., with higher the percentages of Ly6C^{int}. However, the absolute numbers of Ly6C^{hi}, Ly6C^{int} and Ly6C^{-} cells increased by d7p.i. in the CLN, with no response in the ILN and a variable response in the MLN (Figure 3.10C).

The pDC subset (Figure 3.11A and C) and CD8α^{+}DC (Figure 3.11B and D) had a lower percentage of Ly6C^{hi} cells in the CLN, ILN and MLN at d7p.i., compared to d0p.i., with the percentage of Ly6C^{int} cells increasing. In the CLN this translated to significant increases in Ly6C^{hi}, Ly6C^{int} and Ly6C^{-} pDC, relative to d0p.i. (Figure 3.11A), whereas ILN numbers showed negligible changes and MLN Ly6C^{int} pDC had a short-lived increase at d5p.i. Moreover, while there were significant increases in the Ly6C^{hi} and Ly6C^{int} CD8α^{+}DC in the CLN at d7p.i. (Figure 3.11B), relative to d0, the Ly6C^{-} population remained unchanged. As

Figure 3.10 Differential Ly6C subsets in the DC populations of the draining (CLN) and non-draining lymph nodes (MLN, ILN) of the CNS following lethal WNV infection

Leukocytes subsets in the CLN, ILN and MLN were further characterised based on Ly6C expression and subsequently classified as $Ly6C^{hi}$ (square), $Ly6C^{int}$ (triangle) or $Ly6C^{-}$ (circle). Significance, compared to d0, for each subset was defined as follows: ***$Ly6C^{hi}$; $^{+++}Ly6C^{int}$ and $^{ØØØ}Ly6C^{-}$. The number of $Ly6C^{hi/int/-}$ $CD11c^{+}CD11b^{+}$ DC (A), $CD11c^{hi}CD11b^{int}$ DC (B) and $CD11c^{+}CD11b^{-}$ DC (C) in the CLN, ILN and MLN on d0, 3, 5, 6 and 7p.i. following lethal WNV infection ($6x10^{4}$PFU) are shown. Note the change in y-axis for $CD11c^{+}CD11b^{+}$ ($x10^{3}$), $CD11c^{hi}CD11b^{int}$ ($x10^{3}$) and $CD11c^{+}CD11b^{-}$ ($x10^{4}$) cells. Flow cytometry contour plots D-F demonstrate the distributions of Ly6C expression in the CLN, ILN and MLN of WNV-infected mice ($6x10^{4}$PFU) on d7p.i., compared to d0. Since d0 p.i. for CLN, ILN and MLN were similar, only d0p.i. for CLN is shown. Figure D shows the change in Ly6C expression of $CD11c^{+}CD11b^{+}$DC, with figure E demonstrating the change in $CD11c^{hi}CD11b^{int}$ DC and figure F illustrating the $CD11c^{+}CD11b^{-}$ DC. Note the data in panels A-C are averaged from 3 experiments, while those in D, E and F are representative of single animals at single time points. Thus there will inevitably be some disparity between these sets of data.

Data are shown as the mean ±SEM of values from 3 independent experiments, with 2-4 mice/group in each experiment. Statistical analysis was conducted using one-way ANOVA with a Dunnet's multiple comparison post-test (d0 as control), and $Ly6C^{hi}$ =$P\leq0.05$*; $P\leq0.01$**; $P\leq0.001$***. $Ly6C^{int}$ =$P\leq0.05^{+}$; $P\leq0.01^{++}$; $P\leq0.001^{+++}$. $Ly6C^{-}$ =$P\leq0.05^{Ø}$; $P\leq0.01^{ØØ}$; $P\leq0.001^{ØØØ}$.

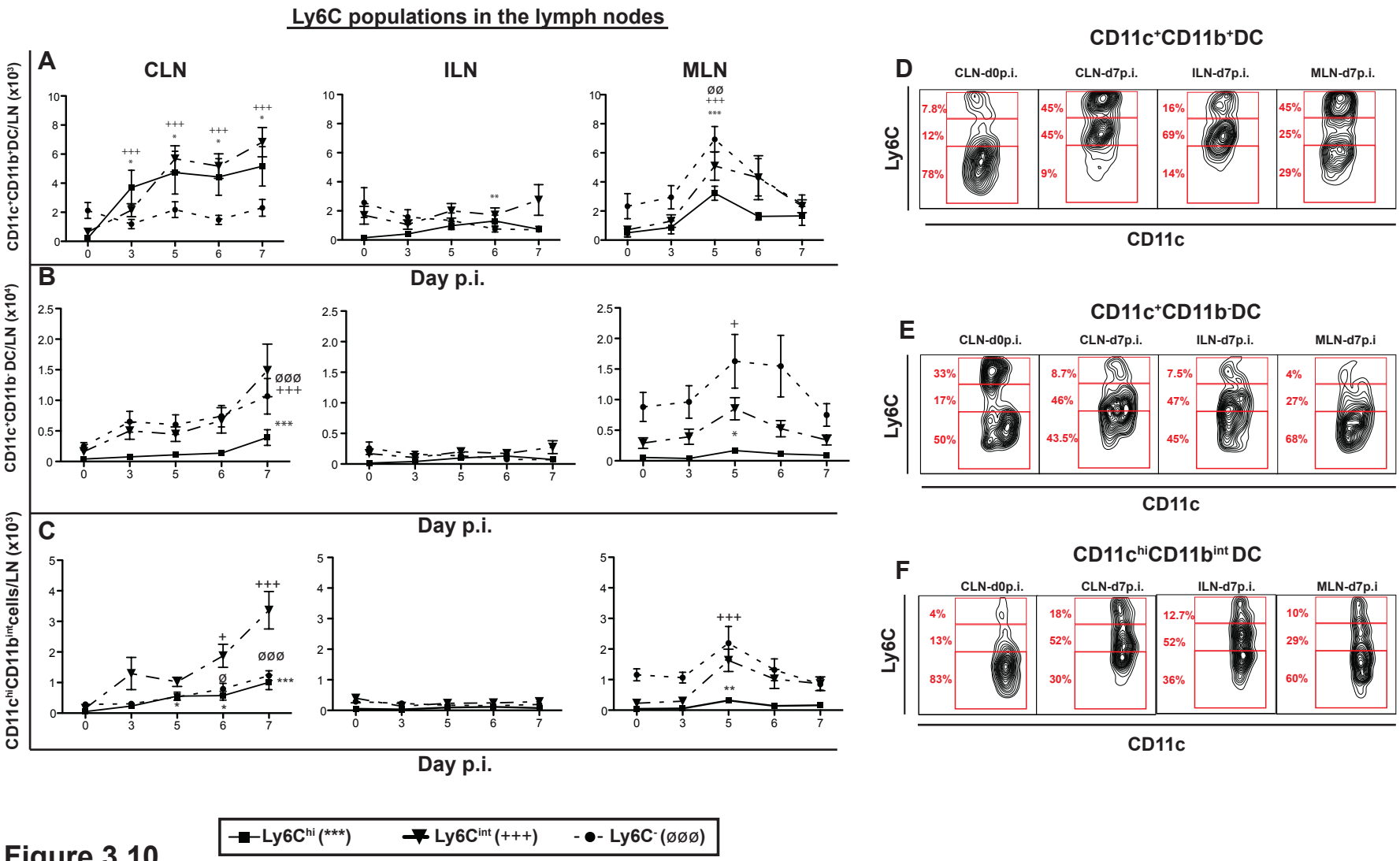
Ly6C populations in the lymph nodes
A
CLN
ILN
MLN
CD11c+CD11b+DC/LN (x10³)
Day p.i.
B
CD11c+CD11b- DC/LN (x10⁴)
Day p.i.
C
CD11chiCD11bintcells/LN (x10³)
Day p.i.
Ly6Chi (***)
Ly6Cint (+++)
Ly6C- (øøø)
D
CD11c+CD11b+DC
CLN-d0p.i.
CLN-d7p.i.
ILN-d7p.i.
MLN-d7p.i.
Ly6C
CD11c
7.8%
12%
78%
45%
45%
9%
16%
69%
14%
45%
25%
29%
E
CD11c+CD11b-DC
CLN-d0p.i.
CLN-d7p.i.
ILN-d7p.i.
MLN-d7p.i
Ly6C
CD11c
33%
17%
50%
8.7%
46%
43.5%
7.5%
47%
45%
4%
27%
68%
F
CD11chiCD11bint DC
CLN-d0p.i.
CLN-d7p.i.
ILN-d7p.i.
MLN-d7p.i
Ly6C
CD11c
4%
13%
83%
18%
52%
30%
12.7%
52%
36%
10%
29%
60%

Figure 3.10

Figure 3.11 Differential Ly6C subsets in the DC populations of the draining (CLN) and non-draining lymph nodes (MLN, ILN) of the CNS following lethal WNV infection

Leukocytes subsets in the CLN, ILN and MLN were further characterised based on Ly6C expression and subsequently classified as $Ly6C^{hi}$ (square), $Ly6C^{int}$ (triangle) or $Ly6C^{-}$ (circle). Significance, compared to d0, for each subset was defined as follows: ***$Ly6C^{hi}$; $^{+++}Ly6C^{int}$ and $^{ØØØ}Ly6C^{-}$. The number of $Ly6C^{hi/int/-}$ $CD11c^{+}B220^{+}$ pDC (A), $CD11c^{+}CD11b^{-}CD8\alpha^{+}$ DC (B) in the CLN, ILN and MLN on d0, 3, 5, 6 and 7p.i. following lethal WNV infection ($6x10^{4}$PFU) are shown. Flow cytometry contour plots C ($CD11c^{+}B220^{+}$ pDC) & D ($CD11c^{+}CD11b^{-}CD8\alpha^{+}$) demonstrate the distribution of Ly6C expression in the CLN, ILN and MLN of WNV-infected mice ($6x10^{4}$PFU) on d7p.i., compared to d0. Since d0 p.i. for CLN, ILN and MLN were similar, only d0p.i. for CLN is shown. Note the data in panels A-B are averaged from 3 experiments, while those in C and D are representative of single animals at single time points. Thus there will inevitably be some disparity between these sets of data.

Data are shown as the mean ±SEM of values from 3 independent experiments, with 2-4 mice/group in each experiment. Statistical analysis was conducted using one-way ANOVA with a Dunnet's multiple comparison post-test (d0 as control), and $Ly6C^{hi}$ =P≤0.05*; P≤0.01**; P≤0.001***. $Ly6C^{int}$ =P≤0.05^{+}; P≤0.01^{++}; P≤0.001^{+++}. $Ly6C^{-}$ =P≤$0.05^{Ø}$; P≤$0.01^{ØØ}$; P≤$0.001^{ØØØ}$.

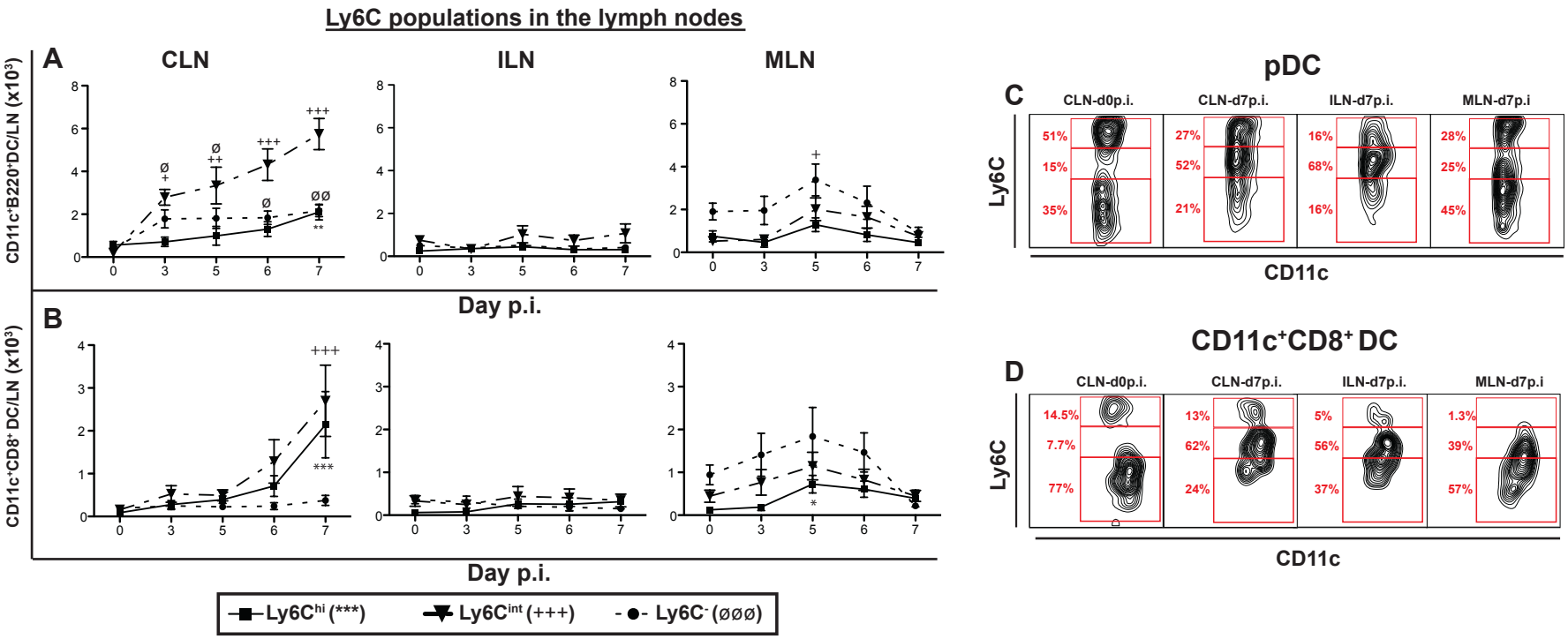
Ly6C populations in the lymph nodes
A
CLN
ILN
MLN
CD11c+B220+DC/LN (x10³)
Day p.i.
B
CD11c+CD8+ DC/LN (x10³)
Day p.i.
Ly6Chi (***)
Ly6Cint (+++)
Ly6C- (øøø)
pDC
C
CLN-d0p.i.
CLN-d7p.i.
ILN-d7p.i.
MLN-d7p.i
Ly6C
CD11c
51%
15%
35%
27%
52%
21%
16%
68%
16%
28%
25%
45%
CD11c+CD8+ DC
D
CLN-d0p.i.
CLN-d7p.i.
ILN-d7p.i.
MLN-d7p.i
Ly6C
CD11c
14.5%
7.7%
77%
13%
62%
24%
5%
56%
37%
1.3%
39%
57%

Figure 3.11

for the other DC subset, numbers in the ILN showed no appreciable changes, whereas MLN Ly6C^{hi} CD8α^{+}DC showed a transient, but significant increase at d5p.i.

In summary, although the numbers of cells in the ILN and MLN did not necessarily increase significantly in response to CNS infection, there were still various increases in the Ly6C populations in these nodes. These data show that the non-draining peripheral lymph nodes are indeed modulated in response to CNS infection. Whether these differential Ly6C populations have functional significance remains to be seen. Nevertheless, similar signals modulating the CNS-draining node may be reaching the peripheral nodes and will likely have additional consequences such as inhibiting or inducing activation and/or proliferation of cells.

3.2.3. Proliferation of leukocyte subsets in the draining and non-draining lymph nodes during WNV encephalitis

It is clear that the downstream effects of CNS inflammation was not limited to the draining lymph node, but had a significant impact on the non-draining lymph nodes. We hypothesised that the signals modulating the decrease in T cell numbers and upregulation of Ly6C, potentially denoting activation, seen in the MLN and ILN, may be reflected in a change in replication status in these nodes. Moreover, to what extent the expansion of CLN cell number was due to infiltration *versus* proliferation, remains to be elucidated. Here, a Bromodeoxyuridine (BrdU) incorporation assay was used to quantify leukocyte proliferation in the CLN, ILN and MLN and determine if the signals modulating the non-draining lymph nodes was also associated with increased cell division. BrdU is an analogue of thymidine that becomes incorporated into cellular DNA when a cell is in S-phase. BrdU was administered i.v. 3 hours prior to sacrificing mice, thus, BrdU^{+} cells only identify the leukocytes that were in S-phase during this time-frame.

As shown in figure 3.12 A, leukocyte proliferation was first detectable from d3 p.i. in the CLN and reached a 6-fold increase by d7 p.i., relative to d0. In contrast, there was no evidence of increased BrdU incorporation in the ILN at any time-point during infection. However, leukocyte proliferation in the MLN showed a significant increase from baseline levels between d6-7 p.i. (Figure 3.12A). Substantial cell division occurred in the T cell population of the CLN with a 4-5-fold rise by d7 p.i. In contrast, the proliferation of T cells in the ILN was reduced to, 30% of baseline levels by d7 p.i. (Figure 3.12B). Both $CD4^+$ (Figure 3.12C) and $CD8^+$ T cell (Figure 3.12D) subsets in the CLN had increased BrdU incorporation from d3 p.i., which resulted in a ~4- and ~5-fold expansion, respectively, by d7 p.i. However, replication of both these subsets in the ILN reduced below baseline levels, while in the MLN these remained stable, apart from an increase seen at d7 p.i.

Increased proliferation of NK cells in the CLN plateaued by d5p.i., remaining high until d7p.i. Significant increases in NK cell proliferation were also seen in the MLN at d5 and d7p.i. (Figure 3.12E), while levels of NK cell proliferation in the ILN remained unchanged throughout infection. Interestingly, NKT cell replication remained at baseline level throughout the disease course in all nodes, with a sudden significant increase at d7 p.i. in the CLN (Figure 3.12F).

The most pronounced increase in proliferation, however, was seen with B cells in the CLN (Figure 3.12G). By d7 p.i. CLN B cells had achieved a 18-fold increase in BrdU incorporation, compared to d0 p.i. This impressive increase in B cell proliferation substantiated the increases seen earlier in cell numbers in the CLN. In the ILN and MLN B cell proliferation remained unchanged, apart from a relatively small but significant increase in the MLN at d7 p.i. (Figure 3.12G).

Monocyte proliferation (Figure 3.13A) increased steadily from d3 p.i. in the CLN of WNV-infected mice, reaching a 10-fold change by d7 p.i., relative to d0. In contrast, the levels of

Figure 3.12 Proliferation of leukocyte subsets in the draining (CLN) and non-draining lymph nodes (MLN, ILN) of the CNS following lethal WNV infection

Proliferation on d0, 3, 5, 6 and 7 p.i. following lethal WNV infection ($6x10^4$ PFU) in the CLN (red), ILN (blue) and MLN (green) of: total leukocytes (A), total T cells (B), $CD4^+$ (C) and $CD8^+$ (D) T cells, NK (E) and NKT (F) cells and B cells (G). Please note the change in y-axis from 1000 to 2500 in figure G. Proliferation was quantified with a BrdU incorporation assay and subsequent analysis of $BrdU^+$ cells by flow cytometry. BrdU was given i.v. 3 hours before sacrifice. Grouped data was normalised using d0 as internal control and is represented as percentage change of $BrdU^+$ cell numbers compared to day 0 (100%).
Data are shown as the mean ±SEM of values from 3 independent experiments, with 2-4 mice/group in each experiment. Statistical analysis was conducted using one-way ANOVA with a Dunnet's multiple comparison post-test (d0 as control), and $P \leq 0.05$*; $P \leq 0.01$**; $P \leq 0.001$***.

Figure 3.12

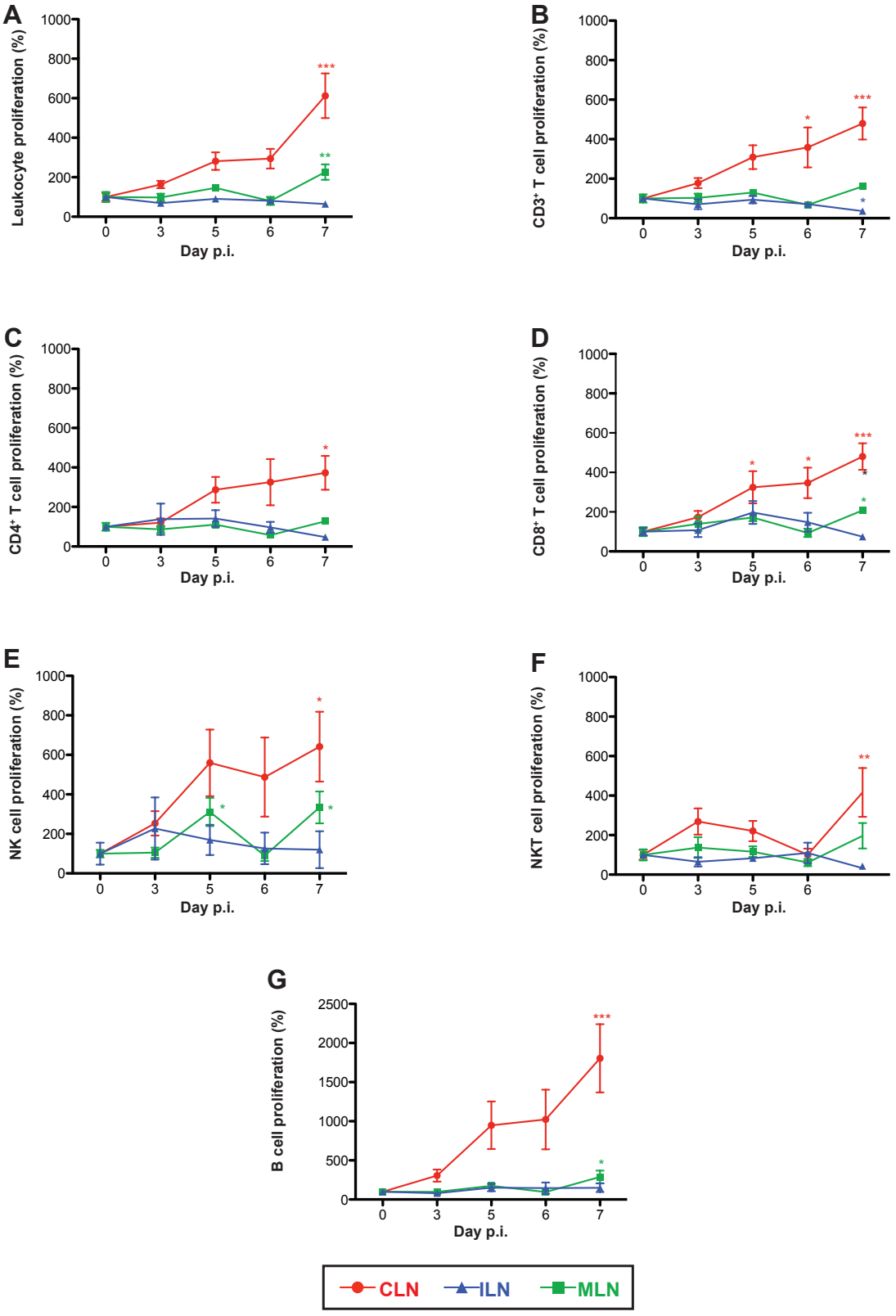
A
Leukocyte proliferation (%)
B
CD3+ T cell proliferation (%)
C
CD4+ T cell proliferation (%)
D
CD8+ T cell proliferation (%)
E
NK cell proliferation (%)
F
NKT cell proliferation (%)
G
B cell proliferation (%)
Day p.i.
CLN
ILN
MLN

Figure 3.13 Proliferation of leukocyte subsets in the draining (CLN) and non-draining lymph nodes (MLN, ILN) of the CNS following lethal WNV infection

Proliferation on d0, 3, 5, 6 and 7 p.i. following lethal WNV infection ($6x10^4$PFU) in the CLN (red), ILN (blue) and MLN (green) of: monocytes (A), $CD11c^+CD11b^+$ DC (B), $CD11c^{hi}CD11b^{int}$ DC, (C) $CD11c^+CD11b^-$ DC (D), $CD11c^+CD8\alpha^+$ DC (E) and pDC (F). Proliferation was quantified with a BrdU incorporation assay and subsequent analysis of $BrdU^+$ cells by flow cytometry. BrdU was given i.v. 3 hours before sacrifice. Grouped data was normalised using d0 as internal control and is represented as percentage change of $BrdU^+$ cell numbers compared to day 0 (100%). Data is shown as the mean ±SEM of values from 3 independent experiments, with 2-4mice/group in each experiment. Statistical analysis was conducted using one-way ANOVA with a Dunnet's multiple comparison post-test (d0 as control), and $P \leq 0.05$*; $P \leq 0.01$**; $P \leq 0.001$***.

Figure 3.13

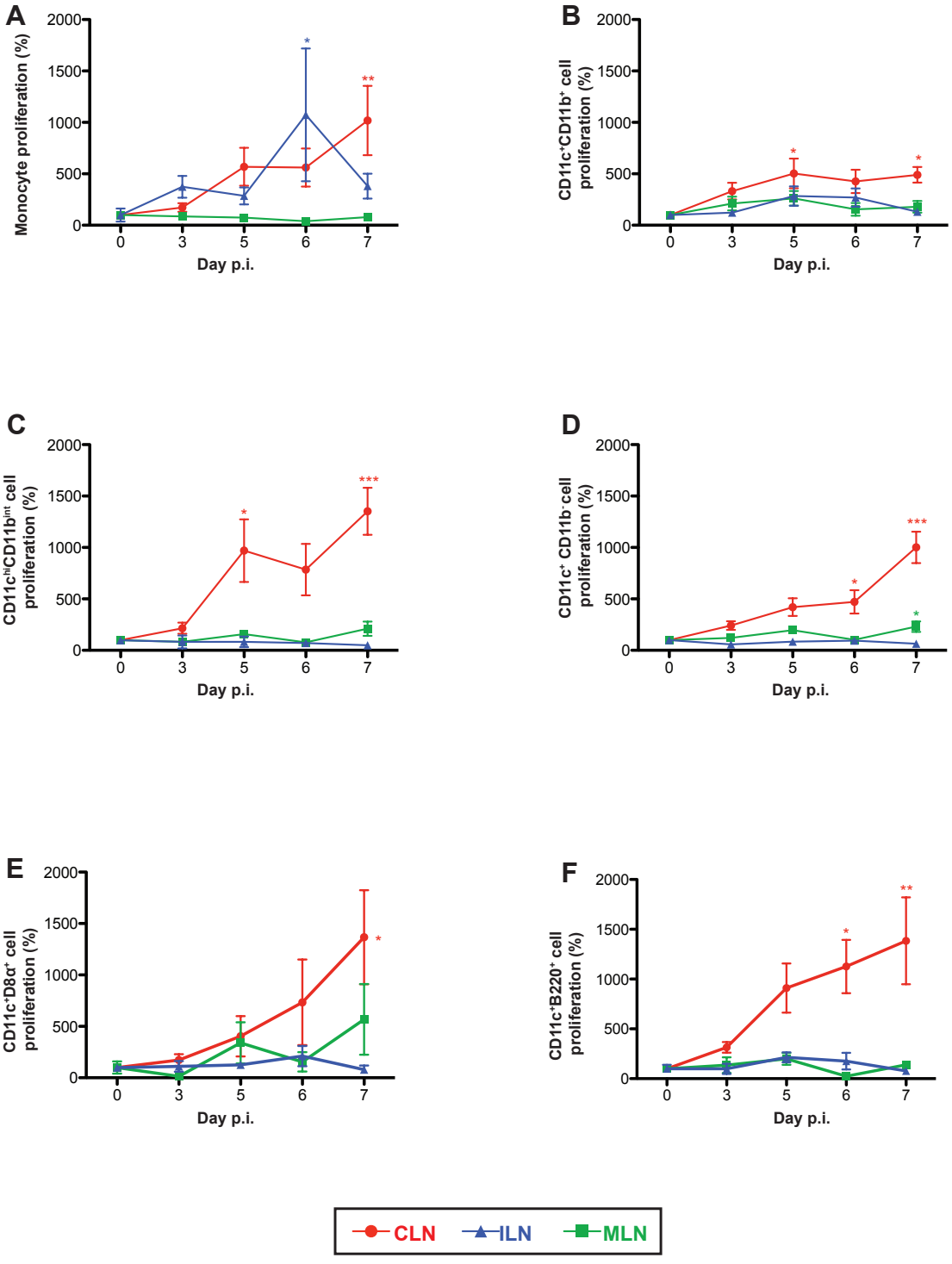
A
Monocyte proliferation (%)
2000
1500
1000
500
0
0
3
5
6
7
Day p.i.
*
**
B
CD11c+CD11b+ cell proliferation (%)
2000
1500
1000
500
0
0
3
5
6
7
Day p.i.
*
*
C
CD11chiCD11bint cell proliferation (%)
2000
1500
1000
500
0
0
3
5
6
7
Day p.i.
*
***
D
CD11c+ CD11b- cell proliferation (%)
2000
1500
1000
500
0
0
3
5
6
7
Day p.i.
*
***
*
E
CD11c+D8α+ cell proliferation (%)
2000
1500
1000
500
0
0
3
5
6
7
Day p.i.
*
F
CD11c+B220+ cell proliferation (%)
2000
1500
1000
500
0
0
3
5
6
7
Day p.i.
*
**
CLN
ILN
MLN

proliferation in monocytes of the MLN remain unchanged. Some elevation in BrdU incorporation occurred in the ILN monocytes, with a statistically significant increase seen at d6 p.i. followed by a subsequent decrease at d7 p.i. Proliferation rose by 5-fold (d7p.i.) in the $CD11c^{+}CD11b^{+}$ DC subset of the CLN and remained at baseline levels in the MLN and ILN (Figure 3.13B). Similarly, replication of the $CD11c^{hi}CD11b^{int}$ DC subset in the CLN rose significantly throughout the course of disease (13-fold by d7 p.i.), but remained at baseline fold increase, relative to d0 p.i., in the CLN and remained unchanged in the ILN and MLN, apart from a relatively small increase at d7 p.i. in the MLN (Figure 3.13D). Moreover, proliferation of the $CD8\alpha^{+}CD11c^{+}$ DC (Figure 3.13E) and pDC (Figure 3.13F) populations of the CLN increased by ~13-fold by d7 p.i., but showed negligible changes in the ILN and MLN.

In order to determine whether there was any correlation between Ly6C expression and proliferation, we examined the Ly6C distribution of $BrdU^{+}$ cells (Figure 3.14). Interestingly, at d0p.i. the majority of $BrdU^{+}$ cells in the CLN (Figure 3.14A) were $Ly6C^{-}$, whereas by d7p.i. this changed to $Ly6C^{+}$(including $Ly6C^{hi}$ and $Ly6C^{int}$). However, this increase in Ly6C expression of $BrdU^{+}$ cells also occurred in the non-draining ILN and MLN (Figure 3.14B and C). Furthermore, this trend was not only present in the total $BrdU^{+}$ leukocyte population, but also applied to the individual leukocyte subsets analysed. As there was little evidence of increased proliferation in the ILN and MLN it suggests that Ly6C upregulation and proliferation is not necessarily biologically linked. However, this does suggests that, during infection, newly proliferated cells in the draining and non-draining lymph nodes of the CNS will be $Ly6C^{+}$, whereas during homeostatic conditions they express lower levels of Ly6C. The functional significance of this will be of great interest for future studies.

Figure 3.14 Ly6C expression of BrdU$^+$ proliferating cells in the draining (CLN) and non-draining lymph nodes (MLN, ILN) of the CNS following lethal WNV infection

Figure A-C are the representative flow cytometry plots illustrating the differential expression of Ly6C on BrdU$^+$ cells in the CLN (A), ILN (B) and MLN (C). The first column demonstrates the gating of total BrdU$^+$ cells in the above lymph node at d0 *versus* d7p.i., following lethal WNV infection ($6x10^4$ PFU). The second column demonstrates the differential Ly6C expression of BrdU$^+$ cells in the above LN at d0 *versus* d7 p.i.

Figure 3.14 Ly6C expression of BrDU⁺ cells

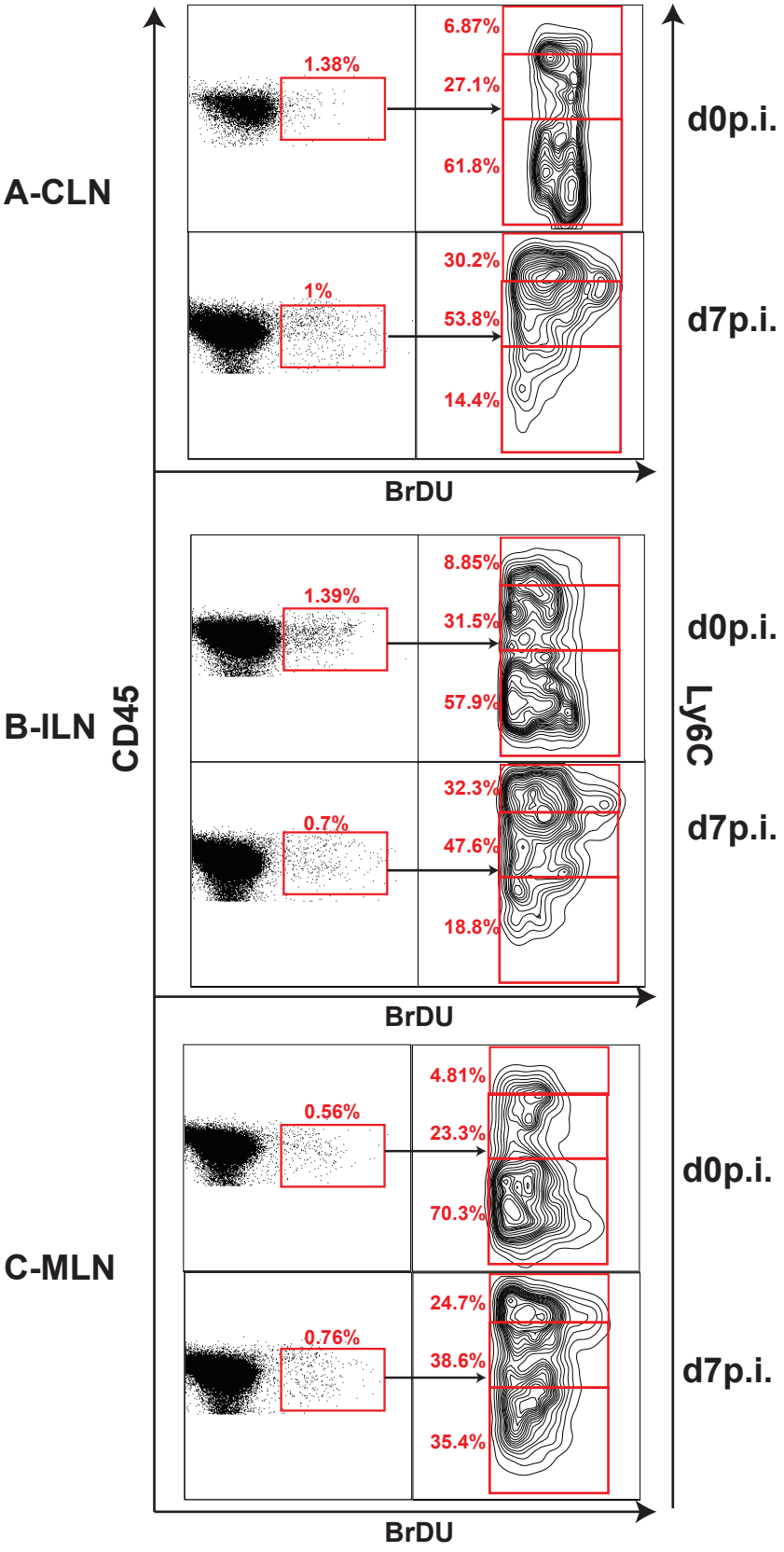

3.2.4. Viral presence in the CNS, draining and non-draining lymph nodes

Cellular proliferation in lymph nodes is often triggered by the presence of pathogen or pathogen-derived products. In order to establish whether or not the substantial proliferation induced in the CLN was due to the presence of virus, we processed the CNS, CLN and ILN of WNV- and mock-infected mice for viral RNA during the course of infection. This allowed us to narrow down the possible factors at play inducing the modification of the non-draining nodes associated with inflammation. Virus was detected with the use of the probes and primers described in Table 2.1.

No viral RNA could be detected in the CNS between d0-3 p.i. WNV RNA was first detected in the CNS at d5 p.i. and remained at the same level of detection until the end of disease course at d7 p.i. (Figure 3.15A columns A2-15). Next, the viral RNA content of the CNS-draining CLN was studied, yielding no appreciable difference between mock-infected (Figure 3.15B columns B4-5) and d3-7p.i. WNV-infected groups (Figure 3.15B columns 6-18). Similarly, the non-draining ILN showed a negligible difference in WNV RNA content between mock-infected (Figure 3.15A columns 16-17) and WNV-infected cohorts (Columns A18-28 and B2-3). Compared to the negative control (Figure 3.15 column A29), there was some signal present in all the lymph nodes (WNV- and mock-infected), however, this was very similar in both mock- and WNV-infected samples, suggesting that this was most likely background signal.

In order to confirm this we performed quantitative RT-PCR (Figure 3.15C) to determine the relative levels of WNV RNA in the CNS, ILN and CLN, at day 0, 1, 3, 5 and 7 p.i. The relative RNA expression in each organ was normalised to mock-infected mice (d0) in terms of 2000ng/µl total RNA and analysed using the $2^{-\Delta\Delta C_T}$ method. There was a

Figure 3.15 Viral RNA presence in the brain, draining and non-draining lymph nodes

Gel electrophoresis (panels A & B) of total viral RNA in isolated mouse brain, CLN and ILN at various time points after infection (Mock, d1, d3, d5 and d7 p.i.). Neat virus stock was used as positive control and uninfected medium as negative control. Panel C demonstrates the results of the RT-PCR for the relative quantity of WNV RNA in the CNS, ILN and CLN at d1, d3, d5 and d7 p.i. with lethal dose of WNV ($6x10^4$ PFU). The relative RNA expression levels were normalised to mock animal (d0) in terms of 2000 ng/µl total RNA and analysed using the $2^{-\Delta\Delta c_T}$ method.

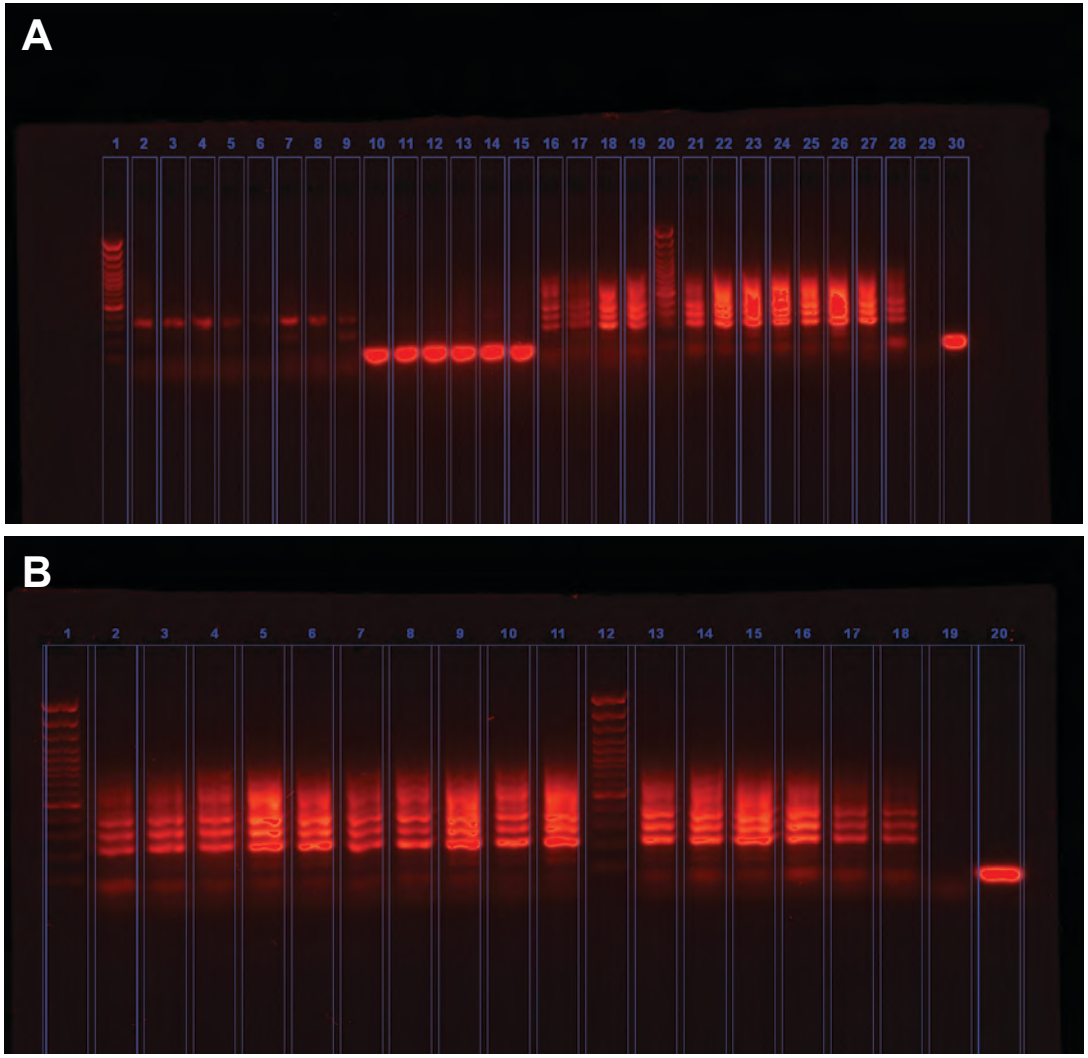

A1	Ladder
A2-3	Mock-infected brain
A4-6	WNV-infected brain d1 p.i.
A7-9	WNV-infected brain d3 p.i.
A10-12	WNV-infected brain d5 p.i.
A13-15	WNV-infected brain d7 p.i.
A16-17	Mock-infected ILN
A18, 19, 21	WNV-infected ILN d1 p.i.
A20	Ladder
A22-24	WNV-infected ILN d3 p.i.
A25-27	WNV-infected ILN d5 p.i.
A28, B2-3	WNV-infected ILN d7 p.i.
A29	Negative control
A30	Positive control (WNV stock)
B1	Ladder
B4-5	Mock-infected CLN
B6-8	WNV-infected CLN d1 p.i.
B9-11	WNV-infected CLN d3 p.i.
B12	Ladder
B13-15	WNV-infected CLN d5 p.i.
B16-18	WNV-infected CLN d7 p.i.
B19	Negative control
B20	Positive control (WNV stock)

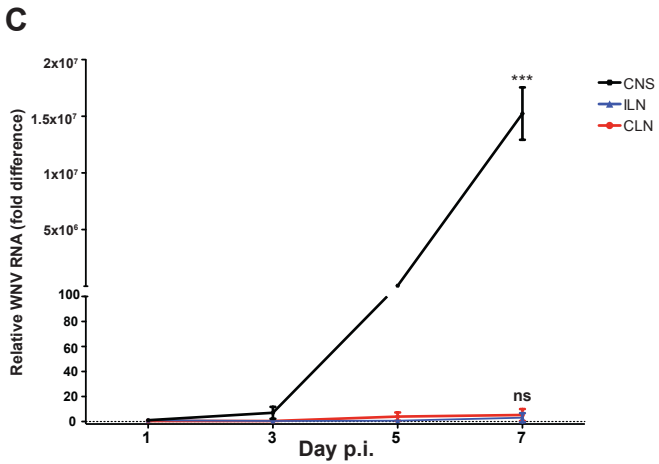

Figure 3.15

significant increase in WNV RNA in the CNS by d7p.i., relative to d0. In contrast, the CLN and ILN both showed negligible change in WNV RNA expression, relative to d0p.i., at all time-points analysed. These results corroborated data from Figure 3.15A and B, confirming the absence of detectable levels of WNV RNA in both the draining and non-draining lymph nodes of the CNS. Therefore, it seems reasonable to conclude that no detectable viral RNA was present in either the draining lymph node (CLN) or non-draining lymph node (ILN) during any of the time points analysed, including the peak of disease at d7 p.i. and that virus-infection was limited to the CNS from d5 p.i. This suggests that the inflammation-associated modulation of these lymph nodes was not due to the presence of virus but likely inflammatory mediators originating in the CNS or perhaps activation by APC migrating from the CNS.

3.2.5. Distribution of cells from a peripheral node to the draining CLN following lethal WNV infection

3.2.5.1. Footpad injection and subsequent distribution of PKH26

We have shown that the non-draining peripheral lymph nodes are undoubtedly modulated by inflammatory signals during the course of WNV-infection, as seen in the reduction of T cells and upregulation of Ly6C in the MLN and ILN. Whether or not these nodes function as a source of lymphoid cells to the upstream nodes, responsible for draining the focus of inflammation, remains to be investigated. Moreover, these nodes may bypass the draining CLN and directly supply lymphoid lineage cells to the CNS. In order to track the extent of lymphatic drainage from a peripheral node to the CLN or CNS during the course of WNV-infection, we performed a footpad injection of a highly fluorescent dye PKH26 (protocol outlined by Figure 3.16 A). PKH26, which is excited at 551mn and has a bright emission at 567nm, was injected on d0 p.i. into the footpad of mice infected i.n. with

Figure 3.16 Injection of PKH26 into the footpad of mock- and WNV-infected mice

Diagram A outlines the protocol followed for the injection of PKH26 into the footpad of WNV- and mock-infected mice. Panels B-E are the representative flow cytometry dot plots showing the distribution of $PKH26^+$ leukocytes ($CD45^+$) in the contra- and ipsilateral PLN (B), ILN (C), CLN (D) and spleen (E) of mock- and WNV-infected mice. The gating for $PKH26^+$ cells was based on the control mice that received no injection.

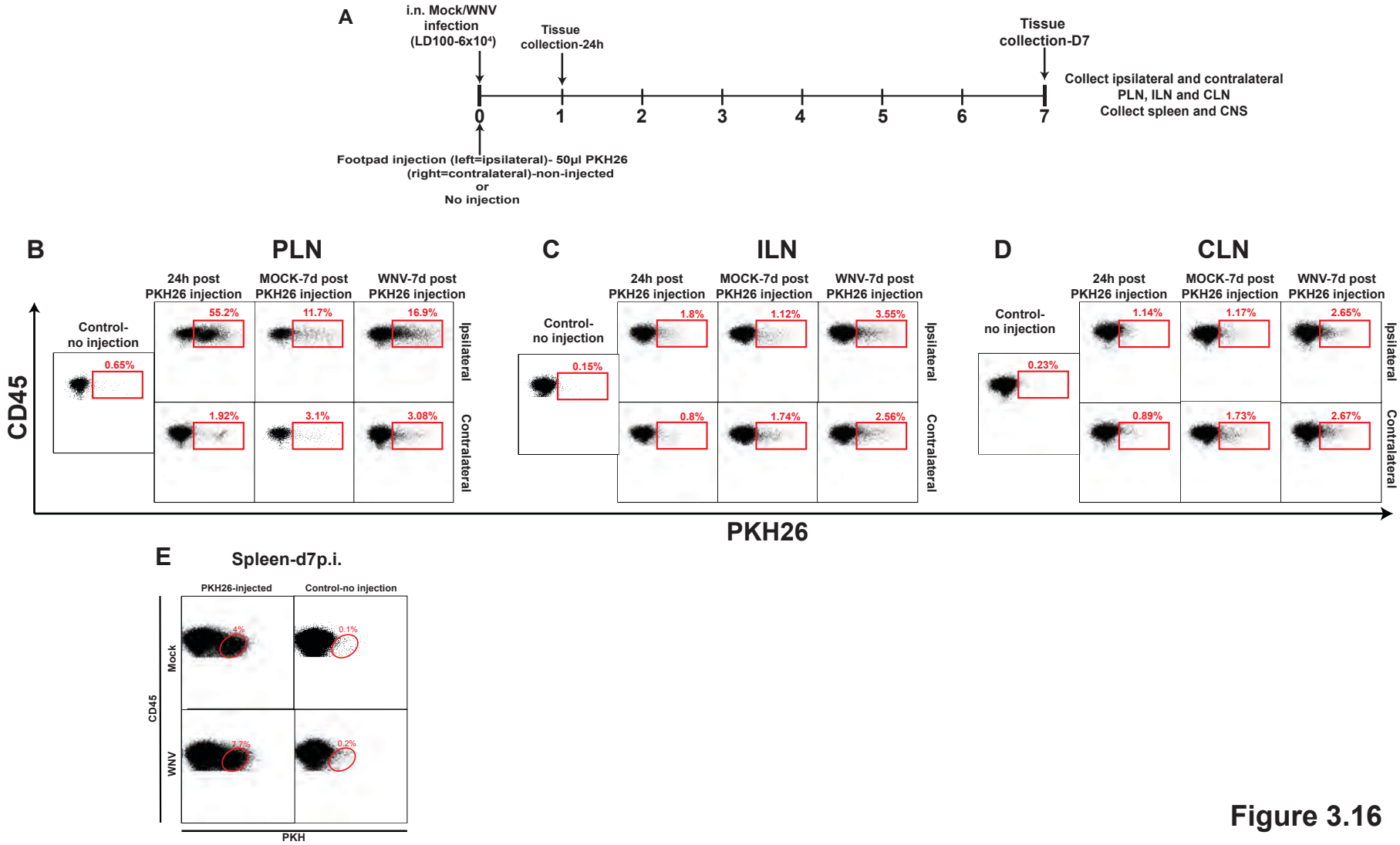
A
i.n. Mock/WNV infection (LD100-6x10⁴)
Tissue collection-24h
Tissue collection-D7
Collect ipsilateral and contralateral PLN, ILN and CLN
Collect spleen and CNS
0
1
2
3
4
5
6
7
Footpad injection (left=ipsilateral)- 50µl PKH26 (right=contralateral)-non-injected or No injection
B
PLN
C
ILN
D
CLN
24h post PKH26 injection
MOCK-7d post PKH26 injection
WNV-7d post PKH26 injection
Control- no injection
Ipsilateral
Contralateral
55.2%
11.7%
16.9%
0.65%
1.92%
3.1%
3.08%
1.8%
1.12%
3.55%
0.15%
0.8%
1.74%
2.56%
1.14%
1.17%
2.65%
0.23%
0.89%
1.73%
2.67%
CD45
PKH26
E
Spleen-d7p.i.
PKH26-injected
Control-no injection
Mock
WNV
4%
0.1%
7.7%
0.2%
CD45
PKH

Figure 3.16

a lethal dose of WNV ($6x10^4$ PFU). The draining node of the footpad, the popliteal lymph node (PLN), was subsequently processed on d7p.i. (i.e. 7 days after PKH26 injection and WNV infection) along with the ILN, CLN, spleen and CNS to determine the extent to which dye^+ cells become distributed in steady state *versus* inflammatory conditions. Furthermore, we also collected control PLN, ILN and CLN, 24h after PKH26 injection of the footpad to determine baseline PKH26 incorporation within 24h in steady state conditions. The steady-state distribution of dye throughout the lymphatic system within 7 days is represented by mock-infected mice, which, in the absence of inflammatory signals, allowed the homeostatic rate of lymphatic distribution throughout the body to be determined. In addition to the ipsilateral nodes, we also collected the contralateral nodes in order to demonstrate the extent to which dye-containing cells can distribute throughout the body.

Figures 3.16 B-D demonstrate the percentage of PKH^+ leukocytes in the contra- and ipsilateral PLN, ILN and CLN within 24h and 7 days post-PKH26 injection in mock- and WNV-infected mice. The PLN, draining the footpad, was the first node to encounter the dye and within 24h ~50% of the ipsilateral node was $PKH26^+$, with very little dye in the contralateral PLN (Figure 3.16B). Within 7 days, some dye had spread to the contralateral PLN in both mock- and WNV-infected mice, with a dramatic reduction in dye^+ cell numbers in the ipsilateral PLN, indicating that the dye or dye-containing cells had distributed elsewhere. Interestingly, by 24h the dye content of the ipsilateral ILN (Figure 3.16C) and CLN (Figure 3.16D) was comparable to that of mock-infected ILN and CLN after 7 days, indicating that 24h was sufficient for distribution of dye or dye-containing cells to reach equilibrium on the ipsilateral side of the body. However, 24h was not sufficient time for $PKH26^+$ leukocytes to distribute evenly to the contralateral nodes, but this had occurred after 7 days. Clearly, additional time-points are needed to estimate exactly how long

equilibration took. Notably, the contra- and ipsilateral ILN and CLN collected from WNV-infected mice had a higher percentage of PKH26$^+$ leukocytes compared to their mock-infected counterparts.

Similarly, the spleen from WNV-infected mice had a higher percentage of PKH26$^+$ leukocytes, compared to mock-infected mice (Fig 3.16E). Lastly, no dye$^+$ cells could be detected in the CNS of either mock or WNV-infected animals (data not shown). These data suggests that WNV infection of the CNS modulates the distribution of cells from a peripheral node, potentially increasing recruitment of cells to the draining node of the CNS.

3.2.5.2. Number and percentage of PKH26$^+$ cells in the ispi- and contralateral PLN, ILN and CLN of mock- *versus* WNV-infected mice

One of the perceived problems of these experiments was that the distribution of dye into the upstream lymph nodes and spleen could occur either as free dye or incorporated into a cell. Therefore, we examined the dynamics of dye distribution in the ipsi- and contralateral PLN, ILN and CLN in more detail.

There was a clear trend for the total number of PKH26$^+$ leukocytes to decrease between 24h and 7days in the ipsilateral PLN (Figure 3.17A-i) and increase in both the contra- and ipsilateral CLN (Figure 3.17A-v) by d7p.i. The percentage of PKH26$^+$ leukocytes in the ipsilateral PLN (Figure 3.17A-ii) also reduced by d7p.i., suggesting that the PKH26$^+$ cells had left the node, potentially dispersing to the CLN or ILN. Indeed, by d7 p.i., the number of PKH26$^+$ leukocytes in the contra- and ipsilateral ILN (Figure 3.17A-iii) of mock-infected mice had increased from 24h. However, the number of PKH26$^+$ leukocytes in the ILN from WNV-infected mice had reduced, compared to mock-infected mice. In contrast, the percentage of PKH26$^+$ leukocytes in the WNV-infected ILN (Figure 3.17A-iv) was

Figure 3.17 Number and percentage of PKH26$^+$ leukocytes, B and T cells in the contra- and ipsilateral PLN, ILN and CLN of mock- and WNV-infected mice

Panel A demonstrates the number (i, iii, v) and percentage (ii, iv, vi) of PKH26$^+$ leukocytes in the contra- and ipsilateral PLN (i,ii), ILN (iii, iv) and CLN (v, vi) of mock- and WNV-infected mice (6x10^4 PFU) 24h and 7 days after PKH injection. Cohorts with no injection (light grey), 24h after injection (dark grey), contralateral mock-infected (light blue), ipsilateral mock-infected (dark blue), contralateral WNV-infected (light green) and ipsilateral WNV-infected (dark green) are shown. Panel B demonstrates the number (i, iii, v) and percentage (ii, iv, vi) of PKH26$^+$ B cells in the contra- and ipsilateral PLN (i,ii), ILN (iii, iv) and CLN (v, vi) of mock- and WNV-infected mice 24h and 7 days after PKH injection. Panel C shows the number (i, iii, v) and percentage (ii, iv, vi) of total PKH26$^+$ T cells in the contra- and ipsilateral PLN (i,ii), ILN (iii, iv) and CLN (v, vi) of mock- and WNV-infected mice 24h and 7 days after PKH injection. Data are shown as the mean ±SEM of values from 2 independent experiments, with 2-3 mice/group in each experiment. The 24h time-point was from one experiment and was not included in the statistical analysis. Statistical analysis was conducted using one-way ANOVA with a Tukey's multiple comparison post-test, and P≤0.05*; P≤0.01**; P≤0.001***.

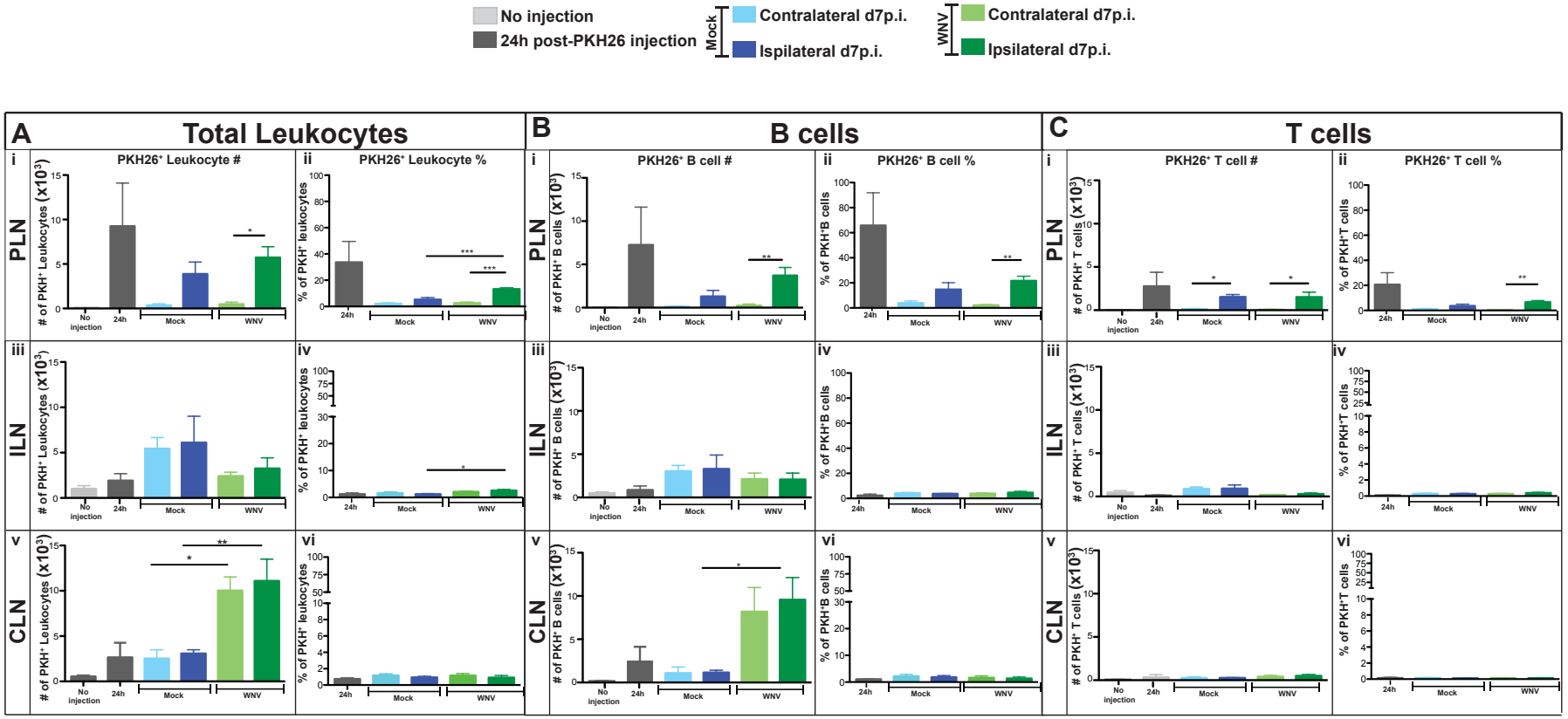
No injection
24h post-PKH26 injection
Mock
Contralateral d7p.i.
Ipsilateral d7p.i.
WNV
Contralateral d7p.i.
Ipsilateral d7p.i.
A
Total Leukocytes
B
B cells
C
T cells
PKH26+ Leukocyte #
PKH26+ Leukocyte %
PKH26+ B cell #
PKH26+ B cell %
PKH26+ T cell #
PKH26+ T cell %
PLN
ILN
CLN
# of PKH+ Leukocytes (x10^3)
% of PKH+ leukocytes
# of PKH+ B cells (x10^3)
% of PKH+B cells
# of PKH+ T cells (x10^3)
% of PKH+T cells
No injection
24h
Mock
WNV

Figure 3.17

significantly higher than in mock-infected ILN. This could indicate that more PKH26$^+$ cells were being recruited from the PLN during infection, or that more cells were incorporating dye during infectious circumstances than in steady-state. Either way, consistent with earlier data showing a decrease in leukocyte number in the ILN, this increased percentage is occurring on a background of reduced PKH26$^-$ cell numbers. The comparable numbers between contra- and ipsilateral sides suggests increased recruitment, rather than incorporation of dye, as the dye would have had to enter the bloodstream and reach the contralateral node undiluted and in similar concentrations to the ipsilateral side for this to occur.

Furthermore, although the number of PKH26$^+$ leukocytes in the WNV-infected CLN (Figure 3.17A-v) was significantly higher than the mock-infected CLN, the percentages of PKH26$^+$ leukocytes (Figure 3.17A-vi) were comparable between mock- and WNV-infected. Data in graph 3.1 F showed a significant increase in CLN leukocyte numbers in response to infection and taken together with the data presented here, is may suggest that the increase in PKH26$^+$ leukocytes occurred in a similar ratio to the increase in total leukocyte number.

B cells accounted for the highest number of PKH26$^+$ cells in the ILN (Figure 3.17B-iii) and CLN (Figure 3.17B-v), although the percentage that the PKH26$^+$ B cells contributed to the total B cell population in both the ILN (Figure 3.17B-iv) and CLN (Figure 3.17B-vi) was very low, both 24h and 7 days after injection. As the B cell population in the ILN and CLN is so large by d7 p.i. the PKH26$^+$ B cells likely became quite dilute. Nevertheless, the trend of PKH26$^+$ B cell distribution throughout the lymph nodes mirrored that of the total PKH26$^+$ leukocyte population, in particular the increase of PKH$^+$ B cells in the contra- and ipsilateral CLN during WNV infection. From this we hypothesised that PKH26$^+$ B cells leave the PLN and possibly the ILN, preferentially trafficking to the WNV-infected contra- and ipsilateral CLN. Higher numbers of PKH26$^+$ B cells in the contra- and ipsilateral ILN (Figure

3.17B-iii) of mock-infected mice indicate that some B cells may be retained there in the absence of an inflammatory stimulus, whereas, during infection they may be recruited to the focus of inflammation and corresponding draining lymph node i.e. the CLN.

There was some incorporation of dye into PLN T cells (Figure 3.17C-i), however the reduction in numbers of PKH26$^+$ T cells between 24h and 7 days was less than in B cells. Considering the large numbers of T cells present in lymph nodes, very few of these were PKH26$^+$ in the ILN (Figure 3.17C-iii) and CLN (Figure 3.17C-v). This was true for both CD4$^+$ (Figure 3.18A i-vi) and CD8$^+$ T cells (Figure 3.18B i-vi), with little difference between mock- and WNV-infected cohorts in terms of PKH26$^+$ T cell content. This suggests that T cells account for a smaller proportion of the PKH26$^+$ population being distributed throughout steady-state conditions and that inflammation does not significantly increase the 'recruitment' of T cells from a peripheral node to the focus of infection in this model of PKH26 injection.

Compared to B and T cells, monocytes are present in relatively low numbers in the lymph node, however ~60% of monocytes in the PLN were PKH26$^+$ 24h after injection (Figure 3.18C-ii). Moreover, homeostatic conditions saw ~20% of monocytes being PKH26$^+$ in both contra- and ipsilateral ILN after 7 days (Figure 3.18C-iv), suggesting that a large proportion of these have been distributed to the ILN from the PLN. Nevertheless, infection did not have a significant effect on the numbers or percentage of PKH26$^+$ monocytes in either the ILN (Figure 3.18C-iii) or the CLN (Figure 3.18C-v).

Similarly, although present in low numbers, a large proportion of CD11b$^+$ DC (~70-80%) in both the contra- and ipsilateral PLN had incorporated PKH26. In addition, the 20-40% of the CD11b$^+$ DC in the contra- and ipsilateral ILN (Figure 3.19A-iv) and CLN (Figure 3.19A-vi) were PKH26$^+$. This suggests that a large proportion of this population in the CLN and ILN was migratory and may be continually redistributed throughout the body. This

Figure 3.18 Number and percentage of PKH26$^+$ CD4$^+$, CD8$^+$ T cells and monocytes in the contra- and ipsilateral PLN, ILN and CLN of mock- and WNV-infected mice

Panel A demonstrates the number (i, iii, v) and percentage (ii, iv, vi) of PKH26$^+$ CD4$^+$ T cells in the contra- and ipsilateral PLN (i,ii), ILN (iii, iv) and CLN (v, vi) of mock- and WNV-infected mice (6x10^4 PFU) 24h and 7 days after PKH injection. Note the 10-fold change in y-axis from x10^3 (figure 3.17) to x10^2. With no injection (light grey), 24h after injection (dark grey), contralateral mock-infected (light blue), ipsilateral mock-infected (dark blue), contralateral WNV-infected (light green) and ipsilateral WNV-infected (dark green) is shown. Panel B demonstrates the number (i, iii, v) and percentage (ii, iv, vi) of PKH26$^+$ CD8$^+$ T cells in the contra- and ipsilateral PLN (i,ii), ILN (iii, iv) and CLN (v, vi) of mock- and WNV-infected mice 24h and 7 days after PKH injection. Panel C shows the number (i, iii, v) and percentage (ii, iv, vi) of PKH26$^+$ monocytes in the contra- and ipsilateral PLN (i, ii), ILN (iii, iv) and CLN (v, vi) of mock- and WNV-infected mice 24h and 7 days after PKH injection. Data are shown as the mean ±SEM of values from 2 independent experiments, with 2-3 mice/group in each experiment. The 24h time-point was from one experiment and was not included in the statistical analysis. Statistical analysis was conducted using one-way ANOVA with a Tukey's multiple comparison post-test, and P≤0.05*; P≤0.01**; P≤0.001***.

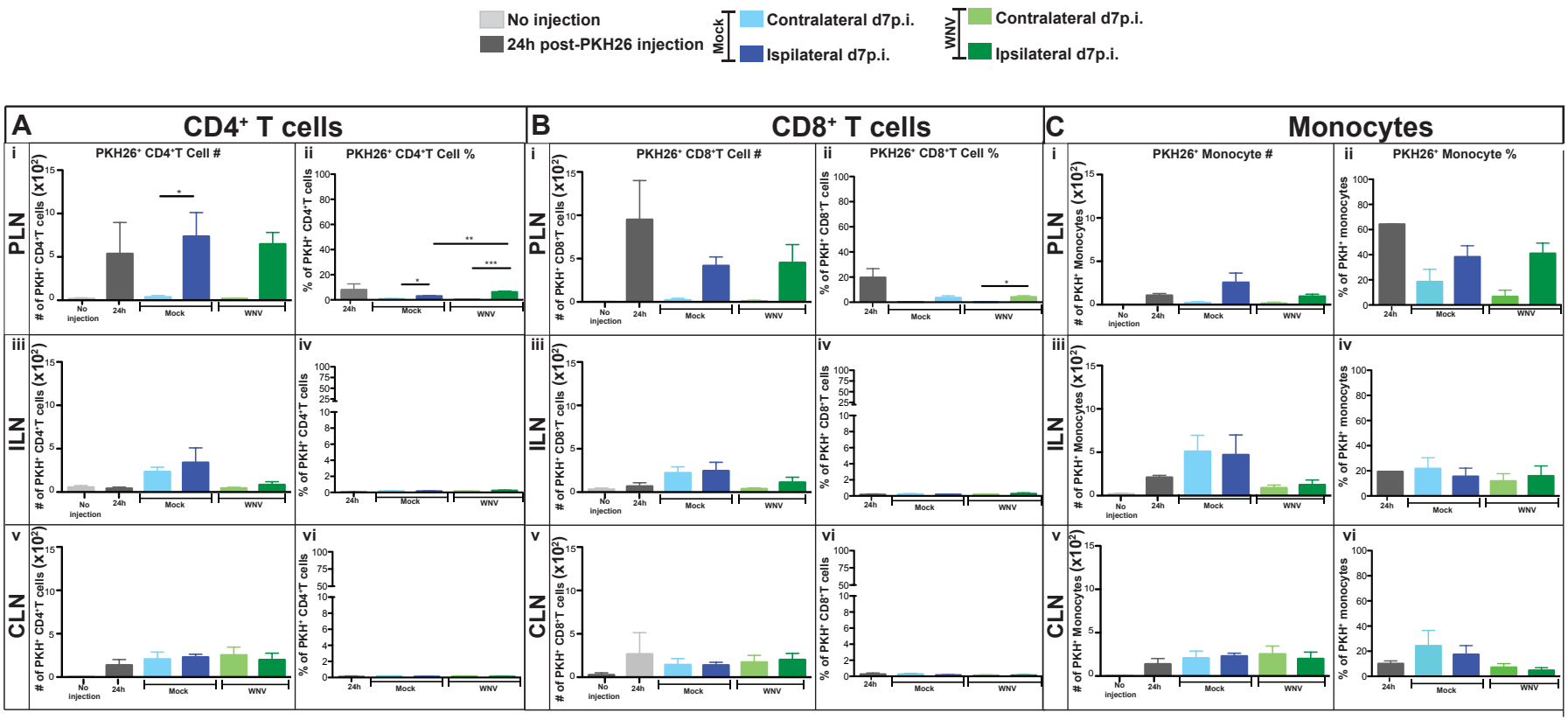
No injection
24h post-PKH26 injection
Mock
Contralateral d7p.i.
Ispilateral d7p.i.
WNV
Contralateral d7p.i.
Ipsilateral d7p.i.
A
CD4+ T cells
B
CD8+ T cells
C
Monocytes
PKH26+ CD4+T Cell #
PKH26+ CD4+T Cell %
PKH26+ CD8+T Cell #
PKH26+ CD8+T Cell %
PKH26+ Monocyte #
PKH26+ Monocyte %
PLN
ILN
CLN
No injection
24h
Mock
WNV

Figure 3.18

Figure 3.19 Number and percentage of PKH26$^+$ CD11c$^+$CD11b$^+$, CD11c$^+$CD11b$^-$ and CD11c$^+$CD8α$^+$ DC in the contra- and ipsilateral PLN, ILN and CLN of mock- and WNV-infected mice

Panel A demonstrates the number (i, iii, v) and percentage (ii, iv, vi) of PKH26$^+$ CD11c$^+$CD11b$^+$ DC in the contra- and ipsilateral PLN (i,ii), ILN (iii, iv) and CLN (v, vi) of mock- and WNV-infected mice ($6x10^4$ PFU) 24h and 7 days after PKH injection. With no injection (light grey), 24h after injection (dark grey), contralateral mock-infected (light blue), ipsilateral mock-infected (dark blue), contralateral WNV-infected (light green) and ipsilateral WNV-infected (dark green) is shown. Panel B demonstrates the number (i, iii, v) and percentage (ii, iv, vi) of PKH26$^+$ CD11c$^+$CD11b$^-$ DC in the contra- and ipsilateral PLN (i,ii), ILN (iii, iv) and CLN (v, vi) of mock- and WNV-infected mice 24h and 7 days after PKH injection. Panel C shows the number (i, iii, v) and percentage (ii, iv, vi) of PKH26$^+$ CD11c$^+$CD8α$^+$ DC in the contra- and ipsilateral PLN (i, ii), ILN (iii, iv) and CLN (v, vi) of mock- and WNV-infected mice 24h and 7 days after PKH injection. Data are shown as the mean ±SEM of values from 2 independent experiments, with 2-3 mice/group in each experiment. The 24h time-point was from one experiment and was not included in the statistical analysis. Statistical analysis was conducted using one-way ANOVA with a Tukey's multiple comparison post-test, and P≤0.05*; P≤0.01**; P≤0.001***.

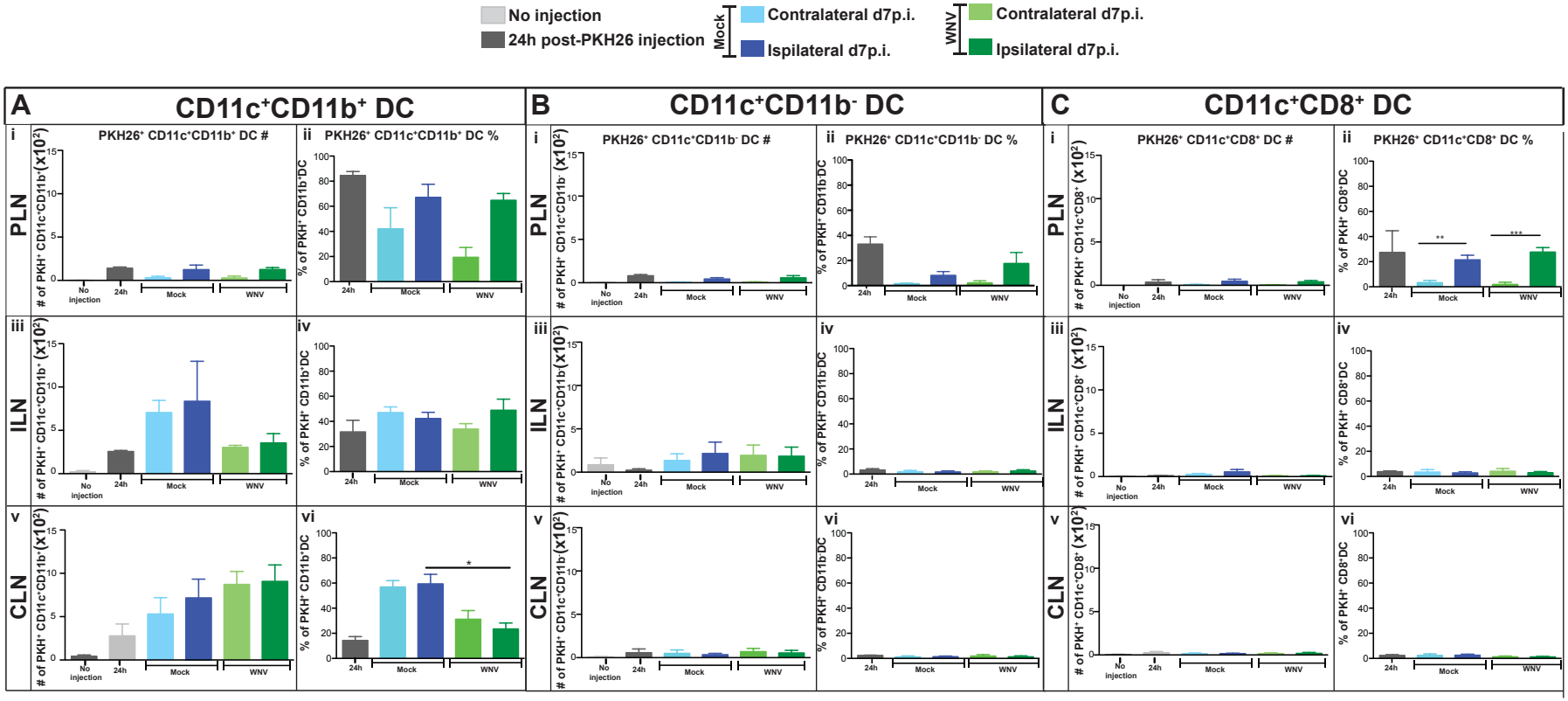
No injection
24h post-PKH26 injection
Mock
Contralateral d7p.i.
Ispilateral d7p.i.
WNV
Contralateral d7p.i.
Ipsilateral d7p.i.
A
CD11c+CD11b+ DC
B
CD11c+CD11b- DC
C
CD11c+CD8+ DC
PLN
ILN
CLN
PKH26+ CD11c+CD11b+ DC #
PKH26+ CD11c+CD11b+ DC %
PKH26+ CD11c+CD11b- DC #
PKH26+ CD11c+CD11b- DC %
PKH26+ CD11c+CD8+ DC #
PKH26+ CD11c+CD8+ DC %
# of PKH+ CD11c+CD11b+ (x10²)
% of PKH+ CD11b+DC
# of PKH+ CD11c+CD11b- (x10²)
% of PKH+ CD11b-DC
# of PKH+ CD11c+CD8+ (x10²)
% of PKH+ CD8+DC
No injection
24h
Mock
WNV
*
**
***

Figure 3.19

notion may be supported by the reduced numbers of these cells in the ILN of infected mice, compared to the mock-infected control, although this difference was not statistically significant. However, as was the case with monocytes, infection did not result in increased numbers of PKH26$^+$ CD11b$^+$DC in the CLN (Figure 3.19A-v) and there was a significant decrease in the percentage (Figure 3.19A-vi) of CD11b$^+$CD11c$^+$ DC that were PKH26$^+$ in the CLN by d7p.i., presumably due to the fact that the total expansion of this subset in the CLN occurred at a much greater rate than the recruitment of PKH26$^+$ CD11b$^+$CD11c$^+$ DC.

Although ~30% of CD11b$^-$ DC in the PLN had incorporated dye by 24h (Figure 3.19B-ii), relatively low distribution of these cells was evident in the ILN (Figure 3.19B-iv) and CLN (Figure 3.19B-vi). Furthermore, there was little evidence for redistribution of PKH26$^+$ CD8α$^+$ DC (Figure 3.19C i-vi) to the ILN and CLN. The CD8α$^+$ DC of the lymph node are classically regarded as the lymphoid tissue resident DC, which do not migrate, explaining the absence of PKH26$^+$CD8α$^+$ DC in the upstream nodes.

Similar to the CD11b$^+$ DC in figure 3.19 A, there were very low numbers, but relatively high percentage of PKH26$^+$CD11c^{hi}CD11b^{int} DC present in both the contra- and ipsilateral ILN and CLN of mock- and WNV-infected mice. Indeed, PKH26$^+$CD11c^{hi}CD11b^{int} DC contributed to ~20% of the total CD11c^{hi}CD11b^{int} population in the steady-state ILN and CLN (Figure 3.20A i-vi). Although the percentage of PKH26$^+$CD11c^{hi}CD11b^{int} DC in the CLN was slightly lower in the WNV-infected cohort, compared to mock-infected, this was not significant. Therefore, WNV infection of the CNS did not significantly modulate the PKH26$^+$CD11b$^+$ or CD11b$^-$ DC response in the CLN or ILN. However, the large proportion of myeloid or CD11b$^+$ DC that were PKH26$^+$ suggests that these cells likely possessed a migratory phenotype, in contrast to the lymphoid resident CD8α$^+$ DC.

Figure 3.20 Number and percentage of PKH26^{+} pDC CD11c^{hi}CD11b^{int} DC and neutrophils in the contra- and ipsilateral PLN, ILN and CLN of mock- and WNV-infected mice

Panel A demonstrates the number (i, iii, v) and percentage (ii, iv, vi) of PKH26^{+} CD11c^{hi}CD11b^{int} DC in the contra- and ipsilateral PLN (i, ii), ILN (iii, iv) and CLN (v, vi) of mock- and WNV-infected mice 24h and 7 days after PKH injection. Figure B demonstrates the number (i, iii, v) and percentage (ii, iv, vi) of PKH26^{+} pDC in the contra- and ipsilateral PLN (i,ii), ILN (iii, iv) and CLN (v, vi) of mock- and WNV-infected mice ($6x10^{4}$ PFU) 24h and 7 days after PKH injection. With no injection (light grey), 24h after injection (dark grey), contralateral mock-infected (light blue), ipsilateral mock-infected (dark blue), contralateral WNV-infected (light green) and ipsilateral WNV-infected (dark green) is shown. Panel C demonstrates the number (i, iii, v) and percentage (ii, iv, vi) of PKH26^{+} neutrophils in the contra- and ipsilateral PLN (i, ii), ILN (iii, iv) and CLN (v, vi) of mock- and WNV-infected mice 24h and 7 days after PKH injection. Data are shown as the mean ±SEM of values from 2 independent experiments, with 2-3 mice/group in each experiment. The 24h time-point was from one experiment and was not included in the statistical analysis. Statistical analysis was conducted using one-way ANOVA with a Tukey's multiple comparison post-test, and $P \leq 0.05$*; $P \leq 0.01$**; $P \leq 0.001$***.

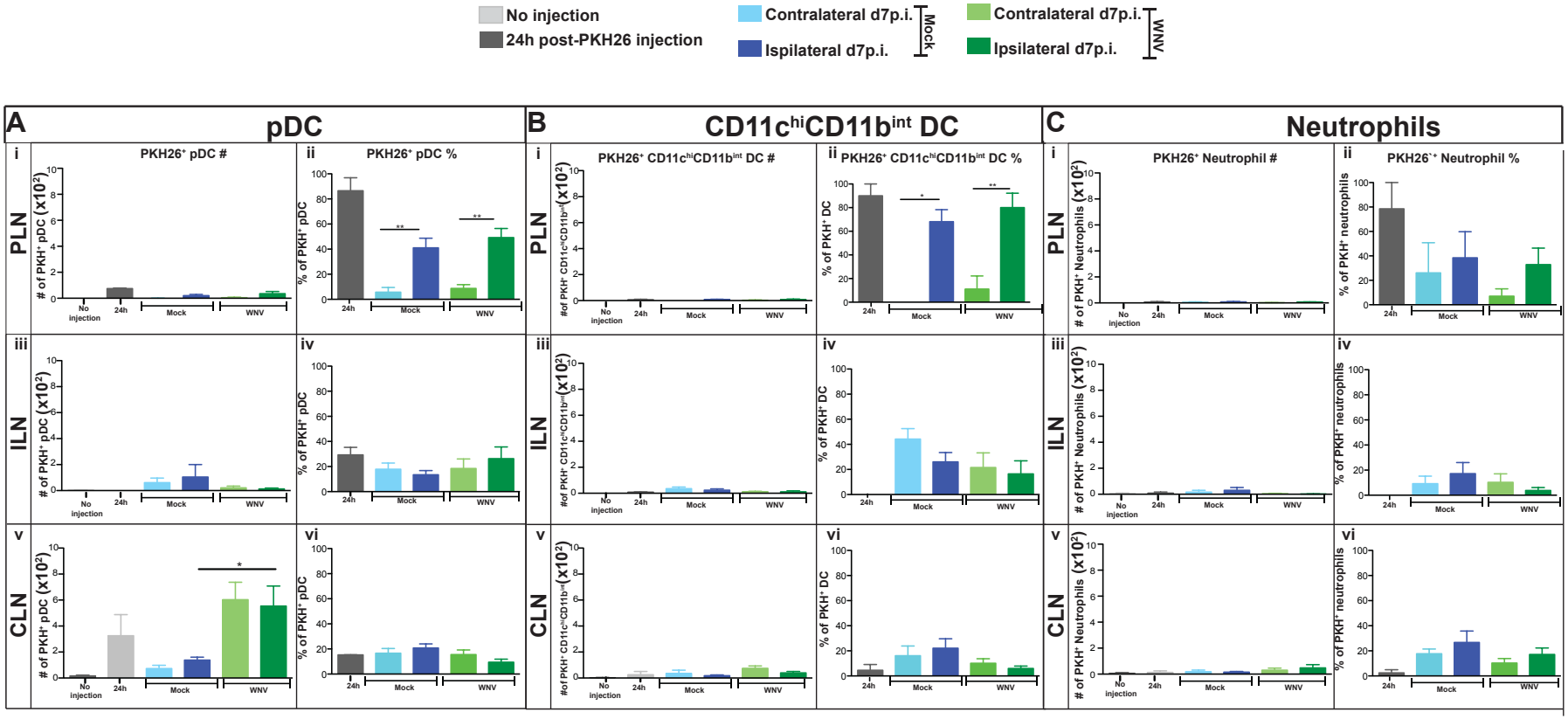
No injection
24h post-PKH26 injection
Contralateral d7p.i.
Ipsilateral d7p.i.
Mock
Contralateral d7p.i.
Ipsilateral d7p.i.
WNV
A
pDC
B
CD11c^hiCD11b^int DC
C
Neutrophils
PLN
ILN
CLN
PKH26+ pDC #
PKH26+ pDC %
PKH26+ CD11c^hiCD11b^int DC #
PKH26+ CD11c^hiCD11b^int DC %
PKH26+ Neutrophil #
PKH26`+ Neutrophil %
# of PKH+ pDC (x10^2)
% of PKH+ pDC
#of PKH+ CD11c^hiCD11b^int (x10^2)
% of PKH+ DC
# of PKH+ Neutrophils (x10^2)
% of PKH+ neutrophils
No injection
24h
Mock
WNV

Figure 3.20

Interestingly, the distribution of PKH26$^+$ pDC was clearly influenced by WNV infection, as there was a significant increase in PKH26$^+$ pDC (Figure 3.20B-v) in the ipsilateral CLN of WNV-infected mice compared to mock-infected. Indeed, the PKH26$^+$ pDC exhibited a similar pattern of distribution throughout the PLN, ILN and CLN to PKH26$^+$ B cells (Figure 3.17B) suggesting that these subsets may be modulated by similar signals.

The number of PKH26$^+$ neutrophils in the PLN (Figure 3.20C-i), ILN (Figure 3.20C-iii) and CLN (Figure 3.20C-v) was extremely low (<100). However, in the CLN, >10% of neutrophils in mock-and WNV-infected mice were PKH26$^+$ suggesting that they originated elsewhere. There were negligible numbers of PKH26$^+$ NK and NKT cells incorporating dye in all 3 nodes examined (Data not shown).

There are two ways in which leukocytes from the ipsilateral ILN could become PKH26$^+$: 1) Free dye, which distributed throughout the lymph and entered the upstream ILN and was subsequently incorporated into leukocytes or 2) Leukocytes that incorporated dye in the PLN and migrated to the ipsilateral ILN. However, there is no direct lymphatic connection from the ipsilateral PLN and ILN to the contralateral PLN and ILN, or for that matter, to the contra- and ipsilateral CLN. Therefore, it is unlikely that free dye spread undiluted to the contralateral node in high enough concentrations to stain cells there. It is much more likely that cells, which have incorporated dye in the ipsilateral ILN or PLN, have travelled via the lymphatics to the bloodstream, and thence to the contralateral ILN and PLN, as well as CLN. If true, then the numbers and percentages of PKH26$^+$ cells in the contralateral ILN and contra- and ipsilateral CLN from mock-infected mice represents the steady-state distribution of cells throughout the body, rather than free dye. Therefore, any changes in this number in the CLN of WNV-infected mice compared to mock-infected, suggests increased recruitment of cells as a result of infectious stimuli. This was mainly evident in the B220$^+$ populations i.e. B cells and pDC, possibly indicating that these two subsets are

being recruited to the CLN by the similar signals. Moreover, the high percentage of $CD11b^+$DC in the CLN highlights the migratory nature of these cells.

There was a substantial presence of dye^+ cells in the mock- and WNV-infected spleen, seven days following PKH26 footpad injection (Figure 3.21B and C). Notably, in both cohorts, the $CD11c^+CD11b^-$ subset had incorporated the majority of PKH26 with 85.8% (mock) and 85% (WNV) of the $PKH26^+$ population identified as $CD11c^+CD11b^-$ cells. The remainder of the $PKH26^+$ population in the spleen from mock-infected mice consisted of B cells (~9%), T cells (~1%) and $CD11b^+$ cells (~5%). The ratio of various leukocytes present in the $PKH26^+$ population in the spleen of WNV-infected cohort differed somewhat to the spleen from mock-infected mice, as the remainder of cells occupied less than 10% of the PKH^+ population. Indeed, when enumerated (Figure 3.21A) there were fewer $PKH26^+$ B cells, T cells and monocytes in the spleen from WNV-infected mice, compared to mock-infected cohort, although this was not statistically significant. Interestingly, there were significantly more $PKH26^+$ neutrophils in the spleen from WNV-infected mice, compared to the mock-infected cohort.

3.2.5.3. Adoptive transfer of CD45.1 and CFSE stained lymph node cells

Although unlikely, the $PKH26^+$ could have spread through the lymphatic or circulatory system as free dye and/or incorporated into cells migrating to the spleen and lymph nodes during homeostatic and inflammatory conditions. In order to confirm that cells from the peripheral nodes, and not free dye, can migrate to the draining CLN during infection we designed an experiment using adoptively-transferred cells. The adoptive transfer of $CD45.1^+$ and CFSE-stained cells from mock-infected peripheral nodes, into the footpad and subsequent examination of PLN, ILN, CLN, spleen and CNS in mock- and WNV-infected mice ($CD45.2^+$), sought to clarify this issue.

Figure 3.21 Number and percentage of PKH26$^+$ cells in the spleen of mock- and WNV-infected mice

Panel A demonstrates the number of PKH26$^+$ leukocytes in the spleen of mock-(blue) and WNV (green)–infected mice 7 days after PKH26 footpad injection and i.n. WNV infection ($6x10^4$ PFU). Panels B and C are the representative flow cytometry plots of PKH26+ leukocyte subsets of mock (B)- and WNV (C) –infected mice. Data are shown as the mean ±SEM of values from 1 experiment, with 3 mice/group. Statistical analysis was conducted using one-way ANOVA with a Tukey's multiple comparison post-test, and P≤0.05*; P≤0.01**; P≤0.001***.

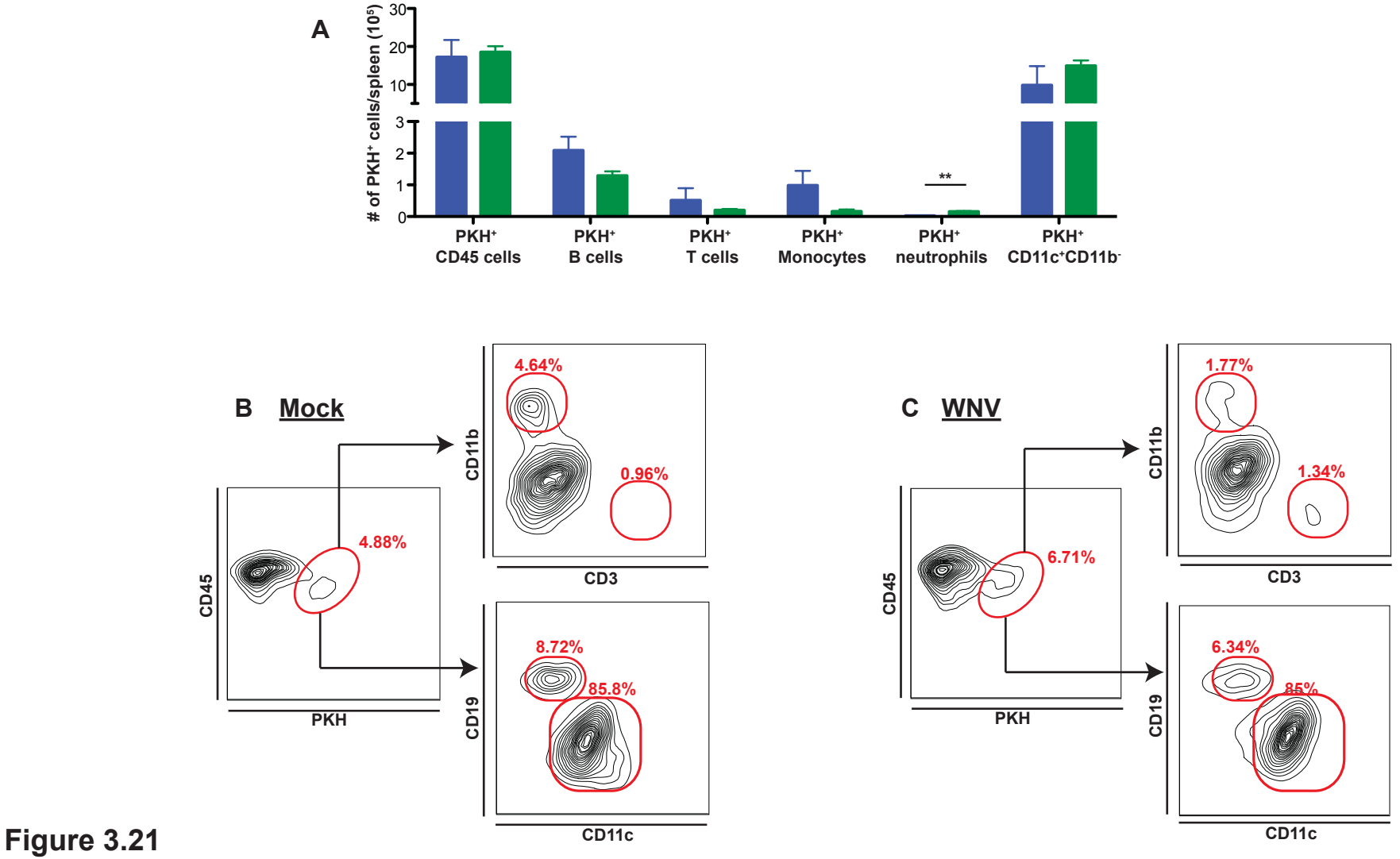
A
# of PKH+ cells/spleen (10^5)
30
20
10
3
2
1
0
**
PKH+ CD45 cells
PKH+ B cells
PKH+ T cells
PKH+ Monocytes
PKH+ neutrophils
PKH+ CD11c+CD11b-
B Mock
4.64%
0.96%
4.88%
CD11b
CD3
CD45
PKH
8.72%
85.8%
CD19
CD11c
C WNV
1.77%
1.34%
6.71%
CD11b
CD3
CD45
PKH
6.34%
85%
CD19
CD11c

Figure 3.21

Seven days following footpad injection, the majority of transferred cells in the PLN of mock- and WNV-infected mice were $CD3^+$ T cells (Figure 3.22A). Interestingly, this was also true for transferred cells migrating into the ILN of mock-infected mice (Figure 3.22B). Very few $CD45.1^+/CFSE^+$ cells could be detected in the ILN of WNV-infected mice at d7 p.i. However, transferred cells could be identified in the CLN of both WNV- and mock-infected mice and these were also identified as being mainly $CD3^+$ T cells (Figure 3.22C). No transferred cells could be detected in the CNS or spleen of mock- or WNV-infected mice (Data not shown). When enumerated (Figure 3.22D), there were increased numbers of transferred cells present in the mock-infected mice of all the nodes examined, compared to the WNV-infected counterpart. The highest number of transferred cells was isolated from the PLN and there was a 2-fold difference between the mock- and WNV-infected cohorts, although this was not significantly significant. On the other hand, the ILN had significantly more (7-fold) $CD45.1^+/CFSE^+$ cells in the mock-infected than WNV-infected node. In contrast, a comparable number of transferred cells were present in the mock- and WNV-infected CLN.

3.3. Discussion

The results from this chapter describe, for the first time, the manner in which CNS inflammation impacts on the cellularity of the draining as well as non-draining lymph nodes of the CNS during WNV encephalitis. Furthermore, these data corroborate published data supporting a role for the CLN in the lymphatic drainage of the CNS (Stern et al. 2014; Louveau et al. 2015). The dramatic expansion of cell numbers in the CLN early during the course of infection indicates that a level of "lymph node shutdown" is likely occurring. Furthermore, it seems that the rate of cellular recruitment, containment and proliferation in the CLN far exceeds the cells emigrating to the area of inflammation, as no reduction was seen in any of the leukocyte subsets analysed, except for T cells on d7 p.i.

Figure 3.22 Adoptive transfer of CD45.1$^+$ and CFSE$^+$ cells into the footpad of mock- and WNV-infected mice

Representative flow cytometry dot plots of leukocytes isolated from the PLN (A), ILN (B) and CLN (C) of mock- and WNV-infected ($6x10^4$ PFU) mice on d7 p.i. and 7 days after adoptive transfer. In panel A, the PLN of mice receiving adoptive transfer of cells (blue) is overlayed onto control non-injected (red) to illustrate the presence of CD45.1$^+$ and CFSE$^+$ adoptively transferred cells in the PLN. Graph D shows the number of adoptively transferred cells in the mock (blue) and WNV- (red) infected PLN, ILN and CLN. Control nodes receiving no cells are represented by the light blue (mock) and orange (WNV) columns.

Data are shown as the mean ±SEM of values from 2 independent experiments, with 2-3 mice/group in each experiment. Statistical analysis was conducted using one-way ANOVA with a Tukey's multiple comparison post-test, and $P \leq 0.05$*; $P \leq 0.01$**; $P \leq 0.001$***.

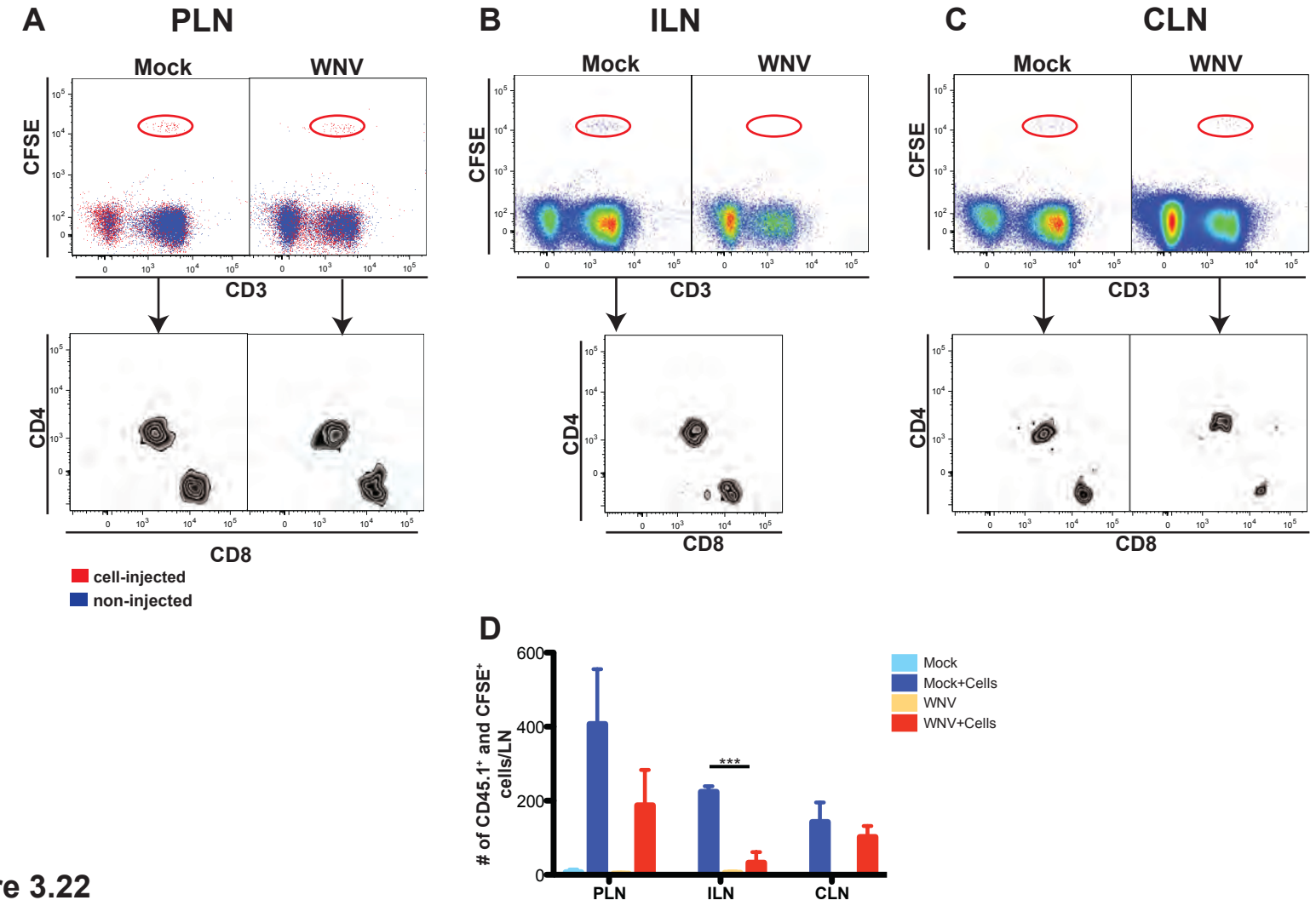
A
PLN
Mock
WNV
CFSE
CD3
CD4
CD8
cell-injected
non-injected
B
ILN
Mock
WNV
CFSE
CD3
CD4
CD8
C
CLN
Mock
WNV
CFSE
CD3
CD4
CD8
D
# of CD45.1+ and CFSE+ cells/LN
600
400
200
0
***
PLN
ILN
CLN
Mock
Mock+Cells
WNV
WNV+Cells

Figure 3.22

Considering the immune-mediated nature of disease, in particular the contribution of bone marrow-derived Ly6C^{hi} monocytes, we hypothesise that the intensity of the disease and immunopathology present, overtakes the ability of the CLN to provide a sufficient adaptive response to resolve infection (Getts et al. 2008), except where the immigration of these Ly6C^{hi} inflammatory monocytes into the CNS can be prevented (Getts et al. 2014). However, it is also possible for the CLN B and T cell response to add to the immunopathology and subsequent mortality present in WNV infection, as RAG KO mice (deficient in B and T cells) have longer MST as a result of reduced Ly6C^{hi} monocyte recruitment (Terry 2012). Furthermore, T cell-derived IFN plays a crucial role in the development of seizures during WNV encephalitis (Getts et al. 2007). Thus, the CLN response may contribute to the intensity of the pathological immune response during WNV encephalitis.

The significant expansion of CLN leukocytes likely occurred as a result of several variables, namely: APC draining from the CNS to the CLN; subsequent proliferation of resident cells in response to antigen presentation and the recruitment of additional cells, particularly naïve T cells, from the periphery. This study further examined the primary source of B and T cells in the CLN and CNS in this model of WNV encephalitis.

In addition to the inflammation-related changes occurring in the CLN, it was also evident that CNS infection and inflammation had an impact on the leukocyte composition of non-draining/peripheral lymph nodes. This was demonstrated by the significant reduction in the T cell numbers, as well as shifts in total leukocyte composition of the ILN and MLN during the course of infection. A few studies have identified changes in cell number and specificity of cells in the lymph nodes, not associated with drainage of the infected area (Ciabattini et al. 2010; Ciabattini et al. 2011). The i.v. adoptive transfer of CD8^{+} T cells into naïve mice prior to i.p. infection with lymphocytic choriomeningitis virus resulted in a

significant reduction in the number and frequency of transferred cells in the non-draining ILN. This occurred in contrast to a significant increase in the draining mediastinal lymph node. However, it should be noted that viral antigen was likely acquired in the ILN due to the systemic spread of virus (Olson et al. 2012).

Ciabattini et al. discovered the presence of primed and proliferative $CD8^+$ and $CD4^+$ T cells in the non-draining mesenteric and iliac nodes following i.n. immunisation with *Streptococcus gordonii* (Ciabattini et al. 2010). However, no evidence of clonal expansion could be detected in the non-draining lymph nodes in our model of i.n. WNV infection, whereas the draining CLN showed a marked increase in cellular replication. The extent to which cellular expansion in the CLN could be attributed to proliferation was studied with a BrdU incorporation assay, to determine whether DNA replication was occurring. The 6-fold expansion in leukocyte numbers of the CLN occurred in parallel to a 6-fold increase in proliferation, relative to baseline. This was also true for B cells, which had a ~15-fold increase in cell numbers and BrdU incorporation alike, compared to d0 p.i. T cell proliferation increased by 5-fold, relative to baseline levels, whilst cell numbers showed a ~50% increase, relative to d0 p.i. It may be that, although CLN T cell numbers do not reduce during infection, cells which are being supplied to the CNS are rapidly replaced by proliferating cells.

It is likely that an early rise in APC numbers in the CLN was due to cells draining from the focus of inflammation. Furthermore, it was clear that inflammatory signals modulating changes in the CLN differed from the signals present in the peripheral nodes (ILN and MLN), as no increased BrdU incorporation occurred in these nodes in response to CNS infection. Although there was a reduction in T cell proliferation in the ILN, this may have been a reflection of the significant reduction in T cell numbers in these nodes by d7 p.i. Whether the increased BrdU incorporation present in some of the leukocyte subsets in the MLN between d6-7p.i. was due to "real proliferation" remains unclear as this occurred at

the height of disease when peripheral organ failure and high rates of cell death were potentially underway. Although this was not directly measured, it seems unlikely that the MLN harboured live virus, as this was not seen in either the ILN or, more importantly, the CLN.

Further evidence for the impact of inflammation on the non-draining lymph nodes was identified in the dramatic alteration in levels of Ly6C expression in various leukocyte subsets during the course of infection, in both the draining and non-draining nodes. The role for Ly6C, a cell surface glycoprotein, is still being investigated and high expression of this marker is used in the identification of inflammatory monocytes (Getts et al. 2008; Sunderkotter et al. 2004). However, it is also expressed on B, $CD8^+$ and $CD4^+$ T cells and increased expression has been associated with the stimulation of T cell proliferation (Walunas et al. 1995; Yamanouchi et al. 1998; Dumont 1987; Wrammert et al. 2002). It has also been implicated as an accessory molecule for the CTL response, as mAb against Ly6C inhibited adhesion between effector and target cells, as well as IFN-γ production and subsequent lysis of target cells (Johnson et al. 1993). Moreover, Ly6C has been shown to increase T cell proliferation and IL-2 secretion. As opposed to the stimulatory role of Ly6C in $CD8^+$ T cells, it inhibits IL-2 secretion from Th1 $CD4^+$ T cells (Yamanouchi et al. 1998). In addition, Ly6C has been identified as a regulator of endothelial adhesion of $CD8^+$ T cells, as it induced the clustering of LFA-1. Evidently, Ly6C is important for the homing of T cells to the lymph node (Hanninen et al. 1997; Jaakkola et al. 2003). A study by Wrammert et al. demonstrated that B cell expression of Ly6C was restricted to plasma cells during steady state conditions and may be used as an additional criterion for plasma cell identification (Wrammert et al. 2002).

We performed a detailed analysis of the Ly6C expression on the various leukocyte subsets present in the CLN, ILN and MLN following lethal WNV infection. The characterisation of lymph node leukocyte subsets into Ly6C^{-}, Ly6C^{int} or Ly6C^{hi} yielded some interesting results. Although the majority of leukocyte populations in the CLN upregulated Ly6C expression in response to infection, certain subsets were clearly restricted in the extent to which they could express Ly6C. For example, CD4^{+} T cells were mainly Ly6C^{int}, even at the height of infection and level of Ly6C upregulation, whereas CD8^{+} T cells clearly possessed a distinct Ly6C^{hi} subset. Similarly, although B cells had significantly upregulated Ly6C expression, the majority of Ly6C^{+} cells were Ly6C^{int}, rather than Ly6C^{hi}. Furthermore, all other leukocyte subsets analysed, including DC and myeloid subsets, increased their expression of Ly6C, obtaining a Ly6C^{hi} phenotype. Notably, the response of the non-draining ILN and MLN was only evident 1-3 days after the CNS-draining CLN. This implies that some of the inflammatory signals modulating the CLN environment likely reached the non-draining nodes over time; however, the exact signals regulating the expression of Ly6C remains to be determined. The functional significance of this is still under investigation and could potentially yield valuable information in terms of understanding the impact of inflammation on the immune system as a whole. It is unlikely that Ly6C solely plays a role in cellular adhesion and migration processes, as lymphoid resident cells such as CD8α^{+} DC also showed increased expression of Ly6C.

A possibility for the disparity in Ly6C expression between B and CD8^{+} T cells, may be the differences in size *versus* the density of Ly6C on the surface of these cells. Nevertheless, in our model of i.n. WNV infection, the upregulation of Ly6C was a clear indicator of inflammation and, albeit CNS-infection-driven, may induce a certain level of activation in leukocytes throughout the lymphatic system in preparation for potential systemic spread of infection.

The presence of pathogen is known to trigger an inflammatory response in lymph nodes and considering the close anatomical relationship between the CNS and CLN it is possible for virus to reach the CLN and elicit an immune response. Furthermore, as the lymphatic system is a continuous network of vessels and nodes, it is also possible for virus to reach peripheral nodes via the circulatory or lymphatic system eliciting a response. Therefore, we analysed the viral RNA content in the CNS, CLN and ILN in order to establish whether any detectable virus was present. However, no virus could be detected in the draining CLN and it is likely that APC, draining from the local site of infection (CNS) to the CLN, presented processed antigen only, subsequently inducing proliferation of leukocytes in the CLN. The absence of virus in the ILN indicates that viral presence was not the primary signal stimulating the changes seen during inflammation. Interestingly, detectable virus was only identified in the CNS from d5 p.i., whereas obvious changes associated with inflammation occurred by d3 p.i. in the draining and non-draining lymph nodes. It is possible that low levels of viral replication or distribution of antigen-primed APC from the CNS or olfactory bulb, to the draining and non-draining nodes occurred. Previous studies from our lab have shown that viral levels in the peripheral organ such as, heart, lungs, kidneys etc. are present in levels less than 0.001% of those found in the brain (Terry 2012), during i.n. WNV infection, reducing the likelihood that APC cells draining from peripheral organs could account for the alteration in cellular composition and cell surface marker expression in the non-draining nodes. A more probable explanation is the transmission and circulation of a stimulus from the draining CLN or CNS to the peripheral nodes via the lymphatic and/or circulatory system. Inflammatory stimuli such as cytokines or chemokines produced by the infected CNS and released into the bloodstream clearly reach the bone marrow and, by inference, the peripheral lymph nodes via the circulatory system. Irrespective, this indicates the extent to which the immune system acts

as a large interconnected network, including the bone marrow, spleen and lymphatic system.

The significant reduction seen in the numbers of T cells in the ILN and MLN led to the hypothesis that T cells from peripheral nodes could traffic to the CLN and even the CNS, adding to the lymphocyte infiltrate. In an attempt to elucidate the ultimate destination of these peripheral T cells emigrating from the non-draining nodes, we attempted to track cells from the ILN and PLN, following lethal WNV infection.

Firstly, we established the extent to which cells, originating from a completely peripheral node distributed throughout the lymphatic system during homeostatic conditions. Secondly, we analysed in detail how this distribution changed during infection. A period of seven days was sufficient for PKH26 and/or cells labelled with PKH26, to move from the draining PLN to the contralateral PLN. Due to the small volume of dye injected and the anatomy of the lymphatic system, it was unlikely that this occurred through spread of free dye via the lymphatics, further than the PLN. In addition, the constant circulation of leukocytes throughout the lymphatic system during homeostatic conditions is a well-known phenomenon and is necessary for the continuous sampling of antigen in the body. Different lymphocyte subsets exhibit different rates of recirculation. $CD4^+$ T cells, followed by $CD8^+$T cells, exhibit the highest rate of turnover (~12h), which is turn followed by B cells, which are replaced within 24h. Indeed, ~70% of steady-state lymph node cells are replaced within 24 h and after 3 days equilibrium is reached throughout the lymphatic system (Tomura et al. 2008). Although, there were still $PKH26^+$ cells in the PLN after 7 days in our model, these were likely cells that incorporated the dye and did not recirculate.

The CLN had significantly more PKH26$^+$ leukocytes in WNV- than mock-infected mice. We hypothesised that this occurred as a direct result of increased recruitment of peripheral lymphocytes from non-draining nodes to the draining CLN during CNS infection. Nevertheless, this increased PKH26$^+$ cell number in the CLN was essentially limited to the B cell and pDC subsets, indicating that they may be recruited by similar signals. TLR-9 stimulation activates both B cells and pDC, however, this would require the presence of virus or pathogen-associated molecular patterns (Jiang et al. 2007; Montoya et al. 2006). Interestingly, the opposite was true for the ILN with fewer PKH26$^+$ B cells and pDC in the WNV- than mock-infected cohort, perhaps suggesting that these cells were bypassing or rapidly leaving the ILN during infectious circumstances, trafficking to the CLN. The PKH26$^+$ content of CD11b$^+$ DC and monocytes was relatively high in both the ILN and CLN, however this ratio did not increase as a result of infection. This highlights the migratory capacity of these subsets during homeostatic conditions throughout the lymphatic system. Interestingly, the contralateral PLN did not obtain the same numbers of PKH26$^+$ cells as the contralateral ILN or CLN in either mock- or WNV-infected cohorts, suggesting that the extent to which these cells are able to spread throughout the lymphatic system was somewhat limited.

Unfortunately, performing dye injection alone could not ultimately verify the migration of cells, rather than dye, from the PLN to the CLN and we were unable to prove that injection of dye did not impair migratory capacity of these cells. Furthermore, dye injection into the footpad raises the possibility that there may be increased cell death of dye$^+$ cells, however, we did not find any significant differences in numbers or percentage of dead cells in PLN that received dye and control PLN to support this. Thus, we designed a preliminary adoptive transfer experiment with cells obtained from mock-infected peripheral lymph nodes in order to clarify this issue. In both mock- and WNV-infected mice the adoptively

transferred cells in the PLN, ILN and CLN were identified as T cells, including $CD8^+$ and $CD4^+$ subsets. The only consistent finding with previous results was the fact that the number of adoptively transferred cells was reduced in the ILN of WNV-infected mice, compared to the mock-infected counterpart. Nevertheless, this study confirms the migration of cells from a peripheral node such as the PLN to the CLN is possible. However, it is likely that we transferred too few cells for detection in the CNS and follow up experiments are needed to conclusively say whether or not peripheral nodes can supply lymphocytes to the CNS. Interestingly, no B cells could be identified in the transferred cells from any of the lymph nodes, suggesting that B cells may not so easily migrate but prefer to proliferate *in situ.* In contrast, T cells likely migrate to the CLN rather than proliferate at the site of injection. Even so, these data provide evidence that the nature of the lymphatic system, associated with the CNS, is not limited to the draining CLN and that CNS inflammation can influence lymph nodes as far removed as the PLN, MLN and ILN.

4. CHAPTER 4 Spleen, WNV infection and IMP treatment

4.1. Introduction

The spleen is the largest secondary lymphoid organ and acts as a crucial phagocytic filter for the circulatory system, protecting the body from invading pathogens and disposing of apoptotic cells (Aichele et al. 2003; Miyake et al. 2007). This organ not only captures particulate antigen, including bacteria, but also removes non-biological nanoparticles present in circulation, in the marginal zone, the location of the MARCO^{+} marginal zone macrophages (Demoy et al. 1997; Demoy et al. 1999). Previous work from our laboratory has shown that Ly6C^{hi} inflammatory monocytes, recruited from the bone marrow to the CNS during WNV infection, significantly contribute to the immunopathology of WNV encephalitis (Getts et al. 2008; Getts et al. 2012). However, several studies have also implicated the spleen as a possible reservoir for these pathogenic Ly6C^{hi} monocytes (Bao et al. 2010; Leuschner et al. 2010).

This laboratory recently developed a treatment, the efficacy of which is primarily based on reducing Ly6C^{hi} inflammatory monocytes infiltrating into the CNS. The distribution of Ly6C^{hi} inflammatory monocyte numbers in the CNS occurred in conjunction with an increase of this subset in the spleen. This strongly suggests that these cells are diverted to and/or detained in the spleen, preventing their migration to the CNS, where they would otherwise have exerted their pathogenic action. This was supported by the distribution of IMP within the mouse as substantial numbers of IMP were found in the spleen, located primarily in the MZM, as well as in Ly6C^{hi} monocytes in the red pulp (Terry 2012; Getts et al. 2014). Thus, considering its prominent role as a filter for the blood, the spleen may be an ideal site for disposing of IMP, or cells that have phagocytosed IMP, and have subsequently travelled to the spleen, where they may be destroyed.

Therefore, to further expand our understanding of the role of the secondary lymphoid organs in CNS infection, we dissected the splenic response to WNV encephalitis. This included looking at changes in cellularity of the spleen, leukocyte composition and whether CNS infection could induce any proliferative changes in the spleen. We further investigated the potential role of the spleen as an additional source to the bone marrow, of the pathogenic Ly6C^{hi} inflammatory monocytes infiltrating the CNS. In addition, we examined the reaction to primary WNV infection in the absence of the spleen and looked at the subsequent development of immunity in splenectomised mice. Lastly, we further explore the role of the spleen in the efficacy of IMP treatment.

4.2. Results

4.2.1. Leukocyte dynamics in the spleen following lethal WNV infection

Chapter 3 demonstrated the significant impact of CNS infection on the draining and non-draining lymph nodes of the CNS following lethal WNV infection. In order to investigate whether or not this holds true for the spleen, we examined the changes in leukocyte number and composition in the spleen following lethal i.n. WNV infection ($6x10^4$ PFU) of female C57BL/6 mice. Note that a detailed flow cytometry gating strategy used for the spleen with isotype and fluorescence minus one controls, can be found in Appendix Figure 5 and 6. .

Total leukocyte (CD45$^+$) and B cell (B220$^+$/CD19$^+$) numbers remained stable throughout the 7-day course of infection and there was a slight, but non-significant, decrease in total T cell numbers (CD3$^+$) (Figure 4.1A). Furthermore, 50% of the spleen was comprised of B cells and this remained unchanged throughout the course of infection. However, there was

Figure 4.1 Cellularity of the spleen following lethal WNV infection- Total leukocyte, B, T cell and DC populations

Graph A shows the number of total leukocytes ($CD45^+$) (circle), B cells ($CD19^+/B220^+$) (triangle) and total T cells ($CD3^+$) (square) in the spleens of mice following lethal WNV infection ($6x10^4$ PFU) on day 0, 3, 5, 6 and 7 p.i. The percentage of B cells ($CD19^+/B220^+$) (triangle) and total T cells ($CD3^+$) (square) in the spleen of mice following lethal WNV infection ($6x10^4$ PFU) is represented by graph B. T cells were further classified into $CD4^+$ and $CD8^+$ subsets, with the number (C) and percentage (D) of $CD4^+$ (circle) and $CD8^+$ T (upside-down triangle) cells in the spleen following WNV infection. DC subsets were classified according to their differential CD11c and CD11b expression to give three subsets, namely $CD11c^+CD11b^+$ (square), $CD11c^+CD11b^-$ (circle) and $CD11c^{hi}CD11b^{int}$ (triangle). Graphs E and F shows the number and percentage change of these DC populations, respectively, following lethal WNV infection. Values of the above leukocyte subsets are expressed as a percentage of total leukocytes in the spleen of each cohort. Data are shown as the mean ±SEM of values from 3 independent experiments, with 3-4 mice/group in each experiment. Statistical analysis was conducted using one-way ANOVA with a Dunnet's multiple comparison post-test (d0 as control), and $P\leq0.05$*; $P\leq0.01$**; $P\leq0.001$***.

Figure 4.1 **Number and percentage of leukocytes/spleen**

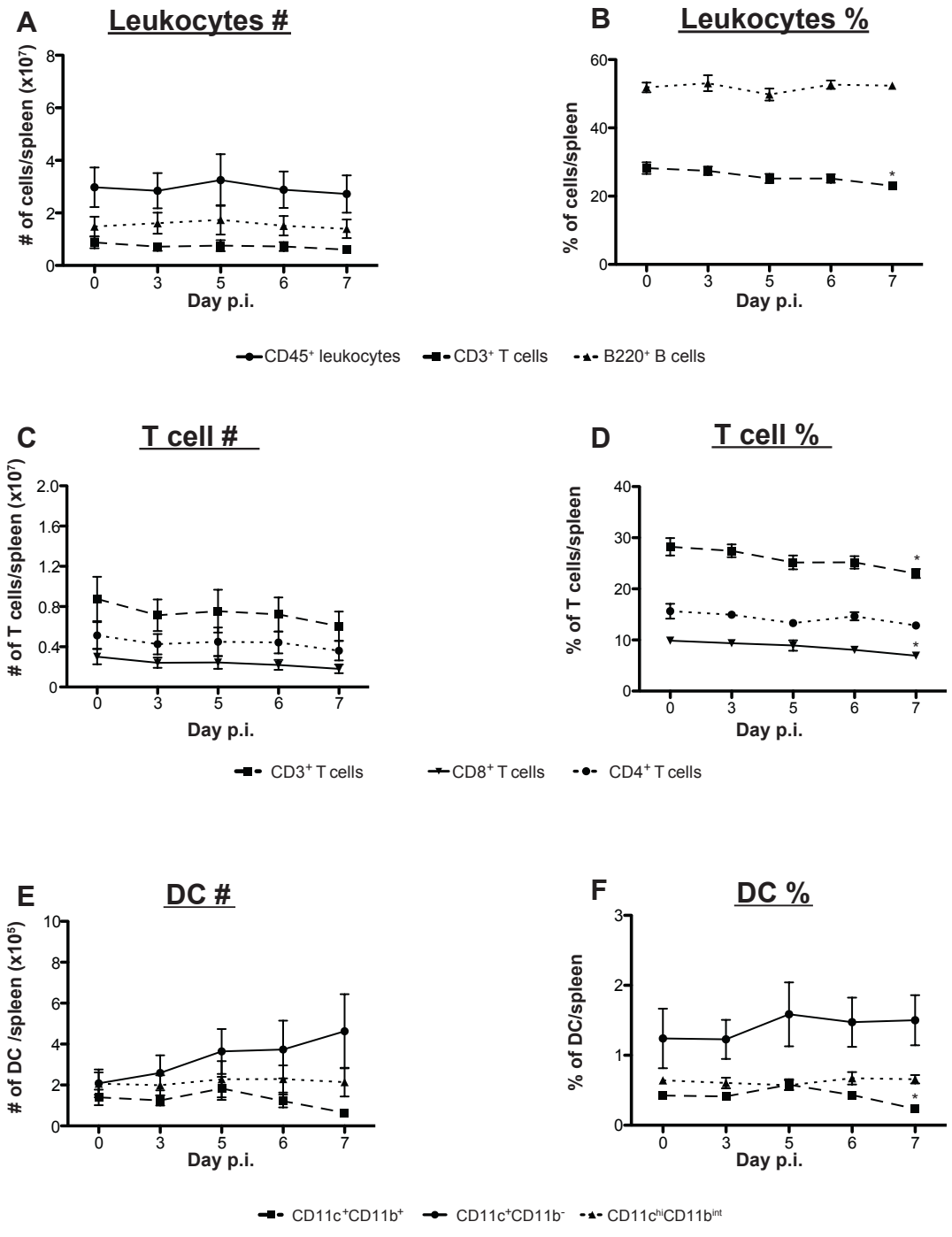

a 5% decrease in the percentage of $CD3^+$ T cells in the spleen by d7 p.i., relative to d0, which was statistically significant (Figure 4.1B). This was comprised of a decrease in the numbers of both $CD4^+$ and $CD8^+$ T cells, although not significant, these subsets had reduced by 30% and 40%, respectively, of the baseline value. Indeed, this accounted for the percentage decrease seen in the total T cell populations and was also evident in the reduction in percentage of both T cell subsets by d7 p.i., compared to d0 (Figure 4.1D).

The DC in the spleen were gated according to the same principles used for lymph node DC gating (Figure 3.5). The $CD11c^{hi}CD11b^{int}$ subset remained stable throughout the disease course, with no change in the numbers (Figure 4.1E) and percentages (Figure 4.1F) of this population. However, $CD11c^+CD11b^-$ numbers (Figure 4.1E) had doubled by d7 p.i., although, the proportion of this subset remained unchanged (Figure 4.1F). In contrast, numbers of the $CD11c^+CD11b^-$ DC (Figure 4.1E) subset had halved by d7p.i., with a significant reduction in percentage (Figure 4.1F) seen on d7p.i.

The $CD11b^+$ populations, namely monocytes ($CD11b^+CD11c^-Ly6G^-$) and neutrophils ($CD11b^{hi}Ly6G^+$), showed opposite responses in the spleen, following WNV infection. Monocyte numbers reduced by 50%, whereas neutrophil numbers doubled (Figure 4.2A) by d7 p.i., relative to d0. Moreover, the percentages (Figure 4.2B) of these subsets mirrored their changes in cell number, with percentage of monocytes in the spleen reducing by half and the percentage of neutrophils increasing significantly, from 1 to 2.7%, by d7 p.i. Neither the number (Figure 4.2C) nor the percentage (Figure 4.2D) of $NK1.1^+$ subsets, namely NK ($NK1.1^+CD3^-$) and NKT ($NK1.1^+CD3^+$) cells, showed significant change during the disease course.

Figure 4.2 Cellularity of the spleen following lethal WNV infection - $CD11b^+$ and $NK1.1^+$ populations

The number (A) and percentage (B) of monocytes ($CD11b^+CD11c^-$) (circle) and neutrophils ($CD11b^{hi}Ly6G^+$) (square) in the spleen, following lethal WNV infection ($6x10^4$ PFU) are shown on day 0, 3, 5, 6 and 7 p.i. Graphs C and D show the number (C) and percentage (D) change in $NK1.1^+$ subsets, including NK ($NK1.1^+CD3^-$) cells (circle) and NKT cells ($NK1.1^+CD3^+$) (square) in the spleen of WNV-infected mice on d0, 3, 5, 6 and 7 p.i. Values of $CD11b^+$ and $NK1.1^+$ subsets are expressed as a percentage of total leukocytes in the spleen in each cohort. Data are shown as the mean ±SEM of values from 3 independent experiments, with 3-4 mice/group in each experiment. Statistical analysis was conducted using one-way ANOVA with a Dunnet's multiple comparison post-test (d0 as control), and $P \leq 0.05$*; $P \leq 0.01$**; $P \leq 0.001$***.

Figure 4.2 **Number and percentage of leukocytes/spleen**

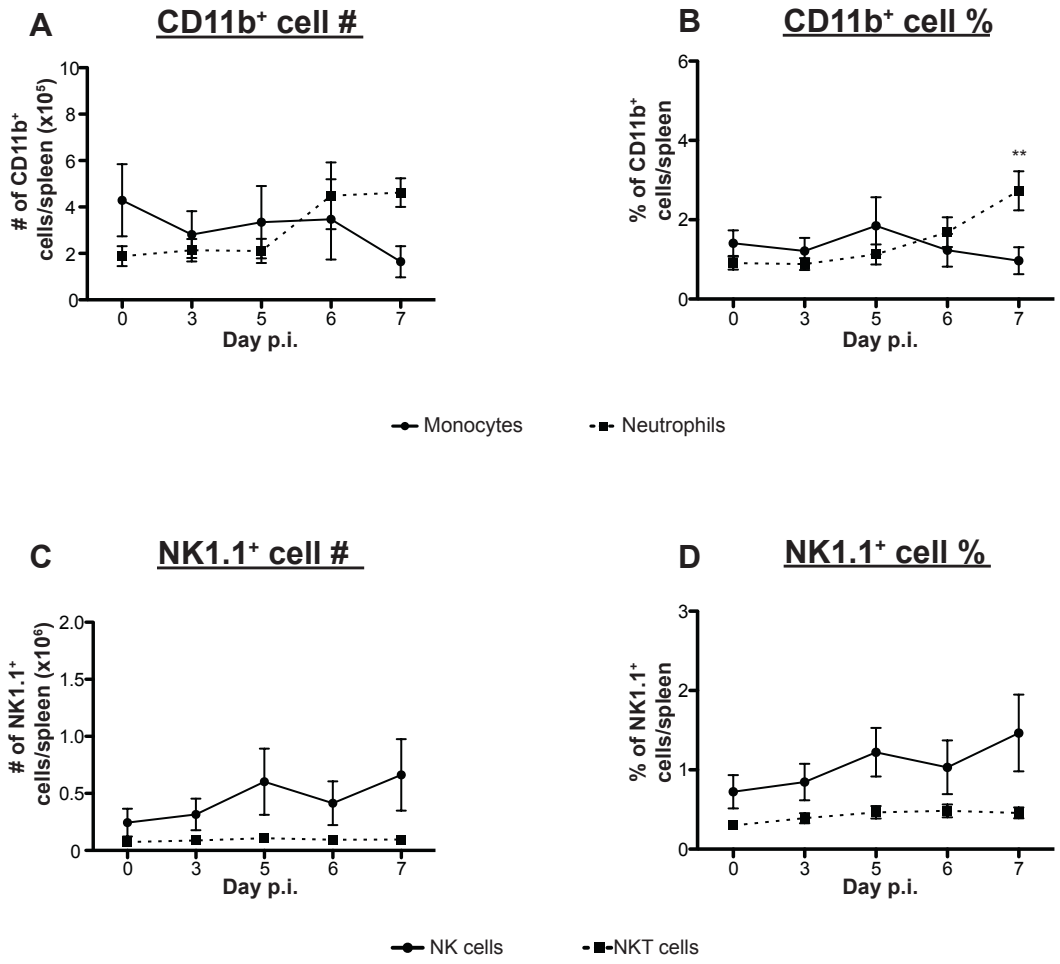

4.2.2. Changes in cell-surface marker expression in various leukocyte subsets of the spleen following lethal WNV infection

Significant upregulation of the cell-surface glycoprotein, Ly6C, was demonstrated in several of the leukocyte populations in the lymph nodes, following WNV infection. Review of the literature also indicated that Ly6C might play an important role in the mobilisation and activation of lymphocytes. Therefore, we analysed the expression of Ly6C in the various splenic leukocyte subsets to determine whether a similar pattern might be present here. Indeed, similar to lymph node data presented in the previous chapter, upregulation of Ly6C occurred in most of the leukocyte subsets analysed in the spleen by d7p.i. (Appendix figure 7), relative to baseline (d0), prompting us to investigate this in further detail.

Flow cytometry histograms demonstrated the expression of Ly6C on B (Figure 4.3A), $CD4^+$ (Figure 4.3D) and $CD8^+$ T cells (Figure 4.3G) on d0, 3, 5, 6 and 7 p.i. As previously seen in the lymph nodes, Ly6C expression marker upregulation was evident in subsets as early as d3p.i. As with the lymph nodes, we characterised these populations into $Ly6C^-$, $Ly6C^{int}$ and $Ly6C^{hi}$, based on FMO and isotype controls. The majority of the B (Figure 4.3C) cells were $Ly6C^-$ at d0p.i., with ~55% becoming $Ly6C^{int}$ by d7p.i., as reflected in the significant increase in $Ly6C^{int}$ B cell numbers (Figure 4.3B) from d5p.i. onwards, relative to d0p.i.

As in the lymph nodes, the $CD4^+$ subset (Figure 4.3F) consisted mainly of $Ly6C^-$ and $Ly6C^{int}$ populations, while the $CD8^+$ T cells were dispersed between $Ly6C^{hi}$, $Ly6C^{int}$ and $Ly6C^-$ populations (Figure 4.3I). In both $CD4^+$ (Figure 4.3E) and $CD8^+$ T cell (Figure 4.3H) subsets, the number of Ly6C-cells reduced significantly, from d3 p.i. onwards in the course of infection.

The upregulation of Ly6C in DC subsets in the spleen was evident from d3 p.i. (Figure 4.4A, D and G). Both the $CD11c^+CD11b^+$ (Figure 4.4C) and $CD11c^+CD11b^-$ (Figure 4.4I) DC

Figure 4.3 Differential Ly6C subsets in the B and T cell populations of the spleen of following lethal WNV infection

Representative flow cytometric histograms (A, D, G) illustrate the change in Ly6C expression of (A) B cells ($B220^{+}/CD19^{+}$), $CD4^{+}$ T cells (D) and $CD8^{+}$ T cells (G) in the spleen on d0, 3, 5, 6 and 7p.i. following lethal WNV infection ($6x10^{4}$ PFU) with isotype control (grey) and WNV infected sample (red). Flow cytometry contour plots C, F and I demonstrate the expression of Ly6C in these subsets in the spleen of WNV-infected mice ($6x10^{4}$ PFU) on d7p.i., compared to d0.

Leukocyte subsets in the spleen were thus characterised based on Ly6C expression as $Ly6C^{hi}$ (square), $Ly6C^{int}$ (triangle) or $Ly6C^{-}$ (circle). The number of $Ly6C^{hi/int/-}$ B cells (B) ($B220^{+}/CD19^{+}$), $CD4^{+}$ (E) and $CD8^{+}$ T (H) cells in the spleen on d0, 3, 5, 6 and 7p.i. following lethal WNV infection ($6x10^{4}$ PFU) are shown. Significance, compared to d0, for each subset was defined as follows: ***$Ly6C^{hi}$-; $^{+++}Ly6C^{int}$ and $^{ØØØ}Ly6C^{-}$.

Data are shown as the mean ±SEM of values from 3 independent experiments, with 3-4 mice/group in each experiment. Statistical analysis was conducted using one-way ANOVA with a Dunnet's multiple comparison post-test (d0 as control), and $Ly6C^{hi}$ =$P\leq0.05$*; $P\leq0.01$**; $P\leq0.001$***. $Ly6C^{int}$ =$P\leq0.05^{+}$; $P\leq0.01^{++}$; $P\leq0.001^{+++}$. $Ly6C^{-}$ =$P\leq0.05^{Ø}$; $P\leq0.01^{ØØ}$; $P\leq0.001^{ØØØ}$.

Figure 4.3

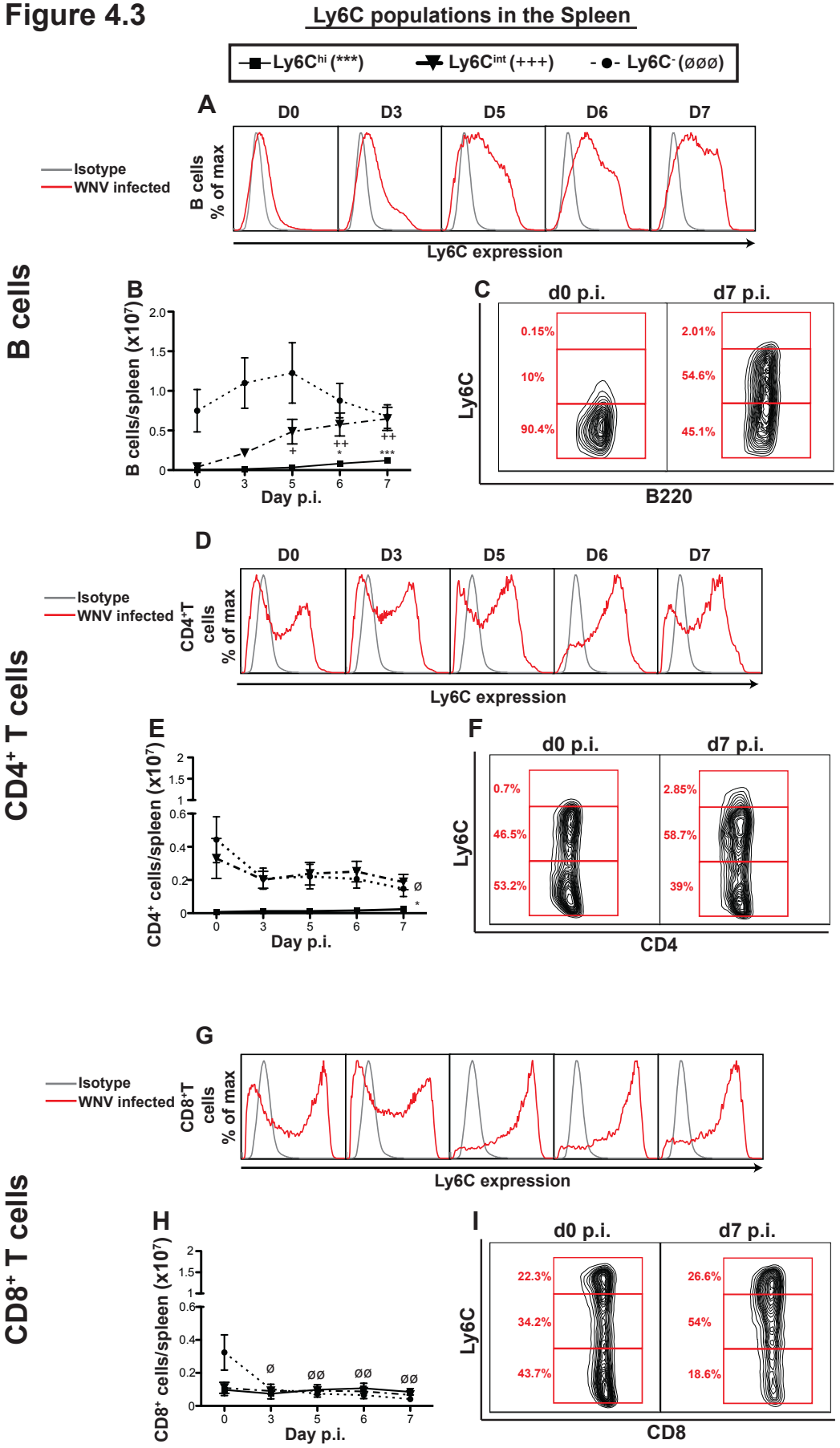
Ly6C populations in the Spleen
Ly6Chi (***)
Ly6Cint (+++)
Ly6C- (øøø)
A
D0
D3
D5
D6
D7
Isotype
WNV infected
B cells
% of max
Ly6C expression
B cells
B
B cells/spleen (x10⁷)
Day p.i.
C
d0 p.i.
d7 p.i.
0.15%
10%
90.4%
2.01%
54.6%
45.1%
Ly6C
B220
CD4⁺ T cells
D
CD4⁺T cells
% of max
Ly6C expression
E
CD4⁺ cells/spleen (x10⁷)
Day p.i.
F
d0 p.i.
d7 p.i.
0.7%
46.5%
53.2%
2.85%
58.7%
39%
Ly6C
CD4
CD8⁺ T cells
G
CD8⁺T cells
% of max
Ly6C expression
H
CD8⁺ cells/spleen (x10⁷)
Day p.i.
I
d0 p.i.
d7 p.i.
22.3%
34.2%
43.7%
26.6%
54%
18.6%
Ly6C
CD8

Figure 4.4 Differential Ly6C subsets in the DC populations of the spleen of following lethal WNV infection

Representative flow cytometric histograms (A, D, G) illustrate the change in Ly6C expression of (A) $CD11c^{+}CD11b^{+}$ DC, $CD11c^{hi}CD11b^{int}$ DC (D) and $CD11c^{+}CD11b^{-}$ DC (G) in the spleen on d0, 3, 5, 6 and 7p.i. following lethal WNV infection ($6x10^{4}$ PFU) with isotype control (grey) and WNV infected sample (red). Flow cytometry contour plots C, F and I demonstrate the expression of Ly6C in the spleen of WNV-infected mice ($6x10^{4}$ PFU) on d7p.i., compared to d0 in $CD11c^{+}CD11b^{+}$ DC (C), $CD11c^{hi}CD11b^{int}$ DC (F) $CD11c^{+}CD11b^{-}$ DC and (I).

Leukocytes subsets in the spleen were further characterised based on Ly6C expression as $Ly6C^{hi}$ (square), $Ly6C^{int}$ (triangle) or $Ly6C^{-}$ (circle). The number of $Ly6C^{hi/int/-}$ $CD11c^{+}CD11b^{+}$ DC (B), $CD11c^{hi}CD11b^{int}$ DC (E) and $CD11c^{+}CD11b^{-}$ DC (H) in the spleen on d0, 3, 5, 6 and 7p.i. following lethal WNV infection ($6x10^{4}$ PFU) are shown. Significance, compared to d0, for each subset was defined as follows: $^{***}Ly6C^{hi}$-; $^{+++}Ly6C^{int}$ and $^{ØØØ}Ly6C^{-}$.

Data are shown as the mean ±SEM of values from 3 independent experiments, with 3-4 mice/group in each experiment. Statistical analysis was conducted using one-way ANOVA with a Dunnet's multiple comparison post-test (d0 as control), and $Ly6C^{hi}$ =$P\leq0.05^{*}$; $P\leq0.01^{**}$; $P\leq0.001^{***}$. $Ly6C^{int}$ =$P\leq0.05^{+}$; $P\leq0.01^{++}$; $P\leq0.001^{+++}$. $Ly6C^{-}$ =$P\leq0.05^{Ø}$; $P\leq0.01^{ØØ}$; $P\leq0.001^{ØØØ}$.

Figure 4.4

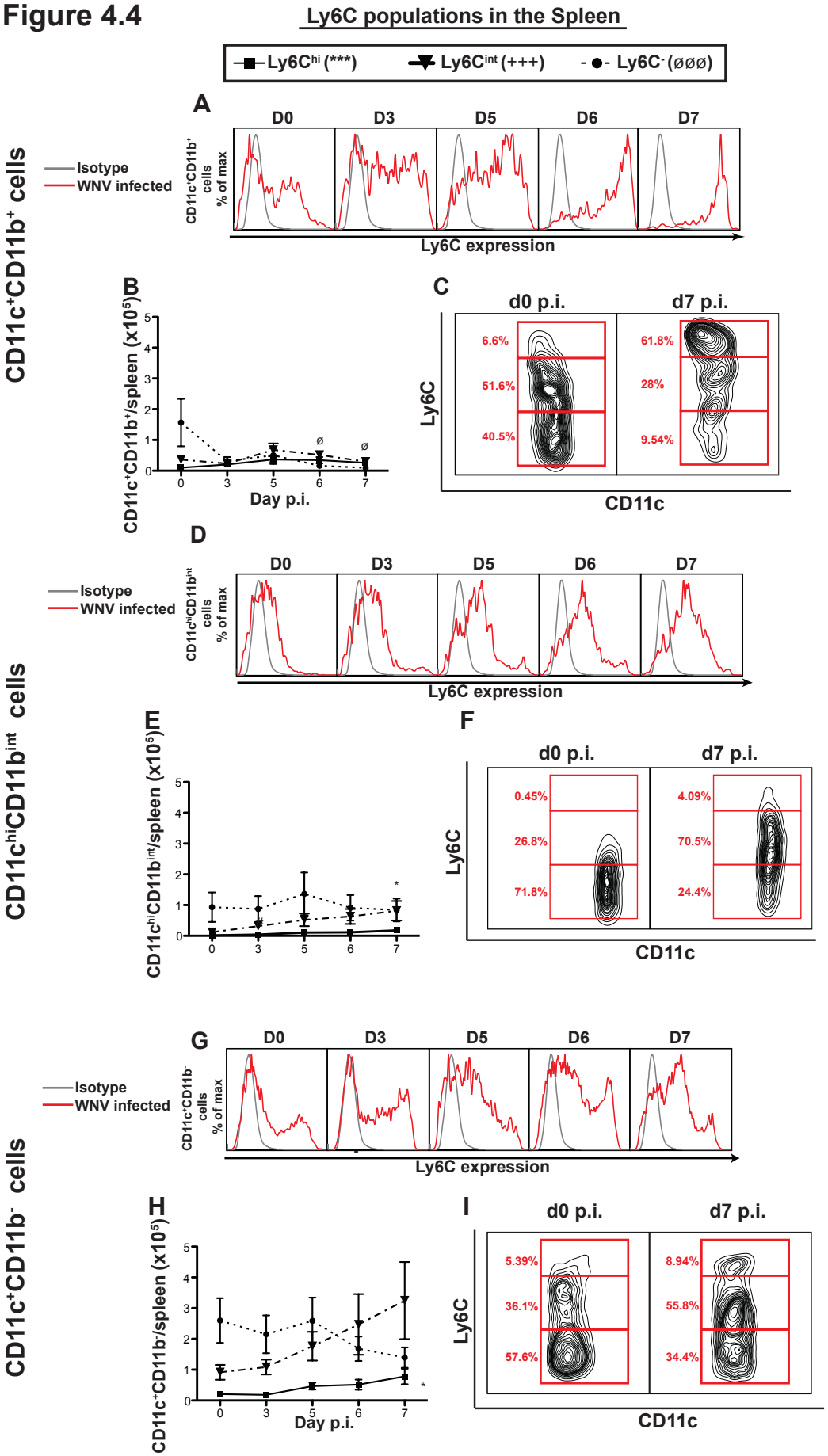
Ly6C populations in the Spleen
Ly6Chi (***)
Ly6Cint (+++)
Ly6C- (øøø)
CD11c+CD11b+ cells
Isotype
WNV infected
A
D0
D3
D5
D6
D7
CD11c+CD11b+ cells % of max
Ly6C expression
B
CD11c+CD11b+/spleen (x10^5)
Day p.i.
C
d0 p.i.
d7 p.i.
6.6%
51.6%
40.5%
61.8%
28%
9.54%
Ly6C
CD11c
CD11c^hiCD11b^int cells
D
CD11c^hiCD11b^int cells % of max
E
CD11c^hiCD11b^int/spleen (x10^5)
F
0.45%
26.8%
71.8%
4.09%
70.5%
24.4%
CD11c+CD11b- cells
G
CD11c+CD11b- cells % of max
H
CD11c+CD11b-/spleen (x10^5)
I
5.39%
36.1%
57.6%
8.94%
55.8%
34.4%

subsets had developed distinct Ly6C^{-}, Ly6C^{int} and Ly6C^{hi} populations by d7 p.i., while the CD11c^{hi}CD11b^{int} DC (Figure 4.4F) mainly showed an increase in Ly6C^{int} cells. The numbers of Ly6C^{-} CD11c^{+}CD11b^{+} cells (Figure 4.4B) had reduced significantly by d6-7 p.i., relative to d0. Enumeration of the CD11c^{hi}CD11b^{int} DC subset showed a significant increase in the number of Ly6C^{hi} CD11c^{hi}CD11b^{int} DC (Figure 4.4E) by d7p.i., relative to d0. Moreover, numbers of Ly6C^{hi} CD11c^{+}CD11b^{-} cells (Figure 4.4.H) increased significantly by d7 p.i.

The CD11b^{+} subsets in the spleen, including neutrophils (Figure 4.5A) and monocytes (Figure 4.5B), expressed relatively high levels of Ly6C, at d0, remaining Ly6C^{int} and Ly6C^{hi}, respectively, throughout the disease course. Numbers of Ly6C^{-} and Ly6C^{int} monocytes (Figure 4.5E) decreased significantly by d7p.i., relative to day 0. Similar to the CD11b^{+} subsets, the NK1.1^{+} subsets, namely NK (Figure 4.5G) and NKT cells (Figure 4.5H), expressed relatively high levels of Ly6C at d0p.i., however, numbers of cells expressing Ly6C^{int} and Ly6C^{hi} increased during infection. This was more distinct in the NKT cell subsets, with the majority of NKT cells becoming Ly6C^{hi} or Ly6C^{int} by d7p.i. Notwithstanding, changes in numbers of Ly6C^{hi}, Ly6C^{int} and Ly6C^{-} NK (Figure 4.5I) and NKT cells (Figure 4.5K) were non-significant.

4.2.3. Proliferation of leukocyte subsets in the spleen following lethal WNV infection

We hypothesised that, although changes in cell numbers in the spleen during infection were small, inflammation may have an impact on the rate at which cells replicate in this organ. The same BrdU incorporation assay, used to determine proliferation in lymph nodes, was applied to the spleen and results displayed as percentage change relative to baseline i.e. d0 p.i. Supporting the stable cell numbers during infection, there was little

Figure 4.5 Differential Ly6C subsets in the CD11b^{+} and NK1.1^{+} populations of the spleen of following lethal WNV infection

Representative flow cytometric histograms (A, B, G, H) illustrate the change in Ly6C expression of (A) neutrophils, monocytes (B), NK cells G) and NKT cells (H) in the spleen on d0, 3, 5, 6 and 7p.i. following lethal WNV infection ($6x10^4$ PFU) with isotype control (grey) and WNV infected sample (red). Flow cytometry contour plots D, F, J and L demonstrate the upregulation of Ly6C in the spleen of WNV-infected mice ($6x10^4$ PFU) on d7p.i., compared to d0 in neutrophils (D), monocytes (F), NK cells (J) and NKT cells (L).
Leukocytes subsets in the spleen were further characterised based on Ly6C expression as Ly6C^{hi} (square), Ly6C^{int} (triangle) or Ly6C^{-} (circle). The number of Ly6C$^{hi/int/-}$ neutrophil (C), monocytes (E), NK cells (I) and NKT cells (K) in the spleen on d0, 3, 5, 6 and 7p.i. following lethal WNV infection ($6x10^4$ PFU) are shown. Significance, compared to d0, for each subset was defined as follows: ***Ly6C^{hi}-; $^{+++}$Ly6C^{int} and ^{øøø}Ly6C^{-}.
Data are shown as the mean ±SEM of values from 3 independent experiments, with 3-4 mice/group in each experiment. Statistical analysis was conducted using one-way ANOVA with a Dunnet's multiple comparison post-test (d0 as control), and Ly6C^{hi} =P≤0.05*; P≤0.01**; P≤0.001***. Ly6C^{int} =P≤0.05^{+}; P≤0.01^{++}; P≤0.001^{+++}. Ly6C^{-} =P≤0.05^{ø}; P≤0.01^{øø}; P≤0.001^{øøø}.

Figure 4.5

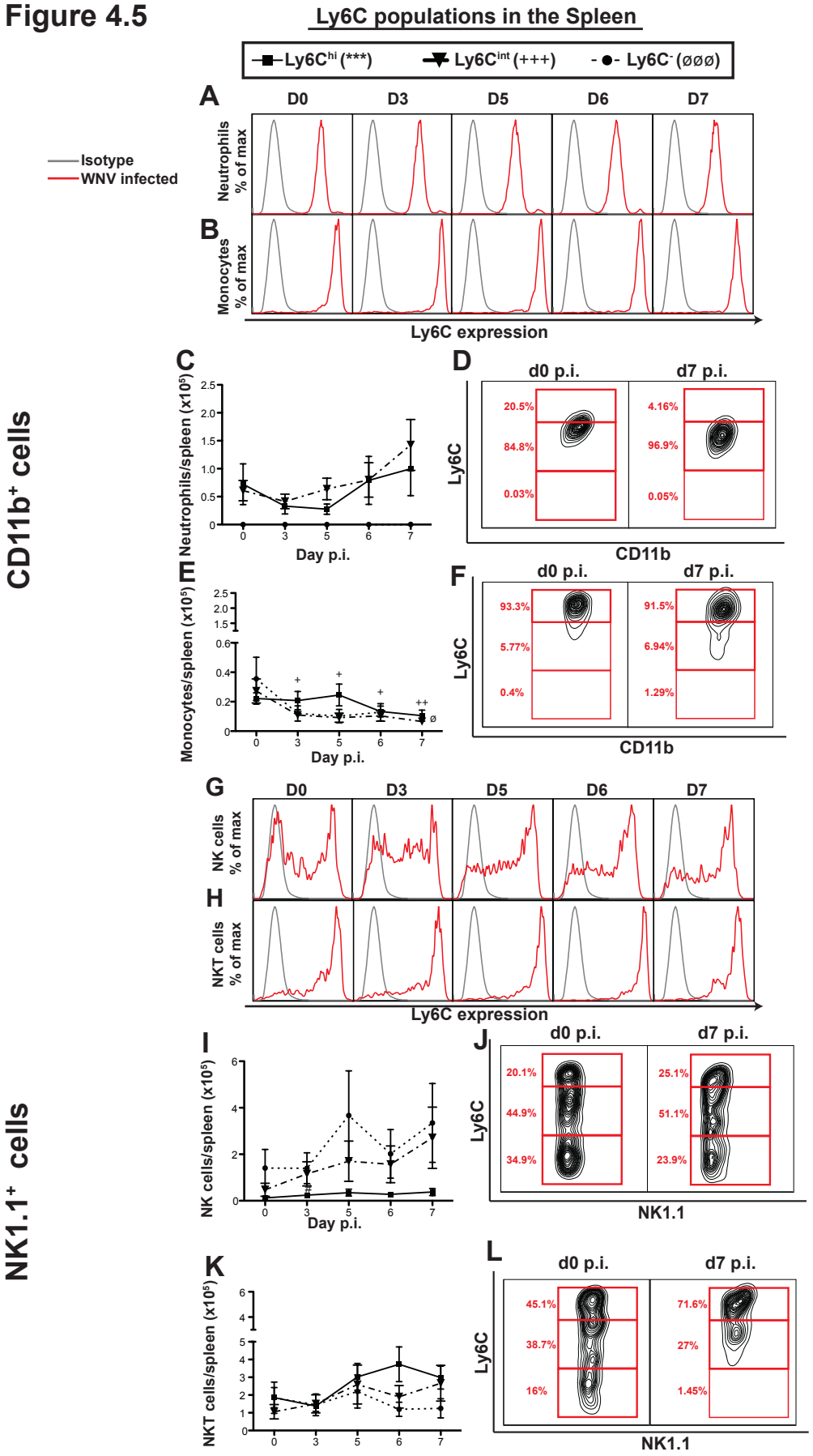
Ly6C populations in the Spleen
Ly6Chi (***)
Ly6Cint (+++)
Ly6C- (øøø)
Isotype
WNV infected
CD11b+ cells
NK1.1+ cells
A
B
D0
D3
D5
D6
D7
Neutrophils % of max
Monocytes % of max
Ly6C expression
C
D
E
F
Neutrophils/spleen (x10⁵)
Monocytes/spleen (x10⁵)
Day p.i.
d0 p.i.
d7 p.i.
20.5%
84.8%
0.03%
4.16%
96.9%
0.05%
93.3%
5.77%
0.4%
91.5%
6.94%
1.29%
Ly6C
CD11b
G
H
I
J
K
L
NK cells % of max
NKT cells % of max
NK cells/spleen (x10⁵)
NKT cells/spleen (x10⁵)
20.1%
44.9%
34.9%
25.1%
51.1%
23.9%
45.1%
38.7%
16%
71.6%
27%
1.45%
NK1.1

evidence of increased BrdU incorporation in any of the cell subsets analysed in the spleen following WNV infection (Figure 4.6A-E).

4.2.4. WNV infection and CNS infiltration in the absence of the spleen

4.2.4.1. Leukocyte infiltration

The spleen plays a crucial role in mounting an effective primary immune response against peripheral bacterial and parasitic. However, there is little information on the role of the spleen in immune responses against a CNS viral infection, or for that matter, in supplying the pathogenic component of this disease, the Ly6C^{hi} inflammatory monocytes. Thus, with a view to establish the extent to which the spleen may be involved in the lethal response found in WNV encephalitis, we used the i.n. model of WNV infection in mice that had their spleen surgically removed. Splenectomised female C57BL/6 mice (7-week old) were allowed to recuperate for 2 weeks, prior to i.n. infection with WNV at 9-11 weeks of age (Reeves et al. 2001). For a detailed gating strategy of the CNS with isotype and fluorescence minus one controls, refer to Appendix Figure 8 and 9.

The resultant changes in CNS cell numbers, following WNV infection of splenectomised mice are shown in Figure 4.7A and B. There was a distinct trend of reduced infiltration of leukocytes into the CNS of splenectomised mice (green), compared to mice that had their spleens intact i.e., normal (blue) mice. Normal, WNV-infected mice had significant infiltration of leukocytes into the CNS, compared to mock-infected mice (grey). There were no differences in CNS leukocyte numbers between mock-infected, normal mice *versus* splenectomised, mock-infected mice (data not shown), thus only normal mock-infected cohort is presented. The largest infiltrating population in all WNV-infected cohorts (splenectomised and normal) consisted of the Ly6C^{hi} inflammatory macrophages (Figure

Figure 4.6 Proliferation of various leukocyte subsets in the spleen, following lethal WNV infection

Graph A represents the percentage change, relative to d0p.i., in BrdU incorporation of the total leukocyte population ($CD45^+$) (circle), B ($B220^+/CD19^+$)(triangle) and total T ($CD3^+$) (square) cells, with graph B demonstrating the percentage change of the $CD4^+$ (circle) and $CD8^+$ (upside-down triangle) T cell subsets. Proliferation of the various DC subsets, namely: $CD11c^+CD11b^+$ (square), $CD11c^{hi}CD11b^{int}$ (triangle) and $CD11c^+CD11b^-$ (circle) is demonstrated by figure C. The percentage change in BrdU incorporation of the $CD11b^+$ $CD11c^-$ subsets, namely: monocytes ($CD11b^+Ly6G^-$) (circle) and neutrophils ($CD11b^{hi}$ $Ly6G^+$) is represented by graph D, with the proliferation of the two $NK1.1^+$ subsets namely: NK cells ($NK1.1^+CD3^-$) (circle) and NKT cells ($NK1.1^+CD3^+$)(square) represented by graph E. Proliferation was quantified with a BrdU incorporation assay and subsequent analysis of $BrdU^+$ cells. Grouped data were normalised using d0 as internal control and is represented as percentage change compared to baseline i.e. d0 p.i. (100%). Data are shown as the mean ±SEM of values from 3 independent experiments, with 3-4 mice/group in each experiment. Statistical analysis was conducted using one-way ANOVA with a Dunnet's multiple comparison post-test (d0 as control), and $P \leq 0.05$*; $P \leq 0.01$**; $P \leq 0.001$***.

Figure 4.6 **Proliferation of Splenic leukocytes**

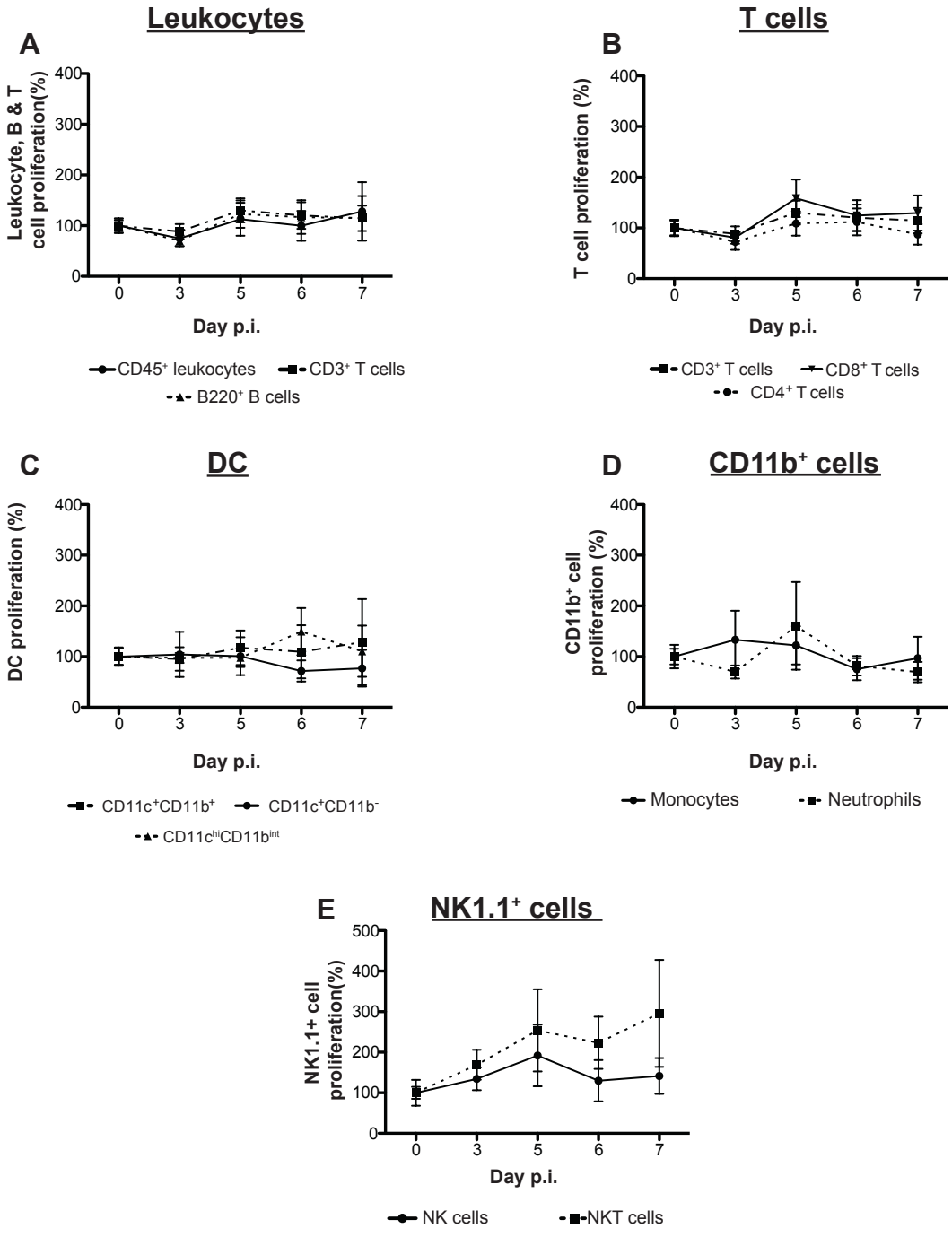

Figure 4.7 Leukocyte infiltration into the CNS of normal *versus* splenectomised mice following lethal WNV infection

Panel A represents the change in number of total leukocytes ($CD45^+$), including resident microglia ($CD11b^+Ly6C^-$) and the $CD11b^+Ly6C^+$ subset, which was further phenotypically characterised as inflammatory macrophages ($CD11b^+Ly6C^{hi}$) and an immigrant/activated microglia ($CD11b^+Ly6C^{int}$) population in mock-infected (grey), WNV-infected (blue) and WNV-infected, splenectomised mice (green). Panel B represents the change in number of neutrophils ($CD11b^{hi}Ly6G^+$) and lymphoid cells, including T cells ($CD3^+$), NK cells ($NK1.1^+$) and B ($B220^+$) cells in the CNS of mock-infected (grey), WNV-infected (blue) and WNV-infected+splenectomised mice (green). Data are shown as the mean ±SEM of values from 3 independent experiments, with 3-4 mice/group in each experiment. Statistical analysis was conducted using one-way ANOVA with a Tukey's multiple comparison post-test, and $P \leq 0.05$*; $P \leq 0.01$**; $P \leq 0.001$***.

Figure 4.7 Number of leukocytes/CNS

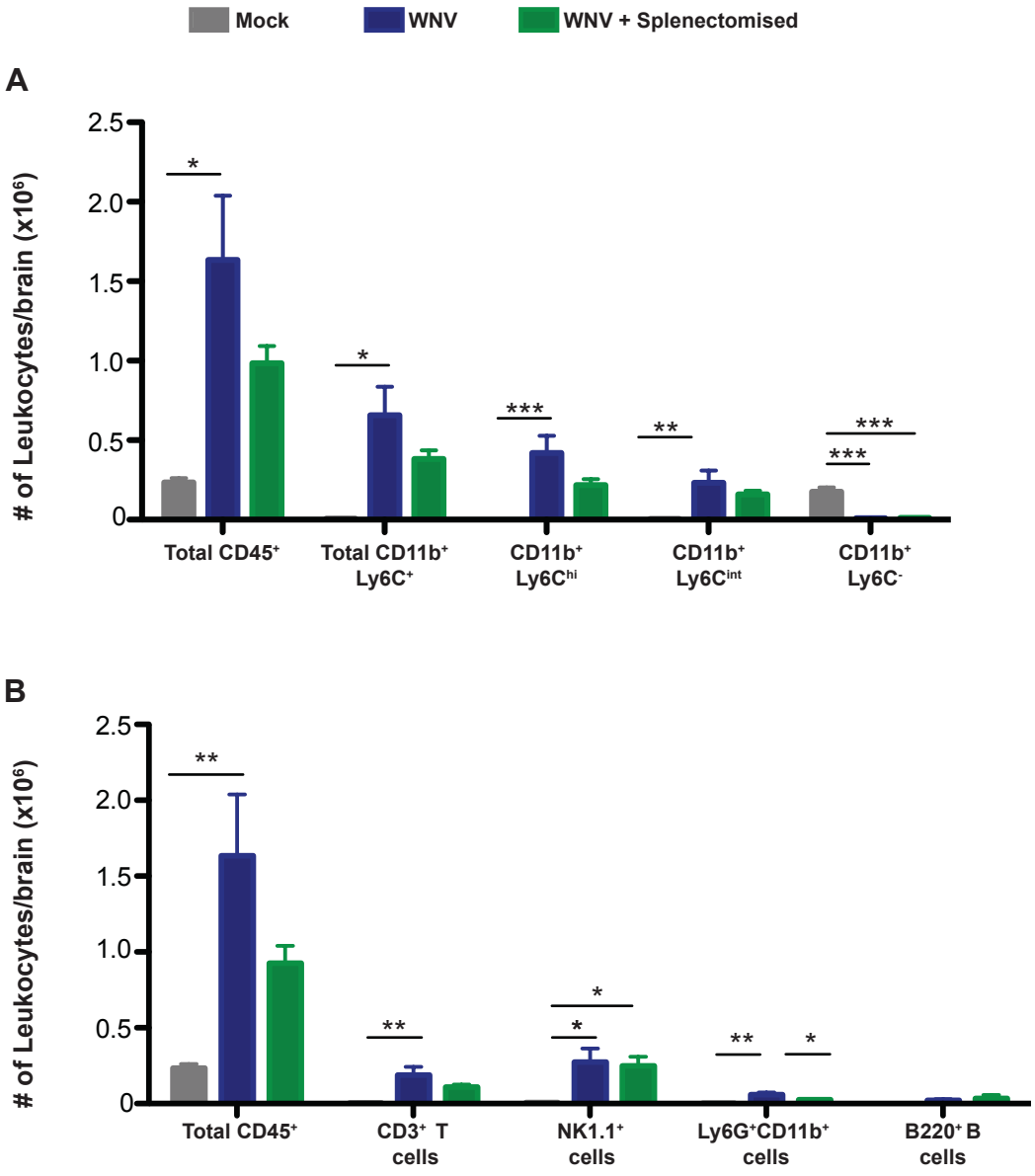

4.7A), followed by the $CD11b^{+}Ly6C^{int}$ immigrant/activated microglia population. Compared to mock-infected mice, there was a reduction in $Ly6C^{-}$ resident microglia following infection, as a proportion of these microglia likely upregulated their Ly6C expression becoming $Ly6C^{int}$. Although a similar pattern of myeloid cell infiltration was present in splenectomised animals, the numbers were reduced compared to normal, WNV-infected mice and not significantly increased relative to mock-infected mice.

Lymphoid lineage cell numbers were also affected in the absence of the spleen, as splenectomised mice had fewer $CD3^{+}$ T cells than normal, WNV-infected mice (Figure 4.7B). In addition, neutrophil infiltration was also decreased. There were comparable numbers of NK cells in the CNS of WNV-infected, normal and splenectomised mice, with both cohorts demonstrating significantly increased numbers of NK cells compared to mock-infected mice. B cells were present in relatively low numbers in the CNS of both normal and splenectomised, WNV-infected mice and there were no significant differences between groups.

4.2.4.2. Percentages

As there was a clear trend for splenectomised mice to have reduced infiltration into the CNS, we examined whether this affected the leukocyte composition of cells infiltrating the WNV-infected CNS. The percentages of various leukocyte subsets in the CNS of WNV-infected, splenectomised (green) mice were compared to the normal, WNV-infected cohort (blue) and normal mock-infected cohort (grey) (Figure 4.8A and B). There were negligible differences in the percentages of $CD11b^{+}Ly6C^{hi}$, $CD11b^{+}Ly6C^{int}$ and $CD11b^{+}Ly6C^{-}$ cells between WNV-infected, normal *versus* splenectomised mice. This indicates that the spleen did not significantly modulate the type of monocyte subset infiltrating the CNS in this model of WNV encephalitis. As expected the, $CD45^{+}$ population in the mock-infected brain

Figure 4.8 Percentage composition of leukocyte subsets infiltrating the CNS of normal *versus* splenectomised mice, following lethal WNV infection

Panel A represents the percentage of resident microglia ($CD11b^{+}Ly6C^{-}$) and the $CD11b^{+}Ly6C^{+}$ subset, which was further phenotypically characterised as inflammatory macrophages ($CD11b^{+}Ly6C^{hi}$) and an immigrant/activated microglia ($CD11b^{+}Ly6C^{int}$) population in mock-infected (grey), WNV-infected (blue) and WNV-infected, splenectomised mice (green). Panel B represents the percentage of neutrophils ($CD11b^{hi}Ly6G^{+}$) and lymphoid lineage cells, including T cells ($CD3^{+}$), NK cells ($NK1.1^{+}$) and B ($B220^{+}$) cells in the CNS of mock-infected (grey), WNV-infected (blue) and WNV-infected, splenectomised mice (green). Percentages of various subsets are expressed as a percentage of total leukocytes in the CNS of each cohort. Data are shown as the mean ±SEM of values from 3 independent experiments, with 3-4 mice/group in each experiment. Statistical analysis was conducted using one-way ANOVA with a Tukey's multiple comparison post-test, and $P \leq 0.05$*; $P \leq 0.01$**; $P \leq 0.001$***.

Figure 4.8 Percentage of leukocyte/CNS

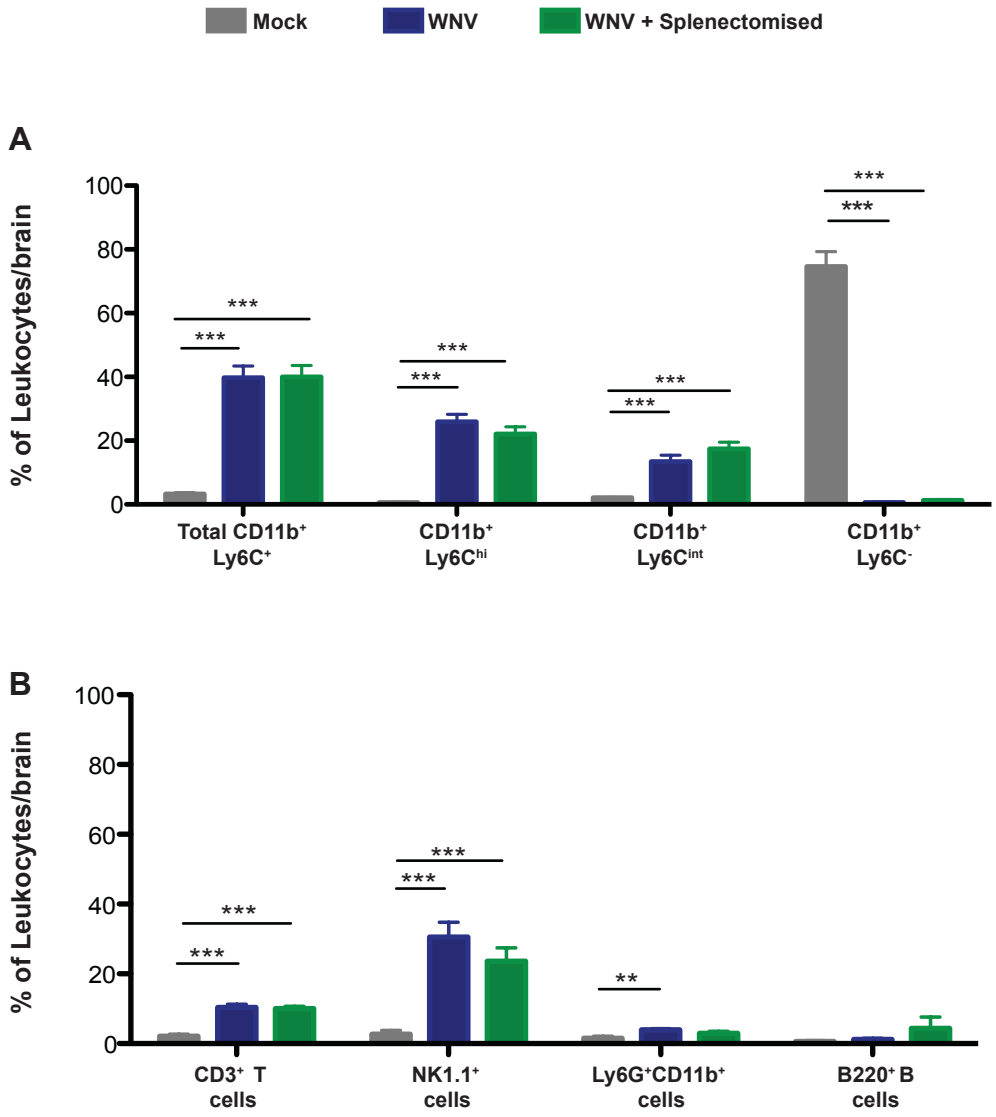

was comprised mainly of $CD11b^{+}Ly6C^{-}$ resident microglia. Both the $CD11b^{+}Ly6C^{hi}$ and $CD11b^{+}Ly6C^{int}$ subsets were increased significantly, compared to mock-infected, and formed 30% and 20%, respectively, of the total leukocyte population in the CNS in both normal and splenectomised cohorts (Figure 4.8A).

Lymphoid lineage cells, such as T and NK cells were distributed in similar fractions in the WNV-infected, normal and splenectomised mice, and were in both cohorts significantly higher than mock-infected mice (Figure 4.8B). Neutrophils contributed to a smaller proportion of leukocytes in the CNS of splenectomised mice than normal mice during WNV encephalitis. Finally, a higher percentage of B cells was present in the inflamed CNS of splenectomised mice, although this was not significant. Both splenectomised and normal, WNV-infected mice had higher percentage of B cells and neutrophils present in the leukocyte population of the CNS than the mock-infected cohort.

4.2.4.3. Weight loss of normal and splenectomised mice following lethal WNV infection

Average weight loss, compared to original weight, was used as a further comparison of disease model between normal and splenectomised animals (Figure 4.9A). C57BL/6 female mice were infected with lethal dose WNV ($6x10^{4}$ PFU) and weighed daily from d0p.i. until the end of disease course on d7 p.i. Firstly, as expected, mock-infected mice (grey) had no significant weight loss at any point during the disease course. Furthermore, both splenectomised and normal, WNV-infected mice started to have significant weight loss from d6p.i., which continued to worsen until d7 p.i. By d7p.i., both normal and splenectomised, WNV-infected cohorts had lost on average 18% of their original weight. Therefore, the normal and splenectomised mice had developed comparable forms of disease following both lethal dose of WNV infection.

Figure 4.9 Survival and average weight loss of naïve normal *versus* splenectomised mice, following WNV infection

Graph A represents the average percentage weight loss, compared to original weight, of mock- (grey) and WNV-infected (blue) *versus* WNV-infected, splenectomised (green) mice following lethal WNV infection ($6x10^4$PFU), from d0-7 p.i. Graph B demonstrates the survival rate of WNV-infected (blue) *versus* WNV-infected, splenectomised (green) mice, following infection with LD50 dose of WNV ($6x10^3$ PFU), from d0-d25 p.i. Graphs C and D show the percentage weight loss of normal and splenectomised mice, respectively, infected with LD50 dose of WNV ($6x10^3$ PFU), from d0-17p.i. Note that graphs C and D are representative of 4 independent experiments, thus, the percentage survival here, may not reflect the average of all four experiments combined, seen in figure B.
The survival study (B) was performed in four separate experiments with 18-25 mice/group. Survival data were graphed in a Kaplan-Meier survival curve and a Log-rank test was used to determine statistical significance. Weight loss data are shown as the mean ±SEM of values from 3 independent experiments, with 3-4 mice/group in each experiment. Statistical analysis was conducted using one-way ANOVA with a Dunnet's multiple comparison post-test (d0 as control), and $P \leq 0.05$*; $P \leq 0.01$**; $P \leq 0.001$***.

Figure 4.9

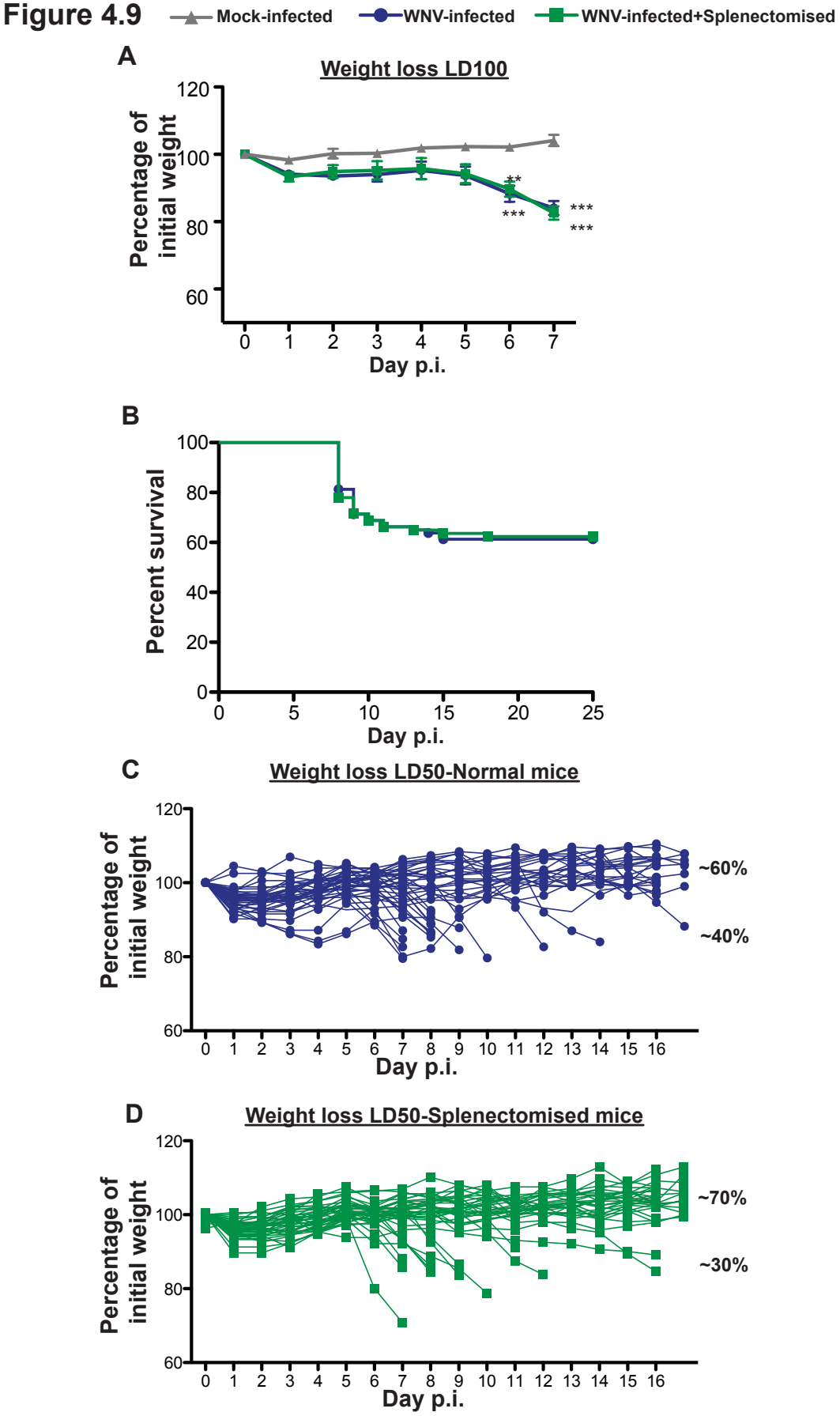
Mock-infected
WNV-infected
WNV-infected+Splenectomised
A
Weight loss LD100
Percentage of initial weight
120
100
80
60
0 1 2 3 4 5 6 7
Day p.i.
**
***
***
***
B
Percent survival
100
80
60
40
20
0
0 5 10 15 20 25
Day p.i.
C
Weight loss LD50-Normal mice
Percentage of initial weight
120
100
80
60
0 1 2 3 4 5 6 7 8 9 10 11 12 13 14 15 16
Day p.i.
~60%
~40%
D
Weight loss LD50-Splenectomised mice
Percentage of initial weight
120
100
80
60
0 1 2 3 4 5 6 7 8 9 10 11 12 13 14 15 16
Day p.i.
~70%
~30%

4.2.4.4. Survival of normal and splenectomised mice following infection with a sublethal dose of WNV

Considering the reduced cell numbers, in particular, the highly pathogenic Ly6C^{hi} inflammatory macrophages, infiltrating the CNS of WNV-infected, splenectomised animals we hypothesised that this may impact on the MST and mortality rate of WNV-infected mice. Thus, we infected normal (blue) and splenectomised (green) mice i.n. with a sublethal (LD50) dose of WNV (6x10^3 PFU) (Figure 4.9B). Both WNV-infected, normal and splenectomised animals started succumbing to disease from d7 p.i. onward. In addition, infection of both cohorts resulted in ~60% mortality, with ~40% of mice surviving infection, without any signs of illness, such as weight loss. The only difference between normal and splenectomised mice was the slightly extended disease course in splenectomised mice, as the last animal to succumb to infection in this cohort occurred on d18 p.i., 3 days later than normal mice. The percentage weight loss of individual, normal (Figure 4.9C) and splenectomised (Figure 4.9D) animals in the LD50 disease course showed no significant differences between these cohorts. However, the extended disease course and reduced infiltration of Ly6C^{hi} inflammatory macrophages in splenectomised mice, raises the question of whether the splenic reservoir of monocytes potentially contributes to the pathology in this model of WNV encephalitis.

4.2.5. The development of immunity in splenectomised mice

Previous work from our laboratory has shown that mice that survive the LD50 dose of WNV infection (6x10^3 PFU) develop immunity to subsequent lethal dose WNV rechallenge. Considering the evident role of the secondary lymphoid organs in the development of immunity, we reinoculated normal and splenectomised mice that had survived the LD50 dose of WNV infection, 90-days after primary infection to test for immunity. Mice were

reinoculated i.n. with a lethal dose of WNV ($6x10^4$ PFU) and monitored for any signs of disease.

All of the re-infected normal mice (blue) were immune to WNV, as none of this cohort succumbed to disease (Figure 4.10A) or lost any significant weight (Figure 4.10B). Two of the splenectomised animals developed signs of illness; one mouse lost a significant amount of weight following infection but recovered fully (Figure 4.10C-a), another developed significant weight loss (Figure 4.10C-b) and ultimately succumbed to infection (Figure 4.10A). While these two mice may not have received the complete dose of virus during primary infection, due to poor technique or experimental variability, it was still nevertheless clear that ~80% of reinoculated splenectomised mice developed no signs of illness and could be considered immune.

4.2.6. Cellularity of the bone marrow of splenectomised *versus* normal mice following lethal WNV infection

The bone marrow of WNV-infected normal and splenectomised animals ($6x10^4$ PFU) was collected on d7 p.i. and processed in order to determine how WNV infection modulates the leukocyte content of the bone marrow in the absence of the spleen. As the bone marrow is contained within a rigid structure with minimal space for expansion, dramatic changes in cell number were not expected in normal mice, however, it was possible for the composition of leukocytes to be altered during infection and potentially in the absence of the spleen. Additionally, the ability of the bone marrow to potentially compensate for the absence of a spleen was of interest. There were no differences in bone marrow leukocyte numbers between mock-infected, normal mice *versus* splenectomised, mock-infected mice (data not shown), thus only the normal mock-infected cohort is presented. A detailed

Figure 4.10 Survival and average weight loss of splenectomised *versus* normal mice, following secondary infection with a lethal dose of WNV

Following primary i.n. infection with a sublethal dose of WNV ($6x10^3$ PFU), surviving mice were kept for 3 months p.i., after which they were re-infected i.n. with a lethal dose (LD100) of WNV ($6x10^4$ PFU) to test for immunity. Graph A demonstrates the survival rate of normal (blue) and splenectomised (green) mice, re-infected with lethal dose of WNV. The percentage weight loss is shown, relative to original weight at reinoculation, of WNV-infected (B-blue) *versus* WNV-infected, splenectomised (C-green) mice following lethal WNV infection ($6x10^4$ PFU). The survival study was performed in one experiment with 7-14 mice/group. Survival data were graphed in a Kaplan-Meier survival curve and a Log-rank test was used to determine statistical significance.

Figure 4.10

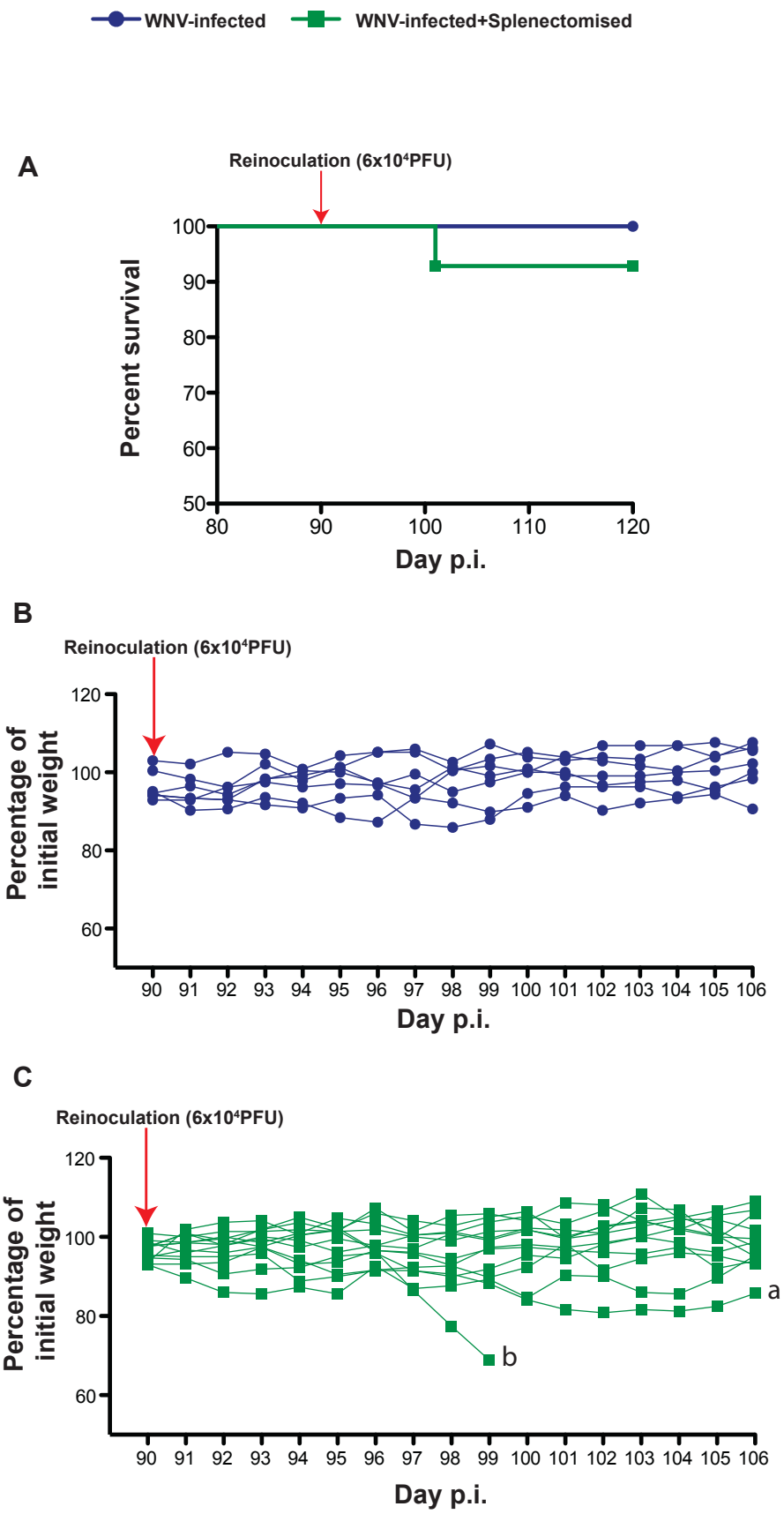
WNV-infected
WNV-infected+Splenectomised
A
Reinoculation (6x10⁴PFU)
Percent survival
100
90
80
70
60
50
80
90
100
110
120
Day p.i.
B
Reinoculation (6x10⁴PFU)
Percentage of initial weight
120
100
80
60
90 91 92 93 94 95 96 97 98 99 100 101 102 103 104 105 106
Day p.i.
C
Reinoculation (6x10⁴PFU)
Percentage of initial weight
120
100
80
60
a
b
90 91 92 93 94 95 96 97 98 99 100 101 102 103 104 105 106
Day p.i.

gating strategy for the bone marrow with isotype and fluorescence minus one controls is outlined by Appendix Figure 10 and 11.

The myeloid lineage cell numbers in the bone marrow of WNV-infected mice did not change appreciably compared to the mock-infected cohort (Figure 4.11A). Furthermore, comparable numbers of myeloid lineage cells were present in the bone marrow of WNV-infected, normal and WNV-infected, splenectomised bone marrow. Myeloid lineage cell subsets analysed included neutrophils ($CD11b^{hi}Ly6G^{+}$) and monocytes ($CD11b^{+}CD11c^{-}Ly6G^{-}$), which were further classified as three separate populations based on Ly6C expression namely: $CD11b^{+}Ly6C^{hi}$, $CD11b^{+}Ly6C^{int}$ and $CD11b^{+}Ly6C^{-}$. Despite a non-significant increase in $CD11b^{+}Ly6C^{hi}$ number of the WNV-infected cohorts, there were no appreciable differences in numbers of the other subsets in any of the cohorts analysed.

In addition, based on the markers available, the DC populations were subdivided into pDC ($CD11c^{+}B220^{+}$) and other DC ($CD11c^{+}B220^{-}$). However, neither of these populations exhibited any difference between any of the cohorts compared. In parallel, there were minor differences in the lymphoid lineage cells of WNV-infected, normal and splenectomised, and mock-infected mice (Figure 4.11B). Similar numbers of B cells were identified in the bone marrow of all three cohorts. WNV-infected, normal and splenectomised mice had higher $CD4^{+}$ and $CD8^{+}$ T cell numbers in the bone marrow than mock-infected mice, although this was not significant. Furthermore, normal WNV-infected mice had significantly more NKT cells present in the bone marrow, compared to mock-infected mice. This trend was also present in WNV-infected, splenectomised mice but was not significant.

In parallel to the cell number data, the percentage composition of leukocytes in the bone marrow changed very little between all of the cohorts (Figure 4.12A and B). Of the myeloid lineage cells analysed, only the $CD11b^{+}Ly6C^{hi}$ subset contributed to a higher fraction of the

Figure 4.11 Number of leukocytes in the bone marrow of normal *versus* splenectomised mice following lethal WNV infection

Panel A represents the number of total leukocytes ($CD45^+$) in the bone marrow of mock (grey), WNV-infected (blue) and WNV-infected, splenectomised (green). This figure includes neutrophils ($CD11b^{hi}Ly6G^+$), monocytes ($CD11b^+CD11c^-Ly6G^-$), pDC ($CD11c^+B220^+$) and other DC ($CD11c^+B220^-$). The monocyte population was further characterised based on Ly6C expression, namely: $Ly6C^{hi}$, $Ly6C^{int}$ and $Ly6C^-$. Panel B represents the number of B cells ($B220^+CD11c^-$), total T cells ($CD3^+NK1.1^-$), $CD4^+$ T cells ($CD3^+CD4^+CD8^-$), $CD8^+$ T cells ($CD3^+CD8^+CD4^-$), NK cells ($NK1.1^+CD3^-$) and NKT cells ($NK1.1^+CD3^+$). Data are shown as the mean ±SEM of values from 3 independent experiments, with 3-4 mice/group in each experiment. Statistical analysis was conducted using one-way ANOVA with a Tukey's multiple comparison post-test, and $P \leq 0.05$*; $P \leq 0.01$**; $P \leq 0.001$***.

Figure 4.11 **Number of leukocytes/bone marrow**

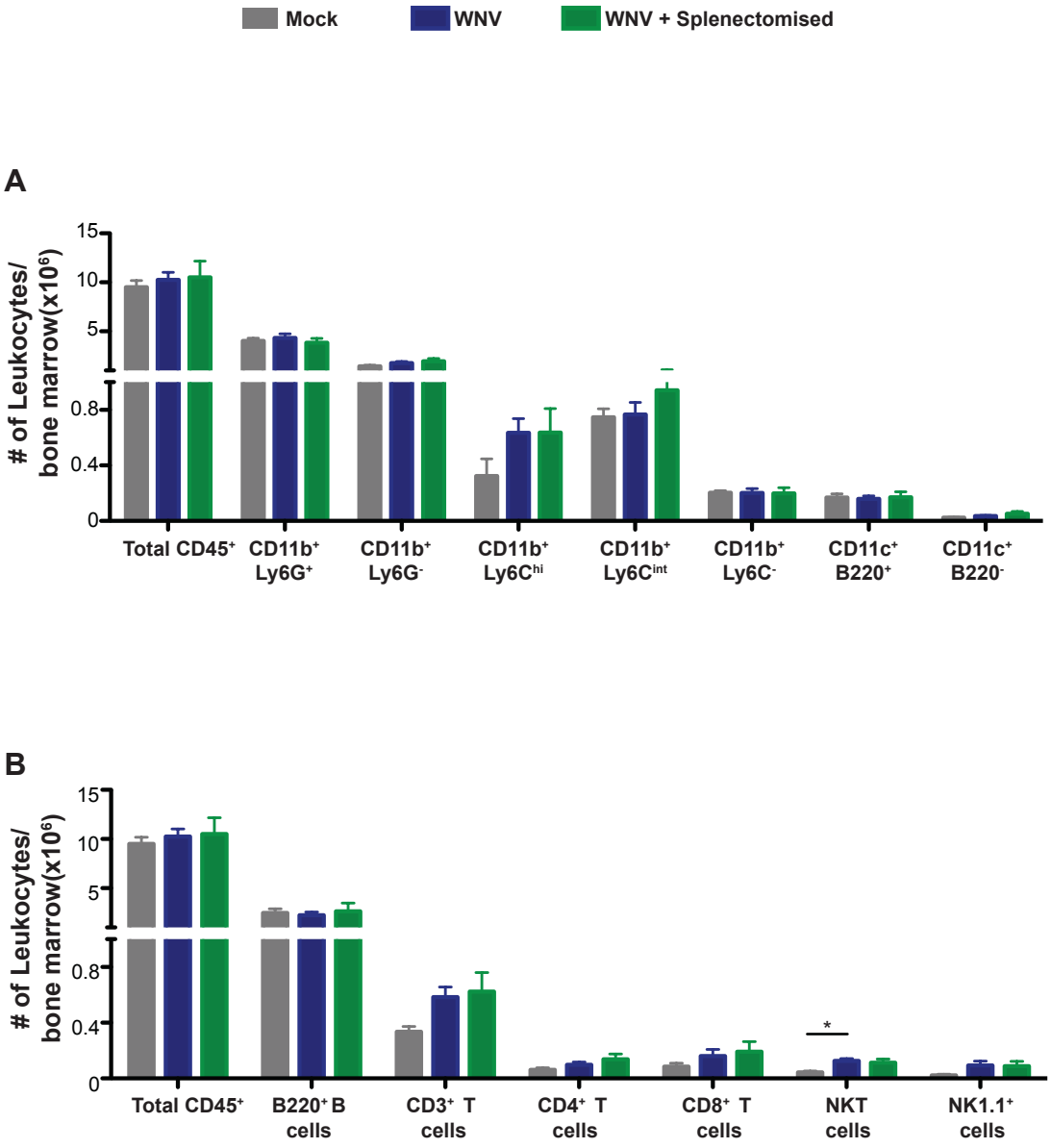

Figure 4.12 Percentage composition of leukocyte subsets in the bone marrow of normal *versus* splenectomised mice following lethal WNV infection

Panel A represents the percentage of total leukocytes ($CD45^+$) in the bone marrow of mock (grey), WNV-infected (blue) and WNV-infected, splenectomised (green). This figure includes the percentage of neutrophils ($CD11b^{hi}Ly6G^+$), monocytes ($CD11b^+Ly6C^{hi}$; $CD11b^+Ly6C^{int}$; $CD11b^+Ly6C^-$), pDC ($CD11c^+B220^+$) and other DC ($CD11c^+B220^-$) in the bone marrow. The monocyte population was further characterised based on Ly6C expression, namely: $Ly6C^{hi}$, $Ly6C^{int}$ and $Ly6C^-$. Panel B represents the percentage of B cells ($B220^+CD11c^-$), total T cells ($CD3^+NK1.1^-$), $CD4^+$ T cells ($CD3^+CD4^+CD8^-$), $CD8^+$ T cells ($CD3^+CD8^+CD4^-$), NK cells ($NK1.1^+CD3^-$) and NKT cells ($NK1.1^+CD3^+$) in the bone marrow. Values of various subsets are expressed as a percentage of total leukocytes in the bone marrow of each cohort. Data are shown as the mean ±SEM of values from 3 independent experiments, with 3-4 mice/group in each experiment. Statistical analysis was conducted using one-way ANOVA with a Tukey's multiple comparison post-test, and $P \leq 0.05$*; $P \leq 0.01$**; $P \leq 0.001$***.

Figure 4.12 Percentage of leukocytes/bone marrow

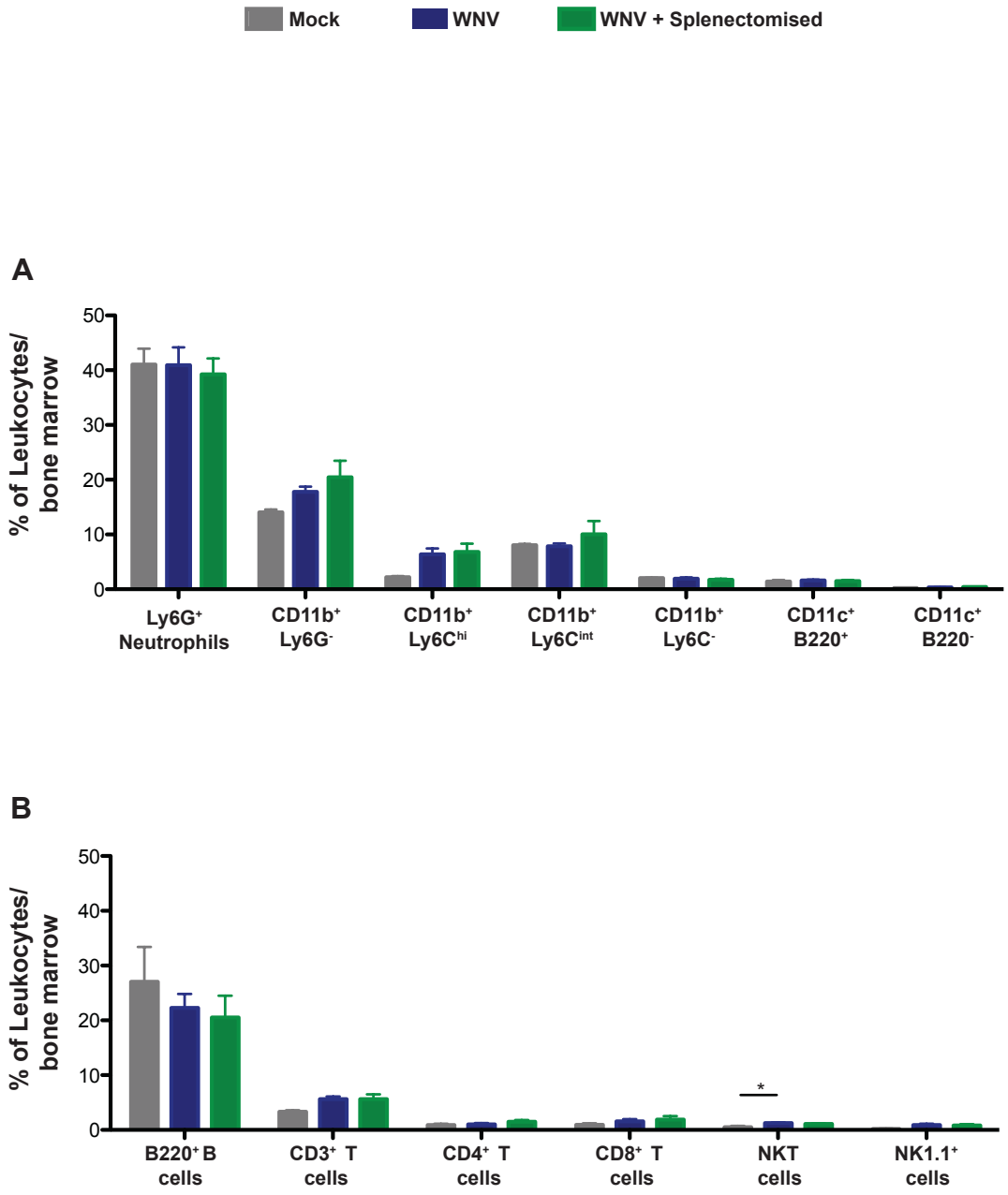

total leukocyte population in WNV-infected, normal and splenectomised mice, compared to mock-infected mice, although this was not statistically significant. The percentage of other myeloid ($CD11b^+Ly6^{int}$, $CD11b^+Ly6C^-$ cells and neutrophils) and DC subsets present in the bone marrow was comparable between mock and WNV-infected.

The population of NKT cells expanded significantly in WNV-infected, normal mice, compared to mock-infected mice (Figure 4.12B). However, no appreciable difference in percentage of T cells, including $CD4^+$ and $CD8^+$, B cells and NK cells was present between mock-infected and WNV-infected, normal or WNV-infected, splenectomised mice. Thus the absence of the spleen produced very little change in the cell number or leukocyte composition of the bone marrow following lethal WNV infection.

4.2.7. Cellularity of the lymph nodes of splenectomised *versus* normal mice following lethal WNV infection

As no significant differences were detected in the leukocyte composition of the bone marrow of WNV-infected, normal *versus* WNV-infected, splenectomised mice, we dissected the leukocyte response of the other secondary lymphoid organ associated with WNV encephalitis, namely the CLN. Results from chapter 3 clearly established a role for the CLN as a draining lymph node of the infected CNS, and whether the removal of the largest secondary lymphoid organ would affect the CLN response to WNV infection was of great interest. The expansion of leukocyte numbers, characteristic of the CLN during WNV infection, was also evident in the CLN of WNV-infected, splenectomised mice (Figure 4.13A). However, this increase in leukocytes including, B and T cells, was significantly higher in CLN isolated from WNV-infected, splenectomised mice than their normal, WNV-infected counterparts. Similarly, significantly higher numbers of monocytes, $CD11c^+CD11b^+$ and $CD11c^+CD11b^-$ cells were identified in the CLN from WNV-infected splenectomised mice, compared to WNV-infected normal mice (Figure 4.13B). The

Figure 4.13 Cell number and percentage of various leukocyte subsets in the CLN and ILN of splenectomised *versus* normal mice following lethal WNV infection

Panel A demonstrates the number of total leukocytes ($CD45^+$), T cells ($CD3^+$) and B cells ($CD19^+/B220^+$) in the CLN mock (grey), WNV-infected normal (blue) and WNV-infected,splenectomised mice (green). The change in monocytes ($CD11b^+CD11c^-$), neutrophil ($CD11b^+Ly6G^+$) and DC subsets, including $CD11c^+CD11b^+$, $CD11c^+CD11b^-$ and $CD11c^{hi}CD11b^{int}$, in the CLN is represented by panel B. The percentage of each of the leukocyte subsets, in the CLN, as described in panel A and B is demonstrated by figure C. Values of various subsets are expressed as a percentage of total leukocytes in the CLN of each cohort. Panel D shows the number of the above leukocytes in the ILN of mock (grey), WNV-infected normal (blue) and WNV-infected splenectomised mice (green). Data for panels A-C are shown as the mean ±SEM of values from 3 independent experiments, with 3-4 mice/group in each experiment. Data for figure D is shown as the mean ±SEM of values from 2 independent experiments, with 3-4 mice/group in each experiment. Statistical analysis was conducted using one-way ANOVA with a Tukey's multiple comparison post-test, and $P \leq 0.05$*; $P \leq 0.01$**; $P \leq 0.001$***.

Figure 4.13 Number and percentage of leukocytes/CLN

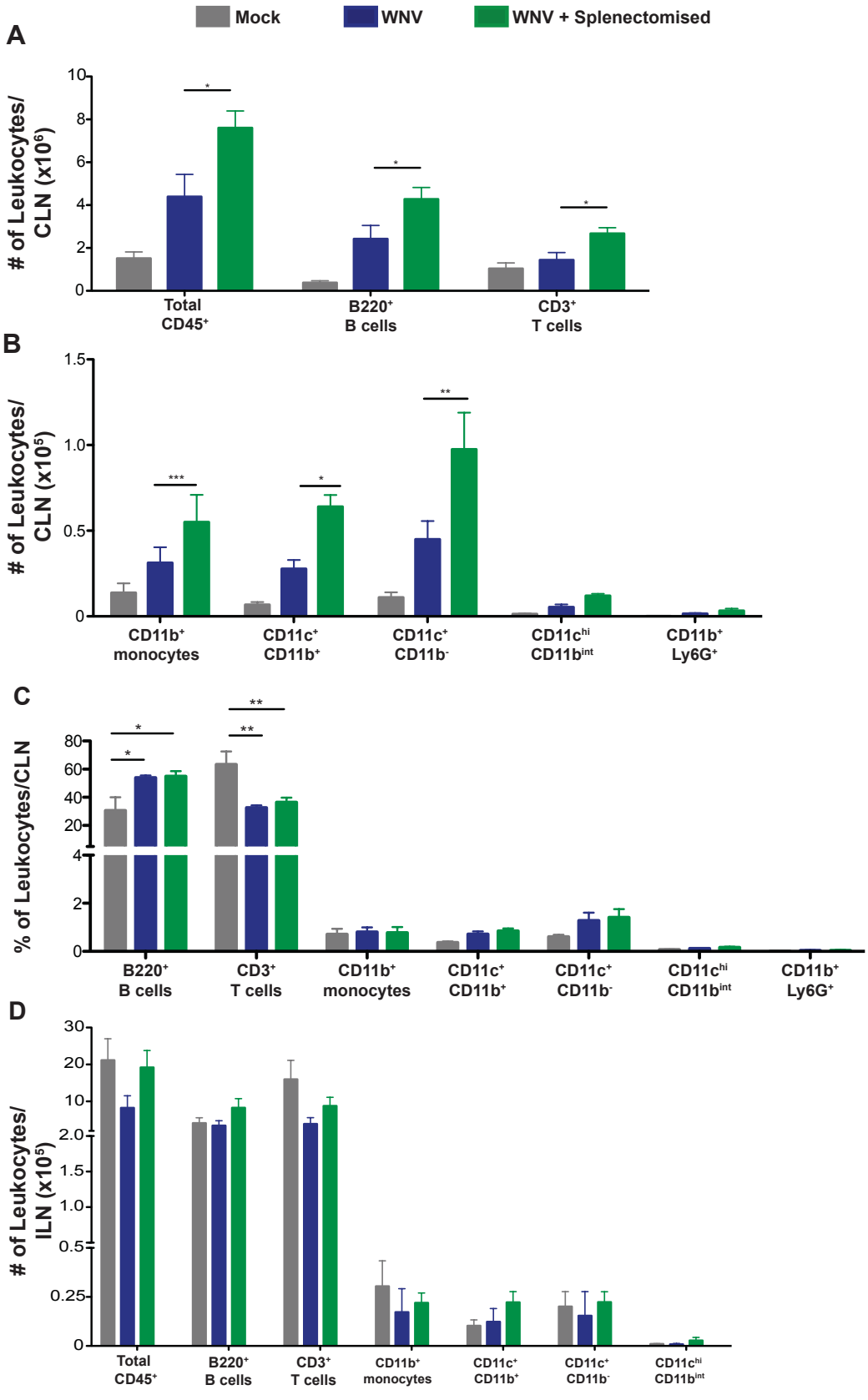

$CD11c^{hi}CD11b^{int}$ subset and neutrophil numbers were also markedly higher in WNV-infected splenectomised mice, however this was not significant.

The percentage composition of leukocytes in the CLN of the two WNV-infected cohorts were comparable, with negligible differences in any of the leukocyte subsets analysed (Figure 4.13C). Furthermore, the splenectomised mice demonstrated similar patterns of B cell expansion and reduction in percentage of T cells seen in normal mice, following lethal WNV infection. Levels of Ly6C expression between splenectomised and normal WNV-infected mice were similar (data not shown). Collectively, the DC subsets comprised less than 4% of the total leukocyte population in all of the cohorts studied, with WNV-infected, normal and splenectomised mice both exhibiting higher percentages of the $CD11c^{+}CD11b^{+}$ and $CD11c^{+}CD11b^{-}$ subsets, compared to mock-infected animals. Whether there were detectable changes in peripheral non-draining nodes, such as the ILN, was also investigated. However, while there was a similar trend for leukocyte subset numbers in the ILN of WNV-infected, splenectomised mice to be higher than that of normal WNV-infected mice, this was not statistically significant (Figure 4.13D).

Thus it is evident that, although the leukocyte composition remained the same, the CLN leukocyte numbers are impacted significantly by the absence of the spleen following CNS infection. Whether or not the increased cell numbers seen in the CLN of splenectomised mice was due to proliferation or increased recruitment of cells is of great interest for future studies.

4.2.8. Cellularity of the blood of splenectomised *versus* normal mice following lethal WNV infection

There is some evidence of mice becoming leukopenic after the spleen has been removed. If this holds true for our model of infection, it may explain the reduction of leukocyte

infiltration seen in the CNS of splenectomised mice following lethal WNV infection. Blood was collected from mock-normal, mock-splenectomised, WNV-normal and WNV-splenectomised mice on d7p.i., in order to establish whether there were any deficiencies in circulatory leukocyte populations when the spleen is removed. On d7 p.i., both WNV-infected, normal and splenectomised mice showed a marked reduction in monocytes, B and T cells, compared to their mock-infected counterparts. However, the numbers of each of the leukocyte subsets in the blood were similar between normal and splenectomised mice in the mock-infected cohort and between these two groups in the WNV-infected cohort (Figure 4.14A).

In parallel to the cell number data, there were negligible differences in percentage composition of these subsets in the blood of mock-normal *versus* mock-splenectomised, and WNV-normal *versus* WNV-splenectomised mice (Figure 4.14B). However, both the T cell and monocyte subsets had halved at d7 p.i. in splenectomised and normal WNV-infected mice, compared to their mock-infected counterparts, while the $CD11c^{+}CD11b^{-}$ subset had increased by ~2-fold. This was presumably due to the recruitment of certain leukocyte subsets from the blood to the CNS or CLN in response to CNS infection.

4.2.9. IMP treatment of normal and splenectomised mice following lethal WNV infection

4.2.9.1. Modulation of CNS leukocyte populations of normal mice following lethal WNV infection and treatment with IMP

Previous work from our laboratory has shown that IMP treatment significantly reduces the infiltration of pathogenic $Ly6C^{hi}$ monocyte in the CNS. This occurred with a concurrent

Figure 4.14 Cell number and percentage composition of leukocytes in the blood of mock- and WNV-infected normal and splenectomised mice following lethal WNV infection

The absolute number (A) and percentage (B) of leukocytes ($CD45^+$), T ($CD3^+$) and B cells ($B220^+$), as well as monocytes ($CD11b^+CD11c^-$) and DC ($CD11c^+$) per millilitre of blood in mock-infected normal (dark grey) *versus* mock-infected, splenectomised (light grey), and WNV-infected normal (blue) *versus* WNV-infected, splenectomised (green). Percentages of various subsets are expressed as a percentage of total leukocytes per millilitre of blood in each cohort. Data are shown as the mean ±SEM of values from 2 independent experiments, with 3-4 mice/group in each experiment. Statistical analysis was conducted using one-way ANOVA with a Tukey's multiple comparison post-test, and $P \leq 0.05$*; $P \leq 0.01$**; $P \leq 0.001$***.

Figure 4.14 **Number and percentage of leukocytes/blood**

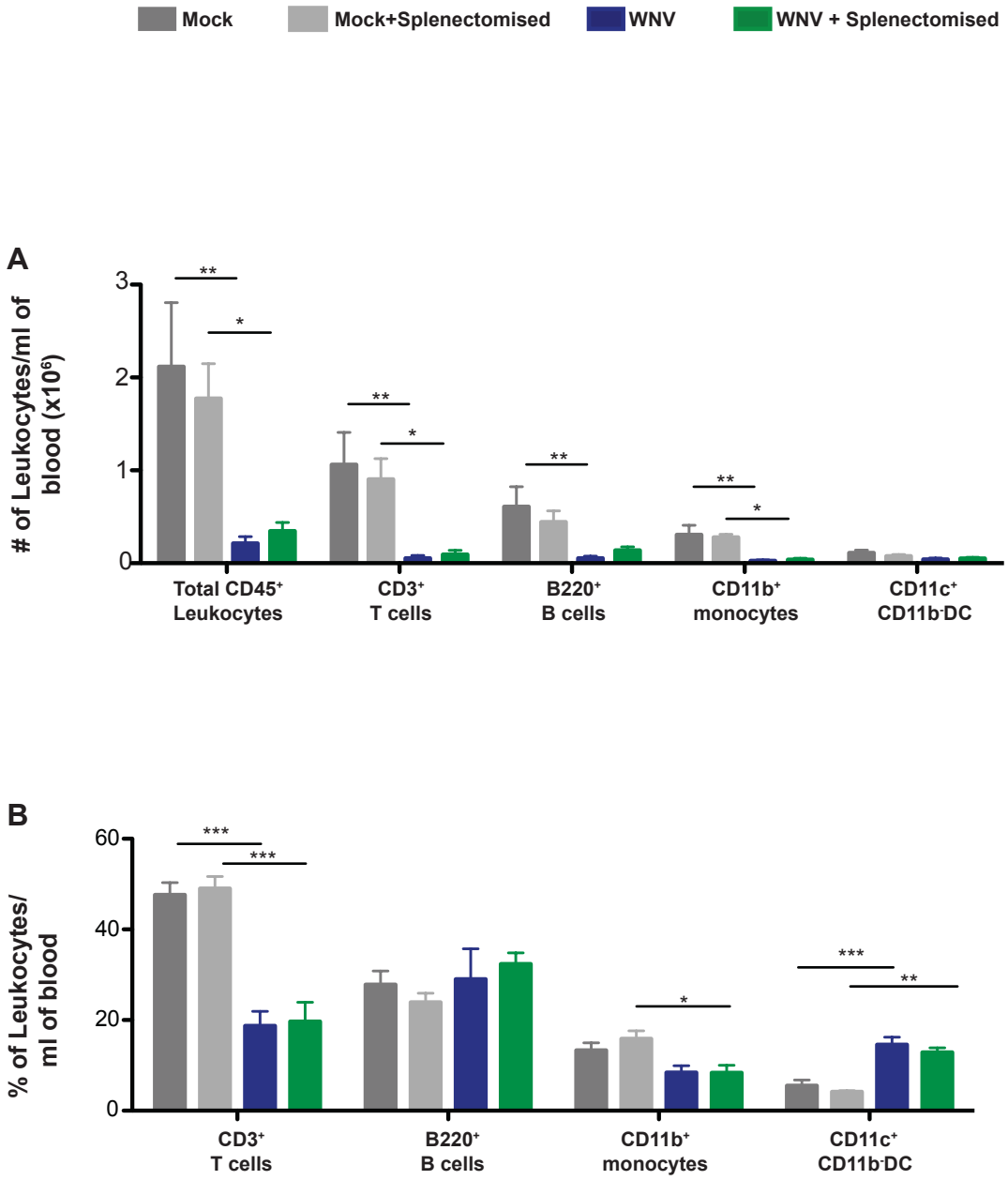

increase in Ly6C^{hi} cell numbers in the spleen and liver (Getts et al. 2014). We hypothesised that, since the spleen was one of the organs evidently most involved in sequestering Ly6C^{hi} inflammatory macrophages, following lethal WNV infection, that the spleen may be crucial for the efficacy of IMP treatment. Figures 4.15 and 4.16 compare the modulation of leukocyte subset infiltration into the CNS following IMP treatment of WNV-infected mice ($6x10^4$ PFU) in normal (Figure 4.15A) and splenectomised (Figure 4.15B) on d7p.i. The significant infiltration of leukocytes in WNV-infected mice (dark blue), compared to mock-infected (grey), was dramatically reduced in IMP-treated, WNV-infected mice (light blue) (Figure 4.15A). Furthermore, IMP treatment significantly reduced the pathogenic Ly6C^{hi} macrophage subset in normal mice with their spleens intact. Although IMP treatment of splenectomised mice (light green) (Figure 4.15B) somewhat reduced the number of leukocytes infiltrating the CNS, compared to vehicle-treated, WNV-infected splenectomised mice (dark green), this was not significant. Nevertheless, compared to the normal cohort presented in Figure 4.15A, the absolute number of Ly6C^{hi} inflammatory macrophages, was at least 50% lower in IMP-treated, splenectomised animals, due to the already reduced numbers as a result of splenectomy.

The infiltration of lymphoid lineage cells, such as T, NK and B cells, was also markedly reduced in IMP-treated WNV-infected normal mice (Figure 4.16A). There was also a decrease in neutrophil numbers following IMP treatment of WNV-infected mice, however this was not significant. Additionally, there was a trend of reduction in lymphoid lineage cell numbers (T, B and NK cells) in the CNS of IMP-treated, WNV-infected splenectomised mice (Figure 4.16B), relative to their vehicle-treated cohort. Similar to neutrophil numbers of normal mice (Figure 4.16A), the numbers of neutrophils in splenectomised animals (Figure 4.16B) had a slight, but non-significant decrease, compared to the vehicle treated cohort. Thus, compared to vehicle-treated splenectomised mice, IMP treatment does not significantly reduce leukocyte infiltration into the CNS of splenectomised mice.

Figure 4.15 CNS leukocyte infiltration following IMP treatment of normal and splenectomised mice infected with a lethal dose of WNV

Panels A represents the change in number of total leukocytes ($CD45^+$), resident microglia ($CD11b^+Ly6C^-$) and the $CD11b^+Ly6C^+$ subset, which can be further subdivided into infiltrating macrophages ($CD11b^+Ly6C^{hi}$) and immigrant/activated microglia ($CD11b^+Ly6C^{int}$) populations in the CNS of mock-infected (grey), WNV-infected, vehicle-treated (dark blue) and WNV-infected, IMP-treated (light blue) mice. Panel B represents the change in number of total leukocytes ($CD45^+$), resident microglia ($CD11b^+Ly6C^-$) and the $CD11b^+Ly6C^+$ subset, which can be further subdivided into infiltrating macrophages ($CD11b^+Ly6C^{hi}$) and immigrant microglia ($CD11b^+Ly6C^{int}$) populations in the CNS of mock-infected (grey), WNV-infected, splenectomised, vehicle-treated (dark green) and WNV-infected, splenectomised, IMP-treated (light green) CNS. Data are shown as the mean ±SEM of values from 3 independent experiments, with 3-4 mice/group in each experiment. Statistical analysis was conducted using one-way ANOVA with a Tukey's multiple comparison post-test, and $P \leq 0.05$*; $P \leq 0.01$**; $P \leq 0.001$***.

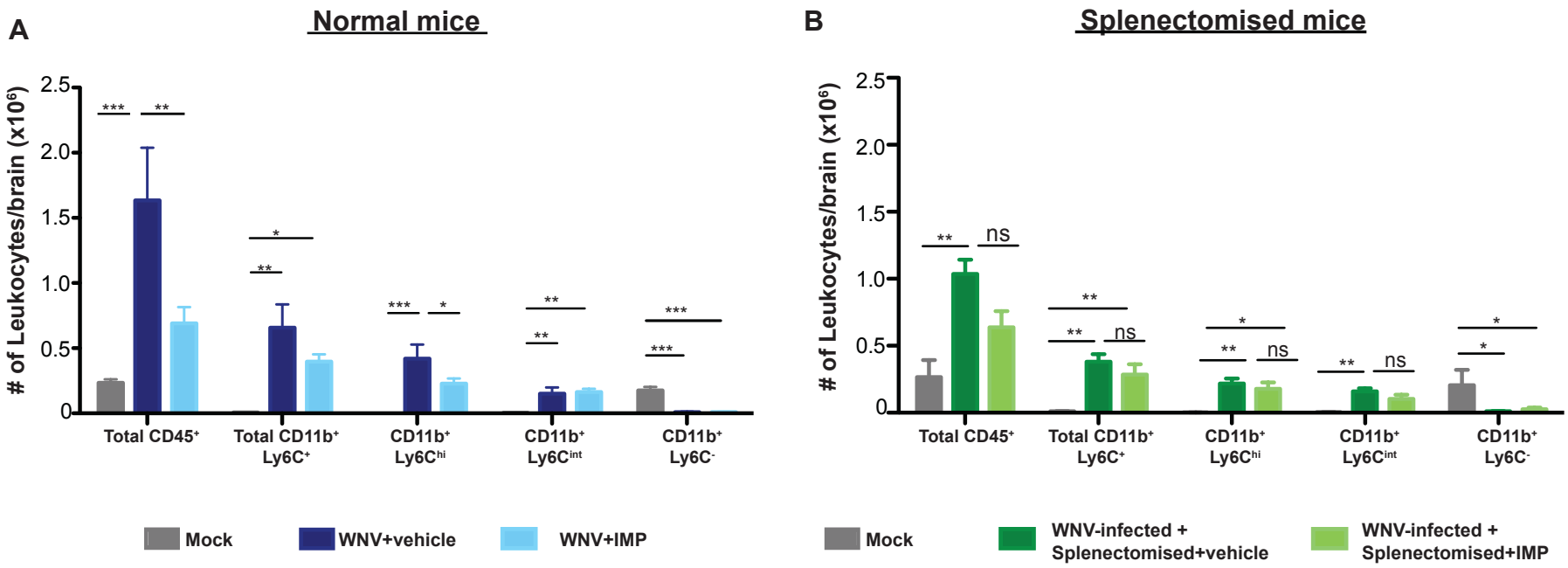
A
Normal mice
# of Leukocytes/brain (x10⁶)
2.5
2.0
1.5
1.0
0.5
0
***
**
*
**
***
*
**
**
***
***
Total CD45⁺
Total CD11b⁺ Ly6C⁺
CD11b⁺ Ly6C^hi
CD11b⁺ Ly6C^int
CD11b⁺ Ly6C⁻
Mock
WNV+vehicle
WNV+IMP
B
Splenectomised mice
# of Leukocytes/brain (x10⁶)
2.5
2.0
1.5
1.0
0.5
0
**
ns
**
**
ns
*
**
ns
**
ns
*
*
Total CD45⁺
Total CD11b⁺ Ly6C⁺
CD11b⁺ Ly6C^hi
CD11b⁺ Ly6C^int
CD11b⁺ Ly6C⁻
Mock
WNV-infected + Splenectomised+vehicle
WNV-infected + Splenectomised+IMP

Figure 4.15

Figure 4.16 CNS leukocyte infiltration following IMP treatment of splenectomised mice infected with a lethal dose of WNV

Panel A represents the change in number of neutrophils ($CD11b^{hi}Ly6G^{+}$) and lymphoid cells, including T cells ($CD3^{+}$), NK cells ($NK1.1^{+}$) and B ($B220^{+}$) cells in the CNS of mock-infected (grey), WNV-infected, vehicle-treated (dark blue) and WNV-infected, IMP-treated (light blue) mice. Panel B represents the change in number of neutrophils ($CD11b^{hi}Ly6G^{+}$) and lymphoid cells, including T cells ($CD3^{+}$), NK cells ($NK1.1^{+}$) and B ($B220^{+}$) cells in the CNS of mock-infected (grey), WNV-infected, splenectomised, vehicle-treated (dark green) and WNV-infected, splenectomised, IMP-treated (light green) mice. Panel C compares the percentage survival between mice that did not lose significant weight (black), i.e. more than 5% of original weight, to mice that have lost more than 5% weight. Normal mice, that did lose significant weight, were given either vehicle (dark blue) or IMP treatment (light blue). Similarly, splenectomised mice, losing significant weight, were given either vehicle (dark green) or IMP treatment (light green). The survival study was performed in four separate experiments with 18-25 mice/group. Survival data were graphed in a Kaplan-Meier survival curve and a Log-rank test was used to determine statistical significance. Cell number data are shown as the mean ±SEM of values from 3 independent experiments, with 3-4 mice/group in each experiment. Statistical analysis was conducted using one-way ANOVA with a Tukey's multiple comparison post-test, and $P \leq 0.05$*; $P \leq 0.01$**; $P \leq 0.001$***.

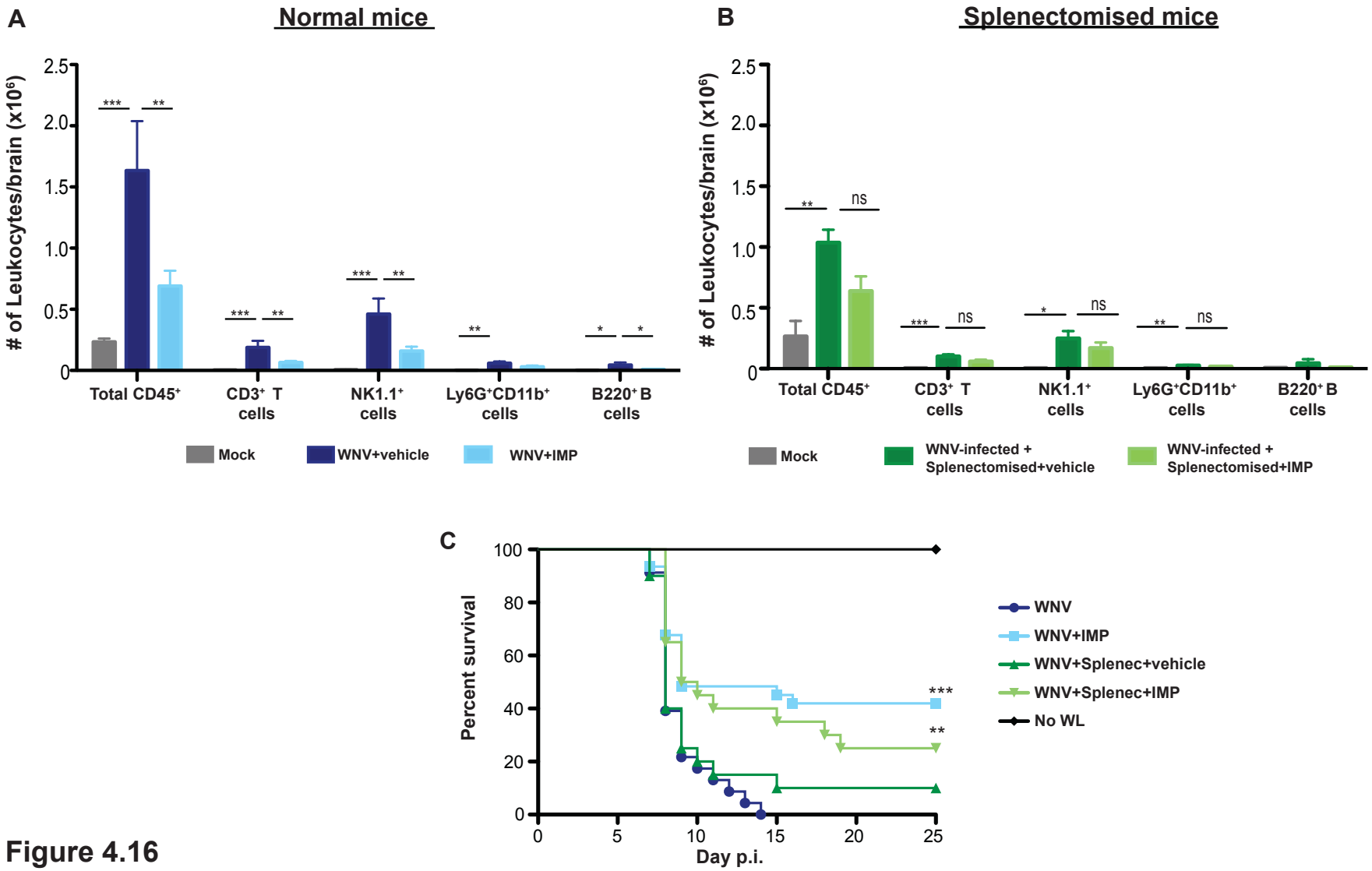
A
Normal mice
# of Leukocytes/brain (x10⁶)
2.5
2.0
1.5
1.0
0.5
0
***
**
***
**
***
**
**
*
*
Total CD45⁺
CD3⁺ T cells
NK1.1⁺ cells
Ly6G⁺CD11b⁺ cells
B220⁺ B cells
Mock
WNV+vehicle
WNV+IMP
B
Splenectomised mice
# of Leukocytes/brain (x10⁶)
2.5
2.0
1.5
1.0
0.5
0
**
ns
***
ns
*
ns
**
ns
Total CD45⁺
CD3⁺ T cells
NK1.1⁺ cells
Ly6G⁺CD11b⁺ cells
B220⁺ B cells
Mock
WNV-infected + Splenectomised+vehicle
WNV-infected + Splenectomised+IMP
C
Percent survival
100
80
60
40
20
0
0
5
10
15
20
25
Day p.i.
***
**
WNV
WNV+IMP
WNV+Splenec+vehicle
WNV+Splenec+IMP
No WL

Figure 4.16

However, with the already reduced leukocyte numbers present in the CNS of WNV-infected splenectomised animals, any additional reduction in cell numbers, induced by IMP treatment, may improve clinical outcome of these animals.

4.2.9.2. Survival of splenectomised versus normal mice following infection with sublethal dose of WNV and IMP treatment

As shown in Figure 4.9, splenectomised and normal mice develop a similar disease course when infected with a sublethal dose of WNV. Therefore, in order to compare the efficacy of IMP treatment in the absence of the spleen, we infected normal and splenectomised mice with the LD50 dose of WNV ($6x10^3$ PFU) and subsequently treated mice displaying clinical symptoms (i.e. >5% of initial pre-infection weight) with IMP or vehicle treatment. Previous work has established that there is a direct correlation between weight loss and CNS involvement of disease, thus, mice losing more than 5% of their initial body weight were assumed to have CNS infiltration of leukocytes.

WNV-infected mice, in both the normal and splenectomised cohorts that had no significant weight loss or showed any signs of illness had a 100% survival rate (black) (Figure 4.16C). Normal WNV-infected animals that received only vehicle treatment, upon losing 5% or more of their original weight, had the worst survival outcome compared to other cohorts, with all of the vehicle-treated, normal mice succumbing to infection (dark blue). However, the vehicle-treated, splenectomised cohort exhibited a marginal improvement in survival rate, with 10% of mice, which had lost significant weight, surviving infection. Interestingly, although IMP treatment did not significantly reduce leukocyte infiltration in splenectomised mice (light green), compared to their vehicle-treated, splenectomised cohort (dark green), it did significantly improve survival outcome. Indeed, 25% of splenectomised mice developing disease survived the infection, when treated with IMP. Nevertheless, normal, WNV-infected mice given IMP treatment (light blue) had the lowest

mortality rate of all the cohorts analysed. IMP treatment of these mice, saved 42% of mice that would have otherwise succumbed to infection, suggesting that, although IMP treatment works in the absence of the spleen, efficacy is reduced compared to normal mice.

4.2.9.3. The location of IMP and IMP-containing cells in the absence of the spleen

As we know from previous studies in our lab, a significant proportion of IMP/IMP-associated cells are destined for the spleen (Getts et al. 2014). Indeed, ~4% of the splenic leukocytes are IMP^+ by d7 p.i. We hypothesised that, in the absence of the spleen, these IMP or IMP-containing cells may be more abundant in other lymphoid and non-lymphoid organs, such as the liver, bone marrow, CLN and in circulation. However, unexpectedly, there was no indication that these organs compensated for the absence of the spleen, with regards to IMP uptake (Figure 4.17). Indeed, there were negligible differences in the absolute number of IMP^+CD45^+ cells identified in the liver, blood and bone marrow of WNV-infected, normal (light blue) and WNV-infected splenectomised mice (light green) (Figure 4.17A). Furthermore, brain and CLN had fewer IMP^+CD45^+ cells in WNV-infected splenectomised mice than the normal cohort.

The distribution of IMP^+CD45^+ cells contained within each organ was also comparable between WNV-infected normal and WNV-infected splenectomised mice (Figure 4.17B). There was no appreciable difference in percentage of IMP^+CD45^+ cells in the either the liver, blood, bone marrow or CNS. Moreover, the fraction of IMP^+CD45^+ cells contained within the leukocyte population of the CLN was significantly reduced. Finally, in the brain, the percentage of IMP^+ $Ly6C^+$ monocytes in both normal and splenectomised WNV-infected mice remained similar at approximately 0.25% of the total $Ly6C^+$ monocyte population.

Figure 4.17 IMP$^+$ leukocytes in the liver, bone marrow, brain, CLN and blood of WNV-infected normal and splenectomised mice following IMP treatment

Panels A and B respectively represents the number and percentage of each leukocyte subset that is IMP$^+$ in the liver, bone marrow, brain, CLN and blood (per ml) of WNV-infected, normal mice (light blue) *versus* WNV-infected, splenectomised mice (light green), 24h after IMP treatment. Data for the brain, bone marrow and CLN are shown as the mean ±SEM of values from 3 independent experiments, with 2-4 mice/group in each experiment. Data for the blood are shown as the mean ±SEM of values from 2 independent experiments, with 3-4 mice/group. Values of IMP$^+$ leukocytes are expressed as a percentage of total leukocytes present in each organ. For reference, IMP+ subpopulations in the spleen are shown in figure 5.14. Data for the liver is shown as the ±SEM of 3-4 mice/group and is representative of 1 experiment. Statistical analysis was conducted using an unpaired, two tailed T-test, and $P \leq 0.05$*; $P \leq 0.01$**; $P \leq 0.001$***.

Figure 4.17

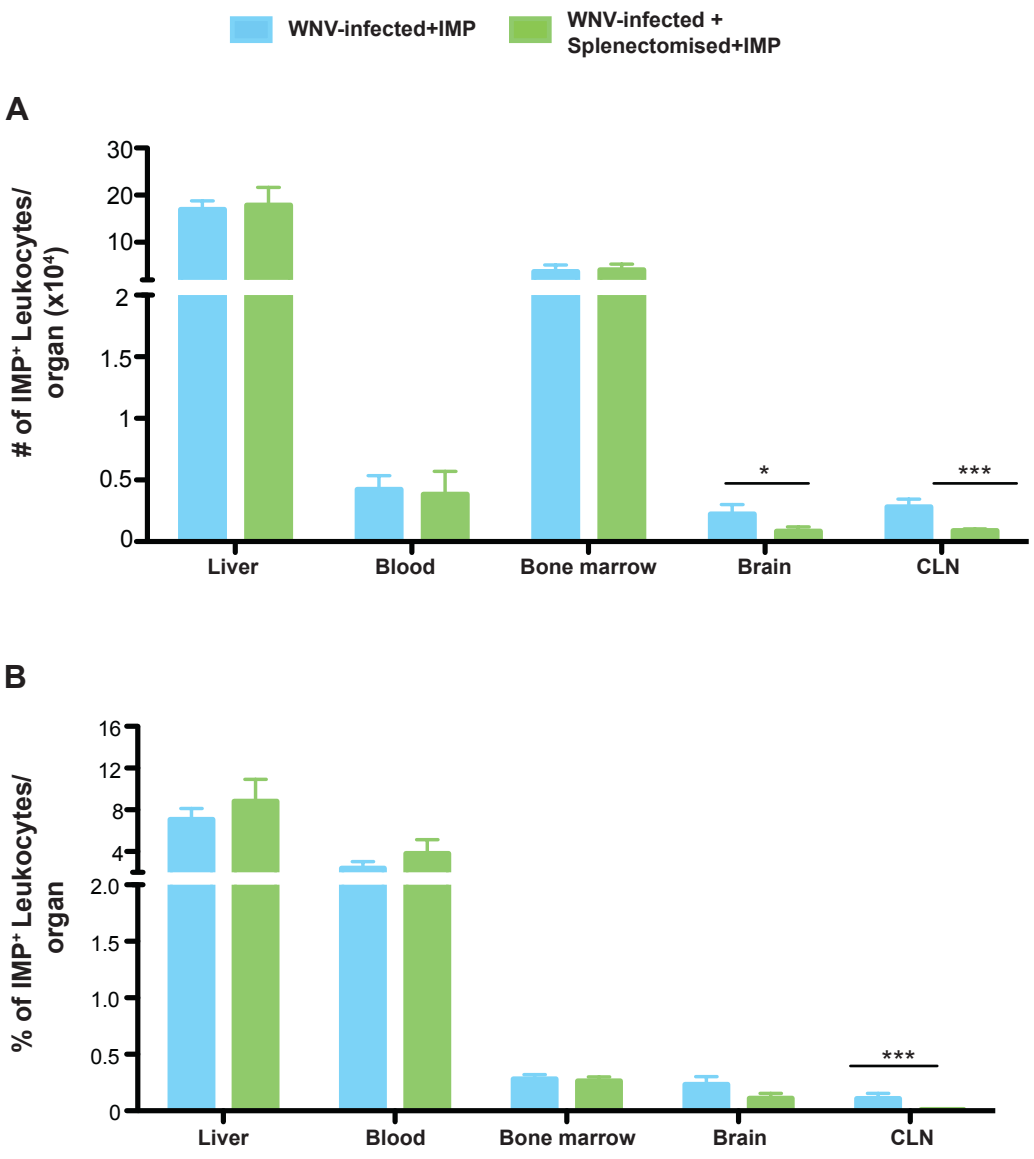
WNV-infected+IMP
WNV-infected + Splenectomised+IMP
A
# of IMP+ Leukocytes/ organ (x10⁴)
30
20
10
2
1.5
1
0.5
0
*
***
Liver
Blood
Bone marrow
Brain
CLN
B
% of IMP+ Leukocytes/ organ
16
12
8
4
2.0
1.5
1.0
0.5
0
***
Liver
Blood
Bone marrow
Brain
CLN

4.2.10. The potential role of the spleen as a splenic reservoir for monocytes infiltrating the WNV-infected CNS: the action of ACE inhibitors.

4.2.10.1. Leukocyte infiltration into the CNS following Enalapril treatment

The reduced infiltration of leukocytes into the CNS of WNV-infected, splenectomised mice led us to examine the possibility of a splenic reservoir of monocytes, which was recently identified as a ready source of undifferentiated monocytes (Swirski et al. 2009) (Bao et al. 2010). The treatment with angiotensin-converting enzyme (ACE) inhibitor Enalapril, has been used with great success to inhibit monocyte recruitment from the spleen in other inflammatory disease models, such as MI (Leuschner et al. 2010). Thus, we tested the hypothesis that the spleen was acting in conjunction with the bone marrow, as an additional source of the leukocyte infiltrate present in the CNS, following WNV infection. Female C57BL/6 mice were infected i.n. with a lethal dose WNV ($6x10^4$ PFU) and subsequently treated daily with i.p. injection of Enalapril administered at a dose of 100 mg/kg/day, from d0 p.i.

A pilot study was initially set up where we treated mice from d5 p.i. with Enalapril, as this is the earliest time-point in which leukocyte infiltration starts significantly increasing in the CNS. However, intervention at this time-point did not result in any clinical improvement, decreased mortality or reduction in monocyte infiltration (data not shown). Intervention at this time-point may have been too late as the mobilisation of splenic reservoir monocyte occurred rapidly after inflammatory stimulus present in the MI model (Leuschner et al. 2010) (Swirski et al. 2009). Therefore, we proceeded to prophylactically treat mice with the ACE inhibitor from d0 onwards to see if this would be more effective.

Enalapril treatment of mock- (light grey) or WNV-infected (purple), from the onset of infection, did not decrease the numbers of leukocyte infiltrating the CNS, compared to mock-infected+vehicle (dark grey) and WNV-infected+vehicle (orange) (Figure 4.18A). In addition, comparable numbers of Ly6C^{hi} inflammatory macrophages infiltrated the CNS in both Enalapril- and vehicle-treated WNV-infected cohorts. Similarly, prophylactic Enalapril treatment had no impact on lymphoid lineage or neutrophil cell numbers in the CNS following WNV-infection (Figure 4.18B).

4.2.10.2. Leukocyte numbers of the spleen following Enalapril treatment

We dissected the spleen to see if any retention in leukocyte subsets, in particular Ly6C^{hi} monocytes, occurred as a result of Enalapril treatment (Swirski et al. 2009). Firstly, differences between mock-infected, vehicle-treated (dark grey) and mock-infected, Enalapril-treated (light grey) were negligible for all the leukocyte subsets analysed in the spleen (Figure 4.19A and B). In particular, there was no notable retention of the population of interest, the pathogenic Ly6C^{hi} monocytes, in the spleen, following Enalapril treatment. Similarly, comparable numbers of DC subsets were present in the spleen of both vehicle- and Enalapril-treated WNV-infected mice (Figure 4.19A). Curiously, neutrophil numbers were slightly lower in the spleen of Enalapril-treated, WNV-infected mice, compared to the vehicle-treated cohort, but this was not significant.

None of the lymphoid lineage subsets (T, B, NK and NKT cells) in the spleen demonstrated any statistically significant changes in response to Enalapril treatment, following WNV infection (Figure 4.19B).

Figure 4.18 Leukocyte number in the CNS of mock- and WNV-infected (6x10^{4}PFU) mice following treatment with Enalapril

Panel A represents the cell number of total leukocytes ($CD45^+$), resident microglia ($CD11b^+Ly6C^-$) and the $CD11b^+Ly6C^+$ subset, which can further be subdivided into infiltrating macrophages ($CD11b^+Ly6C^{hi}$) and immigrant/activated microglia ($CD11b^+Ly6C^{int}$) populations in the CNS of mock-infected, vehicle-treated (dark grey), mock-infected, Enalapril-treated (light grey), WNV-infected, vehicle-treated (purple) and WNV-infected, Enalapril-treated (orange) mice. Panel B shows the number of neutrophils ($CD11b^{hi}Ly6G^+$) and lymphoid cells, including T cells ($CD3^+$), NK cells ($NK1.1^+$) and B ($B220^+$) cells in the CNS of the experimental cohorts described for panel A. Data are shown as the mean ±SEM of values from 2 independent experiments, with 3 mice/group in each experiment. Statistical analysis was conducted using one-way ANOVA with a Tukey's multiple comparison post-test, and P≤0.05*; P≤0.01**; P≤0.001***.

Figure 4.18 **Number of Leukocytes/CNS**

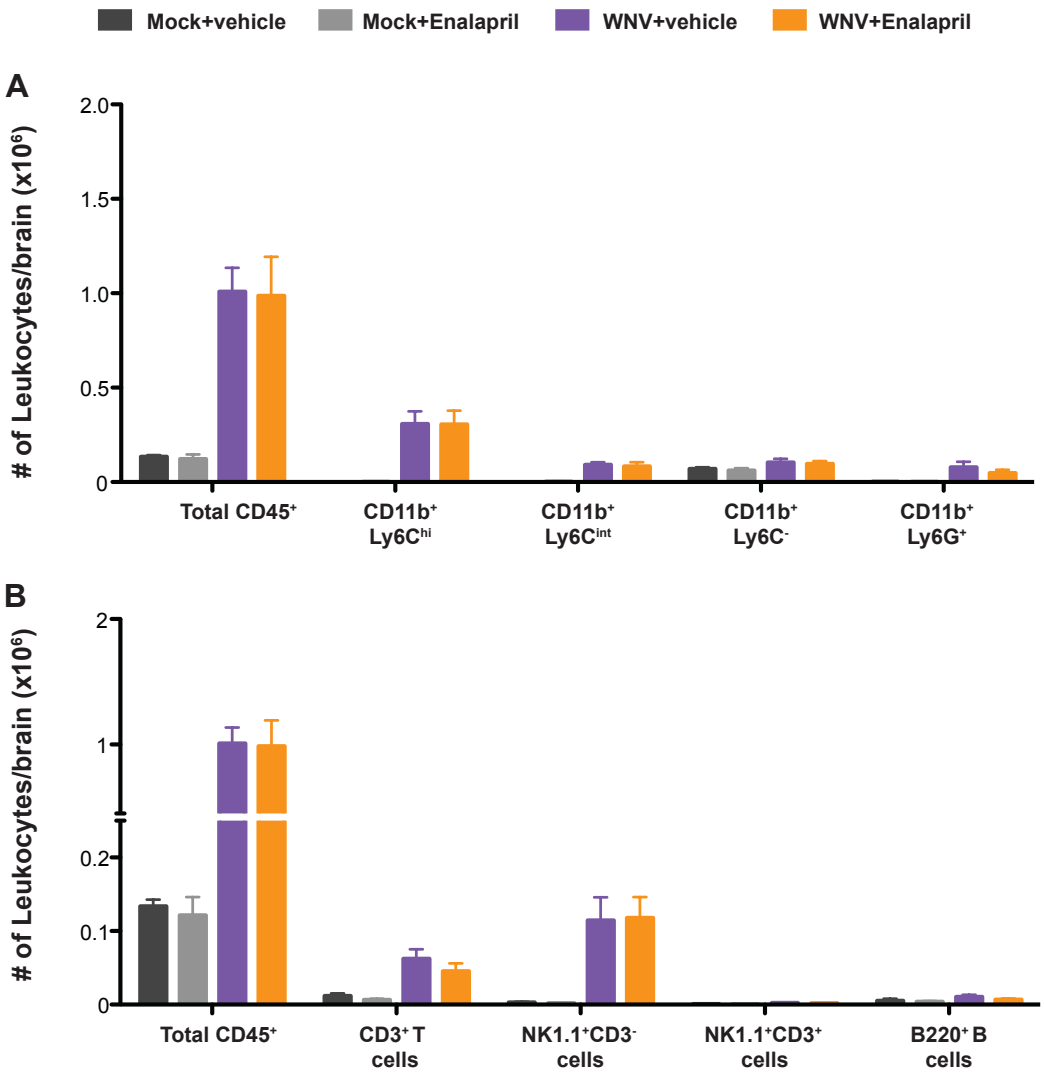

Figure 4.19 Leukocyte number in the spleen of mock- and WNV-infected ($6x10^4$ PFU) mice following treatment with Enalapril

Figure A represents the number of the following leukocyte subsets present in the spleen of mock-infected, vehicle-treated (dark grey), mock-infected, Enalapril-treated (light grey), WNV-infected, vehicle-treated (purple) and WNV-infected, Enalapril-treated (orange) mice: total leukocytes ($CD45^+$) (A), pDC ($B220^+CD11c^+$) and other DC ($CD11c^+B220^-$), neutrophils ($CD11b^{hi}Ly6G^+$) and monocytes, which were classified as $CD11b^+Ly6C^{hi}$, $CD11b^+Ly6C^{int}$, and $CD11b^+Ly6C^-$. The numbers of B ($B220^+CD11c^-$), T ($CD3^+NK1.1^-$), NK ($NK1.1^+CD3^-$) and NKT ($NK1.1^+CD3^+$) cells are shown by panel B, for the same experimental cohorts described in panel A. Data are shown as the mean ±SEM of values from 2 independent experiments, with 3 mice/group in each experiment. Statistical analysis was conducted using one-way ANOVA with a Tukey's multiple comparison post-test, and $P \leq 0.05$*; $P \leq 0.01$**; $P \leq 0.001$***.

Figure 4.19

Number of Leukocytes/Spleen

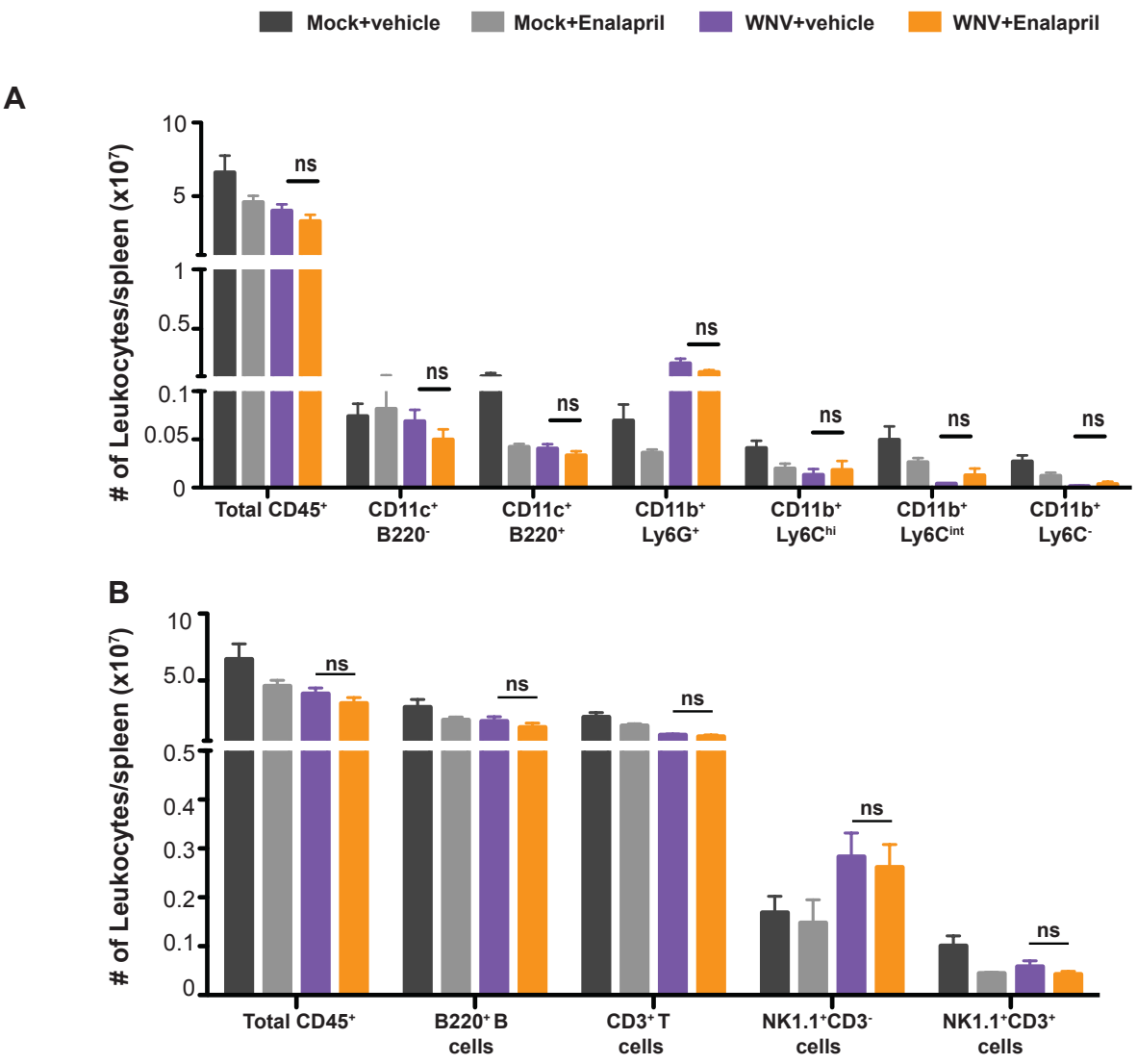

4.2.10.3. Clinical symptoms and weight loss of mice following lethal WNV infection and Enalapril treatment

Even though Enalapril-treated mice had negligible differences in CNS and splenic leukocyte number, compared to vehicle-treated cohorts, we confirmed the absence of a therapeutic effect by closely monitoring clinical symptoms. The classic symptoms of WNV encephalitis are outlined by table 2.2 and include progressive weight loss and seizure development. Although mice were not perceived to exhibit any adverse effects in response to Enalapril treatment, treatment did not produce any remarkable improvement in clinical symptoms in WNV-infected Enalapril-treated mice (Figure 4.20A). Furthermore, both the Enalapril- and vehicle-treated WNV-infected cohorts had comparable weight-loss (Figure 4.20B), with both cohorts losing significant percentage of their original weight from d6p.i. Mock-infected vehicle- and Enalapril-treated mice did not lose any significant weight during the 7-day course of infection

4.2.10.4. Survival outcome following Enalapril treatment of mice infected with a sublethal dose of WNV

Since Enalapril treatment did not result in any clinical improvement or reduction in Ly6C^{hi} macrophage infiltration into the CNS in mice that had been infected with the lethal dose of WNV ($6x10^4$ PFU), we infected mice with a 10-fold lower, sublethal dose of WNV ($6x10^3$ PFU) (Figure 4.20C). However, despite the lower dose of virus, mice receiving Enalapril treatment (orange) did not have improved survival outcomes compared to vehicle-treated mice (purple), nor was there any improvement in MST of animals given Enalapril treatment. These experiments provide no evidence that the use of an ACE inhibitor, widely reported to inhibit the deployment of splenic reservoir monocytes, has any beneficial action in our i.n. model of WNV infection. This either suggests that a splenic reservoir does

Figure 4.20 Clinical score, weight loss and survival of WNV-infected mice treated with Enalapril

The comparative clinical scores (based on table 2.2) for mock-infected, vehicle-treated (dark grey), mock-infected, Enalapril-treated (light grey) and WNV-infected ($6x10^4$ PFU) vehicle-treated (purple) and Enalapril-treated (orange) mice are shown in by panel A. The average percentage weight loss compared to original weight of mice infected with lethal dose of WNV ($6x10^4$ PFU) and given either vehicle (purple) or Enalapril treatment (orange) from day 0-7 p.i. (B). The percentage survival of mice infected with a sublethal dose of WNV ($6x10^3$ PFU) and given either vehicle (purple) or Enalapril (orange) treatment is represented by figure C. Data for the clinical score (A) are shown as the mean ±SEM of values from2 independent experiments, with 3-4 mice/group in each experiment. Data for the weight loss graph (B) is shown as the mean ±SEM of values from 2 independent experiments, with 3 mice/group in each experiment. Statistical analysis was conducted using one-way ANOVA with a Tukey's multiple comparison post-test, and $P \leq 0.05$*; $P \leq 0.01$**; $P \leq 0.001$***. Survival data (C) were graphed in a Kaplan-Meier survival curve and a Log-rank test was used to determine statistical significance. Survival experiment was performed once and is representative of 12-13 mice/group.

Figure 4.20

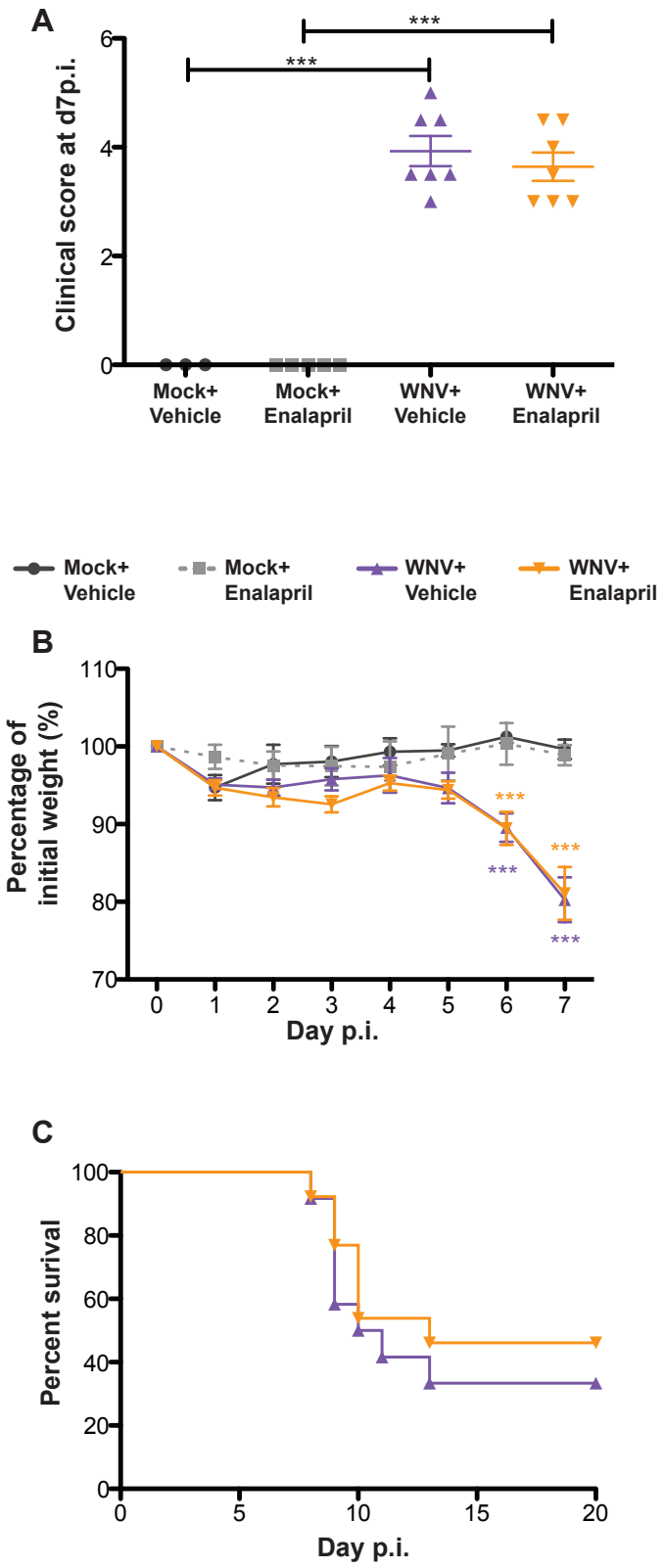
A
Clinical score at d7p.i.
6
4
2
0
***
***
Mock+ Vehicle
Mock+ Enalapril
WNV+ Vehicle
WNV+ Enalapril
Mock+ Vehicle
Mock+ Enalapril
WNV+ Vehicle
WNV+ Enalapril
B
Percentage of initial weight (%)
110
100
90
80
70
0 1 2 3 4 5 6 7
Day p.i.
***
***
***
***
C
Percent surival
100
80
60
40
20
0
0 5 10 15 20
Day p.i.

not contribute to the monocyte infiltration into the CNS during WNV encephalitis or that the infectious stimulus substantially overcomes the effect of this drug. Further studies using a peripheral model of infection such as i.p. or s.c., as a possibly lesser inflammatory stimulus, may produce a different outcome and, in light of the reduction in CNS inflammation seen with splenectomised mice, needs to be investigated.

4.2.11. Locating IMP$^+$ cells in the WNV-infected spleen-Adoptive transfer of spleen cells, MARCO and apoptosis

In order to track the fate of IMP and IMP-associated cells, we adoptively transferred non-sorted spleen cells from C57BL/6 mice i.v., stained with PKH26, into C57BL/6 WNV-infected mice and subsequently treated them with IMP. Previous work has indicated that leukocytes phagocytosing IMP are sequestered by the spleen, localising in the MARCO$^+$ marginal zone macrophages, known for the phagocytic uptake of apoptotic material from circulation (Getts et al. 2014). Thus, we examined the dynamics of IMP-associated myeloid lineage cells within the mock- and WNV-infected spleen 24h following IMP treatment. In particular, we focussed on the distribution of MARCO on IMP$^+$ CD11b$^+$ cells, as well as staining for annexin V. Annexin V has a strong affinity for phosphatidylserine residues, found on the cell surface during the early stages of apoptosis and is therefore used as a probe in the detection of apoptosing cells.

Almost all of the CD45$^+$CD11b$^+$IMP$^+$ transferred cells in the WNV-infected spleen were positive for annexin V (Figure 4.21A-B). It was also clear that the majority of transferred CD45$^+$CD11b$^+$ cells that were annexin V$^+$ (Figure 4.21C) and therefore likely undergoing apoptosis, were MARCO$^+$ (Figure 4.21B)in both mock- and WNV-infected mice. Furthermore, nearly all of the IMP$^+$annexin V$^+$ transferred CD45$^+$CD11b$^+$ cells were MARCO$^+$.

Figure 4.21 Adoptive transfer of PKH$^+$ splenic leukocytes into mock- and WNV-infected mice given IMP treatment

Representative flow cytometric dot plots of adoptively transferred splenic leukocytes on d6 p.i., followed by i.v. IMP or vehicle treatment in mock- and WNV-infected mice ($6x10^4$ PFU). Mice were sacrificed on d7 p.i. and isolated leukocytes stained for apoptosis marker, annexin V, and scavenger receptor MARCO. Panel A represents the portion of adoptively transferred PKH$^+$ splenic total leukocytes identified in the spleen. Panel B demonstrates the portion of CD45$^+$PKH$^+$ cells were CD11b$^+$. Panel C demonstrates which of these CD45$^+$ CD11b$^+$PKH$^+$ splenic leukocytes stained positive for Annexin V (ii) and which were Annexin V negative (i). Panel C, in turn indicates the MARCO distribution of both the annexin V$^+$ (ii) and annexin V$^-$ (i) PKH$^+$ splenic myeloid lineage cells.

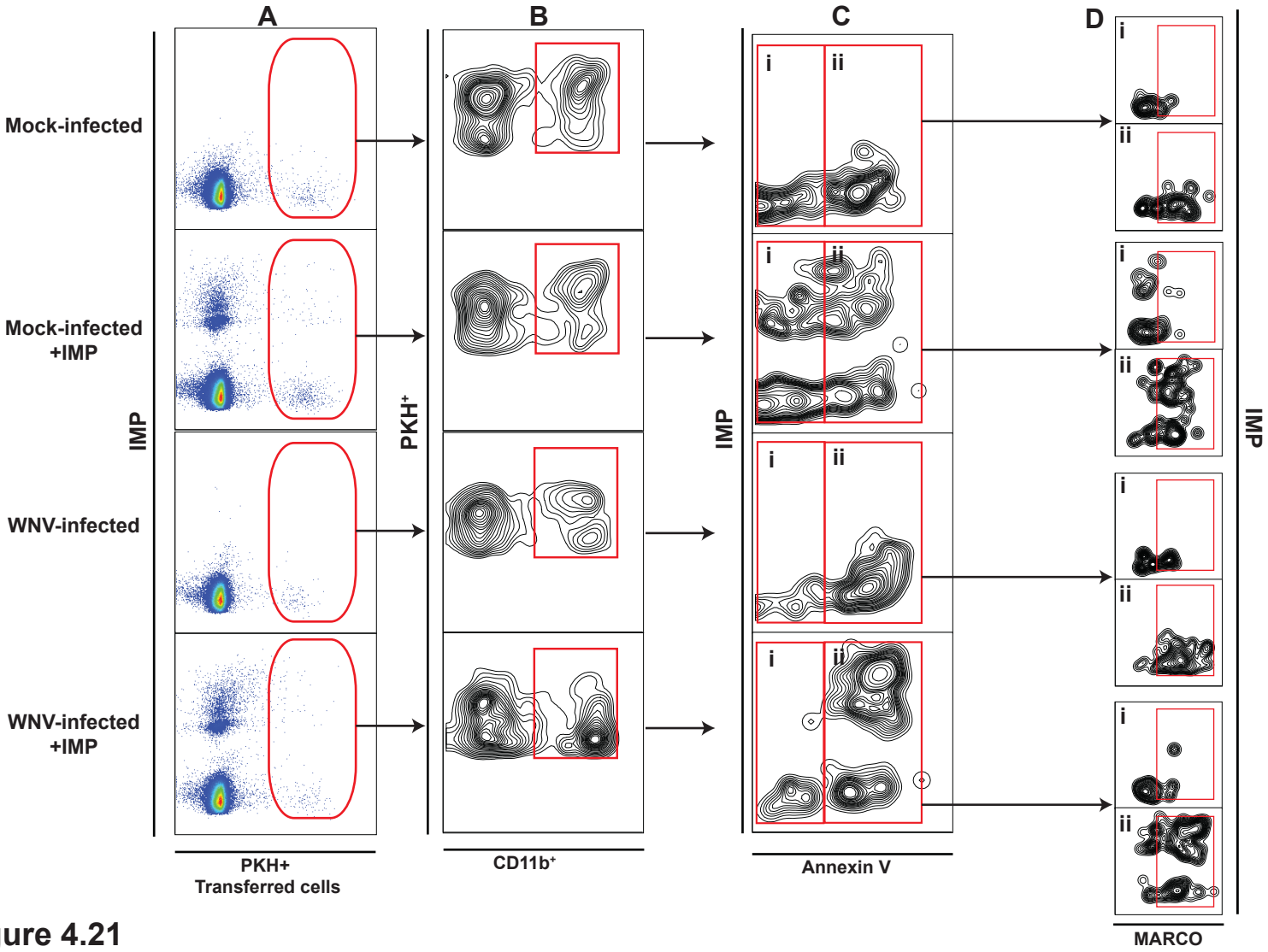
A
B
C
D
Mock-infected
Mock-infected +IMP
WNV-infected
WNV-infected +IMP
IMP
PKH+
IMP
IMP
i
ii
PKH+ Transferred cells
CD11b+
Annexin V
MARCO

Figure 4.21

We further quantified the percentage of total $CD45^+CD11b^+PKH^+$ transferred cells that were IMP^+. It was evident that the association with or possibly phagocytosis of IMP, by myeloid lineage cells was higher in the WNV-infected than mock-infected cohort, although this was not significant (Figure 4.22A). Furthermore, ~90% of the IMP^+ $CD11b^+$ transferred cells were positive for annexin V in WNV-infected spleen, in contrast to 50% in mock-infected spleen (Figure 4.22B), indicating that a larger proportion of IMP^+ cells likely undergo apoptosis under inflammatory conditions. Similarly, there were significantly more IMP^+CD11b^+ transferred cells that were $MARCO^+$ in the WNV-infected spleen (~85%) than mock-infected spleen (~60%) (Figure 4.22C). Thus, CNS viral infection promoted phagocytosis of particles by myeloid lineage cells in the circulation and subsequent transport to the spleen, where these IMP-associated cells likely undergo apoptosis. However, the extent to which MZM take up IMP and undergo apoptosis needs to be investigated.

4.3. Discussion

WNV infection of the CNS did not induce major changes in the cellularity of the spleen. There was little evidence of cell egress or proliferation from the spleen throughout the course of infection, making it unlikely that the spleen contributes significantly to the leukocyte populations infiltrating the CNS. However, the significant upregulation of Ly6C, in direct correlation with disease progression, indicates that CNS inflammation does have some impact on the spleen. Indeed, CNS inflammation has been shown to modulate splenic mRNA profile of various pro- and anti-inflammatory mediators. For example, infection with JEV induced the upregulation of various genes in the CNS and spleen, associated with the anti-viral response. These included pro-inflammatory cytokines and chemokines, such as IFN-γ and CCL2, and also Ly6C, which was upregulated by 4-fold. The authors

Figure 4.22 Annexin V and MARCO distribution of IMP$^+$ CD11b$^+$ transferred cells

Graph A represents the percentage of PKH$^+$ adoptively transferred CD11b$^+$ cells in the mock- and WNV-infected cohorts that are IMP$^+$. The percentage of CD45$^+$ PKH$^+$ CD11b$^+$IMP$^+$ adoptively transferred cells that were positive for annexin V is represented by graph B. Lastly, the fraction of CD45$^+$PKH$^+$CD11b$^+$IMP$^+$ adoptively transferred cells that were positive for MARCO is represented by figure C. Data are shown as the mean ±SEM of 3-4 mice/group and is representative of 1 experiment. Statistical analysis was conducted using an unpaired, two tailed T-test, and P≤0.05*; P≤0.01**; P≤0.001***.

Figure 4.22

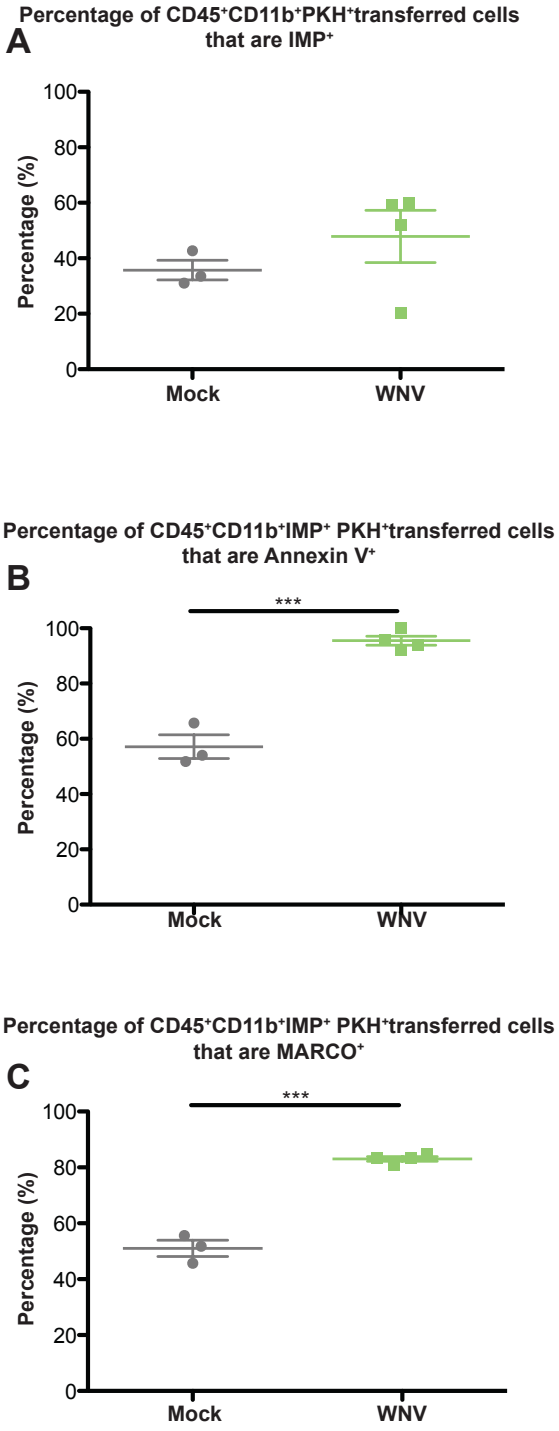
A
Percentage of CD45+CD11b+PKH+transferred cells that are IMP+
Percentage (%)
100
80
60
40
20
0
Mock
WNV
B
Percentage of CD45+CD11b+IMP+ PKH+transferred cells that are Annexin V+
***
Percentage (%)
100
80
60
40
20
0
Mock
WNV
C
Percentage of CD45+CD11b+IMP+ PKH+transferred cells that are MARCO+
***
Percentage (%)
100
80
60
40
20
0
Mock
WNV

hypothesised that the increased expression of splenic factors may aid in the antiviral response or contribute to the pathogenic response (Yang et al. 2011).

It may be possible for inflammatory mediators released by cells of the infected CNS, such as neurons or astrocytes, to enter the circulation and modulate the splenic immune response. In addition, the influence of neuroimmunological connections should be considered, as this has been shown to directly impact the spleen and vice versa following traumatic brain injury. Removal of the spleen immediately after traumatic brain injury in rats directly resulted in decreased levels of pro-inflammatory cytokines in the blood and CNS, suggesting that the spleen played a role in the systemic and CNS immune response. Consequently, rats had improved clinical outcome, which was attributed to the decreased IL-1β, TNF and IL-6, as a result of the splenectomy (Li et al. 2011). Additionally, the spleen was demonstrated to be a potent inducer of neuroinflammation in an experimental model of stroke (Lee et al. 2008). Another link between the CNS and periphery can be found in the increased risk of infection that is frequently seen in stroke patients, in part due to the upregulation of anti-inflammatory signals occurring in reaction to ischemia-reperfusion injury. This suggests that trauma in the brain, the adverse effect of which is also associated with immunopathology, influences the immunological response, although whether this is a consequence of neuroimmunological crosstalk or release of pro- or anti-inflammatory mediators into the circulation, remains to be elucidated. Even so, the rich sympathetic nerve supply to the secondary lymphoid organs, such as the spleen, does highlight the possibility of a neuroimmunological route of communication between the CNS and peripheral organs, rather than solely through circulatory mediators (Chamorro et al. 2007), although, the exact signal/s modulating the expression of Ly6C in the spleen and peripheral lymph nodes remains to be elucidated.

A link between CNS and the spleen is further emphasized by the dramatic reduction in leukocyte infiltration into the WNV-infected CNS of splenectomised mice, compared to normal mice. Notably, the reduction in cell numbers infiltrating the CNS was not due to the development of a leukopenic state in post-splenectomised mice, as there were negligible differences in leukocyte numbers in the blood or bone marrow of normal, compared to splenectomised mice. These results suggest a potential role for the spleen in supplying leukocyte subsets to the CNS, although the static nature of cell numbers in the spleen during the course of infection and stable levels of proliferation seem antithetical to this. Despite this, we wanted to confirm that the diminished leukocyte infiltration in the WNV-infected CNS of splenectomised mice was not due to the spleen acting as a source of cells for the inflamed CNS.

Much like the nervous tissue damage present in WNV encephalitis, cardiac fibrosis, due to tissue remodelling and decreased cardiac function following MI can be attributed to the detrimental actions of an exaggerated immune response. The therapeutic action of ACE inhibitors, such as Enalapril, following MI, has been well documented. However, the cardioprotective action of ACE inhibitors has, in part, been attributed to the inhibition of the renin-angiotensin-aldosterone system and subsequent decrease in blood pressure (Xu et al. 2002). In addition, studies have demonstrated that the improved vascular endothelial function and, specifically NO release, serves as an important mediator of ACE inhibitor function (Liu et al. 2002). However, recent studies have identified the spleen as a reservoir of undifferentiated monocytes, residing in the red pulp, that can rapidly be deployed in response to inflammatory signals, such as those present following MI (Swirski et al. 2009; Goltz et al. 2015). This was supported by post-mortem studies, demonstrating diminished $CD14^+$ cell numbers in the spleen, coinciding with an accumulation of in $CD14^+$ cells in the myocardium, following acute MI (van der Laan et al. 2014). Moreover, ACE

inhibitors were found to abrogate the splenic monocyte response, to the same extent as removal of the spleen, both of which had significant cardioprotective benefits following MI (Leuschner et al. 2010).

The immunopathogenic action of splenic monocytes was not limited to peripheral disease, but also significantly contributed to neuroinflammation and disease severity in the CNS, such as the pathology present in the post-ischemic brain following a stroke (Bao et al. 2010). Removal of the spleen in rats, 2 weeks prior to stroke induction via middle cerebral artery occlusion, resulted in significantly decreased infarct volume and infiltration of leukocytes (Ajmo et al. 2008). Additionally, the splenic contribution of pathogenic Ly6C^{hi} inflammatory monocytes to the spinal cord after injury far outweighed the contribution of the bone marrow, with splenectomy significantly improving post-injury recovery (Blomster et al. 2013).

Thus, we aimed to determine whether there was any evidence of deployment of pathogenic Ly6C^{hi} monocytes from this splenic reservoir, contributing to pathology in response to a CNS viral infection. We treated mice with the ACE inhibitor, Enalapril, prophylactically and at the onset of disease but found no appreciable differences in leukocyte infiltration into the CNS. There was no reduction in Ly6C^{hi} macrophages in the CNS, nor was there any indication that these cells were retained in the spleen following Enalapril administration. Moreover, Enalapril treatment did not improve clinical symptoms, and weight loss occurred at the same rate and extent in both vehicle and Enalapril-treated mice.

As the lethal dose of WNV is severe and results in 100% mortality, we also tested Enalapril treatment at the LD50 dose, which is 10-fold lower. As with the lethal dose of WNV, however, Enalapril treatment of mice infected with the sublethal dose did not improve

survival outcome significantly. Although further studies into titrating the dose of Enalapril and testing different days of intervention may be warranted, these data undoubtedly corroborate the previous studies from our laboratory identifying the bone marrow as a major source of Ly6C^{hi} inflammatory monocytes during WNV encephalitis, rather than the spleen(Getts et al. 2008) .

The nature of viral infection in the CNS is less rapid and immediately severe than an ischemia reperfusion injury, seen in MI and CNS ischemia-reperfusion/stroke injury. It is possible that the rapid deployment of splenic monocytes is required for the immediate response to ischemia-reperfusion injury whereas, in the case of CNS viral infection, signals accumulating in an incremental manner, over a period of several days, mobilises the bone marrow, rather than a splenic response. Thus, the therapeutic efficacy of ACE inhibitors may be limited to acute demand scenarios such as ischemia-reperfusion. Interestingly, however, the IMP treatment developed in this laboratory was successful in the treatment of both ischemia-reperfusion injury, such as cardiac and renal reperfusion injury, as well as CNS viral infection (Getts et al. 2014). This suggests that, IMP may target splenic- and bone marrow-derived monocytes, released into circulation in response to various types of inflammatory disease models.

The absence of the spleen may have led to a reduction of cell numbers infiltrating the CNS, but it did not alter the distribution of leukocyte subsets entering the WNV-infected CNS. Despite the reduction in inflammatory macrophage subsets in the CNS, the disease was not exacerbated nor abrogated in splenectomised mice, as the MST and mortality rate remained comparable to mice with intact spleens. Indeed, mice without spleens showed very similar disease progression to normal mice, with weight loss occurring at the same rate and intensity in both cohorts. The fact that splenectomised mice were able to efficiently clear a sublethal dose of virus to the same extent as normal mice, indicates that

the primary adaptive immune response was not significantly hampered by the absence of the spleen. This suggests that the activation and priming of e.g. T cells occurring in the lymph nodes was sufficient to compensate for the absence of the spleen in primary i.n. WNV infection. We hypothesised that a compensatory reaction may be induced in the other organs involved in the immune response, such as the bone marrow and lymph nodes. However, the absence of the spleen did not significantly alter the cell number or distribution of leukocyte subsets in the bone marrow or the blood. Mice did not become leukopenic, nor was there any sign of increased haematopoiesis and/or leukocyte release into circulation. Thus, a compensatory mechanism for the absence of the spleen in a severe CNS infection was evidently not initiated in the bone marrow.

On the other hand, the absolute leukocyte numbers of all the major subsets in the CLN were nearly doubled in splenectomised mice, indicating a global compensation in the absence of the spleen. Furthermore, the ratio of leukocyte subsets in splenectomised and normal mice also remained unchanged. Interestingly, preliminary data suggested that this also occurred in peripheral nodes, such as the ILN, which are not directly involved in CNS inflammatory response.

Having established that the removal of the spleen had no effect on survival and severity of disease in a primary infection, we investigated the impact on the memory response to a secondary infection by rechallenging with a lethal dose of WNV. Both activation and priming of naïve T cells, and development of memory cells are highly dependent on the environment of the secondary lymphoid organs, including the spleen. Splenectomised mice have been shown to have severely impeded T cell responses to primary and secondary infection with *Listeria monocytogenes* (Kursar et al. 2008). Furthermore, the role of the spleen in the memory response and maintenance of peripheral B cell

homeostasis is highlighted by the decreased frequencies of IgM memory B cells in splenectomised individuals (Martinez-Gamboa et al. 2009; Cameron et al. 2011).

However, surprisingly, all but two splenectomised mice were able to successfully eradicate a secondary i.n. infection with a lethal dose of WNV, without any signs of developing illness. Of the two rechallenged splenectomised animals, the outcome was lethal in one case, with the remaining mouse recovering without any sequelae. There is evidence of enhanced homeostatic proliferation of memory T cells in splenectomised mice (Kim and Harty 2014). The protective capacity of these memory T cells was unaltered and this would explain the ability of splenectomised mice to maintain the memory immune responses. However, this raises the question of where the primary components of the memory response reside, in the lymph nodes or the spleen and to what extent this changes in focussed models of infection, such as with i.n. WNV in the CNS *versus* perhaps more general peripheral models of infection. Future studies, in which mice with intact spleens are infected, resolve infection, and prior to secondary rechallenge undergo splenectomy, may resolve this question. Furthermore, whether splenectomised mice would retain the ability to eradicate primary or secondary WNV infection administered via a peripheral route, i.e. i.p. or s.c., is of interest but remains unknown. It would seem logical that the spleen plays a critical role in the control of viral dissemination, priming of T cells and the development of memory responses in a peripheral rather than CNS infection. Nevertheless, these data demonstrate that the spleen is not required in primary or secondary i.n. WNV infection, limited to the CNS.

Ly6C^{hi} inflammatory monocytes, which would become highly pathogenic macrophages in the CNS during WNV encephalitis, are reduced in the CNS by IMP treatment, which is accompanied by a concurrent increase in this subset in the spleen. Not surprisingly, after IMP treatment, significant numbers of IMP localise to the spleen. We hypothesised that the

spleen may play a crucial role in the efficacy of IMP treatment, and in testing IMP treatment in splenectomised mice, we found that, while IMP treatment reduced leukocyte infiltration into the WNV-infected CNS, this was not statistically significant, compared to WNV-infected, splenectomised, vehicle-treated controls. As shown in this chapter, splenectomised animals infected with WNV had already diminished cell numbers infiltrating the WNV-infected CNS. Thus, further reductions in Ly6C^{hi} macrophages should feasibly have translated into improved clinical outcome. Indeed, improved survival followed sublethal WNV i.n. infection of splenectomised mice, treated with IMP.

Surprisingly, the reduction in infiltrating cell numbers evidently due to splenectomy, did not itself improve the clinical outcome, to the same extent as splenectomy combined with IMP treatment or IMP treatment in normal mice. This indicates a disparity between cell subsets modulated in WNV-infected, splenectomised mice and normal mice receiving IMP treatment only. Nevertheless, the efficacy of IMP treatment remained maximal in mice with intact spleens, strongly suggesting a contribution by the spleen that cannot be fully replicated by other organs where IMP^{+} Ly6C^{hi} monocytes may be sequestered, during WNV encephalitis in splenectomised animals.

Notably, however, there were no differences in the numbers of IMP^{+}leukocytes in the liver, blood, bone marrow and moreover, splenectomised mice had fewer IMP^{+} leukocytes in the brain and CLN, compared to normal mice. Thus, the fate of IMP^{+} leukocytes in the absence of the spleen is currently unclear and further examination will be necessary to resolve the kinetics, distribution and excretion of IMP.

We tried to determine the fate of cells phagocytosing and/or associating with IMP on the cell surface that are subsequently sequestered in the spleen, following IMP treatment of WNV-infected mice. We found that a higher percentage of adoptively transferred PKH26^{+} splenocytes had associated with IMP in the spleens of WNV-infected than mock-infected

mice. This is likely to be due, at least in part, to the fact that during infection cells are more likely to phagocytose particulate matter in the blood (Getts et al. 2014). In addition, the outcome of the annexin V staining suggested that WNV infection created a splenic environment where IMP$^+$ myeloid lineage cells were more likely to undergo apoptosis than cells in a mock-infected mouse spleen. The majority of annexin V$^+$ IMP$^+$CD11b$^+$ cells were identified as being positive for the scavenger receptor MARCO. This may not be surprising, as the MARCO$^+$ marginal zone macrophages readily phagocytose apoptotic or negatively-charged material (McGaha et al. 2011). Moreover, WNV infection increases the expression of MARCO on peripheral blood monocytes and IMP are taken up by fewer monocytes when MARCO is genetically absent (Getts et al. 2014). Thus, it seems to confirm that increased numbers of MARCO$^+$ monocytes pick up IMP in the peripheral blood and become Annexin V$^+$ as a result, subsequently undergoing apoptosis in the marginal zone of the spleen (Getts et al. 2014). This would certainly reduce the number of Ly6Chi inflammatory monocytes available to migrate to the CNS in WNV encephalitis. However, free IMP are also undoubtedly picked up by the marginal zone macrophages themselves. Whether monocytes containing IMP expressing phosphatidyl serine are also taken up by the marginal zone macrophages, as part of clearance of "apoptotic cells" is not demonstrated by these data. Moreover, whether the presence of marginal zone macrophages taking up IMP or apoptotic cells is necessary for the therapeutic effect of IMP is not resolved by these data. This question will be addressed in the next chapter.

5. Chapter 5 Depletion of circulatory and splenic resident macrophages-WNV infection and IMP treatment

5.1. Introduction

The depletion of macrophages with clodronate-encapsulated liposomes has been well documented (Naito et al. 1996; van Rooijen and van Nieuwmegen 1984). These liposomes contain dichloromethylene-bisphosphonate (clodronate) and are designed to mediate intracellular delivery of clodronate via phagocytosis. Once inside the phagocytic cell, the clodronate is released into the aqueous compartments and, after exceeding a threshold concentration, initiates the apoptosis of the cells, although clodronate itself is not directly toxic (van Rooijen and van Nieuwmegen 1984). When administered intravenously, clodronate liposomes deplete all the circulatory macrophages as well as the resident macrophages of the spleen, such as the red pulp, marginal zone and marginal metallophillic macrophages, and liver Kupfer cells (Naito et al. 1996; Yamamoto et al. 1996; van Rooijen et al. 1989), although they spare the microglia in the CNS, even during the highly inflammatory pathogenesis of WNV encephalitis.

As the modulation of Ly6C^{hi} monocytes has shown great therapeutic promise in our model of i.n. WNV encephalitis (Getts et al. 2014), we were interested to determine how clodronate depletion would affect leukocyte infiltration and in particular Ly6C^{hi} monocyte content of the CNS during WNV infection. Indeed, cells of the myeloid lineage are preferentially depleted by clodronate liposomes, with activated macrophages, such as those present in circulation during WNV infection, exhibiting the highest degree of liposome incorporation, compared to resting monocytes (Schmidt-Weber et al. 1996). Furthermore, there is evidence of i.v. clodronate depletion inducing increased production

and release of monocytes into circulation for up to 5 days after administration (Yamamoto et al. 1996). As WNV infection results in significant recruitment of monocytes from the bone marrow, it was of interest to determine how the disease course may be modulated by the combined action of WNV and clodronate depletion on the bone marrow and specifically the production of Ly6C^{hi} monocytes. It is clear that both of these scenarios place immense pressure on the bone marrow to replace monocytes. Our first objective with clodronate depletion was to determine how the depletion of circulatory monocytes would affect WNV disease course and mortality rates.

Secondly, we wished to determine the therapeutic efficacy of IMP treatment following clodronate depletion, after ablation of MARCO^{+} marginal zone macrophages in the spleen. In Chapter 4 our results illustrated that the spleen not only has an impact on leukocyte trafficking to the CNS, but also contributes significantly to the efficacy of IMP treatment.. Furthermore, our laboratory has shown that IMP and/or IMP-associated cells concentrate in the MARCO^{+} marginal zone macrophages (Terry 2012). As these marginal zone macrophages are known to take up nanoparticles and apoptosing cells, we hypothesised that they likely phagocytose IMP and/or IMP-associated cells, which may be undergoing apoptosis. Indeed, the marginal zone macrophages may provide an ideal environment for interactions to take place that are crucial to the therapeutic efficacy of IMP treatment.

5.2. Results

5.2.1. Clodronate depletion and WNV infection

Previous studies indicate that 24-48 h is sufficient to completely deplete the marginal zone macrophages in the spleen, following i.v. administration of clodronate liposomes (CLO) (Naito et al. 1996). Therefore, the splenic response was dissected at various time-points

after i.v. clodronate depletion. We focussed on immunofluorescent staining, as MARCO is a particularly difficult antigen to detect by flow cytometry. Adult C57BL/6 female mice were given i.v. injection of CLO and the spleen was processed for IHC 14, 48 and 72h later, in order to determine at what time-point the majority of $MARCO^+$ marginal zone macrophages were depleted. Figure 5.1 A shows the representative immunofluorescent staining for the $F4/80^+$ red pulp macrophages (green), $MARCO^+$ marginal zone macrophages (red) and nuclei (DAPI-blue) of CLO- and PBS- injected spleen. A reduction in the marginal zone macrophages occurs as early as 14h post-injection of CLO, and these cells are mostly depleted by 48h. By 72h after i.v. CLO administration, there was no positive staining for MARCO in the spleen. Furthermore, a distinct reduction in $F4/80^+$ cells, i.e. the red pulp macrophages, was evident by 48h and these cells were also largely depleted by 72h after CLO administration.

Based on the above, we used a single i.v. dose of CLO liposomes at d5 p.i. in WNV-infected (i.n.) mice, given either LD100 ($6x10^4$ PFU) or LD50 ($6x10^3$ PFU) dose of virus (Figure 5.1B). In the LD100 model of infection, CLO was administered when mice first start losing weight (d5p.i.) and showing signs of leukocyte infiltration into the CNS, i.e., when the pathogenic action of $Ly6C^{hi}$ monocytes starts and where any response to intervention would be most obvious.

5.2.2. CNS leukocyte infiltration in the CNS of WNV-infected mice following CLO depletion

Studies suggest that i.v. CLO depletes monocytes in the circulation, but these are rapidly replaced by the bone marrow in higher numbers than before (Yamamoto et al. 1996). This, so-called 'left shift', induced in the bone marrow, is similar to that seen in WNV encephalitis, as the recruitment of monocytes to the CNS places immense pressure on the

Figure 5.1 Depletion of MARCO$^+$ marginal zone macrophages with clodronate liposomes

Panel A demonstrates the representative immunofluorescent staining for MARCO$^+$ (red) marginal zone macrophages and F4/80$^+$ (green) red pulp macrophages, with nuclei stained with DAPI (blue) in a splenic cross-section of naïve mice 14, 48 and 72h after i.v. clodronate (CLO) depletion, compared to control spleen. Panel B illustrates the protocol followed for CLO depletion of WNV and mock-infected mice. Mice were mock- or WNV-infected, WNV infection was administered at either LD50 ($6x10^3$ PFU) or LD100 ($6x10^4$ PFU) dose and CLO liposomes or vehicle treatment administered at d5 p.i. Mice infected with the LD100 dose of virus were culled at d7p.i. and tissue collected for processing.

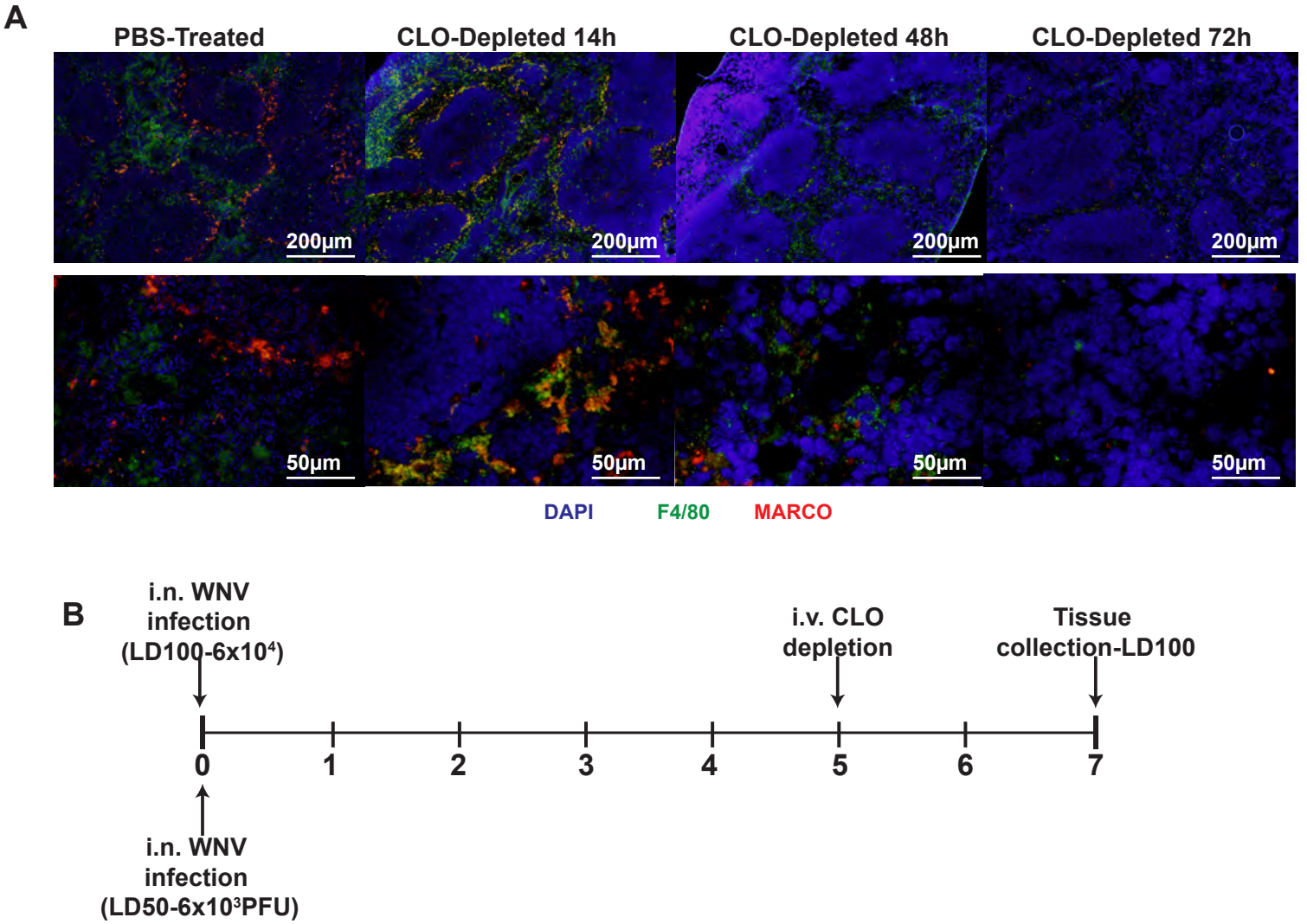
A
PBS-Treated
CLO-Depleted 14h
CLO-Depleted 48h
CLO-Depleted 72h
200μm
200μm
200μm
200μm
50μm
50μm
50μm
50μm
DAPI
F4/80
MARCO
B
i.n. WNV infection (LD100-6x10⁴)
i.v. CLO depletion
Tissue collection-LD100
0
1
2
3
4
5
6
7
i.n. WNV infection (LD50-6x10³PFU)

Figure 5.1

bone marrow for an increased supply of monocytes. Therefore, it was of interest to determine how the combined actions of CNS infection and CLO depletion affected the CNS leukocyte infiltration and immunopathology.

CLO depletion at d5 p.i. in mice infected with lethal dose of WNV ($6x10^4$ PFU) resulted in significantly reduced total leukocyte infiltration into the CNS at d7p.i., compared to control mice (Figure 5.2 A and Figure 5.3 A). Although the CLO-depleted WNV-infected cohort still had significant infiltration compared to mock-infected mice (grey), there was a stark reduction in specific leukocyte subsets relative to the WNV-infected control group. There were negligible differences in the CNS leukocyte numbers of mock-infected mice given CLO, compared to control mock-animals (data not shown), thus only control mock-infected mice are included in these graphs.

Notably, the $Ly6C^{hi}$ inflammatory macrophages, as well as the $Ly6C^{-}$ resident microglia were reduced in the CLO-depleted, WNV-infected cohort, whereas $Ly6C^{int}$ cells were comparable between control and CLO-depleted mice (Figure 5.2A). The reduction in $Ly6C^{hi}$ inflammatory macrophage numbers was likely due to the inability of the bone marrow to keep up with the demand for these cells created by the combined action of CLO depletion and WNV infection. The $Ly6C^{int}$ microglial population in the CNS of WNV-infected mice are described as activated microglia and are contributed to by infiltrating $Ly6C^{hi}$ monocytes, which downregulate Ly6C becoming $Ly6C^{int}$ (Getts et al. 2008). As CLO depletion reduced the $Ly6C^{hi}$ macrophage population in the CNS, the negligible change in $Ly6C^{int}$ numbers was unexpected. However, it may be that a higher percentage of the $Ly6C^{-}$ resident microglia upregulated their Ly6C expression, becoming $Ly6C^{int}$, in order to compensate for the dramatic reduction of infiltrating monocytes. This would account for

Figure 5.2 Leukocyte number and percentage in the CNS of mock- or WNV-infected mice following single or daily clodronate depletion

Graph A shows the number of leukocytes in the CNS following a single clodronate (red) or control (blue) treatment at d5p.i. of WNV-infected mice ($6x10^4$ PFU) and mock-(grey) at d7 p.i. Figure A demonstrates the total leukocyte number ($CD45^+$) and myeloid lineage cells ($CD11b^+$), including the resident microglia ($CD45^{int}CD11b^+Ly6C^-$), immigrant/activated microglia ($CD45^+CD11b^+Ly6C^{int}$) and inflammatory macrophages ($CD45^+CD11b^+Ly6C^{hi}$). Graph B demonstrates the percentage of myeloid lineage cells ($CD11b^+$), including the resident microglia ($CD45^{int}CD11b^+Ly6C^-$), immigrant/activated microglia ($CD45^+CD11b^+Ly6C^{int}$) and inflammatory macrophages ($CD45^+CD11b^+Ly6C^{hi}$) in the CNS.

Data for figure A and B are the mean ±SEM of values from 3 independent experiments, with 2-4 mice/group in each experiment. Statistical analysis was conducted using one-way ANOVA with a Tukey's multiple comparison post-test, and P≤0.05*; P≤0.01**; P≤0.001***.

Figure 5.2 CNS leukocytes - CLO depletion (d5p.i.)

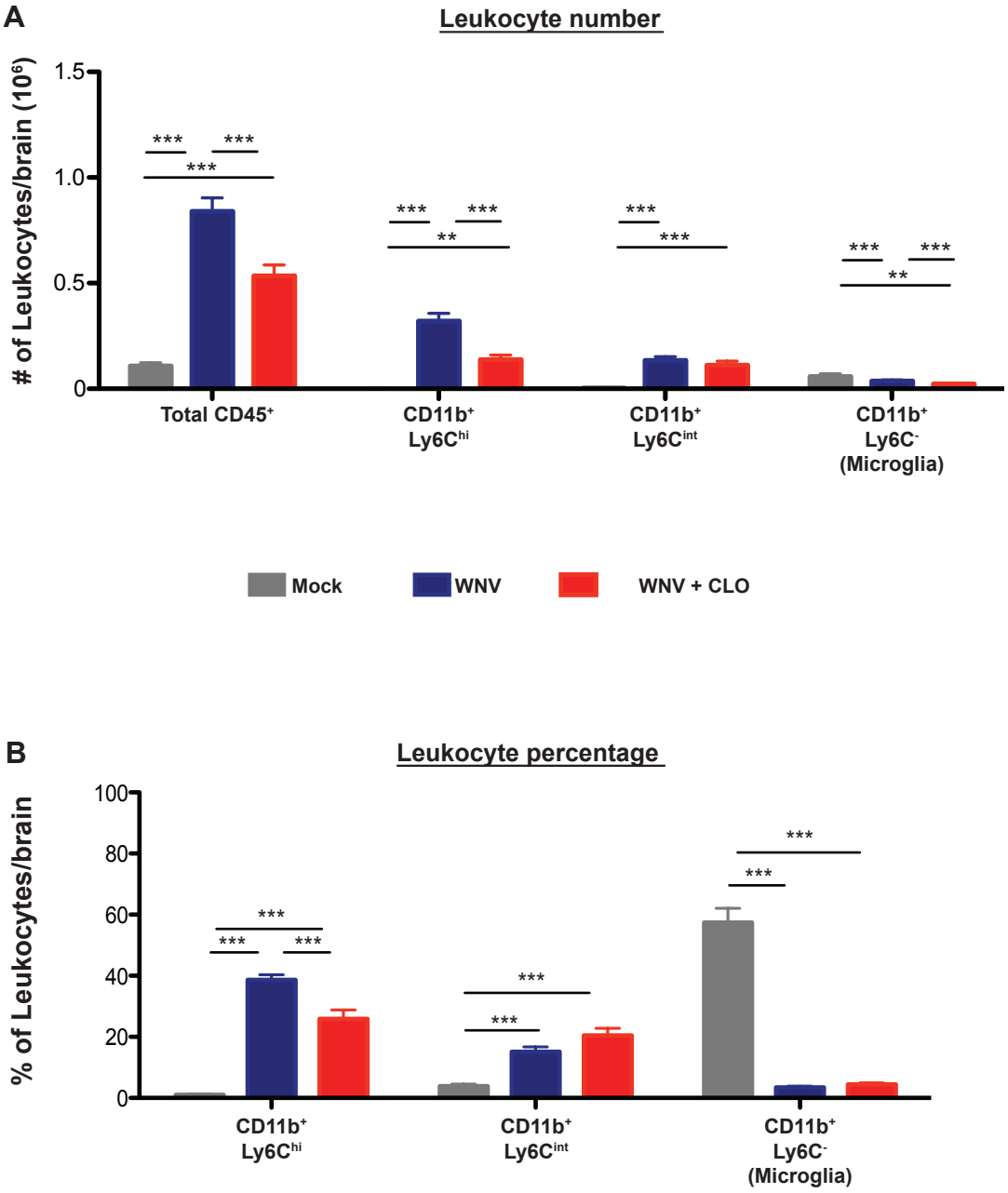

Figure 5.3 Leukocyte number and percentage in the of mock- or WNV-infected mice following single-dose (d5 p.i.) and daily clodronate depletion.

Graphs A and B show the numbers and percentages of cells in the CNS following a single clodronate (CLO) (red) or vehicle treatment (blue) at d5p.i. WNV-infected, control ($6x10^4$ PFU) or mock-infected (grey) mice at d7 p.i. Graph A illustrates the number of neutrophils ($CD11b^{hi}Ly6G^{+}Ly6C^{int}$) and lymphoid lineage cells including T ($CD3^{+}$), B ($B220^{+}/CD19^{+}$) and NK ($NK1.1^{+}$) cells in the CNS. Graph B illustrates the percentage of neutrophils ($CD11b^{hi}Ly6G^{+}Ly6C^{int}$) and lymphoid lineage cells, including T ($CD3^{+}$), B ($B220^{+}/CD19^{+}$) and NK ($NK1.1^{+}$) cells in the CNS following CLO depletion at d5 p.i. (expressed as percentage of total leukocytes).

Graph C demonstrates the number of leukocytes in the CNS following daily clodronate depletion of mock- (grey) or CLO-depleted, WNV–infected (purple) and control, WNV-infected (blue) ($6x10^4$ PFU) mice at d7 p.i.

Data for figures A and B are the mean ±SEM of values from 3 independent experiments, with 2-4 mice/group in each experiment. Data for figure C is the mean ±SEM of 1 experiment with 3-4 mice/group. Statistical analysis was conducted using one-way ANOVA with a Tukey's multiple comparison post-test, and $P \leq 0.05$*; $P \leq 0.01$**; $P \leq 0.001$***.

Figure 5.3 CNS leukocytes - CLO depletion (d5p.i.)

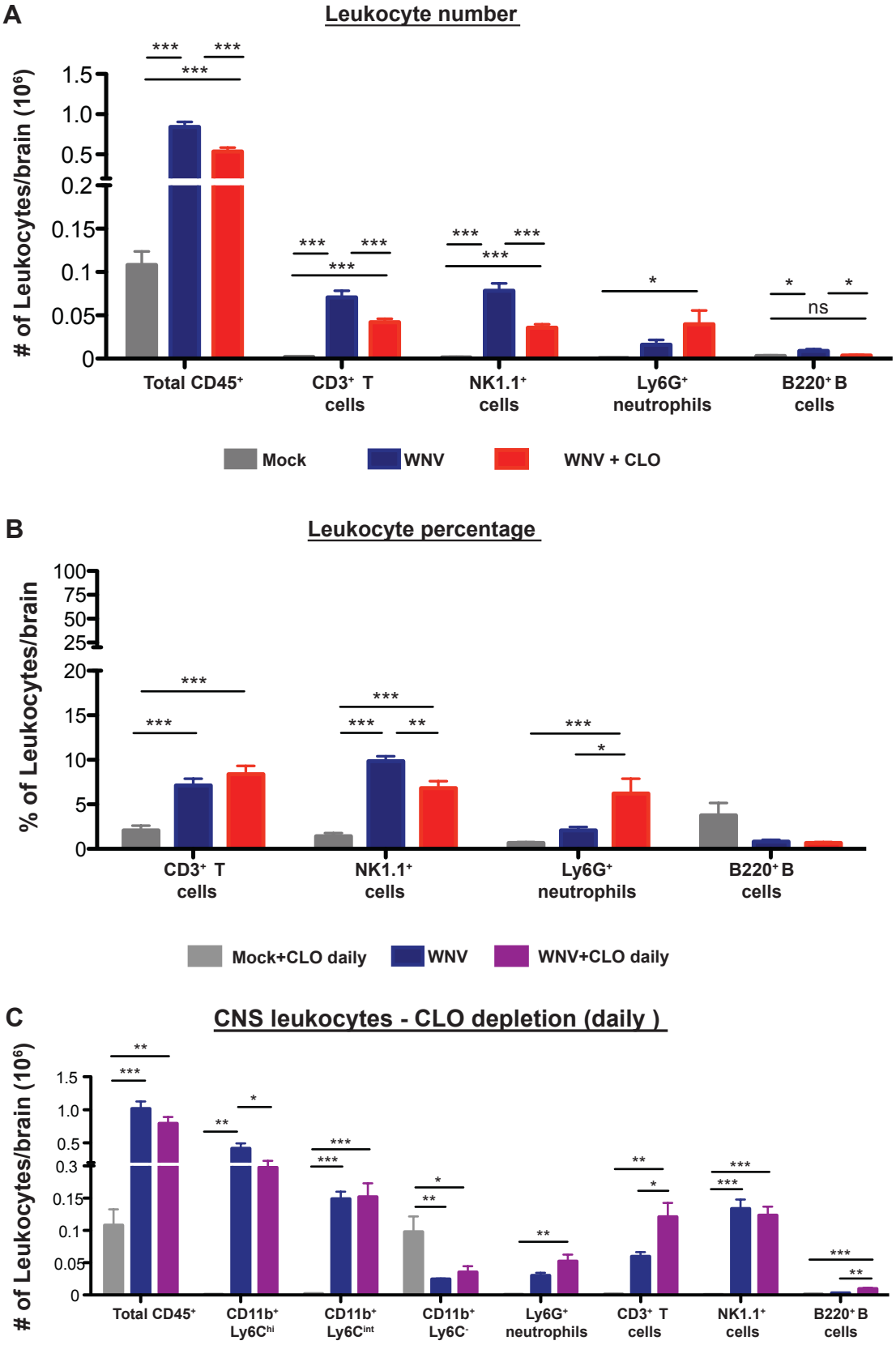

the reduction in Ly6C^{-} microglia in the CNS of CLO-depleted mice, as well as the negligible change in Ly6C^{int} numbers between CLO-depleted and control mice.

CLO depletion not only affected monocyte infiltration, but also significantly reduced lymphoid lineage cell infiltration into the WNV-infected CNS at d7p.i. (Figure 5.3A). These included the number of total T, NK and B cells, however, except for the B cells, these subsets were still present in significantly higher numbers compared to naïve mice. Interestingly, CLO depletion did not reduce neutrophil numbers but rather increased them relative to WNV-infected control, but this was not significant.

The percentage distribution (Figure 5.2B and Figure 5.3B) of leukocytes infiltrating the CNS of CLO-depleted, WNV-infected mice was somewhat modulated compared to WNV-infected controls. Neutrophils were present in a significantly higher percentage in the CLO-depleted cohort (Figure 5.3B), whereas the percentage of NK cells (Figure 5.3B) and Ly6C^{hi} macrophages (Figure 5.2B) was significantly reduced, relative to the control WNV-infected cohort. Nevertheless, the Ly6C^{hi} macrophages remained the largest portion of leukocyte infiltrate in WNV-infected mice of both cohorts (Figure 5.2B).

Although the number and percentage of Ly6C^{hi} inflammatory macrophages infiltrating the CNS of single-dose CLO-depleted mice, was markedly reduced compared to control WNV-infected mice, it was still significantly high relative to the mock-infected cohort. We reasoned that, if a single dose of CLO can result in such a stark reduction, daily injections of CLO may result in further abrogation of the Ly6C^{hi} macrophage population in the WNV-infected CNS (Figure 5.3C). However, despite receiving daily injections of CLO, WNV-infected mice still had significant infiltration of monocytes into the CNS at d7 p.i., relative to naïve mice. Moreover, the number of cells infiltrating the CNS of mice receiving daily

CLO injections was comparable to WNV-infected mice receiving a single dose of CLO at d5 p.i. This indicates that the bone marrow can rapidly replace most of the Ly6C^{hi} monocytes, repeatedly depleted from circulation, for an extended period of time (i.e. 6 days) during infection of the CNS. The phenotypic markers we included in our analysis (CD45^{+}CD11b^{+}Ly6C^{hi}) indicated that the inflammatory monocytes produced by the bone marrow after CLO depletion were similar to what was being produced in control mice. However, future additional markers may specify whether or not these cells vary in their level of activation or maturity.

5.2.3. Clinical outcome of WNV-infected mice following clodronate depletion

Reduced numbers of pathogenic Ly6C^{hi} macrophages in the WNV-infected CNS has been shown to correlate with improved disease outcome (Getts et al. 2012; Getts et al. 2014). Thus, we proceeded to establish whether the significant reduction in Ly6C^{hi} macrophages in the CNS of CLO-depleted, WNV-infected mice might lead to an improved clinical outcome. In contrast to what we have shown with IMP-induced reduction of Ly6C^{hi} inflammatory macrophages, the significant reduction in this subset following CLO-depletion of WNV-infected mice did not reduce mortality in the sublethal dose of infection (6x10^{3} PFU) (Figure-5.4A). Indeed, in the lethal model of infection (6x10^{4} PFU), CLO-depleted mice had similar patterns of weight loss (Figure 5.4B) and comparable clinical scores (Figure 5.4C) at d7 p.i. compared to their WNV-infected control cohort.

Thus, although the absolute number of Ly6C^{hi} inflammatory macrophages in the CNS of CLO-depleted mice reduced significantly, it did not translate to improved clinical outcome. This could indicate that the Ly6C^{hi} inflammatory macrophages, induced from the bone marrow following CLO depletion, differs in their pathogenic nature i.e. are more activated

Figure 5.4 The clinical outcome of mock- or WNV-infected mice following single-dose clodronate depletion at d5 p.i.

Graph A demonstrates the percentage survival of mock-infected (black); mock-infected, CLO-treated (grey); WNV-infected, CLO-treated (red) and WNV-infected, vehicle-treated (blue) mice, following infection with a sublethal dose of WNV ($6x10^3$ PFU). Graph B represents the average percentage weight loss, compared to original weight, of mock- (grey) and WNV-infected, control (blue) *versus* WNV-infected, CLO-depleted (red) mice following lethal WNV infection ($6x10^4$ PFU), from d0-7 p.i. Graph C compares the average clinical score of WNV-infected ($6x10^4$ PFU), CLO-depleted (red) or control (blue) treated mice at d7 p.i.

The survival study was performed in 3 separate experiments with 25-28 mice/group. Survival data (A) was grouped and graphed in a Kaplan-Meier survival curve and a Log-rank test was used to determine statistical significance. The weight loss graph (B) is the mean ±SEM of 3-4 mice/group from one experiment. Statistical analysis for graph B was conducted using a one-way ANOVA with a Dunnet's multiple comparison post-test (d0 as control). Clinical score data (C) is the mean ±SEM of values from 3 independent experiments, with 2-4 mice/group in each experiment. Statistical analysis for figure C was conducted using an unpaired, two tailed T-test, and $P \leq 0.05$*; $P \leq 0.01$**; $P \leq 0.001$***.

Figure 5.4

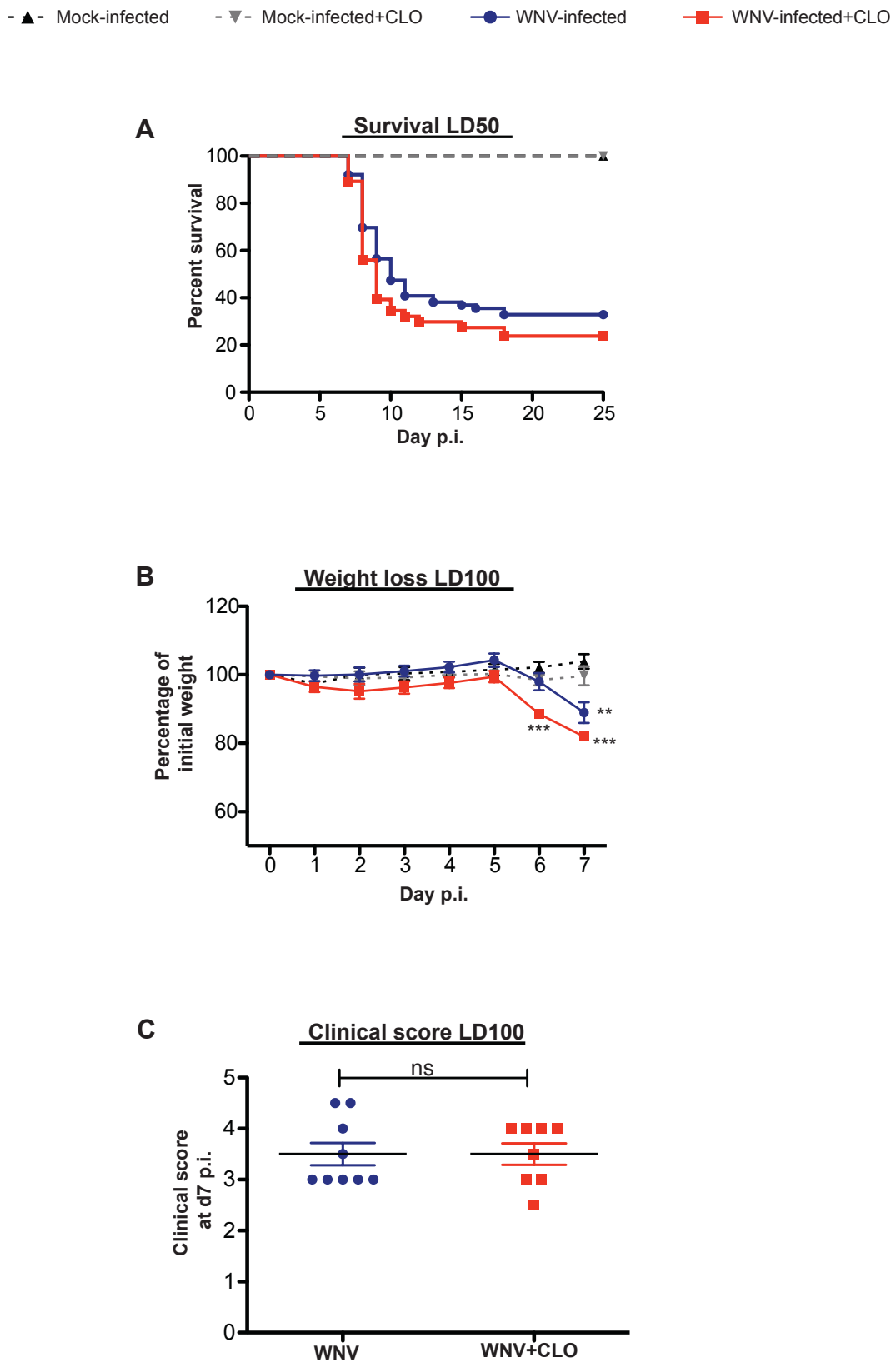
Mock-infected
Mock-infected+CLO
WNV-infected
WNV-infected+CLO
A
Survival LD50
Percent survival
Day p.i.
B
Weight loss LD100
Percentage of initial weight
Day p.i.
**
***
***
C
Clinical score LD100
ns
Clinical score at d7 p.i.
WNV
WNV+CLO

or immature than in control mice. It may be that CLO depletion exhausts the supply of mature monocytes from circulation, inducing the release of highly activated and immature monocytes into circulation to offset the effect of depletion and infection. Therefore, even though there are decreased numbers of Ly6C^{hi} inflammatory macrophages in the CLO-depleted WNV-infected CNS, the Ly6C^{hi} cells which are present could be more neuropathic, abrogating the beneficial effect that the reduction in this subset may otherwise have had.

5.2.3.1. Leukocyte numbers in the spleen following CLO-depletion of WNV-infected mice

Intravenous clodronate depletion is characterised by distinct changes in splenic leukocyte populations. Although macrophages, in particular the marginal zone and red pulp macrophages, are the primary target of clodronate-encapsulated liposomes, other splenic leukocyte subsets, such as the marginal zone lymphocytes and white pulp macrophages, are also affected. Although these subsets are not completely abolished, they do reduce in number and phagocytic activity (van Rooijen and van Nieuwmegen 1984; van Rooijen et al. 1985; van Rooijen et al. 1989). As previous work from our lab has shown, IMP or IMP^{+} cells specifically localise in the marginal zone of the spleen (Getts et al. 2014; Terry 2012). Therefore, in order to determine how CLO-depletion would affect splenic IMP uptake, we needed to establish the baseline changes occurring in the splenic leukocyte populations after CLO depletion of WNV-infected mice without IMP treatment. Since single-dose CLO depletion produced similar outcomes to the daily CLO depletion regime, we used the single-dose depletion approach in these experiments, as shown in Figure 5.1 B.

As shown by the immunofluorescence staining in Figure 5.1 A, MARCO^{+} cells were completely abrogated by single-dose CLO depletion, within 48h. Therefore, in these experiments, FACS analysis focusing on changes in other leukocyte subsets was

conducted, rather than trying to reconfirm MARCO expression, considering the difficulties in identifying MARCO by flow cytometry.

As mentioned previously, the lymphocyte populations in the spleen may also be reduced with CLO depletion and while this was evident in our data, the trend for B and T cells to decrease, but this was not statistically significant, in CLO-depleted, mock- and WNV-infected mice (Figure 5.5A). In addition, the percentage of B cells in the spleen significantly increased in WNV-infected, CLO-depleted mice as a consequence of the depletion of other cells (Figure 5.5B).

As expected, single-dose CLO depletion of mock- and WNV-infected mice had the biggest impact on the F4/80$^+$ red pulp macrophages. Numbers of F4/80$^+$ cells were reduced to less than 3% of the control numbers (Figure 5.6A), with the percentage reducing to <1% of the total leukocyte population (Figure 5.6B). In addition, the DC subsets in the spleen were significantly decreased with CLO depletion. The CD11c$^+$CD11b$^+$ subset of CLO-depleted spleen reduced in number (Figure 5.6A) and percentage (Figure 5.6B) in both mock- and WNV-infected mice, relative to their control-treated cohorts. Similarly, numbers (Figure 5.6A) of pDC in WNV-infected, CLO-treated mice decreased significantly. The representative flow cytometry contour plots (Figure 5.8B) demonstrate the stark reduction in F4/80$^+$ and CD11c$^+$ population in the WNV-infected, CLO-depleted spleen compared to the WNV-infected, control spleen. Additionally, Figure 5.8 A illustrates the modulation of the neutrophil population in the spleen following CLO depletion. Indeed, the percentage of neutrophils in the spleen increased significantly in WNV-infected, CLO-depleted mice (Figure 5.6B). While, this is likely to be due to the decrease in numbers of other leukocyte subsets as a consequence of depletion, it is also possible that increased neutrophil numbers are a result of bone marrow responses in this cell lineage (Figure 5.6A).

Figure 5.5 Leukocyte numbers in the spleen of mock- or WNV-infected mice following clodronate depletion at d5 p.i.

Graphs A and B represent the numbers and percentages of leukocytes in the spleen of ($6x10^4$ PFU) WNV-infected, vehicle-treated (blue) or WNV-infected, CLO-depleted (red) and mock-infected, vehicle-treated (dark grey) or mock-infected, CLO-depleted (light grey) mice at d7 p.i. Figure A demonstrates the change in numbers of B ($B220^+CD11c^-$), T ($CD3^+NK1.1^-$), NK ($NK1.1^+CD3^-$) and NKT ($CD3^+NK1.1^+$) cells following clodronate depletion. Graph B demonstrates the change in percentage of B ($B220^+CD11c^-$), T ($CD3^+NK1.1^-$), NK ($NK1.1^+CD3^-$) and NKT ($CD3^+NK1.1^+$) cells in the spleen following clodronate (CLO) depletion. Percentages of various subsets are expressed as a percentage of total leukocytes in the spleen of each cohort. Data are the mean ±SEM of values from 3 independent experiments, with 2-4 mice/group in each experiment. Statistical analysis was conducted using one-way ANOVA with a Tukey's multiple comparison post-test, and $P \leq 0.05$*; $P \leq 0.01$**; $P \leq 0.001$***.

Figure 5.5

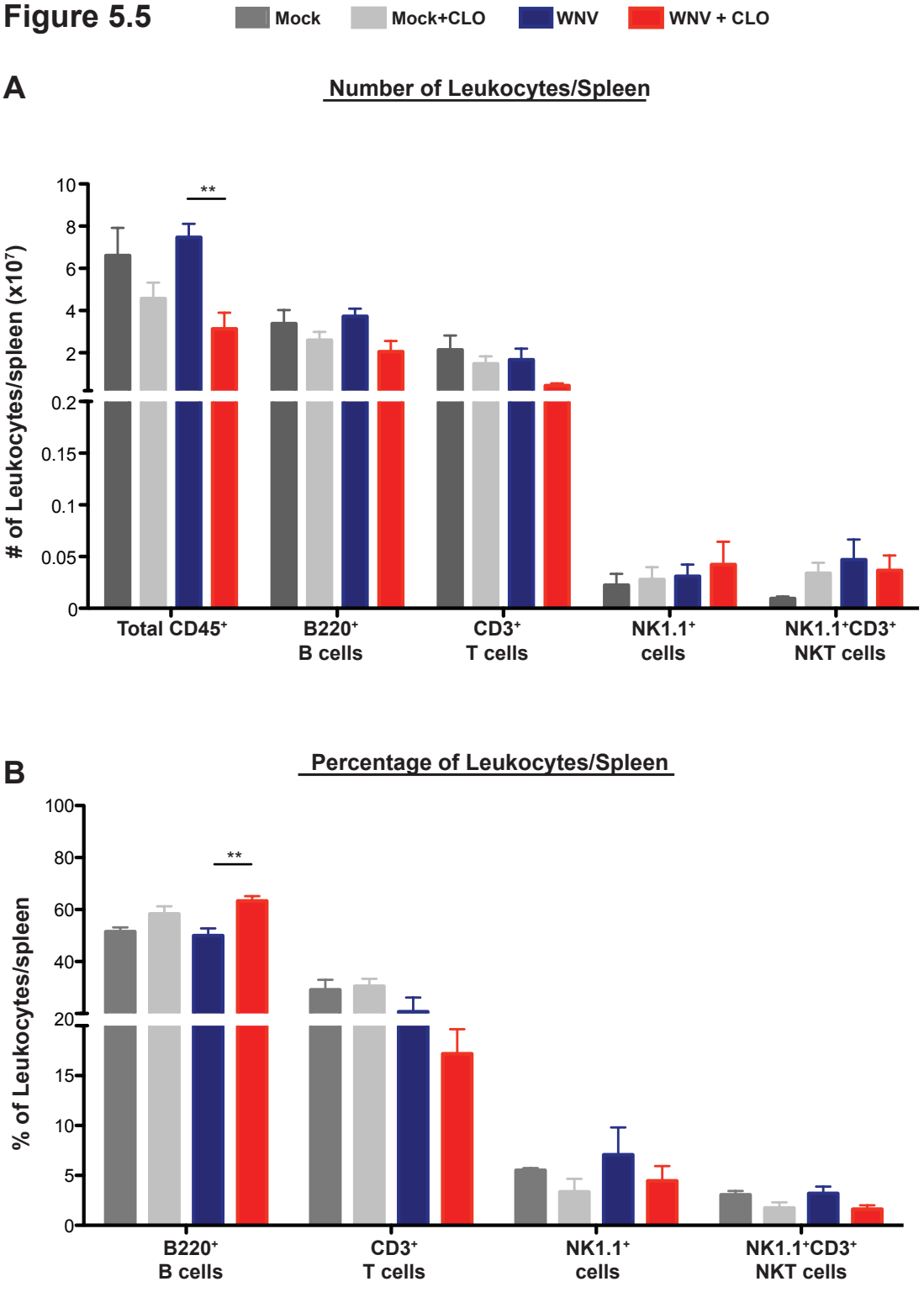
Mock
Mock+CLO
WNV
WNV + CLO
A
Number of Leukocytes/Spleen
# of Leukocytes/spleen (x10⁷)
10
8
6
4
2
0.2
0.15
0.1
0.05
0
**
Total CD45⁺
B220⁺ B cells
CD3⁺ T cells
NK1.1⁺ cells
NK1.1⁺CD3⁺ NKT cells
B
Percentage of Leukocytes/Spleen
% of Leukocytes/spleen
100
80
60
40
20
15
10
5
0
**
B220⁺ B cells
CD3⁺ T cells
NK1.1⁺ cells
NK1.1⁺CD3⁺ NKT cells

Figure 5.6 Leukocyte distribution in the spleen of mock- or WNV-infected mice following clodronate depletion at d5 p.i.

Graphs A and B represent the numbers and percentages of various leukocytes in the spleen of ($6x10^4$ PFU) WNV-infected, vehicle-treated (blue) or WNV-infected, CLO-depleted (red) and mock-infected, vehicle-treated (dark grey) or mock-infected, CLO-depleted (light grey) mice at d7 p.i. Graph A shows the depletion of the red pulp macrophages ($F4/80^+CD11c^{int}$) and various DC subsets in the spleen including $CD11c^+CD11b^+$, $CD11c^+CD11b^-$ and pDC ($CD11c^+B220^-$). It also illustrates the change in neutrophil numbers ($Ly6G^+$ $CD11b^{hi}Ly6C^{int}$). Graph B shows the percentage change of the red pulp macrophages ($F4/80^+CD11c^{int}$) and various DC subsets in the spleen including $CD11c^+CD11b^+$, $CD11c^+CD11b^-$, pDC ($CD11c^+B220^-$) and neutrophils ($Ly6G^+$ $CD11b^{hi}Ly6C^{int}$) following clodronate depletion. Percentages of various subsets are expressed as a percentage of total leukocytes in the spleen of each cohort. Data are the mean ±SEM of values from 3 independent experiments, with 2-4 mice/group in each experiment. Statistical analysis was conducted using one-way ANOVA with a Tukey's multiple comparison post-test, and $P \leq 0.05$*; $P \leq 0.01$**; $P \leq 0.001$***.

Figure 5.6

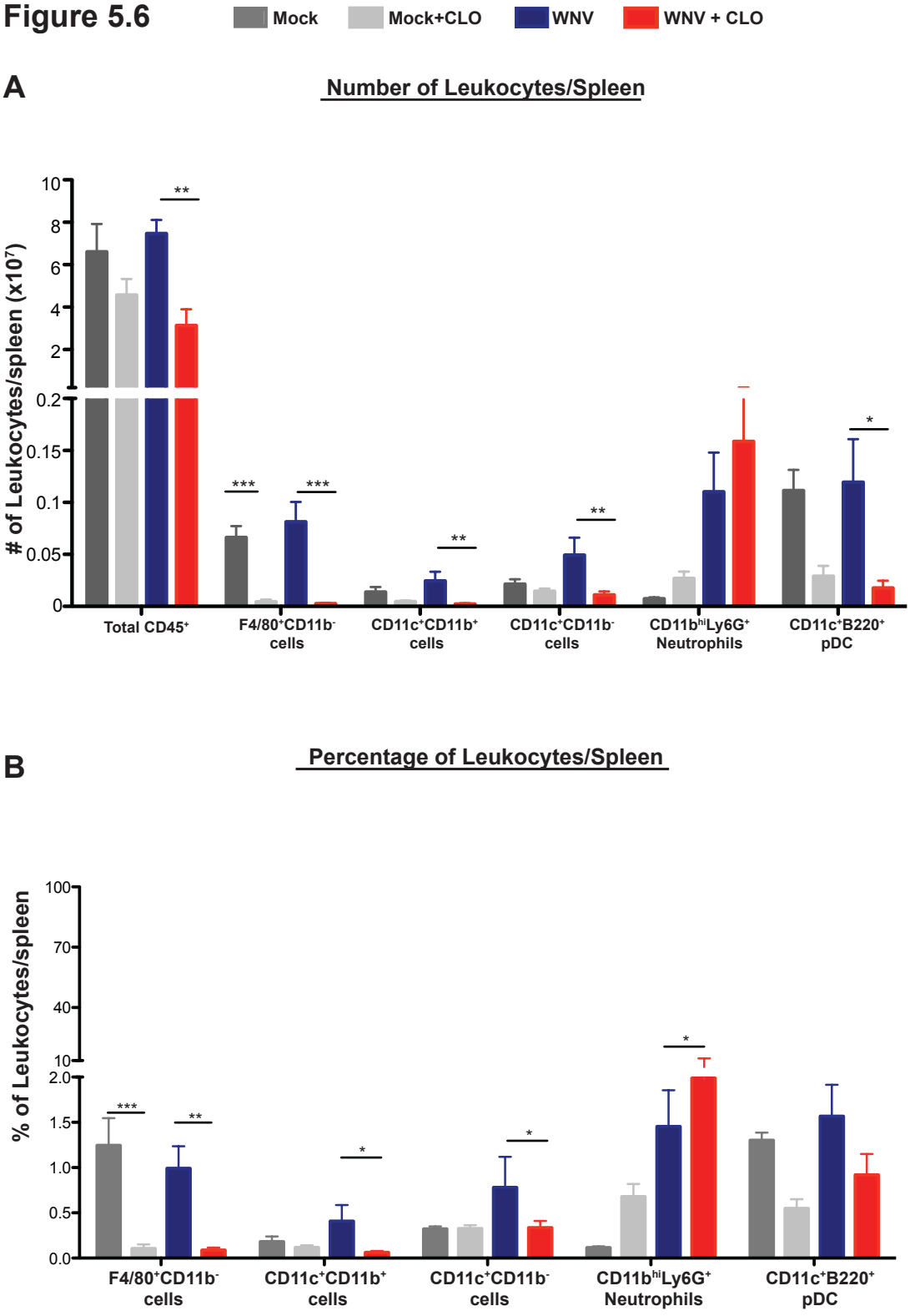
Mock
Mock+CLO
WNV
WNV + CLO
A
Number of Leukocytes/Spleen
# of Leukocytes/spleen (x10⁷)
10
8
6
4
2
0.2
0.15
0.1
0.05
0
**
***
***
**
**
*
Total CD45⁺
F4/80⁺CD11b⁻ cells
CD11c⁺CD11b⁺ cells
CD11c⁺CD11b⁻ cells
CD11b^hiLy6G⁺ Neutrophils
CD11c⁺B220⁺ pDC
B
Percentage of Leukocytes/Spleen
% of Leukocytes/spleen
100
70
40
10
2.0
1.5
1.0
0.5
0.0
***
**
*
*
*
F4/80⁺CD11b⁻ cells
CD11c⁺CD11b⁺ cells
CD11c⁺CD11b⁻ cells
CD11b^hiLy6G⁺ Neutrophils
CD11c⁺B220⁺ pDC

The monocyte populations in the spleen had no significant changes in number (Figure 5.7A) or percentage (Figure 5.7B) and remained more or less comparable between all of the cohorts analysed. This could be because of the spread of replacement of these subsets by the bone marrow, over the time from ablation to analysis in this model.

5.2.4. Leukocyte numbers in the bone marrow following CLO-depletion of WNV-infected mice

Since both CLO depletion and WNV infection likely increases bone marrow production of Ly6C^{hi} monocytes, the combined action of CLO and WNV on the bone marrow might change the leukocyte content. However, although there was a slight increase in the percentage of Ly6C^{hi} monocytes in the bone marrow of CLO-depleted mock- and WNV-infected mice, this was not statistically significant (Figure 5.9B). The only noticeable change in the bone marrow, following CLO depletion of WNV-infected mice, was the significant reduction in F4/80^{+} stromal macrophage number (Figure 5.9A) and percentage (Figure 5.9B and Figure 5.9C). Therefore, despite the dramatic change found within the CNS and splenic leukocyte content, CLO depletion had little effect on the bone marrow cell numbers, other than depleting the stromal macrophages. Nevertheless, these data do not allow us to comment on any proliferative changes or modulation of precursor populations, which may occur as a result of CLO depletion.

5.2.5. Therapeutic efficacy of IMP following clodronate depletion of WNV-infected mice

Having determined the baseline parameters for the depletion of circulatory macrophages by CLO during WNV encephalitis, we wanted to test the therapeutic efficacy of IMP

Figure 5.7 Leukocyte distribution in the spleen of mock- or WNV-infected mice following clodronate depletion at d5 p.i.

Graphs A and B represent the numbers and percentages of various leukocytes in the spleen of ($6x10^4$ PFU) WNV-infected, vehicle-treated (blue) or WNV-infected, CLO-depleted (red) and mock-infected, vehicle-treated (dark grey) or mock-infected, CLO-depleted (light grey) mice at d7 p.i. Graph A demonstrates the number of monocytes ($CD11b^+CD11c^-$), including $Ly6C^{hi}$, $Ly6C^{int}$ and $Ly6C^-$ cells, following clodronate depletion. Graph B demonstrates the percentage of monocytes ($CD11b^+CD11c^-$), including $Ly6C^{hi}$, $Ly6C^{int}$ and $Ly6C^-$ cells, in the spleen following clodronate depletion.

Percentages of various subsets are expressed as a percentage of total leukocytes in the spleen of each cohort. Data are the mean ±SEM of values from 3 independent experiments, with 2-4 mice/group in each experiment. Statistical analysis was conducted using one-way ANOVA with a Tukey's multiple comparison post-test, and $P \leq 0.05$*; $P \leq 0.01$**; $P \leq 0.001$***.

Figure 5.7

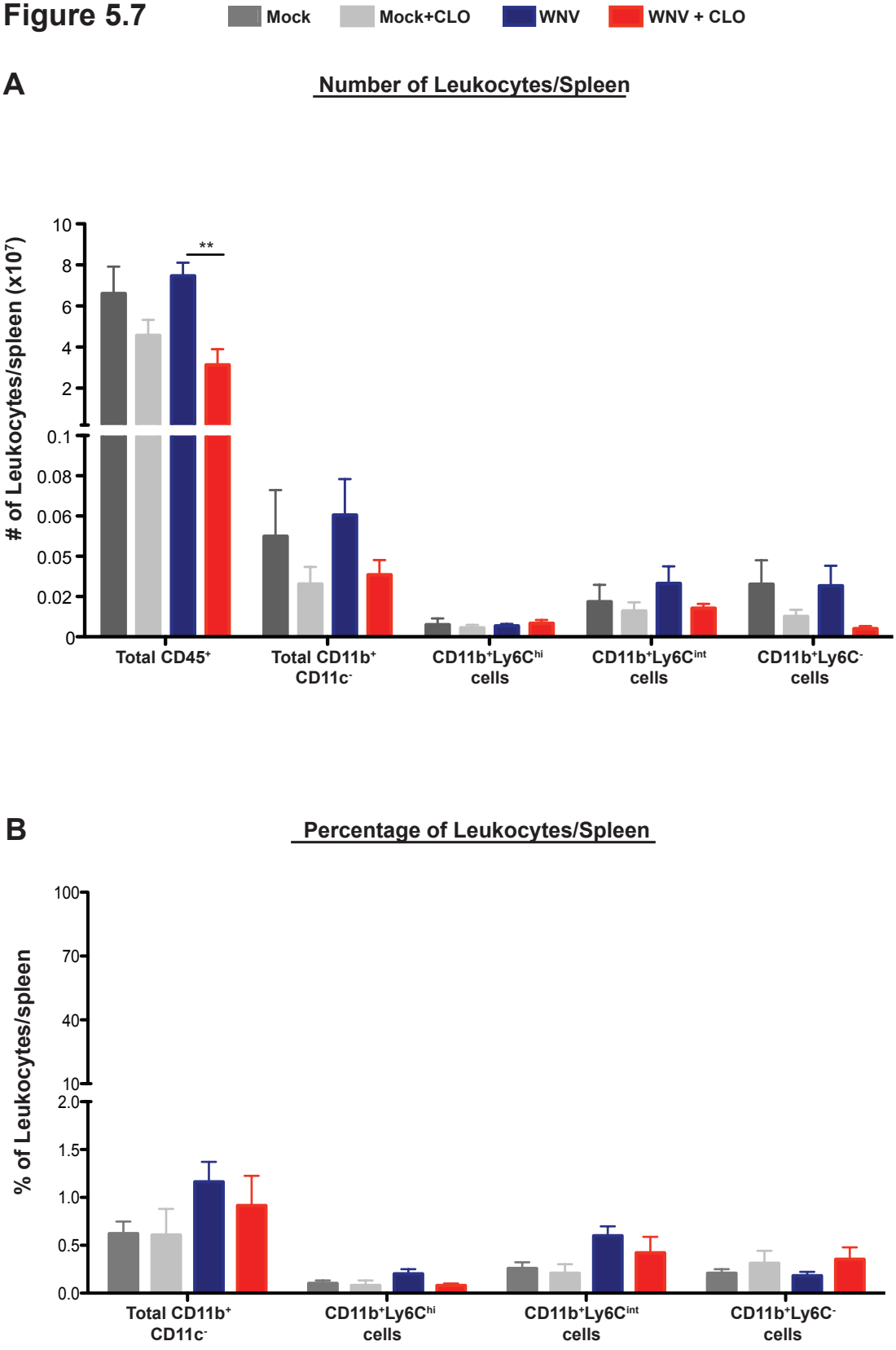
Mock
Mock+CLO
WNV
WNV + CLO
A
Number of Leukocytes/Spleen
# of Leukocytes/spleen (x10⁷)
10
8
6
4
2
0.1
0.08
0.06
0.05
0.02
0
**
Total CD45⁺
Total CD11b⁺ CD11c⁻
CD11b⁺Ly6C^hi cells
CD11b⁺Ly6C^int cells
CD11b⁺Ly6C⁻ cells
B
Percentage of Leukocytes/Spleen
% of Leukocytes/spleen
100
70
40
10
2.0
1.5
1.0
0.5
0.0
Total CD11b⁺ CD11c⁻
CD11b⁺Ly6C^hi cells
CD11b⁺Ly6C^int cells
CD11b⁺Ly6C⁻ cells

Figure 5.8 Clodronate depletion in the spleen following lethal WNV infection

Panels A and B are representative flow cytometry contour plots (10, 000 evts) of the spleen following clodronate depletion (d5 p.i.) of WNV-infected mice ($6x10^4$ PFU) at d7p.i. Panel A illustrates the percentage increase of splenic neutrophils following clodronate depletion. Panel B demonstrates the depletion of the red pulp macrophages ($F4/80^+CD11c^{int}$) and total DC population ($CD11c^+$) in the spleen following clodronate depletion (d5 p.i.). Both panels show the outliers of the contour plots in order to visualise low frequency data, such as the DC and macrophage populations described in this graph (WNV+CLO).

Figure 5.8

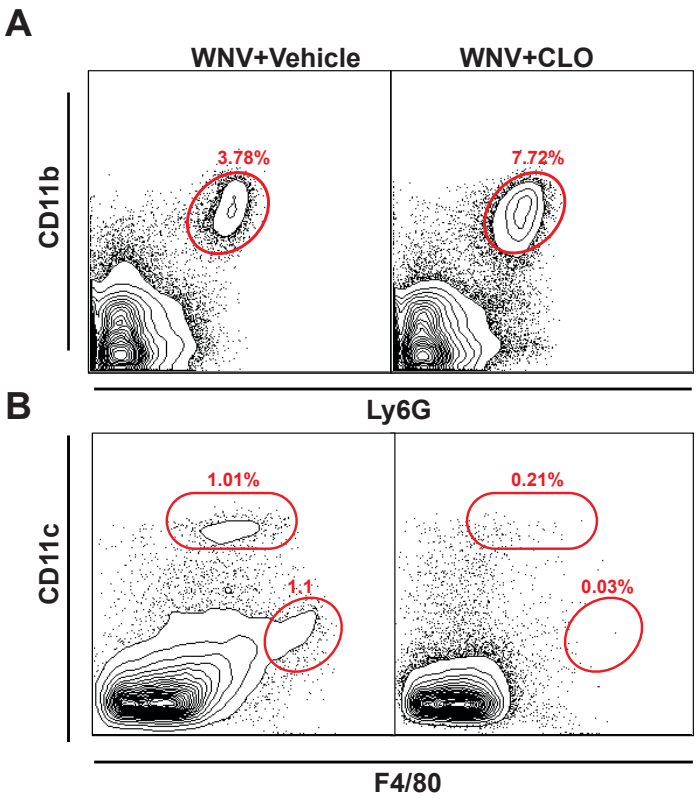
A
WNV+Vehicle
WNV+CLO
CD11b
3.78%
7.72%
Ly6G
B
CD11c
1.01%
1.1
0.21%
0.03%
F4/80

Figure 5.9 Leukocyte numbers and percentage in the bone marrow of mock- or WNV-infected mice following clodronate depletion at d5 p.i.

Figure 5.9 represents the numbers (A) and percentages change (B) of leukocytes in the bone marrow of ($6x10^4$ PFU) WNV-infected, vehicle-treated (blue) or WNV-infected, CLO-depleted (red) and mock-infected, vehicle-treated (dark grey) or mock-infected, CLO-depleted (light grey) mice at d7 p.i. Graph A demonstrates the change in numbers of B cells ($B220^+CD11c^-$), neutrophils ($Ly6G^+$ $CD11b^{hi}Ly6C^{int}$), monocyte subsets ($CD11b^+CD11c^-$), including $Ly6C^{hi}$, $Ly6C^{int}$ and $Ly6C^-$ cells, stromal macrophages ($F4/80^+CD11c^{int}$), DC ($CD11c^+$) and T cells ($CD3^+$) at d7 p.i. Graph B shows the percentage of these cells in the bone marrow. Panel C shows the representative flow cytometry contour plots (10, 000 evts) of the bone marrow following clodronate depletion (d5 p.i.) of WNV-infected mice ($6x10^4$ PFU), demonstrating the depletion of stromal macrophages ($F4/80^+CD11c^{int}$). Percentages of various subsets are expressed as a percentage of total leukocytes in the bone marrow of each cohort. Data for figures A-B is the mean ±SEM of values from 3 independent experiments, with 2-4 mice/group in each experiment. Statistical analysis was conducted using one-way ANOVA with a Tukey's multiple comparison post-test, and $P \leq 0.05$*; $P \leq 0.01$**; $P \leq 0.001$***.

Figure 5.9

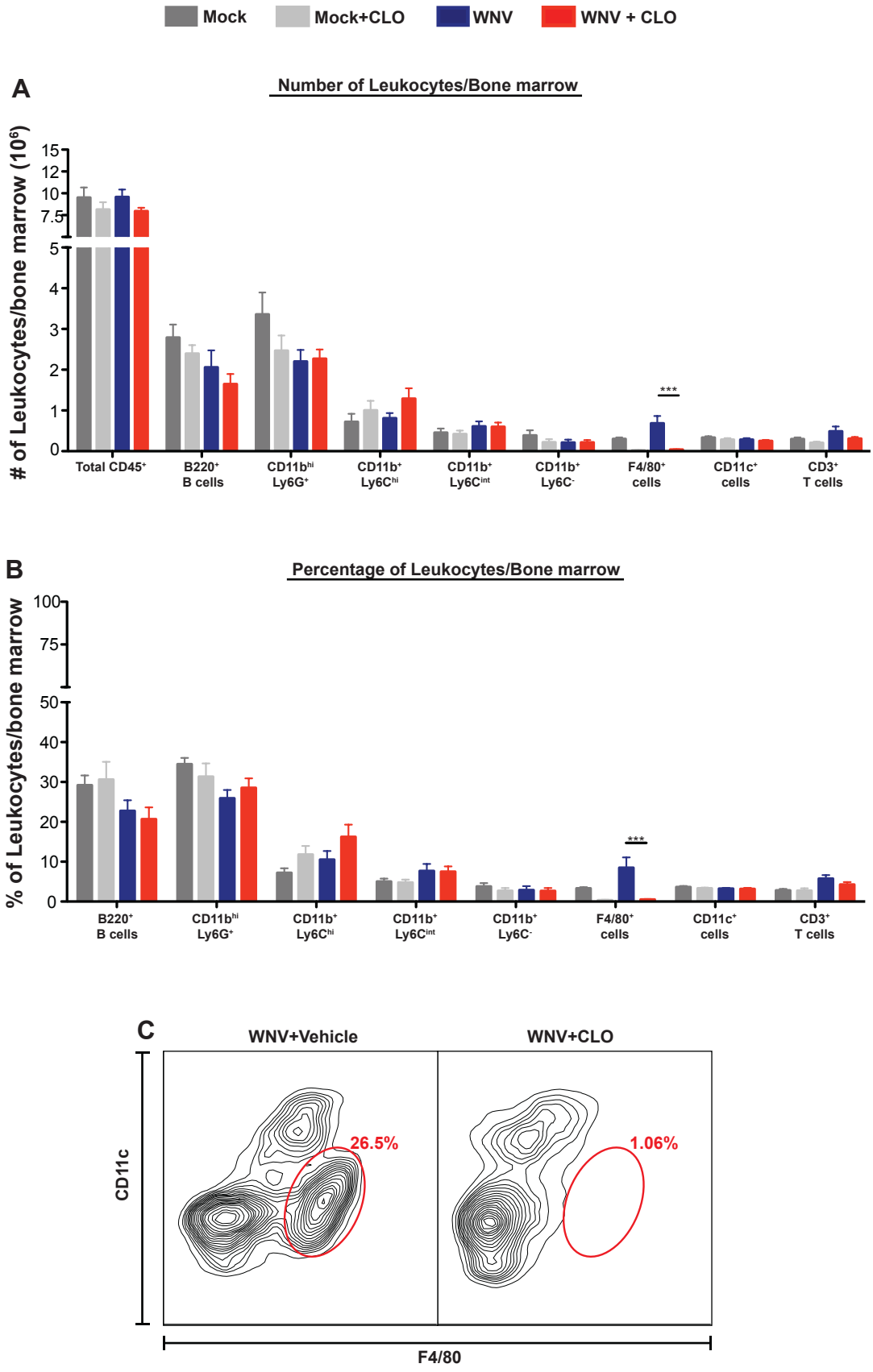
Mock
Mock+CLO
WNV
WNV + CLO
A
Number of Leukocytes/Bone marrow
# of Leukocytes/bone marrow (10^6)
15
12
10
7.5
5
4
3
2
1
0
***
Total CD45+
B220+ B cells
CD11bhi Ly6G+
CD11b+ Ly6Chi
CD11b+ Ly6Cint
CD11b+ Ly6C-
F4/80+ cells
CD11c+ cells
CD3+ T cells
B
Percentage of Leukocytes/Bone marrow
% of Leukocytes/bone marrow
100
75
50
40
30
20
10
0
***
B220+ B cells
CD11bhi Ly6G+
CD11b+ Ly6Chi
CD11b+ Ly6Cint
CD11b+ Ly6C-
F4/80+ cells
CD11c+ cells
CD3+ T cells
C
WNV+Vehicle
WNV+CLO
26.5%
1.06%
CD11c
F4/80

following the depletion of the $MARCO^+$ marginal zone macrophages. As outlined in Figure 5.10A, we infected adult female C57BL/6 mice with either an LD50 ($6x10^3$ PFU) or LD100 ($6x10^4$ PFU) dose of WNV and gave a single i.v. dose of CLO at d5 p.i. Thereafter, LD100 mice were treated i.v. with IMP at d6 p.i., whereas mice infected with the sublethal LD50 dose of WNV were treated with IMP once they had lost 5% or more of their original weight.

Figure 5.10 B and Figure 5.11 A shows the number of leukocytes infiltrating the CNS on d7 p.i. of mock- and WNV-infected, CLO-depleted given either vehicle or IMP treatment. Figure 5.10 C and Figure 5.11 B demonstrates the number of leukocytes infiltrating the CNS on d7 p.i. of mock- and WNV-infected control mice given either vehicle or IMP treatment. Interestingly, similar to control mice (Figure 5.10C), IMP treatment significantly reduced the pathogenic $Ly6C^{hi}$ inflammatory monocytes in the CNS of CLO-depleted mice (Figure 5.10B), compared to the vehicle-treated cohort. The number of T cells in the CNS of CLO-depleted mice was also reduced by IMP treatment (Figure 5.11A). However, neutrophils, $Ly6C^{int}$, B and NK cells remained comparable between IMP- and vehicle-treated, WNV-infected, CLO-depleted mice at d7 p.i.

Considering the pre-existing reduction of $Ly6C^{hi}$ inflammatory macrophage numbers in CLO-depleted compared to control mice, we hypothesised that the additional decrease of this subset, as a result of IMP treatment, might improve survival of WNV-infected mice given a sublethal dose of infection. CLO-depleted, WNV-infected and control, WNV-infected mice that did not lose a significant amount of weight did not receive any treatment nor did any succumb from disease. Furthermore, CLO-depleted mice treated with IMP had significantly improved survival outcome compared to their CLO-depleted, vehicle-treated counterparts (Figure 5.11C). Control WNV-infected, IMP-treated animals (non-CLO-depleted) may have derived more benefit from IMP treatment, as survival of

Figure 5.10 IMP treatment of clodronate-depleted *versus* vehicle-treated mice following WNV infection

Panel A illustrates the protocol followed for IMP treatment (d6p.i-LD100 or >5%WL-LD50) and clodronate depletion (d5 p.i.) of WNV (LD50 or LD100) and mock-infected mice. Graph B demonstrates the effect of IMP treatment on leukocyte numbers in the CNS of mock-infected, CLO-depleted (grey), WNV-infected, CLO-depleted, vehicle-treated (red) and WNV-infected, CLO-depleted, IMP-treated (orange) mice at d7 p.i., following WNV LD100 infection ($6x10^4$ PFU). Graph C demonstrates the effect of IMP treatment on leukocyte numbers in the CNS of mock-infected control (dark grey), WNV-infected control, vehicle-treated (dark blue) and WNV-infected control, IMP-treated (light blue) mice at d7 p.i., following WNV LD100 infection ($6x10^4$ PFU). Graphs B and C show the myeloid lineage cells, including the resident microglia ($CD45^+CD11b^+Ly6C^-$), immigrant/activated microglia ($CD45^+CD11b^+Ly6C^{int}$) and inflammatory macrophages ($CD45^+CD11b^+Ly6C^{hi}$) at d7 p.i. Data for graphs B-C are the mean ±SEM of values from 3 independent experiments, with 2-4 mice/group in each experiment. Statistical analysis was conducted using one-way ANOVA with a Tukey's multiple comparison post-test, and $P \leq 0.05$*; $P \leq 0.01$**; $P \leq 0.001$***.

Figure 5.10

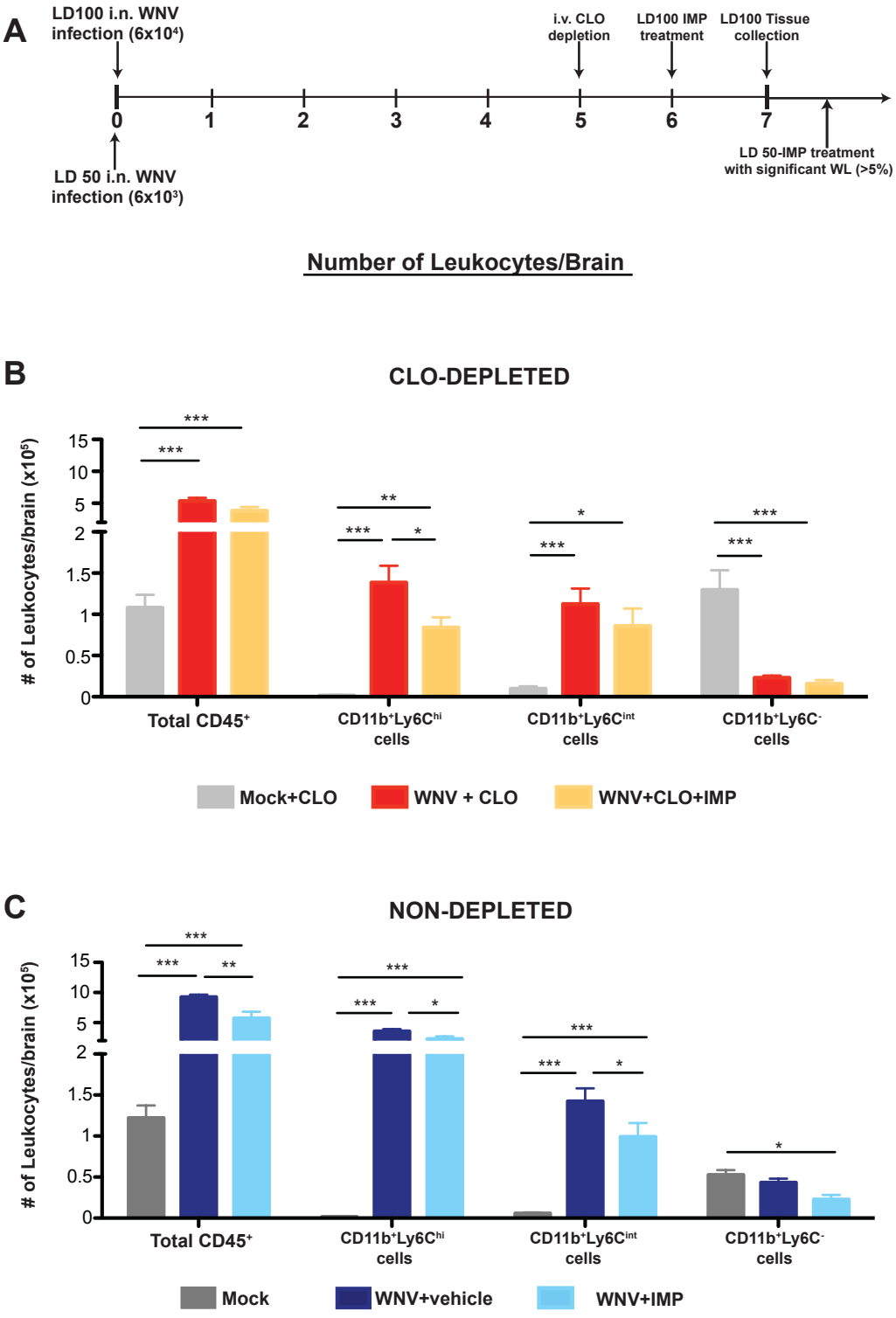
A
LD100 i.n. WNV infection (6x10⁴)
i.v. CLO depletion
LD100 IMP treatment
LD100 Tissue collection
0
1
2
3
4
5
6
7
LD 50-IMP treatment with significant WL (>5%)
LD 50 i.n. WNV infection (6x10³)
Number of Leukocytes/Brain
B
CLO-DEPLETED
# of Leukocytes/brain (x10⁵)
Total CD45⁺
CD11b⁺Ly6C^hi cells
CD11b⁺Ly6C^int cells
CD11b⁺Ly6C⁻ cells
Mock+CLO
WNV + CLO
WNV+CLO+IMP
C
NON-DEPLETED
# of Leukocytes/brain (x10⁵)
Total CD45⁺
CD11b⁺Ly6C^hi cells
CD11b⁺Ly6C^int cells
CD11b⁺Ly6C⁻ cells
Mock
WNV+vehicle
WNV+IMP

Figure 5.11 IMP treatment of clodronate-depleted *versus* vehicle-treated mice following WNV infection

Graph A demonstrates the effect of IMP treatment on leukocyte numbers in the CNS of mock-infected, CLO-depleted (grey), WNV-infected, CLO-depleted, vehicle-treated (red) and WNV-infected, CLO-depleted, IMP-treated (orange) mice at d7 p.i., following WNV LD100 infection ($6x10^4$ PFU). Graph B demonstrates the effect of IMP treatment on leukocyte numbers in the CNS of mock-infected control (dark grey), WNV-infected control (dark blue) and WNV-infected control, IMP-treated (light blue) mice at d7 p.i., following WNV LD100 infection ($6x10^4$ PFU). Graphs A and B illustrate the number of neutrophils ($CD11b^{hi}Ly6G^{+}Ly6C^{int}$) and lymphoid lineage cells including T ($CD3^{+}$), B ($B220^{+}/CD19^{+}$) and NK ($NK1.1^{+}$) cells at d7p.i. Graph C compares the percentage survival of the WNV-infected, CLO-depleted (red) and WNV-infected, vehicle-treated (dark blue) mice, with their IMP-treated cohorts namely WNV-infected, IMP-treated (light blue) and WNV-infected, CLO-depleted, IMP-treated (orange) following infection with a sublethal dose of WNV ($6x10^3$ PFU). The graph includes a no weight loss (WL) cohort i.e. weight loss of <5% (black) that received no treatment. Data for graphs A and B are the mean ±SEM of values from 3 independent experiments, with 2-4 mice/group in each experiment. Statistical analysis was conducted using one-way ANOVA with a Tukey's multiple comparison post-test, and $P \leq 0.05$*; $P \leq 0.01$**; $P \leq 0.001$***. The survival study (C) was performed in 3 separate experiments with 10-14 mice/group. Survival data (C) was grouped and graphed in a Kaplan-Meier survival curve and a Log-rank test was used to determine statistical significance.

Figure 5.11

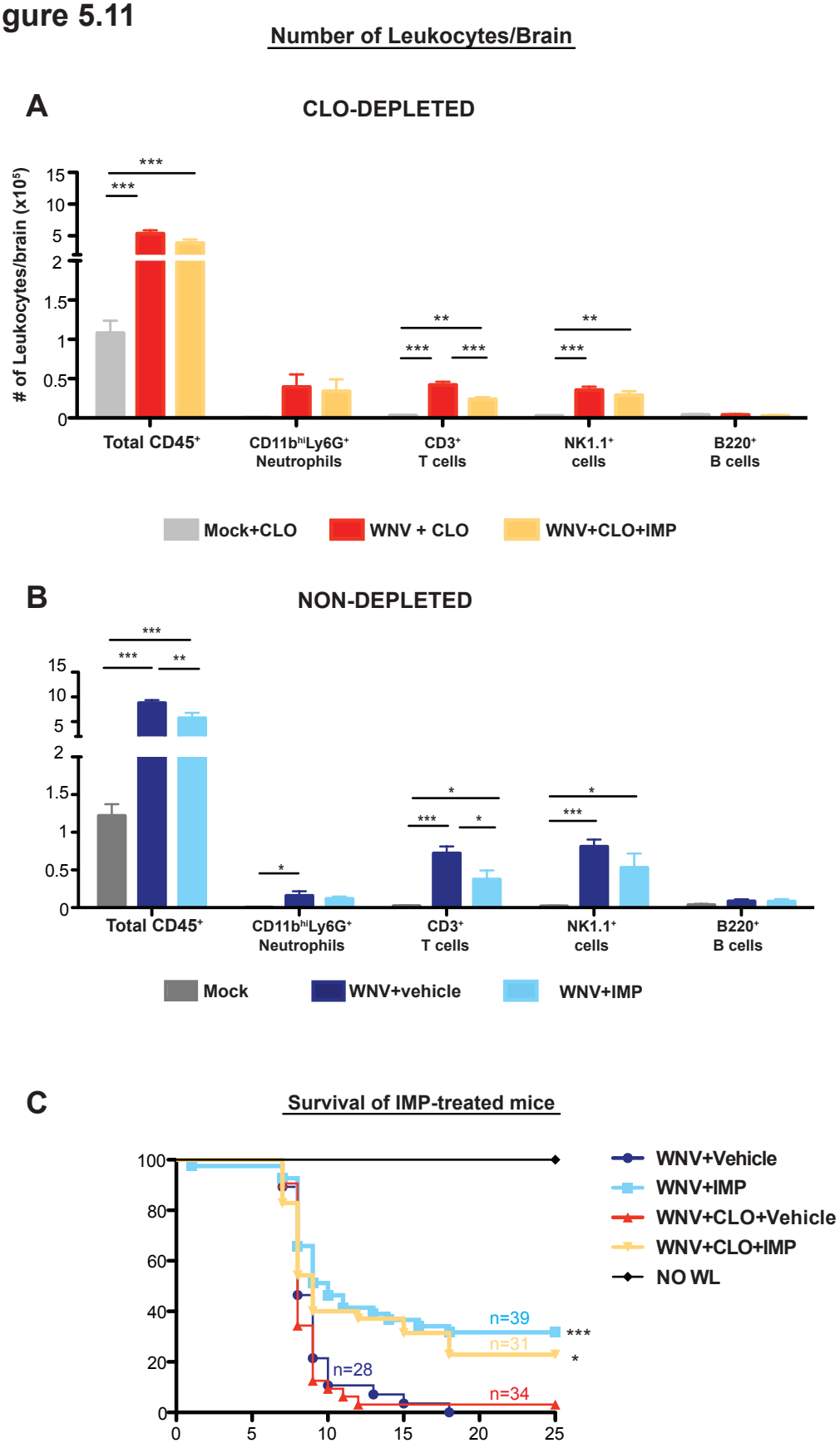
Number of Leukocytes/Brain
A
CLO-DEPLETED
# of Leukocytes/brain (x10⁵)
Total CD45⁺
CD11b^hiLy6G⁺ Neutrophils
CD3⁺ T cells
NK1.1⁺ cells
B220⁺ B cells
Mock+CLO
WNV + CLO
WNV+CLO+IMP
B
NON-DEPLETED
Mock
WNV+vehicle
WNV+IMP
C
Survival of IMP-treated mice
WNV+Vehicle
WNV+IMP
WNV+CLO+Vehicle
WNV+CLO+IMP
NO WL
n=39
n=31
n=28
n=34

this cohort was slightly better than their WNV-infected, CLO-depleted, IMP-treated counterparts. Irrespective, IMP treatment significantly improved survival of CLO-depleted mice. It may be, in the absence of the spleen, that other organs, such as the liver, with high numbers of replenished macrophages after single-dose CLO depletion, can compensate for the absence of the marginal zone macrophages in the spleen as an environment for IMP-containing or IMP-associated cells undergoing apoptosis to be phagocytosed. Nevertheless, this proves that the efficacy of IMP treatment is not solely reliant on the presence of $MARCO^+$ marginal zone macrophages in the spleen.

5.2.6. Distribution of IMP^+ leukocytes in the CNS of WNV-infected mice following clodronate depletion

Following i.v. IMP treatment of control mice there are very few, if any, IMP^+ leukocytes in the CNS of mock- or WNV-infected mice. Thus, it was of interest to discover that a significant number of leukocytes infiltrating the CNS of CLO-depleted mice were IMP^+ (Figure 5.12A). These IMP^+ leukocytes in the CNS of CLO-depleted, WNV-infected mice consisted mainly of $Ly6C^{hi}$ inflammatory macrophages, $Ly6C^{int}$ immigrant/activated microglia and neutrophils. The representative flow cytometry plots in Figure 5.12B illustrate the presence of IMP^+ cells, specifically in the IMP-treated, WNV-infected, CLO-depleted cohort. Table 5.1 describes the percentage of each leukocyte subset that was IMP^+ in the CNS of mock- and WNV-infected control and CLO-depleted mice. Of the total leukocyte population, ~10% of cells were IMP^+ in the CLO-depleted, WNV-infected cohort, compared to <1% in control, WNV-infected and control- and CLO-treated mock groups. Furthermore, ~20% of neutrophils and ~27% of $Ly6C^{hi}$ inflammatory macrophages were IMP^+, within the CLO-depleted, WNV-infected, IMP-treated cohort (Figure 5.12C and Table 5.1). This further indicates that clodronate-encapsulated liposomes not only remove resident and circulatory phagocytic populations, but also modulates the characteristics of

Figure 5.12 Number and distribution of IMP$^+$ leukocytes in the CNS of clodronate-depleted *versus* vehicle treated mice following lethal WNV infection

Graph A demonstrates the number of IMP$^+$ leukocytes in the CNS of WNV-infected, IMP-treated (light blue) and WNV-infected, CLO-depleted, IMP-treated mice at d7 p.i. IMP$^+$ cells in the CNS of both cohorts were mainly found associated with myeloid lineage cells namely: immigrant/activated microglia (CD45$^+$CD11b$^+$Ly6C^{int}), inflammatory macrophages (CD45$^+$CD11b$^+$Ly6C^{hi}) and neutrophils (CD11b^{hi}Ly6G$^+$Ly6C^{int}). Panel B shows the representative flow cytometry contour plots of mock and WNV-infected ($6x10^4$ PFU) CNS from CLO-depleted or vehicle-treated mice receiving IMP treatment. Panel C continues on demonstrating flow cytometry contour plots of the IMP distribution in the CNS of CLO-depleted, WNV-infected mice. Table 5.1 contains the combined percentage values of each major leukocyte population that was IMP$^+$ at d7 p.i., i.e., an average of 10.42% of the total leukocyte population in the CNS of clodronate-depleted and WNV-infected mice was positive for IMP.

Data for graph A are the mean ±SEM of values from 3 independent experiments, with 2-4 mice/group in each experiment. Statistical analysis was conducted using one-way ANOVA with a Tukey's multiple comparison post-test, and P≤0.05*; P≤0.01**; P≤0.001***. Data for table 5.1 are the average percentage from 3 independent experiments, with 2-4 mice/group in each experiment.

Figure 5.12

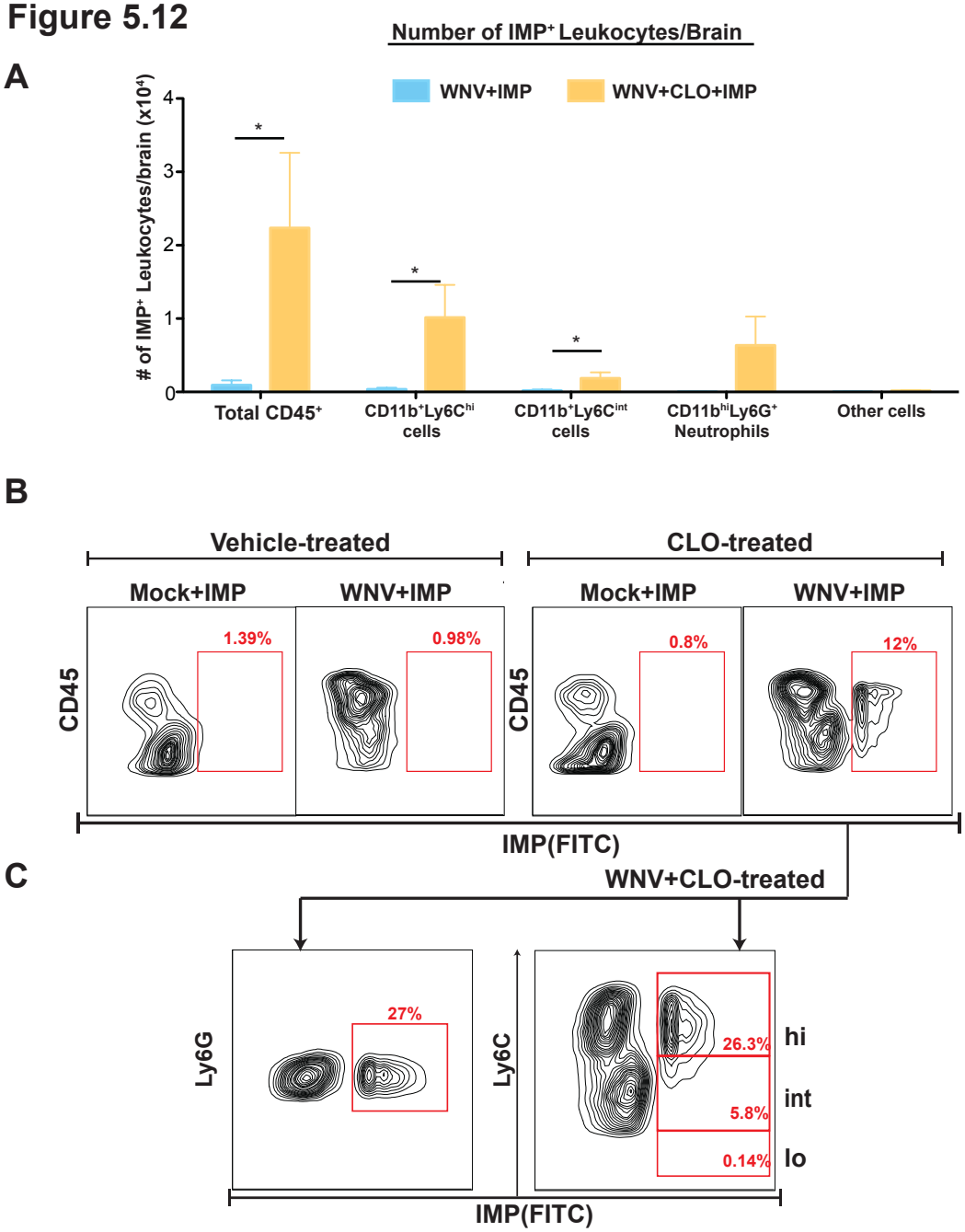

Table 5.1 IMP positivity in the leukocyte populations of the CNS

Average percentage of each population in the CNS that is IMP+				
Cell type	Vehicle-treated		CLO-treated	
	Mock+IMP	WNV+IMP	Mock+IMP	WNV+IMP
Total CD45+ cells	0.69	0.92	0.76	**10.42**
Neutrophils	0.45	1.47	8.67	**20.10**
CD11b+Ly6Chi	2.77	1.14	5.97	**26.71**
CD11b+Ly6Cint	8.48	1.01	4.47	**4.16**
Other	1.88	3.80	1.06	**2.97**

the Ly6C^{hi} inflammatory macrophages, as well as neutrophils, as these cells preferentially phagocytose IMP and traffic to the CNS during WNV infection, as a consequence of clodronate depletion, a phenomenon which is not found in WNV-infected, IMP-treated control animals.

5.2.7. Splenic IMP$^+$ leukocyte content of WNV-infected mice following clodronate depletion

As the spleen and in particular the MARCO$^+$ marginal zone macrophages, evidently sequester IMP and IMP-associated cells, we wanted to determine what the distribution of these IMP$^+$ cells would be in the absence of the marginal zone and red pulp macrophages, due to clodronate depletion. Notably, despite the clodronate-induced reduction in total splenic leukocyte number, shown in figure 5.5, there was an increase in the number of IMP$^+$ leukocytes in the spleen of CLO-depleted mice relative to their control, WNV-infected, IMP-treated counterparts (Figure 5.13A). Moreover, the percentage of IMP$^+$ CD45$^+$ cells was significantly higher in WNV-infected, CLO-depleted mice compared to their WNV-infected counterparts (Figure 5.14A). Therefore, although the numbers of splenic leukocytes are diminished by CLO depletion, evidently their ability to sequester and/or their affinity for IMP or IMP$^+$ cells is increased. Compared to the control mice, there were significantly higher numbers of IMP$^+$ B cells (Figure 5.13A), neutrophils, CD11c$^+$CD11b$^-$ DC (Figure 5.13B) and Ly6C^{hi}CD11b$^+$ monocytes (Figure 5.13C) in the spleen of the CLO-depleted, WNV-infected cohort at d7 p.i.

Clodronate depletion also significantly increased the percentage of B and NK cells (Figure 5.14A and Figure 5.15B and G) that were evidently positive for IMP. This may be due to increased IMP uptake in the spleen and/or IMP$^+$ cell sequestration being greater in

Figure 5.13 IMP$^+$ leukocytes in the spleen of mock- or WNV-infected mice following clodronate depletion (d5 p.i.) and IMP treatment

Graphs A-C represents the number of leukocytes that were IMP$^+$ in the spleen of ($6x10^4$ PFU) WNV-infected, IMP-treated (blue) or WNV-infected, CLO-depleted, IMP-treated (orange) and mock-infected, IMP-treated (dark grey) or mock-infected, CLO-depleted, IMP-treated (light grey) mice at d7 p.i. Graph A demonstrates the number of B ($B220^+CD11c^-$), T ($CD3^+NK1.1^-$), NK ($NK1.1^+CD3^-$) and NKT ($CD3^+NK1.1^+$) cells in the spleen that are IMP$^+$ following CLO depletion. Graph B shows the number of the red pulp macrophages ($F4/80^+CD11c^{int}$), neutrophils ($Ly6G^+$ $CD11b^{hi}Ly6C^{int}$) and various DC subsets, including $CD11c^+CD11b^+$, $CD11c^+CD11b^-$ and pDC ($CD11c^+B220^-$) that are IMP$^+$ in the spleen following CLO depletion. Graph C demonstrates the number of IMP$^+$ monocytes ($CD11b^+CD11c^-$), including $Ly6C^{hi}$, $Ly6C^{int}$ and $Ly6C^-$ cells, in the spleen following CLO depletion. Data for graphs A-C are the mean ±SEM of values from 3 independent experiments, with 2-4 mice/group in each experiment. Statistical analysis was conducted using one-way ANOVA with a Tukey's multiple comparison post-test, and P≤0.05*; P≤0.01**; P≤0.001***.

Figure 5.13

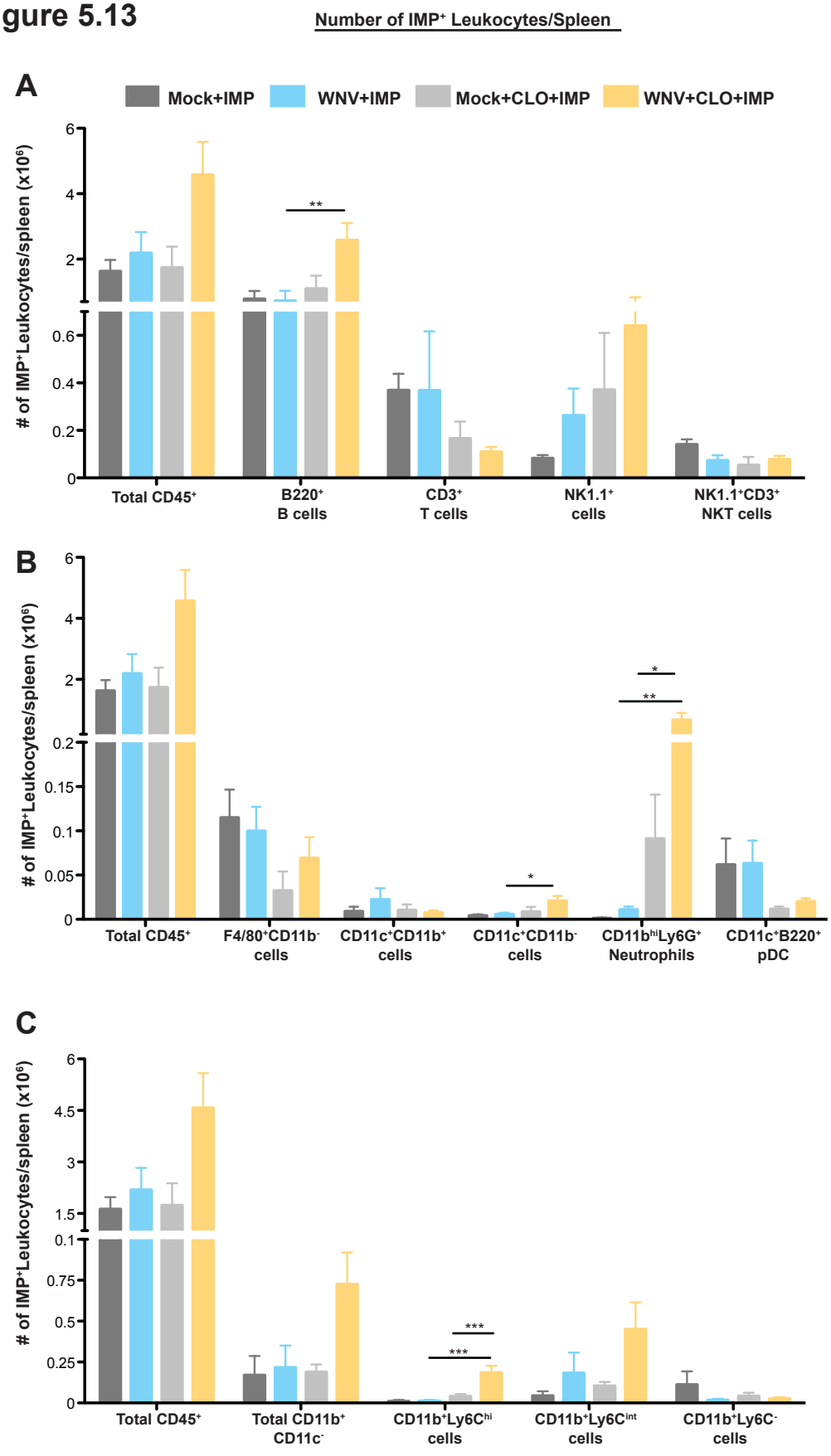
Number of IMP+ Leukocytes/Spleen
A
Mock+IMP
WNV+IMP
Mock+CLO+IMP
WNV+CLO+IMP
# of IMP+Leukocytes/spleen (x10^6)
Total CD45+
B220+ B cells
CD3+ T cells
NK1.1+ cells
NK1.1+CD3+ NKT cells
B
Total CD45+
F4/80+CD11b- cells
CD11c+CD11b+ cells
CD11c+CD11b- cells
CD11bhiLy6G+ Neutrophils
CD11c+B220+ pDC
C
Total CD45+
Total CD11b+ CD11c-
CD11b+Ly6Chi cells
CD11b+Ly6Cint cells
CD11b+Ly6C- cells

Figure 5.14 Percentage of each leukocyte population in the spleen that is IMP$^+$ in of mock- or WNV-infected mice following clodronate depletion (d5 p.i.) and IMP treatment at d6 p.i.

Graphs A-C represents the percentage of each subset of leukocytes that are IMP$^+$ in the spleen of ($6x10^4$ PFU) WNV-infected, IMP-treated (blue) or WNV-infected, CLO-depleted, IMP-treated (orange) and mock-infected, IMP-treated (dark grey) or mock-infected, CLO-depleted, IMP-treated (light grey) mice at d7 p.i. Graph A demonstrates the percentage of B ($B220^+CD11c^-$), T ($CD3^+NK1.1^-$), NK ($NK1.1^+CD3^-$) and NKT ($CD3^+NK1.1^+$) cells in the spleen that are IMP$^+$ following CLO depletion. Graph B shows the percentage of the red pulp macrophages ($F4/80^+CD11c^{int}$), neutrophils ($Ly6G^+$ $CD11b^{hi}Ly6C^{int}$) and various DC subsets, including $CD11c^+CD11b^+$, $CD11c^+CD11b^-$ and pDC ($CD11c^+B220^-$) that are IMP$^+$ in the spleen following CLO depletion. Graph C demonstrates the percentage of IMP$^+$ monocytes ($CD11b^+CD11c^-$), including $Ly6C^{hi}$, $Ly6C^{int}$ and $Ly6C^-$ cells, in the spleen following CLO depletion. Data for panels A-C are the mean ±SEM of values from 3 independent experiments, with 2-4 mice/group in each experiment. Statistical analysis was conducted using one-way ANOVA with a Tukey's multiple comparison post-test, and $P\leq0.05$*; $P\leq0.01$**; $P\leq0.001$***.

Figure 5.14

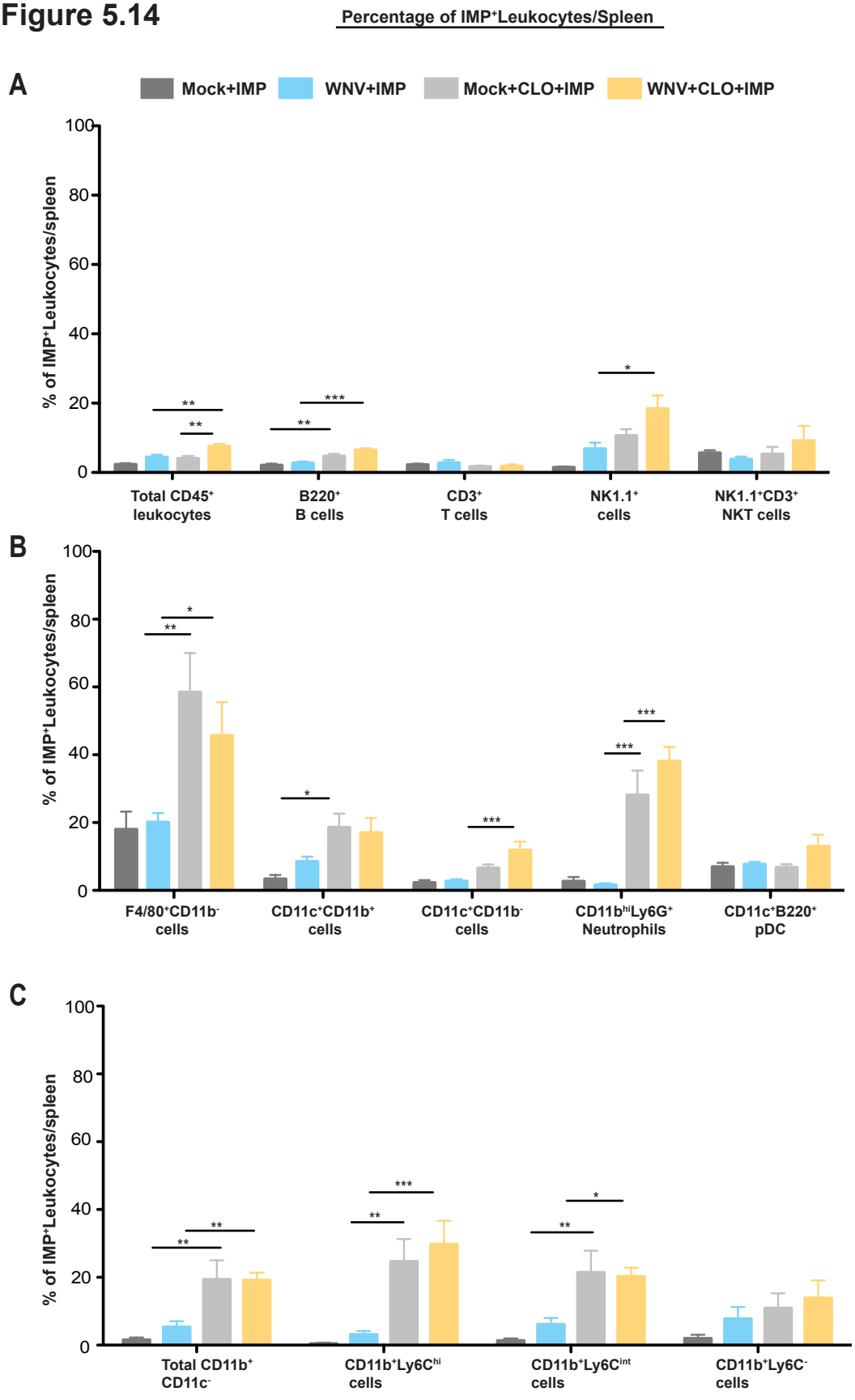
Percentage of IMP+Leukocytes/Spleen
A
Mock+IMP
WNV+IMP
Mock+CLO+IMP
WNV+CLO+IMP
% of IMP+Leukocytes/spleen
100
80
60
40
20
0
**
**
**
***
*
Total CD45+ leukocytes
B220+ B cells
CD3+ T cells
NK1.1+ cells
NK1.1+CD3+ NKT cells
B
% of IMP+Leukocytes/spleen
*
**
*
***
***
***
F4/80+CD11b- cells
CD11c+CD11b+ cells
CD11c+CD11b- cells
CD11bhiLy6G+ Neutrophils
CD11c+B220+ pDC
C
% of IMP+Leukocytes/spleen
**
**
**
***
**
*
Total CD11b+ CD11c-
CD11b+Ly6Chi cells
CD11b+Ly6Cint cells
CD11b+Ly6C- cells

Figure 5.15 Distribution of IMP$^+$ leukocytes in the spleen of clodronate-depleted *versus* vehicle treated mice following lethal WNV infection

Panels A-H are the representative flow cytometry plots of IMP distribution in the various leukocyte populations of the spleen of control (left) and CLO-depleted (right) WNV-infected mice on d7 p.i. These include the IMP distribution of (A) total leukocytes ($CD45^+$); (B) B cells ($CD45^+CD19^+$); (C) neutrophils ($Ly6G^+CD11b^{hi}Ly6C^{int}$); (D) monocytes ($CD11b^+CD11c^-$); (E) CD11b$^-$DC ($CD11c^+CD11b^-$); (F) CD11b$^+$DC ($CD11c^+CD11b^-$); (G) NK cells ($NK1.1^+$) and (H) red pulp macrophages ($F4/80^+CD11c^{int}$).

Figure 5.15

IMP⁺ cells in the spleen

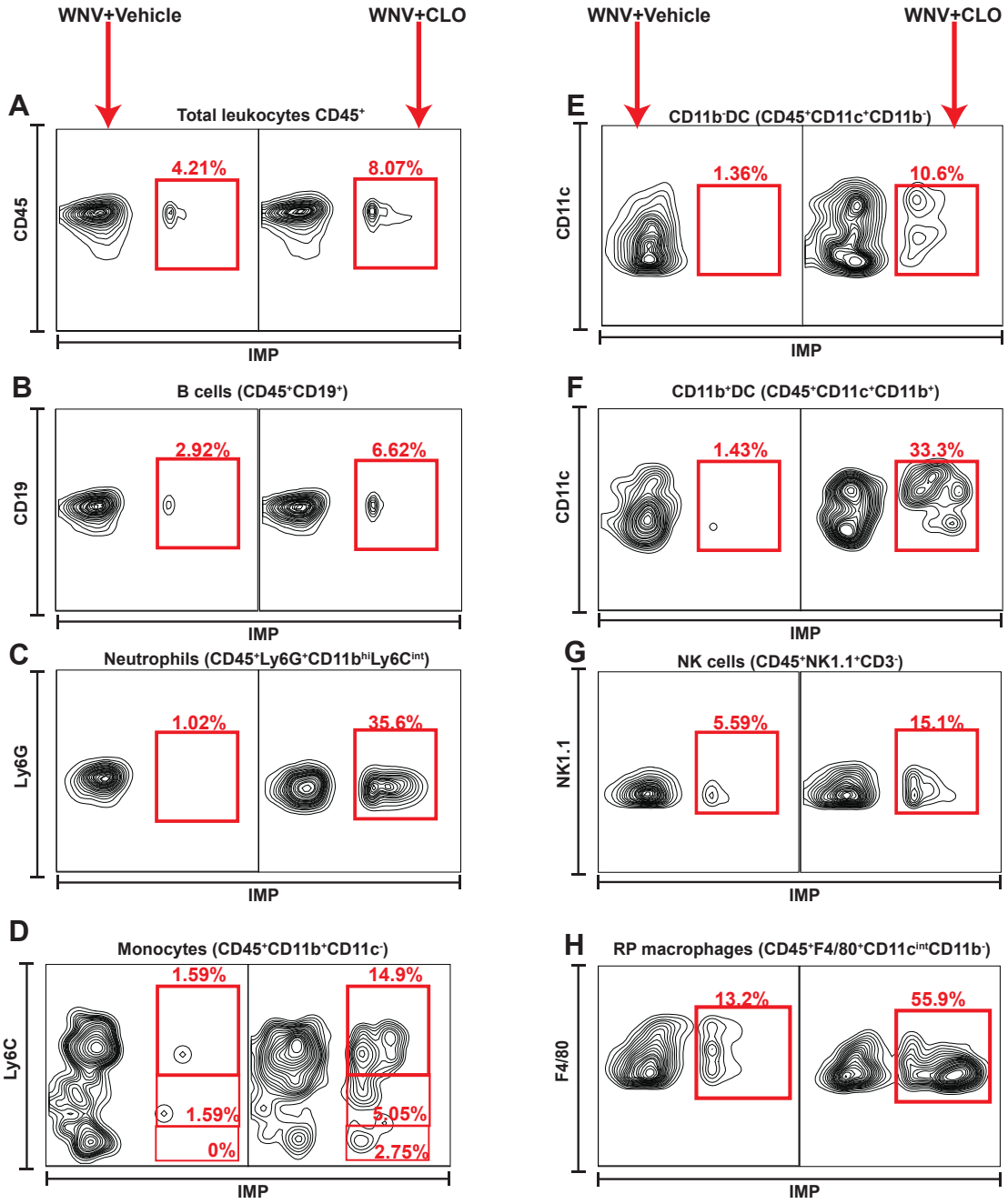

proportion, compared to the IMP$^-$ cell numbers following CLO depletion. Furthermore, there was a significantly larger percentage of F4/80$^+$ red pulp macrophages and other myeloid subsets that were IMP$^+$ in the CLO-depleted, IMP-treated cohorts (both mock- and WNV-infected) (Figure 5.14B and C). Figure 5.15 shows the comparison of IMP-treated mice ±CLO at the individual level, showing markedly increased IMP$^+$ cell numbers in CLO-treated, WNV-infected mice, compared to CLO-untreated. Although a large proportion of these subsets were depleted by clodronate administration (Figure 5.6B), the fact that such large percentages of these subsets were IMP$^+$ suggests that the cells that remained of these subsets after CLO depletion had a significant affinity for IMP. Another noteworthy result was the increased percentage of neutrophils in both mock- and WNV-infected, CLO-depleted mice that were IMP$^+$ (Figure 5.14B and Figure 5.15C). As very few neutrophils associate with IMP in control mice this supports data from the CNS (Figure 5.12) suggesting that clodronate depletion not only resulted in macrophage depletion but also altered the phagocytic activity of other myeloid lineage cells such as neutrophils that normally do not pick up IMP. Furthermore, the percentage of Ly6C^{hi} and Ly6C^{int} monocytes that were positive for IMP also increased in CLO-depleted mice (Figure 5.14C and Figure 5.15D). However, it should be noted again that CLO depletion, without infection, also increased the percentage of IMP$^+$ neutrophils and myeloid lineage cells. The abrogation of resident phagocytic subsets in the spleen with CLO depletion not only leads to higher availability of IMP for possible phagocytosis by other leukocyte populations, but also impacts on the structural organisation of the spleen, allowing access of IMP to areas which would normally be bordered by the marginal zone and red pulp macrophages. As a significant proportion of the phagocytic cells in the marginal zone and red pulp are abolished by CLO depletion, it follows that other leukocytes that would not normally associate with/phagocytose IMP may be able to do so after CLO depletion. Indeed, the

absence of marginal zone cells also allows access of IMP further into the spleen including the white pulp with the B cell follicles and PALS.

Immunofluorescence staining showed IMP$^+$ cells and/or IMP concentrated in the marginal zone of the spleen, surrounding the B cell follicles and PALS of control WNV-infected mice (Figure 5.16A-C). Indeed, there were very few IMP in the white pulp of the spleen and the association of IMP with B cells only occurred at the border of the marginal zone and the B cell follicles in control spleen sections, with very few T cells colocalising with IMP. There were some IMP in the red pulp, likely phagocytosed by the red pulp macrophages, but these were less clustered and more dispersed than those present in the marginal zone. Following clodronate depletion however, it was clear that the anatomy of the spleen had been severely disrupted, leading to IMP being distributed in a much less organised manner throughout the spleen (Figure 5.16A-C). The distinct pattern of T cells, surrounded by B cell staining and IMP localised within the marginal zone is highly disrupted in CLO-depleted splenic sections. In contrast to the tight ring-like distribution of IMP in the marginal zone of control spleen, CLO-depleted spleen sections show the spread of IMP in a much more diffuse distribution. Additionally, the clodronate-depleted spleen had fewer clusters of IMP and IMP were distributed in smaller groups. The ring-like distribution of IMP was occasionally evident in the clodronate-depleted spleen, however as both B and T cell staining was less defined than in control mice it was hard to judge where anatomically IMP or IMP$^+$ cells were located and whether IMP were internalized or merely attached to the cell surface. Nevertheless, in parallel with IMP$^+$ cell number and percentage data, the immunofluorescent staining indicates that CLO-depleted spleen had more IMP$^+$ cells in the spleen compared to control mice.

Figure 5.16 A-C Distribution of IMP$^+$ in the spleen of clodronate-depleted *versus* control mice following lethal WNV infection

Panels A-C are the representative immunofluorescent staining for B220 (red) and/or CD3 and IMP (green), with nuclei stained with DAPI (blue) in a splenic cross-section of WNV-infected, IMP-treated and WNV-infected, CLO-depleted, IMP-treated mice. Mice were infected with LD50 dose of WNV ($6x10^3$ PFU) and clodronate liposomes or vehicle treatment administered at d5 p.i. followed by IMP treatment when >5% WL was reached. Spleen was collected 24-48 h after IMP administration.

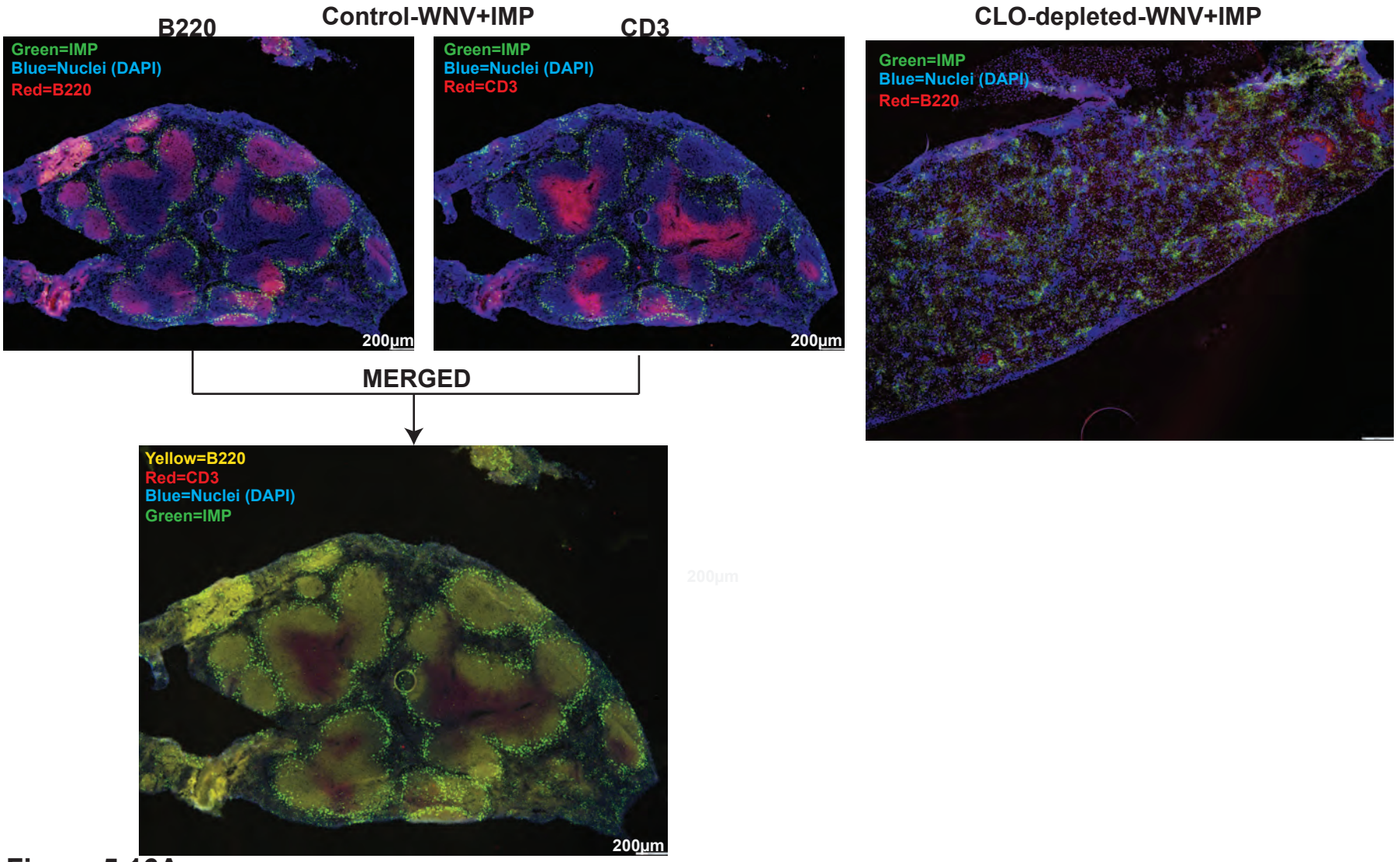
B220
Control-WNV+IMP
CD3
CLO-depleted-WNV+IMP
Green=IMP
Blue=Nuclei (DAPI)
Red=B220
200µm
Green=IMP
Blue=Nuclei (DAPI)
Red=CD3
200µm
Green=IMP
Blue=Nuclei (DAPI)
Red=B220
MERGED
Yellow=B220
Red=CD3
Blue=Nuclei (DAPI)
Green=IMP
200µm

Figure 5.16A

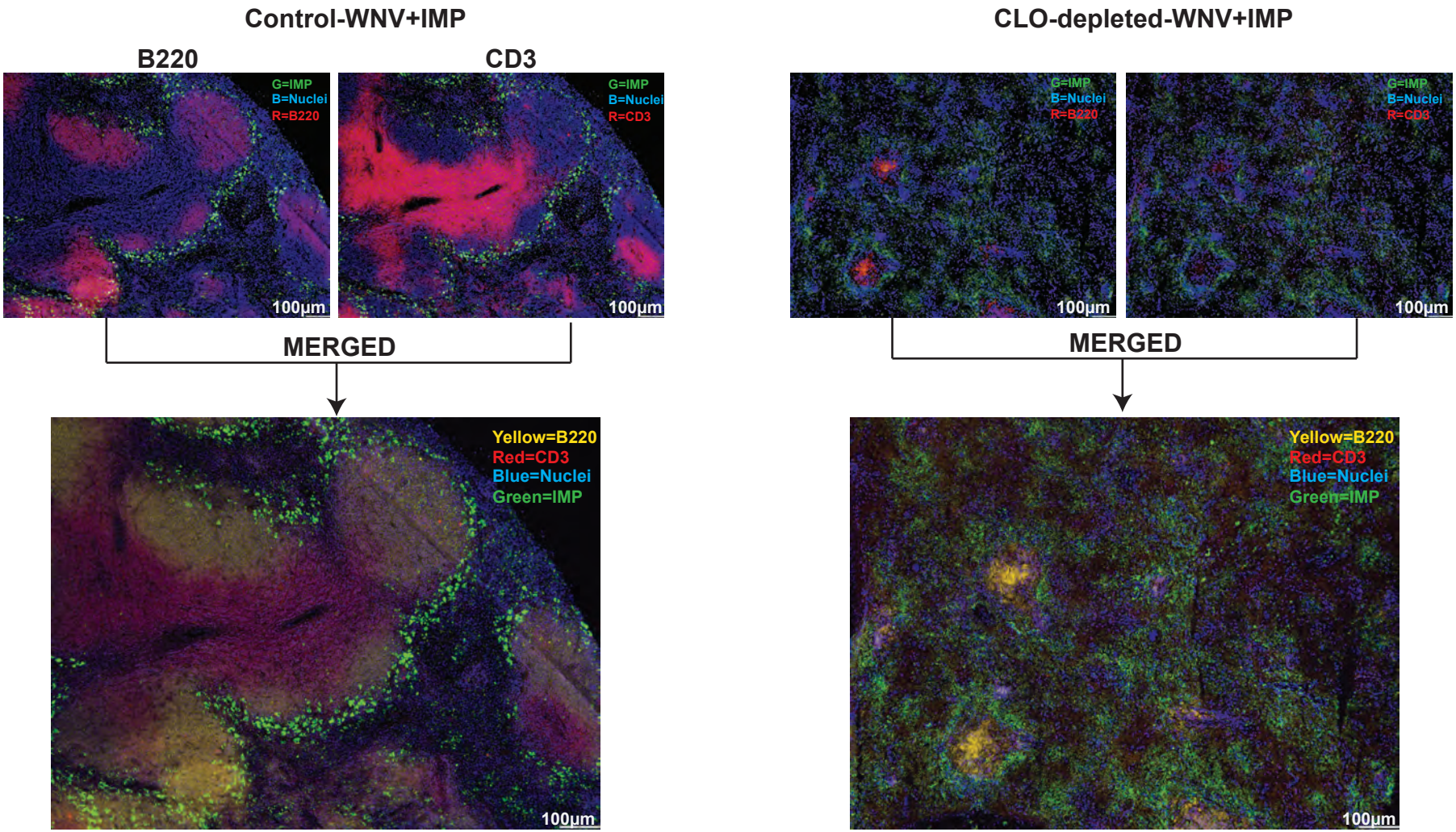
Control-WNV+IMP
B220
CD3
G=IMP
B=Nuclei
R=B220
R=CD3
100µm
MERGED
Yellow=B220
Red=CD3
Blue=Nuclei
Green=IMP
CLO-depleted-WNV+IMP

Figure 5.16B

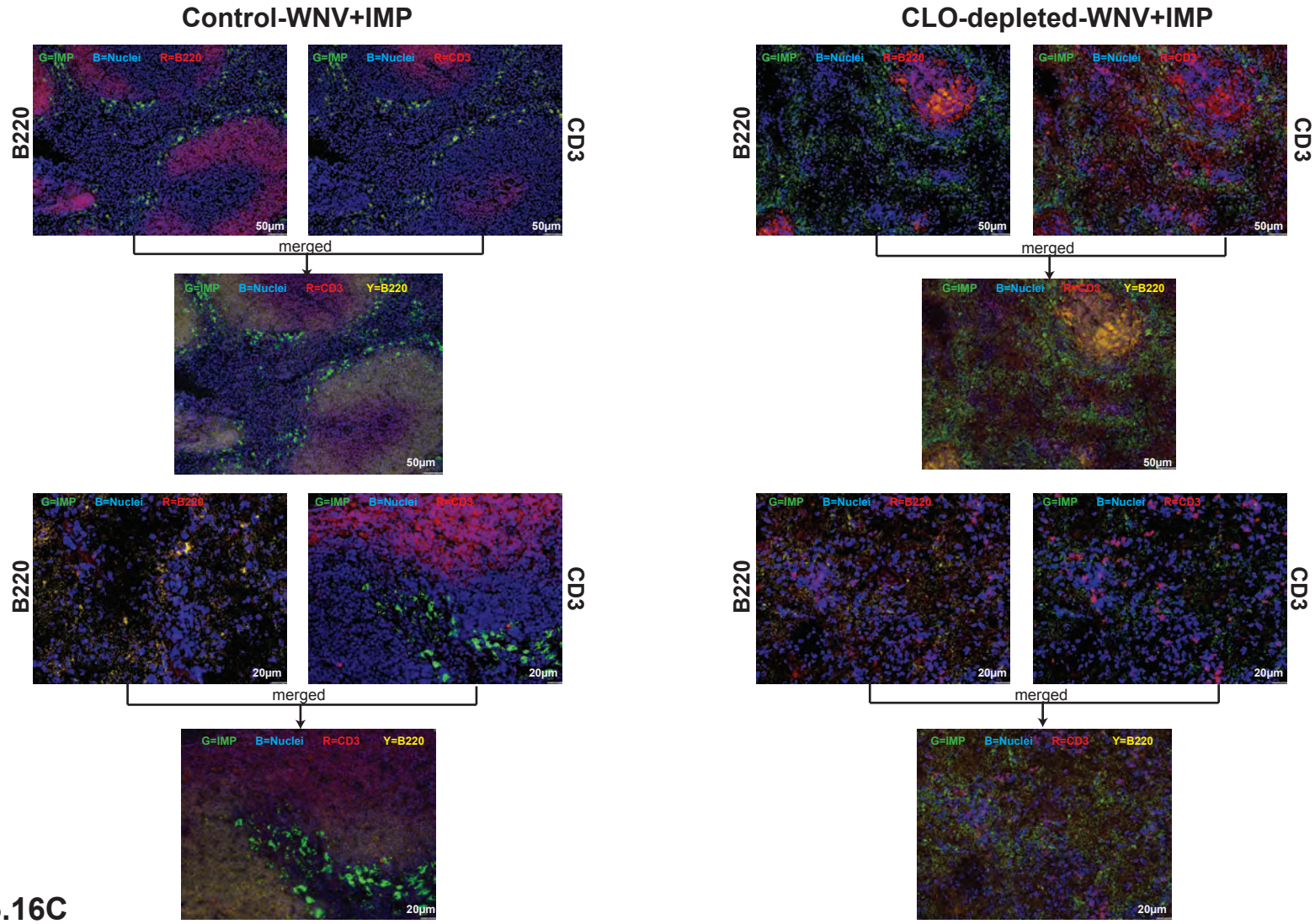
Control-WNV+IMP
CLO-depleted-WNV+IMP
B220
CD3
G=IMP B=Nuclei R=B220
G=IMP B=Nuclei R=CD3
G=IMP B=Nuclei R=CD3 Y=B220
50µm
20µm
merged

Figure 5.16C

5.2.8. IMP$^+$ leukocyte content in the bone marrow of WNV-infected mice following clodronate depletion

Chapter 4 figure 4.17 shows that there were negligible differences in the number of IMP$^+$ cells in the bone marrow of mice that have had their spleens removed, compared to control animals. However, there was a remarkable presence of IMP$^+$ leukocytes in the bone marrow of either mock- or WNV-infected, CLO-depleted mice. Indeed, compared to control mice, there were significantly higher numbers of IMP$^+$ neutrophils and Ly6C^{hi} monocytes in the bone marrow of CLO-depleted, mock- and WNV-infected mice (Figure 5.17A). Clodronate depletion had mostly depleted the F4/80$^+$ stromal macrophages in the bone marrow and, as a consequence, there were also significantly lower numbers of IMP$^+$F4/80$^+$ cells, compared to control cohorts (Figure 5.17A). Nevertheless, the percentage of the remaining F4/80$^+$ stromal macrophages in the bone marrow of CLO-depleted mice that phagocytosed IMP was significantly higher than control mice (Figure 5.17B and Figure 5.18D). As with the spleen, except for the CD11c$^+$ and T cell subsets, most of the leukocyte subsets analysed in the bone marrow contained significantly higher percentages of IMP$^+$ cells than the control animals that had not undergone CLO depletion (Figure 5.17B), including neutrophils (Figure 5.18B) and monocyte subsets (Figure 5.18C). This further supports the notion that, although CLO depletion does not alter the bone marrow distribution or number of leukocytes, it may change the activation status and phagocytic and/or cell surface characteristics of certain leukocyte subsets, in particular the Ly6C^{hi} monocytes and neutrophils. Indeed, preliminary data obtained from an *ex vivo* whole blood phagocytosis assay indicated that the Ly6C^{hi} inflammatory monocytes, isolated 24h after CLO depletion of WNV-infected mice, are much more efficient in phagocytosing IMP than cells isolated from control WNV-infected mice (Appendix Figure 12).

Figure 5.17 IMP$^+$ leukocytes in the bone marrow of mock- or WNV-infected mice following clodronate depletion (d5 p.i.) and IMP treatment

Graph A represents the number of leukocytes that are IMP$^+$ in the bone marrow of ($6x10^4$ PFU) WNV-infected, IMP-treated (blue) or WNV-infected, CLO-depleted, IMP-treated (orange) and mock-infected, IMP-treated (dark grey) or mock-infected, CLO-depleted, IMP-treated (light grey) mice at d7p.i. Graph A demonstrates the number of IMP$^+$ total leukocytes (CD45$^+$), B cells (B220$^+$CD11c$^-$), neutrophils (Ly6G$^+$ CD11b^{hi}Ly6C^{int}), monocytes (CD11b$^+$CD11c$^-$), including Ly6C^{hi}, Ly6C^{int} and Ly6C$^-$ cells, stromal macrophages (F4/80$^+$CD11c^{int}), DC (CD11c$^+$) and T cells (CD3$^+$). Graph B represents the percentage of leukocytes that are IMP$^+$ including total leukocytes (CD45$^+$), B cells (B220$^+$CD11c$^-$), neutrophils (Ly6G$^+$ CD11b^{hi}Ly6C^{int}), monocytes (CD11b$^+$CD11c$^-$), including Ly6C^{hi}, Ly6C^{int} and Ly6C$^-$ cells, stromal macrophages (F4/80$^+$CD11c^{int}), DC (CD11c$^+$) and T cells (CD3$^+$) that are IMP$^+$.

Data for figures A-B are the mean ±SEM of values from 3 independent experiments, with 2-4 mice/group in each experiment. Statistical analysis was conducted using one-way ANOVA with a Tukey's multiple comparison post-test, and P≤0.05*; P≤0.01**; P≤0.001***.

.

Figure 5.17

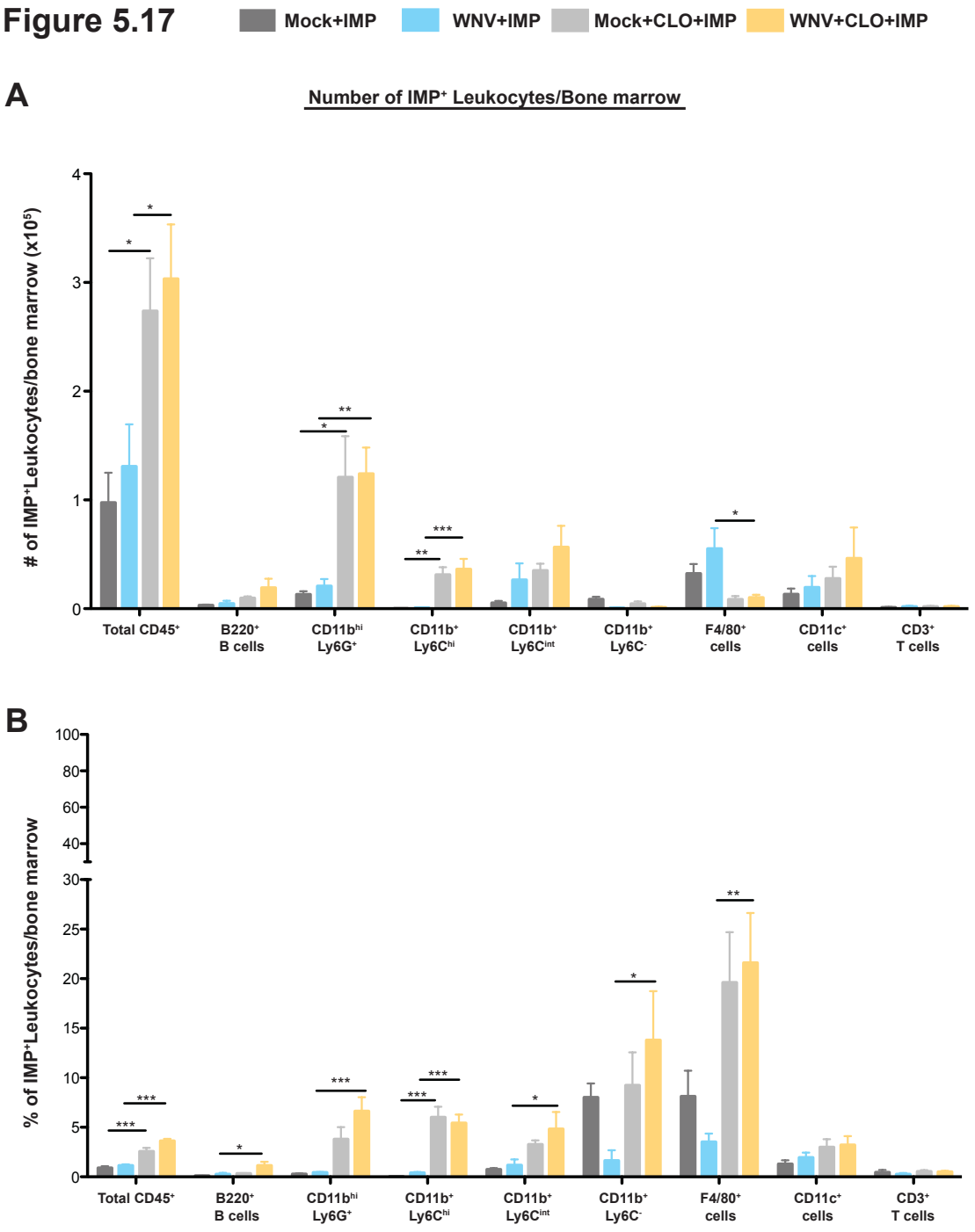
Mock+IMP
WNV+IMP
Mock+CLO+IMP
WNV+CLO+IMP
A
Number of IMP+ Leukocytes/Bone marrow
# of IMP+Leukocytes/bone marrow (x10^5)
0
1
2
3
4
Total CD45+
B220+ B cells
CD11bhi Ly6G+
CD11b+ Ly6Chi
CD11b+ Ly6Cint
CD11b+ Ly6C-
F4/80+ cells
CD11c+ cells
CD3+ T cells
B
% of IMP+Leukocytes/bone marrow
0
5
10
15
20
25
30
40
60
80
100
Total CD45+
B220+ B cells
CD11bhi Ly6G+
CD11b+ Ly6Chi
CD11b+ Ly6Cint
CD11b+ Ly6C-
F4/80+ cells
CD11c+ cells
CD3+ T cells

Figure 5.18 IMP^{+} leukocytes in the bone marrow of mock- or WNV-infected mice following clodronate depletion (d5 p.i.) and IMP treatment

Panels A-D are the representative flow cytometry plots of IMP distribution in the various leukocyte populations of the bone marrow of control (left) and CLO-depleted (right) WNV-infected (6x10^{4} PFU) mice on d7 p.i. These include the IMP distribution of (A) total leukocytes (CD45^{+}); (B) neutrophils (Ly6G^{+}CD11b^{hi}Ly6C^{int}); (C) monocytes (CD11b^{+}CD11c^{-}Ly6C$^{hi/int/-}$); (D) stromal macrophages (F4/80^{+}CD11c^{int}).

Figure 5.18

IMP$^+$ cells in the bone marrow

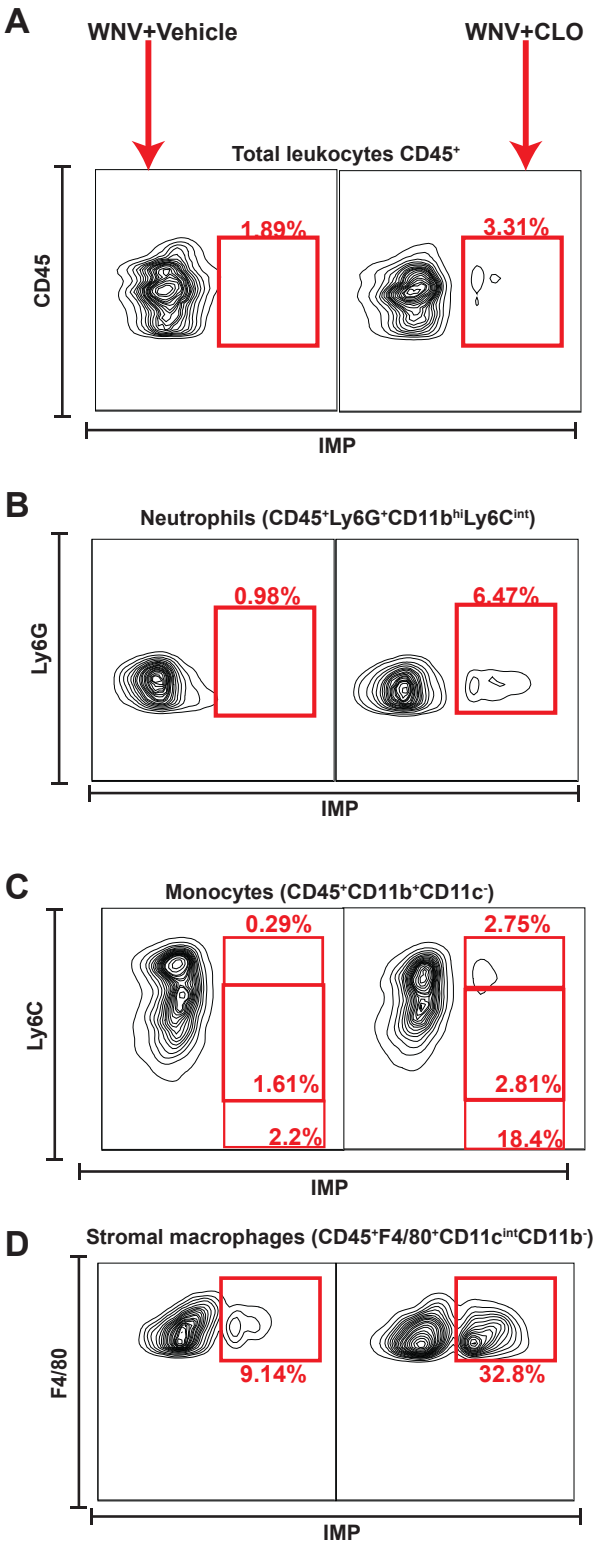

5.2.9. Long-term outcome of clodronate depletion and IMP treatment of WNV-infected mice

The spleens of mice surviving the LD50 dose of WNV infection following clodronate depletion and IMP treatment were investigated to determine the fate of IMP after 90 days. By this time the splenic leukocyte numbers of CLO-depleted mice had returned to that of control mice, with negligible differences in the number of F4/80$^+$ red pulp macrophages in WNV-infected control and CLO-depleted cohorts (Figure 5.19A). Nevertheless, the percentage of IMP$^+$ F4/80$^+$ red pulp macrophages and neutrophils remained higher in the CLO-depleted counterpart (Figure 5.19C), although the numbers of IMP$^+$ splenic leukocyte subsets were similar between groups (Figure 5.19B). This points to retention of the IMP in the spleen over time. There is also an increase in the percentage of these cells, containing IMP. This may suggest that cells taking up IMP have a shorter lifespan necessitating the take up of IMP by surrounding macrophages, eventually leading to a higher percentage of IMP$^+$ cells. Alternatively, there is evidently a redistribution of these IMP. For example, the number of IMP$^+$ B cells reduced from 3 to 1x10^6, while the number of IMP$^+$F4/80 macrophages increased by 10-fold from 0.1 to 1x10^6 over 90 days.

5.3. Discussion

Clodronate depletion has been associated with ameliorating diseases in which pathogenic macrophages play a detrimental role. Indeed, the depletion of specific circulatory macrophages 24 prior to injury, significantly improved clinical outcome in a murine model of renal ischemia (Ferenbach et al. 2012). However, diphtheria toxin-induced CD11b$^+$ cell depletion resulted in a worsened disease outcome in this model, which authors attributed to the depletion of resident renal macrophages by diphtheria toxin. Due to the inability of CLO liposomes injected i.v. to reach these macrophages, they are not depleted. Thus, the

Figure 5.19 Long-term outcome of clodronate depletion and IMP treatment in the spleen of WNV-infected mice

Graph A represents the cell number of total leukocytes ($CD45^+$) in the spleen 90 days p.i. with the LD50 dose ($6x10^3$ PFU) of WNV. Ninety days was sufficient for CLO-depleted animals (red) to have recovered leukocyte number to that of control mice (blue). B cells ($B220^+CD11c^-$), T cells ($CD3^+$), red pulp macrophages ($F4/80^+CD11c^{int}$), monocytes ($CD11b^+CD11c^-$), DC ($CD11c^+$) and neutrophils ($Ly6G^+$ $CD11b^{hi}Ly6C^{int}$) have all recovered in cell number. Graphs B-C demonstrate the numbers (B) and percentages (C) of these leukocytes described in A that are IMP^+ in vehicle-treated (light blue) and CLO-depleted mice (orange). Data are the mean ±SEM of 4 mice/group from 1 experiment. Statistical analysis was conducted using an unpaired, two tailed T-test, and P≤0.05*; P≤0.01**; P≤0.001***.

Figure 5.19

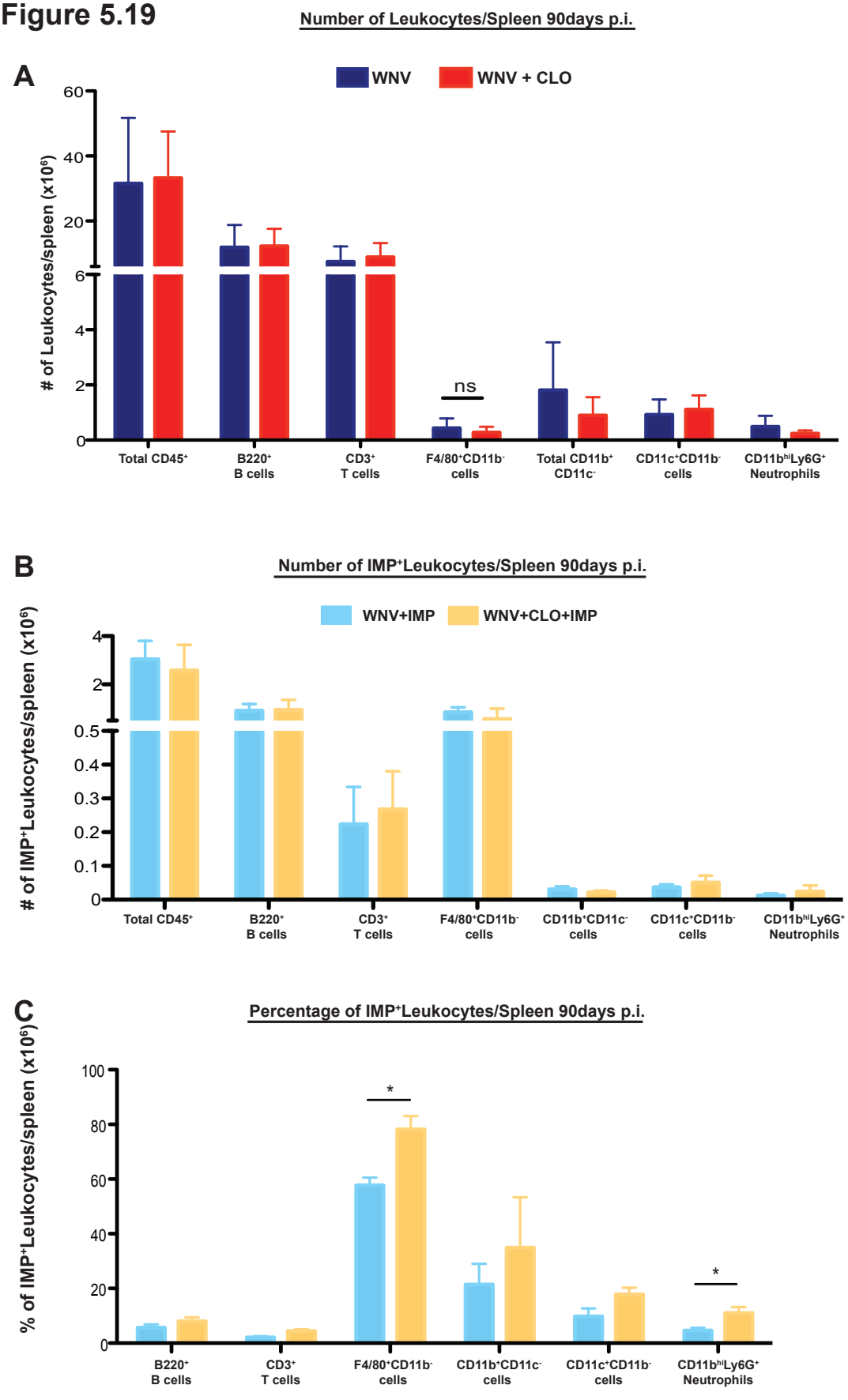
A
Number of Leukocytes/Spleen 90days p.i.
WNV
WNV + CLO
# of Leukocytes/spleen (x10⁶)
60
40
20
6
4
2
0
ns
Total CD45⁺
B220⁺ B cells
CD3⁺ T cells
F4/80⁺CD11b⁻ cells
Total CD11b⁺ CD11c⁻
CD11c⁺CD11b⁻ cells
CD11b^hiLy6G⁺ Neutrophils
B
Number of IMP⁺Leukocytes/Spleen 90days p.i.
WNV+IMP
WNV+CLO+IMP
# of IMP⁺Leukocytes/spleen (x10⁶)
4
2
0.5
0.4
0.3
0.2
0.1
0
Total CD45⁺
B220⁺ B cells
CD3⁺ T cells
F4/80⁺CD11b⁻ cells
CD11b⁺CD11c⁻ cells
CD11c⁺CD11b⁻ cells
CD11b^hiLy6G⁺ Neutrophils
C
Percentage of IMP⁺Leukocytes/Spleen 90days p.i.
% of IMP⁺Leukocytes/spleen (x10⁶)
100
80
60
40
20
0
*
*
B220⁺ B cells
CD3⁺ T cells
F4/80⁺CD11b⁻ cells
CD11b⁺CD11c⁻ cells
CD11c⁺CD11b⁻ cells
CD11b^hiLy6G⁺ Neutrophils

authors hypothesised that, in contrast to circulatory macrophages, these renal macrophages were renoprotective, highlighting the dual pathogenic/protective nature of macrophages (Ferenbach et al. 2012). In contrast, CLO-depletion of circulatory macrophages resulted in increased morbidity and mortality in a vesicular stomatitis virus infection, which causes acute encephalitis (Steel et al. 2010). The data presented in this chapter emphasises that both the method of monocyte depletion and the specific subset targeted are crucial determinants of whether intervention is beneficial.

Clodronate depletion alone did not result in remarkable improvement or worsening of disease in our i.n. model of WNV encephalitis, which was surprising, considering the crucial role of Ly6C^{hi} inflammatory macrophages in the disease pathogenesis. Although a single administration of clodronate liposomes significantly altered the dynamics of leukocyte infiltration into the WNV-infected CNS, in particular reducing Ly6C^{hi} inflammatory macrophages, this did not translate to an improved clinical outcome. Furthermore, daily depletion of circulatory macrophages did not result in further reduced CNS leukocyte numbers of WNV-infected mice, demonstrating the remarkable capacity of the bone marrow to produce a continuous supply of this Ly6C^{hi} macrophage subset.
Interestingly, the significant reduction of Ly6C^{hi} cells occurring in the CNS with clodronate depletion was not seen in the Ly6C^{int} immigrant microglial population, but CLO depletion did decrease the Ly6C^{-} resident microglial population. The possibility that resident microglia become more activated to counterbalance the absence of infiltrating myeloid cells is an interesting one, which needs to be addressed in future experiments.

Interestingly, clodronate depletion did not reduce neutrophil numbers in the CNS but increased this subset. Taken together with data from the spleen, in which neutrophils significantly increased following CLO depletion of WNV-infected mice, this suggests that

the combined action of WNV infection and CLO depletion may alter neutrophil production in the bone marrow. Indeed, as neutrophils and monocytes are both of the myeloid lineage, the effect of CLO on the myeloid progenitor in the bone marrow needs to be further investigated. However, no obvious changes in neutrophil numbers or percentage were present in the bone marrow, with the only subsets significantly altered by CLO being the reduction in F4/80^{+} stromal macrophages. Nevertheless, data from our laboratory supports the notion that Ly6C^{hi} monocyte production is increased in the bone marrow of WNV-infected mice, in order to keep up with the demand for this subset during infection (Thomas Ashhurst, Unpublished). As the bone marrow is a rigid structure limiting large expansion in cell numbers, it is likely that the Ly6C^{hi} monocytes and potentially also the neutrophils are released into the circulation continuously. Thus, it is may be that Ly6C^{hi} monocyte and possibly neutrophil production is increased by the bone marrow in response to the joint action of WNV infection and clodronate depletion but that the release of cells into the circulation matches the rate of proliferation. Proliferation assays, such as the BrdU assay used in chapter 3 and 4, will be useful in determining to what extent clodronate depletion increases the rate of cellular proliferation in the bone marrow of WNV-infected mice.

Moreover, the remarkable presence of IMP^{+} cells in the CNS, in particular IMP^{+}Ly6C^{hi} monocyte and IMP^{+} neutrophils, could be a consequence of the intense left-shift produced by the combined action of WNV infection and clodronate depletion on the bone marrow. It may be that the overwhelming demand for these subsets results in a high output of immature and possibly more activated cells from the bone marrow. Immature Ly6C^{hi} monocytes and neutrophils may be more likely to phagocytose these IMP, but still traffic to the CNS. In the classic model of IMP treatment of WNV-infected mice, the bone marrow supply of mature monocytes is likely released into circulation making their way to the

CNS, whereas the immature monocytes are targeted by IMP treatment, which, once sequestered by the spleen, undergo apoptosis.

Clodronate liposomes deplete any mature (possibly less pathogenic) monocytes in circulation, leaving an abundance of activated and immature Ly6C^{hi} monocytes in circulation, which are highly phagocytic and take up IMP. Studies show that the GR-1^{+} monocyte (i.e. Ly6C^{hi}) populations in circulation completely recover within 24h after i.v. clodronate depletion and reach levels higher than normal by 48h, whereas the GR-1^{-} (Ly6C^{-}) subset has a delayed recovery. Authors excluded neutrophils from these monocyte populations based on Ly6G expression and found that circulatory neutrophils were not depleted by clodronate (Ferenbach et al. 2012).

An overwhelming presence of activated subsets in the blood may traffic to the CNS, accounting for the distinct presence of IMP^{+} cells in the CNS of clodronate-depleted mice. If true, this may explain why the reduction of this subset as a result of clodronate depletion only, does not improve clinical outcome. The absence of mature monocytes and abundance of activated immature Ly6C^{hi} monocytes in the CNS, although reduced, are potentially more pathogenic in nature. It is likely that the ratio of immature-activated *versus* mature monocytes is changed in clodronate-depleted mice, in favour of the activated-immature monocytes. Thus in control animals, IMP may substantially reduce the infiltration of the pathogenic subset of monocytes, whilst allowing the numbers of more mature neuroprotective cells of this lineage migrating into the CNS to supervene.

Importantly, IMP treatment was still effective in clodronate-depleted animals, indicating that the reduction of activated-immature and potentially pathogenic subset mediated by IMP treatment of clodronate-depleted mice was sufficient to enable viral eradication whilst limiting pathogenic action of Ly6C^{hi} macrophages. Irrespective, these data indicate

that, in contrast to our initial hypothesis, that MARCO$^+$ marginal zone macrophages are not essential for the therapeutic efficacy of IMP treatment.

Classically the action of clodronate-encapsulated liposomes is limited to phagocytic cells, in particular circulatory and resident macrophages. However, there were also significant reductions in lymphoid lineage cells such as B, T and NK cells in the CNS of WNV-infected mice following clodronate depletion. Studies have shown the chemokine-dependent recruitment of lymphoid lineage cells to be mediated by inflammatory cytokines produced by macrophages (Pak-Wittel et al. 2013). Thus, it may be that lymphoid lineage cells decrease in response to reduced inflammatory macrophages in the CNS, as a consequence of clodronate depletion.

Dendritic cells in the spleen are also susceptible to clodronate depletion, especially the DC in the marginal zone, which make up the majority of the DC population in the spleen (Leenen et al. 1998). In our model, there was significant depletion of DC in the spleen.

The fact that clodronate depletion did not significantly alter disease outcome might have been markedly different in a peripheral model of infection, as the resident macrophages of the spleen (Seiler et al. 1997) and lymph node are crucial in limiting viral dissemination and systemic spread. The extent to which the macrophages of the spleen may prevent peripheral infection and dissemination of WNV warrants further study.

6. Chapter 6 General discussion

6.1. Role of the draining and non-draining lymph nodes during WNV encephalitis

The data in chapter 3 corroborate studies identifying the CLN as the draining lymph node of the CNS (Louveau et al. 2015; Stern et al. 2014). The absence of detectable virus, paired with the significant clonal expansion in the CLN, but not in the peripheral ILN and MLN suggests that antigen presentation is occurring in the CLN, rather than non-draining lymph nodes, such as the ILN and MLN. Although present in very low numbers, DC from the CNS likely drain to the CLN, inducing the proliferation and activation of local CLN leukocytes. However, whether the innate response generated by the CLN contributes to the lethal immunopathology present in WNV encephalitis remains to be shown.

The results provided in chapter 3 and 4 clearly demonstrate that the response to CNS inflammation is not limited to the CNS draining lymph nodes but that this encompasses the peripheral nodes, as well as the spleen. During homeostatic conditions there is a base level of leukocyte movement throughout the lymphatic system (Tomura et al. 2008). However, this thesis clearly demonstrates that this movement of leukocytes, in particular B cells, from elsewhere to the local DLN is elevated during infection, as there was increased presence of $PKH^{+}B$ cells in the CLN during infection, as shown by the footpad injection of PKH26.

In addition, the significant reduction of T cells in the ILN and MLN following WNV infection suggests that these lymphocytes are recruited to the CNS or CLN, during infection. In contrast to the footpad injection of PKH26, adoptive transfer of $CD45.1^{+}$ leukocytes showed the migration of T cells, from the peripheral PLN to the CLN. This migration of T cells from a peripheral node to the CLN was not significantly modulated by

CNS infection and we could not conclusively demonstrate the recruitment of lymphocytes from the lymph nodes to the CNS. These experiments need to be refined in future studies and will include the adoptive transfer of higher numbers of leukocytes prior to infection, as well as potential lymphadenectomy procedures to shed light on this issue.

The significant upregulation of Ly6C on cells seen in both the draining and non-draining lymph nodes may have a biological function linked to migration (Jaakkola et al. 2003) or it could indicate that these leukocytes are in the preliminary stages of activation, but need a secondary signal such as virus, which would complete this process, for a potential onslaught of virus, should it spread from the CNS to the peripheral organs. The delayed kinetics of increased Ly6C expression in the ILN and MLN (d5 p.i.), compared to the CLN (d3 p.i.), suggests that the signals modulating Ly6C likely originate elsewhere. Studies have shown Th1 cytokines, specifically the IFN group, to directly upregulate Ly6C on B and T cells (Schlueter et al. 2001, 2002). IFN γ production is significantly increased during WNV infection and is also associated with the development of seizures (Getts et al. 2007). It is also reasonable to speculate that cytokines like type I IFN, could emanate from the area of inflammation, reaching the local draining lymph node to induce upregulation of Ly6C. On the other hand, it could also be that, following initial infection of the CNS, low levels of virus spread systemically to initiate a delayed response in the peripheral lymph nodes. However, levels of virus in the ILN and by inference the peripheral organs, are undetectable in this model (Terry 2012), making it unlikely that this is the case. In addition, previous work from our laboratory has shown that CCL2 production by infected neurons and subsequent release into the circulation attracts inflammatory monocytes from the bone marrow to the CNS in WNV infection (Getts et al. 2008). Considering the crucial intimate relationship of the secondary lymphoid organs with the circulatory system, it is reasonable to assume that inflammatory mediators emanating from the

infected CNS and present in circulation in reaching the secondary lymphoid organs, may initiate these changes. It is clear that changes in Ly6C, and leukocyte number and composition in the peripheral nodes are modulated by infection of the CNS, however, whether these leukocytes contribute to the immune response, and if so, in a pathogenic or regulatory manner, remain to be elucidated.

6.2. Role of the spleen in the primary immune response to WNV encephalitis

We further examined the role of the secondary lymphoid organs in CNS inflammation by examining the splenic response to lethal WNV infection. There were negligible changes in cell number and proliferation of leukocytes in the spleen, suggesting that the spleen is not the primary source of lymphoid lineage cells to the inflamed CNS during WNV infection. However, as with the CLN, ILN and MLN, splenic leukocytes showed significant upregulation of Ly6C expression in response to WNV infection and the same distinct $Ly6C^{hi}$ $Ly6C^{int}$ or $Ly6C^{-}$ profiles were also observed in the spleen following infection, in various subsets. Thus, B cells in both the spleen and lymph nodes were $Ly6C^{-}$ during homeostatic conditions, but became more positive as disease progressed, until they were $Ly6C^{int}$.

On the other hand, both $CD4^{+}$ and $CD8^{+}$ T cells possess a $Ly6C^{+}$ subset during homeostatic conditions, with $CD8^{+}$ T cells clearly showing a subset of $Ly6C^{hi}$ cells. This pattern of Ly6C distribution on $CD8^{+}$ T cells seems to suggest that these cells become $Ly6C^{int}$ transiently on their way to become $Ly6C^{hi}$. Interestingly, apart from the $CD4^{+}$ T cells and B cells, all other leukocyte subsets in the lymph nodes and spleen, including DC, monocytes, neutrophils and $NK1.1^{+}$ cells became $Ly6C^{hi}$ at the peak of infection in the spleen. Therefore, the classic characterisation of monocytes and macrophages (Geissmann et al. 2003), based on Ly6C

expression could extend to classification of DC subtypes and even lymphocytes in the future, as a means to describe inflammatory phenotypes. Future experiments using mAb depletion or blockade of Ly6C during infection may prove useful in elucidating the biological significance of Ly6C expression on these subsets.

Whether these changes relate to migration, activation or maturation as previously suggested, will be the aim of future studies (Wrammert et al. 2002). Despite initial results based on proliferation and splenic leukocyte numbers, suggesting that the spleen did not play a role in supplying cells to the CNS during infection, splenectomy prior to WNV infection suggested otherwise. The reduction in pathogenic Ly6C^{hi} inflammatory monocytes in the CNS of WNV-infected splenectomised mice led us to investigate the possibility of the spleen acting as a splenic reservoir of monocytes (Swirski et al. 2009). However, despite the success of ACE inhibitors in reducing the infiltration of Ly6C^{hi} inflammatory macrophages in other disease models, such as MI and stroke (Bao et al. 2010; Leuschner et al. 2010), treatment with ACE inhibitor Enalapril did not reduce the numbers of Ly6C^{hi} monocytes in our model of i.n. WNV infection, nor did it improve survival.

It should be noted that the majority of studies showing successful use of ACE inhibitors to inhibit monocytes from the splenic reservoir, have been limited to acute ischemia-reperfusion injuries. This type of inflammatory insult generally occurs over an acute time-frame compared to the pathogenesis of viral infection of the CNS, suggesting that a more chronic recruitment of monocytes may gradually deplete the splenic reservoir, while simultaneously initiating significant alternative bone marrow production of Ly6C^{hi} monocytes, which quickly overtakes the contribution by the spleen. Indeed, CLO depletion experiments demonstrated the immense the capacity of the bone marrow to continuously supply these cells throughout the course of infection. Thus, these data verify the

importance of the bone marrow as the primary source of pathogenic Ly6C^{hi} inflammatory macrophages during WNV encephalitis.

6.3. The role of the spleen in the development of immunity against lethal WNV infection

Notably, in our i.n. model of WNV infection, splenectomised mice were able to develop sterilising immunity to WNV, raising the issue of where immunity against CNS viral infection resides. The spleen is undoubtedly important for the development of immunity in certain diseases, although whether this applies to CNS infection, has not been investigated in any depth. There is data implicating the spleen as a major reservoir for long-lived memory B cells specific to vaccinia virus (Mamani-Matsuda et al. 2008). In addition, there is a significant reduction in memory B cells against pneumococcal infection in individuals after splenectomy (Rosado et al. 2013). We hypothesise that the relative contribution of the spleen *versus* the draining lymph nodes, likely vary depending on the route of viral infection, with i.n. infection favouring a prominent role for the draining lymph nodes in the development and maintenance of immunity. However, the route of primary and secondary infection in all of these experiments were i.n., therefore the effect of splenectomy and subsequent development of immunity in a peripheral model of infection was not investigated. Future studies will employ different routes of infection, such as i.p. or s.c. in combination with splenectomy after primary infection, followed by lethal dose rechallenge to resolve this question.

6.4. Role of the spleen and the marginal zone macrophages in IMP treatment

Previous studies from this laboratory have implicated the spleen, and in particular the marginal zone macrophages, as a major site of IMP sequestration (Terry 2012; Getts et al. 2014). Thus, we hypothesised that the spleen may be crucial for the efficacy of IMP treatment of WNV encephalitis. Although the IMP treatment of WNV-infected, splenectomised mice did not result in a significant reduction of $Ly6C^{hi}$ inflammatory macrophages in the CNS of LD100 infected mice, it did improve survival outcomes of mice infected with the LD50 dose of virus. Indeed, the already reduced $Ly6C^{hi}$ inflammatory monocyte numbers, as a result of the splenectomy, may have contributed to the improved survival outcome following IMP treatment. Nevertheless, IMP treatment had the best survival outcome in mice with intact spleens. This suggests that; although the absence of the spleen may somewhat impede the beneficial outcome of IMP treatment, the spleen as a whole is not crucial for the efficacy of IMP treatment and that other organs such as the liver, lungs or kidneys may provide similar compensatory environments, promoting the sequestration and phagocytosis of IMP^+ cells.

We therefore focussed on the role of the marginal zone macrophages in the efficacy of IMP treatment, by depleting these macrophages with CLO-encapsulated liposomes prior to IMP administration. Much like the splenectomised mice, CLO-depleted mice showed a significant reduction in the number of leukocytes infiltrating the CNS during WNV infection. Nevertheless, this reduction alone, although significant, did not improve survival outcome. We hypothesise that this was likely due to the fact that CLO depletion also modulated the maturation and activation profile of monocytes in circulation. Thus,

although the Ly6C^{hi} inflammatory macrophages infiltrating the CNS of CLO-depleted mice were reduced, those that did get into the CNS may have been more pathogenic.

IMP treatment of CLO-depleted, WNV-infected mice further reduced the numbers of infiltrating Ly6C^{hi} inflammatory macrophages in the CNS and also resulted in significant improvement in survival. However, similar to the splenectomy model of infection, the maximal benefit of IMP treatment was achieved in mice without CLO-depletion, albeit only marginally. Despite this, these results show that, in contrast to our initial hypothesis, that the spleen and splenic marginal zone macrophages are not critical for the therapeutic efficacy of IMP treatment in our model of i.n. WNV infection.

6.5. Modulation of circulatory and resident macrophages during WNV encephalitis

Clodronate depletion not only abrogated resident splenic macrophages and circulatory monocytes, but also significantly altered the phagocytic capacity and distribution of the myeloid lineage cells in the spleen and CNS, including neutrophils and Ly6C^{hi} inflammatory macrophages. Daily CLO depletion of macrophages demonstrated the remarkable capacity of the bone marrow to continuously and rapidly deploy new monocytes into the circulation. As neutrophils have a shared lineage with monocytes, it is not surprising that this subset was also modulated by CLO depletion. Studies of mice with peritonitis have shown increased neutrophil accumulation in the peritoneal exudate in mice that were CLO-depleted. This increase in neutrophils was attributed to a reduction in monocyte-derived IL-10 as a result of CLO depletion, as IL-10 is known to inhibit neutrophil accumulation (Ajuebor et al. 1999; Chadzinska et al. 2004). In our model, neutrophils were significantly increased in the spleen of CLO-depleted, WNV-infected mice and were also present in the WNV-infected CNS, containing IMP. IMP-containing Ly6C^{hi} inflammatory macrophages were also present in high numbers in the WNV-infected CNS, which is not

seen in the classic model of IMP treatment. These results suggest that the combined action of WNV-infection and CLO depletion amplifies the "left-shift" in the bone marrow, inducing a response which results in the production and release of immature and highly activated monocytes and neutrophils into circulation. Importantly, these results also show that while these IMP^+ cells may change their phenotype to become apoptotic by expressing phosphatidyl serine, to become sequestered in the spleen, they are still capable of migrating to the CNS and diapedesing across the endothelium into the CNS parenchyma. The clinical impact of IMP on other flavivirus infection models, the elucidation of the mechanism(s) by which IMP induce apoptosis markers in MZM and other cell subsets and the subsequent pathophysiological impact on these cells will be of great interest for future studies.

6.6. Conclusion

The results presented in this thesis, show for the first time, the manner in which CNS inflammation modulates the peripheral secondary lymphoid organs. The distinct patterns of Ly6C upregulation occurring in the spleen and non-draining lymph nodes, not only indicates that these organs are likely involved in the immune response, but may also provide new methods of phenotypically characterising leukocyte subsets during inflammation, based on Ly6C expression.

The data from splenectomy and CLO-depletion models highlight the issue that various methods of depletion or abrogation of pathogenic $Ly6C^{hi}$ monocytes can result in different clinical outcomes. Thus, although modulation of pathogenic components of the immune system has shown great promise in the treatment of several disease models, it needs to be done with care, taking into account the nuanced nature of monocytes.

Furthermore, although both splenectomy and CLO-depletion reduced the infiltration of pathogenic $Ly6C^{hi}$ macrophages to the WNV-infected CNS, neither of these models

treatment. Moreover, although the efficacy of IMP treatment was not solely reliant on the spleen or splenic marginal zone macrophages, the absence of these components impeded the therapeutic action of IMP as maximum benefit from IMP treatment was demonstrated in non-CLO-depleted mice, which had their spleens intact.

7. References

Aichele P, Zinke J, Grode L, Schwendener RA, Kaufmann SH, Seiler P (2003) Macrophages of the splenic marginal zone are essential for trapping of blood-borne particulate antigen but dispensable for induction of specific T cell responses. J Immunol 171 (3):1148-1155

Ajmo CT, Jr., Vernon DO, Collier L, Hall AA, Garbuzova-Davis S, Willing A, Pennypacker KR (2008) The spleen contributes to stroke-induced neurodegeneration. Journal of neuroscience research 86 (10):2227-2234. doi:10.1002/jnr.21661

Ajuebor MN, Das AM, Virag L, Flower RJ, Szabo C, Perretti M (1999) Role of resident peritoneal macrophages and mast cells in chemokine production and neutrophil migration in acute inflammation: evidence for an inhibitory loop involving endogenous IL-10. J Immunol 162 (3):1685-1691

Allan RS, Smith CM, Belz GT, van Lint AL, Wakim LM, Heath WR, Carbone FR (2003) Epidermal viral immunity induced by CD8alpha+ dendritic cells but not by Langerhans cells. Science 301 (5641):1925-1928. doi:10.1126/science.1087576

Allan SM, Tyrrell PJ, Rothwell NJ (2005) Interleukin-1 and neuronal injury. Nature reviews Immunology 5 (8):629-640. doi:10.1038/nri1664

Allen CD, Okada T, Cyster JG (2007) Germinal-center organization and cellular dynamics. Immunity 27 (2):190-202. doi:10.1016/j.immuni.2007.07.009

Amaral DCG, Rachid Ma, Vilela MC, Campos RDL, Ferreira GP, Rodrigues DH, Lacerda-Queiroz N, Miranda AS, Costa VV, Campos Ma, Kroon EG, Teixeira MM, Teixeira AL (2011) Intracerebral infection with dengue-3 virus induces meningoencephalitis and behavioral changes that precede lethality in mice. Journal of neuroinflammation 8 (1):23-23. doi:10.1186/1742-2094-8-23

An J, Zhou DS, Zhang JL, Morida H, Wang JL, Yasui K (2004) Dengue-specific CD8+ T cells have both protective and pathogenic roles in dengue virus infection. Immunology letters 95 (2):167-174. doi:10.1016/j.imlet.2004.07.006

Anandasabapathy N, Victora GD, Meredith M, Feder R, Dong B, Kluger C, Yao K, Dustin ML, Nussenzweig MC, Steinman RM, Liu K (2011) Flt3L controls the development of radiosensitive dendritic cells in the meninges and choroid plexus of the steady-state mouse brain. J Exp Med 208 (8):1695-1705. doi:10.1084/jem.20102657

Anderson JF, Rahal JJ (2002) Efficacy of interferon alpha-2b and ribavirin against West Nile virus in vitro. Emerg Infect Dis 8 (1):107-108

Andrews DM, Matthews VB, Sammels LM, Carrello AC, McMinn PC (1999) The severity of murray valley encephalitis in mice is linked to neutrophil infiltration and inducible nitric oxide synthase activity in the central nervous system. J Virol 73 (10):8781-8790

Appler KK, Brown AN, Stewart BS, Behr MJ, Demarest VL, Wong SJ, Bernard KA (2010) Persistence of West Nile virus in the central nervous system and periphery of mice. PLoS One 5 (5):e10649. doi:10.1371/journal.pone.0010649 [doi]

Argall KG, Armati PJ, King NJ, Douglas MW (1991) The effects of West Nile virus on major histocompatibility complex class I and II molecule expression by Lewis rat Schwann cells in vitro. J Neuroimmunol 35 (1-3):273-284

Arjona A, Foellmer HG, Town T, Leng L, McDonald C, Wang T, Wong SJ, Montgomery RR, Fikrig E, Bucala R (2007) Abrogation of macrophage migration inhibitory factor decreases West Nile virus lethality by limiting viral neuroinvasion. 117 (10). doi:10.1172/JCI32218.pools

Arnold SJ, Osvath SR, Hall RA, King NJC, Sedger LM (2004) Regulation of antigen processing and presentation molecules in West Nile virus-infected human skin fibroblasts. Virology 324 (2):286-296

Asano K, Nabeyama A, Miyake Y, Qiu CH, Kurita A, Tomura M, Kanagawa O, Fujii S, Tanaka M (2011) CD169-positive macrophages dominate antitumor immunity by crosspresenting dead cell-associated antigens. Immunity 34 (1):85-95. doi:10.1016/j.immuni.2010.12.011

Asselin-Paturel C, Boonstra A, Dalod M, Durand I, Yessaad N, Dezutter-Dambuyant C, Vicari A, O'Garra A, Biron C, Briere F, Trinchieri G (2001) Mouse type I IFN-producing cells are immature APCs with plasmacytoid morphology. Nat Immunol 2 (12):1144-1150. doi:10.1038/ni736

Ashhurst TM, van Vreden C, Niewold P, King NJ (2014) The plasticity of inflammatory monocyte responses to the inflamed central nervous system. Cellular immunology 291 (1-2):49-57. doi:10.1016/j.cellimm.2014.07.002

Atrasheuskaya AV, Fredeking TM, Ignatyev GM (2003) Changes in immune parameters and their correction in human cases of tick-borne encephalitis. Clin Exp Immunol 131 (1):148-154

Bai F, Kong KF, Dai J, Qian F, Zhang L, Brown CR, Fikrig E, Montgomery RR (2010) A paradoxical role for neutrophils in the pathogenesis of West Nile virus. J Infect Dis 202 (12):1804-1812. doi:10.1086/657416 [doi]

Bajana S, Roach K, Turner S, Paul J, Kovats S (2012) IRF4 Promotes Cutaneous Dendritic Cell Migration to Lymph Nodes during Homeostasis and Inflammation. J Immunol 189 (7):3368-3377. doi:10.4049/jimmunol.1102613

Bajenoff M, Breart B, Huang AY, Qi H, Cazareth J, Braud VM, Germain RN, Glaichenhaus N (2006) Natural killer cell behavior in lymph nodes revealed by static and real-time imaging. J Exp Med 203 (3):619-631. doi:10.1084/jem.20051474

Banchereau J, Briere F, Liu YJ, Rousset F (1994) Molecular control of B lymphocyte growth and differentiation. Stem Cells 12 (3):278-288. doi:10.1002/stem.5530120304

Bankovich AJ, Shiow LR, Cyster JG (2010) CD69 suppresses sphingosine 1-phosophate receptor-1 (S1P1) function through interaction with membrane helix 4. J Biol Chem 285 (29):22328-22337. doi:10.1074/jbc.M110.123299

Bao Y, Kim E, Bhosle S, Mehta H, Cho S (2010) A role for spleen monocytes in post-ischemic brain inflammation and injury. J Neuroinflammation 7:92. doi:10.1186/1742-2094-7-92

Barkho BZ, Song H, Aimone JB, Smrt RD, Nakashima K, Gage FH, Zhao X (2009) NIH Public Access. 15 (3):407-421. doi:10.1089/scd.2006.15.407.Identification

Barrett PN, Schober-Bendixen S, Ehrlich HJ (2003) History of TBE vaccines. Vaccine 21 Suppl 1:S41-49

Batista FD, Harwood NE (2009) The who, how and where of antigen presentation to B cells. Nature reviews Immunology 9 (1):15-27. doi:10.1038/nri2454

Beardsley R, McCannel C (2012) Reactivation West Nile virus infection-related chorioretinitis. Seminars in ophthalmology 27 (3-4):43-45. doi:10.3109/08820538.2011.631512

Belisle C, Saintemarie G (1981) Tridimensional Study of the Deep Cortex of the Rat Lymph-Node .3. Morphology of the Deep Cortex Units. Anat Rec 199 (2):213-226. doi:Doi 10.1002/Ar.1091990206

Belz GT, Heath TJ (1995) Pathways of blood flow to and through superficial lymph nodes in the dog. Journal of anatomy 187 (Pt 2):413-421

Ben-Hur T, Ben-Menachem O, Furer V, Einstein O, Mizrachi-Kol R, Grigoriadis N (2003) Effects of proinflammatory cytokines on the growth, fate, and motility of multipotential neural precursor cells. Molecular and Cellular Neuroscience 24 (3):623-631. doi:10.1016/s1044-7431(03)00218-5

Bennett JL, Elhofy A, Canto MC, Tani M, Ransohoff RM, Karpus WJ (2003) CCL2 transgene expression in the central nervous system directs diffuse infiltration of CD45(high)CD11b(+) monocytes and enhanced Theiler's murine encephalomyelitis virus-induced demyelinating disease. J Neurovirol 9 (6):623-636

Bian G, Xu Y, Lu P, Xie Y, Xi Z (2010) The endosymbiotic bacterium Wolbachia induces resistance to dengue virus in Aedes aegypti. PLoS Pathog 6 (4):e1000833. doi:10.1371/journal.ppat.1000833

Blomster LV, Brennan FH, Lao HW, Harle DW, Harvey AR, Ruitenberg MJ (2013) Mobilisation of the splenic monocyte reservoir and peripheral CX(3)CR1 deficiency adversely affects recovery from spinal cord injury. Experimental neurology 247:226-240. doi:10.1016/j.expneurol.2013.05.002

Blutt SE, Warfield KL, Lewis DE, Conner ME (2002) Early response to rotavirus infection involves massive B cell activation. J Immunol 168 (11):5716-5721

Bode AV, Sejvar JJ, Pape WJ, Campbell GL, Marfin AA (2006) West Nile virus disease: a descriptive study of 228 patients hospitalized in a 4-county region of Colorado in 2003. Clin Infect Dis 42 (9):1234-1240. doi:CID38389 [pii]
10.1086/503038 [doi]

Boonnak K, Dambach KM, Donofrio GC, Tassaneetrithep B, Marovich MA (2011) Cell type specificity and host genetic polymorphisms influence antibody-dependent enhancement of dengue virus infection. J Virol 85 (4):1671-1683. doi:JVI.00220-10 [pii]
10.1128/JVI.00220-10 [doi]

Bowen JL, Olson JK (2013) IFNgamma influences type I interferon response and susceptibility to Theiler's virus-induced demyelinating disease. Viral immunology 26 (4):223-238. doi:10.1089/vim.2013.0004

Braun A, Worbs T, Moschovakis GL, Halle S, Hoffmann K, Bolter J, Munk A, Forster R (2011) Afferent lymph-derived T cells and DCs use different chemokine receptor CCR7-dependent routes for entry into the lymph node and intranodal migration. Nat Immunol 12 (9):879-887. doi:10.1038/ni.2085

Brehin AC, Mouries J, Frenkiel MP, Dadaglio G, Despres P, Lafon M, Couderc T (2008) Dynamics of immune cell recruitment during West Nile encephalitis and identification of a new CD19+B220-BST-2+ leukocyte population. J Immunol 180 (10):6760-6767. doi:180/10/6760 [pii]

Brien JD, Uhrlaub JL, Nikolich-Zugich J (2008) West Nile virus-specific CD4 T cells exhibit direct antiviral cytokine secretion and cytotoxicity and are sufficient for antiviral protection. J Immunol 181 (12):8568-8575. doi:181/12/8568 [pii]

Byrne SN, Halliday GM, Johnston LJ, King NJ (2001) Interleukin-1beta but not tumor necrosis factor is involved in West Nile virus-induced Langerhans cell migration from the skin in C57BL/6 mice. J Invest Dermatol 117 (3):702-709

Calisher CH, Karabatsos N, Dalrymple JM, Shope RE, Porterfield JS, Westaway EG, Brandt WE (1989) Antigenic relationships between flaviviruses as determined by cross-neutralization tests with polyclonal antisera. J Gen Virol 70 (Pt 1):37-43

Camenga DL, Nathanson N (1975) An immunopathologic component in experimental togavirus encephalitis. Journal of neuropathology and experimental neurology 34 (6):492-500

Cameron PU, Jones P, Gorniak M, Dunster K, Paul E, Lewin S, Woolley I, Spelman D (2011) Splenectomy associated changes in IgM memory B cells in an adult spleen registry cohort. PloS one 6 (8):e23164. doi:10.1371/journal.pone.0023164

Cannon MJ, Openshaw PJ, Askonas BA (1988) Cytotoxic T cells clear virus but augment lung pathology in mice infected with respiratory syncytial virus. J Exp Med 168 (3):1163-1168

Cantile C, Del Piero F, Di Guardo G, Arispici M (2001) Pathologic and Immunohistochemical Findings in Naturally Occurring West Nile Virus Infection in Horses. Veterinary Pathology 38 (4):414-431. doi:10.1354/vp.38-4-414

Cardosa MJ, Gordon S, Hirsch S, Springer TA, Porterfield JS (1986) Interaction of West Nile virus with primary murine macrophages: role of cell activation and receptors for antibody and complement. J Virol 57 (3):952-959

Cesta MF (2006) Normal structure, function, and histology of the spleen. Toxicologic pathology 34 (5):455-465. doi:10.1080/01926230600867743

Chadzinska M, Kolaczkowska E, Scislowska-Czarnecka A, Van Rooijen N, Plytycz B (2004) Effects of macrophage depletion on peritoneal inflammation in swiss mice, edible frogs and goldfish. Folia biologica 52 (3-4):225-231

Chamorro A, Urra X, Planas AM (2007) Infection after acute ischemic stroke: a manifestation of brain-induced immunodepression. Stroke; a journal of cerebral circulation 38 (3):1097-1103. doi:10.1161/01.STR.0000258346.68966.9d

Cheeran MC, Hu S, Sheng WS, Rashid A, Peterson PK, Lokensgard JR (2005) Differential responses of human brain cells to West Nile virus infection. J Neurovirol 11 (6):512-524. doi:H0P5M513MRV63803 [pii]
10.1080/13550280500384982

Chen CJ, Ou YC, Lin SY, Raung SL, Liao SL, Lai CY, Chen SY, Chen JH (2010) Glial activation involvement in neuronal death by Japanese encephalitis virus infection. J Gen Virol 91 (Pt 4):1028-1037. doi:vir.0.013565-0 [pii]
10.1099/vir.0.013565-0 [doi]

Cheng Y, King NJC, Kesson AM (2004a) Major histocompatibility complex class I (MHC-I) induction by West Nile virus: involvement of 2 signaling pathways in MHC-I up-regulation. J Infect Dis 189 (4):658-668

Cheng Y, King NJC, Kesson AM (2004b) The role of tumor necrosis factor in modulating responses of murine embryo fibroblasts by flavivirus, West Nile. Virology 329 (2):361-370

Chowers MY, Lang R, Nassar F, Ben-David D, Giladi M, Rubinshtein E, Itzhaki A, Mishal J, Siegman-Igra Y, Kitzes R, Pick N, Landau Z, Wolf D, Bin H, Mendelson E, Pitlik SD, Weinberger M (2001) Clinical characteristics of the West Nile fever outbreak, Israel, 2000. Emerg Infect Dis 7 (4):675-678

Chtanova T, Schaeffer M, Han SJ, van Dooren GG, Nollmann M, Herzmark P, Chan SW, Satija H, Camfield K, Aaron H, Striepen B, Robey EA (2008) Dynamics of neutrophil migration in lymph nodes during infection. Immunity 29 (3):487-496. doi:10.1016/j.immuni.2008.07.012

Chu JJ, Ng ML (2004) Infectious entry of West Nile virus occurs through a clathrin-mediated endocytic pathway. J Virol 78 (19):10543-10555. doi:10.1128/JVI.78.19.10543-10555.2004
78/19/10543 [pii]

Chu JJH (2003) The mechanism of cell death during West Nile virus infection is dependent on initial infectious dose. Journal of General Virology 84 (12):3305-3314. doi:10.1099/vir.0.19447-0

Ciabattini A, Pettini E, Arsenijevic S, Pozzi G, Medaglini D (2010) Intranasal immunization with vaccine vector Streptococcus gordonii elicits primed CD4+ and CD8+ T cells in the genital and intestinal tracts. Vaccine 28 (5):1226-1233. doi:10.1016/j.vaccine.2009.11.021

Ciabattini A, Pettini E, Fiorino F, Prota G, Pozzi G, Medaglini D (2011) Distribution of primed T cells and antigen-loaded antigen presenting cells following intranasal immunization in mice. PLoS One 6 (4):e19346. doi:10.1371/journal.pone.0019346

Cohen SB, Maurer KJ, Egan CE, Oghumu S, Satoskar AR, Denkers EY (2013) CXCR3-dependent CD4(+) T cells are required to activate inflammatory monocytes for defense against intestinal infection. PLoS Pathog 9 (10):e1003706. doi:10.1371/journal.ppat.1003706

Coombes JL, Han SJ, van Rooijen N, Raulet DH, Robey EA (2012) Infection-induced regulation of natural killer cells by macrophages and collagen at the lymph node subcapsular sinus. Cell reports 2 (1):124-135. doi:10.1016/j.celrep.2012.06.001

Costa VV, Fagundes CT, Valadão DF, Cisalpino D, Dias ACF, Silveira KD, Kangussu LM, Ávila TV, Bonfim MRQ, Bonaventura D, Silva Ta, Sousa LP, Rachid Ma, Vieira LQ, Menezes GB, de Paula AM, Atrasheuskaya A, Ignatyev G, Teixeira MM, Souza DG (2012) A model of DENV-3 infection that recapitulates severe disease and highlights the importance of IFN-γ in host resistance to infection. PLoS neglected tropical diseases 6 (5):e1663-e1663. doi:10.1371/journal.pntd.0001663

Cusick MF, Libbey JE, Patel DC, Doty DJ, Fujinami RS (2013) Infiltrating macrophages are key to the development of seizures following virus infection. J Virol 87 (3):1849-1860. doi:10.1128/JVI.02747-12

D'Agostino PM, Gottfried-Blackmore A, Anandasabapathy N, Bulloch K (2012) Brain dendritic cells: biology and pathology. Acta neuropathologica 124 (5):599-614. doi:10.1007/s00401-012-1018-0

Daffis S, Samuel MA, Suthar MS, Gale M, Jr., Diamond MS (2008) Toll-like receptor 3 has a protective role against West Nile virus infection. J Virol 82 (21):10349-10358. doi:JVI.00935-08 [pii]
10.1128/JVI.00935-08 [doi]

Das S, Dutta K, Kumawat KL, Ghoshal A, Adhya D, Basu A (2011) Abrogated inflammatory response promotes neurogenesis in a murine model of Japanese encephalitis. PloS one 6 (3):e17225-e17225. doi:10.1371/journal.pone.0017225

Das S, Mishra MK, Ghosh J, Basu A (2008) Japanese Encephalitis Virus infection induces IL-18 and IL-1beta in microglia and astrocytes: correlation with in vitro cytokine responsiveness of glial cells and subsequent neuronal death. Journal of neuroimmunology 195 (1-2):60-72. doi:10.1016/j.jneuroim.2008.01.009

Davison AM, King NJ (2011) Accelerated dendritic cell differentiation from migrating Ly6C(lo) bone marrow monocytes in early dermal West Nile virus infection. J Immunol 186 (4):2382-2396. doi:jimmunol.1002682 [pii]
10.4049/jimmunol.1002682 [doi]

de Souza KPR, Silva EG, de Oliveira Rocha ES, Figueiredo LB, de Almeida-Leite CM, Arantes RME, de Assis Silva Gomes J, Ferreira GP, de Oliveira JG, Kroon EG, Campos MA (2013) Nitric oxide synthase expression correlates with death in an experimental mouse model of dengue with CNS involvement. Virology journal 10:267-267. doi:10.1186/1743-422x-10-267

Demoy M, Andreux JP, Weingarten C, Gouritin B, Guilloux V, Couvreur P (1999) Spleen capture of nanoparticles: influence of animal species and surface characteristics. Pharmaceutical research 16 (1):37-41

Demoy M, Gibaud S, Andreux JP, Weingarten C, Gouritin B, Couvreur P (1997) Splenic trapping of nanoparticles: complementary approaches for in situ studies. Pharmaceutical research 14 (4):463-468

Denton AE, Roberts EW, Linterman MA, Fearon DT (2014) Fibroblastic reticular cells of the lymph node are required for retention of resting but not activated CD8+ T cells. Proc Natl Acad Sci U S A. doi:10.1073/pnas.1412910111

Després P, Flamand M, Ceccaldi PE, Deubel V, Flamand M, Ceccaldi P-e (1996) Human isolates of dengue type 1 virus induce apoptosis in mouse neuroblastoma cells . These include : Human Isolates of Dengue Type 1 Virus Induce Apoptosis in Mouse Neuroblastoma Cells. 70 (6)

Després P, Frenkiel M-p, Duarte C, Santos D, Deubel V, Ceccaldi P-e, Despre P (1998) Apoptosis in the Mouse Central Nervous System in Response to Infection with Mouse-Neurovirulent Dengue Viruses Apoptosis in the Mouse Central Nervous System in Response to Infection with Mouse-Neurovirulent Dengue Viruses.

Diamond MS, Shrestha B, Marri A, Mahan D, Engle M (2003) B cells and antibody play critical roles in the immediate defense of disseminated infection by West Nile encephalitis virus. J Virol 77 (4):2578-2586

Douglas MW, Kesson AM, King NJ (1994) CTL recognition of west Nile virus-infected fibroblasts is cell cycle dependent and is associated with virus-induced increases in class I MHC antigen expression. Immunology 82 (4):561-570

Dumont FJ (1987) Stimulation of murine T cells via the Ly-6C antigen: lack of proliferative response in aberrant T cells from lpr/lpr and gld/gld mice despite high Ly-6C antigen expression. J Immunol 138 (12):4106-4113

Dunn TB (1954) Normal and pathologic anatomy of the reticular tissue in laboratory mice, with a classification and discussion of neoplasms. Journal of the National Cancer Institute 14 (6):1281-1433

Dutta K, Mishra MK, Nazmi A, Kumawat KL, Basu A (2010) Minocycline differentially modulates macrophage mediated peripheral immune response following Japanese encephalitis virus infection. Immunobiology 215 (11):884-893. doi:10.1016/j.imbio.2009.12.003

Elpek KG, Bellemare-Pelletier A, Malhotra D, Reynoso ED, Lukacs-Kornek V, DeKruyff RH, Turley SJ (2011) Lymphoid organ-resident dendritic cells exhibit unique transcriptional fingerprints based on subset and site. PLoS One 6 (8):e23921. doi:10.1371/journal.pone.0023921

Engle MJ, Diamond MS (2003) Antibody prophylaxis and therapy against West Nile virus infection in wild-type and immunodeficient mice. J Virol 77 (24):12941-12949

Fehniger TA, Cooper MA, Nuovo GJ, Cella M, Facchetti F, Colonna M, Caligiuri MA (2003) CD56bright natural killer cells are present in human lymph nodes and are

activated by T cell-derived IL-2: a potential new link between adaptive and innate immunity. Blood 101 (8):3052-3057. doi:10.1182/blood-2002-09-2876

Ferenbach DA, Sheldrake TA, Dhaliwal K, Kipari TM, Marson LP, Kluth DC, Hughes J (2012) Macrophage/monocyte depletion by clodronate, but not diphtheria toxin, improves renal ischemia/reperfusion injury in mice. Kidney international 82 (8):928-933. doi:10.1038/ki.2012.207

Ferlazzo G, Pack M, Thomas D, Paludan C, Schmid D, Strowig T, Bougras G, Muller WA, Moretta L, Munz C (2004) Distinct roles of IL-12 and IL-15 in human natural killer cell activation by dendritic cells from secondary lymphoid organs. Proc Natl Acad Sci U S A 101 (47):16606-16611. doi:10.1073/pnas.0407522101

Finke S, Conzelmann KK (2005) Replication strategies of rabies virus. Virus Res 111 (2):120-131. doi:S0168-1702(05)00118-8 [pii]
10.1016/j.virusres.2005.04.004 [doi]

Fredericksen BL, Keller BC, Fornek J, Katze MG, Gale M, Jr. (2008) Establishment and maintenance of the innate antiviral response to West Nile Virus involves both RIG-I and MDA5 signaling through IPS-1. J Virol 82 (2):609-616. doi:JVI.01305-07 [pii]
10.1128/JVI.01305-07

Furuya M, Kirschbaum SB, Paulovich A, Pauli BU, Zhang H, Alexander JS, Farr AG, Ruddell A (2010) Lymphatic endothelial murine chloride channel calcium-activated 1 is a ligand for leukocyte LFA-1 and Mac-1. J Immunol 185 (10):5769-5777. doi:10.4049/jimmunol.1002226

Ganusov VV, Auerbach J (2014) Mathematical modeling reveals kinetics of lymphocyte recirculation in the whole organism. PLoS computational biology 10 (5):e1003586. doi:10.1371/journal.pcbi.1003586

Garcia-Tapia D, Loiacono CM, Kleiboeker SB (2006) Replication of West Nile virus in equine peripheral blood mononuclear cells. Veterinary immunology and immunopathology 110 (3-4):229-244. doi:10.1016/j.vetimm.2005.10.003

Gard PR, Mandy A, Sutcliffe MA (1999) Evidence of a possible role of altered angiotensin function in the treatment, but not etiology, of depression. Biological psychiatry 45 (8):1030-1034

Gaya M, Castello A, Montaner B, Rogers N, Reis e Sousa C, Bruckbauer A, Batista FD (2015) Host response. Inflammation-induced disruption of SCS macrophages impairs B cell responses to secondary infection. Science 347 (6222):667-672. doi:10.1126/science.aaa1300

Geissmann F, Jung S, Littman DR (2003) Blood monocytes consist of two principal subsets with distinct migratory properties. Immunity 19 (1):71-82. doi:S1074761303001742 [pii]

Gelpi E, Preusser M, Garzuly F, Holzmann H, Heinz FX, Budka H (2005) Visualization of Central European tick-borne encephalitis infection in fatal human cases. Journal of neuropathology and experimental neurology 64 (6):506-512

Gelpi E, Preusser M, Laggner U, Garzuly F, Holzmann H, Heinz FX, Budka H (2006) Inflammatory response in human tick-borne encephalitis: analysis of postmortem brain tissue. J Neurovirol 12 (4):322-327. doi:10.1080/13550280600848746

German AC, Myint KS, Mai NT, Pomeroy I, Phu NH, Tzartos J, Winter P, Collett J, Farrar J, Barrett A, Kipar A, Esiri MM, Solomon T (2006) A preliminary neuropathological study of Japanese encephalitis in humans and a mouse model. Trans R Soc Trop Med Hyg 100 (12):1135-1145. doi:S0035-9203(06)00107-6 [pii]
10.1016/j.trstmh.2006.02.008 [doi]

Gerner MY, Kastenmuller W, Ifrim I, Kabat J, Germain RN (2012) Histo-cytometry: a method for highly multiplex quantitative tissue imaging analysis applied to dendritic cell subset microanatomy in lymph nodes. Immunity 37 (2):364-376. doi:10.1016/j.immuni.2012.07.011

Getts DR, Matsumoto I, Muller M, Getts MT, Radford J, Shrestha B, Campbell IL, King NJ (2007) Role of IFN-gamma in an experimental murine model of West Nile virus-induced seizures. J Neurochem 103 (3):1019-1030. doi:JNC4798 [pii]
10.1111/j.1471-4159.2007.04798.x [doi]

Getts DR, Terry RL, Getts MT, Deffrasnes C, Müller M, van Vreden C, Ashhurst TM, Chami B, McCarthy D, Wu H, Ma J, Martin A, Shae LD, Witting P, Kansas GS, Kühn J, Hafezi W, Campbell IL, Reilly D, Say J, Brown L, White MY, Cordwell SJ, Chadban SJ, Thorp EB, Bao S, Miller SD, King NJC (2014) Therapeutic inflammatory monocyte modulation using immune-modifying microparticles. Science translational medicine 6 (219):219ra217-219ra217. doi:10.1126/scitranslmed.3007563

Getts DR, Terry RL, Getts MT, Muller M, Rana S, Deffrasnes C, Ashhurst TM, Radford J, Hofer M, Thomas S, Campbell IL, King NJ (2012) Targeted blockade in lethal West Nile virus encephalitis indicates a crucial role for very late antigen (VLA)-4-dependent recruitment of nitric oxide-producing macrophages. J Neuroinflammation 9:246. doi:10.1186/1742-2094-9-246

Getts DR, Terry RL, Getts MT, Muller M, Rana S, Shrestha B, Radford J, Van Rooijen N, Campbell IL, King NJ (2008) Ly6c+ "inflammatory monocytes" are microglial precursors recruited in a pathogenic manner in West Nile virus encephalitis. J Exp Med 205 (10):2319-2337. doi:jem.20080421 [pii]
10.1084/jem.20080421 [doi]

Ghoshal A, Das S, Ghosh S, Kumar Mishra M, Sharma V, Koli P, Sen E, Basu A (2007) Proinflammatory Mediators Released by Activated Microglia Induces Neuronal Death in Japanese Encephalitis. 496 (January):483-496. doi:10.1002/glia

Ginhoux F, Greter M, Leboeuf M, Nandi S, See P, Gokhan S, Mehler MF, Conway SJ, Ng LG, Stanley ER, Samokhvalov IM, Merad M (2010) Fate mapping analysis reveals that adult microglia derive from primitive macrophages. Science 330 (6005):841-845. doi:10.1126/science.1194637

Glass WG, Lim JK, Cholera R, Pletnev AG, Gao JL, Murphy PM (2005) Chemokine receptor CCR5 promotes leukocyte trafficking to the brain and survival in West Nile virus infection. J Exp Med 202 (8):1087-1098. doi:jem.20042530 [pii]
10.1084/jem.20042530

Goldblum N, Sterk VV, Jasinskaklingberg W (1957) The natural history of West Nile fever. II. Virological findings and the development of homologous and heterologous antibodies in West Nile infection in man. Am J Hyg 66 (3):363-380

Goldszmid RS, Caspar P, Rivollier A, White S, Dzutsev A, Hieny S, Kelsall B, Trinchieri G, Sher A (2012) NK cell-derived interferon-gamma orchestrates cellular dynamics and the differentiation of monocytes into dendritic cells at the site of infection. Immunity 36 (6):1047-1059. doi:10.1016/j.immuni.2012.03.026

Goltz D, Huss S, Ramadori E, Buttner R, Diehl L, Meyer R (2015) Immunomodulation by splenectomy or by FTY720 protects the heart against ischemia reperfusion injury. Clinical and experimental pharmacology & physiology. doi:10.1111/1440-1681.12465

Gonzalez SF, Lukacs-Kornek V, Kuligowski MP, Pitcher LA, Degn SE, Kim YA, Cloninger MJ, Martinez-Pomares L, Gordon S, Turley SJ, Carroll MC (2010) Capture of influenza by medullary dendritic cells via SIGN-R1 is essential for humoral immunity in draining lymph nodes. Nat Immunol 11 (5):427-434. doi:10.1038/ni.1856

Graham JB, Da Costa A, Lund JM (2014) Regulatory T cells shape the resident memory T cell response to virus infection in the tissues. J Immunol 192 (2):683-690. doi:10.4049/jimmunol.1202153

Gretz JE, Kaldjian EP, Anderson AO, Shaw S (1996) Sophisticated strategies for information encounter in the lymph node: the reticular network as a conduit of soluble information and a highway for cell traffic. J Immunol 157 (2):495-499

Griffin WST (2006) Inflammation and neurodegenerative diseases. The American journal of clinical nutrition 83 (2):470S-474S

Grigorova IL, Panteleev M, Cyster JG (2010) Lymph node cortical sinus organization and relationship to lymphocyte egress dynamics and antigen exposure. Proc Natl Acad Sci U S A 107 (47):20447-20452. doi:10.1073/pnas.1009968107

Grigorova IL, Schwab SR, Phan TG, Pham TH, Okada T, Cyster JG (2009) Cortical sinus probing, S1P1-dependent entry and flow-based capture of egressing T cells. Nat Immunol 10 (1):58-65. doi:10.1038/ni.1682

Guarner J, Shieh WJ, Hunter S, Paddock CD, Morken T, Campbell GL, Marfin AA, Zaki SR (2004) Clinicopathologic study and laboratory diagnosis of 23 cases with West Nile virus encephalomyelitis. Hum Pathol 35 (8):983-990. doi:S004681770400231X [pii]

Haley M, Retter AS, Fowler D, Gea-Banacloche J, O'Grady NP (2003) The role for intravenous immunoglobulin in the treatment of West Nile virus encephalitis. Clin Infect Dis 37 (6):e88-90. doi:10.1086/377172

Halstead SB, O'Rourke EJ (1977) Dengue viruses and mononuclear phagocytes. I. Infection enhancement by non-neutralizing antibody. J Exp Med 146 (1):201-217

Hanninen A, Jaakkola I, Salmi M, Simell O, Jalkanen S (1997) Ly-6C regulates endothelial adhesion and homing of CD8(+) T cells by activating integrin-dependent adhesion pathways. Proc Natl Acad Sci U S A 94 (13):6898-6903

Hatterer E, Touret M, Belin MF, Honnorat J, Nataf S (2008) Cerebrospinal fluid dendritic cells infiltrate the brain parenchyma and target the cervical lymph nodes under neuroinflammatory conditions. PLoS One 3 (10):e3321. doi:10.1371/journal.pone.0003321

Hayasaka D, Nagata N, Fujii Y, Hasegawa H, Sata T, Suzuki R, Gould Ea, Takashima I, Koike S (2009) Mortality following peripheral infection with tick-borne encephalitis virus results from a combination of central nervous system pathology, systemic inflammatory and stress responses. Virology 390 (1):139-150. doi:10.1016/j.virol.2009.04.026

Hayes CG (2001) West Nile virus: Uganda, 1937, to New York City, 1999. Annals of the New York Academy of Sciences 951:25-37

He X, Ren J, Xu F, Ferguson MR, Li G (2009) Localization of West Nile Virus in monkey brain: double staining antigens immunohistochemically of neurons, neuroglia cells and West Nile Virus. Int J Clin Exp Pathol 3 (2):156-161

Heinz FX, Holzmann H, Essl A, Kundi M (2007) Field effectiveness of vaccination against tick-borne encephalitis. Vaccine 25 (43):7559-7567. doi:10.1016/j.vaccine.2007.08.024

Henri S, Vremec D, Kamath A, Waithman J, Williams S, Benoist C, Burnham K, Saeland S, Handman E, Shortman K (2001) The dendritic cell populations of mouse lymph nodes. J Immunol 167 (2):741-748

Hershkovitz O, Rosental B, Rosenberg LA, Navarro-Sanchez ME, Jivov S, Zilka A, Gershoni-Yahalom O, Brient-Litzler E, Bedouelle H, Ho JW, Campbell KS, Rager-Zisman B, Despres P, Porgador A (2009) NKp44 receptor mediates interaction of the envelope glycoproteins from the West Nile and dengue viruses with NK cells. J Immunol 183 (4):2610-2621. doi:10.4049/jimmunol.0802806

Hickey WF, Hsu BL, Kimura H (1991) T-lymphocyte entry into the central nervous system. Journal of neuroscience research 28 (2):254-260. doi:10.1002/jnr.490280213

Hildner K, Edelson BT, Purtha WE, Diamond M, Matsushita H, Kohyama M, Calderon B, Schraml BU, Unanue ER, Diamond MS, Schreiber RD, Murphy TL, Murphy KM (2008) Batf3 deficiency reveals a critical role for CD8alpha+ dendritic cells in cytotoxic T cell immunity. Science 322 (5904):1097-1100. doi:10.1126/science.1164206

Ho LJ, Wang JJ, Shaio MF, Kao CL, Chang DM, Han SW, Lai JH (2001) Infection of human dendritic cells by dengue virus causes cell maturation and cytokine production. J Immunol 166 (3):1499-1506

Howe CL, Lafrance-Corey RG, Sundsbak RS, Sauer BM, Lafrance SJ, Buenz EJ, Schmalstieg WF (2012) Hippocampal protection in mice with an attenuated inflammatory monocyte response to acute CNS picornavirus infection. Scientific reports 2:545. doi:10.1038/srep00545

Hughes DA, Fraser IP, Gordon S (1995) Murine macrophage scavenger receptor: in vivo expression and function as receptor for macrophage adhesion in lymphoid and

non-lymphoid organs. Eur J Immunol 25 (2):466-473. doi:10.1002/eji.1830250224

Hunsperger E, Roehrig JT (2005) Characterization of West Nile viral replication and maturation in peripheral neurons in culture. J Neurovirol 11 (1):11-22. doi:M507574511822 6Q2 [pii]
10.1080/13550280590900454 [doi]

Hunsperger EA, Roehrig JT (2006) Temporal analyses of the neuropathogenesis of a West Nile virus infection in mice. J Neurovirol 12 (2):129-139. doi:T426J2M58K807767 [pii]
10.1080/13550280600758341 [doi]

Hunsperger EA, Roehrig JT (2009) Nocodazole delays viral entry into the brain following footpad inoculation with West Nile virus in mice. J Neurovirol 15 (3):211-218. doi:911196617 [pii]
10.1080/13550280902913255 [doi]

Iannacone M, Moseman EA, Tonti E, Bosurgi L, Junt T, Henrickson SE, Whelan SP, Guidotti LG, von Andrian UH (2010) Subcapsular sinus macrophages prevent CNS invasion on peripheral infection with a neurotropic virus. Nature 465 (7301):1079-1083. doi:10.1038/nature09118

Irjala H, Johansson EL, Grenman R, Alanen K, Salmi M, Jalkanen S (2001) Mannose receptor is a novel ligand for L-selectin and mediates lymphocyte binding to lymphatic endothelium. J Exp Med 194 (8):1033-1042

Iwamoto M, Jernigan DB, Guasch A, Trepka MJ, Blackmore CG, Hellinger WC, Pham SM, Zaki S, Lanciotti RS, Lance-Parker SE, DiazGranados CA, Winquist AG, Perlino CA, Wiersma S, Hillyer KL, Goodman JL, Marfin AA, Chamberland ME, Petersen LR (2003) Transmission of West Nile virus from an organ donor to four transplant recipients. N Engl J Med 348 (22):2196-2203. doi:10.1056/NEJMoa022987 [doi]
348/22/2196 [pii]

Jaakkola I, Merinen M, Jalkanen S, Hanninen A (2003) Ly6C induces clustering of LFA-1 (CD11a/CD18) and is involved in subtype-specific adhesion of CD8 T cells. J Immunol 170 (3):1283-1290

Jan J-t, Chen B-h, Ma S-h, Liu C-i, Tsai H-p, Wu H-c, Jiang S-y (2000) Potential Dengue Virus-Triggered Apoptotic Pathway in Human Neuroblastoma Cells : Arachidonic Acid , Superoxide Anion , and NF- κ B Are Sequentially Involved Potential Dengue Virus-Triggered Apoptotic Pathway in Human Neuroblastoma Cells : Arachidonic Aci. doi:10.1128/JVI.74.18.8680-8691.2000.Updated

Jiang D, Weidner JM, Qing M, Pan XB, Guo H, Xu C, Zhang X, Birk A, Chang J, Shi PY, Block TM, Guo JT (2010) Identification of five interferon-induced cellular proteins that inhibit west nile virus and dengue virus infections. J Virol 84 (16):8332-8341. doi:JVI.02199-09 [pii]
10.1128/JVI.02199-09

Jiang W, Lederman MM, Harding CV, Rodriguez B, Mohner RJ, Sieg SF (2007) TLR9 stimulation drives naive B cells to proliferate and to attain enhanced antigen presenting function. Eur J Immunol 37 (8):2205-2213. doi:10.1002/eji.200636984

John B, Ricart B, Tait Wojno ED, Harris TH, Randall LM, Christian DA, Gregg B, De Almeida DM, Weninger W, Hammer DA, Hunter CA (2011) Analysis of behavior and trafficking of dendritic cells within the brain during toxoplasmic encephalitis. PLoS Pathog 7 (9):e1002246. doi:10.1371/journal.ppat.1002246

Johnson R, Lancki DW, Fitch FW (1993) Accessory molecules involved in antigen-mediated cytolysis and lymphokine production by cytotoxic T lymphocyte subsets. I. Identification of functions for the T cell surface molecules Ly-6C and Thy-1. J Immunol 151 (6):2986-2999

Johnston LJ, Halliday GM, King NJ (1996) Phenotypic changes in Langerhans' cells after infection with arboviruses: a role in the immune response to epidermally acquired viral infection? Journal of Virology 70 (7):4761-4766

Johnston LJ, Halliday GM, King NJ (2000) Langerhans cells migrate to local lymph nodes following cutaneous infection with an arbovirus. J Invest Dermatol 114 (3):560-568. doi:jid904 [pii]
10.1046/j.1523-1747.2000.00904.x

Jordan I, Briese T, Fischer N, Lau JY, Lipkin WI (2000) Ribavirin inhibits West Nile virus replication and cytopathic effect in neural cells. J Infect Dis 182 (4):1214-1217. doi:JID000690 [pii]
10.1086/315847 [doi]

Junt T, Moseman EA, Iannacone M, Massberg S, Lang PA, Boes M, Fink K, Henrickson SE, Shayakhmetov DM, Di Paolo NC, van Rooijen N, Mempel TR, Whelan SP, von Andrian UH (2007) Subcapsular sinus macrophages in lymph nodes clear lymph-borne viruses and present them to antiviral B cells. Nature 450 (7166):110-114. doi:10.1038/nature06287

K. C. Smithburn MD, T. P. Hughes PD, A. W. Burke MD, J. H. Paul MD (1940) A NEUROTROPIC VIRUS ISOLATED FROM THE BLOOD
OF A NATIVE OF UGANDA. American Journal of Tropical Medicine 20:471-492

Kamenyeva O, Boularan C, Kabat J, Cheung GY, Cicala C, Yeh AJ, Chan JL, Periasamy S, Otto M, Kehrl JH (2015) Neutrophil recruitment to lymph nodes limits local humoral response to Staphylococcus aureus. PLoS Pathog 11 (4):e1004827. doi:10.1371/journal.ppat.1004827

Kang YS, Yamazaki S, Iyoda T, Pack M, Bruening SA, Kim JY, Takahara K, Inaba K, Steinman RM, Park CG (2003) SIGN-R1, a novel C-type lectin expressed by marginal zone macrophages in spleen, mediates uptake of the polysaccharide dextran. International immunology 15 (2):177-186

Kaplan DH (2010) In vivo function of Langerhans cells and dermal dendritic cells. Trends in immunology 31 (12):446-451. doi:10.1016/j.it.2010.08.006

Karman J, Ling C, Sandor M, Fabry Z (2004) Initiation of immune responses in brain is promoted by local dendritic cells. J Immunol 173 (4):2353-2361

Kastenmuller W, Torabi-Parizi P, Subramanian N, Lammermann T, Germain RN (2012) A spatially-organized multicellular innate immune response in lymph nodes limits systemic pathogen spread. Cell 150 (6):1235-1248. doi:10.1016/j.cell.2012.07.021

Kelley TW, Prayson RA, Ruiz AI, Isada CM, Gordon SM (2003) The neuropathology of West Nile virus meningoencephalitis. A report of two cases and review of the literature. Am J Clin Pathol 119 (5):749-753. doi:10.1309/PU4R-76JJ-MG1F-81RP [doi]

Kesson AM, Cheng Y, King NJ (2002) Regulation of immune recognition molecules by flavivirus, West Nile. Viral immunology 15 (2):273-283. doi:10.1089/08828240260066224

Kesson AM, King NJ (2001) Transcriptional regulation of major histocompatibility complex class I by flavivirus West Nile is dependent on NF-kappaB activation. J Infect Dis 184 (8):947-954

Khairallah M, Yahia SB, Letaief M, Attia S, Kahloun R, Jelliti B, Zaouali S, Messaoud R (2007) A prospective evaluation of factors associated with chorioretinitis in patients with West Nile virus infection. Ocul Immunol Inflamm 15 (6):435-439. doi:788618777 [pii]
10.1080/09273940701798488 [doi]

Kim JV, Kang SS, Dustin ML, McGavern DB (2009) Myelomonocytic cell recruitment causes fatal CNS vascular injury during acute viral meningitis. Nature 457 (7226):191-195. doi:10.1038/nature07591

Kim MT, Harty JT (2014) Splenectomy Alters Distribution and Turnover but not Numbers or Protective Capacity of de novo Generated Memory CD8 T-Cells. Frontiers in immunology 5:568. doi:10.3389/fimmu.2014.00568

King IL, Dickendesher TL, Segal BM (2009) Circulating Ly-6C+ myeloid precursors migrate to the CNS and play a pathogenic role during autoimmune demyelinating disease. Blood 113 (14):3190-3197. doi:10.1182/blood-2008-07-168575

King NJ, Kesson AM (1988) Interferon-independent increases in class I major histocompatibility complex antigen expression follow flavivirus infection. J Gen Virol 69 (Pt 10):2535-2543

King NJ, Kesson AM (2003) Interaction of flaviviruses with cells of the vertebrate host and decoy of the immune response. Immunol Cell Biol 81 (3):207-216. doi:1167 [pii]
10.1046/j.1440-1711.2003.01167.x [doi]

King NJC, van Vreden C, Terry RL, Getts DR, Yeung AW, Teague-Getts M, Davison AM, Deffrasnes C, Munoz-Erazo L (2011) The Immunopathogenesis of Neurotropic Flavivirus Infection. In: Ruzek D (ed) Flavivirus Encephalitis. Intech doi:10.5772/22243

Kissenpfennig A, Henri S, Dubois B, Laplace-Builhe C, Perrin P, Romani N, Tripp CH, Douillard P, Leserman L, Kaiserlian D, Saeland S, Davoust J, Malissen B (2005) Dynamics and function of Langerhans cells in vivo: dermal dendritic cells colonize lymph node areas distinct from slower migrating Langerhans cells. Immunity 22 (5):643-654. doi:10.1016/j.immuni.2005.04.004

Kong KF, Delroux K, Wang X, Qian F, Arjona A, Malawista SE, Fikrig E, Montgomery RR (2008) Dysregulation of TLR3 impairs the innate immune response to West Nile virus in the elderly. J Virol 82 (15):7613-7623. doi:JVI.00618-08 [pii]
10.1128/JVI.00618-08 [doi]

Kortekaas J, Ergonul O, Moormann RJ (2010) Interventions against West Nile virus, Rift Valley fever virus, and Crimean-Congo hemorrhagic fever virus: where are we? Vector Borne Zoonotic Dis 10 (7):709-718. doi:10.1089/vbz.2010.0040 [doi]

Kraal G, Mebius R (2006) New insights into the cell biology of the marginal zone of the spleen. International review of cytology 250:175-215. doi:10.1016/S0074-7696(06)50005-1

Kreil TR, Eibl MM (1996) SHORT COMMUNICATION Nitric Oxide and Viral Infection : No Antiviral Activity against a Flavivirus in Vitro , and Evidence for Contribution to Pathogenesis in Experimental Infection in Vivo. 306 (219):304-306

Kumar M, Verma S, Nerurkar VR (2010) Pro-inflammatory cytokines derived from West Nile virus (WNV)-infected SK-N-SH cells mediate neuroinflammatory markers and neuronal death. Journal of neuroinflammation 7 (1):73-73. doi:10.1186/1742-2094-7-73

Kurane I, Innis BL, Nimmannitya S, Nisalak A, Meager A, Janus J, Ennis FA (1991) Activation of T lymphocytes in dengue virus infections. High levels of soluble interleukin 2 receptor, soluble CD4, soluble CD8, interleukin 2, and interferon-gamma in sera of children with dengue. J Clin Invest 88 (5):1473-1480. doi:10.1172/JCI115457

Kursar M, Janner N, Pfeffer K, Brinkmann V, Kaufmann SH, Mittrucker HW (2008) Requirement of secondary lymphoid tissues for the induction of primary and secondary T cell responses against Listeria monocytogenes. Eur J Immunol 38 (1):127-138. doi:10.1002/eji.200737142

Lanciotti RS, Roehrig JT, Deubel V, Smith J, Parker M, Steele K, Crise B, Volpe KE, Crabtree MB, Scherret JH, Hall RA, MacKenzie JS, Cropp CB, Panigrahy B, Ostlund E, Schmitt B, Malkinson M, Banet C, Weissman J, Komar N, Savage HM, Stone W, McNamara T, Gubler DJ (1999) Origin of the West Nile virus responsible for an outbreak of encephalitis in the northeastern United States. Science 286 (5448):2333-2337

Lanteri MC, O'Brien KM, Purtha WE, Cameron MJ, Lund JM, Owen RE, Heitman JW, Custer B, Hirschkorn DF, Tobler LH, Kiely N, Prince HE, Ndhlovu LC, Nixon DF, Kamel HT, Kelvin DJ, Busch MP, Rudensky AY, Diamond MS, Norris PJ (2009) Tregs control the development of symptomatic West Nile virus infection in humans and mice. J Clin Invest 119 (11):3266-3277. doi:39387 [pii]
10.1172/JCI39387 [doi]

Lazear HM, Daniels BP, Pinto AK, Huang AC, Vick SC, Doyle SE, Gale M, Jr., Klein RS, Diamond MS (2015) Interferon-lambda restricts West Nile virus neuroinvasion by tightening the blood-brain barrier. Sci Transl Med 7 (284):284ra259. doi:10.1126/scitranslmed.aaa4304

Lee ST, Chu K, Jung KH, Kim SJ, Kim DH, Kang KM, Hong NH, Kim JH, Ban JJ, Park HK, Kim SU, Park CG, Lee SK, Kim M, Roh JK (2008) Anti-inflammatory mechanism of intravascular neural stem cell transplantation in haemorrhagic stroke. Brain : a journal of neurology 131 (Pt 3):616-629. doi:10.1093/brain/awm306

Leenen PJ, Radosevic K, Voerman JS, Salomon B, van Rooijen N, Klatzmann D, van Ewijk W (1998) Heterogeneity of mouse spleen dendritic cells: in vivo phagocytic activity,

expression of macrophage markers, and subpopulation turnover. J Immunol 160 (5):2166-2173

Leuschner F, Panizzi P, Chico-Calero I, Lee WW, Ueno T, Cortez-Retamozo V, Waterman P, Gorbatov R, Marinelli B, Iwamoto Y, Chudnovskiy A, Figueiredo JL, Sosnovik DE, Pittet MJ, Swirski FK, Weissleder R, Nahrendorf M (2010) Angiotensin-converting enzyme inhibition prevents the release of monocytes from their splenic reservoir in mice with myocardial infarction. Circulation research 107 (11):1364-1373. doi:10.1161/CIRCRESAHA.110.227454

Li L, Barrett AD, Beasley DW (2005) Differential expression of domain III neutralizing epitopes on the envelope proteins of West Nile virus strains. Virology 335 (1):99-105. doi:S0042-6822(05)00104-2 [pii]
10.1016/j.virol.2005.02.011 [doi]

Li M, Li F, Luo C, Shan Y, Zhang L, Qian Z, Zhu G, Lin J, Feng H (2011) Immediate splenectomy decreases mortality and improves cognitive function of rats after severe traumatic brain injury. The Journal of trauma 71 (1):141-147. doi:10.1097/TA.0b013e3181f30fc9

Lieberman aP, Pitha PM, Shin HS, Shin ML (1989) Production of tumor necrosis factor and other cytokines by astrocytes stimulated with lipopolysaccharide or a neurotropic virus. Proceedings of the National Academy of Sciences of the United States of America 86 (16):6348-6352

Lim JK, Obara CJ, Rivollier A, Pletnev AG, Kelsall BL, Murphy PM (2011) Chemokine receptor Ccr2 is critical for monocyte accumulation and survival in West Nile virus encephalitis. J Immunol 186 (1):471-478. doi:jimmunol.1003003 [pii]
10.4049/jimmunol.1003003 [doi]

Lin RJ (2004) Replication-incompetent virions of Japanese encephalitis virus trigger neuronal cell death by oxidative stress in a culture system. Journal of General Virology 85 (2):521-533. doi:10.1099/vir.0.19496-0

Lindsey NP, Hayes EB, Staples JE, Fischer M (2009) West Nile virus disease in children, United States, 1999-2007. Pediatrics 123 (6):e1084-1089. doi:123/6/e1084 [pii]
10.1542/peds.2008-3278 [doi]

Liu TH, Liang LC, Wang CC, Liu HC, Chen WJ (2008) The blood-brain barrier in the cerebrum is the initial site for the Japanese encephalitis virus entering the central nervous system. J Neurovirol 14 (6):514-521. doi:905758679 [pii]
10.1080/13550280802339643 [doi]

Liu X, Yu Y, Li M, Liang G, Wang H, Jia L, Dong G (2011) Study on the protective efficacy of SA14-14-2 attenuated Japanese encephalitis against different JE virus isolates circulating in China. Vaccine 29 (11):2127-2130. doi:10.1016/j.vaccine.2010.12.108

Liu Y, King N, Kesson A, Blanden RV, Mullbacher A (1988) West Nile virus infection modulates the expression of class I and class II MHC antigens on astrocytes in vitro. Annals of the New York Academy of Sciences 540:483-485

Liu Y, King N, Kesson A, Blanden RV, Mullbacher A (1989) Flavivirus infection up-regulates the expression of class I and class II major histocompatibility antigens on and enhances T cell recognition of astrocytes in vitro. J Neuroimmunol 21 (2-3):157-168

Liu Y-P, Lin H-I, Tzeng S-F (2005) Tumor necrosis factor-alpha and interleukin-18 modulate neuronal cell fate in embryonic neural progenitor culture. Brain research 1054 (2):152-158. doi:10.1016/j.brainres.2005.06.085

Liu YH, Xu J, Yang XP, Yang F, Shesely E, Carretero OA (2002) Effect of ACE inhibitors and angiotensin II type 1 receptor antagonists on endothelial NO synthase knockout mice with heart failure. Hypertension 39 (2 Pt 2):375-381

Louveau A, Smirnov I, Keyes TJ, Eccles JD, Rouhani SJ, Peske JD, Derecki NC, Castle D, Mandell JW, Lee KS, Harris TH, Kipnis J (2015) Structural and functional features of central nervous system lymphatic vessels. Nature. doi:10.1038/nature14432

Luna RML, Lee E, Mullbacher A, Blanden RV, Langman R, Lobigs M (2002) Lack of both Fas ligand and perforin protects from flavivirus-mediated encephalitis in mice. Journal of virology 76 (7):3202-3211. doi:Doi 10.1128/Jvi.76.7.3202-3211.2002

Luteijn R, Sciaranghella G, van Lunzen J, Nolting A, Dugast AS, Ghebremichael MS, Altfeld M, Alter G (2011) Early viral replication in lymph nodes provides HIV with a means by which to escape NK-cell-mediated control. Eur J Immunol 41 (9):2729-2740. doi:10.1002/eji.201040886

Mackay CR, Marston WL, Dudler L (1990) Naive and memory T cells show distinct pathways of lymphocyte recirculation. J Exp Med 171 (3):801-817

Mackenzie JS, Gubler DJ, Petersen LR (2004) Emerging flaviviruses: the spread and resurgence of Japanese encephalitis, West Nile and dengue viruses. Nat Med 10 (12 Suppl):S98-109. doi:10.1038/nm1144

Mamani-Matsuda M, Cosma A, Weller S, Faili A, Staib C, Garcon L, Hermine O, Beyne-Rauzy O, Fieschi C, Pers JO, Arakelyan N, Varet B, Sauvanet A, Berger A, Paye F, Andrieu JM, Michel M, Godeau B, Buffet P, Reynaud CA, Weill JC (2008) The human spleen is a major reservoir for long-lived vaccinia virus-specific memory B cells. Blood 111 (9):4653-4659. doi:10.1182/blood-2007-11-123844

Martin-Fontecha A, Thomsen LL, Brett S, Gerard C, Lipp M, Lanzavecchia A, Sallusto F (2004) Induced recruitment of NK cells to lymph nodes provides IFN-gamma for T(H)1 priming. Nat Immunol 5 (12):1260-1265. doi:10.1038/ni1138

Martinez-Gamboa L, Mei H, Loddenkemper C, Ballmer B, Hansen A, Lipsky PE, Emmerich F, Radbruch A, Salama A, Dorner T (2009) Role of the spleen in peripheral memory B-cell homeostasis in patients with autoimmune thrombocytopenia purpura. Clin Immunol 130 (2):199-212. doi:10.1016/j.clim.2008.09.009

Matloubian M, Lo CG, Cinamon G, Lesneski MJ, Xu Y, Brinkmann V, Allende ML, Proia RL, Cyster JG (2004) Lymphocyte egress from thymus and peripheral lymphoid organs is dependent on S1P receptor 1. Nature 427 (6972):355-360. doi:10.1038/nature02284

Matheu MP, Teijaro JR, Walsh KB, Greenberg ML, Marsolais D, Parker I, Rosen H, Oldstone MB, Cahalan MD (2013) Three phases of CD8 T cell response in the lung following H1N1 influenza infection and sphingosine 1 phosphate agonist therapy. PLoS One 8 (3):e58033. doi:10.1371/journal.pone.0058033

Maximova OA, Faucette LJ, Ward JM, Murphy BR, Pletnev AG (2009) Cellular inflammatory response to flaviviruses in the central nervous system of a primate host. J Histochem Cytochem 57 (10):973-989. doi:jhc.2009.954180 [pii]
10.1369/jhc.2009.954180 [doi]

McColl BW, Rothwell NJ, Allan SM (2007) Systemic inflammatory stimulus potentiates the acute phase and CXC chemokine responses to experimental stroke and exacerbates brain damage via interleukin-1- and neutrophil-dependent mechanisms. The Journal of neuroscience : the official journal of the Society for Neuroscience 27 (16):4403-4412. doi:10.1523/jneurosci.5376-06.2007

McGaha TL, Chen Y, Ravishankar B, van Rooijen N, Karlsson MC (2011) Marginal zone macrophages suppress innate and adaptive immunity to apoptotic cells in the spleen. Blood 117 (20):5403-5412. doi:10.1182/blood-2010-11-320028

McGraw HM, Friedman HM (2009) Herpes simplex virus type 1 glycoprotein E mediates retrograde spread from epithelial cells to neurites. J Virol 83 (10):4791-4799. doi:JVI.02341-08 [pii]
10.1128/JVI.02341-08 [doi]

McMahon EJ, Bailey SL, Castenada CV, Waldner H, Miller SD (2005) Epitope spreading initiates in the CNS in two mouse models of multiple sclerosis. Nat Med 11 (3):335-339. doi:10.1038/nm1202

McMeniman CJ, Lane RV, Cass BN, Fong AW, Sidhu M, Wang YF, O'Neill SL (2009) Stable introduction of a life-shortening Wolbachia infection into the mosquito Aedes aegypti. Science 323 (5910):141-144. doi:10.1126/science.1165326

Merad M, Ginhoux F, Collin M (2008) Origin, homeostasis and function of Langerhans cells and other langerin-expressing dendritic cells. Nature reviews Immunology 8 (12):935-947. doi:10.1038/nri2455

Metcalf TU, Griffin DE (2011) Alphavirus-induced encephalomyelitis: antibody-secreting cells and viral clearance from the nervous system. J Virol 85 (21):11490-11501. doi:10.1128/JVI.05379-11

Meyer-Hermann M, Mohr E, Pelletier N, Zhang Y, Victora GD, Toellner KM (2012) A theory of germinal center B cell selection, division, and exit. Cell reports 2 (1):162-174. doi:10.1016/j.celrep.2012.05.010

Michaelis M, Kleinschmidt MC, Doerr HW, Cinatl J (2007) Minocycline inhibits West Nile virus replication and apoptosis in human neuronal cells. The Journal of antimicrobial chemotherapy 60 (5):981-986. doi:10.1093/jac/dkm307

Mishra MK, Basu A (2008) Minocycline neuroprotects, reduces microglial activation, inhibits caspase 3 induction, and viral replication following Japanese encephalitis. Journal of neurochemistry 105 (5):1582-1595. doi:10.1111/j.1471-4159.2008.05238.x

Miyake Y, Asano K, Kaise H, Uemura M, Nakayama M, Tanaka M (2007) Critical role of macrophages in the marginal zone in the suppression of immune responses to apoptotic cell-associated antigens. J Clin Invest 117 (8):2268-2278. doi:10.1172/JCI31990

Moe RE (1963) Fine Structure of Reticulum and Sinuses of Lymph Nodes. Am J Anat 112 (3):311-&. doi:Doi 10.1002/Aja.1001120304

Mohr E, Serre K, Manz RA, Cunningham AF, Khan M, Hardie DL, Bird R, MacLennan IC (2009) Dendritic cells and monocyte/macrophages that create the IL-6/APRIL-rich lymph node microenvironments where plasmablasts mature. J Immunol 182 (4):2113-2123. doi:10.4049/jimmunol.0802771

Monath TP (2010) Suspected yellow fever vaccine-associated viscerotropic adverse events (1973 and 1978), United States. Am J Trop Med Hyg 82 (5):919-921. doi:82/5/919 [pii]
10.4269/ajtmh.2010.10-0001 [doi]

Montoya CJ, Jie HB, Al-Harthi L, Mulder C, Patino PJ, Rugeles MT, Krieg AM, Landay AL, Wilson SB (2006) Activation of plasmacytoid dendritic cells with TLR9 agonists initiates invariant NKT cell-mediated cross-talk with myeloid dendritic cells. J Immunol 177 (2):1028-1039

Moreland NC, Hemmer LB, Koht A (2014) West Nile virus infection and postoperative neurological symptoms: a case report and review of the literature. Journal of clinical anesthesia 26 (5):410-413. doi:10.1016/j.jclinane.2014.02.005

Morrey JD, Olsen AL, Siddharthan V, Motter NE, Wang H, Taro BS, Chen D, Ruffner D, Hall JO (2008) Increased blood-brain barrier permeability is not a primary determinant for lethality of West Nile virus infection in rodents. J Gen Virol 89 (Pt 2):467-473. doi:89/2/467 [pii]
10.1099/vir.0.83345-0 [doi]

Morrey JD, Siddharthan V, Olsen AL, Roper GY, Wang H, Baldwin TJ, Koenig S, Johnson S, Nordstrom JL, Diamond MS (2006) Humanized Monoclonal Antibody against West Nile Virus Envelope Protein Administered after Neuronal Infection Protects against Lethal Encephalitis in Hamsters The Journal of Infectious Diseases 194 (9):1300-1308. doi:10.1086/508293

Morrey JD, Siddharthan V, Olsen AL, Wang H, Julander JG, Hall JO, Li H, Nordstrom JL, Koenig S, Johnson S, Diamond MS (2007) Defining limits of treatment with humanized neutralizing monoclonal antibody for West Nile virus neurological infection in a hamster model. Antimicrob Agents Chemother 51 (7):2396-2402. doi:AAC.00147-07 [pii]
10.1128/AAC.00147-07 [doi]

Mostashari F, Bunning ML, Kitsutani PT, Singer DA, Nash D, Cooper MJ, Katz N, Liljebjelke KA, Biggerstaff BJ, Fine AD, Layton MC, Mullin SM, Johnson AJ, Martin DA, Hayes EB, Campbell GL (2001) Epidemic West Nile encephalitis, New York, 1999: results of a household-based seroepidemiological survey. Lancet 358 (9278):261-264. doi:10.1016/S0140-6736(01)05480-0

Mullbacher A, King NJ (1989) Target cell lysis by natural killer cells is influenced by beta 2-microglobulin expression. Scandinavian journal of immunology 30 (1):21-29

Muller M, Carter SL, Hofer MJ, Manders P, Getts DR, Getts MT, Dreykluft A, Lu B, Gerard C, King NJC, Campbell IL (2007) CXCR3 signaling reduces the severity of experimental autoimmune encephalomyelitis by controlling the parenchymal distribution of effector and regulatory T cells in the central nervous system. J Immunol 179 (5):2774-2786

Muraki Y, Fujita T, Matsuura M, Fuke I, Manabe S, Ishikawa T, Okuno Y, Morita K (2015) The efficacy of inactivated West Nile vaccine (WN-VAX) in mice and monkeys. Virol J 12 (1):54. doi:10.1186/s12985-015-0282-8

Myers JP, Leveque TK, Johnson MW (2005) Extensive chorioretinitis and severe vision loss associated with west nile virus meningoencephalitis. Arch Ophthalmol 123 (12):1754-1756. doi:10.1001/archopht.123.12.1754

Naito M, Nagai H, Kawano S, Umezu H, Zhu H, Moriyama H, Yamamoto T, Takatsuka H, Takei Y (1996) Liposome-encapsulated dichloromethylene diphosphonate induces macrophage apoptosis in vivo and in vitro. J Leukoc Biol 60 (3):337-344

Nazmi A, Dutta K, Das S, Basu A (2011) Japanese encephalitis virus-infected macrophages induce neuronal death. Journal of neuroimmune pharmacology : the official journal of the Society on NeuroImmune Pharmacology 6 (3):420-433. doi:10.1007/s11481-011-9271-x

Neves-Souza PCF, Azeredo EL, Zagne SMO, Valls-de-Souza R, Reis SRNI, Cerqueira DIS, Nogueira RMR, Kubelka CF (2005) Inducible nitric oxide synthase (iNOS) expression in monocytes during acute Dengue Fever in patients and during in vitro infection. BMC infectious diseases 5:64-64. doi:10.1186/1471-2334-5-64

Nolte MA, Belien JA, Schadee-Eestermans I, Jansen W, Unger WW, van Rooijen N, Kraal G, Mebius RE (2003) A conduit system distributes chemokines and small blood-borne molecules through the splenic white pulp. J Exp Med 198 (3):505-512. doi:10.1084/jem.20021801

Nolte MA, Hoen EN, van Stijn A, Kraal G, Mebius RE (2000) Isolation of the intact white pulp. Quantitative and qualitative analysis of the cellular composition of the splenic compartments. Eur J Immunol 30 (2):626-634. doi:10.1002/1521-4141(200002)30:2<626::AID-IMMU626>3.0.CO;2-H

Nossal GJ, Abbot A, Mitchell J (1968) Antigens in immunity. XIV. Electron microscopic radioautographic studies of antigen capture in the lymph node medulla. J Exp Med 127 (2):263-276

Okada S, Albrecht RM, Aharinejad S, Schraufnagel DE (2002) Structural aspects of the lymphocyte traffic in rat submandibular lymph node. Microscopy and microanalysis : the official journal of Microscopy Society of America, Microbeam Analysis Society, Microscopical Society of Canada 8 (2):116-133. doi:10.1017.S1431927601020049

Okada S, Nakamura M, Katoh H, Miyao T, Shimazaki T, Ishii K, Yamane J, Yoshimura A, Iwamoto Y, Toyama Y, Okano H (2006) Conditional ablation of Stat3 or Socs3

discloses a dual role for reactive astrocytes after spinal cord injury. Nat Med 12 (7):829-834. doi:10.1038/nm1425

Oliphant T, Engle M, Nybakken GE, Doane C, Johnson S, Huang L, Gorlatov S, Mehlhop E, Marri A, Chung KM, Ebel GD, Kramer LD, Fremont DH, Diamond MS (2005) Development of a humanized monoclonal antibody with therapeutic potential against West Nile virus. Nat Med 11 (5):522-530. doi:nm1240 [pii]
10.1038/nm1240 [doi]

Olson JK, Miller SD (2004) Microglia initiate central nervous system innate and adaptive immune responses through multiple TLRs. J Immunol 173 (6):3916-3924. doi:173/6/3916 [pii]

Olson MR, McDermott DS, Varga SM (2012) The initial draining lymph node primes the bulk of the CD8 T cell response and influences memory T cell trafficking after a systemic viral infection. PLoS Pathog 8 (12):e1003054. doi:10.1371/journal.ppat.1003054

Pak-Wittel MA, Yang L, Sojka DK, Rivenbark JG, Yokoyama WM (2013) Interferon-gamma mediates chemokine-dependent recruitment of natural killer cells during viral infection. Proc Natl Acad Sci U S A 110 (1):E50-59. doi:10.1073/pnas.1220456110

Pappu R, Schwab SR, Cornelissen I, Pereira JP, Regard JB, Xu Y, Camerer E, Zheng YW, Huang Y, Cyster JG, Coughlin SR (2007) Promotion of lymphocyte egress into blood and lymph by distinct sources of sphingosine-1-phosphate. Science 316 (5822):295-298. doi:10.1126/science.1139221

Park EJ, Peixoto A, Imai Y, Goodarzi A, Cheng G, Carman CV, von Andrian UH, Shimaoka M (2010) Distinct roles for LFA-1 affinity regulation during T-cell adhesion, diapedesis, and interstitial migration in lymph nodes. Blood 115 (8):1572-1581. doi:10.1182/blood-2009-08-237917

Peters NC, Pagan AJ, Lawyer PG, Hand TW, Henrique Roma E, Stamper LW, Romano A, Sacks DL (2014) Chronic parasitic infection maintains high frequencies of short-lived Ly6C+CD4+ effector T cells that are required for protection against re-infection. PLoS Pathog 10 (12):e1004538. doi:10.1371/journal.ppat.1004538

Petersen LR, Carson PJ, Biggerstaff BJ, Custer B, Borchardt SM, Busch MP (2013) Estimated cumulative incidence of West Nile virus infection in US adults, 1999-2010. Epidemiology and infection 141 (3):591-595. doi:10.1017/S0950268812001070

Petersen LR, Marfin AA (2002) West Nile virus: a primer for the clinician. Annals of internal medicine 137 (3):173-179

Petzold A, Groves M, Leis AA, Scaravilli F, Stokic DS (2010) Neuronal and glial cerebrospinal fluid protein biomarkers are elevated after West Nile virus infection. Muscle Nerve 41 (1):42-49. doi:10.1002/mus.21448 [doi]

Phan TG, Grigorova I, Okada T, Cyster JG (2007) Subcapsular encounter and complement-dependent transport of immune complexes by lymph node B cells. Nat Immunol 8 (9):992-1000. doi:10.1038/ni1494

Pijlman GP (2015) Enveloped virus-like particles as vaccines against pathogenic arboviruses. Biotechnology journal 10 (5):659-670. doi:10.1002/biot.201400427

Pineau I, Sun L, Bastien D, Lacroix S (2010) Astrocytes initiate inflammation in the injured mouse spinal cord by promoting the entry of neutrophils and inflammatory monocytes in an IL-1 receptor/MyD88-dependent fashion. Brain, behavior, and immunity 24 (4):540-553. doi:10.1016/j.bbi.2009.11.007

Poidinger M, Hall RA, Mackenzie JS (1996) Molecular characterization of the Japanese encephalitis serocomplex of the flavivirus genus. Virology 218 (2):417-421. doi:S0042-6822(96)90213-5 [pii]
10.1006/viro.1996.0213

Prikhod GG, Prikhod EA, Alexander G, Cohen JI, Pletnev AG (2002) Langat Flavivirus Protease NS3 Binds Caspase-8 and Induces Apoptosis Langat Flavivirus Protease NS3 Binds Caspase-8 and Induces Apoptosis. 76 (11). doi:10.1128/jvi.76.11.5701

Puga I, Cols M, Barra CM, He B, Cassis L, Gentile M, Comerma L, Chorny A, Shan MM, Xu WF, Magri G, Knowles DM, Tam W, Chiu A, Bussel JB, Serrano S, Lorente JA, Bellosillo B, Lloreta J, Juanpere N, Alameda F, Baro T, de Heredia RD, Toran N, Catala A, Torrebadell M, Fortuny C, Cusi V, Carreras C, Diaz GA, Blander JM, Farber CM, Silvestri G, Cunningham-Rundles C, Calvillo M, Dufour C, Notarangelo LD, Lougaris V, Plebani A, Casanova JL, Ganal SC, Diefenbach A, Arostegui JI, Juan M, Yague J, Mahlaoui N, Donadieu J, Chen K, Cerutti A (2012) B cell-helper neutrophils stimulate the diversification and production of immunoglobulin in the marginal zone of the spleen. Nature Immunology 13 (2):170-180. doi:Doi 10.1038/Ni.2194

Purtha WE, Chachu KA, Virgin HWt, Diamond MS (2008) Early B-cell activation after West Nile virus infection requires alpha/beta interferon but not antigen receptor signaling. J Virol 82 (22):10964-10974. doi:10.1128/JVI.01646-08

Purtha WE, Myers N, Mitaksov V, Sitati E, Connolly J, Fremont DH, Hansen TH, Diamond MS (2007) Antigen-specific cytotoxic T lymphocytes protect against lethal West Nile virus encephalitis. Eur J Immunol 37 (7):1845-1854. doi:10.1002/eji.200737192 [doi]

Quintana A, Muller M, Frausto RF, Ramos R, Getts DR, Sanz E, Hofer MJ, Krauthausen M, King NJC, Hidalgo J, Campbell IL (2009) Site-specific production of IL-6 in the central nervous system retargets and enhances the inflammatory response in experimental autoimmune encephalomyelitis. J Immunol 183 (3):2079-2088

Ramakrishna C, Newo AN, Shen YW, Cantin E (2011) Passively administered pooled human immunoglobulins exert IL-10 dependent anti-inflammatory effects that protect against fatal HSV encephalitis. PLoS Pathog 7 (6):e1002071. doi:10.1371/journal.ppat.1002071

Randolph GJ, Sanchez-Schmitz G, Angeli V (2005) Factors and signals that govern the migration of dendritic cells via lymphatics: recent advances. Springer seminars in immunopathology 26 (3):273-287. doi:10.1007/s00281-004-0168-0

Ravi V, Parida S, Desai a, Chandramuki a, Gourie-Devi M, Grau GE (1997) Correlation of tumor necrosis factor levels in the serum and cerebrospinal fluid with clinical

outcome in Japanese encephalitis patients. Journal of medical virology 51 (2):132-136

Ravishankar B, Shinde R, Liu H, Chaudhary K, Bradley J, Lemos HP, Chandler P, Tanaka M, Munn DH, Mellor AL, McGaha TL (2014) Marginal zone CD169+ macrophages coordinate apoptotic cell-driven cellular recruitment and tolerance. Proc Natl Acad Sci U S A 111 (11):4215-4220. doi:10.1073/pnas.1320924111

Reeves JP, Reeves PA, Chin LT (2001) Survival surgery: removal of the spleen or thymus. Current protocols in immunology / edited by John E Coligan [et al] Chapter 1:Unit 1 10. doi:10.1002/0471142735.im0110s02

Reisman NM, Floyd TL, Wagener ME, Kirk AD, Larsen CP, Ford ML (2011) LFA-1 blockade induces effector and regulatory T-cell enrichment in lymph nodes and synergizes with CTLA-4Ig to inhibit effector function. Blood 118 (22):5851-5861. doi:10.1182/blood-2011-04-347252

Rhee C, Eaton EF, Concepcion W, Blackburn BG (2011) West Nile virus encephalitis acquired via liver transplantation and clinical response to intravenous immunoglobulin: case report and review of the literature. Transplant infectious disease : an official journal of the Transplantation Society 13 (3):312-317. doi:10.1111/j.1399-3062.2010.00595.x

Rios M, Zhang MJ, Grinev A, Srinivasan K, Daniel S, Wood O, Hewlett IK, Dayton AI (2006) Monocytes-macrophages are a potential target in human infection with West Nile virus through blood transfusion. Transfusion 46 (4):659-667. doi:TRF00769 [pii]
10.1111/j.1537-2995.2006.00769.x [doi]

Roe K, Kumar M, Lum S, Orillo B, Nerurkar VR, Verma S (2012) West Nile virus-induced disruption of the blood-brain barrier in mice is characterized by the degradation of the junctional complex proteins and increase in multiple matrix metalloproteinases. J Gen Virol 93 (Pt 6):1193-1203. doi:10.1099/vir.0.040899-0

Rosado MM, Gesualdo F, Marcellini V, Di Sabatino A, Corazza GR, Smacchia MP, Nobili B, Baronci C, Russo L, Rossi F, Vito RD, Nicolosi L, Inserra A, Locatelli F, Tozzi AE, Carsetti R (2013) Preserved antibody levels and loss of memory B cells against pneumococcus and tetanus after splenectomy: tailoring better vaccination strategies. Eur J Immunol 43 (10):2659-2670. doi:10.1002/eji.201343577

Ruzek D, Salat J, Palus M, Gritsun TS, Gould EA, Dykova I, Skallova A, Jelinek J, Kopecky J, Grubhoffer L (2009) CD8+ T-cells mediate immunopathology in tick-borne encephalitis. Virology 384 (1):1-6. doi:10.1016/j.virol.2008.11.023

Ruzek D, Salat J, Singh SK, Kopecky J (2011) Breakdown of the blood-brain barrier during tick-borne encephalitis in mice is not dependent on CD8+ T-cells. PloS one 6 (5):e20472. doi:10.1371/journal.pone.0020472

Samuel MA, Diamond MS (2005) Alpha/beta interferon protects against lethal West Nile virus infection by restricting cellular tropism and enhancing neuronal survival. J Virol 79 (21):13350-13361. doi:79/21/13350 [pii]
10.1128/JVI.79.21.13350-13361.2005

Samuel MA, Diamond MS (2009) West Nile Virus Infection of the Central Nervous System. In: Diamond MS (ed) West Nile Encephalitis Virus Infection: Viral Pathogenesis and the Host Immune Response. Emerging Infectious Diseases of the 21st Century. Springer, New York, p 474

Samuel MA, Wang H, Siddharthan V, Morrey JD, Diamond MS (2007) Axonal transport mediates West Nile virus entry into the central nervous system and induces acute flaccid paralysis. Proc Natl Acad Sci U S A 104 (43):17140-17145. doi:0705837104 [pii]
10.1073/pnas.0705837104 [doi]

Sanchez MD, Pierson TC, McAllister D, Hanna SL, Puffer BA, Valentine LE, Murtadha MM, Hoxie JA, Doms RW (2005) Characterization of neutralizing antibodies to West Nile virus. Virology 336 (1):70-82. doi:S0042-6822(05)00141-8 [pii]
10.1016/j.virol.2005.02.020 [doi]

Sasou S, Madarame T, Satodate R (1982) Views of the endothelial surface of the marginal sinus in rat spleens using the scanning electron microscope. Virchows Archiv B, Cell pathology including molecular pathology 40 (2):117-120

Saxena SK, Mathur a, Srivastava RC (2001) Induction of nitric oxide synthase during Japanese encephalitis virus infection: evidence of protective role. Archives of biochemistry and biophysics 391 (1):1-7. doi:10.1006/abbi.2001.2360

Saxena SK, Singh a, Mathur a (2000) Antiviral effect of nitric oxide during Japanese encephalitis virus infection. International journal of experimental pathology 81 (2):165-172

Schlueter AJ, Krieg AM, De Vries P, Li X (2001) Type I interferon is the primary regulator of inducible Ly-6C expression on T cells. Journal of Interferon and Cytokine Research 21 (8):621-629. doi:Doi 10.1089/10799900152547885

Schlueter AJ, Krieg AM, De Vries P, Li X (2002) B cells express Ly-6C in a Th1 but not Th2 cytokine environment. J Interferon Cytokine Res 22 (7):799-806. doi:10.1089/107999002320271396

Schmidt-Weber CB, Rittig M, Buchner E, Hauser I, Schmidt I, Palombo-Kinne E, Emmrich F, Kinne RW (1996) Apoptotic cell death in activated monocytes following incorporation of clodronate-liposomes. J Leukoc Biol 60 (2):230-244

Schneider BS, Soong L, Coffey LL, Stevenson HL, McGee CE, Higgs S (2010) Aedes aegypti saliva alters leukocyte recruitment and cytokine signaling by antigen-presenting cells during West Nile virus infection. PloS one 5 (7):e11704. doi:10.1371/journal.pone.0011704

Schneider BS, Soong L, Girard YA, Campbell G, Mason P, Higgs S (2006) Potentiation of West Nile encephalitis by mosquito feeding. Viral immunology 19 (1):74-82. doi:10.1089/vim.2006.19.74

Schweitzer BK, Kramer WL, Sambol AR, Meza JL, Hinrichs SH, Iwen PC (2006) Geographic factors contributing to a high seroprevalence of West Nile virus-specific antibodies in humans following an epidemic. Clin Vaccine Immunol 13 (3):314-318. doi:13/3/314 [pii]

10.1128/CVI.13.3.314-318.2006

Schwickert TA, Lindquist RL, Shakhar G, Livshits G, Skokos D, Kosco-Vilbois MH, Dustin ML, Nussenzweig MC (2007) In vivo imaging of germinal centres reveals a dynamic open structure. Nature 446 (7131):83-87. doi:10.1038/nature05573

Sedgwick JD, Schwender S, Imrich H, Dorries R, Butcher GW, ter Meulen V (1991) Isolation and direct characterization of resident microglial cells from the normal and inflamed central nervous system. Proc Natl Acad Sci U S A 88 (16):7438-7442

Seiler P, Aichele P, Odermatt B, Hengartner H, Zinkernagel RM, Schwendener RA (1997) Crucial role of marginal zone macrophages and marginal zone metallophils in the clearance of lymphocytic choriomeningitis virus infection. Eur J Immunol 27 (10):2626-2633. doi:10.1002/eji.1830271023

Sejvar JJ, Haddad MB, Tierney BC, Campbell GL, Marfin AA, Van Gerpen JA, Fleischauer A, Leis AA, Stokic DS, Petersen LR (2003) Neurologic manifestations and outcome of West Nile virus infection. JAMA 290 (4):511-515. doi:10.1001/jama.290.4.511 290/4/511 [pii]

Semeraro D, Davies JD (1986) The arterial blood supply of human inguinal and mesenteric lymph nodes. Journal of anatomy 144:221-233

Singh a, Kulshreshtha R, Mathur a (2000) Secretion of the chemokine interleukin-8 during Japanese encephalitis virus infection. Journal of medical microbiology 49 (7):607-612

Sitati EM, Diamond MS (2006) CD4+ T-cell responses are required for clearance of West Nile virus from the central nervous system. J Virol 80 (24):12060-12069. doi:10.1128/JVI.01650-06

Smith HL, Monath TP, Pazoles P, Rothman AL, Casey DM, Terajima M, Ennis FA, Guirakhoo F, Green S (2010) Development of antigen-specific memory CD8+ T cells following live-attenuated chimeric West Nile virus vaccination. J Infect Dis 203 (4):513-522. doi:jiq074 [pii] 10.1093/infdis/jiq074 [doi]

Soderstrom N, Stenstrom A (1969) Outflow paths of cells from the lymph node parenchyma to the efferent lymphatics--observations in thin section histology. Scandinavian journal of haematology 6 (3):186-196

Song H, Stevens CF, Gage FH (2002) Astroglia induce neurogenesis from adult neural stem cells. Nature 417 (6884):39-44. doi:10.1038/417039a

Srivastava R, Ramakrishna C, Cantin E (2015) Anti-inflammatory activity of intravenous immunoglobulins protects against West Nile virus encephalitis. J Gen Virol 96 (Pt 6):1347-1357. doi:10.1099/vir.0.000079

Steel CD, Kim WK, Sanford LD, Wellman LL, Burnett S, Van Rooijen N, Ciavarra RP (2010) Distinct macrophage subpopulations regulate viral encephalitis but not viral clearance in the CNS. J Neuroimmunol 226 (1-2):81-92. doi:10.1016/j.jneuroim.2010.05.034

Steele KE, Linn MJ, Schoepp RJ, Komar N, Geisbert TW, Manduca RM, Calle PP, Raphael BL, Clippinger TL, Larsen T, Smith J, Lanciotti RS, Panella NA, McNamara TS (2000) Pathology of fatal West Nile virus infections in native and exotic birds during the 1999 outbreak in New York City, New York. Vet Pathol 37 (3):208-224

Steer HW, Foot RA (1987) Changes in the medulla of the parathymic lymph nodes of the rat during acute gastro-intestinal inflammation. Journal of anatomy 152:23-36

Steinman RM (1991) The dendritic cell system and its role in immunogenicity. Annu Rev Immunol 9:271-296. doi:10.1146/annurev.iy.09.040191.001415 [doi]

Stern JN, Yaari G, Vander Heiden JA, Church G, Donahue WF, Hintzen RQ, Huttner AJ, Laman JD, Nagra RM, Nylander A, Pitt D, Ramanan S, Siddiqui BA, Vigneault F, Kleinstein SH, Hafler DA, O'Connor KC (2014) B cells populating the multiple sclerosis brain mature in the draining cervical lymph nodes. Sci Transl Med 6 (248):248ra107. doi:10.1126/scitranslmed.3008879

Sticozzi C, Belmonte G, Meini A, Carbotti P, Grasso G, Palmi M (2013) IL-1beta induces GFAP expression in vitro and in vivo and protects neurons from traumatic injury-associated apoptosis in rat brain striatum via NFkappaB/Ca(2)(+)-calmodulin/ERK mitogen-activated protein kinase signaling pathway. Neuroscience 252:367-383. doi:10.1016/j.neuroscience.2013.07.061

Sui Y, Potula R, Dhillon N, Pinson D, Li S, Nath A, Anderson C, Turchan J, Kolson D, Narayan O, Buch S (2004) Neuronal apoptosis is mediated by CXCL10 overexpression in simian human immunodeficiency virus encephalitis. Am J Pathol 164 (5):1557-1566. doi:S0002-9440(10)63714-5 [pii]
10.1016/S0002-9440(10)63714-5 [doi]

Sui Y, Stehno-Bittel L, Li S, Loganathan R, Dhillon NK, Pinson D, Nath A, Kolson D, Narayan O, Buch S (2006) CXCL10-induced cell death in neurons: role of calcium dysregulation. The European journal of neuroscience 23 (4):957-964. doi:10.1111/j.1460-9568.2006.04631.x

Sunderkotter C, Nikolic T, Dillon MJ, Van Rooijen N, Stehling M, Drevets DA, Leenen PJ (2004) Subpopulations of mouse blood monocytes differ in maturation stage and inflammatory response. J Immunol 172 (7):4410-4417

Suthar MS, Ma DY, Thomas S, Lund JM, Zhang N, Daffis S, Rudensky AY, Bevan MJ, Clark EA, Kaja MK, Diamond MS, Gale M, Jr. (2010) IPS-1 is essential for the control of West Nile virus infection and immunity. PLoS Pathog 6 (2):e1000757. doi:10.1371/journal.ppat.1000757 [doi]

Swarup V, Ghosh J, Das S, Basu A (2008) Tumor necrosis factor receptor-associated death domain mediated neuronal death contributes to the glial activation and subsequent neuroinflammation in Japanese encephalitis. Neurochemistry international 52 (7):1310-1321. doi:10.1016/j.neuint.2008.01.014

Sweeney NL, Hanson AM, Mukherjee S, Ndjomou J, Geiss BJ, Steel JJ, Frankowski KJ, Li K, Schoenen FJ, Frick DN (2015) Benzothiazole and Pyrrolone Flavivirus Inhibitors Targeting the Viral Helicase. ACS infectious diseases 1 (3):140-148. doi:10.1021/id5000458

Swirski FK, Nahrendorf M, Etzrodt M, Wildgruber M, Cortez-Retamozo V, Panizzi P, Figueiredo JL, Kohler RH, Chudnovskiy A, Waterman P, Aikawa E, Mempel TR, Libby P, Weissleder R, Pittet MJ (2009) Identification of splenic reservoir monocytes and their deployment to inflammatory sites. Science 325 (5940):612-616. doi:10.1126/science.1175202

Szretter KJ, Daffis S, Patel J, Suthar MS, Klein RS, Gale M, Jr., Diamond MS (2010) The innate immune adaptor molecule MyD88 restricts West Nile virus replication and spread in neurons of the central nervous system. J Virol 84 (23):12125-12138. doi:JVI.01026-10 [pii]
10.1128/JVI.01026-10 [doi]

Shen J, Devery JM, King NJ (1995) Early induction of interferon-independent virus-specific ICAM-1 (CD54) expression by flavivirus in quiescent but not proliferating fibroblasts--implications for virus-host interactions. Virology 208 (2):437-449. doi:S0042-6822(85)71174-9 [pii]
10.1006/viro.1995.1174 [doi]

Shen J, T-To SS, Schrieber L, King NJ (1997) Early E-selectin, VCAM-1, ICAM-1, and late major histocompatibility complex antigen induction on human endothelial cells by flavivirus and comodulation of adhesion molecule expression by immune cytokines. Journal of Virology 71 (12):9323-9332

Shieh WJ, Guarner J, Layton M, Fine a, Miller J, Nash D, Campbell GL, Roehrig JT, Gubler DJ, Zaki SR (2000) The role of pathology in an investigation of an outbreak of West Nile encephalitis in New York, 1999. Emerging infectious diseases 6 (4):370-372. doi:10.3201/eid0604.000407

Shimoni Z, Niven MJ, Pitlick S, Bulvik S (2001) Treatment of West Nile virus encephalitis with intravenous immunoglobulin. Emerg Infect Dis 7 (4):759. doi:10.3201/eid0704.010432

Shiow LR, Rosen DB, Brdickova N, Xu Y, An J, Lanier LL, Cyster JG, Matloubian M (2006) CD69 acts downstream of interferon-alpha/beta to inhibit S1P1 and lymphocyte egress from lymphoid organs. Nature 440 (7083):540-544. doi:10.1038/nature04606

Shrestha B, Gottlieb D, Diamond MS (2003) Infection and injury of neurons by West Nile encephalitis virus. J Virol 77 (24):13203-13213

Shrestha B, Samuel MA, Diamond MS (2006a) CD8+ T cells require perforin to clear West Nile virus from infected neurons. J Virol 80 (1):119-129. doi:10.1128/JVI.80.1.119-129.2006

Shrestha B, Wang T, Samuel MA, Whitby K, Craft J, Fikrig E, Diamond MS (2006b) Gamma interferon plays a crucial early antiviral role in protection against West Nile virus infection. J Virol 80 (11):5338-5348. doi:10.1128/JVI.00274-06

Shrestha B, Zhang B, Purtha WE, Klein RS, Diamond MS (2008) Tumor necrosis factor alpha protects against lethal West Nile virus infection by promoting trafficking of mononuclear leukocytes into the central nervous system. J Virol 82 (18):8956-8964. doi:JVI.01118-08 [pii]
10.1128/JVI.01118-08 [doi]

Tang Y, Anne Hapip C, Liu B, Fang CT (2006) Highly sensitive TaqMan RT-PCR assay for detection and quantification of both lineages of West Nile virus RNA. Journal of clinical virology : the official publication of the Pan American Society for Clinical Virology 36 (3):177-182. doi:10.1016/j.jcv.2006.02.008

Templeton SP, Kim TS, O'Malley K, Perlman S (2008) Maturation and localization of macrophages and microglia during infection with a neurotropic murine coronavirus. Brain Pathol 18 (1):40-51. doi:10.1111/j.1750-3639.2007.00098.x

Terry RL (2012) Inflammatory monocytes and the pathogenesis of West Nile Virus encephalitis. University of Sydney, University of Sydney

Terry RL, Deffrasnes C, Getts DR, Minten C, van Vreden C, Ashhurst TM, Getts MT, Xie RD, Campbell IL, King NJ (2015) Defective inflammatory monocyte development in IRF8-deficient mice abrogates migration to the West Nile virus-infected brain. Journal of innate immunity 7 (1):102-112. doi:10.1159/000365972

Terry RL, Getts DR, Deffrasnes C, van Vreden C, Campbell IL, King NJC (2012) Inflammatory monocytes and the pathogenesis of viral encephalitis. Journal of neuroinflammation 9 (1):270-270. doi:10.1186/1742-2094-9-270

Tobler LH, Cameron MJ, Lanteri MC, Prince HE, Danesh A, Persad D, Lanciotti RS, Norris PJ, Kelvin DJ, Busch MP (2008) Interferon and interferon-induced chemokine expression is associated with control of acute viremia in West Nile virus-infected blood donors. J Infect Dis 198 (7):979-983. doi:10.1086/591466 [doi]

Tomura M, Yoshida N, Tanaka J, Karasawa S, Miwa Y, Miyawaki A, Kanagawa O (2008) Monitoring cellular movement in vivo with photoconvertible fluorescence protein "Kaede" transgenic mice. Proc Natl Acad Sci U S A 105 (31):10871-10876. doi:10.1073/pnas.0802278105

Town T, Bai F, Wang T, Kaplan AT, Qian F, Montgomery RR, Anderson JF, Flavell RA, Fikrig E (2009) Toll-like receptor 7 mitigates lethal West Nile encephalitis via interleukin 23-dependent immune cell infiltration and homing. Immunity 30 (2):242-253. doi:S1074-7613(09)00064-8 [pii]
10.1016/j.immuni.2008.11.012 [doi]

Tsao C-H, Su H-L, Lin Y-L, Yu H-P, Kuo S-M, Shen C-I, Chen C-W, Liao C-L (2008) Japanese encephalitis virus infection activates caspase-8 and -9 in a FADD-independent and mitochondrion-dependent manner. The Journal of general virology 89 (Pt 8):1930-1941. doi:10.1099/vir.0.2008/000182-0

Throsby M, Geuijen C, Goudsmit J, Bakker AQ, Korimbocus J, Kramer RA, Clijsters-van der Horst M, de Jong M, Jongeneelen M, Thijsse S, Smit R, Visser TJ, Bijl N, Marissen WE, Loeb M, Kelvin DJ, Preiser W, ter Meulen J, de Kruif J (2006) Isolation and characterization of human monoclonal antibodies from individuals infected with West Nile Virus. J Virol 80 (14):6982-6992. doi:80/14/6982 [pii]
10.1128/JVI.00551-06 [doi]

Uchide N, Ohyama K, Yuan B, Bessho T, Yamakawa T (2002) Differentiation of monocytes to macrophages induced by influenza virus-infected apoptotic cells. J Gen Virol 83 (Pt 4):747-751

Valero N, Espina LUZM, Añez G, Torres E, Mosquera JA, Virología SD, Inmunología SD, Investigaciones ID, Américo C (2002) SHORT REPORT : INCREASED LEVEL OF SERUM NITRIC OXIDE IN PATIENTS WITH DENGUE. 66 (6):762-764

van der Laan AM, Ter Horst EN, Delewi R, Begieneman MP, Krijnen PA, Hirsch A, Lavaei M, Nahrendorf M, Horrevoets AJ, Niessen HW, Piek JJ (2014) Monocyte subset accumulation in the human heart following acute myocardial infarction and the role of the spleen as monocyte reservoir. European heart journal 35 (6):376-385. doi:10.1093/eurheartj/eht331

van Marle G, Antony J, Ostermann H, Dunham C, Hunt T, Halliday W, Maingat F, Urbanowski MD, Hobman T, Peeling J, Power C (2007) West Nile virus-induced neuroinflammation: glial infection and capsid protein-mediated neurovirulence. Journal of virology 81 (20):10933-10949. doi:10.1128/jvi.02422-06

van Rooijen N, Kors N, Kraal G (1989) Macrophage subset repopulation in the spleen: differential kinetics after liposome-mediated elimination. J Leukoc Biol 45 (2):97-104

van Rooijen N, van Nieuwmegen R (1984) Elimination of phagocytic cells in the spleen after intravenous injection of liposome-encapsulated dichloromethylene diphosphonate. An enzyme-histochemical study. Cell and tissue research 238 (2):355-358

van Rooijen N, van Nieuwmegen R, Kamperdijk EW (1985) Elimination of phagocytic cells in the spleen after intravenous injection of liposome-encapsulated dichloromethylene diphosphonate. Ultrastructural aspects of elimination of marginal zone macrophages. Virchows Archiv B, Cell pathology including molecular pathology 49 (4):375-383

van Vreden C, Niewold P, vu Dinh L, Munoz-Erazo L, Getts DR, King NJC (2015) Flavivirus Encephalitis: Immunopathogenesis of Disease and Immunomodulation. In: Shapshak P, Sinnot JT, Somboonwit C, Kuhn J (eds) Global Virology I-Identifying and Investigating Viral Diseases, vol I. Springer,

Verma S, Kumar M, Gurjav U, Lum S, Nerurkar VR (2010) Reversal of West Nile virus-induced blood-brain barrier disruption and tight junction proteins degradation by matrix metalloproteinases inhibitor. Virology 397 (1):130-138. doi:S0042-6822(09)00660-6 [pii]
10.1016/j.virol.2009.10.036 [doi]

Verma S, Lo Y, Chapagain M, Lum S, Kumar M, Gurjav U, Luo H, Nakatsuka A, Nerurkar VR (2009) West Nile virus infection modulates human brain microvascular endothelial cells tight junction proteins and cell adhesion molecules: Transmigration across the in vitro blood-brain barrier. Virology 385 (2):425-433. doi:S0042-6822(08)00759-9 [pii]
10.1016/j.virol.2008.11.047 [doi]

Verstrepen BE, Fagrouch Z, van Heteren M, Buitendijk H, Haaksma T, Beenhakker N, Palu G, Richner JM, Diamond MS, Bogers WM, Barzon L, Chabierski S, Ulbert S, Kondova I, Verschoor EJ (2014) Experimental infection of rhesus macaques and common marmosets with a European strain of West Nile virus. PLoS Negl Trop Dis 8 (4):e2797. doi:10.1371/journal.pntd.0002797

Victora GD, Dominguez-Sola D, Holmes AB, Deroubaix S, Dalla-Favera R, Nussenzweig MC (2012) Identification of human germinal center light and dark zone cells and their relationship to human B-cell lymphomas. Blood 120 (11):2240-2248. doi:10.1182/blood-2012-03-415380

von Andrian UH, Mempel TR (2003) Homing and cellular traffic in lymph nodes. Nature reviews Immunology 3 (11):867-878. doi:10.1038/nri1222

Wacher C, Muller M, Hofer MJ, Getts DR, Zabaras R, Ousman SS, Terenzi F, Sen GC, King NJC, Campbell IL (2007) Coordinated regulation and widespread cellular expression of interferon-stimulated genes (ISG) ISG-49, ISG-54, and ISG-56 in the central nervous system after infection with distinct viruses. Journal of Virology 81 (2):860-871

Walsh KB, Lanier LL, Lane TE (2008) NKG2D receptor signaling enhances cytolytic activity by virus-specific CD8+ T cells: evidence for a protective role in virus-induced encephalitis. J Virol 82 (6):3031-3044. doi:10.1128/JVI.02033-07

Walunas TL, Bruce DS, Dustin L, Loh DY, Bluestone JA (1995) Ly-6C is a marker of memory CD8+ T cells. J Immunol 155 (4):1873-1883

Wang T, Town T, Alexopoulou L, Anderson JF, Fikrig E, Flavell RA (2004) Toll-like receptor 3 mediates West Nile virus entry into the brain causing lethal encephalitis. Nat Med 10 (12):1366-1373. doi:nm1140 [pii]
10.1038/nm1140

Wang Y, Lobigs M, Lee E, Koskinen A, Mullbacher A (2006) CD8(+) T cell-mediated immune responses in West Nile virus (Sarafend strain) encephalitis are independent of gamma interferon. J Gen Virol 87 (Pt 12):3599-3609. doi:87/12/3599 [pii]
10.1099/vir.0.81306-0 [doi]

Wang Y, Lobigs M, Lee E, Mullbacher A (2003) CD8+ T cells mediate recovery and immunopathology in West Nile virus encephalitis. J Virol 77 (24):13323-13334

Wee JL, Greenwood DL, Han X, Scheerlinck JP (2011) Inflammatory cytokines IL-6 and TNF-alpha regulate lymphocyte trafficking through the local lymph node. Veterinary immunology and immunopathology 144 (1-2):95-103. doi:10.1016/j.vetimm.2011.07.007

Weiss D, Carr D, Kellachan J, Tan C, Phillips M, Bresnitz E, Layton M (2001) Clinical findings of West Nile virus infection in hospitalized patients, New York and New Jersey, 2000. Emerg Infect Dis 7 (4):654-658

Willard-Mack CL (2006) Normal structure, function, and histology of lymph nodes. Toxicologic pathology 34 (5):409-424. doi:10.1080/01926230600867727

Winkelmann ER, Widman DG, Xia J, Johnson AJ, van Rooijen N, Mason PW, Bourne N, Milligan GN (2014) Subcapsular sinus macrophages limit dissemination of West Nile virus particles after inoculation but are not essential for the development of West Nile virus-specific T cell responses. Virology 450-451:278-289. doi:10.1016/j.virol.2013.12.021

Winter PM, Dung NM, Loan HT, Kneen R, Wills B, Thu LT, House D, White NJ, Farrar JJ, Hart CA, Solomon T (2004) Proinflammatory cytokines and chemokines in humans with Japanese encephalitis. The Journal of infectious diseases 190 (9):1618-1626. doi:10.1086/423328

Wrammert J, Kallberg E, Agace WW, Leanderson T (2002) Ly6C expression differentiates plasma cells from other B cell subsets in mice. Eur J Immunol 32 (1):97-103. doi:10.1002/1521-4141(200201)32:1<97::AID-IMMU97>3.0.CO;2-Y

Xiao SY, Guzman H, Zhang H, Travassos da Rosa AP, Tesh RB (2001) West Nile virus infection in the golden hamster (Mesocricetus auratus): a model for West Nile encephalitis. Emerg Infect Dis 7 (4):714-721

Xu J, Carretero OA, Liu YH, Shesely EG, Yang F, Kapke A, Yang XP (2002) Role of AT2 receptors in the cardioprotective effect of AT1 antagonists in mice. Hypertension 40 (3):244-250

Xu Z, Waeckerlin R, Urbanowski MD, van Marle G, Hobman TC (2012) West Nile virus infection causes endocytosis of a specific subset of tight junction membrane proteins. PloS one 7 (5):e37886. doi:10.1371/journal.pone.0037886

Yamada S, DePasquale M, Patlak CS, Cserr HF (1991) Albumin outflow into deep cervical lymph from different regions of rabbit brain. The American journal of physiology 261 (4 Pt 2):H1197-1204

Yamamoto T, Naito M, Moriyama H, Umezu H, Matsuo H, Kiwada H, Arakawa M (1996) Repopulation of murine Kupffer cells after intravenous administration of liposome-encapsulated dichloromethylene diphosphonate. Am J Pathol 149 (4):1271-1286

Yamanouchi S, Kuwahara K, Sakata A, Ezaki T, Matsuoka S, Miyazaki J, Hirose S, Tamura T, Nariuchi H, Sakaguchi N (1998) A T cell activation antigen, Ly6C, induced on CD4+ Th1 cells mediates an inhibitory signal for secretion of IL-2 and proliferation in peripheral immune responses. Eur J Immunol 28 (2):696-707. doi:10.1002/(SICI)1521-4141(199802)28:02<696::AID-IMMU696>3.0.CO;2-N

Yang J-S, Ramanathan MP, Muthumani K, Choo AY, Jin S-H, Yu Q-C, Hwang DS, Choo DK, Lee MD, Dang K, Tang W, Kim JJ, Weiner DB (2002) Induction of inflammation by West Nile virus capsid through the caspase-9 apoptotic pathway. Emerging infectious diseases 8 (12):1379-1384. doi:10.3201/eid0812.020224

Yang T-C, Shiu S-L, Chuang P-H, Lin Y-J, Wan L, Lan Y-C, Lin C-W (2009) Japanese encephalitis virus NS2B-NS3 protease induces caspase 3 activation and mitochondria-mediated apoptosis in human medulloblastoma cells. Virus research 143 (1):77-85. doi:10.1016/j.virusres.2009.03.007

Yang Y, Ye J, Yang X, Jiang R, Chen H, Cao S (2011) Japanese encephalitis virus infection induces changes of mRNA profile of mouse spleen and brain. Virol J 8:80. doi:10.1186/1743-422X-8-80

Yeung AW, Wu W, Freewan M, Stocker R, King NJ, Thomas SR (2012) Flavivirus infection induces indoleamine 2,3-dioxygenase in human monocyte-derived macrophages

via tumor necrosis factor and NF-kappaB. J Leukoc Biol 91 (4):657-666. doi:10.1189/jlb.1011532

Yoshida T, Omatsu T, Saito A, Katakai Y, Iwasaki Y, Iijima S, Kurosawa T, Hamano M, Nakamura S, Takasaki T, Yasutomi Y, Kurane I, Akari H (2012) CD16(+) natural killer cells play a limited role against primary dengue virus infection in tamarins. Arch Virol 157 (2):363-368. doi:10.1007/s00705-011-1178-6

Zink MC, Uhrlaub J, DeWitt J, Voelker T (2005) Neuroprotective and Anti–Human Immunodeficiency Virus Activity of Minocycline. Jama 293 (16):2003-2011

Zhang B, Chan YK, Lu B, Diamond MS, Klein RS (2008) CXCR3 mediates region-specific antiviral T cell trafficking within the central nervous system during West Nile virus encephalitis. J Immunol 180 (4):2641-2649. doi:180/4/2641 [pii]

Zhang M, Daniel S, Huang Y, Chancey C, Huang Q, Lei YF, Grinev A, Mostowski H, Rios M, Dayton A (2010) Anti-West Nile virus activity of in vitro expanded human primary natural killer cells. BMC Immunol 11:3. doi:1471-2172-11-3 [pii]
10.1186/1471-2172-11-3 [doi]

Zhang S, Vogt MR, Oliphant T, Engle M, Bovshik EI, Diamond MS, Beasley DW (2009) Development of resistance to passive therapy with a potently neutralizing humanized monoclonal antibody against West Nile virus. J Infect Dis 200 (2):202-205. doi:10.1086/599794 [doi]

Zhu B, Bando Y, Xiao S, Yang K, Anderson AC, Kuchroo VK, Khoury SJ (2007) CD11b+Ly-6C(hi) suppressive monocytes in experimental autoimmune encephalomyelitis. J Immunol 179 (8):5228-5237

8. Appendix

Appendix Figure 1 General Leukocyte gating of lymph node

Representative flow cytometric dot plots illustrating the gating strategy for leukocytes in the secondary lymphoid organs, in particular the lymph node, of mice infected with lethal dose WNV ($6x10^4$ PFU). In order to obtain a live single cell leukocyte population, the following steps were performed during analysis: Time gate (A), followed by exclusion of doublets with the FSC-H vs FSC-A gate (B). Removal of debris with the SSC-A vs FSC-A gate (C). Negative selection of live cells (D) and finally positive selection of leukocyte (E), based on pan-leukocyte marker (CD45). Specific leukocyte subsets were then identified based on lineage markers. This allowed us to identify the following subsets: total T cells (F) from which we isolated the $CD4^+$ T cells (G) and $CD8^+$ T cells (G). NK cells and NKT cells (F). B cells and pDC (H); Neutrophils (I); Monocytes (J), $CD11c^+CD11c^+$ DC (J), $CD11c^+CD11b^-$ DC (J), $CD11c^{hi}CD11b^{int}$ DC (J). Lastly the $CD8\alpha^+$ DC subset (K) was isolated from the $CD11c^+CD11b^-$ DC gate. Each plot represents 10,000 events.

Appendix Figure 1

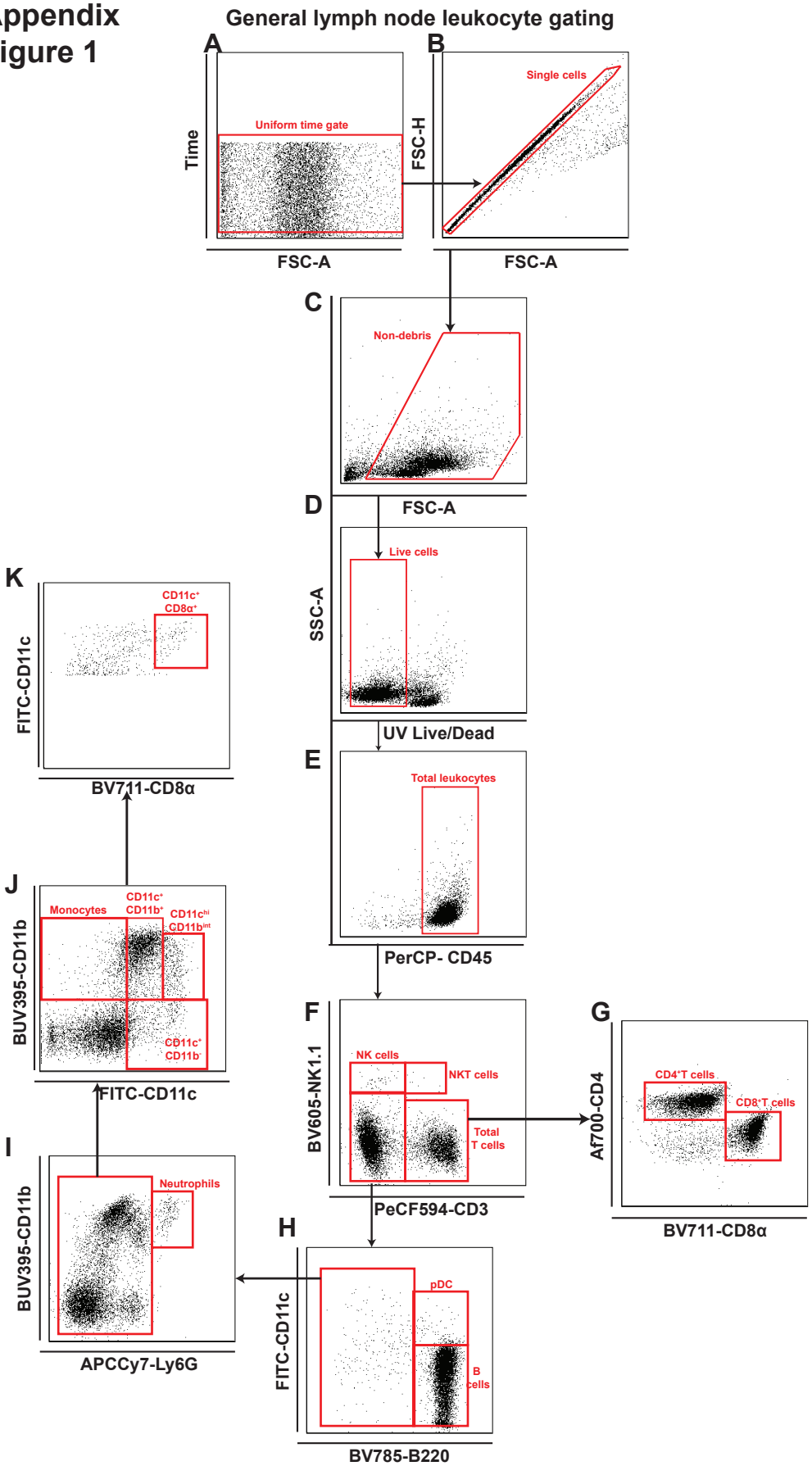

Appendix Figure 2 General Leukocyte gating of lymph node-Fluorescence minus-one and isotype controls

Representative flow cytometric dot plots illustrating the fluorescence minus-one and isotype controls for the gating strategy of leukocytes in the secondary lymphoid organs, in particular the lymph node, of mice infected with lethal dose WNV ($6x10^4$ PFU). Black denotes fluorescence minus-one and red denotes isotype control. In order to obtain a live single cell leukocyte population, the following steps were performed during analysis: Time gate (A), followed by exclusion of doublets with the FSC-H vs FSC-A gate (B). Removal of debris with the SSC-A vs FSC-A gate (C). Negative selection of live cells (D) and finally positive selection of leukocyte (E), based on pan-leukocyte marker (CD45). Specific leukocyte subsets were then identified based on lineage markers. This allowed us to identify the following subsets: total T cells (F) from which we isolated the $CD4^+$ T cells (G) and $CD8^+$ T cells (G). NK cells and NKT cells (F). B cells and pDC (H); Neutrophils (I); Monocytes (J), $CD11c^+CD11c^+$ DC (J), $CD11c^+CD11b^-$ DC (J), $CD11c^{hi}CD11b^{int}$ DC (J). Lastly the $CD8\alpha^+$ DC subset (K) was isolated from the $CD11c^+CD11b^-$ DC gate. Each plot represents 5,000 events.

Appendix Figure 2

General lymph node leukocyte gating-FMO and Isotype controls

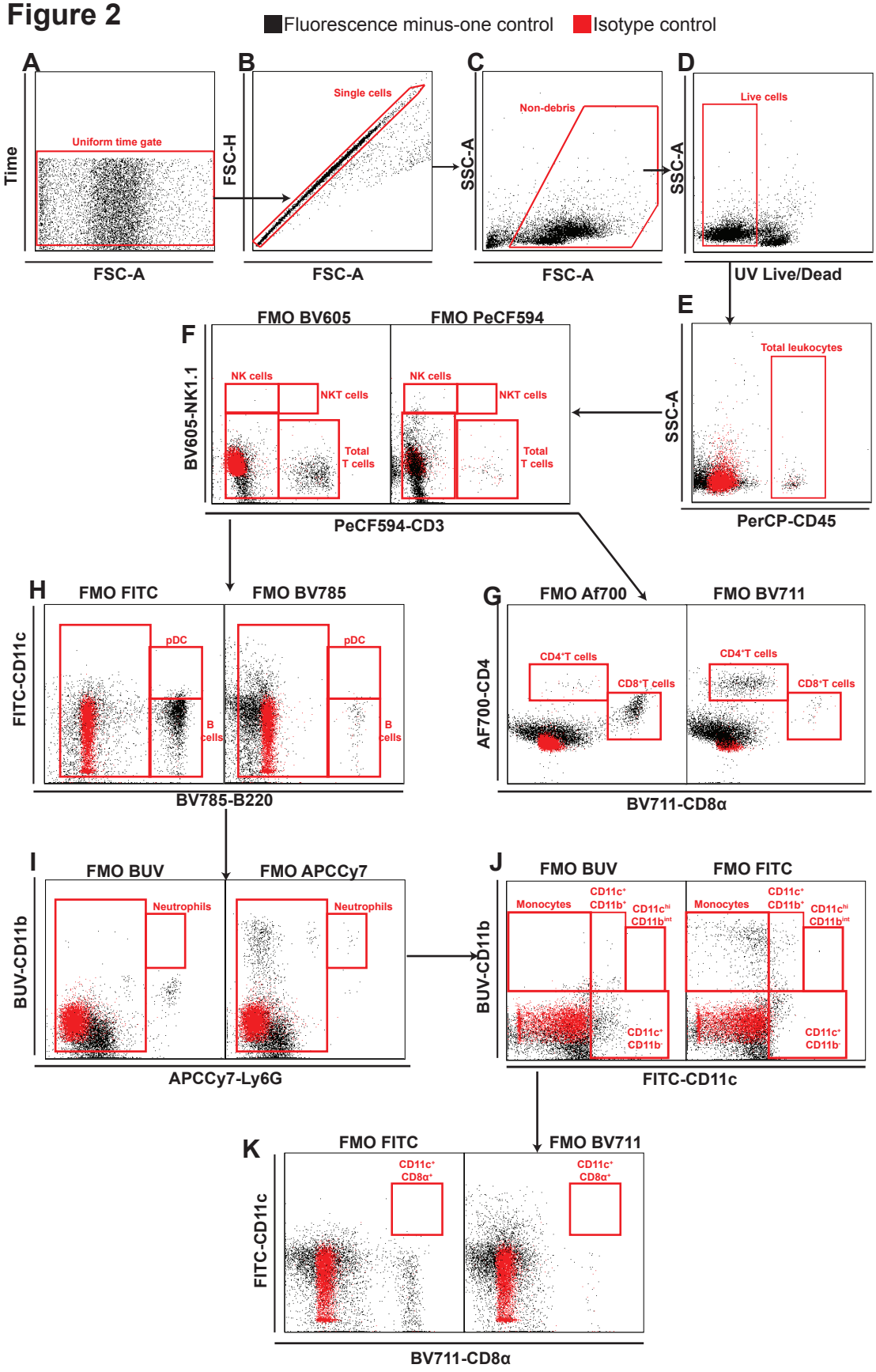

Appendix Figure 3 Expression of Ly6C in leukocyte populations in the draining (CLN) and non-draining lymph nodes (MLN, ILN) of the CNS following lethal WNV infection

Ly6C levels were quantified using the geometric mean of Ly6C expression of whole populations. Ly6C expression of the (A) B cells, (B) $CD4^+$ T, (C) $CD8^+$ T cells, (D) NK cells (E) NKT cells, (F) neutrophils and (G) monocytes in the CLN (red), ILN (blue) and MLN (green) of mice following lethal WNV infection ($6x10^4$ PFU) on d0, 3, 5, 6 and 7 p.i. Grouped data was normalised using d0 as internal control, and is represented as percentage change of the geometric mean of cells compared to day 0 (100%). Data are the mean ±SEM of 3-4 mice/group and is representative of 3 independent experiments. Statistical analysis was conducted using one-way ANOVA with a Dunnet's multiple comparison post-test (d0 as control), and $P \leq 0.05$*; $P \leq 0.01$**; $P \leq 0.001$***.

Appendix Figure 3

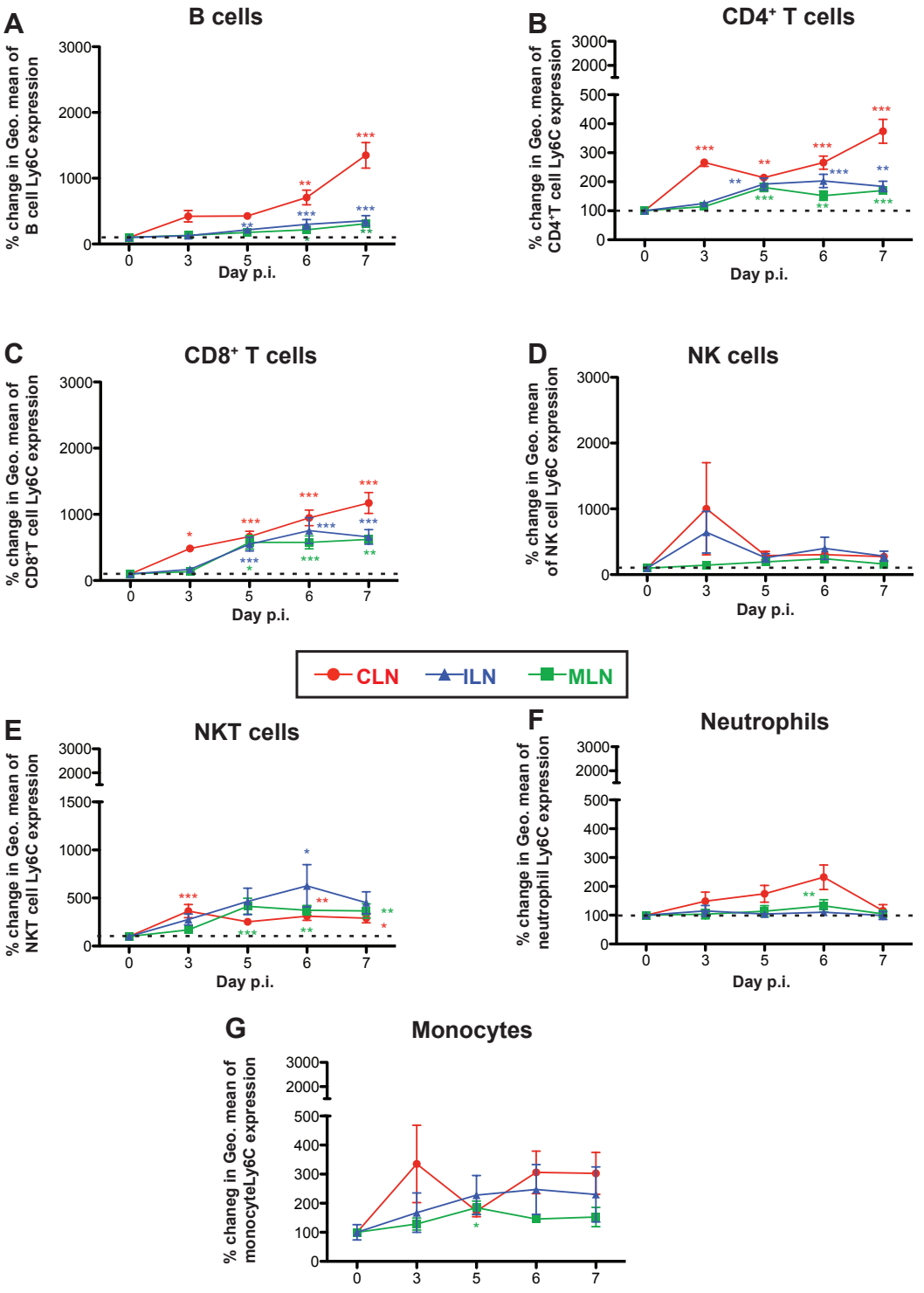

Appendix Figure 4 Expression of Ly6C in leukocyte populations in the draining (CLN) and non-draining lymph nodes (MLN, ILN) of the CNS following lethal WNV infection

Ly6C levels were quantified using the geometric mean of Ly6C expression of whole populations. Ly6C expression of (A) $CD11c^{+}CD11b^{+}$ DC, (B) $CD11c^{hi}CD11b^{int}$ DC, (C) $CD11c^{+}CD11b^{-}$ DC, (D) pDC and $CD11c^{+}CD8\alpha^{+}$ DC (E) in the CLN (red), ILN (blue) and MLN (green) of mice following lethal WNV infection ($6x10^{4}$ PFU) on d0, 3, 5, 6 and 7 p.i. Grouped data was normalised using d0 as internal control, and is represented as percentage change of the geometric mean of cells compared to day 0 (100%). Data are the mean ±SEM of 3-4 mice/group and is representative of 3 independent experiments. Statistical analysis was conducted using one-way ANOVA with a Dunnet's multiple comparison post-test (d0 as control), and $P \leq 0.05$*; $P \leq 0.01$**; $P \leq 0.001$***.

Appendix Figure 4

Percentage change in Geometric mean of Ly6C- CLN, ILN and MLN

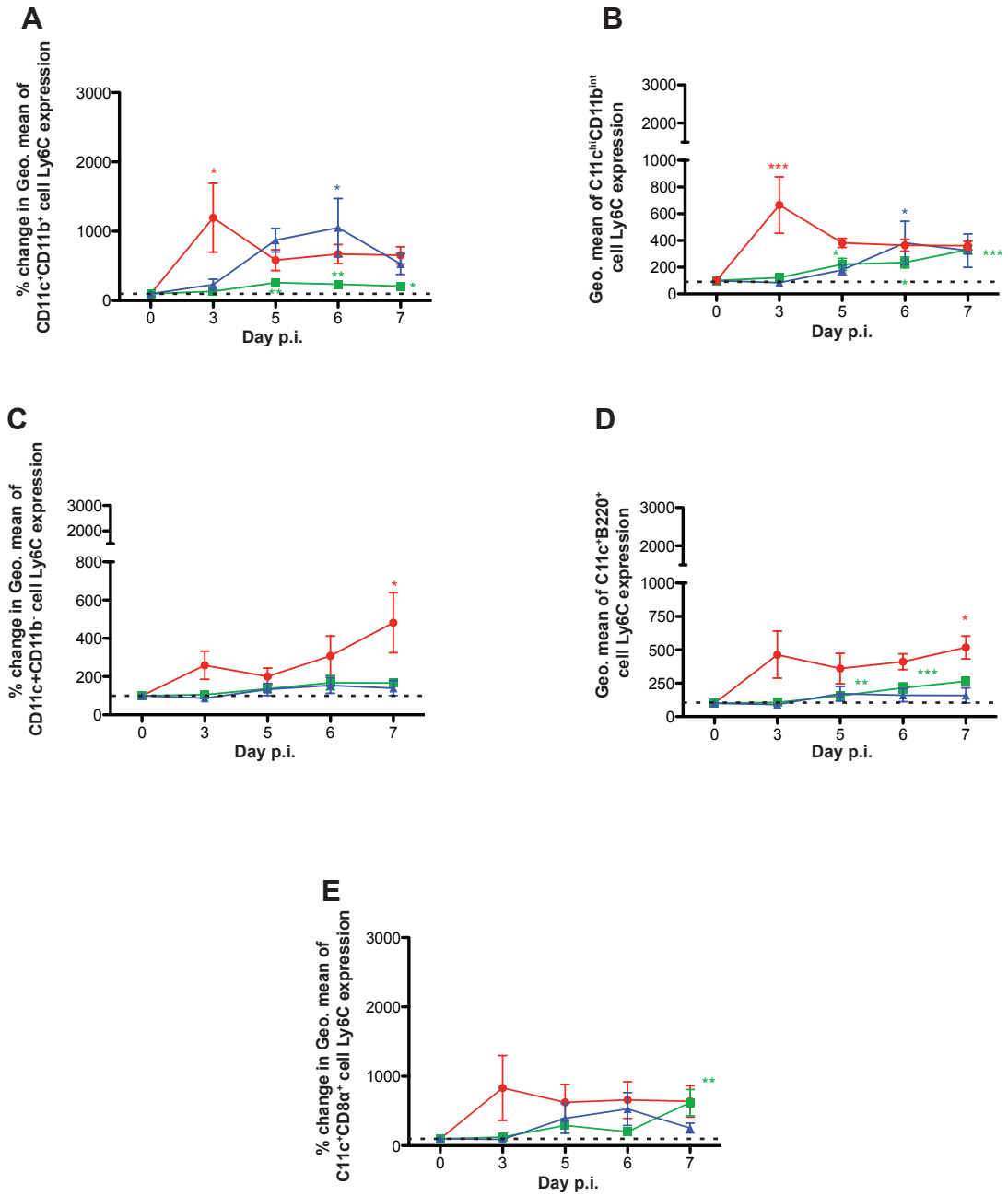

Appendix Figure 5 General Leukocyte gating of spleen

Representative flow cytometric dot plots illustrating the gating strategy for leukocytes in the spleen, of mice infected with lethal dose WNV ($6x10^4$ PFU). In order to obtain a live single cell leukocyte population the following steps were performed during analysis: Time gate (A), followed by exclusion of doublets with the FSC-H vs FSC-A gate (B). Removal of debris with the SSC-A vs FSC-A gate (C). Negative selection of live cells (D) and finally positive selection of leukocyte (E) based on pan-leukocyte marker (CD45). Specific leukocyte subsets were then identified based on lineage markers. This allowed us to identify the following subsets: $B220^+$ cells (F) from which we isolated the B cells and pDC (G); Neutrophils (H); $NK1.1^+$ subsets (I) from which we isolated NK cells and NKT cells (J). Monocytes (K); $CD11c^+CD11c^+$ DC (K); $CD11c^+CD11b^-$ DC (K); $CD11c^{hi}CD11b^{int}$ DC (K). Lastly the total T cell subset (L) including CD4 and CD8 T cell (M). Each plot represents 10, 000 events.

Appendix Figure 5

General spleen leukocyte gating

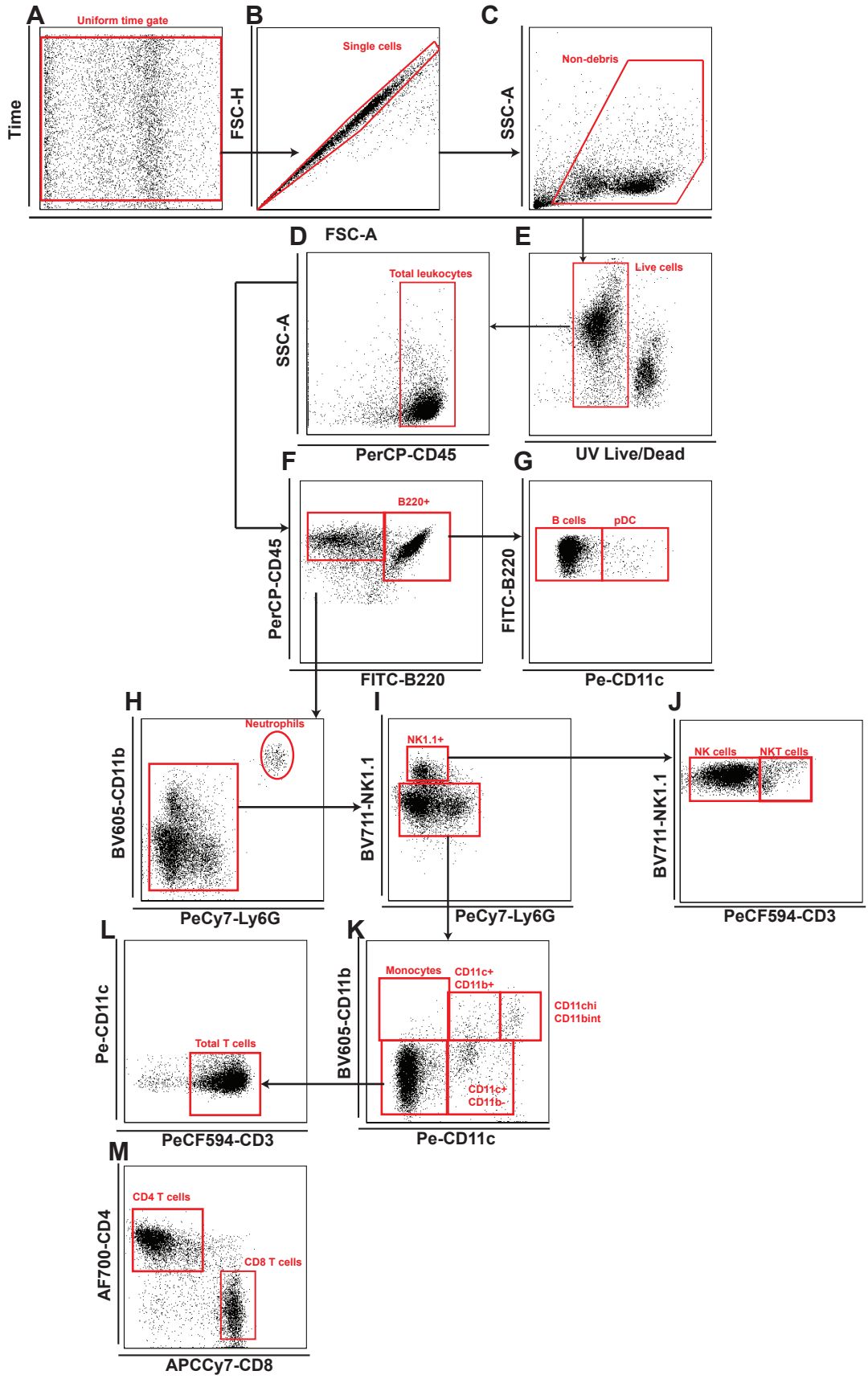

Appendix Figure 6 General Leukocyte gating of spleen-Fluorescence minus one and Isotype controls

Representative flow cytometric dot plots illustrating the fluorescence minus-one and isotype controls for the gating strategy of leukocytes in the spleen, of mice infected with lethal dose WNV ($6x10^4$ PFU). Black denotes fluorescence minus-one and red denotes isotype control. In order to obtain a live single cell leukocyte population the following steps were performed during analysis: Time gate (A), followed by exclusion of doublets with the FSC-H vs FSC-A gate (B). Removal of debris with the SSC-A vs FSC-A gate (C). Negative selection of live cells (D) and finally positive selection of leukocyte (E) based on pan-leukocyte marker (CD45). Specific leukocyte subsets were then identified based on lineage markers. This allowed us to identify the following subsets: $B220^+$ cells (F) from which we isolated the B cells and pDC (G); Neutrophils (H); $NK1.1^+$ subsets (I) from which we isolated NK cells and NKT cells (J). Monocytes (K); $CD11c^+CD11c^+$ DC (K); $CD11c^+CD11b^-$ DC (K); $CD11c^{hi}CD11b^{int}$ DC (K). Lastly the total T cell subset (L) including CD4 and CD8 T cell (M). Each plot represents 5, 000 events.

Appendix Figure 6

General spleen leukocyte gating-FMO and Isotype controls

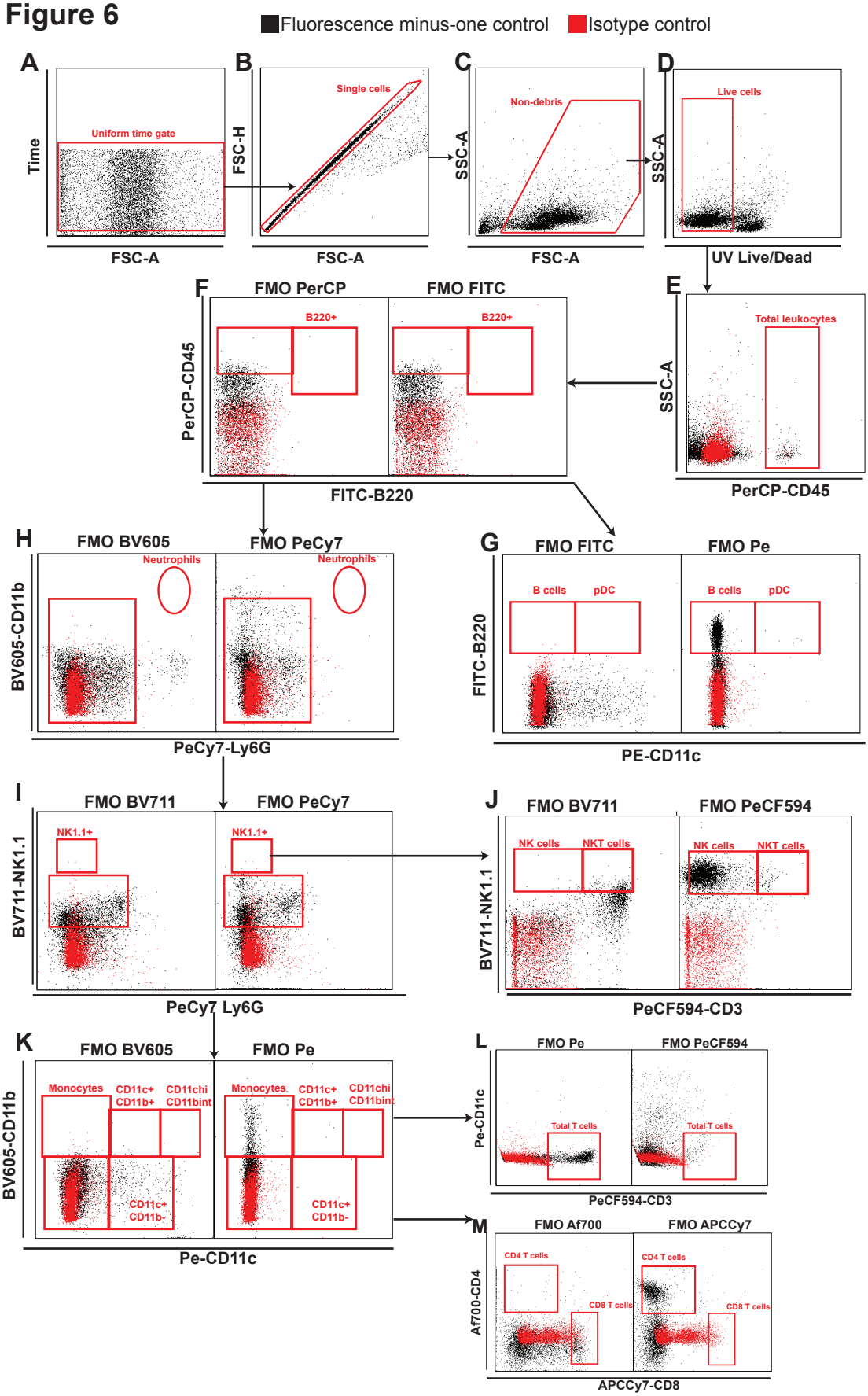

Appendix figure 7 Expression of Ly6C in the leukocyte populations of the spleen, following lethal WNV infection

Graph A demonstrates the change in Ly6C expression between d0-7, following lethal WNV infection ($6x10^4$ PFU) of the total leukocyte population ($CD45^+$) (circle), B cells ($B220^+/CD19^+$) (triangle) and total T ($CD3^+$) (square) cells. T cells were further classified into two subsets based on CD4 or CD8 expression, and Ly6C expression analysed. Figure B represents the change in Ly6C expression between d0-7p.i. of $CD4^+$ (circle) and $CD8^+$ (upside-down triangle) T cells. Ly6C expression of the various DC subsets, namely: $CD11c^+CD11b^+$ (square), $CD11c^+CD11b^-$ (circle) and $CD11c^{hi}CD11b^{int}$ (triangle) is demonstrated by figure C. Furthermore, the change in Ly6C expression between d0-7p.i. of the $CD11b^+$ $CD11c^-$ subsets, namely: monocytes ($CD11b^+Ly6G^-$) (circle) and neutrophils ($CD11b^{hi}$ $Ly6G^+$) (square) is represented by figure D, with the Ly6C expression of the $NK1.1^+$ subsets namely: NK cells ($NK1.1^+CD3^-$) (circle) and NKT cells ($NK1.1^+CD3^+$) (square) represented by figure E. All of the graphs (A-E) show average geometric mean of Ly6C expression, of the relevant splenic leukocyte population, following lethal WNV infection ($6x10^4$ PFU) on d0, 3, 5, 6 and 7 p.i.. Ly6C levels were quantified by averaging the geometric mean of Ly6C expression of whole population. Grouped data was normalised using d0 as internal control and is represented as percentage change compared to baseline i.e. d0 p.i. (100%). Data are the mean ±SEM of 3-4 mice/group and is representative of 3 independent experiments. Statistical analysis was conducted using one-way ANOVA with a Dunnet's multiple comparison post-test (d0 as control), and $P\leq0.05$*; $P\leq0.01$**; $P\leq0.001$***.

Appendix Figure 7

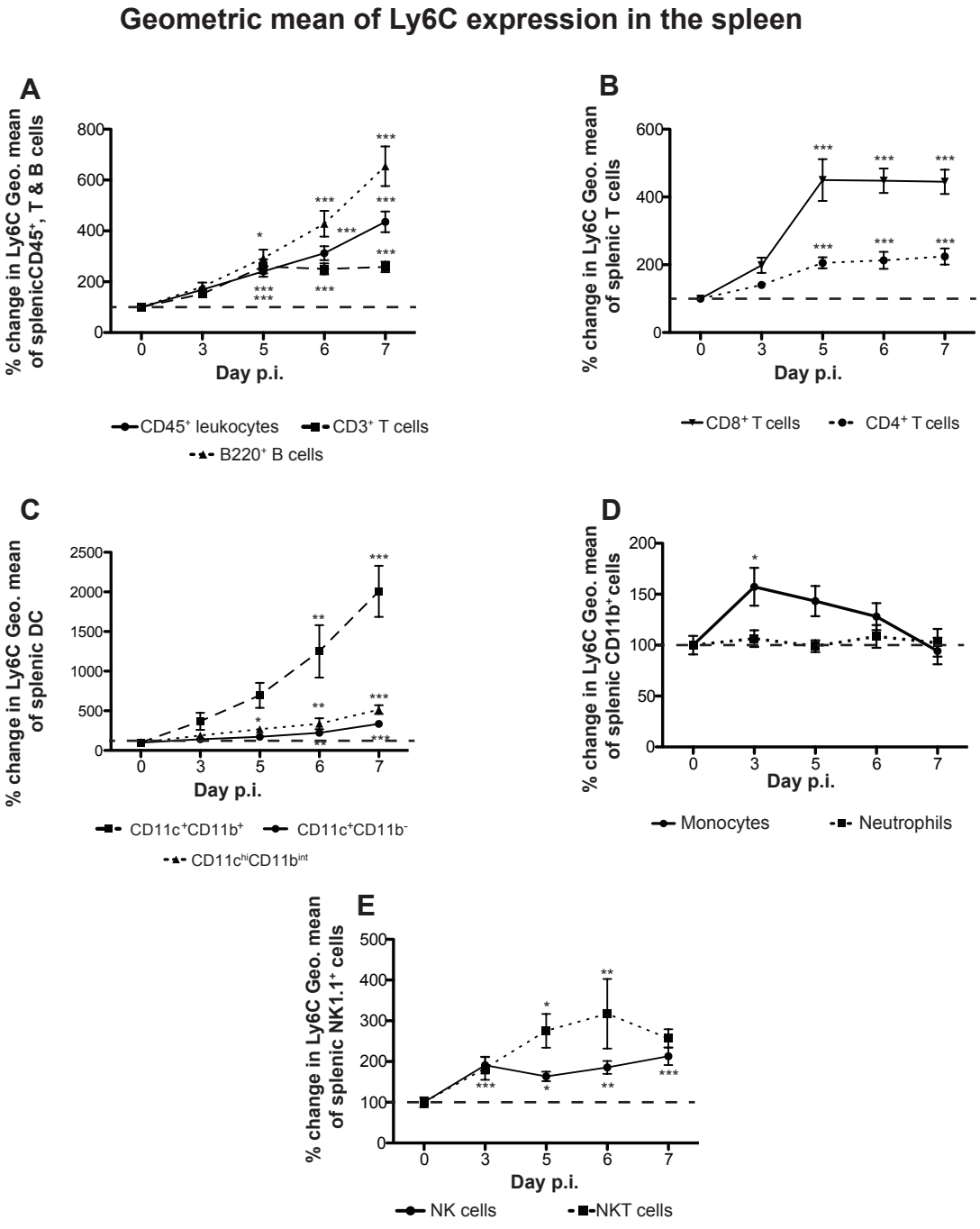

Appendix Figure 8 General Leukocyte gating of the WNV-infected CNS

Representative flow cytometric dot plots illustrating the gating strategy for leukocytes in the CNS, of mice infected with lethal dose WNV ($6x10^4$ PFU). In order to obtain a live single cell leukocyte population the following steps were performed during analysis: Time gate (A), followed by exclusion of doublets with the FSC-H vs FSC-A gate (B). Removal of debris with the SSC-A vs FSC-A gate (C). Negative selection of live cells (D) and finally positive selection of leukocyte (E) based on pan-leukocyte marker (CD45). Specific leukocyte subsets were then identified based on lineage markers. Lymphoid lineage ($CD11b^-$) and myeloid lineage cells ($CD11b^+$) were separated (F). Myeloid lineage cells were further classified as neutrophils ($CD11b^{hi}Ly6G^+$) (G) and resident microglia ($CD11b^+CD45^{int}Ly6C^-$), immigrant microglia ($CD11b^+CD45^-Ly6C^{int}$) and inflammatory macrophages ($CD11b^+CD45^+Ly6C^{hi}$) (H).

Lymphoid lineage cells were further characterised as T cells ($CD3^+NK1.1^-$), NKT cells ($CD3^+NK1.1^+$) and NK cells ($CD3^-NK1.1^+$) (I). Lastly B cells were identified based on B220 expression (J). Each plot represents 10, 000 events.

Appendix Figure 8

General CNS leukocyte gating

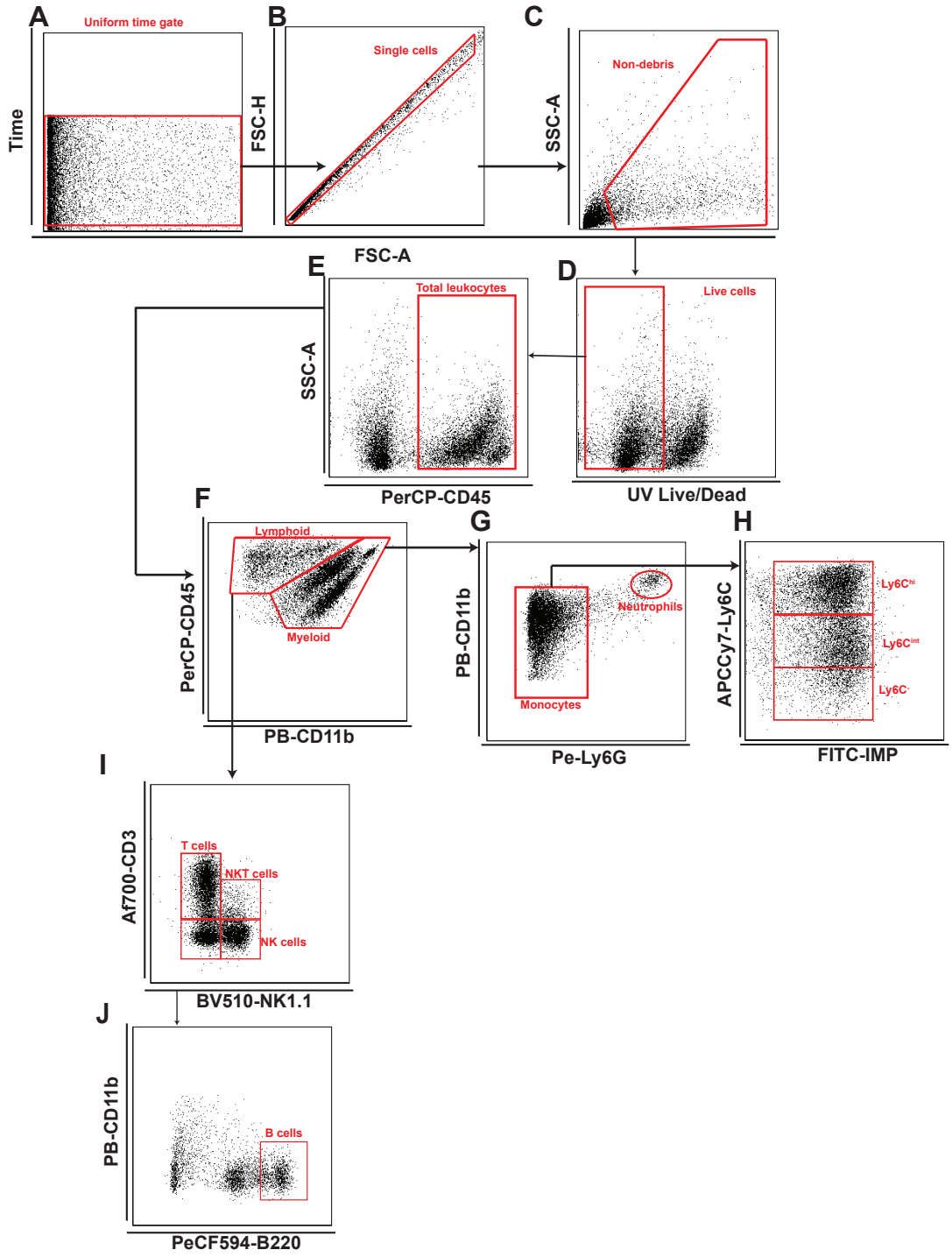

Appendix Figure 9 General Leukocyte gating of the WNV-infected CNS-Fluorescence minus-one and Isotype controls

Representative flow cytometric dot plots illustrating the fluorescence minus-one and isotype controls for the gating strategy of leukocytes in the CNS, of mice infected with lethal dose WNV ($6x10^4$ PFU). Black denotes fluorescence minus-one and red denotes isotype control. In order to obtain a live single cell leukocyte population the following steps were performed during analysis: Time gate (A), followed by exclusion of doublets with the FSC-H vs FSC-A gate (B). Removal of debris with the SSC-A vs FSC-A gate (C). Negative selection of live cells (D) and finally positive selection of leukocyte (E) based on pan-leukocyte marker (CD45). Specific leukocyte subsets were then identified based on lineage markers. Lymphoid lineage ($CD11b^-$) and myeloid lineage cells ($CD11b^+$) were separated (F). Myeloid lineage cells were further classified as neutrophils ($CD11b^{hi}Ly6G^+$) (G) and resident microglia ($CD11b^+CD45^{int}Ly6C^-$), immigrant microglia ($CD11b^+CD45^-Ly6C^{int}$) and inflammatory macrophages ($CD11b^+CD45^+Ly6C^{hi}$) (H).

Lymphoid lineage cells were further characterised as T cells ($CD3^+NK1.1^-$), NKT cells ($CD3^+NK1.1^+$) and NK cells ($CD3^-NK1.1^+$) (I). Lastly B cells were identified based on B220 expression (J). Each plot represents 5, 000 events.

Appendix Figure 9

General CNS leukocyte gating-FMO and Isotype controls

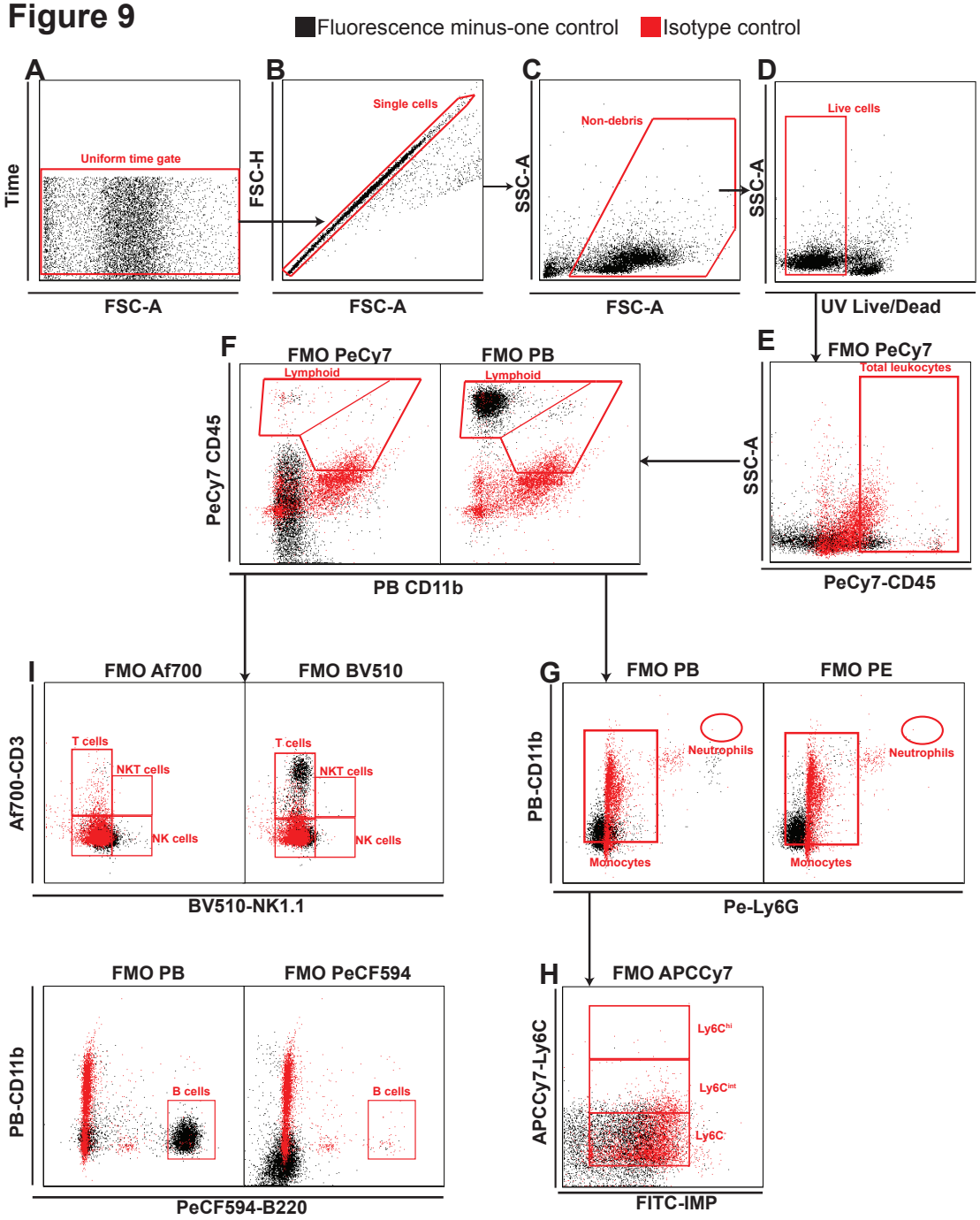

Appendix Figure 10 General Leukocyte gating of the bone marrow

Representative flow cytometric dot plots illustrating the gating strategy for leukocytes in the bone marrow, of mice infected with lethal dose WNV ($6x10^4$ PFU). In order to obtain a live single cell leukocyte population the following steps were performed during analysis: Time gate (A), followed by exclusion of doublets with the FSC-H vs FSC-A gate (B). Removal of debris with the SSC-A vs FSC-A gate (C). Negative selection of live cells (D) and finally positive selection of leukocyte (E) based on pan-leukocyte marker (CD45). Specific leukocyte subsets were then identified based on lineage markers. This allowed us to identify the following subsets: neutrophils ($Ly6G^+$) and total T cells ($CD3^+$) (F) from which we isolated the NKT cells ($CD3^+NK1.1^+$) (G), and $CD4^+$ ($CD3^+NK1.1^-CD4^+$) and $CD8^+$ T cells ($CD3^+NK1.1^-CD8^+$) (H); Monocytes ($CD11b^+$) and $F4/80^+$ stromal macrophages (I); Monocyte subset were further classified as $Ly6C^{hi}$, $Ly6C^{int}$ or $Ly6C^-$ (J).We further identified dendritic cells ($CD11c^+B220^-$), pDC ($CD11c^+B220^+$) and B cells ($CD11c^-B220^+$) (K). Lastly NK cells were gated based on NK1.1 expression (L)

Each plot represents 10, 000 events.

Appendix Figure 10

General bone marrow leukocyte gating

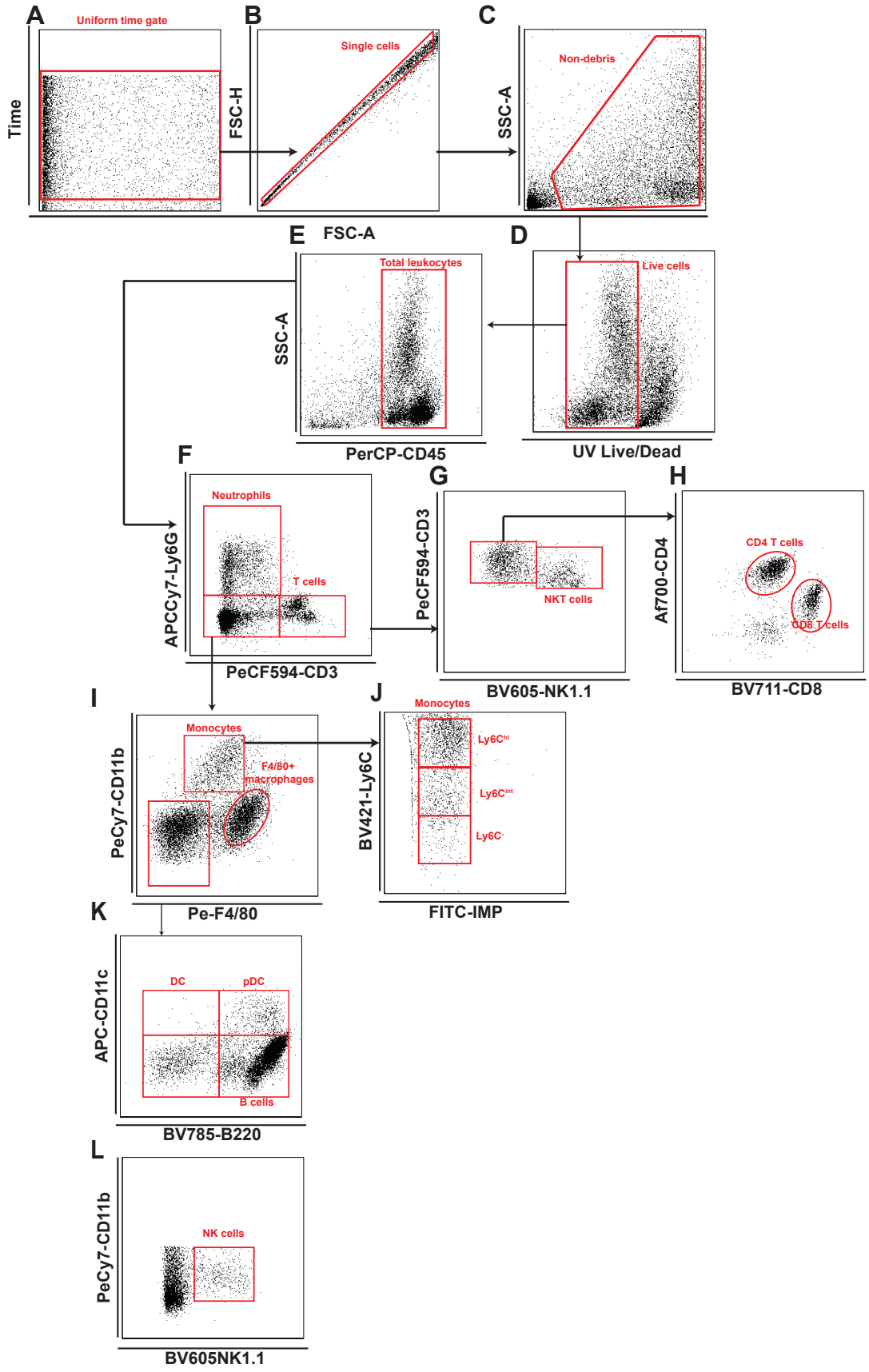

Appendix Figure 11 General Leukocyte gating of the bone marrow-Fluorescence minus-one and Isotype controls

Representative flow cytometric dot plots illustrating the fluorescence minus-one and isotype controls for the gating strategy of leukocytes in the bone marrow, of mice infected with lethal dose WNV ($6x10^4$ PFU). Black denotes fluorescence minus-one and red denotes isotype control. In order to obtain a live single cell leukocyte population the following steps were performed during analysis: Time gate (A), followed by exclusion of doublets with the FSC-H vs FSC-A gate (B). Removal of debris with the SSC-A vs FSC-A gate (C). Negative selection of live cells (D) and finally positive selection of leukocyte (E) based on pan-leukocyte marker (CD45). Specific leukocyte subsets were then identified based on lineage markers. This allowed us to identify the following subsets: neutrophils ($Ly6G^+$) and total T cells ($CD3^+$) (F) from which we isolated the NKT cells ($CD3^+NK1.1^+$) (G), and $CD4^+$ ($CD3^+NK1.1^-CD4^+$) and $CD8^+$ T cells ($CD3^+NK1.1^-CD8^+$) (H); Monocytes ($CD11b^+$) and $F4/80^+$ stromal macrophages (I); Monocyte subset were further classified as $Ly6C^{hi}$, $Ly6C^{int}$ or $Ly6C^-$ (J).We further identified dendritic cells ($CD11c^+B220^-$), pDC ($CD11c^+B220^+$) and B cells ($CD11c^-B220^+$) (K). Lastly NK cells were gated based on NK1.1 expression (L)

Each plot represents 5, 000 events.

Appendix Figure 11 General Bone Marrow leukocyte gating-FMO and Isotype controls

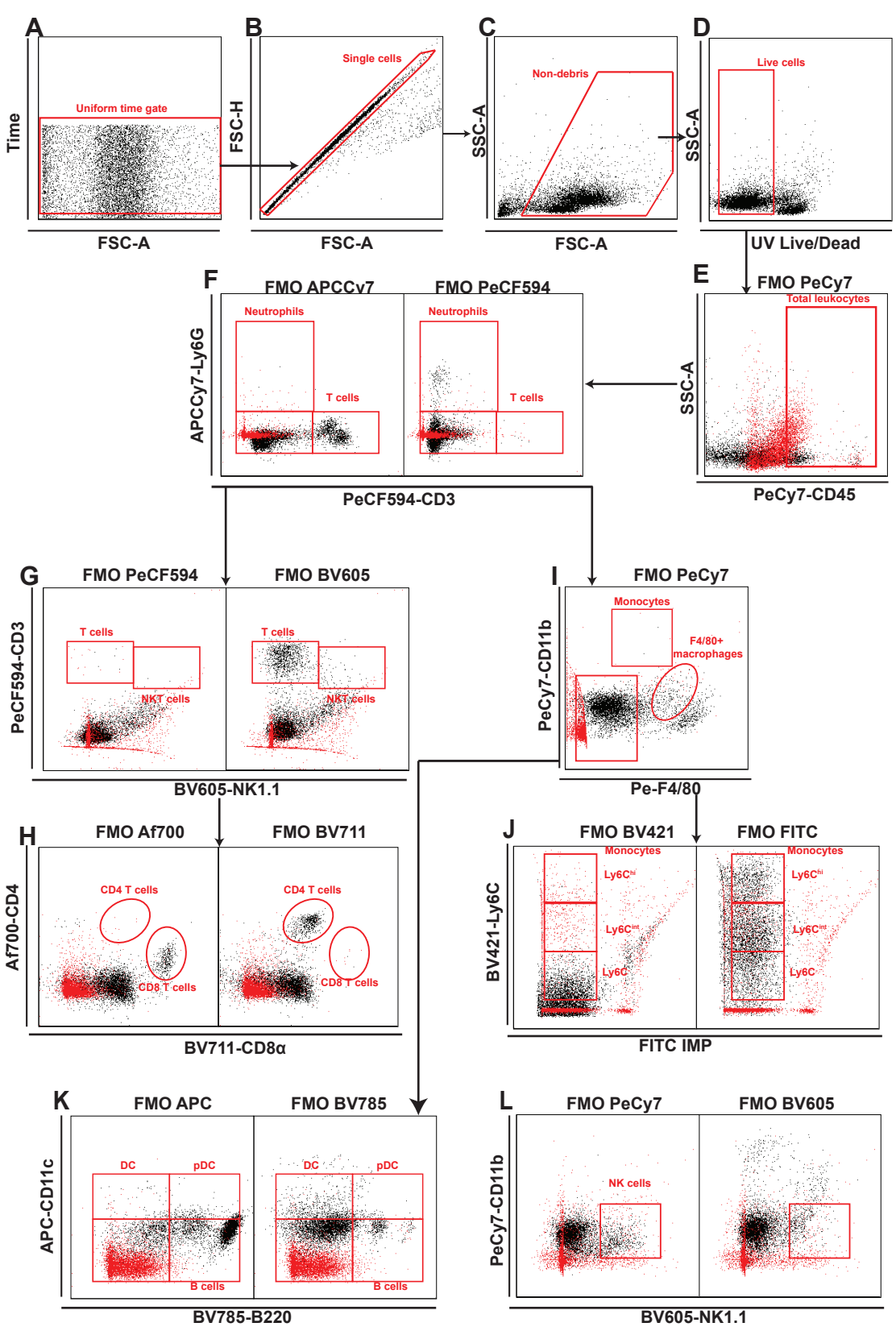

Appendix Figure 12 Whole blood phagocytosis assay of blood from CLO-depleted mice

Graphs A and B show the number (A) and percentage (B) of cells in 1ml of blood that have taken up IMP (undiluted/neat) in WNV-infected+IMP (blue) and WNV-infected+CLO+IMP mice.
Graphs C and D show the number (C) and percentage (D) of cells in 1ml of blood that have taken up IMP, which has been diluted 3x, in WNV-infected+IMP (blue) and WNV-infected+CLO+IMP mice.
Grapsh E and F show the number (E) and percentage (F) of cells in 1ml of blood that have taken up IMP, which has been diluted 9x, in WNV-infected+IMP (blue) and WNV-infected+CLO+IMP mice. Data is representative of 1 sample per group from one experiment.

Appendix Figure 12